frontiers | Research Topics

Metabolic crosstalk between cancer cells and immune cells in the tumor microenvironment: cellular and molecular insights, and their therapeutic implications

Edited by
Parmanand Malvi, Balkrishna Chaube and Shivendra Vikram Singh

Published in
Frontiers in Oncology

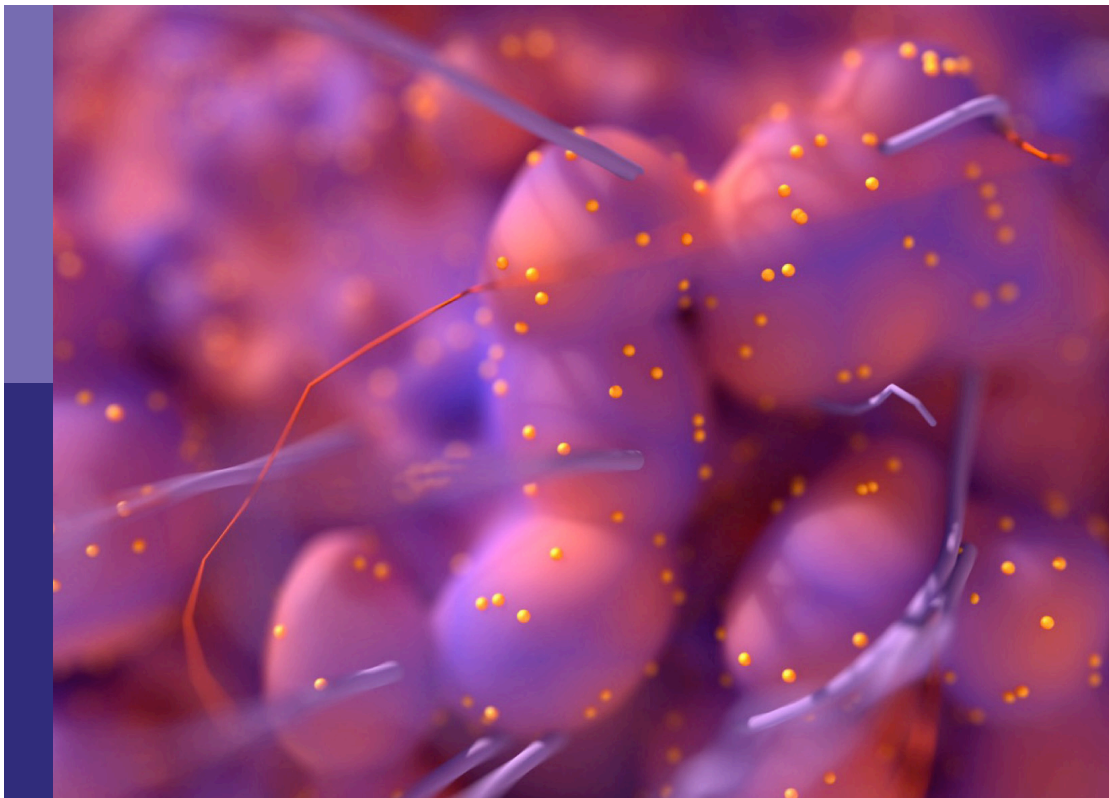

ISSN 1664-8714
ISBN 978-2-8325-7010-4
DOI 10.3389/978-2-8325-7010-4

Generative AI statement
Any alternative text (Alt text) provided alongside figures in the articles in this ebook has been generated by Frontiers with the support of artificial intelligence and reasonable efforts have been made to ensure accuracy, including review by the authors wherever possible. If you identify any issues, please contact us.

About Frontiers

Frontiers is more than just an open access publisher of scholarly articles: it is a pioneering approach to the world of academia, radically improving the way scholarly research is managed. The grand vision of Frontiers is a world where all people have an equal opportunity to seek, share and generate knowledge. Frontiers provides immediate and permanent online open access to all its publications, but this alone is not enough to realize our grand goals.

Frontiers journal series

The Frontiers journal series is a multi-tier and interdisciplinary set of open-access, online journals, promising a paradigm shift from the current review, selection and dissemination processes in academic publishing. All Frontiers journals are driven by researchers for researchers; therefore, they constitute a service to the scholarly community. At the same time, the *Frontiers journal series* operates on a revolutionary invention, the tiered publishing system, initially addressing specific communities of scholars, and gradually climbing up to broader public understanding, thus serving the interests of the lay society, too.

Dedication to quality

Each Frontiers article is a landmark of the highest quality, thanks to genuinely collaborative interactions between authors and review editors, who include some of the world's best academicians. Research must be certified by peers before entering a stream of knowledge that may eventually reach the public - and shape society; therefore, Frontiers only applies the most rigorous and unbiased reviews. Frontiers revolutionizes research publishing by freely delivering the most outstanding research, evaluated with no bias from both the academic and social point of view. By applying the most advanced information technologies, Frontiers is catapulting scholarly publishing into a new generation.

What are Frontiers Research Topics?

Frontiers Research Topics are very popular trademarks of the *Frontiers journals series*: they are collections of at least ten articles, all centered on a particular subject. With their unique mix of varied contributions from Original Research to Review Articles, Frontiers Research Topics unify the most influential researchers, the latest key findings and historical advances in a hot research area.

Find out more on how to host your own Frontiers Research Topic or contribute to one as an author by contacting the Frontiers editorial office: frontiersin.org/about/contact

Metabolic crosstalk between cancer cells and immune cells in the tumor microenvironment: cellular and molecular insights, and their therapeutic implications

Topic editors

Parmanand Malvi — University of Alabama at Birmingham, United States
Balkrishna Chaube — Indian Institute of Technology Dharwad, India
Shivendra Vikram Singh — St. Jude Children's Research Hospital, United States

Citation

Malvi, P., Chaube, B., Singh, S. V., eds. (2025). *Metabolic crosstalk between cancer cells and immune cells in the tumor microenvironment: cellular and molecular insights, and their therapeutic implications*. Lausanne: Frontiers Media SA.
doi: 10.3389/978-2-8325-7010-4

Table of contents

05 Editorial: Metabolic crosstalk between cancer cells and immune cells in the tumor microenvironment: cellular and molecular insights, and their therapeutic implications
Parmanand Malvi, Shivendra Vikram Singh and Balkrishna Chaube

09 Bone marrow adipocytes and lung cancer bone metastasis: unraveling the role of adipokines in the tumor microenvironment
Jian Li, Jialu Wu, Yanni Xie and Xijie Yu

25 Targeting ACAT1 in cancer: from threat to treatment
Tie Sun and Xuan Xiao

32 The causal effects of genetically determined immune cells on gynecologic malignancies: a Mendelian randomization study
Yan Li, Jingting Liu, Qiandan Wang, Yawei Zhou, Chunhua Zhang and Jianying Pei

48 The deregulation of arachidonic acid metabolism in ovarian cancer
Qiuyi Xia, Wen Gao, Jintao Yang, Zhifang Xing and Zhaodong Ji

58 Correlation between fasting blood glucose level and risk of breast cancer in women: a single-center, prospective cohort study
Gefei Li, Mingjie Yin, Zhimin Fan and Fengjiang Qu

65 Gene signatures of copper metabolism related genes may predict prognosis and immunity status in Ewing's sarcoma
Yongqin Chen, Wencan Zhang, Xiao Xu, Biteng Xu, Yuxuan Yang, Haozhi Yu, Ke Li, Mingshan Liu, Lei Qi and Xiejia Jiao

85 Metabolic modulation of melanoma enhances the therapeutic potential of immune checkpoint inhibitors
Zafer Gurel, Michael S. Luy, Qianyun Luo, Nicholas L. Arp, Amy K. Erbe, Aparna H. Kesarwala, Jing Fan and Randall J. Kimple

100 Trace element zinc metabolism and its relation to tumors
Guiping Yao, Zhiwei Wang, Rui Xie, Chenghao Zhanghuang and Bing Yan

110 Integrative analysis of ferroptosis in the hypoxic microenvironment of gastric cancer unveils the immune landscape and personalized therapeutic strategies
Xiao Xu, Liangling Fa, Xiaoxiao Sun, Fangfang Yang, Yongrui Liu, Jifu Song, Yongli Zhao and Jigang Dong

129 Targeting the kynurenine pathway: another therapeutic opportunity in the metabolic crosstalk between cancer and immune cells
Irene Kang, George Theodoropoulos and Medhi Wangpaichitr

137 Bioinformatics and experimental approach reveal potential prognostic and immunological roles of key mitochondrial metabolism-related genes in cervical cancer
Qing Huang, Yang-feng Xu, Hui-ping Li and Ting Zhang

151 Liver kinase B1 expression is associated with improved prognosis and tumor immune microenvironment features in small cell lung cancer
Alessandro Dal Maso, Federica Ferrarini, Giovanni Esposito, Sonia Anna Minuzzo, Anna Maria Puggia, Federica Pezzuto, Elisabetta Zulato, Loc Carlo Bao, Mattia De Nuzzo, Alessandra Ferro, Stefano Frega, Giulia Pasello, Fiorella Calabrese, Matteo Fassan, Federico Rea, Valentina Guarneri, Stefano Indraccolo and Laura Bonanno

161 Unveiling fatty acid subtypes: immunometabolic interplay and therapeutic opportunities in gastric cancer
Huahuan Liu, Xin Hu, Xiangnan Zhang, Yanxin Yao, Liuxing Wu, Ye Tian, Hongji Dai, Kexin Chen and Ben Liu

181 The predictive value of total body PET/CT in high PD-L1 expression and immunotherapy in advanced non-small cell lung cancer patients
Huibin Jin, Bingxin Hu, Jie Zhang, Ye Long, Ang Xuan, Xinyu Wu, Junling Xu and Yongju Gao

frontiers | Frontiers in Oncology

TYPE Editorial
PUBLISHED 11 December 2025
DOI 10.3389/fonc.2025.1751044

OPEN ACCESS

EDITED AND REVIEWED BY
Michael P. Lisanti,
University of Salford, United Kingdom

*CORRESPONDENCE
Parmanand Malvi
parmanandcdri@gmail.com;
pnmalvi@uab.edu
Shivendra Vikram Singh
shivendrasingh5@gmail.com;
shivendra.singh@stjude.org
Balkrishna Chaube
balkrishna@iitdh.ac.in

RECEIVED 21 November 2025
REVISED 21 November 2025
ACCEPTED 01 December 2025
PUBLISHED 11 December 2025

CITATION
Malvi P, Singh SV and Chaube B (2025) Editorial: Metabolic crosstalk between cancer cells and immune cells in the tumor microenvironment: cellular and molecular insights, and their therapeutic implications. *Front. Oncol.* 15:1751044. doi: 10.3389/fonc.2025.1751044

Editorial: Metabolic crosstalk between cancer cells and immune cells in the tumor microenvironment: cellular and molecular insights, and their therapeutic implications

Parmanand Malvi[1]*, Shivendra Vikram Singh[2]* and Balkrishna Chaube[3]*

[1]Department of Biochemistry and Molecular Genetics, University of Alabama at Birmingham, Birmingham, AL, United States, [2]Department of Surgery, St. Jude Children's Research Hospital, Memphis, TN, United States, [3]Department of Biosciences and Bioengineering, Indian Institute of Technology Dharwad, Karnataka, India

KEYWORDS

cancer metabolism, tumor microenvironment, metabolic reprogramming, immune response, immune-cell metabolism, therapeutic target, cancer immunotherapy

Editorial on the Research Topic

Metabolic crosstalk between cancer cells and immune cells in the tumor microenvironment: cellular and molecular insights, and their therapeutic implications

Introduction

Cancer is fundamentally considered as an evolutionary disease characterized by mutation-driven clonal selection, shaped by microenvironmental and therapeutic pressures, leading to heterogeneity, malignant/metastatic progression, and therapy resistance (1–3). Cancer evolution is accompanied by heritable variation (such as point mutations, copy number variation, structural variants, epigenetic changes), selection (e.g., clonal expansion of cells with fitness-enhancing mutations), competition (for example, nutrient/oxygen competition, immune evasion and metabolic competition) and adaptation (such as drug resistance, metastasis and immune escape).

As a part of cancer evolution, metabolic reprogramming is now widely recognized as one of the hallmarks of cancer (4)—not merely as a means by which tumor cells sustain proliferation, but as a central axis by which malignant cells shape their microenvironment and evade immune control (5). Simultaneously, immune cells themselves operate within the metabolic constraints of the tumor microenvironment (TME), adapting—or failing to adapt—to nutrient scarcity, metabolite accumulation, hypoxia, and altered redox states (6). This complex interplay between tumor-cell and immune-cell metabolism forms a dynamic and critical interface—one that presents both mechanistic insight and therapeutic opportunity (5, 6).

The Research Topic *"Metabolic Crosstalk between Cancer Cells and Immune Cells in the Tumor Microenvironment: Cellular and Molecular Insights, and their Therapeutic Implications"* encompasses 14 contributions—nine original research papers, four review articles, and one perspective article— collectively illuminating how metabolic pathways in tumor and immune cells converge, compete, and cooperate—and how these interactions could be harnessed in the clinic.

Articles overview

The contributions to this Research Topic explore how metabolic programs in cancer and immune cells interact in the TME, and how those interactions can be exploited therapeutically. The Research Topic emphasizes lipid, amino-acid and micronutrient metabolism, ferroptosis and redox biology, metabolic biomarkers and gene signatures, and strategies to improve immunotherapy by modulating metabolism. Thus, the Research Topic maps a cross-cutting picture: metabolic programs in tumors are not cell-autonomous — they rewire local and systemic immunity, create metabolic barriers to effective antitumor responses, and offer multiple points for therapeutic intervention (from small-molecule metabolic inhibitors to combination of metabolic and immunotherapy strategies. These works advance our understanding of how metabolism modulates immunity and uncover new therapeutic opportunities for targeting metabolic vulnerabilities.

Mechanistic insights into the tumor–immune metabolic interface

Cancer cells exploit metabolic plasticity to adapt to nutrient-deprived environments and sustain proliferation (7). A key theme emerging across the original research articles is that metabolic reprogramming in tumor cells has dual purpose: supporting the malignant phenotype and actively modulating the immune microenvironment. Several studies in this Research Topic dissect these intertwined processes at multiple biological aspects.

A clinical-translational study by Jin et al. explored the prognostic implications of metabolic imaging in immunotherapy response among non-small cell lung cancer (NSCLC) patients, revealing that elevated total-body PET/CT metabolic activity correlates with high PD-L1 expression and improved outcomes following checkpoint blockade. This clinical link between tumor metabolic phenotype and immune responsiveness highlights the translational potential of metabolic biomarkers. Further mechanistic data explore tumor-intrinsic regulators of metabolism and immune milieu. A study by Dal Maso et al. investigated Liver kinase B1 (LKB1), a master regulator of energy homeostasis, demonstrating its association with favorable prognosis and a remodeled immune microenvironment in small cell lung cancer (SCLC). By linking key metabolic regulators to immune infiltration, this work emphasizes the integrated nature of metabolic and immunological regulation in malignancies. These findings highlight how metabolic gatekeepers may modulate the tumor's immunological landscape.

Mitochondrial metabolism also plays a critical role in cancer (8). A complementary bioinformatics and experimental study by Huang et al. identified mitochondrial metabolism–related genes in cervical cancer that correlate with patient survival and immune infiltration. By integrating transcriptomic and cellular analyses, the authors showcased the mitochondrial–immune axis as a determinant of tumor progression and therapeutic sensitivity. Lipid metabolism is yet another dimension. Liu et al. provided another layer of insight through their integrative analysis of fatty acid metabolic subtypes in gastric cancer, revealing distinct immunometabolic profiles and therapeutic vulnerabilities in these subtypes. Their findings suggest that lipid metabolism may serve as both a biomarker and a therapeutic target in tailoring immunotherapy strategies.

Circulating levels of glucose has been implicated as a major contributor to the occurrence and advancement of malignant tumors. Over a 13-year prospective follow-up study by Li et al., women with higher fasting plasma glucose levels exhibited an increased risk of breast cancer; the study suggests early glucose-control interventions might reduce breast cancer risk. Xu et al. examined ferroptosis—a regulated cell death pathway dependent on lipid peroxidation—within the hypoxic gastric cancer microenvironment. They demonstrated how ferroptosis-related metabolic reprogramming reshapes immune infiltration, offering a framework for combination therapies that exploit ferroptotic sensitivity alongside immune modulation and revealing how regulated cell death mechanisms intersect with immunometabolism.

Using two-sample Mendelian randomization, the study by Li et al. found that genetically predicted levels of various immune cell immunophenotypes causally influence risk of gynecologic malignancies—e.g., B cells panels were protective for cervical cancer, monocyte panels protective for ovarian/vulvar cancer—but reverse causality (cancer → immune cells) was not supported. Adipocytes also play crucial role in various aspects of tumorigenesis (9). The review by Li et al. explores how bone-marrow adipocytes (BMAs) in the bone marrow microenvironment ("soil") facilitate bone metastasis of lung cancer cells ("seed"), via adipokines, provision of lipids, osteoclast/osteoblast regulation and immune modulation, thus emphasizing the adipokines and metabolic interplay between BMAs and tumor cells.

Collectively, these investigations strengthen the concept that tumor and immune cell metabolisms are not separate trajectories but entwined circuits. Tumor cells not only compete for nutrients (such as glucose, amino acids, lipids) but release signaling intermediates/metabolites (e.g., lactate) that actively suppress or reprogram immune effectors. Conversely, immune cell metabolic fitness—and its underlying mitochondrial, lipid and amino-acid metabolism—determines whether immune responses succeed or falter in the TME.

Immunometabolic circuits: translational and therapeutic opportunities

The accompanying articles in this Research Topic also underscore the translational potential of mechanistic insights in oncology. By delineating the molecular and metabolic pathways that drive tumor progression and modulate immune responses, these studies pinpoint actionable vulnerabilities within cancer cells and the tumor microenvironment. Such insights provide a foundation for the rational development of targeted therapies and combination strategies, bridging fundamental biology and clinical implications.

Elevated lactate levels within the TME play a critical role in modulating immune cell function in cancer (10). A preclinical study by Gurel et al. in melanoma showed that combining lactate dehydrogenase inhibitors (LDHIs) with immune checkpoint inhibitors (ICIs) enhanced anti-tumor immune responses and displayed greater efficacy in slowing down the tumor growth, suggesting targeting lactate metabolism may boost ICI efficacy. The review article by Sun and Xiao on acetyl-CoA acetyltransferase 1 (ACAT1) in cancer describes how ACAT1 contributes to tumor initiation, progression, suppression of anti-tumor immunity and proposes ACAT1 inhibition as a therapeutic strategy via targeting cholesterol esterification and tumor immunity. A review on ovarian cancer by Xia et al. discusses how dysregulation of the arachidonic acid metabolic pathways and their metabolites (COX, LOX and CYP450) contributes to tumor initiation, progression, immune-microenvironment alteration, and may serve as a biomarker or therapeutic target.

Aberrant trace-metal metabolism is increasingly recognized as one of the key features of cancer development and progression, influencing proliferation, oxidative stress, immune regulation and therapeutic response (11). A further review by Yao et al. addressed zinc and trace-metal metabolism, an area often overlooked in onco-immunometabolism. Zinc, a critical cofactor for antioxidant and transcriptional processes, exerts context-dependent effects—supporting immune competence at physiological levels but fostering tumor growth when dysregulated. The authors highlight that targeting zinc metalloproteins and modulating zinc transporter function may open novel avenues for cancer therapy. As a key trace element, copper also plays a vital role in mitochondrial energy production, redox homeostasis, and modulation of programmed cell death. A bioinformatic study by Chen et al. developed a five-gene risk signature (TFRC, SORD, SLC11A2, FKBP4 and AANAT) based on copper metabolism-related genes (CMRGs) in Ewing's sarcoma; high-risk patients had significantly worse survival, and the signature also correlated with immune cell infiltration and suggested potential drug sensitivities.

Finally, the perspective article by Kang et al. revisited the kynurenine pathway of tryptophan catabolism—a classic mechanism of tumor-induced immune suppression. The authors propose that dual inhibition of kynurenine pathway's rate-limiting enzymes indoleamine-2,3-dioxygenase 1 (IDO1) and tryptophan 2,3-dioxygenase-2 (TDO2) as well as downstream metabolites could disrupt the metabolic crosstalk between tumor and immune cells. These therapeutic strategies could better reverse immunosuppression in the TME to overcome drug resistance and to improve therapeutic outcomes. Together, these conceptual frameworks point toward a unifying principle: restoring metabolic balance within the TME is central to effective cancer immunotherapy. They emphasize that successful approaches will require careful temporal and spatial tuning of metabolic interventions, as indiscriminate suppression of metabolism may inadvertently impair immune effectors. By understanding how specific pathways influence immune fate decisions, researchers can design interventions that reprogram the TME toward anti-tumor immunity.

Challenges and emerging directions

While the collective findings in this Research Topic provide a powerful snapshot of current progress, they also reveal critical gaps and future challenges. First, the metabolic heterogeneity of tumors remains a major barrier. Spatial and temporal variations in nutrient availability, oxygen tension, and metabolite gradients create complex immunometabolic niches. Advances in single-cell multi-omics and spatial metabolomics will be key to dissecting these interactions *in situ*. Second, metabolic targeting must achieve selectivity to avoid systemic toxicity. Many metabolic enzymes are shared between tumor and immune cells, and indiscriminate inhibition may blunt antitumor immunity. Precision approaches that exploit unique dependencies—such as tumor-specific isoforms, differential transporter expression, or context-driven metabolic states—represent promising frontiers. Third, integrating metabolic interventions with established therapies, including immune checkpoint inhibitors, radiotherapy, and targeted drugs, requires nuanced understanding of timing and sequence. As highlighted by Jin et al., Xu et al., and Gurel et al., metabolic states and metabolites levels can predict and even modulate response to immunotherapy. Prospective trials incorporating metabolic imaging and biomarker-guided treatment are warranted. Finally, the field must expand its translational scope. While many studies in this Research Topic are mechanistic or correlative, translating these insights into robust clinical realities remains challenging. Collaborative efforts that integrate metabolic imaging, metabolite profiling, immune phenotyping, clinical oncology, and computational biology will accelerate the translation of immunometabolic discoveries into therapeutic advances. This integrated approach may allow stratification of patients likely to benefit from metabolic–immunotherapy combinations.

Concluding remarks

The contributions assembled in this Research Topic collectively feature the importance of metabolism as a language of communication within the tumor microenvironment. From

amino acids and lipids to lactate and kynurenine, these metabolites shape the immune landscape, influencing whether tumors thrive or regress.

As the boundaries between cancer cell metabolism and immune regulation blur, it becomes increasingly clear that therapeutic success will depend on decoding—and ultimately rewriting—this metabolic dialogue. The studies presented here provide not only mechanistic insights but also translational pathways to exploit metabolic vulnerabilities for clinical gain.

In summary, this Research Topic reflects the vibrant and rapidly evolving field of cancer immunometabolism. It is our hope that this Research Topic will stimulate deeper cross-disciplinary collaboration among metabolism researchers, immunologists and clinicians. It reaffirms that metabolic crosstalk is not merely a consequence of tumor growth but a driving force of tumor–immune dynamics. Continued integration of metabolic research with immunotherapy promises to unlock new frontiers in precision oncology.

Author contributions

PM: Conceptualization, Formal Analysis, Investigation, Resources, Supervision, Validation, Visualization, Writing – original draft, Writing – review & editing. SS: Conceptualization, Formal Analysis, Investigation, Resources, Supervision, Validation, Visualization, Writing – review & editing. BC: Conceptualization, Formal Analysis, Investigation, Resources, Supervision, Validation, Visualization, Writing – review & editing.

Acknowledgments

We would like to thank the authors of the articles published in this Research Topic for their valuable contributions to the field, and all reviewers for providing peer-review of the manuscripts in a rigorous manner. We would also thank the Frontiers specialists, including Ryan Costello, Amber Cigelske, Tim Rinehart, Kai Thomas, Samuel Oliver, Mark Simões, Rebecca Wood, Philip Elwell and Abigail Rosser, for their initial and ongoing support.

Conflict of interest

The authors declared that this work was conducted in the absence of any commercial or financial relationships that could be construed as a potential conflict of interest.

The authors declared that they were an editorial board member of Frontiers, at the time of submission. This had no impact on the peer review process and the final decision.

Generative AI statement

The author(s) declared that generative AI was not used in the creation of this manuscript.

Any alternative text (alt text) provided alongside figures in this article has been generated by Frontiers with the support of artificial intelligence and reasonable efforts have been made to ensure accuracy, including review by the authors wherever possible. If you identify any issues, please contact us.

Publisher's note

References

1. Merlo LM, Pepper JW, Reid BJ, Maley CC. Cancer as an evolutionary and ecological process. *Nat Rev Cancer*. (2006) 6:924–35. doi: 10.1038/nrc2013

2. Ciriello G, Magnani L, Aitken SJ, Akkari L, Behjati S, Hanahan D, et al. Cancer evolution: A multifaceted affair. *Cancer Discov*. (2024) 14:36–48. doi: 10.1158/2159-8290.CD-23-0530

3. Swanton C, Bernard E, Abbosh C, Andre F, Auwerx J, Balmain A, et al. Embracing cancer complexity: hallmarks of systemic disease. *Cell*. (2024) 187:1589–616. doi: 10.1016/j.cell.2024.02.009

4. Hanahan D, Weinberg RA. Hallmarks of cancer: the next generation. *Cell*. (2011) 144:646–74. doi: 10.1016/j.cell.2011.02.013

5. Pavlova NN, Thompson CB. The emerging hallmarks of cancer metabolism. *Cell Metab*. (2016) 23:27–47. doi: 10.1016/j.cmet.2015.12.006

6. Leone RD, Powell JD. Metabolism of immune cells in cancer. *Nat Rev Cancer*. (2020) 20:516–31. doi: 10.1038/s41568-020-0273-y

7. Al-Masri M, Paliotti K, Tran R, Halaoui R, Lelarge V, Chatterjee S, et al. Architectural control of metabolic plasticity in epithelial cancer cells. *Commun Biol*. (2021) 4:371. doi: 10.1038/s42003-021-01899-4

8. Vasan K, Werner M, Chandel NS. Mitochondrial metabolism as a target for cancer therapy. *Cell Metab*. (2020) 32:341–52. doi: 10.1016/j.cmet.2020.06.019

9. Nieman KM, Romero IL, Van Houten B, Lengyel E. Adipose tissue and adipocytes support tumorigenesis and metastasis. *Biochim Biophys Acta*. (2013) 1831:1533–41. doi: 10.1016/j.bbalip.2013.02.010

10. Wang ZH, Peng WB, Zhang P, Yang XP, Zhou Q. Lactate in the tumour microenvironment: from immune modulation to therapy. *EBioMedicine*. (2021) 73:103627. doi: 10.1016/j.ebiom.2021.103627

11. Gorska A, Markiewicz-Gospodarek A, Trubalski M, Zerebiec M, Poleszak J, Markiewicz R. Assessment of the impact of trace essential metals on cancer development. *Int J Mol Sci*. (2024) 25:13. doi: 10.3390/ijms25136842

frontiers | Frontiers in Oncology

TYPE Review
PUBLISHED 20 March 2024
DOI 10.3389/fonc.2024.1360471

OPEN ACCESS

EDITED BY
Parmanand Malvi,
University of Alabama at Birmingham, United States

REVIEWED BY
Amit Kumar,
University of Maryland, United States
Ajit Prakash,
University of North Carolina at Chapel Hill, United States

*CORRESPONDENCE
Xijie Yu
xijieyu@scu.edu.cn

RECEIVED 23 December 2023
ACCEPTED 08 March 2024
PUBLISHED 20 March 2024

CITATION
Li J, Wu J, Xie Y and Yu X (2024) Bone marrow adipocytes and lung cancer bone metastasis: unraveling the role of adipokines in the tumor microenvironment. *Front. Oncol.* 14:1360471. doi: 10.3389/fonc.2024.1360471

Bone marrow adipocytes and lung cancer bone metastasis: unraveling the role of adipokines in the tumor microenvironment

Jian Li[1,2], Jialu Wu[1], Yanni Xie[1] and Xijie Yu[1]*

[1]Laboratory of Endocrinology and Metabolism/Department of Endocrinology and Metabolism, Rare Disease Center, West China Hospital, Sichuan University, Chengdu, China, [2]Department of Endocrinology and Metabolism, Shandong Second Provincial General Hospital, Jinan, China

Bone is a common site of metastasis for lung cancer. The "seed and soil" hypothesis suggests that the bone marrow microenvironment ("soil") may provide a conducive survival environment for metastasizing tumor cells ("seeds"). The bone marrow microenvironment, comprising a complex array of cells, includes bone marrow adipocytes (BMAs), which constitute about 70% of the adult bone marrow volume and may play a significant role in tumor bone metastasis. BMAs can directly provide energy for tumor cells, promoting their proliferation and migration. Furthermore, BMAs participate in the tumor microenvironment's osteogenesis regulation, osteoclast(OC) regulation, and immune response through the secretion of adipokines, cytokines, and inflammatory factors. However, the precise mechanisms of BMAs in lung cancer bone metastasis remain largely unclear. This review primarily explores the role of BMAs and their secreted adipokines (leptin, adiponectin, Nesfatin-1, Resistin, chemerin, visfatin) in lung cancer bone metastasis, aiming to provide new insights into the mechanisms and clinical treatment of lung cancer bone metastasis.

KEYWORDS

bone marrow adipocytes, adipokines, tumor bone metastasis, lung cancer bone metastasis, immune response

1 Introduction

According to data released by the Global Burden of Disease Study in 2020, an estimated 2.2 million people worldwide are afflicted with lung cancer, with approximately 1.8 million deaths. As the cancer with the highest incidence and mortality rate globally, lung cancer is the leading cause of cancer death among men and the second leading cause among women. Despite substantial regional variations in incidence and mortality rates between men and women, statistics show that rates in men are approximately twice those in women (1).

Compared to other malignancies, lung cancer continues to have a low survival rate, with a 5-year survival rate of only 5% for advanced stages (2). One of the main characteristics of malignant tumors is their ability to metastasize, and over 90% of lung cancer patients die from complications related to metastasis. Bone is among the most common metastasis sites for lung cancer, with an incidence rate of 30-40%. Clinical data indicate that approximately 40-48% of patients with advanced lung cancer exhibit bone metastasis at initial diagnosis (3). Once bone metastasis occurs, the median survival time of patients significantly reduces to only five months (3).Depending on radiological features, lung cancer bone metastasis can be classified into osteolytic, osteoblastic, and mixed types. Studies have shown that approximately 70% of lung cancer bone metastases are osteolytic, with osteoblastic types being less common (4). Following osteolytic bone metastasis in lung cancer, about 50% of patients will experience skeletal-related events (SREs), including intractable bone pain, pathological fractures, spinal cord compression, and hypercalcemia, which accelerate disease deterioration, diminish quality of life, decrease physical abilities, increase medical expenses, and elevate mortality rates. Given that current treatments for lung cancer bone metastasis are limited to symptom relief and cannot effectively slow the progression or fundamentally alter the pathological process, elucidating the pathogenic mechanisms of lung cancer bone metastasis and exploring effective early diagnosis and treatment strategies are crucial.

2 Pathological processes of lung cancer bone metastasis

The occurrence of lung cancer bone metastasis results from a series of complex pathological processes, which can generally be divided into tumor invasion, tumor cell migration, and bone tissue invasion stages. The initiation phase of bone metastasis involves tumor cells escaping the primary site and entering the circulation, forming disseminated tumor cells (DTCs) (5). The epithelial-mesenchymal transition (EMT) plays a key role in this process, where epithelial cells lose polarity and cell-cell adhesion, acquiring mesenchymal characteristics (6). Studies have demonstrated that abnormal activation of the Wnt/β-catenin pathway can induce the onset and progression of tumor EMT (7). Both *in vitro* and *in vivo* studies have observed an increase in β-catenin expression under hypoxic conditions, promoting EMT progression, affecting lung cancer cell migration capabilities, and inducing morphological changes (8). Lung cancer cells can also secrete E-cadherin and matrix metalloproteinases(MMPs), degrading the extracellular matrix, reducing cell adhesion and cross-linking, facilitating tumor cell detachment from the tumor matrix into the circulation as circulating tumor cells (CTCs), and ultimately forming DTCs that migrate to the bone marrow microenvironment (9). Upon reaching the bone marrow microenvironment, tumor cells undergo stages of settlement, survival, and dormancy, eventually reactivating and forming proliferative metastatic foci (5) (Figure 1).

3 The role of the bone marrow microenvironment in lung cancer bone metastasis

The "seed and soil" hypothesis suggests that during the process of bone metastasis, the bone marrow microenvironment ("soil") may provide an "ecological niche" suitable for metastasis, laying the foundation for the seeding, invasion, and proliferation of tumor cells ("seeds") (10). A conducive "soil" may determine whether the "seeds" will germinate, as research has found that less than 0.01% of circulating tumor cells ultimately form distal metastases (11). The activation process of tumor cells within the bone marrow microenvironment (the germination process of "seeds" in the "soil") is the result of bilateral interaction.

On one hand, tumor cells interact with various cells in the bone microenvironment, such as bone marrow stromal cells (BMSCs), osteoclast (OCs), osteoblasts (OBs), endothelial cells (ECs), BMAs, immune cells, etc., causing adaptive changes in the bone marrow microenvironment and providing favorable conditions for tumor cell invasion and growth (12). For instance, *in vivo* studies have found that BMSCs can be chemotactically guided to tumor cells, participating in the construction of the tumor microenvironment (13). Lung cancer cells can also activate OCs, causing bone matrix dissolution and creating conditions for their adhesion and settlement (14). ECs in the microenvironment can enhance tumor metastasis through angiogenesis, providing an energy source and new pathways for tumor cell invasion and migration (15).

On the other hand, various growth factors secreted by lung cancer cells, such as EGF-like domain multiple 6, bone morphogenetic protein-7 (BMP-7), transforming growth factor-beta (TGF-β), endothelin-1 (ET-1), fibroblast growth factors (FGFs), platelet-derived growth factors (PDGF), etc., can directly affect the composition of the tumor microenvironment (16–19). For instance, EGF-like domain multiple 6 secreted by lung adenocarcinoma cells can enhance the EMT process, activate the Wnt/β-catenin and PI3K/AKT/mTOR pathways, promoting lung adenocarcinoma cell proliferation, migration, and invasion capabilities. Overexpression of this factor in a nude mouse model can enhance tumor growth and exacerbate bone resorption. *In vitro* studies have also found that it can increase OC differentiation of mouse bone marrow mononuclear macrophages via the NF-κB and c-Fos/NFATc1 signaling pathways (16). *In vitro* cell studies have shown that downregulating BMP-7 expression can significantly inhibit the invasiveness of lung adenocarcinoma SPC-A1 cells, while upregulating BMP-7 notably promotes the migration ability of A549 cells (17). Clinical studies have also found BMP-7 expression in the tumor cell membrane and cytoplasm of non-small cell lung cancer (NSCLC), with high cytoplasmic BMP-7 expression associated with tumor progression and adverse prognosis. These results all demonstrate that BMP-7 secreted by lung cancer cells, through affecting cell invasiveness and migration capability, promotes its growth and spread in bone tissues (18). *In vitro* cell studies indicate that TGF-β secreted by lung cancer cells can not only promote tumor microenvironment angiogenesis to facilitate lung cancer cell

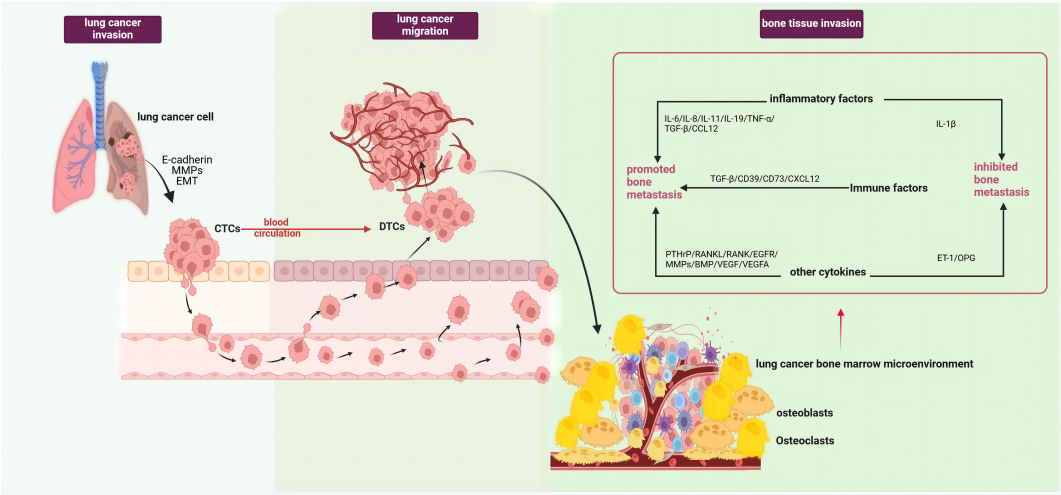

FIGURE 1
Pathological processes of lung cancer bone metastasis (created with BioRender.com.). The occurrence of bone metastasis in lung cancer could be divided into three stages, tumor invasion, tumor cell migration, and bone tissue invasion. In the first stage, lung cancer cells secreted E-cadherin and MMPs, along with EMT of lung cancer cells, enabling their entry into circulation and formation of DTCs. In the second stage, lung cancer cells detached from the tumor matrix and entered circulation to become CTCs. In the third stage, after lung cancer cells migrated to the bone marrow microenvironment, under the combined effects of various interactions between different cell types and factors within the tumor microenvironment, they became reactivated and formed proliferative metastatic lesions. This stage mainly involved the roles of various factors in the tumor microenvironment in bone metastasis,such as pro-metastatic inflammatory factors (IL-6, IL-8, IL-11, IL-19, TNF-α, CCL12), immune factors (TGF-β, CD39, CD73, CXCL12), and other factors (PTHrP, MMPs, RANKL, RANK, BMP, EGFR/VEGF, VEGFA). Factors that inhibited lung cancer bone metastasis included IL-1β, OPG, and ET-1. EMT, epithelial-mesenchymal transition; MMPs, matrix metalloproteinases; DTCs, Disseminated tumor cells; CTCs, Circulating tumor cells; IL-1β, Interleukin 1 beta; IL-6, Interleukin 6; IL-8, Interleukin 8; IL-11, Interleukin 11, IL-19, Interleukin 19; CCL12, C-C motif chemokine ligand 12; TNF-α, Tumor necrosis factor alpha; TGF-β, Transforming growth factor beta; CD39, Cluster of differentiation 39; CD73, Cluster of differentiation 73; CXCL12, C-X-C motif chemokine ligand 12; PTHrP, Parathyroid hormone-related protein; MMPs, Matrix metalloproteinases; RANKL, Receptor activator of nuclear factor kappa B ligand; RANK, Receptor activator of nuclear factor kappa B; BMP, Bone morphogenetic protein; OPG, Osteoprotegerin; ET-1, Endothelin 1.

proliferation and migration but also regulate T cell activity to inhibit the immune system's recognition and attack on tumor cells, helping the tumor evade immune surveillance (19). Additionally, TGF-β can increase the invasive and migratory capabilities of lung cancer cells, thereby promoting bone metastasis (20). Both *in vivo* and *in vitro* studies have confirmed that MMPs and urokinase plasminogen activator secreted by lung cancer cells can specifically degrade bone matrix components (such as collagen and trabeculae), leading to bone tissue destruction and dissolution, facilitating tumor cell invasion into bone tissues (21). A study on microRNA-328 (miR-328) secreted by lung adenocarcinoma A549 cells discovered that miR-328, potentially through the downregulation of neuropilin-2 (Nrp-2) expression in A549-derived extracellular vesicles (A549-Exos) *in vitro*, enhanced OC formation and bone resorption. Meanwhile, the *in vivo* administration of a miR-328 inhibitor in A549-Exos significantly inhibited bone resorption (22). Lastly, the unique invasiveness, infiltrative capability, and rapid growth and migration ability of tumor cells also affect the transformation of the metastatic foci's microenvironment (23). Tumor cells can also engage in inflammatory reactions and a series of complex interactions with immune cells in the microenvironment, enabling tumor cells to evade immune surveillance, thereby promoting their proliferation and migration (24). Additionally, the metabolic decomposition of BMAs can produce a large amount of lipids, providing energy for tumor cells, promoting their proliferation, migration, and invasion. BMAs can also secrete certain adipokines, such as leptin, by activating signaling pathways such as PI3K, HIF, and MAPK, enhancing the proliferation, migration, and invasion capabilities of lung cancer cells (25, 26) (Figure 1).

3.1 The role of OCs in lung cancer bone metastasis

The osteolytic lesions in lung cancer bone metastasis are primarily caused by the activation of OCs. Lung cancer cells can directly influence OCs or indirectly upregulate their function through secreted active factors, thereby promoting lung cancer bone metastasis (27). For instance, lung cancer cells secrete extracellular vesicles containing amphiregulin (AREG), which induces abnormal activation of the EGFR signaling in OCs, upregulating MMP-9 and thus triggering osteolytic metastasis (28). Lung adenocarcinoma secreted miR-21 suppresses programmed cell death 4 (PDCD4), promoting the generation of OCs and hence facilitating osteolytic lesions in lung cancer (29). Additionally, experimental studies with lung cancer cells have found that they secrete parathyroid hormone-related protein (PTHrP), which binds to the PTH/PTHrP receptor, enhances the expression of the receptor activator of nuclear factor-kappa B ligand (RANKL), and inhibits the synthesis of osteoprotegerin (OPG) (30). RANKL binds to the receptor activator of nuclear factor κB (RANK) on the surface of OC precursor cells, inducing OC

aggregation and activation, enhancing their activity, and causing osteolytic destruction (31). The release of insulin-like growth factor-1 (IGF-1) and TGF-β from bone matrix, in turn, acts on tumor cells: IGF-1 promotes tumor cell proliferation and inhibits apoptosis, while TGF-β induces the tumor to secrete more PTHrP, activating more OCs, and dissolving the bone matrix again (32), forming a "vicious cycle" that promotes the occurrence and development of tumor bone metastasis. Furthermore, *in vivo* and *in vitro* studies have discovered that lung adenocarcinoma A549 cells induce OCs to secrete the ligand IL-19 for IL-20RB, activating the downstream JAK1/STAT3 signaling pathway, and promoting lung cancer proliferation in the bone microenvironment (33). Importantly, blocking IL-20RB with neutralizing antibodies can significantly inhibit lung cancer bone metastasis. These data demonstrate the important role played by activated OCs in osteolytic bone metastasis of lung cancer (Figure 2).

3.2 The role of OBs in lung cancer bone metastasis

Compared to osteolytic metastasis, osteoblastic (bone-forming) metastasis of lung cancer is less common (34). Currently, most studies on osteoblastic metastasis suggest that under various influences, OBs participate in tumor bone metastasis through secreting molecules to affect OC formation and tumor progression. Factors promoting osteogenic differentiation of OBs include BMP, ET-1, semaphorin 3A (Sema3A), vascular endothelial growth factor (VEGF), monocyte chemoattractant protein-1 (MCP-1), and interleukin-6 (IL-6), etc. (34–36). For example, Wnt/β-catenin signaling and DKK1 (a Wnt signaling pathway inhibitor) can promote lung cancer metastasis, particularly bone metastasis (37). *In vitro* cell studies discovered that ET-1 significantly downregulates DKK1 in OBs, while also upregulates osteogenic genes (such as IL-6, Wnt5a, RANKL, etc.) (38). Thus, ET-1, as a key tumor factor, can not only upregulate genes promoting osteogenesis but also downregulate negative regulators of osteogenesis, participating in tumor osteoblastic metastasis. Additionally, miR-139-5p was found to positively regulate the osteogenic differentiation of mesenchymal stem cells (MSCs) (39). However, Feng et al. found that miR-139-5p inhibits osteogenic differentiation. *In vivo* model studies showed that upregulation of miR-139-5p reduced cell proliferation and osteogenic differentiation in MSCs by targeting NOTCH1 and inhibiting the Wnt/β-catenin signaling pathway (40). *In vitro* cell studies also found that hypoxia-inducible factor-1α (HIF-1α) can inhibit osteogenic differentiation by upregulating Sema4D, thus participating in lung cancer bone metastasis (41). Engblom et al. found that OBs also have a distal regulatory role in lung cancer

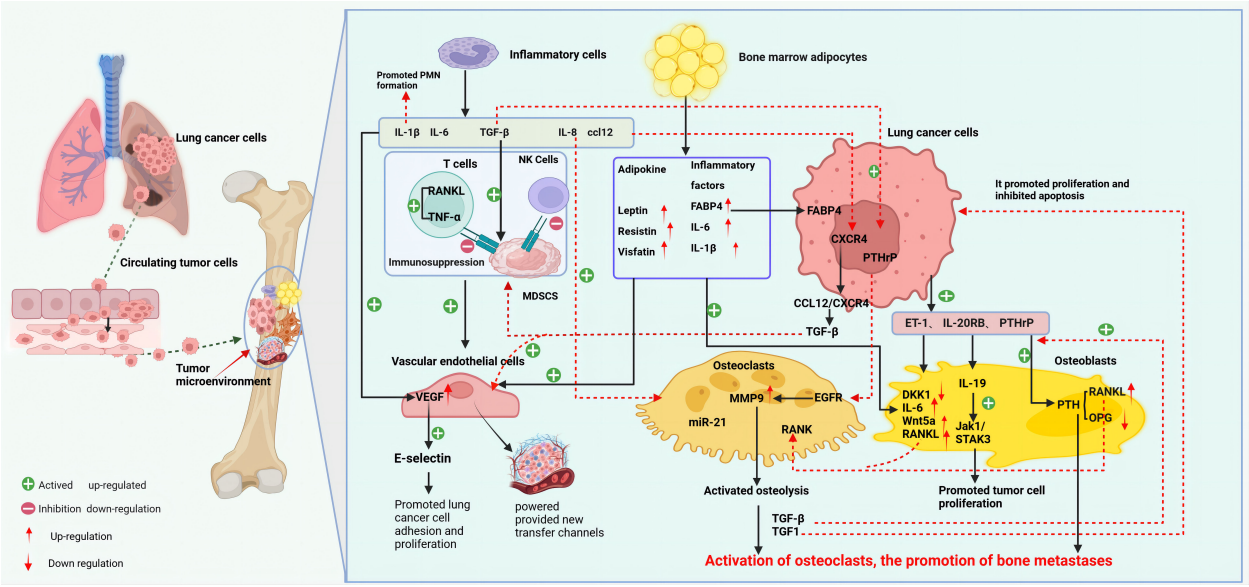

FIGURE 2
Mechanism of bone metastasis in lung cancer (created with BioRender.com.). The main mechanism of bone metastasis in lung cancer is the interaction between various cells (OC, OB, EC, BMA, inflammatory cells, etc.) in the bone microenvironment and lung cancer cells, which leads to adaptive changes in the bone marrow microenvironment for tumor cell invasion and growth. At the same time, various factors secreted by lung cancer cells also participate in and affect the composition of the tumor microenvironment. Bone metastasis in lung cancer mainly manifests as osteolytic lesions. Lung cancer cells can directly or indirectly activate OC, initiating a vicious cycle of bone resorption, promoting bone matrix dissolution and lung cancer bone metastasis. OB metastasis is relatively rare in lung cancer, mainly through the downregulation of DKK1 in OB by ET-1 secreted by lung cancer cells, upregulation of osteogenic genes such as IL-6 and RANKL, and promotion of OB metastasis. Lung cancer cells, inflammatory cells, and BMA in the bone tumor microenvironment release inflammatory factors, participate in the construction of an immune-suppressive and tumor angiogenesis microenvironment, and provide conditions for lung cancer cells to evade immune surveillance, proliferate,and migrate. BMA, bone marrow adipocytes; ccl12, chemokine 12; CXCR4, CXC chemokine receptor 4; DKK1, Dickkopf-1; ET-1, endothelin-1; EC, endothelial cells; EGFR, epidermal growth factor receptor; IL-19, Interleukin-19; IL-20R, interleukin 20 receptor; MDSCs, myeloid-derived suppressor cells; MMP9, matrix metalloproteinase 9; OB, osteoblasts; OC, osteoclasts; PTHrP, parathyroid hormone-related protein; PTH, parathyroid hormone; RANK, receptor activator of nuclear factor κ B; RANKL, RANK ligand; sVCAM1, soluble vascular cell adhesion molecule-1.

progression (42). However, the specific mechanisms of OBs in lung cancer bone metastasis are still not fully understood and require further in-depth research (Figure 2).

3.3 The role of inflammatory cells in bone metastasis of lung cancer

It is well-documented that inflammation plays a critical role in tumor progression. Both lung cancer cells and inflammatory cells secrete pro-inflammatory cytokines, which not only directly participate in the formation of the pre-metastatic niche (PMN) but also engage in the activation, proliferation, and migration of tumor cells in the microenvironment, thereby facilitating bone metastasis (43). Evidence suggests that cytokines such as interleukin-1β (IL-1β), IL-6, interleukin-7 (IL-7), interleukin-8 (IL-8), interleukin-11 (IL-11), tumor necrosis factor-alpha (TNF-α), TGF-β, and C-C motif chemokine ligand 12 (CCL12) play significant roles in the bone metastasis of lung cancer (43–46). For instance, studies have shown that blocking IL-1β in K-ras mutant lung adenocarcinoma (KM-LUAD) mice, which express high levels of IL-1β in the lungs, significantly reduces tumor load when IL-1β monoclonal antibodies are administered at 6 and 14 weeks of age (47). Clinical research also confirms that inhibiting IL-1β significantly reduces the incidence rate of lung cancer in a dose-dependent manner (48). Lung cancer cells secrete IL-6 and IL-11, which can activate various signaling pathways such as PI3K/Akt and MAPK, promoting cell proliferation and migration (49–52). *In vitro* studies reveal that IL-11 can stimulate OC formation and activation, accelerate bone resorption, and release growth factors such as TGF-β in the bone matrix, thereby promoting the growth and metastasis of lung cancer cells (53). Additionally, IL-8 has been found to increase the invasive capabilities of tumor cells and promote OC maturation and activation, leading to the release of key enzymes such as acid phosphatase and MMPs that degrade the bone matrix and further enhance bone dissolution (54). IL-8 also induces BMSC to secrete RANKL while inhibiting OPG secretion, leading to RANKL/OPG dysregulation, thus promoting OC activation and maturation and subsequent bone resorption (55). Moreover, IL-1, IL-6, IL-8, TNF-α, and TGF-β secreted by lung cancer cells can activate downstream signaling pathways to increase VEGF expression, thereby promoting angiogenesis in the bone tumor microenvironment and indirectly facilitating bone metastasis (56). These inflammatory cytokines can also recruit and induce immune cells, notably myeloid-derived suppressor cells (MDSCs), tumor-associated macrophages, and neutrophils, creating an immunosuppressive local milieu that promotes tumor cell survival and thereby indirectly facilitating bone metastasis (57). *In vitro* cell studies have shown that activation of the KRAS signaling pathway can upregulate tumor cell secretion of CCL12, which promotes tumor cell recruitment to target organs through binding to its receptor CXCR4 (46). Research has confirmed that upregulation of CXCL12 promotes cancer cell metastasis and growth in bone metastases of breast and prostate cancers (58, 59). The expression of CXCR4 is elevated in bone destruction areas of NSCLC bone metastasis patients (60). Furthermore, clinical studies have found TGF-β promoting CD39 and CD73 expression on MDSCs, which can suppress T cell and NK cell activity, thus contributing to the formation of an immunosuppressive microenvironment and enabling tumor cells to evade immune surveillance (61). These findings underscore the pivotal role of inflammatory cells and their secreted cytokines in lung cancer bone metastasis, though the complex inflammatory response mechanisms involved in lung cancer bone metastasis require further research (Figure 2).

3.4 The role of the RANK/RANKL signaling axis in bone metastasis of lung cancer

The RANK/RANKL signaling axis, crucial for maintaining bone homeostasis, plays a key role in tumor bone metastasis. RANKL, a critical regulator of OC differentiation, is chiefly secreted by OBs, osteocytes, and activated T cells. Binding of RANKL to RANK activates signaling pathways in OC precursors, promoting OC formation and enhancing bone resorption (62). OPG, a competitive receptor for RANKL, inhibits the RANKL-RANK interaction, thereby reducing OC formation and activity (63).

3.4.1 Direct effects of the RANKL/RANK signaling pathway on bone metastasis of lung cancer

The RANKL/RANK signaling pathway directly affects the functionality of lung cancer cells and OCs, playing a role in bone metastasis of lung cancer. *In vitro* studies have revealed that RANKL, by activating the RANK receptor, can promote lung cancer cell proliferation and growth while inhibiting apoptosis (64). Other research has shown that activation of the RANKL/RANK signaling pathway enhances OC functionality within the bone marrow microenvironment, aiding bone resorption and consequently facilitating bone metastasis (65).

3.4.2 Indirect effects of the RANKL/RANK signaling pathway on bone metastasis of lung cancer

The indirect mechanisms in bone metastasis include: 1) Activation of NF-κB, MAPK, and other signaling pathways to promote lung cancer proliferation and growth (66). 2) Release of inflammatory cytokines and other cellular factors, altering the composition of the tumor microenvironment and indirectly facilitating bone metastasis (62). 3) Regulation of the activation and function of immune cells within the tumor microenvironment. In certain cases, activation of the RANKL/RANK signaling pathway induces immunosuppressive molecules (e.g., TGF-β from Treg cells), regulating the immune response balance, allowing lung cancer cells to evade immune surveillance and promote bone metastasis (67). Moreover, RANKL can stimulate the maturation and activation of dendritic cells, macrophages, and other immune cells, enhancing their cytokine and chemokine production, thus boosting antigen presentation and T cell activation capabilities (65, 68). Additionally, RANKL/RANK signaling activation can regulate the NF-κB signaling

pathway to inhibit B cell apoptosis, promoting B cell survival and proliferation capacity, providing a protective environment for lung cancer cells to escape immune surveillance, thereby inhibiting lung cancer cell apoptosis and promoting bone metastasis (69). In summary, RANKL/RANK maintains immune homeostasis through various immune regulation mechanisms, indirectly participating in bone metastasis. 4) Regulation of VEGF receptor activation and tumor angiogenesis. It also promotes EC growth, migration, and lumen formation, contributing to tumor microenvironment angiogenesis (70, 71). The RANK/RANKL signaling axis plays a complex role in lung cancer bone metastasis, with the specific mechanisms requiring further in-depth study.

3.5 The role of lung cancer cell apoptosis in bone metastasis

Apoptosis functions as a critical protective mechanism within organisms, which eliminates aberrant cells and prevents tumor genesis. When apoptosis of tumor cells is inhibited, cells may evade immune surveillance, thereby enhancing their survival and propagation (72). *In vitro* studies have revealed that lung cancer cells can suppress the initiation of apoptosis by upregulating the anti-apoptotic protein Bcl-2, which blocks the release of apoptogenic cytochrome c; they can also inhibit apoptosis by downregulating pro-apoptotic proteins, such as Bax and Bak, thus promoting their survival within the bone marrow microenvironment (73, 74). Furthermore, lung cancer cells can interact with other cells in the bone microenvironment (such as OBs, OCs, and BMAs), not only augmenting the anti-apoptotic capabilities of lung cancer cells but also enhancing the function of OCs (73). For instance, proteins of the Bcl-2 family can inhibit the apoptosis of lung cancer cells and promote the differentiation and function of OCs. Cytokines released during the apoptosis of lung cancer cells, such as TNF-α, TGF-β, and VEGF, can indirectly promote bone metastasis by fostering inflammation and angiogenesis within the tumor microenvironment (75). Additionally, the release of lactate and ATP post-apoptosis can upregulate the metabolic state of bone cells and increase acidification of the tumor microenvironment, indirectly facilitating bone resorption in the context of lung cancer bone metastasis (76).

3.6 Mechanisms of angiogenesis and VEGF in bone metastasis

During tumor metastasis, lung cancer cells and ECs release VEGF to promote the formation of new blood vessels, supplying the tumor with additional nutrients and growth factors, and providing new physical pathways for tumor metastasis. For example, MDSCs, as critical molecules in PMN formation, can produce VEGFA, which upregulates E-selectin, thereby enhancing the adhesion of tumor cells, and facilitating the homing and proliferation of circulating tumor cells (77). Furthermore, MDSCs can secrete MMP9 to regulate the function of VEGF to promote angiogenesis and tumor cell extravasation and migration (78, 79). Increasing research indicates that adipokines (such as leptin, resistin, visfatin, etc.) and inflammatory factors (such as IL-1β, IL-6, chemokines, FABP4, etc.) secreted by BMA can also regulate angiogenesis, indirectly facilitating the progression of tumor bone metastasis (80–83). Occupying 70% of the bone marrow cavity volume, BMAs constitute a major component of the bone marrow microenvironment, and their role in tumor bone metastasis is gaining increasing attention, particularly the regulatory effects of secreted adipokines on energy metabolism, endocrine functions, and inflammatory responses in influencing tumor growth and migration (81, 83). Despite numerous studies on tumor bone metastasis and the bone marrow microenvironment, the mechanisms linking BMAs and lung cancer bone metastasis remain largely unexplored. This text will next focus on elucidating the mechanisms underlying the role of BMAs and their secreted adipokines in lung cancer bone metastasis (Figure 2).

4 The role of BMAs in lung cancer bone metastasis

4.1 Origin and distribution of BMAs

BMAs originate from a distinct cell population within the bone marrow, comprising MSCs and preadipocytes of the marrow adipogenic lineage (84). While historically regarded as an inert adipose tissue, recent studies have identified unique characteristics and functions of BMAs, distinguishing them from white, brown, and beige adipose tissues (85, 86). In humans, BMAs are primarily located in the marrow of long bones, especially within the trabecular bone at the epiphyses and metaphyses, and near the endosteal surface of the bone shaft (87). The abundance of BMAs in the bone marrow increases with aging, obesity, the application of peroxisome proliferator-activated receptor γ (PPARγ), and radiation exposure (85, 88). Studies in ovariectomized mouse models have shown that estrogen deficiency leads to an increase in BMAs, which can be reversed by estrogen supplementation (89). Clinical research on osteoporosis has revealed that the age-related increase in BMAs is associated with bone loss, suggesting BMAs as negative regulators of bone mass (90). However, this correlation is not uniformly observed across studies. In C57BL/6 mice (with the lowest trabecular and cortical bone density among all mouse strains), BMAs are scarce, whereas they are abundant in C3H/He mice (a unique strain with higher bone density) (91, 92), implying genetic regulation of BMA distribution and the need for further comprehensive analysis (Figure 2).

4.2 The role of BMAs as key components of the bone marrow microenvironment in lung cancer bone metastasis

4.2.1 The effect of BMAs on OCs in lung cancer bone metastasis

BMAs can secrete factors like RANKL, IL-6, and TNF-α, which activate OCs to promote bone resorption within the bone

microenvironment (93, 94). *In vitro* studies have shown that BMAs can upregulate the RANK expression on OCs, leading to increased OC formation (95). Research on breast cancer bone metastasis demonstrated that activated OCs release acid phosphatase, acidifying the bone microenvironment (96, 97). This acidic environment upregulates matrix MMPs, and BMAs further contribute to bone matrix degradation by upregulating expression of OC-specific genes such as cathepsin K, facilitating tumor cell growth (98). IL-1β and IL-6 can induce EMT in breast cancer cells via the STAT3 pathway and promote angiogenesis, which suggests that BMAs may similarly exacerbate bone destruction in lung cancer bone metastasis (Figure 2).

4.2.2 The effect of BMAs on OBs in lung cancer bone metastasis

Studies have shown that enhanced adipogenic differentiation of bone marrow MSCs in the bone marrow microenvironment leads to a decrease in their osteogenic potential (99). BMAs contribute to the regulation of OB function by secreting inflammatory factors such as IL-6, IL-1β, and TNF-α (100–102). Both tumor cells and BMAs can produce IL-6, which promotes tumor cell proliferation, induces OC activation, and downregulates OB activity (102). Additionally, IL-6 promotes adipogenic differentiation of MSCs while inhibiting osteogenesis (103). An increase in palmitic acid and arachidonic acid, associated with increased BMAs, heightens the cytotoxic effects on OBs. *In vitro* studies indicate that palmitate-induced lipotoxicity in OBs and osteocytes is mediated by autophagy dysregulation, leading to OB apoptosis (104). Given that lung cancer cells also secrete IL-6 and TNF-α, it is speculated that lung cancer cells and BMAs, by regulating OB function and inhibiting osteogenic differentiation, indirectly disrupt bone remodeling and promote lung cancer bone metastasis (Figure 2).

4.2.3 The effect of BMAs on ECs in lung cancer bone metastasis

BMAs can regulate EC function through both direct and indirect mechanisms. Directly, they secrete cytokines and metabolic products influencing EC growth, proliferation, and migration (105–107). *In vitro* studies have found that adiponectin secreted by BMAs affects EC growth and migration and influences the expression of EC adhesion molecules, facilitating closer proximity and invasion by tumor cells into bone (107, 108). Indirectly, cytokines secreted by BMAs activate multiple signaling pathways affecting ECs. Studies on breast cancer bone metastasis showed that BMAs-secreted IL-1β activates the p38-MAPK pathway, increasing EC permeability and vasculogenesis (108). Additionally, the impact of BMAs-secreted IL-6 on HIF-1α and VEGF levels participates in the regulation of angiogenesis (109). The presence of adiponectin and IL-6 in the bone marrow microenvironment of lung cancer bone metastasis suggests that BMAs may promote EC growth and new blood vessel formation, providing additional nutrients and pathways for cancer metastasis (Figure 2).

4.2.4 The role of inflammatory factors secreted by BMAs in lung cancer bone metastasis

BMAs are capable of secreting pro-inflammatory cytokines such as IL-1β, IL-6, TNF-α, and leptin, and they induce BMSCs to participate in the inflammatory immune response by regulating B cell responses and lymphocyte production (110). For instance, the inflammatory cytokine IL-1β, secreted by BMAs, can upregulate the expression of leptin (111). A clinical study involving 116 lung cancer patients with bone metastasis found significantly higher levels of leptin and its receptor in patients with bone metastases compared to those without, suggesting that the formation of lung adenocarcinoma bone metastatic lesions is closely related to leptin (112). Leptin can inhibit the activity of macrophages and natural killer cells, reducing their ability to kill lung cancer cells. It can also regulate the expression of immune checkpoint molecules on the surface of lung cancer cells, such as programmed death-ligand 1 (PD-L1), to inhibit the immune cells' ability to kill tumor cells. PD-L1, in conjunction with its receptor PD-1, forms an immune checkpoint that suppresses the activation and proliferation of effector T cells and promotes the increase and upregulation of regulatory T cells (Tregs) (113, 114). Ultimately, lung cancer cells can escape immune surveillance by regulating the leptin signaling pathway, thereby promoting the occurrence and development of lung cancer bone metastases. Additionally, IL-6, TNF-α, CXCL12, and leptin are considered to significantly promote tumor cell migration and proliferation, as well as inhibit apoptosis and activate autophagy, facilitating the development of tumor bone metastasis (115, 116) (Figure 2).

4.2.5 The role of BMAs as an energy source in lung cancer bone metastasis

Current research posits that BMAs, through their metabolic processes, produce a substantial quantity of lipids, including fatty acids, triglycerides, phospholipids, and cholesterol (117, 118). These lipids serve as an effective energy source for tumor cells, promoting their proliferation, migration, and invasion (118). Lipids are not only essential components of tumor cell membranes but also serve as energy sources during high metabolic demands (117). Fatty acids, fundamental components of lipids, have been found to be released from triacylglycerol in BMAs through lipolysis. These fatty acids can supply energy for tumor cell growth and metabolism via the microcirculation (119). Furthermore, fatty acid-binding protein 4 (FABP4) secreted by BMAs can increase the stability of fatty acids. FABP4 facilitates lipid transport and the transfer of free fatty acids to tumor cells, playing a role in the process of tumor bone metastasis (120, 121). Studies utilizing BMA-enriched mouse models found upregulated levels of FABP4 in Prostate Cancer(PCa) cells directly in contact with BMAs, suggesting a bidirectional interaction between FABP4 and the PPARγ pathway may enhance the invasiveness of tumor cells in bone metastasis (121). Additionally, co-culture studies inducing lipolysis in adipocytes and beta-oxidation in cancer cells have demonstrated that adipocytes can act as an energy source for cancer cells (122). In PCa, *in vitro* studies showed that adipocytes could enhance *PCa* cell migration. Breast cancer research found that adipocytes near invasive cancer cells promoted the migration and growth of breast tumor cells (119). These studies collectively underscore the significant role of BMAs as an energy source in the process of tumor bone metastasis (123). Given the metabolic secretion of a large amount of lipids by BMAs in the bone marrow microenvironment of lung cancer bone metastasis, it is speculated

that BMAs, as an energy source, facilitate the development of lung cancer bone metastasis.

Furthermore, certain immunomodulatory adipokines secreted by BMAs may participate in the process of tumor bone metastasis through interactions with adipocytes, immune cells, and tumor cells (110, 124). The following sections will discuss the mechanisms of action of leptin, adiponectin, Nesfatin-1, Resistin, chemerin, and visfatin in lung cancer bone metastasis.

5 The action of adipokines secreted by BMAs in lung cancer bone metastasis

5.1 Leptin

Leptin is a protein composed of 146 amino acids encoded by the *ob* gene, acting as a neuromodulatory, immunoregulatory, and endocrine hormone with multifunctional roles across various organs (125). By binding to specific leptin receptors, leptin activates intracellular signaling pathways, regulating the transcription of target genes to exert biological effects (125). The interaction of leptin with central and peripheral receptors yields divergent, sometimes opposing effects; while binding to peripheral receptors may increase bone mass, interaction with central receptors can induce bone loss (126).

5.1.1 Direct effects of leptin in lung cancer bone metastasis

The binding of leptin to its receptor can activate several signaling pathways associated with tumor progression, including TGF-β, JAK/STAT, PI3K, HIF, and MAPK pathways (127). *In vitro* studies on lung cancer bone metastasis have shown that leptin promotes metastasis of the A549 human lung cancer cell line through a TGF-β-dependent induction of EMT (128). Leptin can also block the endoplasmic reticulum stress-related pathway, preventing apoptosis and promoting proliferation in lung adenocarcinoma A549 cells (129). Inhibition of the leptin-related pathway significantly induces apoptosis in these cells. Ieptin can regulate apoptosis-related factors, such as members of the Bcl-2 family and caspases, to inhibit apoptosis in lung cancer cells (130). This evidence confirms that leptin enhances lung cancer cell growth and migration through suppressing apoptosis (Table 1).

5.1.2 Indirect effects of leptin in lung cancer bone metastasis

Leptin's indirect effects in lung cancer bone metastasis mainly involve regulation of OCs and OBs. Leptin inhibits the expression of RANKL in OBs, thereby suppressing OC differentiation; it also increases the expression of OPG, preventing the RANKL/RANK binding and indirectly inhibiting bone resorption (131). Leptin can regulate other factors and pathways affecting bone resorption, such as matrix MMP2 and MMP9, which are involved in extracellular matrix remodeling, tumor progression, and bone absorption (131, 153). Clinical studies on lung cancer bone metastasis have found that overactivation of MMP2/MMP9 promotes osteolytic metastasis and bone destruction in advanced cancer (154). *In vitro* studies showed that leptin enhanced production of soluble intercellular adhesion molecule-1 (ICAM-1) in lung cancer cells through triggering a signaling cascade involving JAK1/2, STAT3, FAK, ERK, and GSK3αβ (154). Leptin-stimulated production of soluble ICAM-1, in coordination with RANKL activation, synergistically induces OC formation, suggesting that leptin indirectly promotes tumor-induced bone resorption. Animal experiments have shown that leptin promotes proliferation and differentiation of OBs and enhances bone matrix synthesis and secretion, including collagen, alkaline phosphatase, and osteocalcin (155, 156). Further research is needed to determine whether this effect is similarly active in lung cancer bone metastasis (Table 1).

5.1.3 Immune modulation by leptin in lung cancer bone metastasis

Leptin directly influences the proliferation, differentiation, and activity of various immune cells (such as monocytes, T cells, B cells, and macrophages) and interacts with other cytokines in the tumor microenvironment (157). Leptin indirectly regulates immune function in the lung cancer bone metastasis microenvironment by affecting the function of other cells (158). Cell studies have demonstrated that leptin promotes monocyte proliferation, induces macrophage phagocytosis and pro-inflammatory cytokine secretion, and acts as a nutritional factor to prevent apoptosis, playing a role in adaptive immunity by regulating T and B cell populations (159). Leptin dose-dependently promotes naïve CD4+ T cell proliferation and polarizes CD4+ T cells towards a Th1 phenotype (160), which in turn facilitates lung cancer secretion of inflammatory cytokines such as TNF-α and IL-6, promoting lung cancer bone metastasis. Beyond its effects on T cells, leptin maintains the homeostasis of murine B cells by inducing Bcl-2 and cyclin D1, promoting cell cycle entry and preventing apoptosis, thereby promoting lung cancer cell proliferation (161). Leptin interacts with inflammatory cytokines, such as VEGF and TGF-β, to establish and maintain an inflammatory immune state within the tumor microenvironment (162). Leptin can also upregulate the function of MDSCs, which suppress T cell activation and proliferation through the release of immunosuppressive factors and direct interaction with T cells (163), allowing lung cancer cells to evade immune surveillance (Table 1).

It is crucial to note that the specific mechanisms of leptin in lung cancer bone metastasis require further investigation due to the complexity of tumor metastasis and individual variability, which may lead to diverse leptin response patterns. Additionally, factors such as lung cancer type (e.g., adenocarcinoma, squamous cell carcinoma), molecular subtypes, and the microenvironment may also influence the effects of leptin.

5.2 Adiponectin

While previous studies suggested adiponectin was primarily secreted by white adipose tissue (WAT), recent research shows that BMAs produce more adiponectin than WAT, especially in cancer

TABLE 1 Leptin, Adiponectin, Nesfatin-1, Resistin, Chemerin, Visfatin: Mechanisms of action in tumor bone metastasis - Literature table.

BMAs	Tumor types	Promote or inhibit tumor bone metastasis	Impacts	Mechanisms of action	References
Leptin	Lung cancer	Promote	Promotion of tumor cell migration	Induction of EMT via TGF-β	(128)
			Promotion of tumor cell survival	Inhibition of endoplasmic reticulum stress and apoptosis	(129)
			Promotion of tumor cell survival	Regulation of apoptotic factors such as Bcl-2 family, cysteine proteases,inhibiting apoptosis	(130)
			Promotion of osteolysis	Increase in ICAM-1 expression,combination with NF-κB inducing OC formation	(131)
		inhibit	Inhibition of osteolysis	Inhibition of OB production of RANKL and inhibition of OC differentiation	(131)
			Inhibition of osteolysis	Up-regulation of OPG expression and hindering of RANKL/RANK binding	(131)
Adiponectin	Lung cancer	Promote	Promotion of tumor microenvironment angiogenesis	Regulation of VEGF expression and signaling pathways	(132, 133)
			Promotion of osteolysis	Direct action on OC to promote OC formation and activation	(134)
			Promotion of osteolysis	Regulation of OC differentiation through the RANK/RANKL, JAK/STAT, and MAPK signaling pathways	(135–139)
		inhibit	Inhibition of tumor proliferation	Regulation of OC differentiation through the PI3K/Akt and mTOR signaling pathways	(140)
			Promotion of tumor cell apoptosis	Induction of apoptosis by activating AMPK signaling to increase the BAX/Bcl-2 ratio	(141)
Nesfatin-1	Colon cancer	Promote	Promotion of tumor cell migration and invasion	Induction of EMT-associated proteins	(142)
Resistin	Lung cancer	Promote	Promotion of osteolysis	Activation of NF-κB signaling pathway to promote OC activation and function enhancement	(143)
			Promotion of osteolysis	Inhibition of OB differentiation and promotion of OC activation, leading to bone destruction	(144)
			Promotion of tumor microenvironment inflammation	Promotion of activation of immune inflammatory cells, regulation of cytokines, and affecting the tumor microenvironment	(145, 146)
			Promotion of tumor microenvironment angiogenesis	Activation of signals such as JAK/STAT and PI3K/AKT to promote angiogenesis	(146, 147)
Chemerin	Oral cancer	Promote	Promotion of angiogenesis	Recruitment of immune cells,promotion of angiogenesis, and regulation of bone remodeling through Wnt/β-catenin signaling	(148–150)
	Breast cancer	inhibit	Inhibition of osteolysis	Blocking of RANKL inducing OC formation	(151)
Visfatin	Chondrosarcoma	Promote	Promotion of tumor migration	Synthesis of MMPs-2 via pro-inflammatory signaling pathways	(152)

TGF-β, Transforming Growth Factor Beta; EMT, Epithelial-Mesenchymal Transition; Bcl-2, B-cell lymphoma 2; ICAM-1, Intercellular Adhesion Molecule 1; NF-κB, Nuclear Factor Kappa-Light-Chain-Enhancer of Activated B Cells; OC, Osteoclast; OB - Osteoblast; RANK, Receptor Activator of Nuclear Factor Kappa-B; RANKL, Receptor Activator of Nuclear Factor Kappa-B Ligand; OPG, Osteoprotegerin; VEGF, Vascular Endothelial Growth Factor; JAK/STAT, Janus kinase/signal transducer and activator of transcription; MAPK, Mitogen-activated protein kinase; PI3K/Akt, Phosphoinositide 3-kinase/protein kinase B; AMPK, AMP-activated protein kinase; BAX/Bcl-2 ,Bcl-2-associated X protein/B-cell lymphoma 2; Wnt/β-catenin, Wingless-related integration site/beta- catenin; MMPs-2, Matrix Metalloproteinases-2.

patients. Adiponectin's role in the tumor microenvironment contrasts with that of leptin, sparking debate over its impact on cancer (164). Although earlier results pointed towards anti-tumor effects, recent studies have highlighted adiponectin's significant role in promoting tumor metastasis (165).

5.2.1 Direct effects of adiponectin in lung cancer bone metastasis

Adiponectin primarily exerts its influence by inhibiting the proliferation of lung cancer cells and inducing their apoptosis. An *in vitro* study on lung cancer revealed that adiponectin can suppress the proliferation of lung cancer cells by inhibiting the PI3K/Akt signaling pathway and the phosphorylation of mTOR (mammalian target of rapamycin) (140). Additionally, it induces cell apoptosis by activating the AMPK signaling pathway and increasing the BAX/Bcl-2 ratio (140, 141) (Table 1). Animal experimental studies have also discovered adiponectin's role in prohibiting lung cancer cell proliferation through inhibiting the Wnt/β-catenin signaling pathway (166).

5.2.2 Indirect effects of adiponectin in lung cancer bone metastasis

Adiponectin indirectly participates in lung cancer bone metastasis by regulating angiogenesis, influencing OC activities, and impacting immune functions. Research indicates that adiponectin affects vessel formation by regulating the expression of VEGF and its signaling pathways (165). Adiponectin can enhance the expression of VEGFs (including VEGF-A, VEGF-B, VEGF-C, and VEGF-D) in ECs. VEGFs operate on receptors on ECs, such as VEGFR-1 and VEGFR-2, promoting EC proliferation and tubule formation through activating the VEGFR-2 signaling pathway. Moreover, adiponectin promotes angiogenesis by inhibiting angiogenesis inhibitors, such as Angiopoietin-1 (132, 133).

Adiponectin directly and indirectly partakes in the development and maturation of OCs, influencing bone metastasis in lung cancer. On one side, *in vitro* experiments have shown that adiponectin can directly influence OCs, promoting their formation, activation, and increasing the release of lysosomal enzymes, thereby enhancing bone resorption (134). On the other hand, it indirectly contributes to the formation and maturation of OCs mainly through binding to receptors on cell types such as OBs and OCs (167). Receptors include Ob-Rb (long-form receptor primarily distributed in MSCs); upon binding, adiponectin can activate multiple signaling pathways and regulate the expression of related genes, contributing to the differentiation of hematopoietic stem cells (HSCs) into OCs (166). Pathways implicated include RANK/RANKL, JAK/STAT, and MAPK, promoting bone metastasis by influencing OC formation and maturation (135–139) (Table 1). In summary, adiponectin exerts an indirect influence on osteolytic metastasis in lung cancer primarily through modulating angiogenesis within the tumor microenvironment, participating in the regulation of OC activity, and affecting the equilibrium of bone remodeling.

5.2.3 Impact on immune regulation

Adiponectin might play a role in lung cancer bone metastasis through regulating immune cell functions. *In vitro* studies indicate that adiponectin can increase the quantity and function of regulatory T cells (Tregs) while reducing the activity of natural killer (NK) cells, diminishing attacks on cancer cells, thus creating a favorable environment for lung cancer bone metastasis (168). However, differing studies suggest adiponectin possesses anti-inflammatory properties, inhibiting the NF-κB signaling pathway and cytokine release, thereby reducing the production of inflammatory mediators. Consequently, it suppresses the inflammatory response surrounding lung cancer cells, reducing their survival and proliferation capabilities (169, 170).

5.3 Nesfatin-1

Discovered in 2006, Nesfatin-1 is an anorexigenic neuropeptide initially associated with food intake and energy regulation, hence being considered as a hormone regulating body weight and appetite. Beyond the central system, Nesfatin-1 is also present in various organs and tissues, such as the stomach, intestines, spleen, and adipose tissue (171). However, research on Nesfatin-1 secreted by BMAs in lung cancer bone metastasis is lacking. Recent studies have predominantly focused on Nesfatin-1 secreted by white adipose tissue, observing elevated expression levels of Nesfatin-1 in lung cancer, breast cancer, and other tumors. It has been found that Nesfatin-1 is associated with tumor invasion, metastasis, and prognosis (172, 173).

5.3.1 Direct role of Nesfatin-1 in tumor bone metastasis

Nesfatin-1 secreted by adipose tissue in the tumor microenvironment might directly influence tumor bone metastasis by regulating the expression and function of EMT-related proteins like E-cadherin, N-cadherin, and Vimentin (174). Some studies have demonstrated that Nesfatin-1/Nucleobindin-2 can suppress the expression of E-cadherin and increase the expression of N-cadherin and Vimentin, thereby inducing migration, invasion, and EMT of colon cancer cells (142) (Table 1). Since both peripheral and bone marrow fat can secrete Nesfatin-1, it can be inferred that in the bone marrow microenvironment of lung cancer bone metastasis, Nesfatin-1 secreted by BMAs might promote the migration and invasion of lung cancer cells by inducing EMT.

5.3.2 Indirect role of Nesfatin-1 in tumor bone metastasis

Nesfatin-1 might indirectly affect the invasion and metastasis of tumor cells in bone tissue by influencing the activity of immune cells and the production of inflammatory cytokines (175). Clinical research has shown that Nesfatin-1 can induce an increase in CCL2 expression in human synovial tissues, favoring M1 macrophage polarization, thereby increasing the expression of pro-inflammatory cytokines like IL-1β, IL-6, and TNF-α, and promoting the progression of inflammatory responses (176). This, consequently, indirectly affects the invasion and metastasis of tumor cells in bone tissue. Additionally, studies in rats have found that Nesfatin-1 can

inhibit cell apoptosis induced by IL-1β inflammation and promote angiogenesis by inhibiting neutrophil recruitment, cell apoptosis, and activating VEGF, mechanisms that can indirectly promote tumor bone metastasis (177, 178). There is currently no direct evidence regarding Nesfatin-1's mechanisms in lung cancer bone metastasis, further research to clarify these mechanisms is required.

5.4 Resistin

Resistin, a peptide hormone, is primarily secreted by white adipose tissue but also produced by other tissues such as bone marrow adipose, liver, and muscle (179). Initial studies suggested its association with insulin resistance and type 2 diabetes (180). Recent research, however, has linked Resistin to bone marrow fat and bone metabolism, suggesting it may influence OC and osteoblast OB functions, participate in inflammatory responses and immune regulation, and affect the tumor microenvironment in tumor bone metastasis.

5.4.1 Direct role of resistin in lung cancer bone metastasis

Resistin may directly promote lung cancer bone metastasis by activating OC function. *In vitro* studies have revealed that resistin can activate the NF-κB signaling pathway, leading to the release of inflammatory cytokines like TNF-α and IL-6, which further enhance OC activation and functionality, accelerating bone tissue destruction and bone metastasis (143). Additionally, resistin has been found to inhibit OB differentiation and bone-forming functions while promoting OC activation and functionality, resulting in bone tissue destruction and remodeling (144) (Table 1).

5.4.2 Indirect role of resistin in lung cancer bone metastasis

By regulating the production of inflammatory cytokines and the activity of immune cells, as well as activating tumor-associated signaling pathways like JAK/STAT and PI3K/AKT, resistin can indirectly promote cellular growth, angiogenesis, and immune response in the tumor microenvironment, facilitating lung cancer bone metastasis (145). Resistin can promote the production and activation of inflammatory cells like macrophages and lymphocytes and regulate the inflammatory response by modulating cytokine release (146) (Table 1). These immune cells play an essential role in lung cancer bone metastasis, including promoting inflammatory responses, regulating immune responses, and affecting tumor cell invasion and migration. Moreover, animal models of lung cancer have shown that mice treated with anti-resistin antibodies exhibited reduced rates of lung cancer development and metastasis (181), further proving that resistin, by modulating inflammatory responses in the tumor microenvironment, indirectly facilitates lung cancer bone metastasis.

Resistin can activate signaling pathways such as JAK/STAT and PI3K/AKT, thereby influencing cell growth and angiogenesis within the tumor microenvironment, as well as suppressing the body's anti-tumor immune response, indirectly facilitating the occurrence and progression of tumor bone metastasis. Studies have found that resistin activates the PI3K and Akt signaling pathways, while inhibitors of PI3K and Akt, or siRNA, can reduce the expression of VEGF-A induced by resistin (146). Concurrently, both *in vitro* and *in vivo* studies have demonstrated that resistin promotes the expression of VEGF-A and angiogenesis within the tumor microenvironment by inhibiting the expression of miR-5-3p through the PI3K/Akt signaling cascade, thus affecting tumor bone metastasis (146, 147) (Table 1).

5.5 Chemerin

Chemerin is a small peptide hormone predominantly secreted by adipose tissue, with subsequent production noted in the liver, kidneys, and other tissues. Initially identified for its roles in inflammation and immune regulation, recent clinical studies have unveiled Chemerin's capability to inhibit osteogenic differentiation in favor of adipogenesis (182). The Wnt pathway plays a crucial role in bone biology and the regulation of bone tumors, especially the classic Wnt/β-catenin signaling pathway is closely related to tumor bone metastasis. Relevant studies on mouse bone structure have shown that inhibiting the Wnt/β-catenin signaling pathway and activating the RANK signal promote bone resorption. Simultaneously, it has been demonstrated that Chemerin participates in the progression of bone tumors (151, 183). However, the role of Chemerin in cancer remains contentious, with a majority of studies highlighting its anticancer effects, while a minority suggest its protumorigenic capabilities. These effects derive from its regulation of angiogenesis and modulation of the immune-inflammatory response in the bone marrow microenvironment, indirectly contributing to the osteolytic metastasis of lung cancer.

Antitumor activities of Chemerin have been identified in a murine model of breast cancer, where it binds to its receptor ChemR23/CMKLR1 and inhibits neovascularization, thereby suppressing growth and invasion of breast cancer cells (148). Moreover, in Chemerin-treated media derived from metastatic breast cancer cells, an increase in the RANKL/OPG ratio and a reduction in the secretion of MMPs (e.g., MMP-2, MMP-9) and Cathepsin K were observed (148) (Table 1), thus inhibiting RANKL-induced OC formation and consequentially suppressing bone dissolution and tumor bone metastasis.

On the contrary, protumorigenic activity is evidenced through the recruitment of innate immune defenses and activation of endothelial vasculogenesis, as well as the suppression of Wnt/β-catenin signaling, reducing OB differentiation and stimulating OC differentiation and proliferation through RANK signaling activation (149). This mechanism plays a crucial role in tumor bone metastasis. Furthermore, studies in oral squamous cell carcinoma (OSCC) have shown that Chemerin enhances the formation of human umbilical vein ECs (HUVECs), promoting angiogenesis and subsequently tumor growth and migration. Additionally, Chemerin can upregulate pro-angiogenic factors such as VEGF-A, MMP-9, MMP-2, and S100A9 in neutrophils through the activation of the MEK/ERK signaling pathway (150, 184) (Table 1), thereby facilitating tumor vascularization and bone metastasis in lung cancer. Hence, the balance between Chemerin's anticancer and

protumorigenic effects ultimately dictates tumor progression, underscoring the need for further research into Chemerin's role within the lung cancer bone metastasis.

5.6 Visfatin

Visfatin, an inflammatory adipokine also known as pre-B cell colony-enhancing factor (PBEF), plays a pivotal role in NAD+ biosynthesis as the rate-limiting enzyme in nicotinamide metabolism, implicating its involvement in B-cell development, apoptosis, and glucose metabolism. Initially discovered in visceral adipose tissue, Visfatin has been widely recognized for its compensatory response in obesity-induced insulin resistance (185). Recent studies have expanded our understanding of Visfatin's functionality, uncovering its significant role in the genesis and development of tumors as well as bone metabolism. Elevated levels of Visfatin expression have been associated with certain tumor types, correlating with aggressiveness, migration, and prognosis (152). By promoting the synthesis of MMP-2 and activation of the AP-1 transcription factor through the ERK, p38, and JNK signaling pathways, Visfatin enhances tumor cell migration (186) (Table 1). Additionally, overexpression of Visfatin has been linked to increased pulmonary metastasis in a murine model of chondrosarcoma. In the mouse bone marrow, it disrupts the balance between bone resorption and formation, tilting towards a pro-inflammatory phenotype in MSCs differentiating towards BMAs and OBs (144). As an adipokine, Visfatin's exact action in bone regulation and immune modulation remains to be fully elucidated. However, its capacity to induce pro-inflammatory transcription factors, such as NF-kB, and modulate pathways including MAPK, PI3K, and ROS (187), suggests that Visfatin might act as a potential tumor-promoting factor in lung cancer bone metastasis through upregulation of MMP-2, enhanced differentiation of OBs, and the promotion of inflammatory responses in MSCs, thereby indirectly facilitating osteolysis and the progression of pulmonary cancer bone metastasis.

6 Conclusion and future perspectives

This review primarily explored how BMAs directly or indirectly interact with various cells within the bone microenvironment of lung cancer, as well as its pathological role in modulating the tumor microenvironment and thus influencing bone metastasis in lung cancer. The contributions of BMAs are summarized through three main aspects: (1) BMAs provide direct energy supply to lung cancer cells through lipid metabolites and FABP4, with lipids also serving as building blocks for the cancer cell membrane; (2) Direct effects of BMAs in bone metastasis of lung cancer include secretion of pro-inflammatory cytokines like IL-1β that participate in PMN formation and CCL12 which directly interacts with CXCR4 on lung cancer cells, promoting cell proliferation and invasion. Secreted adipokines like leptin activate TGF-β, PI3K/Akt, and MAPK signaling pathways, upregulating MMP2/MMP9 secretion and facilitating EMT, thereby promoting bone metastasis; (3) Indirect effects of BMAs are mediated through interactions with OCs, OBs, ECs, and MSCs, indirectly aiding lung cancer bone metastasis. For instance, leptin secreted by BMAs may regulate osteogenesis and osteolysis by inhibiting OC activity, suppressing RANKL production and enhancing OPG secretion. Adiponectin influences OC activity, increases regulatory T cells, and inhibits NK cell activity, contributing to immune evasion by cancer cells. Resistin could activate the NF-κB pathway, releasing inflammatory cytokines like TNF-α and IL-6, thus promoting OC activation and inhibiting OB differentiation, essential for lung cancer bone metastasis.

Despite the existence of both metastasis-promoting and inhibitory factors secreted by BMAs, they predominantly exert a pro-metastatic role in lung cancer bone metastasis. Reducing BMAs in the bone microenvironment could represent a novel approach to inhibit lung cancer bone metastasis. Considering the shared origin and mutual regulation during differentiation between BMAs and OBs, promoting osteogenic differentiation to decrease BMAs might suppress lung cancer bone metastasis. Z-DNA binding protein 1 (ZBP1) has been identified as a novel regulator of osteogenic and adipogenic differentiation through the Wnt/β-catenin signaling pathway (188). Therefore, ZBP1 could serve as a novel therapeutic target for treating lung cancer bone metastasis. Additionally, inhibiting the actions of BMA-secreted factors could indirectly repress lung cancer bone metastasis. For instance, clinical research on metastatic renal cell carcinoma (RCC) patients undergoing tyrosine kinase inhibitor (TKI) therapy revealed that the adiponectin-AdipoR1 axis inhibits tumor cell migration and invasion by blocking the GSK3β/β-Catenin pathway (189). This raises the possibility that adiponectin-AdipoR1 might exhibit similar effects in lung cancer bone metastasis, potentially serving as a therapeutic target for further verification.

In summary, BMAs and their secreted adipokines present effective therapeutic targets for lung cancer bone metastasis, paving new directions for future research in this field.

Author contributions

JL: Writing – original draft, Writing – review & editing. JW: Writing – original draft. YN: Writing – review & editing. XY: Writing – review & editing.

Funding

The author(s) declare financial support was received for the research, authorship, and/or publication of this article. Fund program: The National Natural Science Foundation of China (Grant Number 82273294).

Conflict of interest

The authors declare that the research was conducted in the absence of any commercial or financial relationships that could be construed as a potential conflict of interest.

Publisher's note

References

1. Sung H, Ferlay J, Siegel RL, Laversanne M, Soerjomataram I, Jemal A, et al. Global cancer statistics 2020: GLOBOCAN estimates of incidence and mortality worldwide for 36 cancers in 185 countries. *CA: Cancer J Clin*. (2021) 71:209–49. doi: 10.3322/caac.21660

2. Qin N, Ma H, Jin G. Annual progress in epidemiological research on lung cancer in 2022. *Chin Med J*. (2023) 103:1068–73. doi: 10.3760/cma.j.cn112137-20221213-02640

3. Riihimaki M, Hemminki A, Fallah M. Metastatic sites and survival in lung cancer. *Lung Cancer*. (2014) 86:78–84. doi: 10.1016/j.lungcan.2014.07.020

4. Katakami N, Kunikane H, Takeda K. Prospective study on the incidence of bone metastasis (BM) and skeletal-related events (SREs) in patients (pts) with stage IIIB and IV lung cancer-CSP-HOR 13. *J Thorac Oncol*. (2014) 9:231–8. doi: 10.1097/JTO.0000000000000051

5. Mohme M, Riethdorf S, Pantel K. Circulating and disseminated tumour cells - mechanisms of immune surveillance and escape. Nature reviews. *Clin Oncol*. (2017) 14:155–67. doi: 10.1038/nrclinonc.2016.144

6. Dongre A, Weinberg RA. New insights into the mechanisms of epithelial-mesenchymal transition and implications for cancer. *Nat Rev Mol Cell Biol*. (2019) 20:69–84. doi: 10.1038/s41580-018-0080-4

7. Tang Q, Chen J, Di Z, Yuan W, Zhou Z, Liu Z, et al. TM4SF1 promotes EMT and cancer stemness via the Wnt/β-catenin/SOX2 pathway in colorectal cancer. *J Exp Clin Cancer Res*. (2020) 39:232. doi: 10.1186/s13046-020-01690-z

8. Wang S, Cheng Y, Gao Y, He Z, Zhou W, Chang R, et al. SH2B1 promotes epithelial-mesenchymal transition through the IRS1/β-catenin signaling axis in lung adenocarcinoma. *Mol carcinogenesis*. (2018) 57:640–52. doi: 10.1002/mc.22788

9. Hamilton G, Rath B. Circulating tumor cell interactions with macrophages: implications for biology and treatment. *Trans Lung Cancer Res*. (2017) 6:418–30. doi: 10.21037/tlcr.2017.07.04

10. Fidler IJ. The pathogenesis of cancer metastasis: the 'seed and soil' hypothesis revisited. Nature reviews. *Cancer*. (2003) 06:453–8. doi: 10.1038/nrc1098

11. Rucci N, Teti A. Osteomimicry: how the seed grows in the soil. *Calcified Tissue Int*. (2018) 102:131–40. doi: 10.1007/s00223-017-0365-1

12. Zhang X. Interactions between cancer cells and bone microenvironment promote bone metastasis in prostate cancer. *Cancer Commun (London England)*. (2019) 39:76. doi: 10.1186/s40880-019-0425-1

13. Zhang W, Xu Z, Hao X, He T, Li J, Shen Y, et al. Bone metastasis initiation is coupled with bone remodeling through osteogenic differentiation of NG2+ Cells. *Cancer Discovery*. (2023) 13:474–95. doi: 10.1158/2159-8290.CD-22-0220

14. Zhao M-N, Zhang L-F, Sun Z, Qiao L-H, Yang T, Ren Y-Z, et al. A novel microRNA-182/Interleukin-8 regulatory axis controls osteolytic bone metastasis of lung cancer. *Cell Death Dis*. (2023) 14:298. doi: 10.1038/s41419-023-05819-8

15. Anderson NM, Simon MC. The tumor microenvironment. *Curr Biol*. (2020) 30: R921–5. doi: 10.1016/j.cub.2020.06.081

16. Yang M, Sun Yi, Sun J, Wang Z, Zhou Y, Yao G, et al. Differentially expressed and survival-related proteins of lung adenocarcinoma with bone metastasis. *Cancer Med*. (2018) 7:1081–92. doi: 10.1002/cam4.1363

17. Song X, Cheng Xu, Jin X, Ruan S, Xu X, Lu F, et al. EGFL6 promotes bone metastasis of lung adenocarcinoma by increasing cancer cell Malignancy and bone resorption. *Clin Exp metastasis*. (2023) 40:357–71. doi: 10.1007/s10585-023-10219-5

18. Liu Y, Chen J, Yang Y, Zhang L, Jiang WG. Molecular impact of bone morphogenetic protein 7, on lung cancer cells and its clinical significance. *Int J Mol Med*. (2012) 29:1016–24. doi: 10.3892/ijmm.2012.948

19. Aoki M, Umehara T, Kamimura Go, Imamura N, Morizono S, Nonaka Y, et al. Expression of bone morphogenetic protein-7 significantly correlates with non-small cell lung cancer progression and prognosis: A retrospective cohort study. Clinical medicine insights. *Oncology*. (2019) 13:1179554919852087. doi: 10.1177/1179554919852087

20. Juárez P, Guise TA. TGF-β in cancer and bone: implications for treatment of bone metastases. *Bone*. (2011), 48:23–9. doi: 10.1016/j.bone.2010.08.004

21. Liu L, Chen X, Wang Y, Qu Z, Lu Q, Zhao J, et al. Notch3 is important for TGF-β-induced epithelial-mesenchymal transition in non-small cell lung cancer bone metastasis by regulating ZEB-1. *Cancer Gene Ther*. (2014) 21:364–72. doi: 10.1038/cgt.2014.39

22. Wu M, Kong D, Zhang Y. SPON2 promotes the bone metastasis of lung adenocarcinoma via activation of the NF-κB signaling pathway. *Bone*. (2023) 167:116630. doi: 10.1016/j.bone.2022.116630

23. Zhang C, Qin J, Yang Lu, Zhu Z, Yang J, Su W, et al. Exosomal miR-328 originated from pulmonary adenocarcinoma cells enhances osteoclastogenesis via downregulating Nrp-2 expression. *Cell Death Discovery*. (2022) 8:405. doi: 10.1038/s41420-022-01194-z

24. Kang J, Manna FLa, Bonollo F, Sampson N, Alberts IL, Mingels C, et al. Tumor microenvironment mechanisms and bone metastatic disease progression of prostate cancer. *Cancer Lett*. (2022) 530:156–69. doi: 10.1016/j.canlet.2022.01.015

25. Yuan Z, Li Y, Zhang S, Wang X, Dou He, Yu Xi, et al. Extracellular matrix remodeling in tumor progression and immune escape: from mechanisms to treatments. *Mol Cancer*. (2023) 22:48. doi: 10.1186/s12943-023-01744-8

26. Shin E, Koo JaS. The role of adipokines and bone marrow adipocytes in breast cancer bone metastasis. *Int J Mol Sci*. (2020) 21. doi: 10.3390/ijms21144967

27. Wu S, Pan Y, Mao Y, Chen Yu, He Y. Current progress and mechanisms of bone metastasis in lung cancer: a narrative review. *Trans Lung Cancer Res*. (2021) 10:439–51. doi: 10.21037/tlcr-20-835

28. Taverna S, Pucci M, Giallombardo M, Bella MADi, Santarpia M, Reclusa P, et al. Amphiregulin contained in NSCLC-exosomes induces osteoclast differentiation through the activation of EGFR pathway. *Sci Rep*. (2017) 7:3170. doi: 10.1038/s41598-017-03460-y

29. Xu Z, Liu X, Wang H, Li J, Dai L, Li J, et al. Lung adenocarcinoma cell-derived exosomal miR-21 facilitates osteoclastogenesis. *Gene*. (2018) 666:116–22. doi: 10.1016/j.gene.2018.05.008

30. Kir S, Komaba H, Garcia AP, Economopoulos KP, Liu W, Lanske B, et al. PTH/PTHrP receptor mediates cachexia in models of kidney failure and cancer. *Cell Metab*. (2016) 23:315–23. doi: 10.1016/j.cmet.2015.11.003

31. Dou C, Li J, Kang F, Cao Z, Yang X, Jiang H, et al. Dual effect of cyanidin on RANKL-induced differentiation and fusion of osteoclasts. *J Cell Physiol*. (2016) 231:558–67. doi: 10.1002/jcp.24916

32. Chappard D, Bouvard B, Baslé M-F, Legrand E, Audran M. Bone metastasis: histological changes and pathophysiological mechanisms in osteolytic or osteosclerotic localizations. A review. *Morphol: Bull l'Association Des anatomistes*. (2011) 95:65–75. doi: 10.1016/j.morpho.2011.02.004

33. He Y, Luo W, Liu Y, Wang Y, Ma C, Wu Q, et al. IL-20RB mediates tumoral response to osteoclastic niches and promotes bone metastasis of lung cancer. *J Clin Invest*. (2022), 132:20. doi: 10.1172/JCI157917

34. Han Y, You X, Xing W, Zhang Z, Zou W. Paracrine and endocrine actions of bone-the functions of secretory proteins from osteoblasts, osteocytes, and osteoclasts. *Bone Res*. (2018) 6:16. doi: 10.1038/s41413-018-0019-6

35. Rahim F, Hajizamani S, Mortaz E, Ahmadzadeh A, Shahjahani M, Shahrabi S, et al. Molecular regulation of bone marrow metastasis in prostate and breast cancer. *Bone Marrow Res*. (2014), 405920. doi: 10.1155/2014/405920

36. Jeong HM, Cho SW, Park SI. Osteoblasts are the centerpiece of the metastatic bone microenvironment. *Endocrinol Metab (Seoul)*. (2016) 31:485–92. doi: 10.3803/EnM.2016.31.4.485

37. Pang H, Ma N, Jiao Mi, Shen W, Xin Bo, Wang T, et al. The biological effects of dickkopf1 on small cell lung cancer cells and bone metastasis. *Oncol Res*. (2017) 25:35–42. doi: 10.3727/096504016X14719078133249

38. Clines GA, Mohammad KS, Bao Y, Stephens OW, Suva LJ, Shaughnessy JD, et al. Dickkopf homolog 1 mediates endothelin-1-stimulated new bone formation. *Mol Endocrinol (Baltimore Md.)*. (2007) 21:486–98. doi: 10.1210/me.2006-0346

39. Xu S, Yang F, Liu R, Li X, Fan H, Liu J, et al. Serum microRNA-139-5p is downregulated in lung cancer patients with lytic bone metastasis. *Oncol Rep*. (2018) 39:2376–84. doi: 10.3892/or.2018.6316

40. Feng Y, Wan P, Yin L, Lou X. The inhibition of microRNA-139-5p promoted osteoporosis of bone marrow-derived mesenchymal stem cells by targeting wnt/beta-catenin signaling pathway by NOTCH1. *J Microbiol Biotechnol*. (2020) 30:448–58. doi: 10.4014/jmb.1908.08036

41. Chen WG, Sun J, Shen WW, Yang SZ, Zhang Y, Hu X, et al. Sema4D expression and secretion are increased by HIF-1alpha and inhibit osteogenesis in bone metastases of lung cancer. *Clin Exp Metastasis*. (2019) 36:39–56. doi: 10.1007/s10585-018-9951-5

42. Engblom C, Pfirschke C, Zilionis R, Martins JDaS, Bos SA, Courties G, et al. Osteoblasts remotely supply lung tumors with cancer-promoting SiglecFhigh neutrophils. *Science*. (2017) 358:6367. doi: 10.1126/science.aal5081

43. Giese MA, Hind LE, Huttenlocher A. Neutrophil plasticity in the tumor microenvironment. *Blood*. (2019) 133:2159–67. doi: 10.1182/blood-2018-11-844548

44. Zhou J, Lu X, Zhu H, Ding N, Zhang Y, Xu X, et al. Resistance to immune checkpoint inhibitors in advanced lung cancer: Clinical characteristics, potential prognostic factors and next strategy. *Front Immunol*. (2023) 14:1089026. doi: 10.3389/fimmu.2023.1089026

45. Renaud S, Falcoz PE, Schaeffer M. Prognostic value of the KRAS G12V mutation in 841 surgically resected Caucasian lung adenocarcinoma cases. *Br J Cancer*. (2015) 113:1206–15. doi: 10.1038/bjc.2015.327

46. D'Oronzo S, Coleman R, Brown J, Silvestris F. Metastatic bone disease: Pathogenesis and therapeutic options: Up-date on bone metastasis management. *J Bone Oncol*. (2019) 15:004–4. doi: 10.1016/j.jbo.2018.10.004

47. Yuan Bo, Clowers MJ, Velasco WV, Peng S, Peng Q, Shi Y, et al. Targeting IL-1β as an immunopreventive and therapeutic modality for K-ras-mutant lung cancer. *JCI Insight*. (2022) 7:11. doi: 10.1172/jci.insight.157788

48. Pretre V, Papadopoulos D, Regard J, Pelletier M, Woo J. Interleukin-1 (IL-1) and the inflammasome in cancer. *Cytokine*. (2022) 153:155s850. doi: 10.1016/j.cyto.2022.155850

49. Maimon A, Levi-Yahid V, Ben-Meir K, Halpern A, Talmi Z, Priya S, et al. Myeloid cell-derived PROS1 inhibits tumor metastasis by regulating inflammatory and immune responses via IL-10. *J Clin Invest*. (2021) 131:10. doi: 10.1172/JCI126089

50. Zhao X, Lin Y, Jiang B, Yin J, Lu C, Wang J, et al. Icaritin inhibits lung cancer-induced osteoclastogenesis by suppressing the expression of IL-6 and TNF-a and through AMPK/mTOR signaling pathway. *Anti-canc Drugs*. (2020) 31:1004–11. doi: 10.1097/CAD.0000000000000976

51. Gross AC, Cam H, Phelps DA, Saraf AJ, Bid HK, Cam M, et al. IL-6 and CXCL8 mediate osteosarcoma-lung interactions critical to metastasis. *JCI Insight*. (2018) 3:16. doi: 10.1172/jci.insight.99791

52. Liu N-N, Yi C-X, Wei L-Q, Zhou J-A, Jiang T, Hu C-C, et al. The intratumor mycobiome promotes lung cancer progression via myeloid-derived suppressor cells. *Cancer Cell*. (2023) 41:1927–1944.e9. doi: 10.1016/j.ccell.2023.08.012

53. Amarasekara DS, Yun H, Kim S, Lee N, Kim H, Rho J. Regulation of osteoclast differentiation by cytokine networks. *Immune Net*. (2018) 18:e8. doi: 10.4110/in.2018.18.e8

54. Raimondo S, Saieva L, Vicario E, Pucci M, Toscani D, Manno M, et al. Multiple myeloma-derived exosomes are enriched of amphiregulin (AREG) and activate the epidermal growth factor pathway in the bone microenvironment leading to osteoclastogenesis. *J Hematol Oncol*. (2019) 12:2. doi: 10.1186/s13045-018-0689-y

55. Bendre MS, Margulies AG, Walser B, Akel NS, Bhattacharrya S, Skinner RA, et al. Tumor-derived interleukin-8 stimulates osteolysis independent of the receptor activator of nuclear factor-kappaB ligand pathway. *Cancer Res*. (2005) 65:11001–9. doi: 10.1158/0008-5472.CAN-05-2630

56. Tung Y-T, Huang P-W, Chou Y-C, Lai C-W, Wang H-P, Ho H-C, et al. Lung tumorigenesis induced by human vascular endothelial growth factor (hVEGF)-A165 overexpression in transgenic mice and amelioration of tumor formation by miR-16. *Oncotarget*. (2015) 12:10222–38. doi: 10.18632/oncotarget.3390

57. Lee H-M, Lee H-J, Chang J-E. Inflammatory cytokine.An attractive target for cancer treatment. *Biomedicines*. (2022) 10:9. doi: 10.3390/biomedicines10092116

58. Gandhi S, Opyrchal M, Grimm MJ, Slomba RT, Kokolus KM, Witkiewicz A, et al. Systemic infusion of TLR3-ligand and IFN-α in patients with breast cancer reprograms local tumor microenvironments for selective CTL influx. *J Immunother Cancer*. (2023) 11:11. doi: 10.1136/jitc-2023-007381

59. Heidegger I, Fotakis G, Offermann A, Goveia J, Daum S, Salcher S, et al. Comprehensive characterization of the prostate tumor microenvironment identifies CXCR4/CXCL12 crosstalk as a novel antiangiogenic therapeutic target in prostate cancer. *Mol Cancer*. (2022) 21:132. doi: 10.1186/s12943-022-01597-7

60. Liao T, Chen W, Sun J, Zhang Y, Hu X, Yang S, et al. CXCR4 accelerates osteoclastogenesis induced by non-small cell lung carcinoma cells through self-potentiation and VCAM1 secretion. *Cell Physiol Biochem*. (2018) 50:1084–99. doi: 10.1159/000494533

61. Li J, Wang L, Chen X, Li L, Li Yu, Ping Yu, et al. CD39/CD73 upregulation on myeloid-derived suppressor cells via TGF-β-mTOR-HIF-1 signaling in patients with non-small cell lung cancer. *Oncoimmunology*. (2017) 6:e1320011. doi: 10.1080/2162402X.2017.1320011

62. Yasuda H. Discovery of the RANKL/RANK/OPG system. *J Bone mineral Metab*. (2021) 39:2–11. doi: 10.1007/s00774-020-01175-1

63. Yao Z, Getting SJ, Locke IC. Regulation of TNF-induced osteoclast differentiation. *Cells*. (2021) 11:1. doi: 10.3390/cells11010132

64. Brouns AJWM, Hendriks LEL, Berge IJR-vd, Driessen AJHM, Roemen GMJM, van Herpen BLJ, et al. Association of RANKL and EGFR gene expression with bone metastases in patients with metastatic non-small cell lung cancer. *Front Oncol*. (2023) 13:1145001. doi: 10.3389/fonc.2023.1145001

65. Ono T, Hayashi M, Sasaki F, Nakashima T. RANKL biology: bone metabolism, the immune system, and beyond. *Inflammation Regenerat*. (2020) 40:2. doi: 10.1186/s41232-019-0111-3

66. Zhang Y, Liang J, Liu P, Wang Q, Liu L, Zhao H. The RANK/RANKL/OPG system and tumor bone metastasis: Potential mechanisms and therapeutic strategies. *Front Endocrinol*. (2022) 13:1063815. doi: 10.3389/fendo.2022.1063815

67. Leon-Oliva DDe, Barrena-Blázquez S, Jiménez-Álvarez L, Fraile-Martinez O, García-Montero C, López-González L, et al. The RANK-RANKL-OPG system: A multifaceted regulator of homeostasis, immunity, and cancer. *Med (Kaunas Lithuania)*. (2023) 59:10. doi: 10.3390/medicina59101752

68. Deng J, Lu C, Zhao Q, Chen K, Ma S, Li Z. The Th17/Treg cell balance: crosstalk among the immune system, bone and microbes in periodontitis. *J periodontal Res*. (2022) 57:246–55. doi: 10.1111/jre.12958

69. Titanji K. Beyond antibodies: B cells and the OPG/RANK-RANKL pathway in health, non-HIV disease and HIV-induced bone loss. *Front Immunol*. (2017) 8:1851. doi: 10.3389/fimmu.2017.01851

70. Rochette L, Meloux A, Rigal E, Zeller M, Cottin Y, Vergely C. The role of osteoprotegerin and its ligands in vascular function. *Int J Mol Sci*. (2019) 20:3. doi: 10.3390/ijms20030705

71. Romeo SG, Alawi KM, Rodrigues J, Singh A, Kusumbe AP, Ramasamy SK. Endothelial proteolytic activity and interaction with non-resorbing osteoclasts mediate bone elongation. *Nat Cell Biol*. (2019) 21:430–41. doi: 10.1038/s41556-019-0304-7

72. Madeddu C, Donisi C, Liscia N, Lai E, Scartozzi M, Macciò A. EGFR-mutated non-small cell lung cancer and resistance to immunotherapy. Role of the tumor microenvironment. *Int J Mol Sci*. (2022) 23:12. doi: 10.3390/ijms23126489

73. Chen J, Zhao L, Xu M-F, Huang Di, Sun X-L, Zhang Y-X. Novel isobavachalcone derivatives induce apoptosis and necroptosis in human non-small cell lung cancer H1975 cells. *J Enzyme inhibition Medic Chem*. (2024) 39:2292006. doi: 10.1080/14756366.2023.2292006

74. Liu J-H, Li C, Cao L, Zhang C-H, Zhang Z-H. Cucurbitacin B regulates lung cancer cell proliferation and apoptosis via inhibiting the IL-6/STAT3 pathway through the lncRNA XIST/miR-let-7c axis. *Pharm Biol*. (2022) 60:154–62. doi: 10.1080/13880209.2021.2016866

75. Su L, Chen Y, Huang C, Wu S, Wang X, Zhao X, et al. Targeting Src reactivates pyroptosis to reverse chemoresistance in lung and pancreatic cancer models. *Sci Trans Med*. (2023) 15:678:eabl7895. doi: 10.1126/scitranslmed.abl7895

76. Pennington Z, Goodwin ML, Westbroek EM, Cottrill E, Ahmed AK, Sciubba DM. Lactate and cancer: spinal metastases and potential therapeutic targets (part 2). *Ann Trans Med*. (2019) 10:221. doi: 10.21037/atm.2019.01.85

77. Hiratsuka S, Goel S, Kamoun WS, Maru Y, Fukumura D, Duda DG, et al. Endothelial focal adhesion kinase mediates cancer cell homing to discrete regions of the lungs via E-selectin up-regulation. *Proc Natl Acad Sci U.S.A*. (2011) 108:3725–30. doi: 10.1073/pnas.1100446108

78. Gyamfi J, Eom M, Koo JS, Choi J. Multifaceted roles of interleukin-6 in adipocyte–breast cancer cell interaction. *Trans Oncol*. (2018) 11:275–85. doi: 10.1016/j.tranon.2017.12.009

79. Tacchio MDi, Macas J, Weissenberger J, Sommer K, Bähr O, Steinbach JP, et al. Tumor vessel normalization, immunostimulatory reprogramming, and improved survival in glioblastoma with combined inhibition of PD-1, angiopoietin-2, and VEGF. *Cancer Immunol Res*. (2019) 7:1910–27. doi: 10.1158/2326-6066.CIR-18-0865

80. Rami AZA, Hamid AA, Anuar NNM, Aminuddin A, Ugusman A. Exploring the relationship of perivascular adipose tissue inflammation and the development of vascular pathologies. *Mediators Inflammation*. (2022) 2022:2734321. doi: 10.1155/2022/2734321

81. Li Y, Cao S, Gaculenko A, Zhan Y, Bozec A, Chen X. Distinct metabolism of bone marrow adipocytes and their role in bone metastasis. *Front Endocrinol*. (2022) 13:90 2033. doi: 10.3389/fendo.2022.902033

82. Galley JC, Singh S, Awata WMC, Alves JV, Bruder-Nascimento T. Adipokines. Deciphering the cardiovascular signature of adipose tissue. *Biochem Pharmacol*. (2022) 206:115324. doi: 10.1016/j.bcp.2022.115324

83. Hardaway AL, Herroon MK, Rajagurubandara E, Podgorski I. Bone marrow fat: linking adipocyte-induced inflammation with skeletal metastases. *Cancer Metastasis Rev*. (2014) 33:527–43. doi: 10.1007/s10555-013-9484-y

84. Rendina-Ruedy E, Rosen CJ. Lipids in the bone marrow: an evolving perspective. *Cell Metab*. (2020) 31:219–31. doi: 10.1016/j.cmet.2019.09.015

85. Wang H, Leng Y, Gong Y. Bone marrow fat and hematopoiesis. *Front Endocrinol*. (2018) 9:694. doi: 10.3389/fendo.2018.00694

86. Horowitz MC, Berry R, Holtrup B, Sebo Z, Nelson T, Fretz JA, et al. Bone marrow adipocytes. *Adipocyte*. (2017) 6:193–204. doi: 10.1080/21623945.2017.1367881

87. Li Q, Wu Y, Kang N. Marrow adipose tissue: its origin, function, and regulation in bone remodeling and regeneration. *Stem Cells Int*. (2018) 2018:7098456. doi: 10.1155/2018/7098456

88. Hawkes CP, Mostoufi-Moab S. Fat-bone interaction within the bone marrow milieu: Impact on hematopoiesis and systemic energy metabolism. *Bone*. (2019) 119:57–64. doi: 10.1016/j.bone.2018.03.012

89. Ali D, Figeac F, Caci A, Ditzel N, Schmal C, Kerckhofs G, et al. High-fat diet-induced obesity augments the deleterious effects of estrogen deficiency on bone: Evidence from ovariectomized mice. *Aging Cell*. (2022) 21:e13726. doi: 10.1111/acel.13726

90. Beekman KM, Duque G, Corsi A, Tencerova M, Bisschop PH, Paccou J. Osteoporosis and bone marrow adipose tissue. *Curr osteoporosis Rep*. (2023) 21:45–55. doi: 10.1007/s11914-022-00768-1

91. Gawronska-Kozak B, Staszkiewicz J, Gimble JM, Kirk-Ballard H. Recruitment of fat cell precursors during high fat diet in C57BL/6J mice is fat depot specific. *Obesity*. (2014) 22:1091–102. doi: 10.1002/oby.20671

92. Hardouin P, Pansini V, Cortet B. Bone marrow fat. *Joint Bone Spine*. (2014) 81:313–9. doi: 10.1016/j.jbspin.2014.02.013

93. Oliveira MC, Vullings J, van de Loo FAJ. Osteoporosis and osteoarthritis are two sides of the same coin paid for obesity. *Nutrition*. (2020) 70:110486. doi: 10.1016/j.nut.2019.04.001

94. Histing T, Andonyan A, Klein M, Scheuer C, Stenger D, Holstein JH. N T Veith, et al.Obesity does not affect the healing of femur fractures in mice. *Injury*. (2016) 47:1435–44. doi: 10.1016/j.injury.2016.04.030

95. Xu F, Du Yu. Shilong Hang, Anmin Chen, Fengjin Guo, Tao Xu.Adipocytes regulate the bone marrow microenvironment in a mouse model of obesity. *Mol Med Rep*. (2013) 8:823–8. doi: 10.3892/mmr.2013.1572

96. Gall CélineLe, Bellahcène A, Bonnelye E, Gasser JürgA, Castronovo V, Green J, et al. A cathepsin K inhibitor reduces breast cancer induced osteolysis and skeletal tumor burden. *Cancer Res*. (2007) 67:9894–902. doi: 10.1158/0008-5472.CAN-06-3940

97. Duong L, Wesolowski GA, Leung P, Oballa R, Pickarski M. Efficacy of a cathepsin K inhibitor in a preclinical model for prevention and treatment of breast cancer bone metastasis. *Mol Cancer Ther*. (2014) 13:2898–909. doi: 10.1158/1535-7163.MCT-14-0253

98. Cheng M, Liu P, Xu LX. Iron promotes breast cancer cell migration via IL-6/JAK2/STAT3 signaling pathways in a paracrine or autocrine IL-6-rich inflammatory environment. *J inorganic Biochem*. (2020) 210:111159. doi: 10.1016/j.jinorgbio.2020.111159

99. Lin Z, He H, Wang M, Liang J. MicroRNA-130a controls bone marrow mesenchymal stem cell differentiation towards the osteoblastic and adipogenic fate. *Cell proliferation*. (2019) 52:e12688. doi: 10.1111/cpr.12688

100. Liu Yu, Almeida M, Weinstein RS, O'Brien CA, Manolagas SC, Jilka RL. Skeletal inflammation and attenuation of Wnt signaling, Wnt ligand expression, and bone formation in atherosclerotic ApoE-null mice. American journal of physiology. *Endocrinol Metab*. (2016) 310:E762–73. doi: 10.1152/ajpendo.00501.2015

101. Huang M, Liu H, Zhu L, Li X, Li J, Yang S, et al. Mechanical loading attenuates breast cancer-associated bone metastasis in obese mice by regulating the bone marrow microenvironment. *J Cell Physiol*. (2021) 236:6391–406. doi: 10.1002/jcp.30314

102. Xie C, Chen Q. Adipokines: new therapeutic target for osteoarthritis? *Curr Rheumatol Rep*. (2019) 21:71. doi: 10.1007/s11926-019-0868-z

103. Singh L, Tyagi S, Myers D, Duque G. Good, bad, or ugly: the biological roles of bone marrow fat. *Curr Osteoporos Rep*. (2018) 16:130–7. doi: 10.1007/s11914-018-0427-y

104. Gunaratnam K, Vidal C, Boadle R, Thekkedam C, Duque G. Mechanisms of palmitate-induced cell death in human osteoblasts. *Biol Open*. (2013) 2:1382–9. doi: 10.1242/bio.20136700

105. Favaretto F, Bettini S, Busetto L, Milan G, Vettor R. Adipogenic progenitors in different organs: Pathophysiological implications. *Rev endocrine Metab Disord*. (2022) 23:71–85. doi: 10.1007/s11154-021-09686-6

106. Archivum Immunologiae et. Therapiae Experimentalis. Annual report for 1964. *Arch Immunol Ther Exp (Warsz)*. (1965) 13:Suppl:1–15.

107. Lu Y, Gao X, Wang R, Sun J, Guo B, Wei R, et al. Adiponectin inhibits proliferation of vascular endothelial cells induced by Ox-LDL by promoting dephosphorylation of Caveolin-1 and depolymerization of eNOS and up-regulating release of NO. *Int Immunopharmacol*. (2019) 73:424–34. doi: 10.1016/j.intimp.2019.05.017

108. Tulotta C, Ottewell P. The role of IL-1B in breast cancer bone metastasis. *Endocr Relat Cancer*. (2018) 25:R421–34. doi: 10.1530/ERC-17-0309

109. Gyamfi J, Eom M, Koo JS, Choi J. Multifaceted roles of interleukin-6 in adipocyte-breast cancer cell interaction. *Transl Oncol*. (2018) 11:275–85. doi: 10.1016/j.tranon.2017.12.009

110. Aaron N, Costa S, Rosen CJ, Qiang Li. The implications of bone marrow adipose tissue on inflammaging. *Front Endocrinol*. (2022) 13:853765. doi: 10.3389/fendo.2022.853765

111. Evangelista GCM, Salvador PA, Soares SMA, Barros LRC, Xavier FHdaC, Abdo LM, et al. 4T1 mammary carcinoma colonization of metastatic niches is accelerated by obesity. *Front Oncol*. (2019) 9:685. doi: 10.3389/fonc.2019.00685

112. Feng HL, Guo P, Wang J, Liu QY, Xu JF, Yang HC, et al. Association of the expression of leptin and leptin receptor with bone metastasis in pulmonary adenocarcinoma. *Chin J Oncol*. (2016) 38:840–4. doi: 10.3760/cma.j.issn.0253-3766.2016.11.008

113. Oyanagi J, Koh Y, Sato K, Mori K, Teraoka S, Akamatsu H, et al. Predictive value of serum protein levels in patients with advanced non-small cell lung cancer treated with nivolumab. *Lung Cancer*. (2019) 6:107–13. doi: 10.1016/j.lungcan.2019.03.020

114. Olea-Flores M, Juárez-Cruz JC, Zuñiga-Eulogio MD, Acosta E, García-Rodríguez E, Zacapala-Gomez AE, et al. New actors driving the epithelial-mesenchymal transition in cancer the role of leptin. *Biomolecules*. (2020) 10:12. doi: 10.3390/biom10121676

115. Morris EV, Edwards CM. Adipokines, adiposity, and bone marrow adipocytes: Dangerous accomplices in multiple myeloma. *J Cell Physiol*. (2018) 233:9159–66. doi: 10.1002/jcp.26884

116. Hardaway AL, Herroon MK, Rajagurubandara E, Podgorski I. Marrow adipocyte-derived CXCL1 and CXCL2 contribute to osteolysis in metastatic prostate cancer. *Clin Exp Metastasis*. (2015) 32:353–68. doi: 10.1007/s10585-015-9714-5

117. Koundouros N, Poulogiannis G. Reprogramming of fatty acid metabolism in cancer. *Br J Cancer*. (2020) 122:4–22. doi: 10.1038/s41416-019-0650-z

118. Samimi A, Ghanavat M, Shahrabi S, Azizidoost S, Saki N. Role of bone marrow adipocytes in leukemia and chemotherapy challenges. *Cell Mol Life Sci*. (2019) 76:2489–97. doi: 10.1007/s00018-019-03031-6

119. Wang C, Wang J, Chen K, Pang H, Li X, Zhu J, et al. Caprylic acid (C8:0) promotes bone metastasis of prostate cancer by dysregulated adipo-osteogenic balance in bone marrow. *Cancer Sci*. (2020) 111:3600–12. doi: 10.1111/cas.14606

120. Luis Géraldine, Godfroid A, Nishiumi S, Cimino J, Blacher S, Maquoi E, et al. Tumor resistance to ferroptosis driven by Stearoyl-CoA Desaturase-1 (SCD1) in cancer cells and Fatty Acid Biding Protein-4 (FABP4) in tumor microenvironment promote tumor recurrence. *Redox Biol*. (2021) 07:102006. doi: 10.1016/j.redox.2021.102006

121. Herroon MK, Rajagurubandara E, Hardaway AL, Powell K, Turchick A, Feldmann D, et al. Bone marrow adipocytes promote tumor growth in bone via FABP4-dependent mechanisms. *Oncotarget*. (2013) 4:2108–23. doi: 10.18632/oncotarget.1482

122. Cao Y. Adipocyte and lipid metabolism in cancer drug resistance. *J Clin Invest*. (2019) 129:3006–17. doi: 10.1172/JCI127201

123. Yip RKH, Rimes JS, Capaldo BD, Vaillant François, Mouchemore KA, Pal B, et al. Mammary tumour cells remodel the bone marrow vascular microenvironment to support metastasis. *Nat Commun*. (2021) 12:6920. doi: 10.1038/s41467-021-26556-6

124. Wang K, Jiang L, Hu A, Sun C, Zhou L, Huang Y, et al. Vertebral-specific activation of the CX3CL1/ICAM-1 signaling network mediates non-small-cell lung cancer spinal metastasis by engaging tumor cell-vertebral bone marrow endothelial cell interactions. *Theranostics*. (2021) 11:4770–89. doi: 10.7150/thno.54235

125. Zhang Y, Chua S. Leptin function and regulation. *Compr Physiol*. (2017) 8:351–69. doi: 10.1002/cphy.c160041

126. Sáinz N, Barrenetxe J, Moreno-Aliaga MaríaJ, Martínez JoséA. Leptin resistance and diet-induced obesity: central and peripheral actions of leptin. *Metabolism: Clin Exp*. (2015) 64:35–46. doi: 10.1016/j.metabol.2014.10.015

127. Münzberg H. Christopher D Morrison.Structure, production and signaling of leptin. *Metabolism: Clin Exp*. (2015) 64:13–23. doi: 10.1016/j.09.010.metabol.2014

128. Xu M, Cao F-L, Li N, Gao X, Su X, Jiang X. Leptin induces epithelial-to-mesenchymal transition via activation of the ERK signaling pathway in lung cancer cells. *Oncol letters*. (2018) 16:4782–8. doi: 10.3892/ol.2018.9230

129. Wang W, Yan H, Dou C, Su Y. Human leptin triggers proliferation of A549 cells via blocking endoplasmic reticulum stress-related apoptosis. *Biochemistry*. (2013) 78:1333–41. doi: 10.1134/S0006297913120031

130. Zheng X-J, Yang Z-X, Dong Y-J, Zhang G-Y, Sun M-F, An X-K, et al. Downregulation of leptin inhibits growth and induces apoptosis of lung cancer cells via the Notch and JAK/STAT3 signaling pathways. *Biol Open*. (2016) 5:794–800. doi: 10.1242/bio.017798

131. Maroni P. Leptin, adiponectin, and sam68 in bone metastasis from breast cancer. *Int J Mol Sci*. (2020) 21:3. doi: 10.3390/ijms21031051

132. Boura P, Loukides S, Grapsa D, Achimastos A, Syrigos K. The diverse roles of adiponectin in non-small-cell lung cancer: current data and future perspectives. *Future Oncol*. (2015) 11:2193–203. doi: 10.2217/fon.15.96

133. Roger Lijnen H, Scroyen I. Effect of vascular endothelial growth factor receptor 2 antagonism on adiposity in obese mice. *J Mol endocrinology*. (2013) 50:319–24. doi: 10.1530/JME-12-0244

134. Maroni P, Luzzati A, Perrucchini G, Cannavò L, Bendinelli P. Leptin receptor, KHDRBS1 (KH RNA binding domain containing, signal transduction associated 1), and adiponectin in bone metastasis from breast carcinoma. *Immunohistochemical Study. Biomedicines*. (2020) 8:11. doi: 10.3390/biomedicines8110510

135. Zhang H-Q, Wang L-J, Liu S-H, Li J, Xiao L-G, Yang G-T. Adiponectin regulates bone mass in AIS osteopenia via RANKL/OPG and IL6 pathway. *J Trans Med*. (2019) 17:64. doi: 10.1186/s12967-019-1805-7

136. Sharma D, Wang J, Fu PP, Sharma S, Nagalingam A, Mells J, et al. Adiponectin antagonizes the oncogenic actions of leptin in hepatocellular carcinogenesis. *Hepatology*. (2010) 52:1713–22. doi: 10.1002/hep.23892

137. Akifusa S, Kamio N, Shimazaki Y, Yamaguchi N, Nonaka K, Yamashita Y. Involvement of the JAK-STAT pathway and SOCS3 in the regulation of adiponectin-generated reactive oxygen species in murine macrophage RAW 264 cells. *J Cell Biochem*. (2010),111, 597–606. doi: 10.1002/jcb.22745

138. Luo X-H, Guo L-J, Xie H, Yuan L-Q, Wu X-P, Zhou H-D, et al. Adiponectin stimulates RANKL and inhibits OPG expression in human osteoblasts through the MAPK signaling pathway. *J Bone mineral research: Off J Am Soc Bone Mineral Res*. (2006) 21:1648–56. doi: 10.1359/jbmr.060707

139. Fang H, Judd RL. Adiponectin regulation and function. *Compr Physiol*. (2018) 8:1031–63. doi: 10.1002/cphy.c170046

140. Fogarty S, Hardie DG. Development of protein kinase activators: AMPK as a target in metabolic disorders and cancer. *Biochim Biophys Acta*. (2010) 1804:581–91. doi: 10.1016/j.bbapap.2009.09.012

141. Kim AY, Lee YS, Kim KH, Lee JH, Lee HK, Jang SH, et al. Adiponectin represses colon cancer cell proliferation via AdipoR1-and-R2-mediated AMPK activation. *Mol Endocrinol*. (2010) 24:1441–52. doi: 10.1210/me.2009-0498

142. Ren Le, Bao D, Wang L, Xu Q, Xu Y, Shi Z. Nucleobindin-2/nesfatin-1 enhances the cell proliferation, migration, invasion and epithelial-mesenchymal transition in gastric carcinoma. *J Cell Mol Med*. (2022) 26:4986–94. doi: 10.1111/jcmm.17522

143. Sudan SK, Deshmukh SK, Poosarla T, Holliday NP, Dyess DL, Singh AP, et al. Resistin: An inflammatory cytokine with multi-faceted roles in cancer. Biochimica et biophysica acta. *Rev cancer*. (2020) 1874:188419. doi: 10.1016/j.bbcan.2020.188419

144. Muruganandan S, Ionescu AM, Sinal CJ. At the crossroads of the adipocyte and osteoclast differentiation programs: future therapeutic perspectives. *Int J Mol Sci*. (2020) 21:7. doi: 10.3390/ijms21072277

145. Ntikoudi E, Kiagia M, Boura P, Syrigos KN. Hormones of adipose tissue and their biologic role in lung cancer. *Cancer Treat Rev*. (2014) 40:22–30. doi: 10.1016/j.ctrv.2013.06.005

146. Tzanavari T, Tasoulas J, Vakaki C, Mihailidou C, Tsourouflis G, Theocharis S. The role of adipokines in the establishment and progression of head and neck neoplasms. *Curr Medic Chem*. (2019) 26:4726–48. doi: 10.2174/0929867325666180713154505

147. Chen S-S, Tang C-H, Chie M-J, Tsai C-H, Fong Y-C, Lu Y-C, et al. Resistin facilitates VEGF-A-dependent angiogenesis by inhibiting miR-16-5p in human chondrosarcoma cells. *Cell Death Dis*. (2019) 10:31. doi: 10.1038/s41419-018-1241-2

148. Kim H, Lee J-H, Lee SK, Song N-Y, Son SH, Kim KiR, et al. Chemerin treatment inhibits the growth and bone invasion of breast cancer cells. *Int J Mol Sci*. (2020) 21:8. doi: 10.3390/ijms21082871

149. Ostrowska Z, Morawiecka-Pietrzak Małgorzata, Pluskiewicz W, Świętochowska Elżbieta, Strzelczyk J, Gołąbek K, et al. The relationship between chemerin, bone metabolism, the RANKL/RANK/OPG system, and bone mineral density in girls with anorexia nervosa. *Endokrynologia Polska*. (2022) 73:26–34. doi: 10.5603/EP.a2021.0103

150. Hu X, Xiang F, Feng Y, Gao F, Ge S, Wang C, et al. Neutrophils promote tumor progression in oral squamous cell carcinoma by regulating EMT and JAK2/STAT3 signaling through chemerin. *Front Oncol*. (2022) 12:812044. doi: 10.3389/fonc.2022.812044

151. Han L, Zhang Yu, Wan S, Wei Q, Shang W, Huang G, et al. Loss of chemerin triggers bone remodeling in vivo and in *vitro*. *Mol Metab*. (2021) 53:101322. doi: 10.1016/j.molmet.2021.101322

152. Dahl TB, Holm S, Aukrust Pål, Halvorsen B. Visfatin/NAMPT: a multifaceted molecule with diverse roles in physiology and pathophysiology. *Annu Rev Nutr*. (2012) 32:229–43. doi: 10.1146/annurev-nutr-071811-150746

153. Olea-Flores M, Zuñiga-Eulogio M, Tacuba-Saavedra A, Bueno-Salgado M, Sánchez-Carvajal A, Vargas-Santiago Y, et al. Leptin promotes expression of EMT-related transcription factors and invasion in a src and FAK-dependent pathway in MCF10A mammary epithelial cells. *Cells*. (2019) 8:10. doi: 10.3390/cells8101133

154. Tsai CF, Chen JH, Wu CT, Chang PC, Wang SL, Yeh WL. Induction of osteoclast-like cell formation by leptin-induced soluble intercellular adhesion molecule secreted from cancer cells. *Ther Adv Med Oncol(2019)*. (2019) 14:1758835919846806. doi: 10.1177/1758835919846806

155. Reid IR, Baldock PA, Cornish J. Effects of leptin on the skeleton. *Endocrine Rev*. (2018) 39:938–59. doi: 10.1210/er.2017-00226

156. Mei L, Li M, Zhang T. MicroRNA miR-874-3p inhibits osteoporosis by targeting leptin (LEP). *Bioengineered*. (2021) 12:11756–67. doi: 10.1080/21655979.2021.2009618

157. Vita E, Stefani A, Piro G, Mastrantoni L, Cintoni M, Cicchetti G, et al. Leptin-mediated meta-inflammation may provide survival benefit in patients receiving maintenance immunotherapy for extensive-stage small cell lung cancer (ES-SCLC). *Cancer immunology Immunother: CII*. (2023) 72:3803–12. doi: 10.1007/s00262-023-03533-0

158. Kim J-W, Mahiddine FY, Kim GA. Leptin modulates the metastasis of canine inflammatory mammary adenocarcinoma cells through downregulation of lysosomal protective protein cathepsin A (CTSA). *Int J Mol Sci*. (2020) 21:23. doi: 10.3390/ijms21238963

159. Sanchez-Margalet V, Martin-Romero C. Human leptin signaling in human peripheral blood mononuclear cells: activation of the JAK-STAT pathway. *Cell Immunol*. (2001) 211:30–6. doi: 10.1006/cimm.2001.1815

160. Maurya R, Sebastian P, Namdeo M, Devender M, Gertler A. COVID-19 severity in obesity: leptin and inflammatory cytokine interplay in the link between high morbidity and mortality. *Front Immunol*. (2021) 12:649359. doi: 10.3389/fimmu.2021.649359

161. Lam QLK, Wang S, Ko OKH, Kincade PW, Lu L. Leptin signaling maintains B-cell homeostasis via induction of Bcl-2 and Cyclin D1. *Proc Natl Acad Sci United States America*. (2010) 107:13812–7. doi: 10.1073/pnas.1004185107

162. Skrypnik D, Skrypnik K, Suliburska J, Bogdański Paweł. Leptin-VEGF crosstalk in excess body mass and related disorders: A systematic review. *Obes reviews: an Off J Int Assoc Study Obes*. (2023) 24:e13575. doi: 10.1111/obr.13575

163. Clements VK, Long T, Long R, Figley C, Smith DMC, Ostrand-Rosenberg S. Frontline Science: High fat diet and leptin promote tumor progression by inducing myeloid-derived suppressor cells. *J leukocyte Biol*. (2018) 103:395–407. doi: 10.1002/JLB.4HI0517-210R

164. Luo G, He Y, Yu X. Bone marrow adipocyte: an intimate partner with tumor cells in bone metastasis. *Front Endocrinol*. (2018) 9:339. doi: 10.3389/fendo.2018.00339

165. Man K, Ng KTP, Xu A, Cheng Q, Lo CM, Xiao JW, et al. Suppression of liver tumor growth and metastasis by adiponectin in nude mice through inhibition of tumor angiogenesis and downregulation of Rho kinase/IFN-inducible protein 10/matrix metalloproteinase 9 signaling. *Clin Cancer research: an Off J Am Assoc Cancer Res*. (2010) 16:967–77. doi: 10.1158/1078-0432.CCR-09-1487

166. Wang Y, Zhang X, Shao J, Liu H, Liu X, Luo En. Adiponectin regulates BMSC osteogenic differentiation and osteogenesis through the Wnt/β-catenin pathway. *Sci Rep*. (2017) 7:3652. doi: 10.1038/s41598-017-03899-z

167. Mukohira H, Hara T, Abe S, Tani-Ichi S, Sehara-Fujisawa A, Nagasawa T, et al. Mesenchymal stromal cells in bone marrow express adiponectin and are efficiently targeted by an adiponectin promoter-driven Cre transgene. *Int Immunol*. (2019) 131:729–42. doi: 10.1093/intimm/dxz042

168. Illiano M, Nigro E, Sapio L, Caiafa I, Spina A, Scudiero O, et al. Adiponectin down-regulates CREB and inhibits proliferation of A549 lung cancer cells. *Pulmonary Pharmacol Ther*. (2017) 45:114–20. doi: 10.1016/j.pupt.2017.05.009

169. Tsai J-R, Liu P-L, Chen Y-H, Chou S-H, Cheng Y-J, Hwang J-J, et al. Curcumin inhibits non-small cell lung cancer cells metastasis through the adiponectin/NF-κb/MMPs signaling pathway. *PloS One*. (2015) 10:e0144462. doi: 10.1371/journal.pone.0144462

170. Jian M, Kwan JS-C, Bunting M, Ng RC-L, Chan KHo. Adiponectin suppresses amyloid-β oligomer (AβO)-induced inflammatory response of microglia via AdipoR1-AMPK-NF-κB signaling pathway. *J Neuroinflamm*. (2019) 16:110. doi: 10.1186/s12974-019-1492-6

171. Rupp SK, Stengel A. Interactions between nesfatin-1 and the autonomic nervous system-An overview. *Peptides*. (2022) 149:170719. doi: 10.1016/j.peptides.2021.170719

172. Suzuki S, Takagi K, Miki Y, Onodera Y, Akahira JI, Ebata A, et al. Nucleobindin 2 in human breast carcinoma as a potent prognostic factor. *Cancer Sci*. (2012) 103:136–43. doi: 10.1111/j.1349-7006.2011.02119.x

173. Altan B, Kaira K, Okada S, Saito T, Yamada E, Bao H, et al. High expression of nucleobindin 2 is associated with poor prognosis in gastric cancer. *Tumor Biol*. (2017) 39:1–7. doi: 10.1177/1010428317703817

174. Akrida I, Papadaki H. Adipokines and epithelial-mesenchymal transition (EMT) in cancer. *Mol Cell Biochem*. (2023) 1:30. doi: 10.1007/s11010-023-04670-x

175. Kmiecik AM, Dzięgiel P, Podhorska-Okołów M. Nucleobindin-2/nesfatin-1-A new cancer related molecule? *Int J Mol Sci*. (2021) 22:15. doi: 10.3390/ijms22158313

176. Chang J-W, Liu S-C, Lin Y-Y, He X-Y, Wu Y-S, Su C-M, et al. Nesfatin-1 stimulates CCL2-dependent monocyte migration and M1 macrophage polarization: implications for rheumatoid arthritis therapy. *Int J Biol Sci*. (2023) 19:281–93. doi: 10.7150/ijbs.77987

177. Jiang L, Xu K, Li J, Zhou X, Xu L, Wu Z, et al. Nesfatin-1 suppresses interleukin-1β-induced inflammation, apoptosis, and cartilage matrix destruction in chondrocytes and ameliorates osteoarthritis in rats. *Aging*. (2020) 12:1760–77. doi: 10.18632/aging.102711

178. Solmaz A, Bahadır E, Gülçiçek OB, Yiğitbaş H, Çelik A, Karagöz Ayça, et al. Nesfatin-1 improves oxidative skin injury in normoglycemic or hyperglycemic rats. *Peptides*. (2016) 78:1–10. doi: 10.1016/j.peptides.2015.12.006

179. Tripathi D, Kant S, Pandey S, Ehtesham NZ. Resistin in metabolism, inflammation, and disease. *FEBS J*. (2020) 287:3141–9. doi: 10.1111/febs.15322

180. Deepika F, Bathina S, Armamento-Villareal R. Novel adipokines and their role in bone metabolism: A narrative review. *Biomedicines*. (2023) 11:2. doi: 10.3390/biomedicines11020644

181. Kuo C-H, Chen K-F, Chou S-H, Huang Y-F, Wu C-Y, Cheng D-E, et al. Lung tumor-associated dendritic cell-derived resistin promoted cancer progression by increasing Wolf-Hirschhorn syndrome candidate 1/Twist pathway. *Carcinogenesis*. (2013) 34:2600–9. doi: 10.1093/carcin/bgt281

182. Wang X, Tang Y, Xiao R. Chemerin contributes to inflammatory responses and suppresses osteogenic differentiation in chronic periodontitis. *Oral Dis*. (2023) 29:1706–14. doi: 10.1111/odi.14130

183. Wani AK, Prakash A, Sena S, Akhtar N, Singh R, Chopra C, et al. Unraveling molecular signatures in rare bone tumors and navigating the cancer pathway landscapes for targeted therapeutics. *Crit Rev oncology/hematology*. (2024) 196:104291. doi: 10.1016/j.critrevonc.2024.104291

184. Gao F, Feng Y, Hu X, Zhang X, Li T, Wang Y, et al. Neutrophils regulate tumor angiogenesis in oral squamous cell carcinoma and the role of Chemerin. *Int Immunopharmacol*. (2023) 121:110540. doi: 10.1016/j.intimp.2023.110540

185. Dakroub A, Nasser SA, Younis N, Bhagani H, Al-Dhaheri Y, Pintus G, et al. Visfatin: A possible role in cardiovasculo-metabolic disorders. *Cells*. (2020) 9:11. doi: 10.3390/cells9112444

186. Hung S-Y, Lin C-Y, Yu C-C, Chen H-T, Lien M-Y, Huang Y-W, et al. Visfatin promotes the metastatic potential of chondrosarcoma cells by stimulating AP-1-dependent MMP-2 production in the MAPK pathway. *Int J Mol Sci*. (2021) 22:16. doi: 10.3390/ijms22168642

187. Zhang Z, Xiao Ke, Wang S, Ansari AR, Niu X, Yang W, et al. Visfatin is a multifaceted molecule that exerts regulation effects on inflammation and apoptosis in RAW264.7 cells and mice immune organs. *Front Immunol*. (2022) 13:1018973. doi: 10.3389/fimmu.2022.1018973

188. Zhao X, Xie L, Wang Z, Wang J, Xu H, Han X, et al. ZBP1 (DAI/DLM-1) promotes osteogenic differentiation while inhibiting adipogenic differentiation in mesenchymal stem cells through a positive feedback loop of Wnt/β-catenin signaling. *Bone Res*. (2020) 8:12. doi: 10.1038/s41413-020-0085-4

189. Sun G, Zhang X, Liu Z, Zhu S, Shen P, Zhang H, et al. The adiponectin-adipoR1 axis mediates tumor progression and tyrosine kinase inhibitor resistance in metastatic renal cell carcinoma. *Neoplasia*. (2019) 21:921–31. doi: 10.1016/j.neo.2019.07.004

frontiers | Frontiers in Oncology

TYPE Mini Review
PUBLISHED 24 April 2024
DOI 10.3389/fonc.2024.1395192

OPEN ACCESS

EDITED BY
Parmanand Malvi,
University of Alabama at Birmingham, United States

REVIEWED BY
Chunming Cheng,
University of Oklahoma, United States
Elena Sacco,
University of Milano-Bicocca, Italy
Uri Nir,
Bar-Ilan University, Israel

*CORRESPONDENCE
Xuan Xiao
brex@sina.com

RECEIVED 03 March 2024
ACCEPTED 12 April 2024
PUBLISHED 24 April 2024

CITATION
Sun T and Xiao X (2024) Targeting ACAT1 in cancer: from threat to treatment.
Front. Oncol. 14:1395192.
doi: 10.3389/fonc.2024.1395192

Targeting ACAT1 in cancer: from threat to treatment

Tie Sun and Xuan Xiao*

Department of Thyroid and Breast Surgery, People's Hospital of China Medical University (Liaoning Provincial People's Hospital), Shenyang, China

Altered cholesterol metabolism has been identified as a critical feature of cancers. Cholesterol functions as the main component of cell membrane, cholesterol and is required for sustaining membrane integrity and mediating signaling transduction for cell survival. The intracellular level of cholesterol is dynamically regulated. Excessive cholesterol could be converted to less toxic cholesteryl esters by acyl-coenzyme A:cholesterol acyltransferases (ACATs). While ACAT2 has limited value in cancers, ACAT1 has been found to be widely participated in tumor initiation and progression. Moreover, due to the important role of cholesterol metabolism in immune function, ACAT1 is also essential for regulating anti-tumor immunity. ACAT1 inhibition may be exploited as a potential strategy to enhance the anti-tumor immunity and eliminate tumors. Herein, a comprehensive understanding of the role of ACAT1 in tumor development and anti-tumor immunity may provide new insights for anti-tumor strategies.

KEYWORDS

metabolism, immunity, ACAT (acyl-CoA:cholesterol acyltransferase), cancer, cholesterol

Introduction

A hallmark of cancer is the deregulated metabolism (1). As an integral component of cell membrane, cholesterol is crucial for maintaining membrane integrity and signaling transduction for cell survival (2). Besides, cholesterol also participates in the regulation of multiple biological processes, including lipid metabolism, inflammation, apoptosis, and cell survival (3–5). Cholesterol-derived metabolites exert a wide variety of biological effects in tumor development and anti-tumor immunity responses (6). As fast-proliferating cells, tumor cells rely on cholesterol for membrane biogenesis and various biological processes (7). Therefore, targeting cholesterol metabolism may provide novel therapeutic strategies for cancer management.

Intracellular cholesterol is dynamically transported for maintaining membrane integrity (8). Excessive cholesterol is either exported by ATP-binding cassette proteins, or converted to less toxic cholesteryl esters by acyl-coenzyme A: cholesterol acyltransferases (ACATs) to store in the form of lipid droplets or lipoproteins (3). ACATs belong to membrane-bound O-acyltransferase family, are composed of two enzymes localizing in the mitochondria and cytoplasm, respectively (9). ACAT1 and ACAT2 catalyze acyl transfer from acyl-coenzyme A (CoA) to cholesterol and produce cholesterol esters that are used for

storage and intercellular transport of sterol, which is important for cellular cholesterol homeostasis (10). ACAT1 is expressed in nucleated eukaryotic cells and its products are incorporated into lipid droplets (LDs) in the cytoplasm (11). ACAT2 is primarily expressed in intestinal epithelial cells and hepatocytes, and its products are incorporated into lipoproteins in the endoplasmic reticulum (12). While ACAT2 has limited value in tumors, ACAT1 has been found to be implicated in tumor occurrence and development. Recent studies introduced the complex role of ACAT1 in tumor development and anti-tumor immunity, which may provide new insights for anti-tumor strategies.

ACAT1 structure, regulation, and function

Structure analysis has identified human ACAT1 as a tetramer with two homodimers (13). Each monomer is composed of nine transmembrane segments, which enclose a cytosolic tunnel and a transmembrane tunnel that converge at the predicted catalytic site (14). ACAT1 tetramers, but not monomers, are phosphorylated and stabilized by enhanced Y407 phosphorylation observed in multiple human cancer cells. It has also been indicated that CoA could enter through the cytosolic tunnel, while cholesterol enters via the transmembrane tunnel (13). The structure of ACAT1 has been deciphered previously (13, 14). ACAT1 exerts its catalytic role in ketolysis, ketogenesis, fatty acid oxidation and isoleucine degradation (12). ACAT1 senses free cholesterol by its allosteric site. ACAT1 cannot exert its catalytic role for esterification with high efficiency under low cholesterol concentrations, whereas high amounts of cholesterol could facilitate esterification allosterically under high cholesterol concentrations (13). Herein, ACAT1 activity is determined by the level of free cholesterol to regulate cholesterol homeostasis of the endoplasmic reticulum (15). In addition to mediating cholesterol homeostasis, ACAT1 exerts its acetyltransferase activity capable of specifically acetylating various enzymes. For instance, ACAT1 regulates pyruvate dehydrogenase complex (PDC) by acetylating pyruvate dehydrogenase (PDH) and PDH phosphatase to promote glycolysis (16). ACAT1-mediated K128 acetylation of GNPAT could protect FASN from degradation and promote lipid metabolism (17). ACAT1-mediated K337 acetylation of ME1 dimerize and activate ME1 to regulate NADPH generation and lipid metabolism (18). The structure and function of ACAT1 has been illustrated in Figure 1.

ACAT1 and immunity

Cholesterol metabolism has been identified to be essential for immune function (4, 19). Cholesterol biosynthesis is critical for T cell growth, activation, and anti-tumor function (4, 20, 21). It has been demonstrated that elevated levels of cholesterol in T cells could boost the anti-tumor immunity of T cells (22). CD8+ T cells play an essential role in anti-tumor immunity, but their function is always abrogated in the context of cancers (23). Therefore, remodeling the anti-tumor ability of CD8+ T cells is a key strategy for improving the efficacy of immunotherapy. ACAT1 inhibition could impair cholesterol esterification, therefore potentiating anti-tumor effect and strengthening cell proliferation of CD8+ T cells (22). Mechanistically, elevated cholesterol level of CD8+ T cells could enhance T-cell receptor clustering and signaling. ACAT1-deleted CD8+ T cells exhibited impaired tumor growth and metastasis of melanoma (22). An avasimibe-induced inhibition of cholesterol esterification has been shown to improve the antitumor response of CD8+ T cells in mice (24). Avasimibe exerted significant anti-tumor effect. Moreover, avasimibe combined with PD-1 inhibitor exhibited greater anti-tumor capabilities compared with PD-1 inhibitor alone. Avasimibe could be restrained on the T cell surface to induce rapid T cell receptor clustering and sustaine T cell activation (25). In addition, paclitaxel and immunoadjuvant αGC were co-encapsulated in liposomes modified with pH sensitive TH peptide (PTX/αGC-TH-Lip). Avasimibe could elevate the level of free cholesterol and relieve the inhibition of CD8+ T cells resulted from PTX/αGC-TH-Lip. The combination of avasimibe and PTX/αGC-TH-Lip could enhance immune responses and cytotoxic effects in xenografts of melanoma, which is a potential strategy to improve the anti-tumor effects of immune-chemotherapy (26) (Figure 2).

ACAT1 in different tumor types

The role of metabolic enzymes in various biological processes has been gradually discovered. It has been well-established that multiple metabolic enzymes could participate in epigenetic

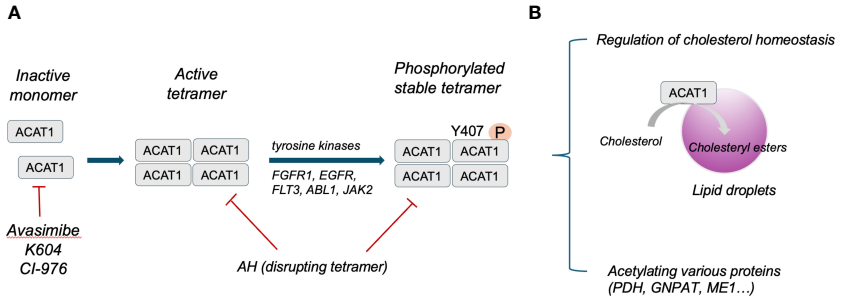

FIGURE 1
(A), Schematic illustration of ACAT1 structure. **(B)**, Primary function of ACAT1 in cells.

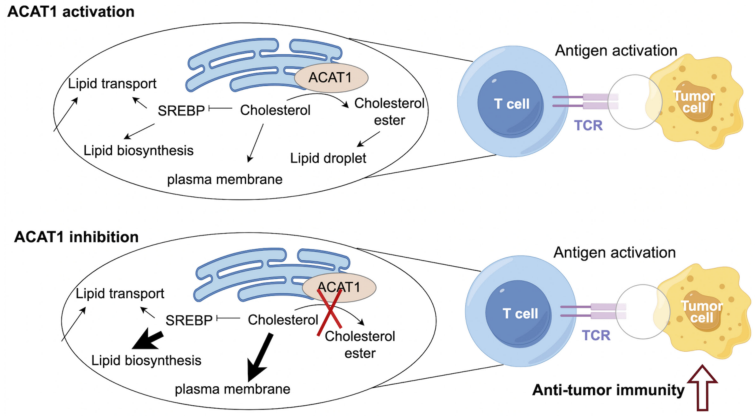

FIGURE 2
ACAT1 is a potential target to enhance the anti-tumor strategy.

remodeling by providing substrates such as acetyl-CoA (27, 28). Considering the catalytic role of ACAT1 in mediating acyl transfer from CoA to cholesterol, ACAT1 may exert complex and dynamic role in tumorigenesis and progression. Mounting evidence has elucidated the significance of ACAT1 in multiple malignances. Here, we summarized the role of ACAT1 in the contexts of different cancers.

ACAT1 and colorectal cancer

Colorectal cancer (CRC) is the third most diagnosed tumor worldwide (29). 25% of newly diagnosed CRC patients are diagnosed at the metastatic stage (30). The crosstalk between cholesterol metabolism and CRC has been under vast investigations. An elevated cholesterol level could accelerate CRC progression by activating β-catenin oncogenic signaling pathway (29). Specific liver metastases of CRC display an aberration of cholesterol biosynthesis (31). Thus, aberrant cholesterol metabolism is a hallmark of CRC, which may be exploited as potential therapeutic targets.

Numerous evidence illustrated that various molecular mechanisms are engaged in the tumorigenesis and development of CRC (32). The cytoplasmic form of malic enzymes (ME), ME1, has been identified as a primary source of NADPH for lipogenesis and glutamine biosynthesis. In CRC cells, depletion of ACAT1 could dramatically impair ME1 acetylation without influencing its protein level, whereas ACAT1 overexpression exerts the opposite effect. Moreover, ACAT1 overexpression enhances ME1 dimerization whereas deletion of ACAT1 expression impair ME1 dimerization. This ACAT1-mediated K337 acetylation positively regulates ME1 dimerization. PGAM5, a mitochondrial serine/threonine phosphatase, could dephosphorylate ME1 at S336, further promoting acetylation by ACAT1 at the adjacent K337. ACAT1-mediated ME1 K337 acetylation could enhance NADPH generation, lipogenesis, and CRC tumorigenesis (18). β-hydroxybutyrate (BHB) was previously identified as an oncogenic metabolite of CRC, which was also found to be elevated in CRC tissues. BHB has been found to promote CRC progression by ACAT1 by mediating acetylation of isocitrate dehydrogenase 1. ACAT1 abrogation could impair CRC tumorigenesis and abrogate the tumorigenic effects of BHB (33, 34). Small molecule inhibitors that target ACAT1-mediated ME1 acetylation may be a potential anti-tumor strategy for CRC patients. Besides, the development of CRC is correlated with hyperinsulinemia. Insulin-induced tumor progression of CRC is regulated by ACAT1. Insulin enhanced CRC development by upregulating ACAT1, which can be exploited as a promising therapeutic target for CRC (35). Collectively, the understanding of CRC biological features associated with ACAT1 may be beneficial for diagnosis and treatment of CRC in the clinical settings (36).

ACAT1 and hepatocellular carcinoma

Liver cancer is the sixth most diagnosed cancer worldwide (29). Notably, it is highly refractory to most chemotherapeutic regimens. Hepatocellular carcinoma (HCC) is the most common type of liver cancer (37). In HCC cells, ACAT1 could stabilize and dimerize glyceronephosphate O-acyltransferase (GNPAT), a rate-limiting enzyme in plasmalogen synthesis and lipogenesis, by acetylation at K128. Precisely, ACAT1-mediated GNPAT acetylation could inhibit GNPAT degradation by repressing TRIM21-mediated GNPAT ubiquitination, ultimately promoting tumor growth in HCC xenografts. ACAT1 overexpression enhanced tumor growth in HCC xenografts and GNPAT deletion could attenuate ACAT1-induced HCC growth, and ACAT1 overexpression with GNPAT inhibition diminish fatty acid synthesis and lipogenesis. Combination treatment of ACAT1 inhibitor and sorafenib could significantly inhibit tumor growth in HCC xenografts, indicating that pharmaceutical inhibition of ACAT1 could be a promising target in anti-HCC strategy (17). In HEK293 cells, ACAT1 has been identified as a substrate of E3 ubiquitin ligase UBE3A/E6AP. High-fat diet could downregulate UBE3A expression, while UBE3A overexpression could lead to decreased ACAT1 protein level (38).

Future studies may require combination regimens that include systemic therapies and molecularly targeted treatments, such as ACAT1.

ACAT1 and glioblastoma

Glioblastoma (GBM) are the most frequently diagnosed malignant primary brain tumors that originate from neuroglial progenitor cells (39). Conventional treatment could bring limited improvements in the survival of glioma patients, leading to poor survival outcomes for GBM patients (40). Herein, it is desperately required for effective molecularly targeted therapy to improve prognosis of GBM patients. In GBM patients, ACAT1 has been found to be upregulated and correlated with poor prognosis. Moreover, pharmacological inhibition of ACAT1 in GBM cells demonstrated that ACAT1 is required for GBM proliferation (41). Upon inhibition of mTORC1, ACAT1 could catalyze acetylation of glycine decarboxylase (GLDC), a critical enzyme of glycine metabolism that catalyzes the conversion of glycine into one-carbon units. The acetylation of GLDC at K514 inhibits its enzymatic activity, which promoted K33-linked polyubiquitination at K544 by NF-X1, resulting in GLDC degradation by the proteasomal pathway (42). Acetylation of GLDC at K514 could suppress glycine catabolism, pyrimidines synthesis and GBM development. K604, a potent ACAT1 inhibitor, could impair the proliferation of U251−MG cells and inactivate Akt signaling pathway in GBM cells (43). Avasimibe, another specific inhibitor of ACAT, exerts anti-tumor effect on U87, A172 and GL261 GBM cells. In GBM cell lines, avasimibe could inhibit the expression of ACAT1 and biosynthesis of cholesterol ester. Moreover, avasimibe could impair the proliferation of GBM cells resulted from caspase-8 and caspase-3 activation (44). Herein, ACAT1 functions as a novel target for HCC, providing effective assistance to the treatment of GBM.

ACAT1 and lung cancer

Lung cancer is a heterogenous disease composed of multiple genetic and molecular subtypes, which is still the leading cause of cancer-related death worldwide (45). Considering that molecularly defined subtypes are potentially targetable, novel anti-tumor strategies in for lung cancer are required to be explored. Excessive intracellular cholesterol is catalyzed to cholesteryl esters via ACAT1 and exported via the cholesterol transporter ABCA1. In a cohort of patients with lung adenocarcinoma, ACAT1 has been found to be upregulated, while ABCA1 is downregulated in the lung cancer tissues. In H1299 cells, ACAT1 has been identified as the acetyltransferase of PDHA1 and PDP1. Mechanistically, PDP1 phosphorylation at Y381 recruits ACAT1 and dissociates SIRT3 to promote lysine acetylation of PDP1 and PDHA1. ACAT1 predominantly signals through inhibition of PDC by PDP1 and PDHA acetylation to enhance glycolysis and tumor growth, indicating the ACAT1-PDP1-PDHA axis a promising anti-cancer target (46). lncRNA DARS-AS1 inhibition attenuated non-small cell lung cancer development by activating miR-302a-3p to inhibit ACAT1 expression (47). It has been demonstrated that Kras-specific antigenic peptides in combination of avasimibe could promote CD8+ T cell infiltration and impair lung tumor progression (48). Collectively, ACAT1 may function as a promising therapeutic target for lung cancer.

ACAT1 and breast cancer

Breast cancer is a heterogeneous malignancy with multiple molecular subtypes based on histological and genomic features (49). Gene expression profiling has proposed four intrinsic molecular subtypes: Luminal A, Luminal B, HER 2+ and basal like (50). It has been demonstrated that ER-negative breast cancer cells display accumulation of LDs, increased LDL uptake, a higher ratio of cholesteryl ester to triacylglycerol, lower cholesterol biosynthesis, increased expression of ACAT1, higher ACAT activity as compared to ER-positive breast cancer cells (51). CP-113,818, a ACAT inhibitor, could inhibit proliferation of breast tumor cells and reduce LDL-mediated proliferation of ER-negative cells. In MDA-MB-231 cells, LDL receptor (LDLR) mRNA could be markedly impaired by ACAT inhibition, indicating that high ACAT1 activity is correlated with higher LDLR expression (52). It has been found that ACAT1 upregulation in breast tumor cells could promote tumor initiation and metastasis, indicating ACAT1 as a metabolic tumor promoter (53). Nuclear receptor subfamily 2 group F member 6 (NR2F6) could transcriptionally activate ACAT1 and enhance the suppressive role of ACAT1-induced METTL3 acetylation on cell migration and invasion of breast cancer (54).

ACAT1 and leukemia

Leukemia is a heterogeneous malignancy with different genetic, morphologic and molecular feature, which is composed of multiple subtypes including acute myeloid leukemia (AML) and chronic myeloid leukemia (CML) (55). ACAT1 and SIRT3 have been identified as the upstream acetyltransferase and deacetylase of mutant isocitrate dehydrogenase 2 (mIDH2) in AML to regulate K413-acetylation of mIDH2 and inhibit mIDH2 activity (56). Spectromicroscopic analysis in multiple leukemia cell lines has revealed that aberrant accumulation of CE was found in CML (chronic myelogenous leukemia), which may be resulted from altered BCR-ABL kinase activity. Inhibiting cholesterol esterification via avasimibe could significantly suppress CML cell proliferation. Besides, combinational treatment of avasimibe and imatinib brought synergistic effects on blocking cell proliferation in K562R cells (57).

Implications for targeting ACAT1 in anti-tumor therapy

Targeting ACAT1 has been identified as a potential anti-tumor strategy (58). Avasimibe, also named as avasimin, has been developed as a potent non-specific ACAT1 inhibitor to impair cholesterol esterification in multiple cancer models. *In vitro* studies

TABLE 1 Current ACAT1 inhibitors tested in human cancers.

Inhibitors	Disease	Struture	Binding sites	Mechanism of action	Target	Models	Combined therapy	Reference
Arecoline hydrobromide	Hepatocellular carcinoma	–	Cysteine residue (C126) in the ACAT1 catalytic site	Binds to and disrupts ACAT1 tetramers	Cancer cell proliferation and tumor growth	Cellular or mice models	Sorafenib	(16)
Avasimibe	Melanoma, Lewis lung adenocarcinoma	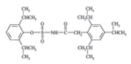	–	A chemical group that conferred ACAT inhibitory properties (the 2,6-diisopropylphenyl moiety)	Tumor growth	Mice models	Anti-PD-1 antibody	(23)
	Chronic myeloid leukemia		–		Tumor growth	Mice models	Imatinib	(57)
K604	Glioblastoma	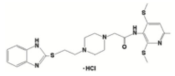	–	–	Cancer cell proliferation	Cellular models	–	(43)

have elucidated that avasimibe could reduce cholesteryl-ester storage in LDs and increase levels of free cholesterol, leading to cell apoptosis and impaired proliferation (59). ACAT1 inhibitor could also enhance the cytotoxic effects of CD8+ T cells by reprogramming cholesterol metabolism. A combination of avasimin and anti-PD-1 treatment exhibited synergistic cytotoxic effects in suppressing melanoma development (22). Avasimin combined with nanoparticles of doxorubicin showed better anti-tumor efficacy in impairing breast cancer progression (60). The combination of avasimibe and immune-chemotherapy could enhance the anti-tumor effects of immune-chemotherapy. The combinational treatment could increase the level of free cholesterol and relieve the inhibition of CD8+ T cells resulted from PTX/αGC-TH-Lip. The combination of avasimibe and PTX/αGC-TH-Lip could enhance immune responses and cytotoxic effects in xenografts of melanoma, which is a potential strategy to improve the anti-tumor effects of immune-chemotherapy (26). It has been demonstrated that vaccine of Kras-specific antigenic peptides combines with avasimibe could eliminate regulatory T cells and promote CD8+ T cell infiltration (48).

Targeting tetrameric ACAT1 has been proposed as a promising anti-tumor strategy. Arecoline hydrobromide (AH) is a covalent ACAT1 inhibitor that specifically binds to and disrupts ACAT1 tetramers, thereby AH treatment leads to impaired ACAT1 activity. Due to the inhibitory effect of ACAT1 on PDC by acetylating PDH and PDH phosphatase, AH treatment could enhance PDC flux and oxidative phosphorylation to impair tumor growth, making ACAT1 a potential anti-tumor target. Combination treatment of AH with other anti-tumor strategy have shown greater anti-tumor efficacy. In HCC, AH treatment combined with sorafenib could significantly inhibit tumor growth in HCC xenografts (16). CI-976, a small molecule ACAT1 inhibitor, can bind inside the catalytic chamber and blocks the accessibility of the active site residues of ACAT1. CI-976 has been found to reduce atherosclerotic plaques and decrease plasma cholesterol levels in animals fed with high cholesterol diet (61). Another selective ACAT1 inhibitor K604 has been found to impair the proliferation of U251−MG cells and inhibit Akt signaling in glioblastoma cells (43). The current reported ACAT1 inhibitors have been illustrated in Table 1. The anti-tumor effect of ACAT1 inhibitors should be further verified in more cancer types *in vitro* and vivo models to explore the cancer types that can be effectively treated with ACAT1 inhibitors. Clinical trials should be accelerated to evaluate the anti-tumor effects of more ACAT1 inhibitors in different cancer types (62).

Author contributions

TS: Writing – original draft, Writing – review & editing. XX: Writing – original draft, Writing – review & editing.

Funding

The author(s) declare that no financial support was received for the research, authorship, and/or publication of this article.

Conflict of interest

The authors declare that the research was conducted in the absence of any commercial or financial relationships that could be construed as a potential conflict of interest.

Publisher's note

References

1. Kroemer G, Pouyssegur J. Tumor cell metabolism: cancer's Achilles' heel. *Cancer Cell*. (2008) 13:472–82. doi: 10.1016/j.ccr.2008.05.005

2. Maxfield FR, van Meer G. Cholesterol, the central lipid of mammalian cells. *Curr Opin Cell Biol*. (2010) 22:422–9. doi: 10.1016/j.ceb.2010.05.004

3. Luo J, Yang H, Song BL. Mechanisms and regulation of cholesterol homeostasis. *Nat Rev Mol Cell Biol*. (2020) 21:225–45. doi: 10.1038/s41580-019-0190-7

4. Tall AR, Yvan-Charvet L. Cholesterol, inflammation and innate immunity. *Nat Rev Immunol*. (2015) 15:104–16. doi: 10.1038/nri3793

5. Li K, Deng Y, Deng G, Chen P, Wang Y, Wu H, et al. High cholesterol induces apoptosis and autophagy through the ROS-activated AKT/FOXO1 pathway in tendon-derived stem cells. *Stem Cell Res Ther*. (2020) 11:131. doi: 10.1186/s13287-020-01643-5

6. Huang B, Song BL, Xu C. Cholesterol metabolism in cancer: mechanisms and therapeutic opportunities. *Nat Metab*. (2020) 2:132–41. doi: 10.1038/s42255-020-0174-0

7. Kuzu OF, Noory MA, Robertson GP. The role of cholesterol in cancer. *Cancer Res*. (2016) 76:2063–70. doi: 10.1158/0008-5472.CAN-15-2613

8. SChade DS, Shey L, Eaton RP. Cholesterol review: A metabolically important molecule. *Endocr Pract*. (2020) 26:1514–23. doi: 10.4158/EP-2020-0347

9. Antonenkov VD, Croes K, Waelkens E, Van Veldhoven PP, Mannaerts GP. Identification, purification and characterization of an acetoacetyl-CoA thiolase from rat liver peroxisomes. *Eur J Biochem*. (2000) 267:2981–90. doi: 10.1046/j.1432-1327.2000.01314.x

10. Chang TY, Li BL, Chang CC, Urano Y. Acyl-coenzyme A:cholesterol acyltransferases. *Am J Physiol Endocrinol Metab*. (2009) 297:E1–9. doi: 10.1152/ajpendo.90926.2008

11. Shibuya Y, Chang CC, Chang TY. ACAT1/SOAT1 as a therapeutic target for Alzheimer's disease. *Future Med Chem*. (2015) 7:2451–67. doi: 10.4155/fmc.15.161

12. Goudarzi A. The recent insights into the function of ACAT1: A possible anti-cancer therapeutic target. *Life Sci*. (2019) 232:116592. doi: 10.1016/j.lfs.2019.116592

13. Qian H, Zhao X, Yan R, Yao X, Gao S, Sun X, et al. Structural basis for catalysis and substrate specificity of human ACAT1. *Nature*. (2020) 581:333–8. doi: 10.1038/s41586-020-2290-0

14. Long T, Sun Y, Hassan A, Qi X, Li X. Structure of nevanimibe-bound tetrameric human ACAT1. *Nature*. (2020) 581:339–43. doi: 10.1038/s41586-020-2295-8

15. Lee-Rueckert M, Lappalainen J, Leinonen H, Plihtari R, Nordström T, Åkerman K, et al. Acidic extracellular pH promotes accumulation of free cholesterol in human monocyte-derived macrophages via inhibition of ACAT1 activity. *Atherosclerosis*. (2020) 312:1–7. doi: 10.1016/j.atherosclerosis.2020.08.011

16. Fan J, Lin R, Xia S, Chen D, Elf SE, Liu S, et al. Tetrameric acetyl-coA acetyltransferase 1 is important for tumor growth. *Mol Cell*. (2016) 64:859–74. doi: 10.1016/j.molcel.2016.10.014

17. Gu L, Zhu Y, Lin X, Tan X, Lu B, Li Y. Stabilization of FASN by ACAT1-mediated GNPAT acetylation promotes lipid metabolism and hepatocarcinogenesis. *Oncogene*. (2020) 39:2437–49. doi: 10.1038/s41388-020-1156-0

18. Zhu Y, Gu L, Lin X, Liu C, Lu B, Cui K, et al. Dynamic regulation of ME1 phosphorylation and acetylation affects lipid metabolism and colorectal tumorigenesis. *Mol Cell*. (2020) 77:138–149.e5. doi: 10.1016/j.molcel.2019.10.015

19. King RJ, Singh PK, Mehla K. The cholesterol pathway: impact on immunity and cancer. *Trends Immunol*. (2022) 43:78–92. doi: 10.1016/j.it.2021.11.007

20. Ma X, Bi E, Lu Y, Su P, Huang C, Liu L, et al. Cholesterol induces CD8+ T cell exhaustion in the tumor microenvironment. *Cell Metab*. (2019) 30:143–156.e5. doi: 10.1016/j.cmet.2019.04.002

21. Ma X, Xiao L, Liu L, Ye L, Su P, Bi E, et al. CD36-mediated ferroptosis dampens intratumoral CD8+ T cell effector function and impairs their antitumor ability. *Cell Metab*. (2021) 33:1001–1012.e5. doi: 10.1016/j.cmet.2021.02.015

22. Rashkovan M, Albero R, Gianni F, Perez-Duran P, Miller HI, Mackey AL, et al. Intracellular cholesterol pools regulate oncogenic signaling and epigenetic circuitries in early T-cell precursor acute lymphoblastic leukemia. *Cancer Discovery*. (2022) 12:856–71. doi: 10.1158/2159-8290.CD-21-0551

23. Yang W, Bai Y, Xiong Y, Zhang J, Chen S, Zheng X, et al. Potentiating the antitumour response of CD8(+) T cells by modulating cholesterol metabolism. *Nature*. (2016) 531:651–5. doi: 10.1038/nature17412

24. Hao M, Hou S, Li W, Li K, Xue L, Hu Q, et al. Combination of metabolic intervention and T cell therapy enhances solid tumor immunotherapy. *Sci Transl Med*. (2020) 12:eaaz6667. doi: 10.1126/scitranslmed.aaz6667

25. Zhao L, Li J, Liu Y, Kang L, Chen H, Jin Y, et al. Cholesterol esterification enzyme inhibition enhances antitumor effects of human chimeric antigen receptors modified T cells. *J Immunother*. (2018) 41:45–52. doi: 10.1097/CJI.0000000000000207

26. Li M, Yang Y, Wei J, Cun X, Lu Z, Qiu Y, et al. Enhanced chemo-immunotherapy against melanoma by inhibition of cholesterol esterification in CD8 + T cells. *Nanomedicine*. (2018) 14:2541–50. doi: 10.1016/j.nano.2018.08.008

27. Mews P, Donahue G, Drake AM, Luczak V, Abel T, Berger SL. Acetyl-CoA synthetase regulates histone acetylation and hippocampal memory. *Nature*. (2017) 546:381–6. doi: 10.1038/nature22405

28. Pietrocola F, Galluzzi L, Bravo-San Pedro JM, Madeo F, Kroemer G. Acetyl coenzyme A: a central metabolite and second messenger. *Cell Metab*. (2015) 21:805–21. doi: 10.1016/j.cmet.2015.05.014

29. Sung H, Ferlay J, Siegel RL, Laversanne M, Soerjomataram I, Jemal A, et al. Global cancer statistics 2020: GLOBOCAN estimates of incidence and mortality worldwide for 36 cancers in 185 countries. *CA Cancer J Clin*. (2021) 71:209–49. doi: 10.3322/caac.21660

30. Andrei P, Battuello P, Grasso G, Rovera E, Tesio N, Bardelli A. Integrated approaches for precision oncology in colorectal cancer: The more you know, the better. *Semin Cancer Biol*. (2022) 84:199–213. doi: 10.1016/j.semcancer.2021.04.007

31. Jun SY, Brown AJ, Chua NK, Yoon JY, Lee JJ, Yang JO, et al. Reduction of squalene epoxidase by cholesterol accumulation accelerates colorectal cancer progression and metastasis. *Gastroenterology*. (2021) 160:1194–1207.e28. doi: 10.1053/j.gastro.2020.09.009

32. Zhang KL, Zhu WW, Wang SH, Gao C, Pan JJ, Du ZG, et al. Organ-specific cholesterol metabolic aberration fuels liver metastasis of colorectal cancer. *Theranostics*. (2021) 11:6560–72. doi: 10.7150/thno.55609

33. Mao T, Qin F, Zhang M, Li J, Li J, Lai M. Elevated serum β-hydroxybutyrate, a circulating ketone metabolite, accelerates colorectal cancer proliferation and metastasis via ACAT1. *Oncogene*. (2023) 42:1889–99. doi: 10.1038/s41388-023-02700-y

34. Liu Z, Gomez CR, Espinoza I, Le TPT, Shenoy V, Zhou X. Correlation of cholesteryl ester metabolism to pathogenesis, progression and disparities in colorectal Cancer. *Lipids Health Dis*. (2022) 21:22. doi: 10.1186/s12944-022-01629-7

35. Chen X, Liang H, Song Q, Xu X, Cao D. Insulin promotes progression of colon cancer by upregulation of ACAT1. *Lipids Health Dis*. (2018) 17:122. doi: 10.1186/s12944-018-0773-x

36. Xu H, Xia H, Zhou S, Tang Q, Bi F. Cholesterol activates the Wnt/PCP-YAP signaling in SOAT1-targeted treatment of colon cancer. *Cell Death Discovery*. (2021) 7:38. doi: 10.1038/s41420-021-00421-3

37. Gilles H, Garbutt T, Landrum J. Hepatocellular carcinoma. *Crit Care Nurs Clin North Am*. (2022) 34:289–301. doi: 10.1016/j.cnc.2022.04.004

38. Peng K, Wang S, Liu R, Zhou L, Jeong GH, Jeong IH, et al. Effects of UBE3A on cell and liver metabolism through the ubiquitination of PDHA1 and ACAT1. *Biochemistry*. (2023) 62:1274–86. doi: 10.1021/acs.biochem.2c00624

39. Le Rhun E, Preusser M, Roth P, Reardon DA, van den Bent M, Wen P, et al. Molecular targeted therapy of glioblastoma. *Cancer Treat Rev*. (2019) 80:101896. doi: 10.1016/j.ctrv.2019.101896

40. Ou A, Yung WKA, Majd N. Molecular mechanisms of treatment resistance in glioblastoma. *Int J Mol Sci*. (2020) 22:351. doi: 10.3390/ijms22010351

41. Chi KC, Tsai WC, Wu CL, Lin TY, Hueng DY. An adult drosophila glioma model for studying pathometabolic pathways of gliomagenesis. *Mol Neurobiol*. (2019) 56:4589–99. doi: 10.1007/s12035-018-1392-2

42. Liu R, Zeng LW, Gong R, Yuan F, Shu HB, Li S. mTORC1 activity regulates post-translational modifications of glycine decarboxylase to modulate glycine metabolism and tumorigenesis. *Nat Commun*. (2021) 12:4227. doi: 10.1038/s41467-021-24321-3

43. Ohmoto T, Nishitsuji K, Yoshitani N, Mizuguchi M, Yanagisawa Y, Saito H, et al. K604, a specific acyl−CoA:cholesterol acyltransferase 1 inhibitor, suppresses proliferation of U251−MG glioblastoma cells. *Mol Med Rep*. (2015) 12:6037–42. doi: 10.3892/mmr.2015.4200

44. Bemlih S, Poirier MD, El Andaloussi A. Acyl-coenzyme A: cholesterol acyltransferase inhibitor Avasimibe affect survival and proliferation of glioma tumor cell lines. *Cancer Biol Ther*. (2010) 9:1025–32. doi: 10.4161/cbt.9.12.11875

45. Bade BC, Dela Cruz CS. Lung cancer 2020: epidemiology, etiology, and prevention. *Clin Chest Med*. (2020) 41:1–24. doi: 10.1016/j.ccm.2019.10.001

46. Fan J, Shan C, Kang HB, Elf S, Xie J, Tucker M, et al. Tyr phosphorylation of PDP1 toggles recruitment between ACAT1 and SIRT3 to regulate the pyruvate dehydrogenase complex. *Mol Cell*. (2014) 53:534–48. doi: 10.1016/j.molcel.2013.12.026

47. Li J, Li Y, Sun X, Wei L, Guan J, Fu L, et al. Silencing lncRNA-DARS-AS1 suppresses nonsmall cell lung cancer progression by stimulating miR-302a-3p to inhibit ACAT1 expression. *Mol Carcinog*. (2024) 63(4):757–71. doi: 10.1002/mc.23686

48. Pan J, Zhang Q, Palen K, Wang L, Qiao L, Johnson B, et al. Potentiation of Kras peptide cancer vaccine by avasimibe, a cholesterol modulator. *EBioMedicine*. (2019) 49:72–81. doi: 10.1016/j.ebiom.2019.10.044

49. Harbeck N, Gnant M. Breast cancer. *Lancet*. (2017) 389:1134–50. doi: 10.1016/S0140-6736(16)31891-8

50. Waks AG, Winer EP. Breast cancer treatment: A review. *JAMA*. (2019) 321:288–300. doi: 10.1001/jama.2018.19323

51. Antalis CJ, Uchida A, Buhman KK, Siddiqui RA. Migration of MDA-MB-231 breast cancer cells depends on the availability of exogenous lipids and cholesterol esterification. *Clin Exp Metastasis*. (2011) 28:733–41. doi: 10.1007/s10585-011-9405-9

52. Antalis CJ, Arnold T, Rasool T, Lee B, Buhman KK, Siddiqui RA. High ACAT1 expression in estrogen receptor negative basal-like breast cancer cells is associated with LDL-induced proliferation. *Breast Cancer Res Treat*. (2010) 122:661–70. doi: 10.1007/s10549-009-0594-8

53. Ozsvari B, Sotgia F, Simmons K, Trowbridge R, Foster R, Lisanti MP. Mitoketoscins: Novel mitochondrial inhibitors for targeting ketone metabolism in cancer stem cells (CSCs). *Oncotarget*. (2017) 8:78340–50. doi: 10.18632/oncotarget.21259

54. Zhang G, Huang R, Zhao H, Xia Y, Huang H, Qian M, et al. ACAT1-mediated METTL3 acetylation inhibits cell migration and invasion in triple negative breast cancer. *Genes Immun*. (2023) 24:99–107. doi: 10.1038/s41435-023-00202-1

55. Estey E, Döhner H. Acute myeloid leukaemia. *Lancet*. (2006) 368:1894–907. doi: 10.1016/S0140-6736(06)69780-8

56. Chen D, Xia S, Zhang R, Li Y, Famulare CA, Fan H, et al. Lysine acetylation restricts mutant IDH2 activity to optimize transformation in AML cells. *Mol Cell*. (2021) 81:3833–3847.e11. doi: 10.1016/j.molcel.2021.06.027

57. Bandyopadhyay S, Li J, Traer E, Tyner JW, Zhou A, Oh ST, et al. Cholesterol esterification inhibition and imatinib treatment synergistically inhibit growth of BCR-ABL mutation-independent resistant chronic myelogenous leukemia. *PloS One*. (2017) 12:e0179558. doi: 10.1371/journal.pone.0179558

58. Tu T, Zhang H, Xu H. Targeting sterol-O-acyltransferase 1 to disrupt cholesterol metabolism for cancer therapy. *Front Oncol*. (2023) 13:1197502. doi: 10.3389/fonc.2023.1197502

59. Lee SS, Li J, Tai JN, Ratliff TL, Park K, Cheng JX. Avasimibe encapsulated in human serum albumin blocks cholesterol esterification for selective cancer treatment. *ACS Nano*. (2015) 9:2420–32. doi: 10.1021/nn504025a

60. Lei J, Wang H, Zhu D, Wan Y, Yin L. Combined effects of avasimibe immunotherapy, doxorubicin chemotherapy, and metal-organic frameworks nanoparticles on breast cancer. *J Cell Physiol*. (2020) 235:4814–23. doi: 10.1002/jcp.29358

61. Guan C, Niu Y, Chen SC, Kang Y, Wu JX, Nishi K, et al. Structural insights into the inhibition mechanism of human sterol O-acyltransferase 1 by a competitive inhibitor. *Nat Commun*. (2020) 11:2478. doi: 10.1038/s41467-020-16288-4

62. Bhattacharjee P, Rutland N, Iyer MR. Targeting sterol O-Acyltransferase/Acyl-CoA:Cholesterol acyltransferase(ACAT): A perspective on small-molecule inhibitors and their therapeutic potential. *J Med Chem*. (2022) 65:16062–98. doi: 10.1021/acs.jmedchem.2c01265

frontiers | Frontiers in Oncology

TYPE Original Research
PUBLISHED 30 April 2024
DOI 10.3389/fonc.2024.1371309

OPEN ACCESS

EDITED BY
Parmanand Malvi,
University of Alabama at Birmingham,
United States

REVIEWED BY
Jia Li,
University of North Carolina at Charlotte,
United States
Zeliha Selamoglu,
Niğde Ömer Halisdemir University, Türkiye

*CORRESPONDENCE
Jianying Pei
peijianying1989@163.com

†These authors have contributed equally to this work

RECEIVED 16 January 2024
ACCEPTED 10 April 2024
PUBLISHED 30 April 2024

CITATION
Li Y, Liu J, Wang Q, Zhou Y, Zhang C and Pei J (2024) The causal effects of genetically determined immune cells on gynecologic malignancies: a Mendelian randomization study. *Front. Oncol.* 14:1371309. doi: 10.3389/fonc.2024.1371309

The causal effects of genetically determined immune cells on gynecologic malignancies: a Mendelian randomization study

Yan Li[1†], Jingting Liu[2†], Qiandan Wang[2], Yawei Zhou[2], Chunhua Zhang[2] and Jianying Pei[2*]

[1]Department of Biochemistry and Molecular Biology, Medical College of Northwest Minzu University, Lanzhou, China, [2]Maternal and Child Health Care Research Center, Gansu Provincial Maternity and Child Care Hospital, Lanzhou, China

Background: Evidence from observational studies suggested a connection between immune cells and gynecologic malignancies. To investigate potential causative associations between immunophenotype traits and gynecologic malignancies, we used a two-sample Mendelian randomization analysis.

Methods: The genetic instrumental variables of 731 immunophenotypes of peripheral blood were obtained by the GWAS database; the GWAS data of common gynecologic cancers were obtained from FinnGen study. The main statistic method was the inverse-variance weighted method. We also used the weighted mode, weighted median, and MR Egger for evaluations. The MR Steiger directionality test was further used to ascertain the reverse causal relationship between immune cells and gynecologic cancers.

Results: We identified 50 highly probable immunophenotypes and 65 possible ones associated with gynecologic malignancies. The majority of the B cell panel was protective factors in cervical cancer. However, there was a correlation found in the B cells panel with a probable factor associated with an elevated risk of endometrial cancer. Immunophenotypes in the monocyte panel were linked to a lower probability of ovarian cancer and vulvar cancer. All of the gynecologic cancers in our study had no statistically significant impact on immune cells, according to reverse MR analysis.

Conclusion: Our study firstly emphasized the genetically predicted causality between immune cells and gynecologic malignancies. This knowledge will be critical to formulating the measures to prevent malignancies in female at risk in future clinical practice.

KEYWORDS

gynecologic malignancies, immunophenotype, Mendelian randomization, causality, immune system

1 Introduction

Gynecological malignancies (including cervical cancer, endometrial cancer, ovarian cancer and vulvar cancer) are estimated with 1,353,361 new cases, account for 7% of total new case, and 654,448 cancer deaths (6.6%) globally by the 2020 GLOBOCAN Statistic (1). Of them, ovarian cancer is one of the deadliest gynecological malignancies that affect women (2), and cervical cancer makes up the greatest fraction with an incidence rate of 3.1%. Furthermore, the burden could be made worse by the world's population expansion and the increasing prevalence of risk factors (3). It highlighted how urgently effective preventative measures must be developed in order reduce the burden of gynecological cancer on the general public's health. As a consequence, a lot of work needs to be done to cultivate novel interventions in order to find new cases and raise patient survival rates.

Tumor metabolism involves multiple metabolic pathways, and cancer is a complex pathological disease with an abnormal metabolic profile. Cancer cells have a different metabolic profile due to changes in these signal transduction pathways and the enzymatic machinery that goes along with them (4, 5). Surgery, radiation, and chemotherapy are the primary methods used for the treatment in cancer. Recently, however, targeted treatment and immunotherapy have all become significant tools in the battle anti-cancer. Recent research has gradually demonstrated that immune cells in the tumor microenvironment (TME) predict overall survival and play a substantial part in the progression of gynecologic malignancies (6, 7). Since cervical cancer is brought on by a chronic human papillomavirus (HPV) infection, it has been referred to as an immunogenic tumor. Myeloid-derived suppressor cells (MDSCs) created a premetastatic microenvironment in cervical cancer by expressing high levels of Cxcl2, S100a8/9, Bv8, and MMP-9. This niche promotes visceral organ metastasis (8). Tumor-infiltrating MDSCs and arginase-1 expression were also elevated in endometrial cancer (9). According to a study, activated memory $CD4^+$ T cells and mast cells were independent predictors of overall survival for patients with cervical cancer. The majority of tumor-infiltrating immune cells (TICs) in cervical cancer were found to be $CD8^+$ T cells and macrophages (10). According to a retrospective study, higher expression of Treg, M2 macrophages, and CD4 naïve T cells during immunotherapy was found to be predictive of worse overall survivals by Ni Y and colleagues. They also discussed the role of M2 macrophages, T-regulatory cells, and eosinophils, which are known to produce TGF-β in the TME (11). In a recent study, patients with cervical cancer who had higher levels of infiltration of naïve $CD4^+$ T cells had a worse prognosis, but higher levels of M0 macrophage infiltration was associated with tumor stage and a better prognosis. The correlation between M0 macrophages and naïve $CD4^+$ T cells was also confirmed by the results (12). Higher $CD4^+$ ($p = 0.0028$) and $CD45^+$ ($p = 0.0221$) infiltration was associated with a longer overall survival for patients with ovarian cancer, based on an observational study (13). However, most of the results mentioned above were obtained from observational or retrospective research, which might be constrained by the small sample size and heterogeneous patient organization. They had merely noted the connections between various immune cells and gynecologic cancers; it is unclear whether these relationships are causative. Owing to confounding factors and limited sample size, the results may be biased. Furthermore, the existing studies did not comprehensively investigate the associations between gynecologic malignancies and immunophenotype traits.

Mendelian randomization (MR), a statistical technique that has gained broad popularity, assesses the causal relationship between exposure and outcome by using genetic variants as instrumental variables (IVs) (14, 15). The MR analysis might not be affected by reverse causality and confounders because genetic variants are randomly distributed at conception (16).

Many MR studies that have been undertaken recently with a focus on gynecologic malignancies have emphasized the relationship between the risk of gynecologic cancers and lifestyle habits (e.g. coffee consumption (17), smoking (18, 19), alcohol consumption (18, 19), obesity (20), vitamin D (21)). Inspired by MR analysis's non-confounding character, this study conducted the first thorough two-sample Mendelian randomization analysis to evaluate the causal relationships between immunophenotype traits and gynecologic cancers. Our findings may influence clinical practice, offer relevant risk factors and preventative hints. Our study aims to assist clinicians in identifying people who are very susceptible to gynecologic cancers, enabling more frequent follow-up and timely intervention.

2 Materials and methods

2.1 Study design

Figure 1 displayed the overview of the study design. In this study we performed a Mendelian randomization (MR) analysis to assess the causal relationship between 731 immunophenotypes and gynecologic malignancies. Three important assumptions must be met when choosing instrumental variables (IVs) (Figure 1A): Three requirements must be met for the genetic variations to be considered as IVs: (1) they must be strongly correlated with the exposure; (2) they cannot be linked to any confounders; and (3) the variants chosen should only influence the risk of the outcome by the risk factor independently not through other pathways (22).

2.2 Exposure and outcome data sources

The 731 immunophenotypes of peripheral blood were published by the genome wide association studies (GWAS) and are accessible to the general public through the GWAS database (GCST90001391-GCST90002121) (23). The original GWAS on immunophenotypes used information from 3,757 European individuals. It contains 4 trait types,7 panels, and 731 traits. Supplementary Table 1 provided an immunophenotype characterization. We selected four most common gynecologic malignancies including cervical cancer, ovarian cancer, endometrial cancer, and vulvar cancer as outcome. To obtain a more comprehensive conclusion of the causal links, we also took the

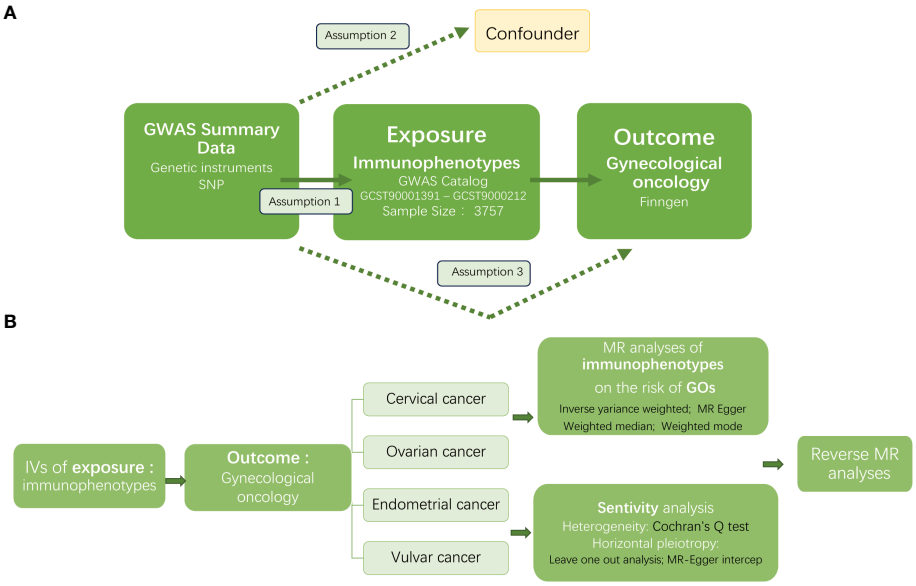

FIGURE 1
The workflow of this study design. GWAS, the genome wide association studies; SNPs, single-nucleotide polymorphisms; IVs, instrumental variables; GO, gynecologic oncology; MR, Mendelian randomization.

carcinoma *in situ* into consideration. The GWAS summary data of the gynecologic cancer were accessed from the FinnGen study (24) (https://www.finngen.fi/en). Table 1 presented the detailed information of datasets used in this study. The analysis was based on summary-level data from large genome wide association studies that were made available in public. Therefore, ethical approval was not needed.

2.3 Instrumental variable selection

The IVs that met the strict significance threshold ($P < 1 \times 10^{-8}$) were chosen. SNPs with linkage disequilibrium were excluded concurrently ($r^2 > 0.001$, window size < 10,000 kb). In order to minimize the bias caused by weak IVs, SNPs with F-statistics < 10 were also eliminated. Next, we looked through and eliminated SNPs corresponding to confounders via the PhenoScanner website (25). The confounders included (age at menarche (26), trunk fat mass, body mass index (27), obesity, treatment with ovestin 0.1% vaginal cream, and treatment with estrogen product). Finally, 251independent SNPs were obtained as IVs for immunophenotypes.

2.4 Statistical analysis

In measuring the causal relationships between immunophenotypes and gynecologic malignancies, four MR methods (inverse variance weighted (IVW) (28), MR Egger (29), Weighted median (30), and Weighted mode) were utilized, including. The primary analysis was the IVW. The Benjamini-Hochberg, which regulates the false discovery rate (FDR), was used to modify multiple testing. The heterogeneity was evaluated using the Cochran's Q test. MR-Egger intercept and leave one out analysis were used to determine horizontal pleiotropy. Immunophenotypes with adj.P value <0.05 were deemed to have a highly probable relationship with gynecologic malignancies(statistically significant), while those that displayed P value <0.05 after MR analyzes, but 0.05< adj.P value <0.2 were considered possible factors. After excluding IVs that exhibited pleiotropic effects, we performed the primary MR analysis once more. To investigate if exposure was directionally causal for the outcome, we applied the MR Steiger directionality test (31). All analyses were carried out in R software 4.3.1 utilizing the "Two Sample MR" and "Mendelian Randomization" packages.

3 Results

3.1 Overview

For an insight into the relationship between immunophenotypes and four gynecologic cancers, we applied a tow-sample MR analysis. This study identified 252 independent SNPs linked to immunophenotypes (Supplementary Table 2). By applying IVW methods, there were 50 highly probable immunophenotype traits (adj.P value <0.05, Tables 2, 3, Supplementary Table 5) and 65 possible immunophenotypes (P value <0.05, 0.05< adj.P value <0.2, Supplementary Tables 4, 5) linked with gynecologic malignancies. When the highly probable immunophenotypes were classified in 7 panels (B cell, cDC, maturation stages of T cell, monocyte, myeloid cell, TBNK, Treg), 19 traits belonged to B cell, 8 from TBNK, 6 from cDC, monocyte, and maturation stages of T cell respectively, 4 from myeloid cell, and 2 from Treg. Sensitivity studies were performed to guarantee the robustness of the causal associations because IVW approaches are prone to weak IVs bias.

TABLE 1 The GWAS datasets used for analyses.

Trait/Disease		Data Type	Consortium	Sample Size	Case	Control	GWAS_ID	Population
Immunophenotypes		Exposure	GWAS Catalog	3757	-	-	GCST90001391 - GCST9000212	European
Cervical cancer	Adenocarcinomas of cervix	Outcome	Finngen	167301	112	167189	finngen_R9_C3_CERVIX_ADENO_EXALLC	European
	Squamous cell neoplasms and carcinoma of cervix	Outcome	Finngen	167353	164	167189	finngen_R9_C3_CERVIX_SQUAM_EXALLC	European
	Malignant neoplasm of cervix uteri	Outcome	Finngen	167558	369	167189	finngen_R9_C3_CERVIX_UTERI_EXALLC	European
Endometrial cancer	Malignant neoplasm of corpus uteri	Outcome	Finngen	169156	1967	167189	finngen_R9_C3_CORPUS_UTERI_EXALLC	European
	Endometroid carcinoma of ovary	Outcome	Finngen	167411	222	167189	finngen_R9_C3_OVARY_ENDOMETROID_EXALLC	European
Ovarian cancer	Malignant neoplasm of ovary	Outcome	Finngen	168214	1025	167189	finngen_R9_C3_OVARY_EXALLC	European
	Serous carcinoma of ovary	Outcome	Finngen	168041	852	167189	finngen_R9_C3_OVARY_SEROUS_EXALLC	European
Vulvar cancer	Malignant neoplasm of vulva	Outcome	Finngen	167379	190	167189	finngen_R9_C3_VULVA_EXALLC	European
Carcinoma in situ	Carcinoma in situ of cervix uteri	Outcome	Finngen	167637	2236	165401	finngen_R9_CD2_INSITU_CERVIX_UTERI_EXALLC	European
	Carcinoma in situ of endometrium	Outcome	Finngen	167267	106	167161	finngen_R9_CD2_INSITU_ENDOMETRIUM_EXALLC	European
	Carcinoma in situ of vulva	Outcome	Finngen	167252	155	167097	finngen_R9_CD2_INSITU_VULVA_EXALLC	European

10.3389/fonc.2024.1371309

3.2 Cervical cancer

Table 2 and Figure 8 demonstrated that 32 pairs had highly probable causal effects (adj.P <0.05) between immunophenotypes and cervical cancer. The causal effect of immunophenotypes on adenocarcinomas of cervix was shown in Figure 2A. The B-cell panel showed the highest number of significant associations when compared to other panels, and the majority of B cells were protective factors against cervical cancer. In the study we conducted, B-cell activating factor receptor (BAFF-R) was the most frequently expressed molecule in our analysis. It expresses on several B cell subtypes, such as $CD24^+$ $CD27^+$ B cell, IgD^+ $CD24^+$ B cell, IgD^+ CD24- B cell, IgD^+ $CD38^-$ B cell, memory B cell, and naive-mature B cell. However, CD20 on IgD+ CD38+ B cell (OR=1.887, 95%CI:1.078-3.306, P=0.026) had a significant association with the probability of cervical cancer (Table 2, Figure 2B). In cDC panels, CD123 on plasmacytoid Dendritic Cell (OR=2.48, 95%CI:1.229-5.003, P=0.011), CD123 on $CD62L^+$ plasmacytoid Dendritic Cell (OR=2.5, 95%CI:1.231-5.077, P=0.011), CD80 on plasmacytoid Dendritic Cell (OR=2.62, 95% CI:1.244-5.515, P=0.011), CD80 on $CD62L^+$ plasmacytoid Dendritic Cell (OR=2.641, 95%CI:1.246-5.596, P=0.011) had a disadvantageous association with cervical cancer(Table 2, Figure 2B). The causal effect of immunophenotypes on Malignant neoplasm of cervix uteri was shown in Figure 3.

3.3 Endometrial cancer

No immunophenotype was found at the criterion "adj.P value <0.05" after FDR correction. Nevertheless, 18 immunophenotypes that fit the requirements of P value <0.05 and 0.05< adj.P value <0.2 are possible factors in our study (Figures 4, 9). B cells were also vital in endometrial cancer, similarly to how they were in cervical cancer. But all possible factors in B cell panel, namely, CD38 on IgD^+ $CD24^-$ B cell (OR=1.286, 95%CI; 1.038-1.594, P=0.021), IgD on IgD^+ CD24- B cell (OR=1.09, 95%CI; 1-1.188, P=0.049), IgD on IgD^+ CD38dim B cell (OR=1.096, 95%CI; 1.001-1.199, P=0.046), BAFF-R on IgD^+ $CD24^+$ B cell (OR=1.219, 95%CI; 1.003-1.483, P=0.047), BAFF-R on IgD- CD24- B cell (OR=1.249, 95%CI; 1.019-1.532, P=0.032), BAFF-R on IgD^- $CD27^-$ B cell (OR=1.249, 95%CI; 1.02-1.529, P=0.032), BAFF-R on IgD- $CD38^+$ B cell (OR=1.915, 95%CI; 1.12-3.273, P=0.018) were correlated with increased risk of

TABLE 2 The highly probable effects of immunophenotypes on cervical cancer by IVW method.

Outcome	Exposure	SNP(n)	OR (95%CI)	P value	adj.P value
Malignant neoplasm of cervix uteri	Terminally Differentiated CD4-CD8- T cell Absolute Count	2	5.989 (2.51, 14.29)	5.470E-05	0.002
	FSC-A on Natural Killer T	2	0.235 (0.095, 0.584)	0.002	0.027
Squamous cell neoplasms and carcinoma of cervix	Effector Memory CD4+ T cell %CD4+ T cell	3	2.131 (1.114, 4.077)	0.022	0.046
	Effector Memory CD4-CD8- T cell % T cell	3	0.378 (0.163, 0.879)	0.024	0.046
	Terminally Differentiated CD4-CD8- T cell Absolute Count	2	8.017 (2.232, 28.798)	0.001	0.021
	BAFF-R on CD24+ CD27+ B cell	8	0.745 (0.581, 0.953)	0.019	0.045
	BAFF-R on IgD+ CD24+ B cell	6	0.745 (0.613, 0.905)	0.003	0.021
	BAFF-R on IgD+ CD24- B cell	10	0.769 (0.641, 0.923)	0.005	0.021
	BAFF-R on IgD+ CD38- B cell	9	0.755 (0.626, 0.909)	0.003	0.021
	BAFF-R on IgD+ CD38- naive B cell	8	0.768 (0.64, 0.92)	0.004	0.021
	BAFF-R on IgD+ CD38+ B cell	10	0.761 (0.629, 0.92)	0.005	0.021
	BAFF-R on IgD+ CD38dim B cell	10	0.763 (0.636, 0.915)	0.004	0.021
	BAFF-R on IgD- CD38- B cell	7	0.758 (0.594, 0.966)	0.025	0.047
	BAFF-R on memory B cell	7	0.734 (0.595, 0.904)	0.004	0.021
	BAFF-R on naive-mature B cell	10	0.762 (0.634, 0.916)	0.004	0.021
	BAFF-R on unswitched memory B cell	7	0.733 (0.596, 0.902)	0.003	0.021
	BAFF-R on switched memory B cell	9	0.749 (0.591, 0.95)	0.017	0.045
	BAFF-R on IgD+ B cell	10	0.764 (0.636, 0.917)	0.004	0.021
	BAFF-R on transitional B cell	8	0.749 (0.612, 0.916)	0.005	0.021

(Continued)

TABLE 2 Continued

Outcome	Exposure	SNP(n)	OR (95%CI)	P value	adj.P value
	CD19 on CD24+ CD27+ B cell	2	0.577 (0.369, 0.902)	0.016	0.045
	CD19 on memory B cell	2	0.538 (0.325, 0.89)	0.016	0.045
	CD20 on IgD+ CD38+ B cell	5	1.887 (1.078, 3.306)	0.026	0.047
	BAFF-R on B cell	10	0.768 (0.638, 0.923)	0.005	0.021
	CD3 on HLA DR+ CD4+ T cell	2	1.843 (1.085, 3.131)	0.024	0.046
	CD3 on activated CD4 regulatory T cell	4	1.465 (1.05, 2.043)	0.024	0.046
	CD3 on activated & secreting CD4 regulatory T cell	4	1.457 (1.05, 2.023)	0.024	0.046
	CD123 on plasmacytoid Dendritic Cell	2	2.48 (1.229, 5.003)	0.011	0.039
	CD123 on CD62L+ plasmacytoid Dendritic Cell	2	2.5 (1.231, 5.077)	0.011	0.039
	CD80 on plasmacytoid Dendritic Cell	2	2.62 (1.244, 5.515)	0.011	0.039
	CD80 on CD62L+ plasmacytoid Dendritic Cell	2	2.641 (1.246, 5.596)	0.011	0.039
	SSC-A on plasmacytoid Dendritic Cell	5	2.508 (1.243, 5.059)	0.010	0.039
	HLA DR on B cell	8	0.674 (0.499, 0.909)	0.010	0.039

TABLE 3 The highly probable effects of immunophenotypes on ovarian and vulvar cancer by IVW method.

Outcome	Exposure	SNP(n)	OR (95%CI)	P value	adj.P value
Malignant neoplasm of ovary	HLA DR++ monocyte %leukocyte	2	0.648 (0.5, 0.84)	0.001	0.011
	Monocytic Myeloid-Derived Suppressor Cells Absolute Count	5	1.205 (1.067, 1.361)	0.003	0.018
	CD45 on B cell	2	1.855 (1.146, 3.001)	0.012	0.046
	HLA DR on CD14+ CD16- monocyte	5	0.823 (0.74, 0.916)	3.381E-04	0.006
	HLA DR on CD14+ monocyte	5	0.819 (0.734, 0.913)	3.365E-04	0.006
	HLA DR on monocyte	4	0.824 (0.73, 0.93)	0.002	0.016
	HLA DR on myeloid Dendritic Cell	6	0.862 (0.77, 0.964)	0.009	0.042
	HLA DR on CD33+ HLA DR + CD14dim	3	0.769 (0.646, 0.915)	0.003	0.019
	HLA DR on CD33- HLA DR+	2	0.855 (0.76, 0.962)	0.009	0.042
	HLA DR++ monocyte %leukocyte	2	0.443 (0.248, 0.793)	0.006	0.036
	Terminally Differentiated CD4+ T cell Absolute Count	2	3.135 (1.247, 7.883)	0.015	0.043
	CD20 on IgD+ CD24+ B cell	2	0.326 (0.139, 0.765)	0.010	0.037
	CD4 on HLA DR+ CD4+ T cell	2	0.239 (0.099, 0.579)	0.002	0.029
	HLA DR on CD14+ CD16- monocyte	5	0.69 (0.543, 0.876)	0.002	0.029
	HLA DR on CD14+ monocyte	5	0.682 (0.533, 0.873)	0.002	0.029
	HLA DR on monocyte	4	0.706 (0.537, 0.928)	0.013	0.039
	HLA DR on CD33+ HLA DR+ CD14-	2	0.642 (0.466, 0.884)	0.007	0.036

(Continued)

TABLE 3 Continued

Outcome	Exposure	SNP(n)	OR (95%CI)	P value	adj.P value
	HLA DR on B cell	9	1.391 (1.115, 1.736)	0.003	0.032
Carcinoma in situ of vulva	Terminally Differentiated CD4-CD8- T cell Absolute Count	2	8.095 (2.206, 29.699)	0.002	0.039

endometrial cancer. In other panels, $CD25^{++}$ $CD45RA^{+}CD4^{+}$ T cell, $CD28^{-}$ $CD8^{+}$ T cell, CCR7 on naive $CD8^{+}$ T cell, myeloid Dendritic Cell, Natural Killer cell, Basophil cell had positive links with endometrial cancer. However, CD62L on $CD62L^{+}$ plasmacytoid Dendritic Cell (OR=0.831, 95%CI; 0.699-0.989, P=0.037) and $CD14^{-}$ $CD16^{+}$ monocyte %monocyte (OR=0.465, 95%CI; 0.227-0.953, P=0.036) were negatively associated with the risk of endometrial cancer.

3.4 Ovarian cancer

We noticed 9 highly probable immunophenotype traits were connected to ovarian cancer in IVW test (Figure 8, Table 3). In the Monocyte panel, reduction in the risk of ovarian cancer was associated with HLA DR on $CD14^{+}$ CD16- monocyte (OR=0.823, 95%CI:0.74-0.916, P=3.381E-04), HLA DR on $CD14^{+}$ monocyte (OR=0.819, 95%CI:0.734-0.913, P=3.365E-04), and HLA DR on

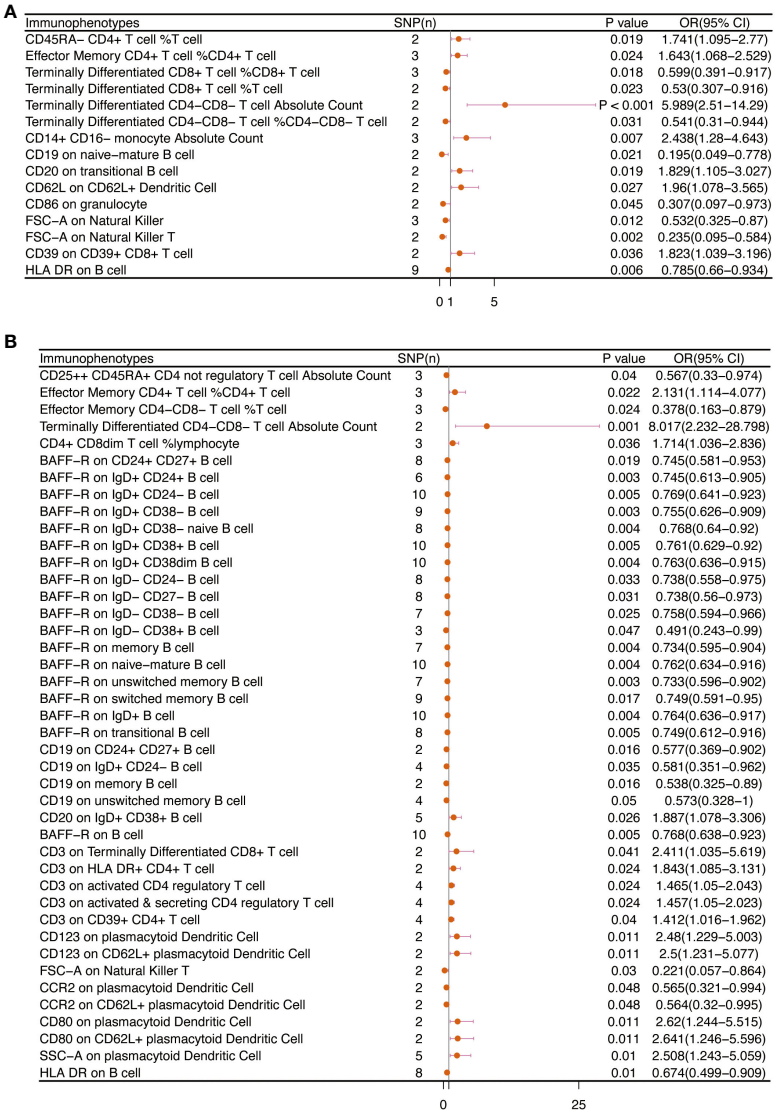

FIGURE 2
The causal effect of immunophenotypes on cervical cancer. **(A)** Adenocarcinomas of cervix; **(B)** Squamous cell neoplasms and carcinoma of cervix; SNP(n), the number of single-nucleotide polymorphisms; OR, odds ratio; CI, confidence interval.

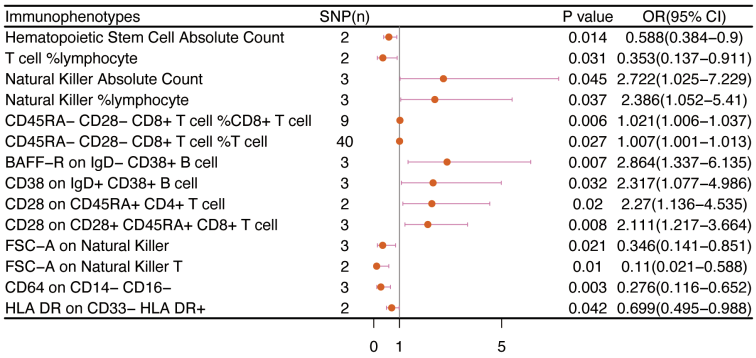

FIGURE 3
The causal effect of immunophenotypes on cervical cancer (Malignant neoplasm of cervix uteri). SNP(n), the number of single-nucleotide polymorphisms; OR, odds ratio; CI, confidence interval.

monocyte (OR=0.824, 95%CI:0.73-0.93, P=0.002). However, immune cells of different traits had opposing effects on ovarian cancer in TBNK and Myeloid cell panels. HLA DR^{++} monocyte, HLA DR on $CD33^{+}$ HLA DR^{+} CD14dim, and HLA DR on $CD33^{-}$ HLA DR^{+} exhibited favorable effects. On the other hand, Monocytic Myeloid-Derived Suppressor Cells and CD45 on B cell were positively associated with the increasing risk of ovarian cancer. The causal effect of immunophenotypes on ovarian cancer was shown in Figure 5.

3.5 Vulvar cancer

The IVW analysis indicated that 9 highly probable immunophenotype traits had causal relationship with vulvar cancer (Figure 8, Table 3). Terminally Differentiated $CD4^{+}$ T cell Absolute Count (OR=3.135, 95%CI:1.247-7.883, P=0.015) and HLA DR on B cell (OR=1.391, 95%CI:1.115-1.736, P=0.003) were correlated with increased vulvar cancer risk. Whereas HLA DR^{++} monocyte %leukocyte (OR=0.443, 95%CI:0.248-0.793, P=0.006), CD20 on IgD^{+} $CD24^{+}$ B cell (OR=0.326, 95%CI:0.139-0.765, P=0.010), CD4 on HLA DR^{+} $CD4^{+}$ T cell (OR=0.239, 95% CI:0.099-0.579, P=0.002), HLA DR on $CD14^{+}$ $CD16^{-}$ monocyte (OR=0.69, 95%CI:0.543-0.876, P=0.002), HLA DR on $CD14^{+}$ monocyte (OR=0.682, 95%CI:0.533-0.873, P=0.002), HLA DR on monocyte (OR=0.706, 95%CI:0.537-0.928, P=0.013), HLA DR on $CD33^{+}$ HLA DR^{+} $CD14^{-}$ (OR=0.642, 95%CI:0.466-0.884, P=0.007) were related to a reduced risk of vulvar cancer. In addition, we also screened 5 possible immunophenotypes for vulvar cancer. Figure 6 and Supplementary Table 3 presented the detailed data.

3.6 Gynecologic carcinoma *in situ*

There are 65 possible immunophenotypes for gynecologic cancer *in situ*, but we found only one highly probable immunophenotype trait after FDR correction. There are 65 possible immunophenotypes

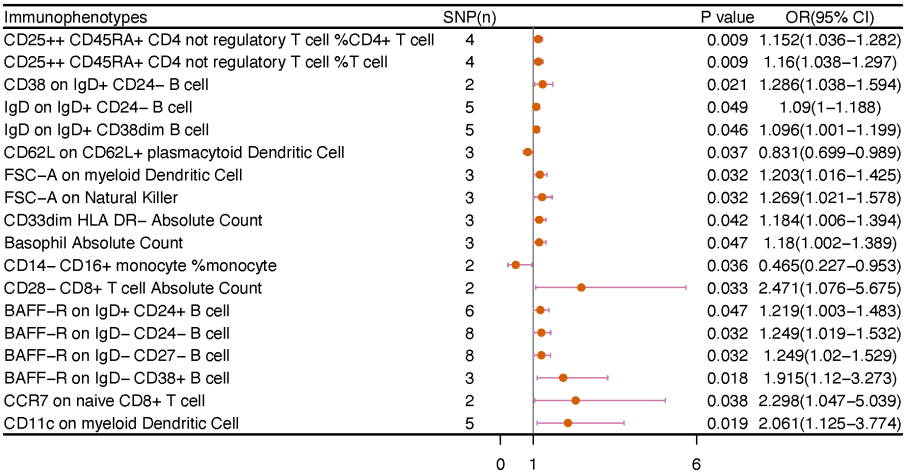

FIGURE 4
The causal effect of immunophenotypes on endometrial cancer. SNP(n), the number of single-nucleotide polymorphisms; OR, odds ratio; CI, confidence interval.

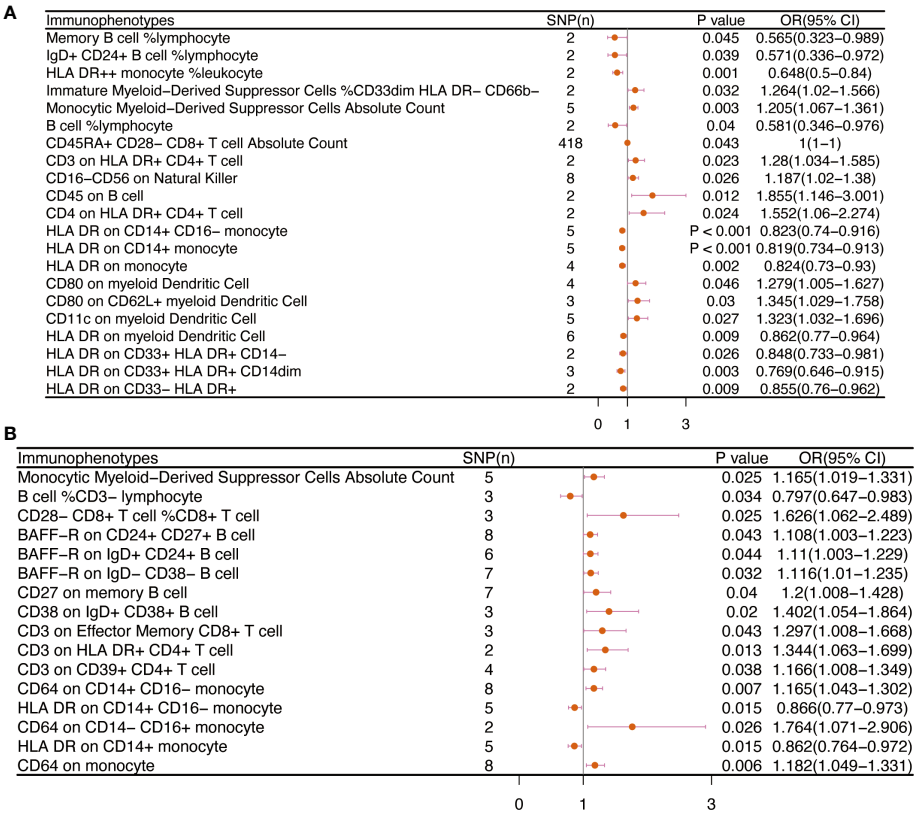

FIGURE 5
The causal effect of immunophenotypes on ovarian cancer. **(A)** Malignant neoplasm of ovary; **(B)** Serous carcinoma of ovary; SNP(n), the number of single-nucleotide polymorphisms; OR, odds ratio; CI, confidence interval.

for gynecologic cancer in situ, but we found only one highly probable immunophenotype trait after FDR correction (Figure 10). Terminally Differentiated $CD4^{-}CD8^{-}$ T cell (OR=8.095, 95CI%: 2.206-29.699, adj.P= 0.039) was significantly positive link with carcinoma *in situ* of vulva risk.

In carcinoma *in situ* of cervix uteri, 26 causative links between the immune cells and cervical carcinoma *in situ* have been identified (Figure 7A, Supplementary Table 5). Compared to other panels, TBNK had the greatest number of possible associations. CD8dim T cell was linked in a higher incidence of cervical carcinoma *in situ*, but NKT cell, HLA DR^{+} $CD4^{+}$ T cell, and HLA DR^{+} NK cell were protective immune factors. Treg cells also play an important role. $CD39^{+}$ $CD8^{+}$ T cell %$CD8^{+}$ T cell (OR=1.14, 95%CI:1.012-1.284, P=0.032), CD3 on activated CD4 regulatory T cell (OR=1.103, 95% CI:1.007-1.208, P=0.035), CD3 on activated & secreting CD4 regulatory T cell (OR=1.1, 95%CI:1.006-1.204, P=0.036), CD3 on $CD39^{+}$ $CD4^{+}$ T cell (OR=1.112, 95%CI:1.016-1.216, P=0.021) were linked in a higher incidence of cervical carcinoma *in situ*.

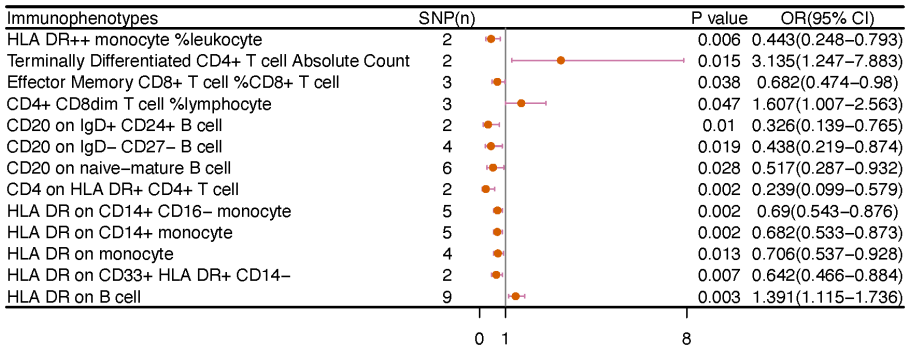

FIGURE 6
The causal effect of immunophenotypes on vulvar cancer. SNP(n), the number of single-nucleotide polymorphisms; OR, odds ratio; CI, confidence interval.

10.3389/fonc.2024.1371309

Endometrial carcinoma *in situ* was revealed to be causally related to 28 possible immunophenotypes (Figure 7B, Supplementary Table 5). The Treg panel's characteristics were still prominent in endometrial cancer *in situ*, similar to carcinoma *in situ* of the cervix uteri.CD3 on T cell (OR=0.463, 95%CI:0.26-0.827, P=0.009), CD3 on activated CD4 regulatory T cell (OR=0.576, 95%CI:0.377-0.882, P=0.011), CD3 on $CD39^+$ activated CD4 regulatory T cell (OR=0.538, 95%CI:0.347-0.835, P=0.006), CD3 on activated & secreting CD4 regulatory T cell (OR=0.582, 95%CI:0.382-0.884, P=0.011), CD3 on $CD39^+$ $CD4^+$ T cell (OR=0.598, 95%CI:0.394-0.909, P=0.016), CD3 on $CD28^+$ $CD4^+$ T cell (OR=0.482, 95%CI:0.276-0.842, P=0.01), CD3 on $CD28^+$ $CD45RA^-$ $CD8^+$ T cell (OR=0.416, 95%CI:0.215-0.804, P=0.009), and CD8 on $CD28^+$ $CD45RA^+$ $CD8^+$ T cell (OR=0.621, 95%CI:0.415-0.931, P=0.021) were inversely correlated with the incidence of endometrium carcinoma *in situ*. In Myeloid cell panel, CD45 on Immature Myeloid-Derived Suppressor Cells (OR=1.65, 95%CI:1.016-2.679, P=0.043) was linked in a higher incidence risk, while $CD33^+$ HLA DR^+ CD14dim, Granulocytic Myeloid-Derived Suppressor Cells, CD33 on $CD14^+$ monocyte, CD33 on $CD33^{dim}$ HLA DR^+ $CD11b^+$, CD33 on CD33dim HLA DR^+ $CD11b^-$, and CD33 on basophil were protective factors for carcinoma *in situ* of endometrium. We also found that there were causal links between B cells, T cell and cDC.

In carcinoma *in situ* of vulva, we identified 11 possible immunophenotypes (Figure 7C, Supplementary Table 5). HLA DR^{++} monocyte, CD20 on IgD^+ $CD24^+$ B cell, CD4 on HLA DR^+ $CD4^+$ T cell, HLA DR on $CD14^+$ $CD16^-$ monocyte, HLA DR on

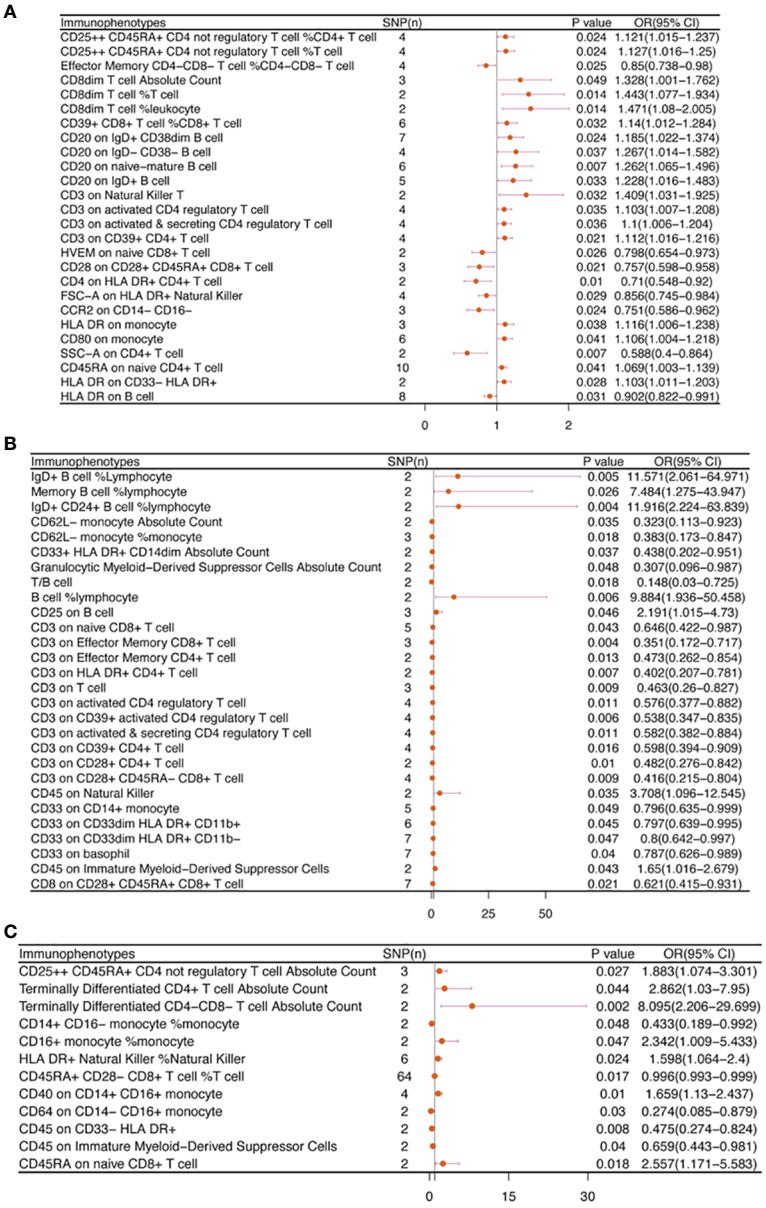

FIGURE 7
The causal effect of immunophenotypes on gynecologic carcinoma *in situ*. **(A)** Carcinoma *in situ* of cervix uteri; **(B)** Carcinoma *in situ* of endometrium; **(C)** Carcinoma *in situ* of vulva; SNP(n), the number of single-nucleotide polymorphisms; OR, odds ratio; CI, confidence interval.

10.3389/fonc.2024.1371309

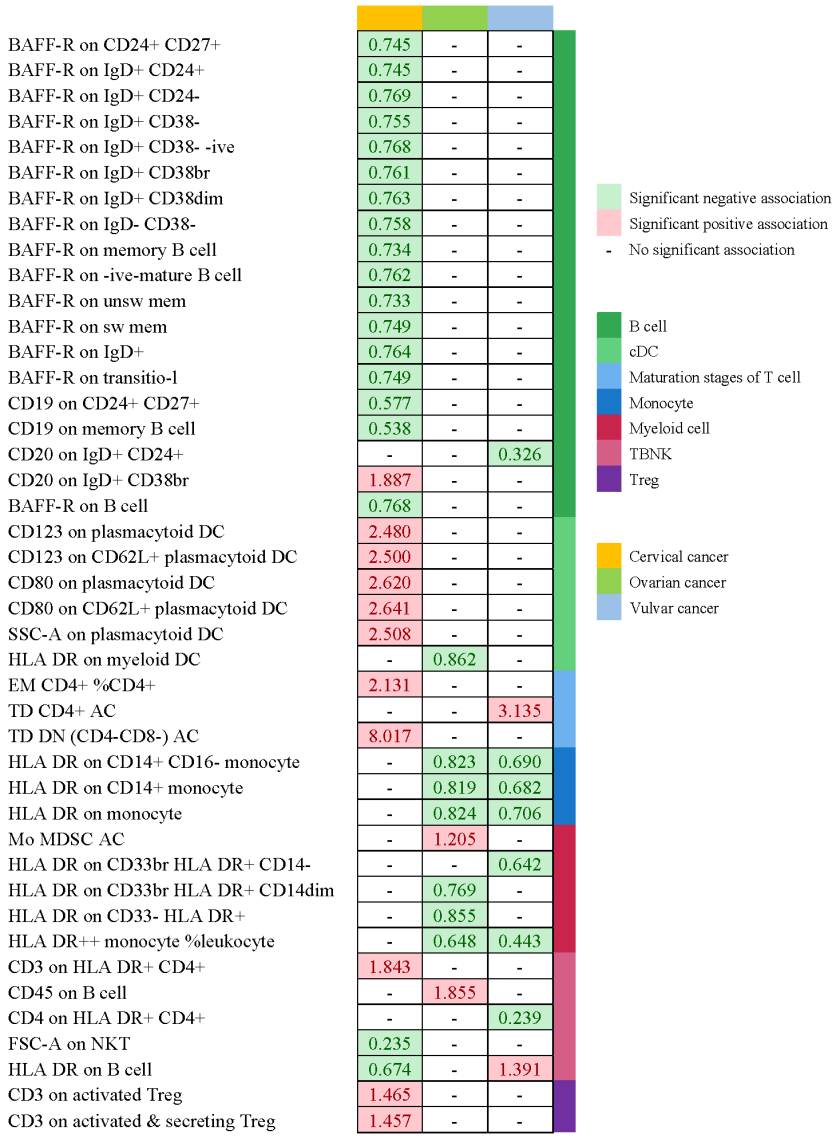

FIGURE 8
Summary of associations of genetically predicted immunophenotype traits with cervical cancer, ovarian cancer and vulvar cancer.

$CD14^+$ monocyte, HLA DR on monocyte, and HLA DR on $CD33^+$ HLA DR^+ $CD14^-$ had a negative association with vulvar carcinoma *in situ*. The following factors might raise the incidence of vulvar cancer *in situ*: $CD25^{++}$ $CD45RA^+$ CD4 not regulatory T cell, Terminally Differentiated $CD4^+$ T cell, $CD16^+$ monocyte, HLA DR^+ Natural Killer cell, CD40 on $CD14^+$ $CD16^+$ monocyte, and CD45RA on naive $CD8^+$ T cell.

3.7 Sensitivity analysis

Sensitivity analysis was performed to ensure the robustness of the causal evaluation because IVW methods are prone to weak instrumental bias. The highly probable or possible immunophenotypes showed no evidence of horizontal pleiotropy when examined using the MR-Egger intercept method (all $P > 0.05$). Cochran's Q statistic test did not reveal any evidence of heterogeneity (all $P > 0.05$). The MR Steiger directionality test additionally demonstrated the causative links between immune cells and gynecologic malignancies. In our results, reverse causality was not observed. (Supplementary Tables 7).

4 Discussion

The three most prevalent types of gynecological malignancies are cervical cancer, endometrial cancer, and ovarian cancer (1). Besides endangering a woman's ability to conceive, the gynecological cancers can be fatal in their advanced stages. In addition, female patients will suffer serious psychological harm as a result of the lesion's location. More research is showing that immunological imbalance is necessary for cancer developing, but

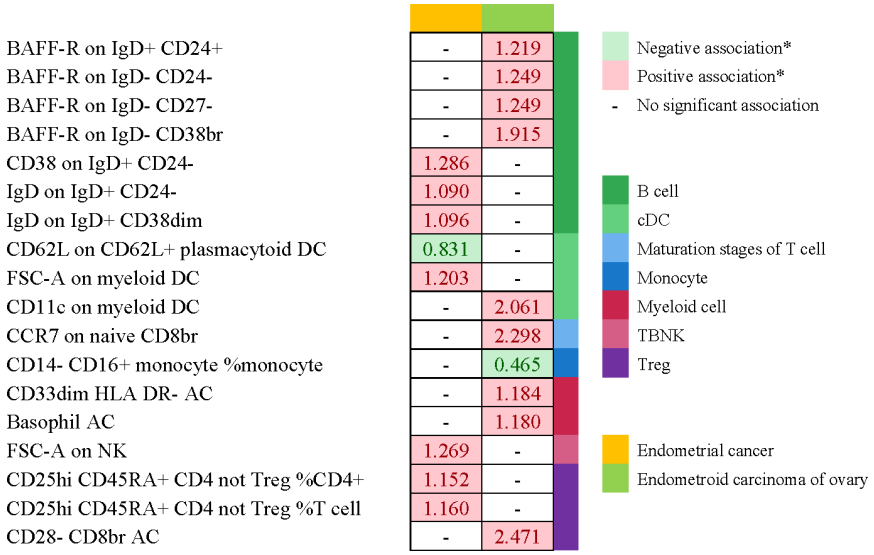

FIGURE 9
Summary of associations of genetically predicted immunophenotype traits with endometrial cancer. * means "P value <0.05, but 0.05< adj.P value <0.2 after FDR correction.

the function of the immune system in the progression of gynecological cancers is still unknown. In this study, we used a two-sample MR analysis to acquire information about the genetic evidence links between immunophenotypes and four gynecologic malignancies. With IVW techniques, we successfully managed to determine 65 possible immunophenotype traits and 50 highly probable ones. 19 traits in B cell panel, 8 in TBNK, 6 in cDC, monocyte, and maturation stages of T cell, 4 in myeloid cell, and 2 in Treg composed the highly probable immunophenotypes. In order to help the general public understand the excellent outcomes, we also plotted a schematic summary figure in Figure 11. The study revealed a more thorough and trustworthy causation of immunophenotype in gynecologic cancers than we anticipated.

We used 4 distinct MR analysis methods to conduct a large-scale MR analysis for this work. Initially, we searched into the potential connection between immune cells and four gynecologic cancers, including preinvasive carcinoma. 206 pairs of significant (P<0.05) causal associations were confirmed by the results of the MR analysis (Supplementary Table 2). Nevertheless, we modified the P-value to adj.P-value (FDR adjusted with Benjamini-Hochberg method) in regard to multiple comparisons. Our research revealed that 32 pairs had highly probable causative effects for cervical cancer, 9 for ovarian cancer, and 9 for vulvar cancer. Unfortunately, the findings failed to confirm a high probability of a causal link between immunophenotype traits and endometrial cancer. Thus, we identified the immunophenotypes that showed P value <0.05; and 0.05< adj. P value <0.2 was considered to be possible factors. Subsequently, 18 possible immunophenotypes for endometrial cancer and 65 for *in situ* gynecologic carcinoma were identified.

In assessing immunological components in the TME, T cells and myeloid cells have been the subject of numerous investigations. But little research has been done on the function of B cells. In our study, the B-cell panel showed the highest number of significant associations in cervical cancer when compared to other panels, and the majority of B cells panel (e.g. BAFF-R on $CD24^+$ $CD27^+$ B cell, BAFF-R on IgD^+ $CD24^+$ B cell, BAFF-R on IgD^+ CD24- B cell, BAFF-R on IgD^+ CD38- B cell, CD19 on $CD24^+$ $CD27^+$ B cell, and CD19 on memory B cell) were protective factors against cervical cancer. A recent investigation provided evidence that B-cells performed an anti-tumorigenic effect on squamous cell carcinomas associated with HPV. Furthermore, the findings demonstrated that B-cell specific molecule (CD19) was a predictive survival biomarker in head and neck squamous cell carcinoma and cervical squamous cell carcinomas (32). Additionally, Kim SS et al. discovered that B-cell depleted mice had larger tumors and grew at a faster rate than matched mice with controls, indicating a critical function for B-cells in the progression of squamous cell carcinoma (32). Cao and colleagues mapped the immunological landscape of cervical cancer using single-cell RNA sequencing. The findings demonstrated that germinal center B cells improved clinical outcomes and have anti-tumor abilities (33). The diversity of B-cell subsets in anti-tumor responses was also demonstrated by Cao et al. Our findings were consistent with the aforementioned studies, which show that B cells significantly improved the prognosis of cervical cancer patients.

Prior studies have indicated that the lymphocyte-to-monocyte ratio (LMR) has been explored as a potential predictive marker for ovarian cancer. Similarly, we discovered that monocytes (such as HLA DR on $CD14^+$ CD16-monocyte, HLA DR on $CD14^+$ monocyte, and HLA DR on monocyte) were linked to a lower risk of ovarian cancer. According to a clinical trial, patients with a high LMR typically respond better to chemotherapy, and the complete response (CR) rate differed significantly between the LMR-low and LMR-high groups. (48.9% vs. 75.3%, P < 0.0001) (34). In patients with ovarian cancer, low LMR was

10.3389/fonc.2024.1371309

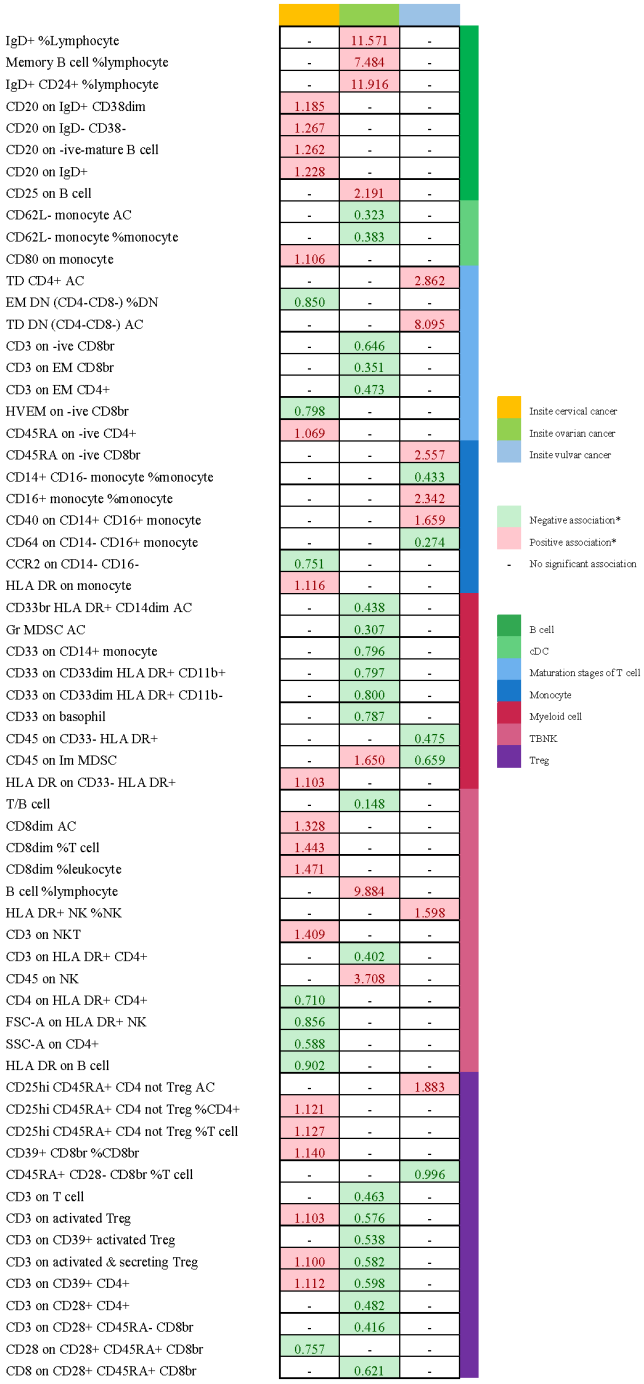

FIGURE 10
Summary of associations of genetically predicted immunophenotype traits with gynecologic carcinoma *in situ*. * means "P value <0.05, but 0.05< adj.P value <0.2 after FDR correction.

linked with poor survival outcomes, particularly poor OS and PFS, based on the findings of a meta-analysis (35). Consistent with previous research, our results showed that monocytes were positively correlated with survival and may contribute to maintaining the equilibrium between anti-tumor immune response and tumor promoting capacity.

This study is the first to investigate the causative relationships between immunophenotype traits and gynecologic malignancies via a two-sample Mendelian randomization. The study's main strength is the MR method, which eliminated bias from other variables and reverse causality. Our analysis's broad coverage of immune cells and large sample size, which outperformed comparable observational studies in terms of statistical efficiency, are two of its main advantages. An additional benefit is that our study was limited to European participants, thereby decreasing the possibility of heterogeneity. Thirdly, all IVs satisfied the criterion that F-statistics > 10, confirming no weak IVs bias. Yet it is also

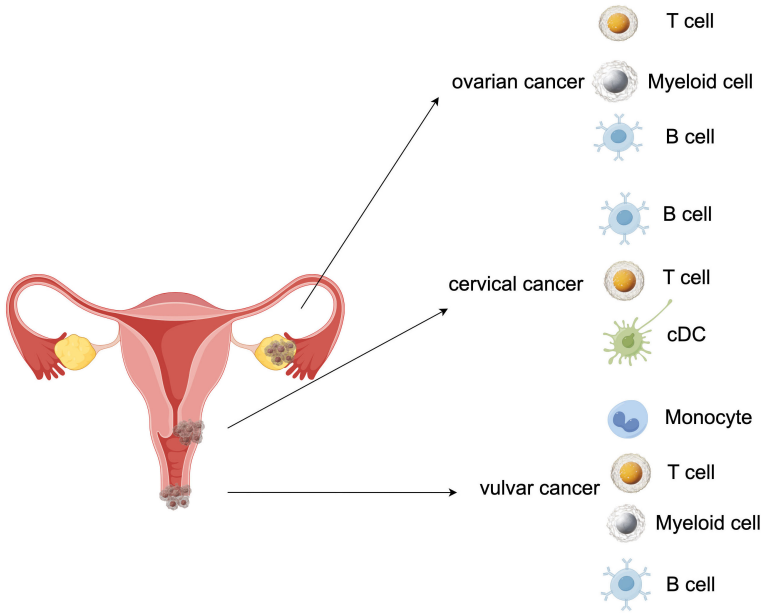

FIGURE 11
A schematic summary figure for the positive results after the Bonferroni method. (Created with Figdraw). **(A)** Three important assumptions for choosing instrumental variables (IVs); **(B)** The overview of the study design.

essential to note our study's limitations. First off, since all the GWAS summary data were from European populations, more research is needed to determine whether our findings apply to other racial or ethnic groups. Second, we are unable to do a stratified analysis of the population in the absence of baseline information (such as age, gender, TNM stage, and grade), which could potentially muddy the causal link due to hidden population structure. Thirdly, there are fewer SNPs accessible for some immunophenotype features in this because of the stringent screening IV cut-off, which could have resulted in bias.

5 Conclusions

To sum up, we discovered that the level of various immunophenotypes was connected to a risk of gynecologic malignancies based on a bidirectional two-sample MR study. Our study presented intriguing results on the causative relationship between immunological factors and gynecologic cancers. According to our findings, immune cell-targeting lymphocyte subset harmonies may be a viable intervention strategy for the prevention of gynecologic cancers. These findings also offer compelling justification for the creation of new immune cell-targeting therapies and additional methods for diagnosis.

Data availability statement

The datasets presented in this study can be found in online repositories. The names of the repository/repositories and accession number(s) can be found in the article/Supplementary Material.

Ethics statement

All studies included in cited genome-wide association studies had approved by a relevant review board. All participants had provided the inform consent. FinnGen research project is based on samples from Finnish biobanks and data from national health registers and applies the permissions to utilize the register data for research purposes from national authorities. All studies were conducted in accordance with the Declaration of Helsinki.

Author contributions

YL: Conceptualization, Formal analysis, Funding acquisition, Supervision, Writing – review & editing. JL: Formal analysis, Methodology, Software, Visualization, Writing – original draft. QW: Data curation, Software, Writing – review & editing. YZ: Visualization, Writing – original draft. CZ: Data curation, Writing – review & editing. JP: Funding acquisition, Methodology, Supervision, Validation, Writing – review & editing.

Funding

The author(s) declare financial support was received for the research, authorship, and/or publication of this article. This work was supported by grants from the Natural Science Foundation of Gansu Province (22JR5RA191, 23JRRA1381), grants from the National Natural Science Foundation of China (82360469), and grants from the Lanzhou Science and Technology Bureau (2022-ZD-62).

Conflict of interest

The authors declare that the research was conducted in the absence of any commercial or financial relationships that could be construed as a potential conflict of interest.

Publisher's note

All claims expressed in this article are solely those of the authors and do not necessarily represent those of their affiliated organizations, or those of the publisher, the editors and the reviewers. Any product that may be evaluated in this article, or claim that may be made by its manufacturer, is not guaranteed or endorsed by the publisher.

Supplementary material

The Supplementary Material for this article can be found online at: https://www.frontiersin.org/articles/10.3389/fonc.2024.1371309/full#supplementary-material

References

1. Sung H, Ferlay J, Siegel RL, Laversanne M, Soerjomataram I, Jemal A, et al. Global cancer statistics 2020: GLOBOCAN estimates of incidence and mortality worldwide for 36 cancers in 185 countries. *CA Cancer J Clin*. (2021) 71:209–49. doi: 10.3322/caac.21660

2. Stewart C, Ralyea C, Lockwood S. Ovarian cancer: an integrated review. *Semin Oncol Nurs*. (2019) 35:151–6. doi: 10.1016/j.soncn.2019.02.001

3. Cibula D, Pötter R, Planchamp F, Avall-Lundqvist E, Fischerova D, Haie Meder C, et al. The European Society of Gynaecological Oncology/European Society for Radiotherapy and Oncology/European Society of Pathology guidelines for the management of patients with cervical cancer. *Radiother Oncol*. (2018) 127:404–16. doi: 10.1016/j.radonc.2018.03.003

4. Sarfraz I, Rasul A, Hussain G, Shah MA, Zahoor AF, Asrar M, et al. 6-Phosphogluconate dehydrogenase fuels multiple aspects of cancer cells: From cancer initiation to metastasis and chemoresistance. *Biofactors*. (2020) 46:550–62. doi: 10.1002/biof.1624

5. Sarfraz I, Rasul A, Hussain G, Hussain SM, Ahmad M, Nageen B, et al. Malic enzyme 2 as a potential therapeutic drug target for cancer. *IUBMB Life*. (2018) 70:1076–83. doi: 10.1002/iub.1930

6. Salman L, Sabah G, Jakobson-Setton A, Raban O, Yeoshoua E, Eitan R. Neutrophil-to-lymphocyte ratio as a prognostic factor in advanced stage ovarian carcinoma treated with neoadjuvant chemotherapy. *Int J Gynaecol Obstet*. (2020) 148:102–6. doi: 10.1002/ijgo.12986

7. Lieber S, Reinartz S, Raifer H, Finkernagel F, Dreyer T, Bronger H, et al. Prognosis of ovarian cancer is associated with effector memory CD8+ T cell accumulation in ascites, CXCL9 levels and activation-triggered signal transduction in T cells. *Oncoimmunology*. (2018) 7:e1424672. doi: 10.1080/2162402X.2018.1424672

8. Sasano T, Mabuchi S, Kozasa K, Kuroda H, Kawano M, Takahashi R, et al. The highly metastatic nature of uterine cervical/endometrial cancer displaying tumor-related leukocytosis: clinical and preclinical investigations. *Clin Cancer Res*. (2018) 24:4018–29. doi: 10.1158/1078-0432.CCR-17-2472

9. Vanderstraeten A, Luyten C, Verbist G, Tuyaerts S, Amant F. Mapping the immunosuppressive environment in uterine tumors: implications for immunotherapy. *Cancer Immunol Immunother*. (2014) 63:545–57. doi: 10.1007/s00262-014-1537-8

10. Wang J, Li Z, Gao A, Wen Q, Sun Y. The prognostic landscape of tumor-infiltrating immune cells in cervical cancer. *BioMed Pharmacother*. (2019) 120:109444. doi: 10.1016/j.biopha.2019.109444

11. Ni Y, Soliman A, Joehlin-Price A, Rose PG, Vlad A, Edwards RP, et al. High TGF-β signature predicts immunotherapy resistance in gynecologic cancer patients treated with immune checkpoint inhibition. *NPJ Precis Oncol*. (2021) 5:101. doi: 10.1038/s41698-021-00242-8

12. Chen H, Ma R, Zhou B, Yang X, Duan F, Wang G. Integrated immunological analysis of single-cell and bulky tissue transcriptomes reveals the role of interactions between M0 macrophages and naïve CD4(+) T cells in the immunosuppressive microenvironment of cervical cancer. *Comput Biol Med*. (2023) 163:107151. doi: 10.1016/j.compbiomed.2023.107151

13. Barna AJ, Herold Z, Acs M, Bazsa S, Gajdacsi J, Garay TM, et al. High tumor-infiltrating lymphocyte count is associated with distinct gene expression profile and longer patient survival in advanced ovarian cancer. *Int J Mol Sci*. (2023) 24. doi: 10.3390/ijms241813684

14. Davey Smith G, Hemani G. Mendelian randomization: genetic anchors for causal inference in epidemiological studies. *Hum Mol Genet*. (2014) 23:R89–98. doi: 10.1093/hmg/ddu328

15. Evans DM, Davey Smith G. Mendelian randomization: new applications in the coming age of hypothesis-free causality. *Annu Rev Genomics Hum Genet*. (2015) 16:327–50. doi: 10.1146/annurev-genom-090314-050016

16. Grover S, Del Greco MF, Stein CM, Ziegler A. Mendelian randomization. *Methods Mol Biol*. (2017) 1666:581–628. doi: 10.1007/978-1-4939-7274-6_29

17. Ong JS, Hwang LD, Cuellar-Partida G, Martin NG, Chenevix-Trench G, Quinn MCJ, et al. Assessment of moderate coffee consumption and risk of epithelial ovarian cancer: a Mendelian randomization study. *Int J Epidemiol*. (2018) 47:450–9. doi: 10.1093/ije/dyx236

18. Larsson SC, Carter P, Kar S, Vithayathil M, Mason AM, Michaëlsson K, et al. Smoking, alcohol consumption, and cancer: A mendelian randomisation study in UK Biobank and international genetic consortia participants. *PloS Med*. (2020) 17:e1003178. doi: 10.1371/journal.pmed.1003178

19. Ong J-S, Derks EM, Eriksson M, An J, Hwang L-D, Easton DF, et al. Evaluating the role of alcohol consumption in breast and ovarian cancer susceptibility using population-based cohort studies and two-sample Mendelian randomization analyses. *Int J Cancer*. (2021) 148:1338–50. doi: 10.1002/ijc.33308

20. Dimou NL, Papadimitriou N, Mariosa D, Johansson M, Brennan P, Peters U, et al. Circulating adipokine concentrations and risk of five obesity-related cancers: A Mendelian randomization study. *Int J Cancer*. (2021) 148:1625–36. doi: 10.1002/ijc.33338

21. Ye Y, Yang H, Wang Y, Zhao H. A comprehensive genetic and epidemiological association analysis of vitamin D with common diseases/traits in the UK Biobank. *Genet Epidemiol*. (2021) 45:24–35. doi: 10.1002/gepi.22357

22. Emdin CA, Khera AV, Kathiresan S. Mendelian randomization. *JAMA*. (2017) 318:1925–6. doi: 10.1001/jama.2017.17219

23. Orrù V, Steri M, Sidore C, Marongiu M, Serra V, Olla S, et al. Complex genetic signatures in immune cells underlie autoimmunity and inform therapy. *Nat Genet*. (2020) 52:1036–45. doi: 10.1038/s41588-020-0684-4

24. Kurki MI, Karjalainen J, Palta P, Sipilä TP, Kristiansson K, Donner KM, et al. FinnGen provides genetic insights from a well-phenotyped isolated population. *Nature*. (2023) 613:508–18. doi: 10.1038/s41586-022-05473-8

25. Staley JR, Blackshaw J, Kamat MA, Ellis S, Surendran P, Sun BB, et al. PhenoScanner: a database of human genotype-phenotype associations. *Bioinformatics*. (2016) 32:3207–9. doi: 10.1093/bioinformatics/btw373

26. Yang H, Dai H, Li L, Wang X, Wang P, Song F, et al. Age at menarche and epithelial ovarian cancer risk: A meta-analysis and Mendelian randomization study. *Cancer Med*. (2019) 8:4012–22. doi: 10.1002/cam4.2315

27. Dixon SC, Nagle CM, Thrift AP, Pharoah PD, Pearce CL, Zheng W, et al. Adult body mass index and risk of ovarian cancer by subtype: a Mendelian randomization study. *Int J Epidemiol*. (2016) 45:884–95. doi: 10.1093/ije/dyw158

28. Burgess S, Small DS, Thompson SG. A review of instrumental variable estimators for Mendelian randomization. *Stat Methods Med Res*. (2017) 26:2333–55. doi: 10.1177/0962280215597579

29. Burgess S, Thompson SG. Interpreting findings from Mendelian randomization using the MR-Egger method. *Eur J Epidemiol*. (2017) 32:377–89. doi: 10.1007/s10654-017-0255-x

30. Bowden J, Davey Smith G, Haycock PC, Burgess S. Consistent estimation in Mendelian randomization with some invalid instruments using a weighted median estimator. *Genet Epidemiol*. (2016) 40:304–14. doi: 10.1002/gepi.21965

31. Hemani G, Tilling K, Davey Smith G. Orienting the causal relationship between imprecisely measured traits using GWAS summary data. *PloS Genet*. (2017) 13:e1007081. doi: 10.1371/journal.pgen.1007081

32. Kim SS, Shen S, Miyauchi S, Sanders PD, Franiak-Pietryga I, Mell L, et al. B cells improve overall survival in HPV-associated squamous cell carcinomas and are activated by radiation and PD-1 blockade. *Clin Cancer Res*. (2020) 26:3345–59. doi: 10.1158/1078-0432.CCR-19-3211

33. Cao G, Yue J, Ruan Y, Han Y, Zhi Y, Lu J, et al. Single-cell dissection of cervical cancer reveals key subsets of the tumor immune microenvironment. *EMBO J*. (2023) 42:e110757. doi: 10.15252/embj.2022110757

34. Eo WK, Chang HJ, Kwon SH, Koh SB, Kim YO, Ji YI, et al. The lymphocyte-monocyte ratio predicts patient survival and aggressiveness of ovarian cancer. *J Cancer*. (2016) 7:289–96. doi: 10.7150/jca.13432

35. Gong J, Jiang H, Shu C, Hu MQ, Huang Y, Liu Q, et al. Prognostic value of lymphocyte-to-monocyte ratio in ovarian cancer: a meta-analysis. *J Ovarian Res*. (2019) 12:51. doi: 10.1186/s13048-019-0527-z

frontiers | Frontiers in Oncology

TYPE Review
PUBLISHED 02 May 2024
DOI 10.3389/fonc.2024.1381894

OPEN ACCESS

EDITED BY
Shivendra Vikram Singh,
St. Jude Children's Research Hospital,
United States

REVIEWED BY
Shafiq Khan,
Clark Atlanta University, United States
Mauricio Rodriguez-Dorantes,
National Institute of Genomic Medicine
(INMEGEN), Mexico

*CORRESPONDENCE
Zhaodong Ji
ntjzd_1990@163.com

†These authors have contributed equally to this work

RECEIVED 04 February 2024
ACCEPTED 19 April 2024
PUBLISHED 02 May 2024

CITATION
Xia Q, Gao W, Yang J, Xing Z and Ji Z (2024) The deregulation of arachidonic acid metabolism in ovarian cancer.
Front. Oncol. 14:1381894.
doi: 10.3389/fonc.2024.1381894

The deregulation of arachidonic acid metabolism in ovarian cancer

Qiuyi Xia[1†], Wen Gao[2†], Jintao Yang[3†], Zhifang Xing[1] and Zhaodong Ji[1*]

[1]Department of Laboratory Medicine, Huashan Hospital, Fudan University, Shanghai, China, [2]Cancer Hospital of the University of Chinese Academy of Sciences (Zhejiang Cancer Hospital), Institute of Basic Medicine and Cancer (IBMC), Chinese Academy of Sciences, Hangzhou, Zhejiang, China, [3]Key Laboratory of Digital Technology in Medical Diagnostics of Zhejiang Province, Hangzhou, Zhejiang, China

Arachidonic acid (AA) is a crucial polyunsaturated fatty acid in the human body, metabolized through the pathways of COX, LOX, and cytochrome P450 oxidase to generate various metabolites. Recent studies have indicated that AA and its metabolites play significant regulatory roles in the onset and progression of ovarian cancer. This article examines the recent research advancements on the correlation between AA metabolites and ovarian cancer, both domestically and internationally, suggesting their potential use as biological markers for early diagnosis, targeted therapy, and prognosis monitoring.

KEYWORDS

arachidonic acid, ovarian cancer, metabolic pathway, biological marker, targeted therapy

1 Lipid metabolites in ovarian cancer

Ovarian cancer(OC) is a common gynecological malignant tumor with a hidden onset, high degree of malignancy, and high mortality rate (1). Globally, there are nearly 240,000 new cases annually, with the ovarian cancer mortality rate expected to significantly increase by 2040 (2). However, the lack of specific markers for ovarian cancer means that most patients are diagnosed in the late stages of the disease (51% in stage III or 29% in stage IV), missing the optimal timing for surgery, resulting in a 5-year survival rate of only 26-42% (3). Therefore, there is an urgent need to develop new molecular markers for the prevention and treatment of ovarian cancer. Extensive research indicates a close relationship between abnormal lipid metabolism and tumor development, increasing the possibility of detecting subtle metabolic changes in early tumor formation, making it a promising candidate as an ideal biomarker for ovarian cancer diagnosis (4–6). Among them, arachidonic acid is considered a key lipid metabolism product, playing a significant role in cell proliferation, apoptosis, invasion, and metastasis. Therefore, research on arachidonic acid and other lipid

metabolites can not only help us better understand the pathogenesis of ovarian cancer but also offer new insights and methods for the treatment and prevention of this disease.

2 Arachidonic acid metabolism in cancer

Arachidonic acid (AA) is an essential omega-6 polyunsaturated fatty acid in the human body (7). The endogenous generation of arachidonic acid (AA) is derived from phospholipids in the cell membrane, which is catalyzed by the superfamily of phospholipase A2 (PLA2). This process is induced by various cellular activation signals, including stimulation of tumor necrosis factor receptor (TNFR) and toll-like receptor 4 (TLR4) in the course of inflammation or infection. Among the members of the PLA2 enzyme superfamily, three contribute to eicosanoid production and are involved in distinct functions within eicosanoid metabolism (8–10). The cytosolic calcium-dependent PLA2 alpha (cPLA2α) primarily facilitates the production of free fatty acids (FFAs) and generation of AA, which plays a crucial role in cellular signaling (11). The cytosolic calcium-independent PLA2 alpha (iPLA2α) contributes to cellular homeostasis through synthesis of specialized pro-resolving mediators (SPMs) and reacylation of free AA, while secretory PLA2 (sPLA2), operating in a paracrine manner, controls the release of free AA and induces local inflammatory responses. In addition to PLA2 enzymes, other enzymes known as phospholipase C (PLC) and phospholipase D (PLD), generate AA via intermediate products such as diacylglycerol(DAG) (12–14). Free AA is converted in three ways: ① Cyclooxygenase (COX) enzymes catalyze the metabolic conversion of arachidonic acid to prostanoids including prostaglandins (PGs), prostacyclin, and thromboxane(TXs). ② Lipoxygenase (LOX) pathways catalyze the conversion of arachidonic acid to leukotrienes and lipoxins. ③ Cytochrome P450 enzyme (CYP) pathway (15) (Figure 1). Previous studies have demonstratedthat AA and its metabolites promote the occurrence and development of tumors by regulating the process of cell carcinogenesis, progression, and differentiation such as cell proliferation, chemotaxis, mitosis, migration, and apoptosis (16–18). Therefore, AA metabolism is considered to be one of the active metabolisms in tumor metabolism.

2.1 The action of COX pathway in tumor

The COX enzyme is the initial catalyst in the arachidonic acid pathway for prostaglandin (PG) and thromboxane (Tx) synthesis, existing in three isomeric forms: COX-1, COX-2, and COX-3 (19). Both COX-1 and COX-2 enzymes facilitate the conversion of cell membrane phospholipids to arachidonic acid via phospholipase A2, followed by its conversion to PGH2 through PGG2 (20) (Figure 2).COX-1 is a constitutive enzyme essential for normal physiological functions and widely distributed across various tissues to safeguard cellular integrity (21). There is no significant difference in the expression level of COX-1 between tumor tissues and normal tissues (22).

COX-2 is an inducible enzyme that performs a crucial function in the pathophysiological process of various cancers, including pancreatic, breast, prostate, lung, liver, cervical, bowel, and skin cancer (23–28). It is either not expressed or expressed at low levels in most normal tissues. The expression of COX-2 is associated with inflammation, cell survival, proliferation, angiogenesis, invasion, and metastasis. In response to growth factors and endotoxins, COX-2 is briefly but strongly expressed. The overexpression of COX-2 significantly enhances the production of PGE2, leading to increased cell aggressiveness (29). PGE2 contributes to the development and progression of many cancers by activating the

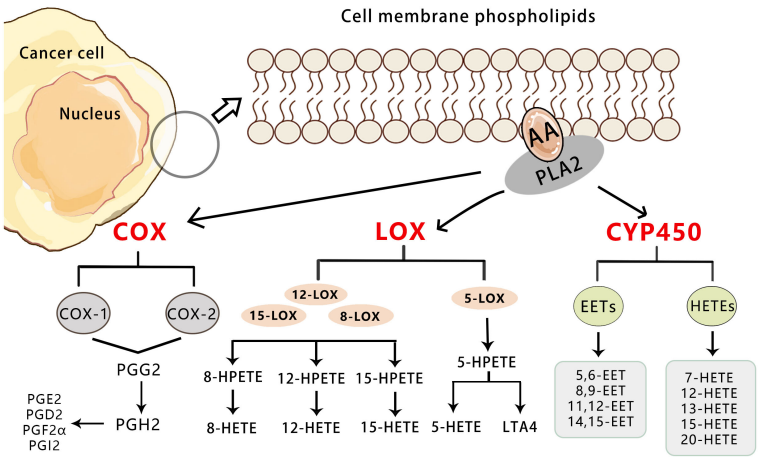

FIGURE 1
Overview of the three pathways for AA metabolism in cancer. Upon cell stimulation, phospholipase A2 induces FFAs, primarily AA derived from the lipid bilayer. The released AA is metabolized into bioactive lipid signaling molecules by three different enzymatic pathways. COX-1/2 metabolize AA to a series of prostaglandins (PGD2, PGE2, PGF2, PGH2, and PGI2).5-LO metabolizes AA to 5-HETE, LTB4, and cysteine leukotrienes, and 12-LO metabolizes AA to 12-HETE. Both subtypes of 15-LO metabolize AA to 15-HETE and, to a lesser extent, 12-HETE. Cytochrome P450 metabolizes AA to 19-/20-HETEand so on.

membrane receptors EP (including EP1, EP2, EP3, and EP4 receptors) and the nuclear receptor PPARδ of target cells (30). Other studies have indicated that high expression of COX-2 can hinder the apoptosis of tumor cells, which is crucial in the early stages of tumor formation (31). The overexpression of COX-2 can result in increased synthesis of PG, which plays a significant biological role in tumor growth and proliferation. PGE2 can impede apoptosis induced by selective COX-2 inhibitors by upregulating the anti-apoptotic protein bc-l2 (32). Kajita et al. discovered that the level of specific enzymes in the PG synthesis pathway, such as TXA2 synthetase, increased in papillary thyroid carcinoma. Additionally, the expression of COX-2 protein in papillary thyroid carcinoma was higher than in normal thyroid tissue and varied greatly, indicating that COX-2 could promote the growth of the thyroid papillary gland (33). These findings suggest that the increased expression of these enzymes may contribute to the pathogenesis of tumors.

What's more, angiogenesis is the physiological basis of solid cancer growth and metastasis (34). The high expression of COX-2 and its metabolite PGE2 promotes angiogenesis by up-regulating angiogenic factors such as vascular endothelial growth factor (VEGF) and basic fibroblast growth factor (bFGF) (35). COX-2 also promotes the metastasis and invasion of ovarian cancer by inducing matrix metalloproteinases (MMPs) in the extracellular matrix and the decomposition of collagen matrix, which may be involved in the activation of the PI3K/AKT signaling pathway (36–38). Inhibition of COX-2 with its specific inhibitor NS-398 can increase the expression of E-cadherin and inhibit the expression of slug, vimentin, MMP2, and MMP9, thereby suppressing the invasion and metastasis of ovarian cancer cells under estrogen treatment (39–41). Moreover, overexpression of COX-2 in ovarian cancer cells can directly up-regulate Bcl-2 expression through the increased synthesis of PGs. In addition, COX-2 can inhibit the proliferation of T and B lymphocytes through its product PGE2, and also inhibit the synthesis of cytokines to reduce the cytotoxicity of natural killer cells (42). Therefore, the role of COX-2 and PGE2 in promoting tumor proliferation and invasion, reducing tumor cell apoptosis, and promoting tumor angiogenesis has been confirmed, and it proved that they play an important role in carcinogenesis, and have the function of promoting tumor by inhibiting the body's immunity (43).

2.2 The action of LOX pathway in tumor

LOX is the initial enzyme in the leukotriene (LT) pathway of arachidonic acid. Isoenzymes of LOX consist of 5-LOX, 12-LOX, and two isomers of 15-LOX (15-LOX-1, 15-LOX-2). However, 5-LOX, 12-LOX, and 15-LOX-1 have pro-tumor effects, while 15-LOX-2 appears to have anticancer effects (44).

LOX catalyzes the oxidation of arachidonic acid to 5-HPETE, which is subsequently metabolized to 5-HETE (5-hydroxyeicosatetraenoic acid) and LTB4 (leukotriene B4) (45). As a member of the arachidonic acid oxygenase family, 5-LOX is composed of 674 amino acids and is a monomeric enzyme containing iron ions. 5-LOX can be transcriptionally regulated by transcription factor Er, Sp1, nuclear factor-κB (NF-κB), and GATA (46). 5-LOX is activated by 5-LOX activating protein (FLAP) to catalyze arachidonic acid, which is released from the phospholipid bilayer by phospholipase A2 (47). Arachidonic acid is transformed into 5-HPETE, which can be metabolized by glutathione peroxidase into 5-HETE (48). The activity of 5-LOX leads to the formation of unstable LTA4, which can be converted to LTB4, LTC4,LTD4 and LTE4 (49). More significantly, the average endogenous level of LOX metabolites such as 12-HETE (12-hydroxyeicosatetraenoic acid) in primary prostate cancer were found to be significantly higher than that in non-neoplastic prostate tissue. It is suggested that 12-HETE is crucial in the progression of prostate cancer and the LOX pathway may be a target for the treatment and prevention of prostate cancer (50). 12-HETE has also been shown to play an important role in cancer adhesion, invasion, and metastasis. It stimulates NF-κB activation and NF-κB-dependent ICAM-1 expression through RhoA and PKCα signaling pathways, and the Rho/Rac family of GTases also play a role in cell adhesion and migration. 12-HETE can also promote the secretion of protease and enhance the motor capacity of tumor cells (51)(Figure 3).

Various environmental and chemical carcinogens activate pro-tumor mediators during carcinogenesis, including 5-LOX, whose

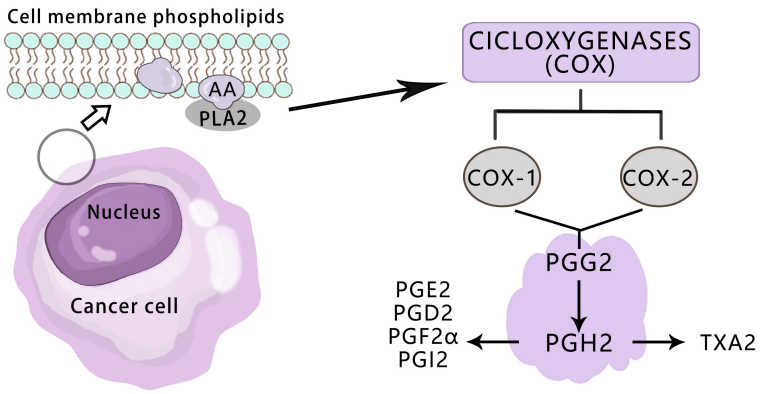

FIGURE 2
Overview of the pathways for the COX-mediated AA metabolism in cancer.

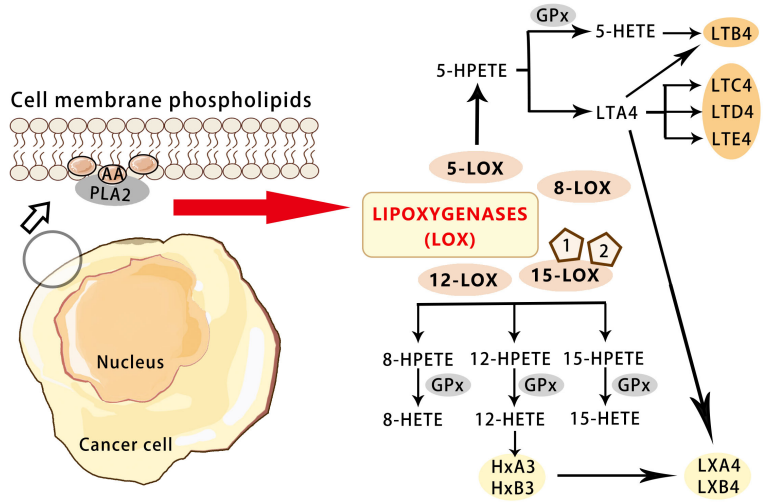

FIGURE 3
Overview of the pathways for the LOX-mediated AA metabolism in cancer.

metabolite 5S-HERE acts as a substrate for COX-2 to form bicyclic and is further transformed into two pro-angiogenic mediators (52). However, the specific role of these products in cancer development needs better understanding, given the pro-angiogenic role of these enzymes. As a result, 5-LOX is considered a new target for cancer prevention and treatment, while LETA4 hydrolase is considered a tumor promoter whose inhibitors can reduce tumor growth and development (53). Although most of the metabolites synthesized by the COX and LOX pathways can promote tumorigenesis. Additionally, CYP450 monooxygenase-derived metabolites can also regulate the occurrence and growth of cancer, playing both a pro-tumor and anti-tumor role (54).

2.3 The action of CYP pathway in tumor

Cytochrome P450 (CYP) belongs to the group of hemoglobin enzymes. It is a super-family gene encoding isoenzymes with a structure and function related to CYP. The combination of reduced CYP and carbon monoxide (CO) has a special light absorption peak at 450 nm (55). The expression of CYP surface oxidase is significantly high in cancer tissues, while almost no expression is found in adjacent normal tissues. This confirms that CYP surface oxidase and its metabolites can regulate the occurrence and growth of cancer, playing both a pro-tumor and anti-tumor role. It has been shown that reducing the expression and activity of CYP450 has anti-tumor effects, making it a promising anti-cancer treatment method (56) (Figure 4).

Arachidonic acid produces epoxyeicosatrienoic acid (EETs) and hydroxyeicosatetraenoic acid (HETEs) through the catalysis of cytochrome P450 surface oxidase. EETs are further categorized into four types: 5,6-EET, 8,9-EET, 11,12-EET, and 14,15-EET (57, 58). Recent studies have focused on the role and mechanism of EETs in important biological processes of tumors, including proliferation, apoptosis, and metastasis (59). These studies have revealed that EETs can significantly enhance the proliferation of

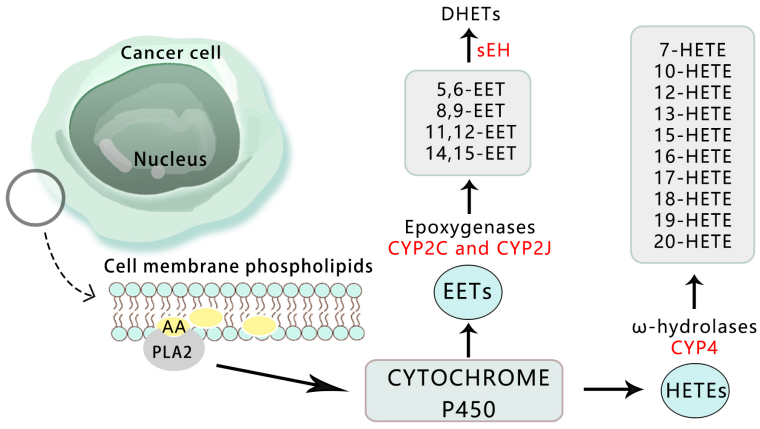

FIGURE 4
Overview of the pathways for the CYP450-mediated AA metabolism in cancer.

tumor cells and protect them from TNF-α-induced apoptosis by up-regulating anti-apoptotic proteins Bcl-2 and Bcl-XL, while down-regulating pro-apoptotic proteins Bax and Bak, thereby reducing the activity of caspase-3 protein (60).

In light of the characteristics of the CYP gene superfamily, research on the correlation between CYP and gynecologic tumors primarily focuses on specific CYP polymorphisms involved in sterol hormone metabolism. The polymorphisms of CYPlAl, CYPlBl, CYPl7, and CYPl9 have garnered increasing attention in relation to gynecologic tumors (61, 62). CYPlAl is an enzyme involved in the metabolism of polycyclic aromatic hydrocarbons (PAHs), which are significant metabolically active chemical carcinogens, and is expressed in various sterol hormone-reactive tissues such as the ovary, mammary gland, and prostate. Studies have shown that the CYPlAl Ile/Val and Val/Val genotypes are significantly more common in patients with epithelial ovarian tumors, indicating that women with these genotypes are at higher risk for ovarian cancer (63). CYP and its lipid metabolites play a role in the development of ovarian tumors, and their expression may be a crucial marker for tumor development (64).

3 Arachidonic acid metabolism in OC

3.1 Cox pathway in ovarian cancer

AA catalyzes the synthesis of prostaglandins (PGs) and thromboxanes (TXs) through cyclooxygenase (COX). There are two subtypes of COX: COX-1 and COX-2. COX-1 is widely distributed in tissues, with no significant difference in expression levels between tumor tissues and normal tissues. On the other hand, COX-2 is closely associated with the development of inflammation and tumors. Overexpression of COX-2 significantly promotes the biosynthesis of prostaglandin E2 (PGE2). PGE2 stimulates the occurrence and progression of various cancers by activating membrane receptors EP and nuclear receptor PPARδ in target cells.

Recently, Mauricio A. Cuello discussed the impact of COX-2 on the immune spectrum of high-grade serous ovarian cancer (HGSOC). Elevated levels of COX-2 may hinder NK cell activity, promote the expression of cytotoxic T lymphocyte-associated protein-4 (CTLA-4), affecting the efficacy of anti-CTLA-4 immunotherapy in HGSOC patients. Targeting COX-2 before anti-CTLA-4 immunotherapy could be a promising strategy to enhance the effectiveness of immunotherapy in ovarian cancer patients (42). Additionally, Ning Ding's research found that the overexpression of COX-2 in SKOV3 cells (human ovarian cancer cells) is associated with the acquisition of stem cell properties, inflammatory microenvironment, enhanced tumor sphere formation, increased cell proliferation, and enhanced metastatic potential, all contributing to ovarian cancer progression and metastasis (65). Based on current research, the roles of COX- and LOX-derived class of diterpenes in cancer have been fairly well studied. COX-1, COX-2, mPGES-1, EP1, and EP2 are mainly expressed in epithelial cells of human epithelial ovarian cancer (66). The expression of COX-2 in ovarian cancer cells is regulated by various cytokines, such as EGF, vitamin D, IL-1β, which can stimulate the proliferation, migration, and angiogenesis of ovarian cancer cells. It mainly enhances the proliferation and migration of human ovarian cancer CAOV-3 cells by activating the phosphatidylinositol 3 kinase/protein kinase B (PI3-k/Akt) pathway (67). Moreover, by analyzing epithelial ovarian cancer tissues and cell lines, COX-2 also regulates cell growth and apoptosis through the PI3K/AKT signaling pathway in ovarian cancer tissues (68).

3.2 LOX pathway family in ovarian cancer

In the Lipoxygenase (LOX) pathway, AA is catalyzed by the LOX enzyme, undergoing an oxidation reaction at specific sites to form hydroxyl-containing products, namely Hydroxyeicosatetraenoic acid (HETEs, including 5-, 8-, 12-HETE, etc.). Additionally, there are lipoxins (LXs), leukotrienes (LTs), and other products, which will not be the focus here.

Research in ovarian cancer has found an increased expression level of 5-LOX in the immune stroma of tissues, suggesting a specific impact on the tumor microenvironment during tumor initiation and progression (47). Under hypoxic conditions, the transcription levels of 5-LOX and ALOX5AP in ovarian cancer cell lines also increase, significantly correlating with poor overall survival, progression-free survival, lymphatic infiltration after initial treatment, rapid relapse, and other adverse clinical pathological features. Current studies have discovered that various LOX pathway metabolites, such as HETEs, play a role in inhibiting tumor cell apoptosis, stimulating angiogenesis, enhancing cell proliferation, and promoting metastasis. The presence of 12-HETE has been identified in high-grade serous ovarian cancer and normal ovarian epithelial tissues. The 12-LOX - 12-HETE system is present in two epithelial ovarian cancer cell lines, OVCAR-3 and SK-OV-3, with high levels of 12-LOX mRNA and protein (69, 70). Exposure to arachidonic acid increases the production of 12-HETE in both epithelial ovarian cancer cell lines. Numerous studies have confirmed its ability to promote the proliferation, adhesion, migration, and angiogenesis of various cancer cells such as breast, prostate, and colon cancer. These findings collectively indicate that metabolites produced by the LOX pathway can play a role in the development of ovarian cancer through different isoenzymes (71).

3.3 CYP450 pathway in ovarian cancer

Most studies on gynecologic malignant tumors have focused on the arachidonic acid oxygenase pathway, particularly examining the roles of PGE2 and PGF2a along with their respective receptors. While some research has touched upon the P450 cytochrome epoxygenase pathway in ovarian cancer, there is a lack of in-depth mechanistic studies in this area (72). Research indicates that CYP2C8 and CYP3A5 are prominently expressed in the majority of ovarian tumors, showing higher IHC staining intensity of CYP3A5 and other CYP enzymes in primary ovarian cancer tissues. In contrast, CYP3A4 is expressed at significantly lower levels in ovarian cancer (73, 74).

Arachidonic acid is converted into four eicosanoids (EETs) by cytochrome P450 oxygenases (CYP oxygenases). Human EETs are synthesized by the CYP2 family, including the CYP2C and CYP2J families. EETs are intermediate products downstream of the VEGF signaling pathway, regulating vascular tone and maintaining vascular homeostasis. They have been shown to promote endothelial cell proliferation, enhance endothelial cell migration through pathways such as eNOS, MEK/MAPK, and PI3K, and boost VEGF-mediated angiogenesis. Angiogenesis plays a crucial role in tumor development, enabling tumors to access more nutrients and oxygen for continued growth, spread, and metastasis by providing pathways for tumor cells to travel through the bloodstream to distant sites.

4 The arachidonic acid metabolism in tumor microenvironment of ovarian cancer

AA is a highly concentrated polyunsaturated fatty acid present in the microenvironment of ovarian cancer, with multiple research findings indicating its association with adverse clinical outcomes (75). Enzymes and metabolites related to the AA metabolic pathway regulate various pathophysiological processes in the cellular system, establishing the tumor microenvironment (TME) (76). The progression, metastasis, and spread of cancer, as well as the evasion of tumor cells from immune surveillance, crucially depend on the signaling network of the tumor microenvironment. In ovarian cancer, ascites is a significant component of the peritoneal TME, containing numerous tumor spheroids and immune cells, particularly tumor-associated macrophages (TAMs), T cells, and NK cells (77). Studies have reported a correlation between ovarian cancer survival and the abundance of immunosuppressive CD163-CD206-high tumor-associated macrophages (TAMs) and high levels of arachidonic acid (AA) in the tumor microenvironment. A research also indicates that the high expression of CD163 and CD206/MRC1 in TAMs is closely related to the inhibition of cytokine-triggered signals, reflecting impaired interferon and IL-6 transcriptional responses in monocyte-derived macrophages by AA (78). How does arachidonic acid affect the cytokine-triggered signals in macrophages? It influences the signal transduction of cytokine-triggered signals in macrophages by inhibiting the transcriptional responses to interferon and IL-6. This inhibition of pro-inflammatory signals is caused by dysfunction of homologous receptors, manifested as inhibition of JAK1, JAK2, STAT1, and STAT3 phosphorylation, as well as the relocation of interferon receptor IFNAR1, STAT1, and other immune regulatory proteins in lipid rafts. Exposure to AA leads to significant accumulation of free AA in lipid rafts, which appears to be a crucial mechanism, as inhibiting its binding to phospholipids does not affect AA-mediated interference with STAT1 phosphorylation. Therefore, the association between arachidonic acid and TAMs in the ovarian cancer microenvironment involves high levels of arachidonic acid impairing the signal transduction and transcriptional responses of TAMs, leading to an immunosuppressive environment. Additionally, macrophages play a key role in tumor growth, metastasis, immune suppression, and chemoresistance, contributing significantly to the progression and treatment of drug resistance in ovarian cancer (79).

5 Targeted therapy and drugs for arachidonic acid metabolism

An article entitled "Targeting LTA4H facilitates the reshaping of the immune microenvironment mediated by CCL5 and sensitizes ovarian cancer to Cisplatin" discusses the establishment of a prognosis model for ovarian cancer based on pufa-related genes, the role of the downstream LTA4H gene in the progression and drug resistance of ovarian cancer, and potential treatment strategies for ovarian cancer (80). The article highlights the significant role of LTA4H in influencing tumor characteristics and the immune microenvironment in the context of ovarian cancer. Positive correlation between LTA4H and poor prognosis in ovarian cancer has been observed, with the lack of LTA4H enhancing sensitivity to Cisplatin. Knockdown of LTA4H has been shown to inhibit the proliferation of ovarian cancer cells, while high expression of LTA4H leads to a decrease in infiltrating CD8+ T cells, which are crucial for anti-tumor immune responses. Furthermore, LTA4H is associated with abnormal metabolism in the arachidonic acid (AA) pathway, resulting in a reduction of certain chemokines such as CCL5. The decrease in chemokines may lead to changes in the composition of immune cells in the tumor microenvironment. LTA4H has been identified as a potential therapeutic target. Targeting LTA4H, whether through genetic manipulation or chemical inhibition, can yield favorable therapeutic effects for ovarian cancer. However, targeted therapies and drug researches related to arachidonic acid metabolism in ovarian cancer are still in the exploratory stage and have not yet been widely applied in clinical settings. Due to the complexity of the biochemical properties of AA and its metabolites, inhibitors of AA have been continuously discovered to have effects in tumors. Additionally, COX-2, HETEs, and key enzymes in their metabolic pathways may become potential targets for early cancer detection and treatment.

COX-2, LOX-5, and HETEs, along with the key enzymes in their metabolic pathways, could be potential targets for the early detection and treatment of cancer. The standard initial treatment for ovarian cancer is a combination of platinum and taxane (81, 82). However, due to the complexity of the biochemical properties of AA and its metabolites, the role of its inhibitors in tumors is continually being uncovered.

The COX inhibitor SC-560 was initially used as a pharmacological tool to study the role of COX-1-derived prostaglandins in inflammation and pain. It was later found that at specific doses of COX-1 inhibition, SC-560 exhibited mild to moderate inhibitory effects on tumor growth. Its anti-tumor activity has been demonstrated in various ovarian and colorectal cancer *in vitro* models and other types of tumor tissue. SC-560 also enhanced the sensitivity of paclitaxel-resistant ovarian cancer cell lines with MDR1/p-glycoprotein upregulation to paclitaxel. It belongs to a group of small molecules that may target specific genes in ovarian cancer stem cells (OVCSC), suggesting that SC-560 could be a promising lead compound for ovarian cancer (83).

Reduced expression of COX-2 and PGE is positively associated with decreased severity and occurrence of ovarian cancer. Currently, COX-2 has been recognized as a new cancer chemoprevention and therapeutic target. Selective COX-2 inhibitors like celecoxib, when used in combination with anti-cancer drugs, can overcome multidrug resistance in various cancers. They can also reduce cell growth, increase cleaved caspase-3 activity, and induce cell cycle G1 phase arrest in a dose-dependent manner in ovarian cancer cells (84).

Additionally, recent studies shown that the CYP4A/F-20-HETE pathway has a positive feedback regulatory effect (85). The AA pathway inhibits tumor cell migration and invasion by inhibiting 20-HETE synthesis. This is achieved by using the selective 20-HETE inhibitor N-hydroxy-N'-(4-butyl-2-methylphenyl)formamidine (HET0016), which significantly reduces the levels of vascular endothelial growth factor responsible for tumor cell communication with the microenvironment (86, 87), whether used alone or in combination. It is worth noting that ovarian cancer shows upregulation of CYP4A/F family enzymes involved in 20-HETE production and widespread use of HET0016 as a therapeutic approach against excessive proliferation (88).

Studies have also indicated that berberine, a natural compound with low cytotoxicity in normal cells, effectively inhibits the regeneration of post-chemotherapy ovarian cancer cells, particularly SKOV3 cells induced by VP16 (82, 89). Berberine can lower AA levels while increasing PGE2 levels, thus reversing the caspase-3-iPLA2-AA-COX-2-PGE2 pathway induced by chemotherapy drugs in SKOV-3 cells (90). This confirms that berberine can prevent recurrence of ovarian cancer, suggesting that combining chemotherapy drugs with berberine may prove to be an effective approach for preventing its recurrence (89).

6 Functional and signaling pathway enrichment analysis of AA metabolism related genes in OC

To comprehensively evaluate the function and signaling pathways of AA metabolism related genes in OC, we obtained transcriptome expression profile data from TCGA-OV cohort and normal ovarian tissues, and after analysis, a total of 8885 differentially expressed genes (DEGs) were identified (Figure 5A).Then, veen analysis was utilized to identify the above DEGs and AA metabolism related genes,resulting in a total of 34 overlapping DEGs (Figure 5B). To further determine the function of 34 candidate genes with related signaling pathways in OC, enrichment analysis was performed. Gene Ontology (GO)-biological process (BP) analysis showed that candidate genes were primarily involved in carboxylic acid metabolic process and monocarboxylic acid biosynthetic process, while GO-cellular component (CC) analysis showed that candidate genes were mainly located in endomembrane system and organelle membrane, with molecular functions (MF) mainly including aromatase activity, metal ion binding, and cation binding (Figure 5C).

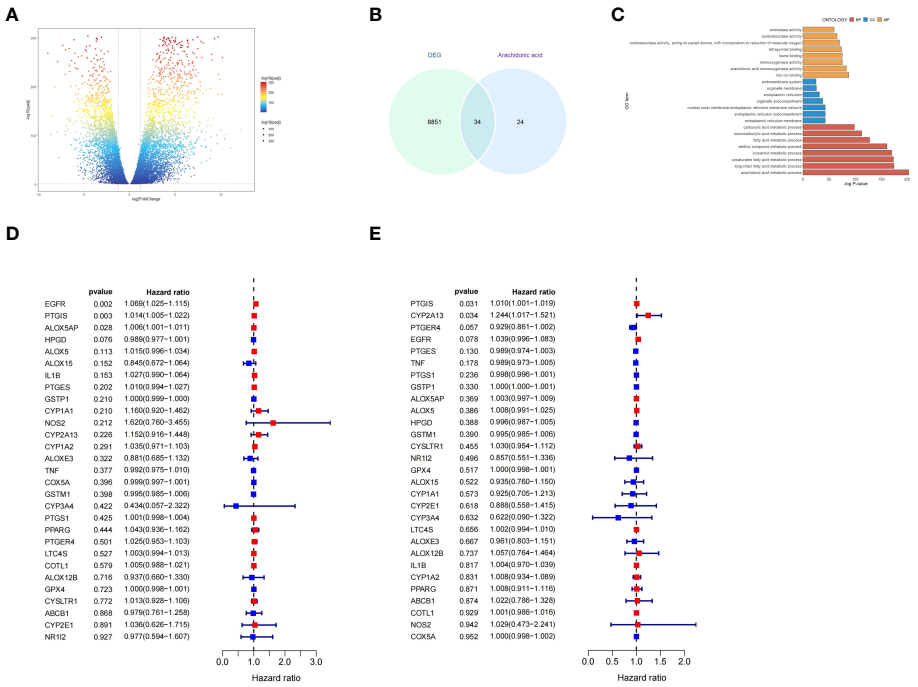

FIGURE 5
Functional and signaling pathway enrichment analysis of AA metabolism related genes in OC. **(A)** Volcano plot of DEGs between ovarian cancer and non-tumor tissues based on the TCGA (OV for ovarian cancer, accessed on 20240329) and GTEx (Ovary, accessed on 20240329) database. **(B)** Venn diagram showing the number of DEGs and AA metabolism related genes; the intersection part is the total number of genes in the two datasets. **(C)** Results of GO analysis of overlapping DEGs. **(D, E)** Forest plot demonstrating the univariate Cox model results of 34 OS/PFS-related key genes of AA metabolism.

To discover the potential prognostic significance of key genes of AA metabolism, we performed a univariate Cox hazard regression analysis. The expressions of 3 genes were found to be significantly associated with OC patient with overall survival(OS) and 2 genes associated with OC patient with progression-free survival (PFS) (Figures 5D, E).

7 Prospect

With the continuous development of research methods and tools, it has been gradually discovered that AA and its metabolites play important roles in the proliferation, metastasis, apoptosis, angiogenesis, and inflammatory responses of various tumor cells such as ovarian cancer, as well as in treatment and prognosis. High levels of COX, LOX, CYP, and key enzymes in related metabolic pathways may serve as potential targets for early detection and treatment of ovarian cancer. These pathways have been utilized to assess the progression of ovarian cancer, which is crucial for clinical diagnosis of the disease, especially early diagnosis. As an important metabolite of AA metabolism, an increased level of 15(S)-HETE has been identified in various cancers, including non-small cell lung cancer and breast cancer, which suggests that 15(S)-HETE could be served as a potential biomarker for cancer diagnosis (44).245 epithelial ovarian cancer samples were explored by tissue microarray and revealed a higher expression of 12-LOX. Furthermore, it was found that free fatty acid metabolism via LOX pathway leads to an elevated level of 8-HETE in women at risk for developing ovarian cancer. Therefore, measuring levels of 8-HETE could be proposed as an important indicator for assessing the risk of ovarian cancer (91).

This review emphasizes the critical role of AA and its metabolites in the occurrence, development, and metastasis of ovarian cancer. However, due to the complex biochemical nature of AA and its metabolites, their role in ovarian cancer remains challenging. Further research into the relationship between AA and tumor development is essential, requiring a more comprehensive and systematic exploration of the association between inhibitors and combination therapy efficacy. It is anticipated that with the discovery of more biomarkers, AA will usher in a new era of gene-targeted cancer therapy.

Author contributions

QX: Visualization, Writing – original draft. WG: Conceptualization, Writing – review & editing. JY: Formal Analysis, Writing – review & editing. ZX: Project administration, Writing – review & editing. ZJ: Funding acquisition, Writing – review & editing.

Funding

The author(s) declare financial support was received for the research, authorship, and/or publication of this article. This study was supported by grants from the Yangfan Plan of Shanghai Science and Technology Commission (No. 22YF1404700 for ZJ), the Research Start Up Fund of Huashan Hospital (No.2021QD043 for ZJ),the Medical Health Science and Technology Project of Zhejiang Province (No.2022KY627 and 2024KY793 for WG).

Conflict of interest

The authors declare that the research was conducted in the absence of any commercial or financial relationships that could be construed as a potential conflict of interest.

Publisher's note

Supplementary material

The Supplementary Material for this article can be found online at: https://www.frontiersin.org/articles/10.3389/fonc.2024.1381894/full#supplementary-material

References

1. Zhang R, Siu MKY, Ngan HYS, Chan KKL. Molecular biomarkers for the early detection of ovarian cancer. *Int J Mol Sci*. (2022) 23(19):12041. doi: 10.3390/ijms231912041

2. Bray F, Ferlay J, Soerjomataram I, Siegel RL, Torre LA, Jemal A. Global cancer statistics 2018: GLOBOCAN estimates of incidence and mortality worldwide for 36 cancers in 185 countries. *CA Cancer J Clin*. (2018) 68:394–424. doi: 10.3322/caac.21492

3. Torre LA, Trabert B, DeSantis CE, Miller KD, Samimi G, Runowicz CD, et al. Ovarian cancer statistics, 2018. *CA Cancer J Clin*. (2018) 68:284–96. doi: 10.3322/caac.21456

4. Beeghly-Fadiel A, Wilson AJ, Keene S, El Ramahi M, Xu S, Marnett LJ, et al. Differential cyclooxygenase expression levels and survival associations in type I and type II ovarian tumors. *J Ovarian Res*. (2018) 11(1):17. doi: 10.1186/s13048-018-0389-9

5. Yu W, Lei Q, Yang L, Qin G, Liu S, Wang D, et al. Contradictory roles of lipid metabolism in immune response within the tumor microenvironment. *J Hematol Oncol*. (2021) 14:187. doi: 10.1186/s13045-021-01200-4

6. Yin X, Xu R, Song J, Ruze R, Chen Y, Wang C, et al. Lipid metabolism in pancreatic cancer: emerging roles and potential targets. *Cancer Commun (Lond)*. (2022) 42:1234–56. doi: 10.1002/cac2.12360

7. Zhang Y, Liu Y, Sun J, Zhang W, Guo Z, Ma Q. Arachidonic acid metabolism in health and disease. *MedComm (2020)*. (2023) 4:e363. doi: 10.1002/mco2.363

8. Rangwala SM, Lazar MA. Peroxisome proliferator-activated receptor gamma in diabetes and metabolism. *Trends Pharmacol Sci*. (2004) 25:331–6. doi: 10.1016/S0165-6147(04)00115-4

9. McFadyen MC, Cruickshank ME, Miller ID, McLeod HL, Melvin WT, Haites NE, et al. Cytochrome P450 CYP1B1 over-expression in primary and metastatic ovarian cancer. *Br J Cancer*. (2001) 85:242–6. doi: 10.1054/bjoc.2001.1907

10. Lynes MD, Leiria LO, Lundh M, Bartelt A, Shamsi F, Huang TL, et al. The cold-induced lipokine 12,13-diHOME promotes fatty acid transport into brown adipose tissue. *Nat Med*. (2017) 23:631–7. doi: 10.1038/nm.4297

11. Moran JH, Weise R, Schnellmann RG, Freeman JP, Grant DF. Cytotoxicity of linoleic acid diols to renal proximal tubular cells. *Toxicol Appl Pharmacol*. (1997) 146:53–9. doi: 10.1006/taap.1997.8197

12. Medina-Gomez G, Gray S, Vidal-Puig A. Adipogenesis and lipotoxicity: role of peroxisome proliferator-activated receptor gamma (PPARgamma) and PPARgammacoactivator-1 (PGC1). *Public Health Nutr*. (2007) 10:1132–7. doi: 10.1017/S1368980007000614

13. Rett BS, Whelan J. Increasing dietary linoleic acid does not increase tissue arachidonic acid content in adults consuming Western-type diets: a systematic review. *Nutr Metab (Lond)*. (2011) 8:36. doi: 10.1186/1743-7075-8-36

14. Yarla NS, Bishayee A, Sethi G, Reddanna P, Kalle AM, Dhananjaya BL, et al. Targeting arachidonic acid pathway by natural products for cancer prevention and therapy. *Semin Cancer Biol*. (2016) 40-41:48–81. doi: 10.1016/j.semcancer.2016.02.001

15. Bosma KJ, Kaiser CE, Kimple ME, Gannon M. Effects of arachidonic acid and its metabolites on functional beta-cell mass. *Metabolites*. (2022) 12(4):342. doi: 10.3390/metabo12040342

16. Wang B, Wu L, Chen J, Dong L, Chen C, Wen Z, et al. Metabolism pathways of arachidonic acids: mechanisms and potential therapeutic targets. *Signal Transduct Target Ther*. (2021) 6:94. doi: 10.1038/s41392-020-00443-w

17. Cui L, Zhao Y, Pan Y, Zheng X, Shao D, Jia Y, et al. Chemotherapy induces ovarian cancer cell repopulation through the caspase 3-mediated arachidonic acid metabolic pathway. *Onco Targets Ther*. (2017) 10:5817–26. doi: 10.2147/OTT

18. Ma Y, Zheng L, Wang Y, Gao Y, Xu Y. Arachidonic acid in follicular fluid of PCOS induces oxidative stress in a human ovarian granulosa tumor cell line (KGN) and upregulates GDF15 expression as a response. *Front Endocrinol (Lausanne)*. (2022) 13:865748. doi: 10.3389/fendo.2022.865748

19. Yoshimura. Arachidonic acid pathway: A molecular target in human testicular cancer (Review). *Mol Med Rep*. (2009) 2(4):527–31. doi: 10.3892/mmr

20. Wang T, Fu X, Chen Q, Patra JK, Wang D, Wang Z, et al. Arachidonic acid metabolism and kidney inflammation. *Int J Mol Sci*. (2019) 20(15):3683. doi: 10.3390/ijms20153683

21. Pannunzio A, Coluccia M. Cyclooxygenase-1 (COX-1) and COX-1 inhibitors in cancer: A review of oncology and medicinal chemistry literature. *Pharm (Basel)*. (2018) 11(4):101. doi: 10.3390/ph11040101

22. Uddin MJ, Wilson AJ, Crews BC, Malerba P, Uddin MI, Kingsley PJ, et al. Discovery of furanone-based radiopharmaceuticals for diagnostic targeting of COX-1 in ovarian cancer. *ACS Omega*. (2019) 4:9251–61. doi: 10.1021/acsomega.9b01093

23. Renaldi K, Simadibrata M, Rahadiani N, Handjari DR, William A, Sinuraya F, et al. Prognostic value of COX-2, NF-κB, and sp1 tissue expressions in pancreatic ductal adenocarcinoma: A systematic review and meta-analysis. *Turk J Gastroenterol*. (2021) 32:956–70. doi: 10.5152/tjg

24. Balamurugan K, Poria DK, Sehareen SW, Krishnamurthy S, Tang W, McKennett L, et al. Stabilization of E-cadherin adhesions by COX-2/GSK3β signaling is a targetable pathway in metastatic breast cancer. *JCI Insight*. (2023) 8(6):e156057. doi: 10.1172/jci.insight.156057

25. Musalam A, Andarawi M, Osman M, Al-Shriam M, Elrefaie A, Mahfouz AA, et al. Alterations of COX-2, HER-2/neu and E-Cadherin protein expression in the prostatic adenocarcinoma: preliminary findings. *Am J Transl Res*. (2019) 11:1653–67.

26. Desind SZ, Iacona JR, Yu CY, Mitrofanova A, Lutz CS. PACER lncRNA regulates COX-2 expression in lung cancer cells. *Oncotarget*. (2022) 13:291–306. doi: 10.18632/oncotarget.v13

27. Alves AF, Baldissera VD, Chiela ECF, Cerski CTS, Fontes PRO, Fernandes MDC, et al. Altered expression of COX-2 and TNF-α in patients with hepatocellular carcinoma. *Rev Esp Enferm Dig*. (2019) 111:364–70. doi: 10.17235/reed.2019.5898/2018

28. Tudor DV, Bâldea I, Lupu M, Kacso T, Kutasi E, Hopârtean A, et al. COX-2 as a potential biomarker and therapeutic target in melanoma. *Cancer Biol Med*. (2020) 17:20–31. doi: 10.20892/j.issn.2095-3941.2019.0339

29. Xin C, Chu L, Zhang L, Geng D, Wang Y, Sun D, et al. Expression of cytosolic phospholipase A2 (cPLA2)-arachidonic acid (AA)-cyclooxygenase-2 (COX-2) pathway factors in lung cancer patients and its implication in lung cancer early detection and prognosis. *Med Sci Monitor*. (2019) 25:5543–51. doi: 10.12659/MSM.915314

30. Ye Y, Wang X, Jeschke U, von Schönfeldt V. COX-2-PGE(2)-EPs in gynecological cancers. *Arch Gynecol Obstet*. (2020) 301:1365–75. doi: 10.1007/s00404-020-05559-6

31. Lai ZZ, Yang HL, Ha SY, Chang KK, Mei J, Zhou WJ, et al. Cyclooxygenase-2 in endometriosis. *Int J Biol Sci*. (2019) 15:2783–97. doi: 10.7150/ijbs.35128

32. Sato N, Yako Y, Maruyama T, Ishikawa S, Kuromiya K, Tokuoka SM, et al. The COX-2/PGE(2) pathway suppresses apical elimination of RasV12-transformed cells from epithelia. *Commun Biol*. (2020) 3:132. doi: 10.1038/s42003-020-0847-y

33. Kajita S, Ruebel KH, Casey MB, Nakamura N, Lloyd RV. Role of COX-2, thromboxane A2 synthase, and prostaglandin I2 synthase in papillary thyroid carcinoma growth. *Modern Pathol*. (2005) 18:221–7. doi: 10.1038/modpathol.3800285

34. Hyde CA, Missailidis S. Inhibition of arachidonic acid metabolism and its implication on cell proliferation and tumour-angiogenesis. *Int Immunopharmacol*. (2009) 9:701–15. doi: 10.1016/j.intimp.2009.02.003

35. Xu L, Croix BS. Improving VEGF-targeted therapies through inhibition of COX-2/PGE2 signaling. *Mol Cell Oncol*. (2014) 1:e969154. doi: 10.4161/23723548.2014.969154

36. Cheng HW, Chen YF, Wong JM, Weng CW, Chen HY, Yu SL, et al. Cancer cells increase endothelial cell tube formation and survival by activating the PI3K/Akt signalling pathway. *J Exp Clin Cancer Res*. (2017) 36:27. doi: 10.1186/s13046-017-0495-3

37. Ghoneum A, Said N. PI3K-AKT-mTOR and NFκB pathways in ovarian cancer: implications for targeted therapeutics. *Cancers (Basel)*. (2019) 11(7):949. doi: 10.3390/cancers11070949

38. Liu L, Wu N, Wang Y, Zhang X, Xia B, Tang J, et al. TRPM7 promotes the epithelial-mesenchymal transition in ovarian cancer through the calcium-related PI3K / AKT oncogenic signaling. *J Exp Clin Cancer Res*. (2019) 38:106. doi: 10.1186/s13046-019-1061-y

39. Joki T, Heese O, Nikas DC, Bello L, Zhang J, Kraeft SK, et al. Expression of cyclooxygenase 2 (COX-2) in human glioma and in vitro inhibition by a specific COX-2 inhibitor, NS-398. *Cancer Res*. (2000) 60:4926–31.

40. Zhang X, Qu P, Zhao H, Zhao T, Cao N. COX−2 promotes epithelial −mesenchymal transition and migration in osteosarcoma MG−63 cells via PI3K/AKT/NF−κB signaling. *Mol Med Rep*. (2019) 20:3811–9. doi: 10.3892/mmr

41. Seo JM, Park S, Kim JH. Leukotriene B4 receptor-2 promotes invasiveness and metastasis of ovarian cancer cells through signal transducer and activator of transcription 3 (STAT3)-dependent up-regulation of matrix metalloproteinase 2. *J Biol Chem*. (2012) 287:13840–9. doi: 10.1074/jbc.M111.317131

42. Gómez-Valenzuela F, Wichmann I, Suárez F, Kato S, Ossandón E, Hermoso M, et al. Cyclooxygenase-2 Blockade Is Crucial to Restore Natural Killer Cell Activity before Anti-CTLA-4 Therapy against High-Grade Serous Ovarian Cancer. *Cancers (Basel)*. (2023) 16(1):80. doi: 10.3390/cancers16010080

43. Frejborg E, Salo T, Salem A. Role of cyclooxygenase-2 in head and neck tumorigenesis. *Int J Mol Sci*. (2020) 21(23):9246. doi: 10.3390/ijms21239246

44. Hada M, Edin ML, Hartge P, Lih FB, Wentzensen N, Zeldin DC, et al. Prediagnostic serum levels of fatty acid metabolites and risk of ovarian cancer in the prostate, lung, colorectal, and ovarian (PLCO) cancer screening trial. *Cancer Epidemiol Biomarkers Prev*. (2019) 28:189–97. doi: 10.1158/1055-9965.EPI-18-0392

45. Korbecki J, Rębacz-Maron E, Kupnicka P, Chlubek D, Baranowska-Bosiacka I. Synthesis and significance of arachidonic acid, a substrate for cyclooxygenases, lipoxygenases, and cytochrome P450 pathways in the tumorigenesis of glioblastoma multiforme, including a pan-cancer comparative analysis. *Cancers (Basel)*. (2023) 15 (3):946. doi: 10.3390/cancers15030946

46. Xia C, Sadeghi L, Strååt K, Merrien M, Wright AP, Sander B, et al. Intrinsic 5-lipoxygenase activity regulates migration and adherence of mantle cell lymphoma cells. *Prostaglandins Other Lipid Mediat*. (2021) 156:106575. doi: 10.1016/j.prostaglandins.2021.106575

47. Smith PG, Roque D, Ching MM, Fulton A, Rao G, Reader JC. The role of eicosanoids in gynecological Malignancies. *Front Pharmacol*. (2020) 11:1233. doi: 10.3389/fphar.2020.01233

48. Moore GY, Pidgeon GP. Cross-talk between cancer cells and the tumour microenvironment: the role of the 5-lipoxygenase pathway. *Int J Mol Sci*. (2017) 18 (2):236. doi: 10.3390/ijms18020236

49. Poczobutt JM, Nguyen TT, Hanson D, Li H, Sippel TR, Weiser-Evans MCM, et al. Deletion of 5-lipoxygenase in the tumor microenvironment promotes lung cancer progression and metastasis through regulating T cell recruitment. *J Immunol*. (2016) 196:891–901. doi: 10.4049/jimmunol.1501648

50. Yang P, Cartwright CA, Li J, Wen S, Prokhorova IN, Shureiqi I, et al. Arachidonic acid metabolism in human prostate cancer. *Int J Oncol*. (2012) 41:1495–503. doi: 10.3892/ijo.2012.1588

51. Liu Q, Tan W, Che J, Yuan D, Zhang L, Sun Y, et al. 12-HETE facilitates cell survival by activating the integrin-linked kinase/NF-κB pathway in ovarian cancer. *Cancer Manage Res*. (2018) 10:5825–38. doi: 10.2147/CMAR.S180334

52. Wasilewicz MP, Kołodziej B, Bojułko T, Kaczmarczyk M, Sulzyc-Bielicka V, Bielicki D, et al. Overexpression of 5-lipoxygenase in sporadic colonic adenomas and a possible new aspect of colon carcinogenesis. *Int J Colorectal Dis*. (2010) 25:1079–85. doi: 10.1007/s00384-010-0980-z

53. Bishayee K, Khuda-Bukhsh AR. 5-lipoxygenase antagonist therapy: a new approach towards targeted cancer chemotherapy. *Acta Biochim Biophys Sin (Shanghai)*. (2013) 45:709–19. doi: 10.1093/abbs/gmt064

54. Alzahrani AM, Rajendran P. The multifarious link between cytochrome P450s and cancer. *Oxid Med Cell Longev*. (2020) 2020:3028387. doi: 10.1155/2020/3028387

55. Elfaki I, Mir R, Almutairi FM, Duhier FMA. Cytochrome P450: polymorphisms and roles in cancer, diabetes and atherosclerosis. *Asian Pac J Cancer Prev*. (2018) 19:2057–70. doi: 10.22034/APJCP.2018.19.8.2057

56. Shi Z, He Z, Wang DW. CYP450 epoxygenase metabolites, epoxyeicosatrienoic acids, as novel anti-inflammatory mediators. *Molecules*. (2022) 27(12):3873. doi: 10.3390/molecules27123873

57. Reddy KK, Vidya Rajan VK, Gupta A, Aparoy P, Reddanna P. Exploration of binding site pattern in arachidonic acid metabolizing enzymes, Cyclooxygenases and Lipoxygenases. *BMC Res Notes*. (2015) 8:152. doi: 10.1186/s13104-015-1101-4

58. Kim HS, Moon SJ, Lee SE, Hwang GW, Yoo HJ, Song JW. The arachidonic acid metabolite 11,12-epoxyeicosatrienoic acid alleviates pulmonary fibrosis. *Exp Mol Med*. (2021) 53:864–74. doi: 10.1038/s12276-021-00618-7

59. Zhang Z, Hu D, Zhou M, Liu H, Wu J, Huang S, et al. 14,15-Epoxyeicosatrienoic acid induces the proliferation and anti- apoptosis of human carcinoma cell. *Daru*. (2011) 19:462–8.

60. Rand AA, Barnych B, Morisseau C, Cajka T, Lee KSS, Panigrahy D, et al. Cyclooxygenase-derived proangiogenic metabolites of epoxyeicosatrienoic acids. *Proc Natl Acad Sci*. (2017) 114:4370–5. doi: 10.1073/pnas.1616893114

61. Wang F, Chen J, Wang L, Ma Y, Mayinuer N. CYP1A1 genetic polymorphisms and uterine leiomyoma risk: a meta-analysis. *Int J Clin Exp Med*. (2015) 8:3590–4.

62. Bozina N, Bradamante V, Lovrić M. Genetic polymorphism of metabolic enzymes P450 (CYP) as a susceptibility factor for drug response, toxicity, and cancer risk. *Arh Hig Rada Toksikol*. (2009) 60:217–42. doi: 10.2478/10004-1254-60-2009-1885

63. Androutsopoulos VP, Tsatsakis AM, Spandidos DA. Cytochrome P450 CYP1A1: wider roles in cancer progression and prevention. *BMC Cancer*. (2009) 9:187. doi: 10.1186/1471-2407-9-187

64. Al-Saraireh YM, Alshammari F, Abu-Azzam OH, Al-Dalain SM, Al-Sarayra YM, Haddad M, et al. Targeting cytochrome P450 enzymes in ovarian cancers: new approaches to tumor-selective intervention. *Biomedicines*. (2023) 11(11):2898. doi: 10.20944/preprints202309.0152.v1

65. Ding Y, Zhuang S, Li Y, Yu X, Lu M, Ding N. Hypoxia-induced HIF1α dependent COX2 promotes ovarian cancer progress. *J Bioenergetics Biomembranes*. (2021) 53:441–8. doi: 10.1007/s10863-021-09900-9

66. Sun H, Zhang X, Sun D, Jia X, Xu L, Qiao Y, et al. COX-2 expression in ovarian cancer: an updated meta-analysis. *Oncotarget*. (2017) 8:88152–62. doi: 10.18632/oncotarget.v8i50

67. Song JH, Lee CJ, An HJ, Yoo SM, Kang HC, Lee JY, et al. Magnolin targeting of ERK1/2 inhibits cell proliferation and colony growth by induction of cellular senescence in ovarian cancer cells. *Mol Carcinog*. (2019) 58:88–101. doi: 10.1002/mc.22909

68. Song G, Cai QF, Mao YB, Ming YL, Bao SD, Ouyang GL. Osteopontin promotes ovarian cancer progression and cell survival and increases HIF-1alpha expression through the PI3-K/Akt pathway. *Cancer Sci*. (2008) 99:1901–7. doi: 10.1111/j.1349-7006.2008.00911.x

69. Liu Q, Tan W, Che J, Yuan D, Zhang L, Sun Y, et al. 12-HETE facilitates cell survival by activating the integrin-linked kinase/NF-κB pathway in ovarian cancer. *Cancer Manag Res*. (2018) 10:5825–38. doi: 10.2147/CMAR

70. Zheng Z, Li Y, Jin G, Huang T, Zou M, Duan S. The biological role of arachidonic acid 12-lipoxygenase (ALOX12) in various human diseases. *BioMed Pharmacother*. (2020) 129:110354. doi: 10.1016/j.biopha.2020.110354

71. Guo AM, Liu X, Al-Wahab Z, Maddippati KR, Ali-Fehmi R, Scicli AG, et al. Role of 12-lipoxygenase in regulation of ovarian cancer cell proliferation and survival. *Cancer Chemother Pharmacol*. (2011) 68:1273–83. doi: 10.1007/s00280-011-1595-y

72. Chistyakov DV, Kovalenko LV, Donnikov MY, Sergeeva MG. Blood oxylipin profiles as markers of oncological diseases. *Biochem (Moscow)*. (2023) 88:621–9. doi: 10.1134/S000629792305005X

73. Gréen H, Khan MS, Jakobsen-Falk I, Åvall-Lundqvist E, Peterson C. Impact of CYP3A5*3 and CYP2C8-HapC on paclitaxel/carboplatin-induced myelosuppression in patients with ovarian cancer. *J Pharm Sci*. (2011) 100:4205–9. doi: 10.1002/jps.22680

74. van Eijk M, Boosman RJ, Schinkel AH, Huitema ADR, Beijnen JH. Cytochrome P450 3A4, 3A5, and 2C8 expression in breast, prostate, lung, endometrial, and ovarian tumors: relevance for resistance to taxanes. *Cancer Chemother Pharmacol*. (2019) 84:487–99. doi: 10.1007/s00280-019-03905-3

75. Schoutrop E, Moyano-Galceran L, Lheureux S, Mattsson J, Lehti K, Dahlstrand H, et al. Molecular, cellular and systemic aspects of epithelial ovarian cancer and its tumor microenvironment. *Semin Cancer Biol*. (2022) 86:207–23. doi: 10.1016/j.semcancer.2022.03.027

76. Dietze R, Hammoud MK, Gomez-Serrano M, Unger A, Bieringer T, Finkernagel F, et al. Phosphoproteomics identify arachidonic-acid-regulated signal transduction pathways modulating macrophage functions with implications for ovarian cancer. *Theranostics*. (2021) 11:1377–95. doi: 10.7150/thno.52442

77. Bamias A, Koutsoukou V, Terpos E, Tsiatas ML, Liakos C, Tsitsilonis O, et al. Correlation of NK T-like CD3+CD56+ cells and CD4+CD25+(hi) regulatory T cells with VEGF and TNFalpha in ascites from advanced ovarian cancer: Association with platinum resistance and prognosis in patients receiving first-line, platinum-based chemotherapy. *Gynecol Oncol*. (2008) 108:421–7. doi: 10.1016/j.ygyno.2007.10.018

78. Hammoud MK, Dietze R, Pesek J, Finkernagel F, Unger A, Bieringer T, et al. Arachidonic acid, a clinically adverse mediator in the ovarian cancer microenvironment, impairs JAK-STAT signaling in macrophages by perturbing lipid raft structures. *Mol Oncol*. (2022) 16:3146–66. doi: 10.1002/1878-0261.13221

79. Nowak M, Klink M. The role of tumor-associated macrophages in the progression and chemoresistance of ovarian cancer. *Cells*. (2020) 9(5):1299. doi: 10.3390/cells9051299

80. Guo Z, Huang J, Huo X, Huang C, Yu X, Sun Y, et al. Targeting LTA4H facilitates the reshaping of the immune microenvironment mediated by CCL5 and sensitizes ovarian cancer to Cisplatin. *Sci China Life Sci*. (2024). doi: 10.1007/s11427-023-2444-5

81. Sørensen BH, Thorsteinsdottir UA, Lambert IH. Acquired cisplatin resistance in human ovarian A2780 cancer cells correlates with shift in taurine homeostasis and ability to volume regulate. *Am J Physiology-Cell Physiol*. (2014) 307:C1071–80. doi: 10.1152/ajpcell.00274.2014

82. Zhang Q, Yan G, Lei J, Chen Y, Wang T, Gong J, et al. The SP1-12LOX axis promotes chemoresistance and metastasis of ovarian cancer. *Mol Med*. (2020) 26:39. doi: 10.1186/s10020-020-00174-2

83. Li W, Wan L, Zhai LY, Wang J. Effects of SC-560 in combination with cisplatin or taxol on angiogenesis in human ovarian cancer xenografts. *Int J Mol Sci*. (2014) 15:19265–80. doi: 10.3390/ijms151019265

84. Spyra S, Meisner A, Schaefer M, Hill K. COX-2-selective inhibitors celecoxib and deracoxib modulate transient receptor potential vanilloid 3 channels. *Br J Pharmacol*. (2017) 174:2696–705. doi: 10.1111/bph.13893

85. Capdevila JH, Wang W, Falck JR. Arachidonic acid monooxygenase: Genetic and biochemical approaches to physiological/pathophysiological relevance. *Prostaglandins Other Lipid Mediat*. (2015) 120:40–9. doi: 10.1016/j.prostaglandins.2015.05.004

86. Chen L, Ackerman R, Saleh M, Gotlinger KH, Kessler M, Mendelowitz LG, et al. 20-HETE regulates the angiogenic functions of human endothelial progenitor cells and contributes to angiogenesis in vivo. *J Pharmacol Exp Ther*. (2014) 348:442–51. doi: 10.1124/jpet.113.210120

87. Pascale JV, Wolf A, Kadish Y, Diegisser D, Kulaprathazhe MM, Yemane D, et al. 20-Hydroxyeicosatetraenoic acid (20-HETE): Bioactions, receptors, vascular function, cardiometabolic disease and beyond. *Adv Pharmacol*. (2023) 97:229–55. doi: 10.1016/bs.apha.2023.01.002

88. Borin T, Angara K, Rashid M, Achyut B, Arbab A. Arachidonic acid metabolite as a novel therapeutic target in breast cancer metastasis. *Int J Mol Sci*. (2017) 18(12):2661. doi: 10.3390/ijms18122661

89. Zhao Y, Cui L, Pan Y, Shao D, Zheng X, Zhang F, et al. Berberine inhibits the chemotherapy-induced repopulation by suppressing the arachidonic acid metabolic pathway and phosphorylation of FAK in ovarian cancer. *Cell Prolif*. (2017) 50(6):e12393. doi: 10.1111/cpr.12393

90. Liu L, Fan J, Ai G, Liu J, Luo N, Li C, et al. Berberine in combination with cisplatin induces necroptosis and apoptosis in ovarian cancer cells. *Biol Res*. (2019) 52:37. doi: 10.1186/s40659-019-0243-6

91. Oktem EK, Aydin B, Gulfidan G, Arga KY. A transcriptomic and reverse-engineering strategy reveals molecular signatures of arachidonic acid metabolism in 12 cancers. *OMICS: A J Integr Biol*. (2023) 27:127–38. doi: 10.1089/omi.2022.0185

frontiers | Frontiers in Oncology

TYPE Original Research
PUBLISHED 01 July 2024
DOI 10.3389/fonc.2024.1359839

OPEN ACCESS

EDITED BY
Parmanand Malvi,
University of Alabama at Birmingham, United States

REVIEWED BY
Navneet Kaur,
Yale University, United States
Ashish Toshniwal,
The University of Utah, United States

*CORRESPONDENCE
Zhimin Fan
fanzm@jlu.edu.cn
Fengjiang Qu
qufengjiang@jlu.edu.cn

RECEIVED 22 December 2023
ACCEPTED 11 June 2024
PUBLISHED 01 July 2024

CITATION
Li G, Yin M, Fan Z and Qu F (2024) Correlation between fasting blood glucose level and risk of breast cancer in women: a single-center, prospective cohort study. *Front. Oncol.* 14:1359839. doi: 10.3389/fonc.2024.1359839

Correlation between fasting blood glucose level and risk of breast cancer in women: a single-center, prospective cohort study

Gefei Li[1], Mingjie Yin[2], Zhimin Fan[1]* and Fengjiang Qu[3]*

[1]Department of Breast Surgery, General Surgery Center, The First Hospital of Jilin University, Xinmin, Changchun, Jilin, China, [2]Tangshan Workers' Hospital Affiliated to Hebei Medical University, Wenhua, Tangshan, Hebei, China, [3]Department of Emergency Surgery, The First Hospital of Jilin University, Xinmin, Changchun, Jilin, China

Purpose: We prospectively analyzed the correlation between fasting plasma glucose (FPG) and the risk of breast cancer in women; explored the independent risk factors for breast cancer in women, and compared the effect of FPG level on the risk of young and non-young breast cancer. Our study provides new evidence and ideas for research into breast cancer etiology in China, improves the accuracy of secondary prevention of breast cancer, and provides options for the clinical diagnosis and treatment of breast cancer patients with diabetes.

Materials and methods: Three cohorts of women participating in the first health examination of the Kailuan Group in 2006, 2008 and 2010 were assembled to conduct a descriptive analysis of the baseline data on FPG. The cumulative incidence of breast cancer in different groups over 13 years was calculated using the Kaplan-Meier method and groups were compared using the log-rank test. A Cox proportional hazards regression model was used to analyze the association between FPG level and the risk of breast cancer.

Results: The cumulative incidence of breast cancer increased in people with FPG higher than 5.29 mmol/L, but there was no significant difference in the effect of different levels of FPG on the risk of young breast cancer in the population. Different degrees of fasting glucose can affect the risk of non-young breast cancer in the population.

Conclusion: The results of this study suggest that the risk of breast cancer can be reversed by early intervention to control levels of FPG. Regular monitoring of FPG may reduce the misdiagnosis rate of breast cancer in the population.

KEYWORDS

breast cancer, fasting blood glucose, TyG index, prospective cohort, young breast cancer

1 Background

As the "first killer" of women's physical health, the risk factors for the occurrence and development of breast cancer have always held the attention of investigators. The occurrence of malignant tumors in women is the result of various risk factors, one of which is elevated fasting blood glucose (fasting plasma glucose, FPG), which has been found to be a high-risk factor for the occurrence and development of malignant tumors (1–4). There is a linear correlation between elevated FPG levels and the risk of breast cancer (5–7). In addition, high levels of FPG also increase the risk of postoperative recurrence (8) and distant metastasis in women (9), and they significantly affect the efficacy of postoperative chemotherapy in breast cancer patients (10). Meanwhile, a high level of the triglyceride-glucose index (TyG) is an independent risk factor for type 2 diabetes, and indirectly may also be one of the potential risk factors for breast cancer. At present, research concerning FPG and the cumulative incidence of female breast cancer is still incomplete, as there are few comparative studies on the cumulative incidence of young and non-young breast cancer; furthermore, the conclusions of these studies are not consistent, requiring further data support. The present study aims to prospectively explore the cumulative risk for breast cancer caused by elevated FPG, covering a follow-up period of 13 years. Moreover, we sought to determine if controlling blood sugar may help prevent breast cancer and lower recurrence and metastasis measures (11, 12). We further examined whether timely detection of FPG and regular physical examinations can improve the detection rate of female breast cancer and increase secondary prevention of breast cancer. Finally, we studied the relationship between the diabetes and breast cancer treatment, which may provide perspective for the clinical diagnosis and treatment of diabetic breast cancer patients.

2 Research method

2.1 Study participants and subgroups

We selected women who participated in the first physical examination of the Kailuan Group in 2006, 2008 and 2010. Patients with abnormal FPG caused by various factors were excluded (see Figure 1).

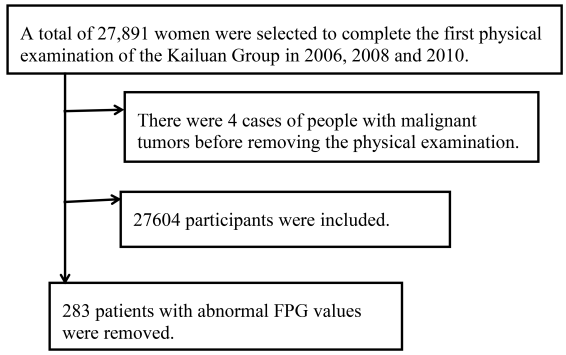

FIGURE 1
Inclusion and exclusion flowchart.

Based on the large number of single-center clinical studies at home and abroad, the participants were divided into three groups according to FPG levels: Q1 (fasting glucose <4.72 mmol/L); Q2 (fasting glucose 4.72–5.29 mmol/L) and Q3 (fasting glucose >5.29 mmol/L). In addition, based on the TyG index, the participants were also divided into three groups: W1 group: TyG index <8.17 mg/dl; W2 group: TyG index 8.17 mg/dl–8.70 mg/dl; and W3 group: TyG index >8.70 mg/dl.

2.2 Data collection

Epidemiological data collected included demographic data (age, gender), health behavioral habits (smoking, alcohol consumption, physical exercise, salt intake), anthropometric indicators (height, weight, systolic and diastolic blood pressure), and blood biochemical indicators, including FPG, triglycerides, total cholesterol, high-density lipoprotein cholesterol, and low-density lipoprotein cholesterol.

2.3 Relevant definitions

TyG index = Ln (fasting blood glucose * triglycerides/2) in mg/dl. Waist-to-hip ratio = waist/hip circumference. Smoking: average numbers of cigarettes per day in the previous year. Alcohol consumption: in the previous 1 year, women drank on average one standard alcohol drink/day (consisting of 100 g beer alcohol, 5.0 g alcohol; 100 g wine alcohol, 12.0 g; 100 g liquor alcohol, 40.0 g, 1 standard alcohol 14.0 g). Regular physical exercise was defined as exercise three times per week for at least 30 min duration. Salt intake: light daily intake of sodium chloride, <6 g; normal daily intake of sodium chloride, 6–10 g; heavy daily intake of sodium chloride, >10 g. Young breast cancer: breast cancer with an age of onset <35 years of age; non-young breast cancer: ≥35 years (13).

2.4 Follow-up starting point and endpoint events

The completion of the first health examination of the Kailuan Group in 2006, 2008 or 2010 was adopted as the starting point of the follow-up, while the endpoint event was breast cancer occurring during the follow-up period. The definition and diagnostic criteria were adopted from the World Health Organization criteria, namely, the National Comprehensive Cancer Network guidelines. The time of the starting point event and endpoint event were recorded, with the endpoint event occurring no later than December 31, 2020. If the participant did not have an endpoint event but died during the follow-up period, the time of death was considered the end of follow-up.

2.5 Statistical methods

For descriptive analysis of baseline data of study participants, normal measurement data were expressed as means ± standard

deviation (x ± s) for variance analysis; as medians (M [P25, P75]) for Kruskal-Wallis rank-sum tests for group comparisons; count data were expressed by n (%); and comparisons between groups (2 test). Missing values of covariates were filled by multiple interpolation.

The cumulative incidence of breast cancer in different groups was calculated using the Kaplan-Meier method and compared using the log-rank test. The Cox proportional hazards regression model was used to analyze the association of FPG levels with the risk of breast cancer disease. To test the stability of the results, we performed a sensitivity analysis, using the Cox proportional hazards regression model to analyze the role of the TyG index on the risk of breast cancer disease. Two-sided tests at $P < 0.05$ were considered to indicate statistically significant differences.

3 Results

3.1 Comparison of baseline data on breast cancer disease in different groups

In the study population of 27,604 women, the mean age was 47.53 ± 11.95 years. Compared with the Q1 group, age, triglycerides, total cholesterol, LDL cholesterol, systolic blood pressure, diastolic blood pressure, alcohol consumption and the smoking rate were higher in the Q2 group, while measures of HDL cholesterol, physical exercise frequency and salt intake was lower in the Q2 vs Q1 group. Compared with the Q1 group, age, triglycerides, total cholesterol, LDL cholesterol, systolic BP, diastolic blood pressure, smoking rate, and physical exercise frequency were higher in the Q3 group, while measures of HDL cholesterol, alcohol consumption and salt intake were lower (see Table 1 for details).

3.2 Cumulative incidence and incidence density of breast cancer disease in different groups

During the mean follow-up period of 12.90 ± 2.03 years, 375 of the participants included in the study developed breast cancer during the follow-up period. The cumulative incidence of breast cancer in the three groups was 1.20% (103/9,091), 1.53% (126/9,243) and 1.70% (146/9,270) in groups Q1, Q2 and Q3, respectively, ($\chi 2 = 7.65$, $P = 0.02$, see Table 2 and Figure 2). The incidence density was 0.87/thousand, 1.06/thousand and 1.24/thousand in groups Q1, Q2 and Q3, respectively (see Table 2 for details).

3.3 Multivariate Cox regression analysis of the effect of participant groups on disease risk of breast cancer

In the entire population, the Q2 and Q3 groups had hazard ratios (HR) of 1.21 (95% confidence interval [CI]: 0.93–1.57) and 1.30 (95% CI: 1.00–1.68; (see Table 3 for details).

3.4 Multivariate Cox regression analysis of the effect of FPG on disease risk of young and non-young breast cancer

The risk of young breast cancer (age of onset of breast cancer <35 years) was not significantly correlated with FPG. For the population with non-young breast cancer (>=35 years), the risk of breast cancer was significantly increased in the Q2 and Q3 groups

TABLE 1 Baseline data (N = 27,604).

Variable	Q1	Q2	Q3	F/χ^2 rate	P rate
Age ($\bar{x}$± s, year)	45.82 ± 12.53	45.99 ± 11.96	50.74 ± 11.35	503.62	<0.01
Waist-to-hipratio ($\bar{x}$ ± s)	0.86 ± 0.08	0.86 ± 0.08	0.87 ± 0.08	132.95	<0.01
Fasting blood-glucose ($\bar{x}$± s, mmol/L)	4.32 ± 0.33	4.99 ± 0.16	6.57 ± 2.14	7,818.21	<0.01
Glycerin trilaurate [M (P_{25}, P_{75}), mmol/L]	1.03 (0.72, 1.50)	1.07 (0.75, 1.55)	1.34 (0.93, 1.99)	1,097.63	<0.01
Cholesterol total ($\bar{x}$ ± s, mmol/L)	4.78 ± 1.04	4.87 ± 1.02	5.12 ± 1.14	247.02	<0.01
High density lipoprotein cholesterol ($\bar{x}$ ± s, mmol/L)	1.59 ± 0.47	1.55 ± 0.38	1.57 ± 0.43	15.76	<0.01
Low density lipoprotein cholesterol [M (P_{25}, P_{75}), mmol/L]	2.09 (1.60, 2.65)	2.23 (1.74, 2.78)	2.44 (1.92, 3.02)	816.88	<0.01
Systolic pressure ($\bar{x}$ ± s, mmHg)	119.16 ± 19.79	120.66 ± 19.47	129.00 ± 21.76	624.69	<0.01
Diastolic pressure ($\bar{x}$ ± s, mmHg)	77.16 ± 10.78	78.01 ± 10.65	81.56 ± 11.13	426.72	<0.01
Smoke [n (%)]	172 (1.89)	158 (1.71)	192 (2.07)	3.27	<0.01
Drink [n (%)]	601 (6.61)	630 (6.82)	517 (5.58)	13.75	<0.01
Do physical exercise regularly [n (%)]	1,199 (13.19)	1,048 (11.34)	1,407 (15.18)	59.44	<0.01
Salt habit the taste is light [n (%)]	1,036 (11.40)	974 (10.54)	1,012 (10.92)	10.33	<0.01

TABLE 2 Cumulative incidence and incidence density of breast cancer disease among different participant groups.

Groups	Number of incident cases/ total number	Disease onset density (/thousand person-years)	Cumulative incidence rate (%)	P rate
Breast cancer disease				
Q1	103/9,091	0.87	1.20	0.01
Q2	126/9,243	1.06	1.53	
Q3	146/9,270	1.24	1.70	

compared with the Q1 group, with HR values of 1.21 (95% CI: 0.92–1.59) and 1.28 (95% CI: 0.98–1.67, respectively; see Table 4 for details).

3.5 Sensitivity analysis: multivariate Cox regression analysis of the effect of TyG index on disease risk in breast cancer

Compared with the W1 group, the HRs for the W2 and W3 groups were 1.19 (95% CI: 0.91–1.55) and 1.21 (95% CI: 0.91–1.60), respectively; see Table 5.

4 Discussion

According to the latest statistics from the World Health Organization, breast cancer has become the most frequent malignant tumor in the world (14), which seriously damages the physical and mental health of women and places a great burden due to its social and economic aspects. Therefore, the exploration of risk factors for breast cancer and secondary prevention strategies for early intervention have received increasing attention. The latest research has shown that FPG level is closely related to the onset and prognosis of breast cancer. In our study, women with healthy physical examinations were classified according to FPG values. After follow-up, it was found that the incidence and density of breast cancer were positively associated with FPG levels. Multivariate analysis showed that elevated FPG was a risk factor for breast cancer. At the molecular level, hyperglycemia glycosylates protein structures non-enzymatically and promotes the production of various factors which affect the growth of tumor cells. Hyperglycemia can also activate the polyol pathway by increasing the expression and activity of aldose reductase, which subsequently increases the metabolic activity of breast cancer cells. In the process of catabolism, sugar produces reactive oxygen clusters such as superoxide anions which aggravate the oxygen stress in tumor cells, causing the obstruction or disorder of cell DNA and enzyme synthesis, thus inducing carcinogenesis and promoting the occurrence and development of breast cancer through a variety of pathways. In breast cancer cells, insulin-like growth factor (IGF)-I and IGF-II exert biological activity mainly through the IGF-1 receptor. After ligand and receptor binding, the IGFs exert antiproliferation and pro-phosphorylation effects on specific binding proteins and reduce their binding to the IGF-I receptor, thus promoting breast cancer development. It is well known that the specific components of the IGF system are ubiquitous, and the interference or disruption of any link in this system may cause growth retardation, atherosclerosis, insulin resistance and even cancer. Influencing mechanisms may involve

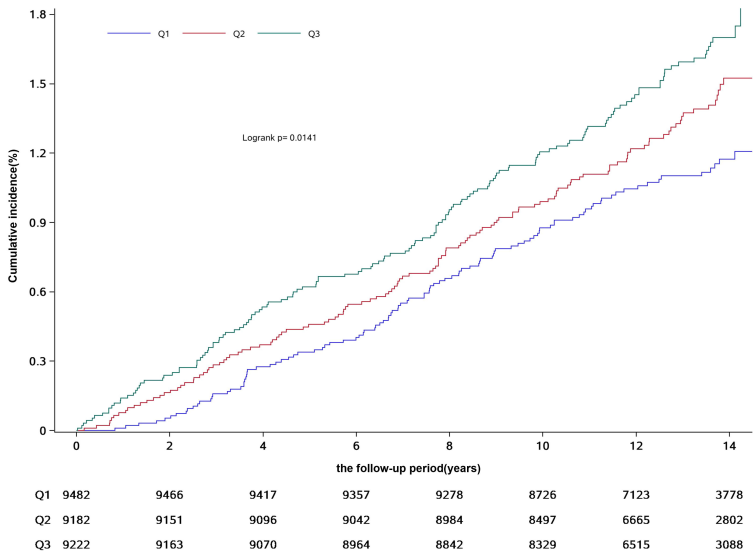

FIGURE 2
Cumulative incidence of breast cancer in participants from different groups.

TABLE 3 Multivariate Cox regression analysis of the effect of FPG on the risk of breast cancer.

Groups	Model 1		Model 2	
	HR rate (95% CI)	P rate	HR rate (95% CI)	P rate
The whole crowd (n = 27,604)				
Triple tile of fasting blood glucose				
Q1	1		1	
Q2	1.22 (0.94, 1.58)	0.14	1.21 (0.93, 1.57)	0.15
Q3	1.32 (1.03, 1.71)	0.03	1.30 (1.00, 1.68)	0.05
	P for trend = 0.03		P for trend = 0.05	
For every 1 mmol/L increase in fasting blood glucose	1.03 (0.98, 1.09)	0.26	1.03 (0.97, 1.09)	0.40
For every 1 standard deviation increase in fasting blood glucose[a]	1.05 (0.96, 1.15)	0.26	1.04 (0.95, 1.14)	0.40

Model 1 corrected for age; model 2 corrected for systolic blood pressure, waist-hip ratio <0.8 or waist-hip ratio = 0.8), triglycerides, total cholesterol, frequency of physical exercise (infrequent or frequent), smoking (yes or no), alcohol consumption (yes or no), and salt intake (light or moderate). [a]1.57.

insulin, IGF-1, insulin resistance (15, 16), endogenous hormones (17), leptin (18), adiponectin (19), inflammatory factors and other factors. Moreover, both Chinese and international researchers have found that FPG level is closely related to the efficacy of breast cancer and systemic therapy, metastasis and death risk (20–23). Nevertheless, the long-term impact of FPG on breast cancer risk and the specific biological mechanism need further analysis.

We divided the breast cancer study population into young and non-young breast cancer cohorts according to the age of onset, then performed Cox regression analysis based on FPG levels. The results suggest that FPG levels are not a risk factor for young breast cancer, which may be due to the relatively small population base in the young group, leading to some bias. The psychological neglect of malignant tumor diseases in young people may also reduce the diagnosis rate. Breast cancer is also associated with individual differences in diet and exercise habits and family history (24, 25). For patients with non-young breast cancer, FPG levels are a high-risk factor for morbidity, and for every 1 mmol/L increase in FPG, the risk increases (26). The average age of abnormal glucose metabolism is between 40 and 50 years (27), while the average

TABLE 4 Multivariate Cox regression analysis of the effect of FPG on the risk of early-onset and late-onset breast cancer.

Groups	Model 1 (age)		Model 2 (Others)	
	HR rate (95% CI)	P rate	HR rate (95% CI)	P rate
Early onset breast cancer				
Q1	1		1	
Q2	0.92 (0.33, 2.55)	0.88	0.90 (0.33, 2.50)	0.84
Q3	1.04 (0.31, 3.46)	0.95	0.96 (0.28, 3.27)	0.94
	P for trend = 0.99		P for trend = 0.91	
For every 1 mmol/L increase in fasting blood glucose	0.98 (0.49, 1.95)	0.95	0.92 (0.46, 1.87)	0.83
For every 1 standard deviation increase in fasting blood glucose[a]	0.99 (0.64, 1.52)	0.95	0.95 (0.61, 1.48)	0.83
Late onset breast cancer				
Q1	1		1	
Q2	1.22 (0.93, 1.59)	0.16	1.21 (0.92, 1.59)	0.17
Q3	1.30 (1.00, 1.69)	0.05	1.28 (0.98, 1.67)	0.07
	P for trend = 0.05		P for trend = 0.07	
For every 1 mmol/L increase in fasting blood glucose	1.03 (0.97, 1.09)	0.29	1.02 (0.97, 1.09)	0.43
For every 1 standard deviation increase in fasting blood glucose[b]	1.05 (0.96, 1.16)	0.29	1.04 (0.94, 1.15)	0.43

Model 1 corrected for age; model 2 corrected for systolic blood pressure, waist-hip ratio (<0.8 or ≥0.8), triglycerides, total cholesterol, frequency of physical exercise (infrequent or frequent), smoking (yes or no), alcohol consumption (yes or no), and salt intake (light or moderate). [a]0.63, [b]1.68.

TABLE 5 Multivariate Cox regression analysis of the effect of TyG index on disease risk in breast cancer.

Groups	Model 1 (age)		Model 2 (Others)	
	HR rate (95% CI)	P rate	HR rate (95% CI)	P rate
Breast cancer disease				
W1	1		1	
W2	1.19 (0.91,1.55)	0.21	1.19 (0.91,1.55)	0.21
W3	1.20 (0.91,1.57)	0.19	1.21 (0.91,1.60)	0.19
	P for trend=0.21		P for trend=0.21	
For every 1 mmol/L increase in TyG indexC	1.14 (0.98,1.33)	0.1	1.15 (0.98,1.36)	0.09
For every 1 mmol/L increase in TyG index[d]	1.09 (0.98,1.21)	0.1	1.10 (0.99,1.23)	0.09

Model 1 corrected for age; model 2 corrected for systolic blood pressure, waist-hip ratio (<0.8 or ≥0.8), triglycerides, total cholesterol, frequency of physical exercise (infrequent or frequent), smoking (yes or no), alcohol consumption (yes or no), and salt intake (light or moderate). [d]0.67.

age of early type II diabetes is around 33 (28), and studies have shown that the FPG level increases the risk of breast cancer (29). We can therefore conclude that routine testing of FPG in women aged 35 to 50 may be helpful for screening and early diagnosis and treatment of breast cancer.

The TyG index takes the logarithm of FPG and lipid indices and conducts multivariate analysis for the risk of breast cancer. Many domestic and foreign studies have shown that an elevated TyG index is independently associated with the increased risk of diabetes and cardiovascular disease in adults, indicating that it may be a reliable predictor of diabetes in high-risk groups (30–32). However, the results of the present study showed that the TyG index is not a risk factor for breast cancer, while FPG is a risk factor for the cumulative incidence of breast cancer. Therefore, we can infer that while blood lipids may affect the prognosis of breast cancer disease (33), they are not a risk factor for breast cancer development (34).

In conclusion, we found an increased cumulative incidence of breast cancer disease in people with high FPG but no significant difference in the effect of different FPG levels on the risk of young breast cancer among the population. It is rather a risk factor for non-young breast cancer.

Data availability statement

The original contributions presented in the study are included in the article/supplementary material. Further inquiries can be directed to the corresponding authors.

Ethics statement

The studies involving humans were approved by Kailuan LC Hospital Ethics Committee. The studies were conducted in accordance with the local legislation and institutional requirements. The participants provided their written informed consent to participate in this study.

Author contributions

GL: Writing – original draft, Writing – review & editing. MY: Writing – original draft, Writing – review & editing. ZF: Writing – original draft, Writing – review & editing. FQ: Writing – original draft, Writing – review & editing.

Funding

The author(s) declare that no financial support was received for the research, authorship, and/or publication of this article.

Conflict of interest

The authors declare that the research was conducted in the absence of any commercial or financial relationships that could be construed as a potential conflict of interest.

Publisher's note

References

1. Feng X. *A prospective cohort study of fasting blood glucose and the risk of Malignancy*. Peking Union Medical College: Chinese Academy of Medical Sciences (2020).

2. Xie Y. Exploring the relationship between serum tumor marker levels and fasting blood glucose and HbA hemoglobin in type 2 diabetes mellitus. *Diabetes New World*. (2020) 23(9):30–1, 34. doi: 10.16658/j.cnki.1672-4062.2020.09.030

3. Mubarik S, Cao J, Wang F, Hussain SR, Liu Q, Wang S, et al. Lifestyle and socioeconomic transition and health consequences of breast cancer in the East Asia region, from 1990 to 2019. *Front Nutr*. (2022) 9:817836. doi: 10.3389/fnut.2022.817836

4. Ge X, Hu J, Bai T, Lu W, Song L. A nested case-control study of the association between the triacylglycerol-glucose index and its derived index and the onset of type 2 diabetes mellitus. *Chin Gen Med*. (2023) 26(12):1456–62. doi: 10.12114/j.issn.1007-9572.2022.0737

5. Hu R, Pan J, Lu F, He Q, Cao N, Wang Y, et al. [Study on the relationship between level of glucose metabolism and risk of cancer incidents]. *Zhonghua Liu Xing Bing Xue Za Zhi*. (2014) 35(7):759–63. doi: 10.3760/cma.j.issn.0254-6450.2014.07.001

6. Zhang M, Cui Y, Wang C, Xu K, Xing J. Trend analysis of the disease burden and risk factors in Chinese women from 1990 to 2019. *Chin J Cancer Prev Treat*. (2022) 29 (7):456–62. doi: 10.16073/j.cnki.cjcpt.2022.07.02

7. Zhan YS, Feng L, Tang SH, Li WG, Xu M, Liu TF, et al. Glucose metabolism disorders in cancer patients in a Chinese population. *Med Oncol*. (2010) 27:177–84. doi: 10.1007/s12032-009-9189-9

8. Zhang R. Effect of elevated fasting blood glucose on breast cancer recurrence in women. *Hebei Med Univ*. (2016). doi: 10.7666/d.D845120

9. Liu Y, Liu B, He Y, Li Z, Li X, Wang D, et al. Analysis of risk factors related to breast cancer metastasis: A retrospective nested case-control study. *J BUON*. (2021) 26(4):1415–21.

10. Arici S, Geredeli C, Secmeler S, Cekin R, Sakin A, Cihan S. The effects of diabetes and fasting plasma glucose on treatment of breast cancer with neoadjuvant chemotherapy. *Curr Probl Cancer*. (2020) 44:100485. doi: 10.1016/j.currproblcancer.2019.05.007

11. Mubarik S, Liu X, Malik SS, Wang L, Yu Y, Yu C. Evaluation of lifestyle risk factor differences in global patterns of breast cancer mortality and DALYs during 1990–2017 using hierarchical age-period-cohort analysis. *Environ Sci pollut Res Int*. (2021) 28:49864–76. doi: 10.1007/s11356-021-14165-1

12. Li N, Deng Y, Zhou L, Tian T, Yang S, Wu Y, et al. Global burden of breast cancer and attributable risk factors in 195 countries and territories, from 1990 to 2017: Results from the Global Burden of Disease Study 2017. *J Hematol Oncol*. (2019) 12:140. doi: 10.1186/s13045-019-0828-0

13. Zhang B, Zhang Q, Sivasubramaniam PG, Gao J, Yi F, Xiang W, et al. Risk factors for young breast cancer in China-a multi-decade retrospective study. *Tumor China*. (2015) 24:1042–7. doi: 10.11735/j.issn.1004-0242.2015.12.A018

14. Johnson JA, Moore BJ, Syrnioti G, Eden CM, Wright D, Newman LA. Landmark series: The cancer genome atlas and the study of breast cancer disparities. *Ann Surg Oncol*. (2023) 30:6427–40. doi: 10.1245/s10434-023-13866-w

15. Pearson-Stuttard J, Papadimitriou N, Markozannes G, Cividini S, Kakourou A, Gill D, et al. Type 2 diabetes and cancer: An umbrella review of observational and Mendelian randomization studies. *Cancer Epidemiol Biomarkers Prev*. (2021) 30:1218–28. doi: 10.1158/1055-9965.EPI-20-1245

16. Contiero P, Berrino F, Tagliabue G, Mastroianni A, Di Mauro MG, Fabiano S, et al. Fasting blood glucose and long-term prognosis of non-metastatic breast cancer: A cohort study. *Breast Cancer Res Treat*. (2013) 138:951–9. doi: 10.1007/s10549-013-2519-9

17. Wang L, Ruan X. Progress in the relationship between hormonal therapy and the risk of developing breast cancer development. *China Med J*. (2018) 53(5):469–72. doi: 10.3969/j.issn.1008-1070.2018.05.002

18. Yi F, Diao S, Yuan X, Lijia Y. Correlation study of plasma leptin and soluble leptin receptor and breast cancer in women. *Chin J Prev Med*. (2018) 52:253–9. doi: 10.3760/cma.j.issn.0253-9624.2018.03.007

19. Hu H, Liu R, Sun R, Qi Q, Jiang L, Wang Y, et al. The relation between adiponectin and type 2 diabetic breast cancer and its mechanism study. *Chin J Diabetes*. (2021) 13:162–8. doi: 10.3760/cma.j.cn115791-20200706-00421

20. Minicozzi P, Berrino F, Sebastiani F, Falcini F, Vattiato R, Cioccoloni F, et al. High fasting blood glucose and obesity significantly and independently increase risk of breast cancer death in hormone receptor-positive disease. *Eur J Cancer*. (2013) 49:3881–8. doi: 10.1016/j.ejca.2013.08.004

21. Lu Y, Wang P, Lan N, Kong F, Abdumijit A, Tu S, et al. Metabolic syndrome predicts response to neoadjuvant chemotherapy in breast cancer. *Front Oncol*. (2022) 12:899335. doi: 10.3389/fonc.2022.899335

22. Isaac-Lam MF, DeMichael KM. Calorie restriction and breast cancer treatment: A mini-review. *J Mol Med (Berl)*. (2022) 100:1095–109. doi: 10.1007/s00109-022-02226-y

23. Liu W, Wang LJ, Qi JL, Liu JM, You JL, Lin L, et al. [Disease burden of breast cancer in women in China, 1990–2017]. *Zhonghua Liu Xing Bing Xue Za Zhi*. (2021) 42 (7):1225–30. doi: 10.3760/cma.j.cn112338-20200908-01139

24. Simões LMFR, Tavares NAR, Ferreira-Pêgo C. Plant-based diet and IGF-1 modulation on HER2-positive breast cancer: A lifestyle medicine nutrition approach in oncology. *Am J Lifestyle Med*. (2021) 16(1):36–45. doi: 10.1177/15598276211023048

25. Yuan S, Kar S, Carter P, Vithayathil M, Mason AM, Burgess S, et al. Is type 2 diabetes causally associated with cancer risk? Evidence from a two-sample Mendelian randomization study. *Diabetes*. (2020) 69:1588–96. doi: 10.2337/db20-0084

26. Ekinci O, Eren T, Kurtoglu Yakici M, Gapbarov A, Aydemir MA, Saglam ZA, et al. Relationship between metabolic syndrome and postmenopausal breast cancer. *Cir Esp (Engl Ed)*. (2020) 98:540–6. doi: 10.1016/j.cireng.2020.06.009

27. Gu J, Yu Z. (2010). Factors associated with abnormal glucose metabolism and breast cancer, in: *Proceedings of the 2010 National Academic Conference on Parenteral Nutrition*, (Hefei, Anhui, China.: Chinese Medical Association). pp. 245–50.

28. Yu H, Xie LF, Chen K, Yang GY, Xing XY, Zhao JJ, et al. Initiating characteristics of early-onset type 2 diabetes mellitus in Chinese patients. *Chin Med J (Engl)*. (2016) 129:778–84. doi: 10.4103/0366-6999.178959

29. Haseen SD, Khanam A, Sultan N, Idrees F, Akhtar N, Imtiaz F. Elevated fasting blood glucose is associated with increased risk of breast cancer: Outcome of case-control study conducted in Karachi, Pakistan. *Asian Pac J Cancer Prev*. (2015) 16:675–8. doi: 10.7314/APJCP.2015.16.2.675

30. Li X, Li G, Cheng T, Liu J, Song G, Ma H. Association between triglyceride-glucose index and risk of incident diabetes: A secondary analysis based on a Chinese cohort study: TyG index and incident diabetes. *Lipids Health Dis*. (2020) 19:236. doi: 10.1186/s12944-020-01403-7

31. Liu X, Tan Z, Huang Y, Zhao H, Liu M, Yu P, et al. Relationship between the triglyceride-glucose index and risk of cardiovascular diseases and mortality in the general population: A systematic review and meta-analysis. *Cardiovasc Diabetol*. (2022) 21:124. doi: 10.1186/s12933-022-01546-0

32. Zhao Y, Lv X, Chen C, Li K, Wang Y, Liu J. The association between triglyceride-glucose index and hyperferritinemia in patients with type 2 diabetes mellitus. *Hormones (Athens)*. (2023) 22:403–12. doi: 10.1007/s42000-023-00453-7

33. Ademi-Islami D, Manxhuka-Kerliu S, Tarifa-Koroveshi D, Koliqi R, Mujaj B. Metabolic syndrome and breast cancer molecular subtypes: An observational patient study. *Breast Cancer (Auckl)*. (2022) 16:11782234221080555. doi: 10.1177/11782234221080555

34. Panigoro SS, Sutandyo N, Witjaksono F, Siregar NC, Ramli R, Hariani R, et al. The association between triglyceride-glucose index as a marker of insulin resistance and the risk of breast cancer. *Front Endocrinol (Lausanne)*. (2021) 12:745236. doi: 10.3389/fendo.2021.745236

frontiers | Frontiers in Oncology

TYPE Original Research
PUBLISHED 09 July 2024
DOI 10.3389/fonc.2024.1388868

OPEN ACCESS

EDITED BY
Shivendra Vikram Singh,
St. Jude Children's Research Hospital,
United States

REVIEWED BY
Yasen Maimaitiyiming,
Xinjiang Medical University, China
Amit Kumar,
University of Maryland, United States

*CORRESPONDENCE
Xiejia Jiao
jiaoxiejia@163.com
Lei Qi
qilei_spine@hotmail.com

†These authors have contributed equally to this work

RECEIVED 20 February 2024
ACCEPTED 12 June 2024
PUBLISHED 09 July 2024

CITATION
Chen Y, Zhang W, Xu X, Xu B, Yang Y, Yu H, Li K, Liu M, Qi L and Jiao X (2024) Gene signatures of copper metabolism related genes may predict prognosis and immunity status in Ewing's sarcoma.
Front. Oncol. 14:1388868.
doi: 10.3389/fonc.2024.1388868

Gene signatures of copper metabolism related genes may predict prognosis and immunity status in Ewing's sarcoma

Yongqin Chen[1†], Wencan Zhang[1†], Xiao Xu[2], Biteng Xu[1], Yuxuan Yang[1], Haozhi Yu[1], Ke Li[1], Mingshan Liu[1], Lei Qi[1*] and Xiejia Jiao[3*]

[1]Department of Orthopedics, Qilu Hospital of Shandong University, Jinan, Shandong, China, [2]Sterile Supply Department, The First People Hospital of Jinan, Jinan, Shandong, China, [3]Department of Orthopedics, The Second Hospital of Shandong University, Jinan, Shandong, China

Background: Cuproptosis is copper-induced cell death. Copper metabolism related genes (CMRGs) were demonstrated that used to assess the prognosis out of tumors. In the study, CMRGs were tested for their effect on TME cell infiltration in Ewing's sarcoma (ES).

Methods: The GEO and ICGC databases provided the mRNA expression profiles and clinical features for downloading. In the GSE17674 dataset, 22prognostic-related copper metabolism related genes (PR-CMRGs) was identified by using univariate regression analysis. Subsequently, in order to compare the survival rates of groups with high and low expression of these PR-CMRGs,Kaplan-Meier analysis was implemented. Additionally, correlations among them were examined. The study employed functional enrichment analysis to investigate probable underlying pathways, while GSVA was applied to evaluate enriched pathways in the ES (Expression Set). Through an unsupervised clustering algorithm, samples were classified into two clusters, revealing significant differences in survival rates and levels of immune infiltration.

Results: Using Lasso and step regression methods, five genes (TFRC, SORD, SLC11A2, FKBP4, and AANAT) were selected as risk signatures. According to the Kaplan-Meier survival analysis, the high-risk group had considerably lower survival rates than the low-risk group(p=6.013e-09). The area under the curve (AUC) values for the receiver operating characteristic (ROC) curve were 0.876, 0.883, and 0.979 for 1, 3, and 5 years, respectively. The risk model was further validated in additional datasets, namely GSE63155, GSE63156, and the ICGC datasets. To aid in outcome prediction, a nomogram was developed that incorporated risk levels and clinical features. This nomogram's performance was effectively validated through calibration curves.Additionally, the study evaluated the variations in immune infiltration across different risk groups, as well as high-expression and low-

expression groups. Importantly, several drugs were identified that displayed sensitivity, offering potential therapeutic options for ES.

Conclusion: The findings above strongly indicate that CMRGs play crucial roles in predicting prognosis and immune status in ES.

KEYWORDS

Ewing's sarcoma, copper metabolism related genes, prognostic-related copper metabolism related genes, functional enrichment, immune infiltration, risk model, clinical features

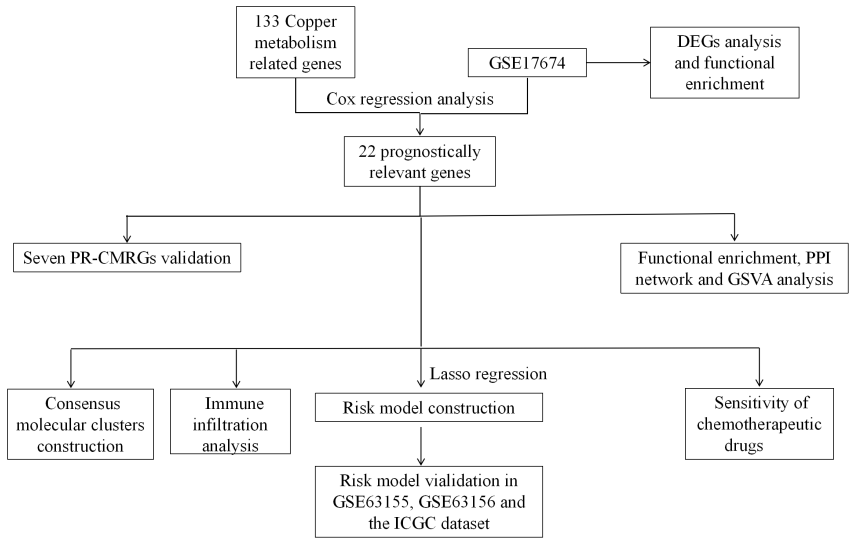

GRAPHICAL ABSTRACT
Flow chart. PR-CMRGs: prognostic-related copper metabolism related genes. DEGs, differentially expressed genes; GSVA, Gene Set Variation Analysis; PPI, protein-protein interaction.

1 Introduction

Ewing's sarcoma (ES) is a very aggressive cancer that mostly impacts the skeletal system and soft tissues in individuals who are in their childhood or teenage years (1). The documented prevalence of ES is 2.9 occurrences per million individuals annually (2). ES was distinguished by the merging of the EWSR1 gene with the FLI1 gene in previous researches (3, 4). The FLI1 gene belongs to the ETS gene group. A novel inhibitor of ETS proteins called TK216 has shown clinical benefits for almost half of the patients (5). The dedication of researchers and clinicians has advanced ES therapy. Traditionally, the main approach for treating ES has been a combination of surgery and radiation. However, despite comprehensive therapy, approximately 30–40% of patients continue to encounter recurrence or metastases. Less than 10% of ES patients with metastases still survive after five years. Currently, treating ES patients remains immensely challenging, necessitating the urgent identification of dependable intervention biomarkers to advance therapy.

Copper plays a crucial role in mitochondrial respiration, antioxidant defense, and programmed cell death (6). Maintaining an appropriate copper concentration is crucial for the survival of living organisms. Oxidative stress and cytotoxicity result from excessive copper levels, while copper deficiency can also be detrimental (7, 8). Cuproptosis is a novel kind of cellular demise induced by copper. In the tricarboxylic acid (TCA) cycle, copper ions bind to lipoylated components and engage in certain cellular interactions. This leads to the clustering of these copper-bound lipoylated proteins in the mitochondria, which in turn reduces the levels of iron-sulfur (Fe-S) clusters. This process causes proteotoxic stress and eventually leads to the death of the cell (6). Cu fills an essential function in the advancement and growth of cancer by stimulating the multiplication of cells, the formation of new blood vessels, and the spread of cancer cells to

other parts of the body. Recent research indicates that the Cu-complex might be a promising target for cancer treatment. Cu has been found to induce apoptosis and/or the formation of free radicals, leading to the death of cancer cells (9, 10). Notable advancements in copper metabolism have been made in recent years. Several studies have revealed significant regulation of metabolism by proteins involved in copper handling and utilization in proliferating cells (11, 12). Cuproplasia, a novel kind of copper-dependent cell growth and proliferation, has been discovered (13). Both neoplasia and hyperplasia are included under this phrase. Growing evidence underscores the deep involvement of copper metabolism in cancer proliferation, angiogenesis, and metastasis (14, 15). Copper dysregulation is observed in cancer tissue than normal tissue (16–18). Various cancers have exhibited elevated amounts of copper (19). Additionally, copper imbalance is closely associated with weakened immune responses in cancer. Hence, a potential prognostic model based on CMRGs could effectively predict the prognosis and immune status of ES.

There is no study suggested that the mechanism of TFRC, SORD, SLC11A2, FKBP4, and AANAT in cuproptosis. In this study, we identified five signatures (TFRC, SORD, SLC11A2, FKBP4, and AANAT) based on CMRGs, which robustly predict ES prognosis. TFRC, SLC11A2, FKBP4, and AANAT were demonstrated associated with increased risk, while SORD was a favorable prognostic factor. Furthermore, we elucidated the correlation between these signatures and immune status. Ultimately, we concluded that CMRGs play a pivotal role in ES prognosis and immunity, providing valuable guidance for future research.

2 Manuscript formatting

2.1 Material and methods

2.1.1 Data collection and preprocessing

Using the Molecular Signatures Database (MSigDB: https://www.gsea-msigdb.org/gsea/msigdb), we were able to identify 133 copper metabolism-related genes (Supplementary Table 1).Using the "GEOquery" software, we extracted profile matrices and clinical/survival data for this investigation from the GSE17674, GSE63155, and GSE63156 datasets in the Gene Expression Omnibus (GEO) database. We standardized all probe information to corresponding gene symbols based on annotation files using a consistent approach: when one gene symbol matched more than one probe, we eliminated the probes that had multiple gene symbols and chose the probe with the greatest expression value. GSE17674, comprised of 44 ES and 18 muscle samples, used the GPL570 platform. The GSE63155 and GSE63157 datasets, each containing 39 and 46 ES samples, respectively, were generated by the GPL5175 platform. Additionally, we obtained clinical data and expression profiles for 49 ES samples from the database of International Cancer Genome Consortium (ICGC). We designated GSE17674 as the training dataset, and GSE63155, GSE63156, and ICGC datasets as external test datasets. The flow chart of the study as follows (Graphical Abstract).

2.1.2 Landscape of prognostic related CMRGs in ES

To assess the prognostic significance of CMRGs, we conducted univariate Cox regression analysis. We identified 22 CMRGs as prognostically relevant (PR-CMRGs). Using the "ggplot2" package, we visualized the results through a forest plot. Using the point_cut function to determine the cutoff value for PR-CMRGs, we classified the samples into categories based on their level of expression, distinguishing between high and low expression. We performed Kaplan-Meier analysis between these two expression groups using the "tinyarray" package. Utilizing the same package, we investigated the expression levels of PR-CMRGs in skeletal muscle and ES samples. To analyze correlations among these prognostic genes, we employed the "Pearson" method. The "corrplot" and "circlize" packages were used to present the correlation analysis results. We constructed a network of the 22 CMRGs using the "igraph" package and visualized the chromosomal positions of PR-CMRGs using the "RCircos" package.

2.1.3 Functional enrichment, PPI network and GSVA

Using the "clusterProfiler" package, we performed functional enrichment analysis (GO/KEGG) to uncover potential mechanisms involving PR-CMRGs in ES. The results of the analysis were visualized using the ggplot package. To gain insight into potential interactions among PR-CMRGs, we identify protein interaction networks (with a minimum required interaction score > 0.150) by utilizing the STRING database (http://string-db.org/), and then depicted these results using the "igraph" package.

Gene Set Variation Analysis (GSVA) was conducted based on the "h.all.v7.5.1.symbols.gmt" gene set from the Molecular Signature Database. Using the "limma" package, we identified the differentially enriched scores of 50 pathways between ES and normal tissue, and illustrated these findings with bar plots.

2.1.4 Construction of consensus molecular clusters

Based on the PR-CMRGs matrix to identify distinct molecular patterns that provide insight into the potential involvement of CMRGs in ES, unsupervised clustering was employed. For this task, we utilized the "ConsensusClusterPlus" package, known for its interpretability. We utilized PCA and t-SNE methods to confirm the differentiation of molecular clusters. To assess the survival differences among these clusters, we employed Kaplan-Meier curves. Additionally, we conducted an analysis of immune infiltration to gain insights into the status of the tumor microenvironment within these two clusters.

2.1.5 Establishment and validation of risk model

To streamline the PR-CMRGs, we conducted Lasso regression analysis through the "glmnet" package. Utilizing the "survival" package, we then employed stepwise regression to identify the risk signature with the lowest Akaike's information criterion (AIC). In addition, we used the "ggplot2" package to present the prognostic model via a forest plot.

The subsequent equation: the prognostic risk model was developed by conducting a study to calculate the risk score, which is determined by multiplying the Ei coefficient of a gene with its corresponding gene expression [risk score = Ei coefficient (gene i) × expression (gene i)]. Using the "survminer" package, the samples in the datasets were classified into high risk and low risk groups based on a predetermined cutoff value. Heatmaps, scatter plots, and PCA plots showed signature expression, survival status distribution, and risk score in different risk groups. Applying the Kaplan-Meier analysis with log-rank testing, survival curves were produced for these categories. Furthermore, using the "timeROC" package, the reliability of the risk model was confirmed by utilizing AUC values and time-dependent ROC curves.

Additionally, we evaluated the AUC of clinical features and risk model effectiveness in different clinical subgroups. Wilcoxon test was used to examine risk scores distribution in clusters and clinical subgroups. An alluvial diagram was employed to depict the link among risk groups, molecular clusters and clinical features.

2.1.6 Establishment and validation of nomogram

We used Cox regression analysis to see if the risk score could act as a prognostic indication apart from clinical data(including gender, age, and stage status).Subsequently, using the "rsm" package, a nomogram was developed at risk level and clinical data, which facilitated prognosis prediction. Finally, evaluate the nomogram's prediction accuracy at one, three, and five years, calibration curves were used.

2.1.7 Analysis of immune infiltration

We utilized the ssGSEA method, implemented using the "GSVA" package to evaluate the differing amounts of 13 immunological pathways and 28 immune cells across groups classified as high and low risk. Additionally, we investigated immune cells variations in different signature expression groups.

We employed Spearman correlation analysis to explore how the risk score, different immune cells, and the signature were connected. These results were presented using lollipop diagrams created with the "ggplot" package. Lastly, we used the mantel approach in conjunction with the "ggcor" package to assess the link between the risk signature matrix and PR-CMRGs.

2.1.8 Sensitivity of chemotherapeutic drugs

The "pRRophetic" package is designed for predicting clinical chemotherapeutic responses based on gene expression levels in various cancers, facilitating the evaluation of measured drug responses. The sensitivity of chemotherapeutic medications was tested across groups with high and low risk using this package. Using the expression profile of ES from the training dataset and expression data from Genomics of Drug Sensitivity in Cancer (GDSC, www.cancerrxgene.org/), we predicted the half-maximal inhibitory concentration (IC50) of drugs with a significance threshold of $p < 0.001$.

2.1.9 Differentially expressed genes between risk groups, functional enrichment and GSVA

Using the "limma" package, we detected differentially expressed genes (DEGs) in different risk groups in the GSE17674 dataset ($|LogFC| > 1$, $p < 0.05$). For a deeper understanding of DEGs functions, based on $|log2FC| > 1$ and FDR value < 0.05, GO/KEGG analysis was conducted by using the "clusterProfiler" software. Visualization of the analysis results was done using the "ggplot" package. For KEGG pathways with $|NES| > 1$, NOM p value < 0.05, and FDR (p.adj) < 0.25, Gene Set Enrichment Analysis(GSEA) was conducted. Visualization of the results was accomplished using the "gseaplot2" and "ridgeplot" tools. We also conducted GSVA, comparing the enriched scores of pathways between risk groups using the Wilcoxon test. Heatmaps and boxplots were utilized to display the results.

2.2 Validation of Hub PR-CMRGs by RT-PCR

2.2.1 Cell source

For this experiment, American Type Cell Culture (ATCC) provided RD-ES and A673 cells, and mesenchymal stem cells (MSCs) from Cyagen (Guangzhou, China).

2.2.2 Real Time-PCR

Total RNA was extracted from cells using Trizol (Sigma, United States) and reverse transcribed into cDNA using a reverse transcription kit (Takara, Japan). The SYBR Premix Ex Taq

TABLE 1 The sequences of the primers.

Gene Symbol	Forward primer	Reverse primer
DAXX	ACGTGCCCACTCTCTGTTTT	CAGAGGGCTCATTGGAGGTG
CCS	GGGAACTATTGACGGCCTGG	GTCAGCATCAGCACGGACAT
MTF2	GCATGTGGCGAAAAATACCG	GCAGTTGCTCCTTCCCATTC
F8	GGCCATCAGTGGACTCTCTTT	TAGCGAGTCAGTAACGGTGG
SLC11A2	GAGTGGTTACTGGGCTGCAT	CACAGGATGACTCGTGGGAC
IL1A	CTTCTGGGAAACTCACGGCA	AGCACACCCAGTAGTCTTGC
FKBP4	TGCTATCGTGGAGGTTGCAC	CTCCTTTCTCCATGCGCTGA

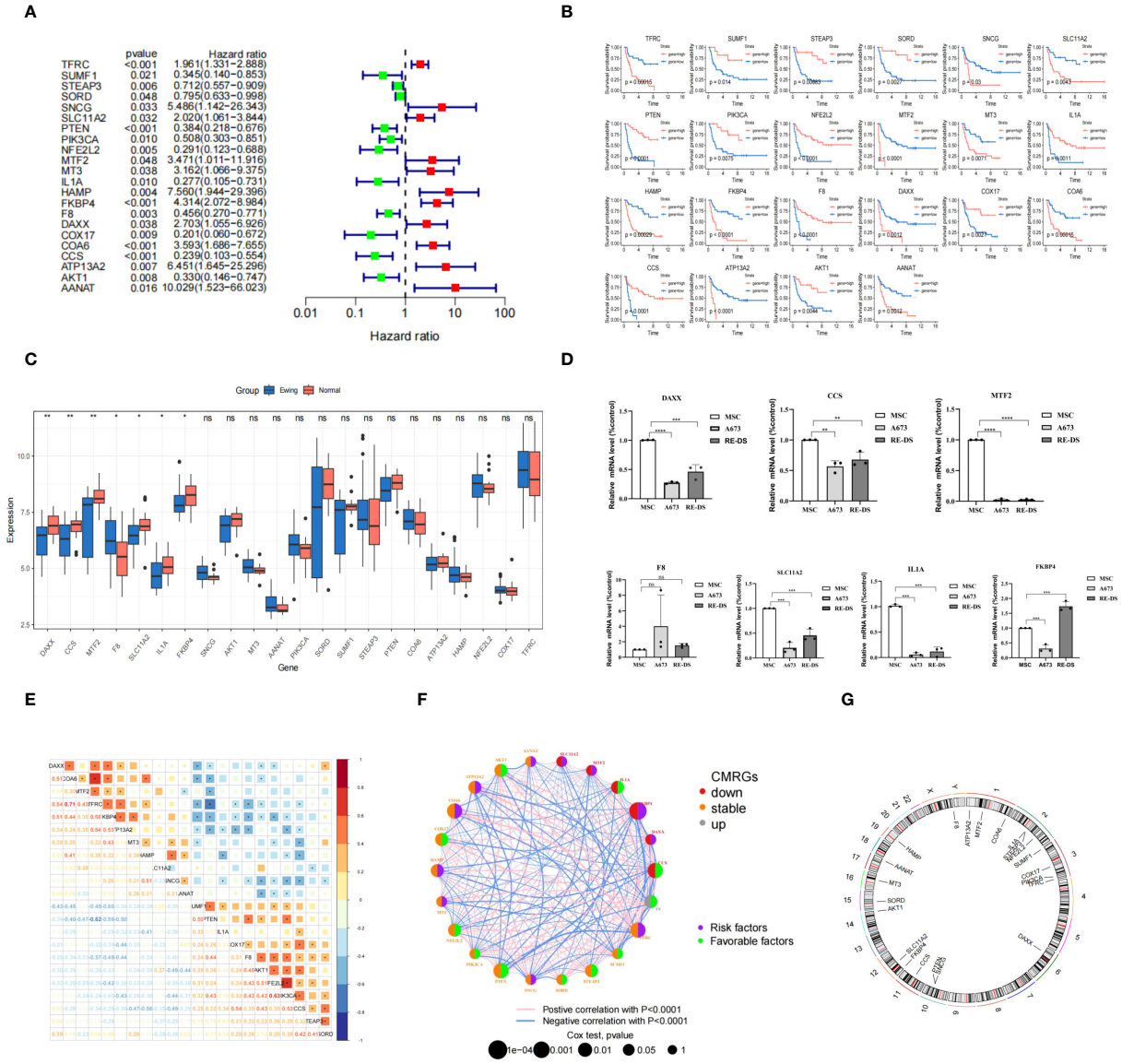

FIGURE 1
Construction of the CMRGS in ES and validation of hub PR-CMRGs. **(A)** The forest map of hazard ratios displayed the outcomes of univariate regression. **(B)** The result from the Kaplan-Meier analysis. **(C)** Boxplot of differentially expressed PR-CMRGs between Ewing and normal groups. **(D)** RT-PCR results of DAXX, CCS, MTF2, F8, SLC11A2, IL1A, and FKBP4. **(E, F)** PR-CMRGs correlation in ES. **(G)** Chromosomal positions of PR-CMRGs. * means p < 0.05, ** means p < 0.01, *** means p < 0.001, **** means p < 0.0001 and ns means no significance (p>0.05).

(Takara, Japan) was utilized for real-time PCR, and the protocol provided by the manufacturer was adhered. Primer design was done using the "primerBank" website (pga.mgh.harvard.edu), and the primer sequences are provided in Table 1. The data analysis employed the 2-ΔΔCT method. At least three replications of each experiment were conducted.

2.3 Statistical methods

R was utilized to execute bioinformatic analyses, and the Wilcoxon rank sum test was employed to analyze data between two groups. Spearman's rank correlation was employed for the correlation study. Statistics were considered significant if P<0.05.R 4.1.3 (https://www.r-project.org) and GraphPad Prism 9.0 (GraphPad Software) were used for all statistical analyses.

3 Result

3.1 Landscape of prognostic related CMRGs in ES

In our study, we investigated 133 CMRGs in GSE17674. Initially, the p-value and hazard ratio for each gene were calculated using univariate Cox regression. Subsequently, we identified 22 CMRGs with p-values < 0.05 as prognostically relevant genes (PR-CMRGs). A forest plot visualized the results, highlighting that among the 22

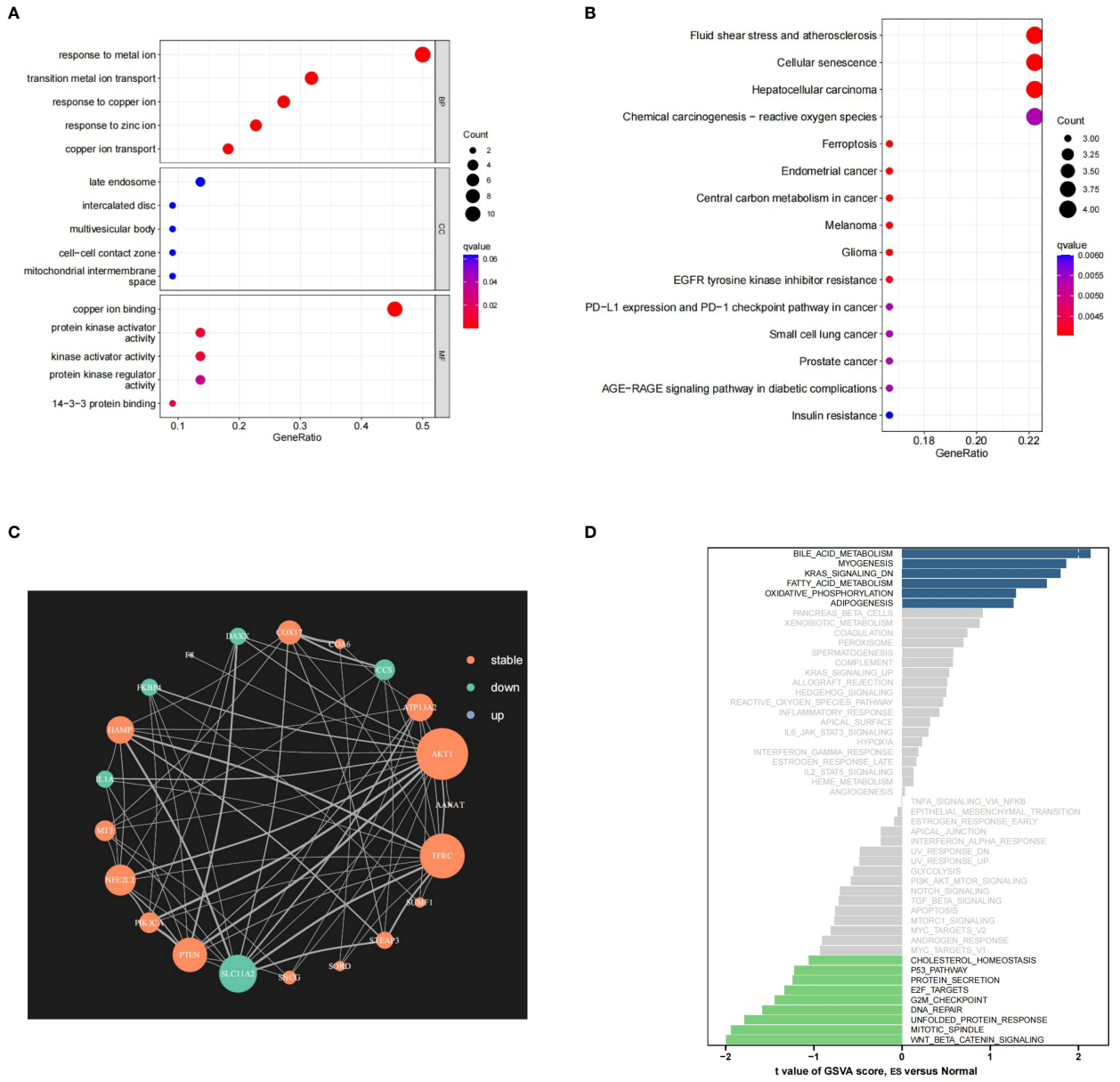

FIGURE 2
The outcomes of the enrichment analysis. **(A, B)** The outcomes of GO and KEGG study of PR-CMRGs. **(C)** The PPI network of PR-CMRGs. **(D)** Pathways alteration in ES by GSVA.

CMRGs, 11 genes including TFRC, SNCG, SLC11A2, MTF2, MT3, HAMP, FKBP4, DAXX, COA6, ATP13A2, and AANAT with HR > 1 were associated with worse survival (Figure 1A). The remaining 11 PR-CMRGs, which included SUMF1, STEAP3, SORD, PTEN, PIK3CA, NFE2L2, IL1A, F8, COX17, CCS, and AKT1 with HR < 1, were related to beneficial survival. Based on the levels of PR-CMRGs, the samples were divided into two groups: high expression and low expression. Kaplan-Meier analysis showed that there was a significant difference in survival rates between the two groups (Figure 1B).

Among the 22 PR-CMRGs, 7 (DAXX, CCS, MTF2, F8, SLC11A2, IL1A, and FKBP4) exhibited differential expression in the training dataset. Specifically, F8 was found to be enriched, while DAXX, CCS, MTF2, SLC11A2, IL1A, and FKBP4 were significantly down-regulated in ES samples compared to skeletal muscle tissue (Figure 1C).

RT-PCR results demonstrated that in A673 cells, the relative expression levels of seven hub PR-CMRGs were lower compared to MSCs, except for F8 which was higher. But the expression of F8 has not significant difference between them. In the RD-ES cell line, five of the hub genes were also significantly down-regulated in tumors, except for F8 and FKBP4 (Figure 1D).

Considering their biological function similarity, we explored the correlation among these PR-CMRGs. Notably, TFRC exhibited positive correlation with COA6 (r=0.71) while showing a negative

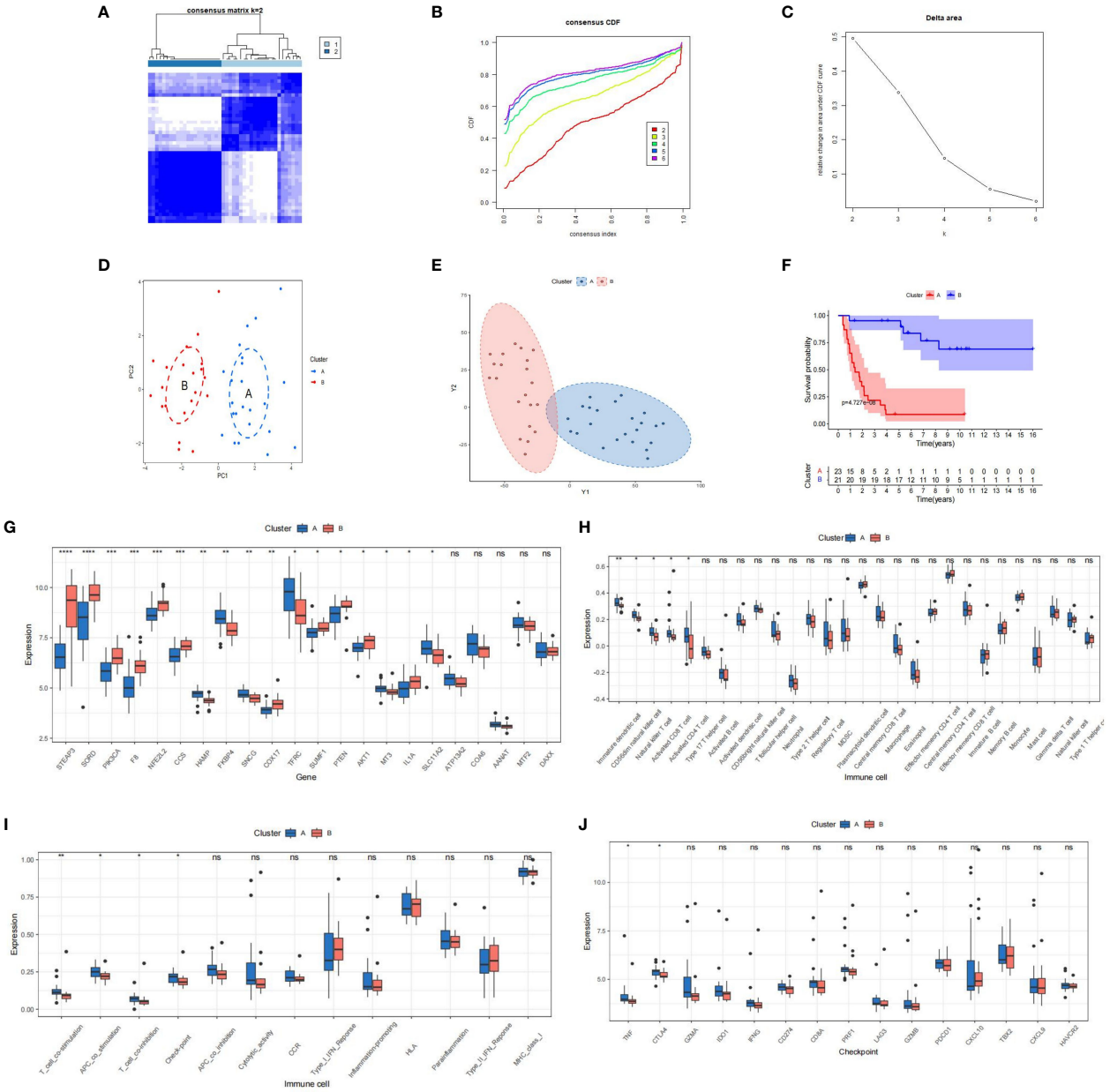

FIGURE 3
The outcomes of the consensus clusters, CRGs, and immune infiltration in clusters [**(A)**: blue vs. **(B)**: red] are as follows. **(A–C)** Two molecular clusters constructed using PR-CMRGs. The findings of **(D, E)** PCA and t-SNE show two distinct clusters. **(F)** Kaplan-Meier curves plotted for several molecular groupings. **(G–I)** A boxplot displaying the differential expression of PR-CMRGs and immune cells is shown. **(J)** A box diagram illustrating the distribution of checkpoint genes in clusters. * means $p < 0.05$, ** means $p < 0.01$, *** means $p < 0.001$, **** means $p < 0.0001$ and ns means no significance ($p>0.05$).

correlation with PTEN (r=-0.62), underscoring TFRC's central role in ES progression (Figure 1E).

The gene network of PR-CMRGs depicted their expression levels, correlations, and prognostic values in ES (Figure 1F). Chromosomal positions were visualized, revealing that F8 was located on the X chromosome, while the others were on autosomes. Chromosomes 1 (ATP13A2, MTF2, and COA6), 2 (IL1A, STEAP3, and NFE2L2), and 3 (COX17, PIK3CA, and TFRC) harbored the most genes, with no genes found on chromosomes 4, 5, 7, 8, 9, 13, 18, 20, 21, 22, and Y (Figure 1G).

3.2 Functional enrichment, PPI network and GSVA

The PR-CMRGs were subjected to functional enrichment analysis, revealing involvement in processes like transition metal ion transport, response to copper ion and copper ion transport. In terms of cellular components, these genes were primarily located in the late endosome, intercalated disc, and multivesicular body. Molecular function analyses indicated participation in copper ion binding, protein kinase activator activity, and kinase activator

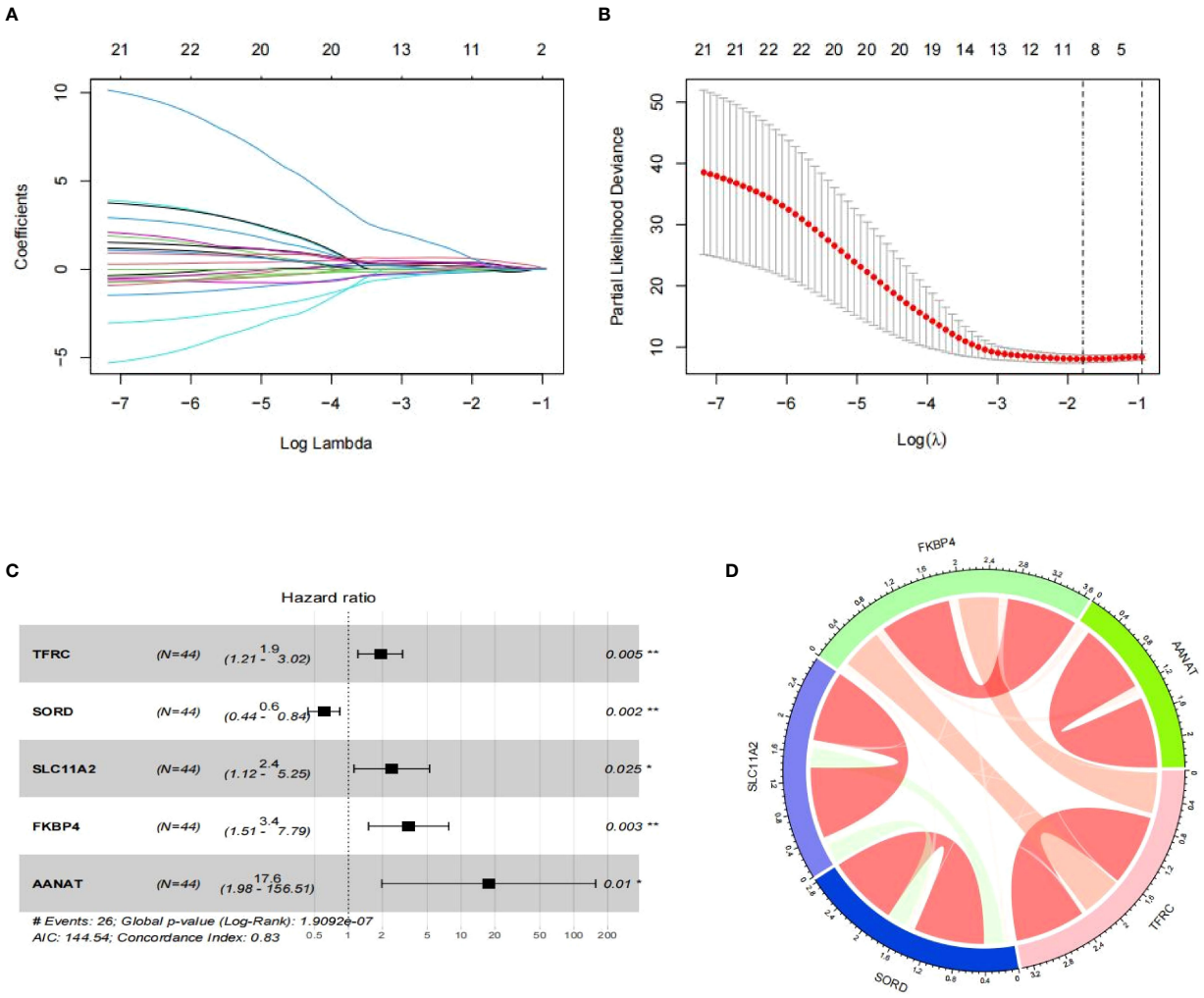

FIGURE 4
Development of a risk model. **(A, B)** The outcomes of Lasso regression. **(C)** Risk model depicted as a forest map. **(D)** Chord diagram of signature correlation. * means p < 0.05, ** means p < 0.01.

activity (Figure 2A). KEGG analysis highlighted associations with various human cancers such as hepatocellular carcinoma, melanoma, and glioma. These enrichment results strongly emphasize the essential role of PR-CMRGs in carcinogenesis and cancer progression (Figure 2B). The PPI network of PR-CMRGs underscored the core positions of AKT1, TFRC, and SLC11A2 (Figure 2C). GSVA results demonstrated enriched scores for pathways like oxidative_phosphorylation, fatty_acid_metabolism, and kras_signaling_dn, with t-values>1, as well as pathways like wnt_beta_catenin_signaling, mitotic_spindle,andnfolded_protein_response with t-values < -1, when comparing ES and normal tissue (Figure 2D).

3.3 Consensus molecular clusters construction

We conducted unsupervised clustering based on PR-CMRGs to discern distinct patterns. The optimal number of patterns was determined as K=2. Consequently, the 44 ES samples in GSE17674 were categorized into cluster A (n=23) and cluster B (n=21) (Figures 3A-C). The separation between these clusters was evident through PCA and t-SNE analyses (Figures 3D, E). In terms of survival advantage, cluster B outperformed cluster A, showing noticeably longer survival times.(p=4.727e−08) (Figure 3F). Dysregulated PR-CMRGs were observed in both clusters, as indicated by box plots (Figure 3G).

An analysis of immune infiltration unveiled that cluster A was characterized by higher levels of infiltration of Immature dendritic cells, Natural killer T cells, CD56dim natural killer cells, and Activated CD8 T cells (Figures 3H, I). Significant differences were observed between the two clusters in terms of immune function and checkpoints such as T-cell co-stimulation, APC co-stimulation, T-cell co-inhibition, and checkpoint genes (Figure 3J). Additionally, TNF and CTLA4 were enriched in cluster A. These findings collectively suggest that cluster A exhibited greater immunogenicity but worse prognosis.

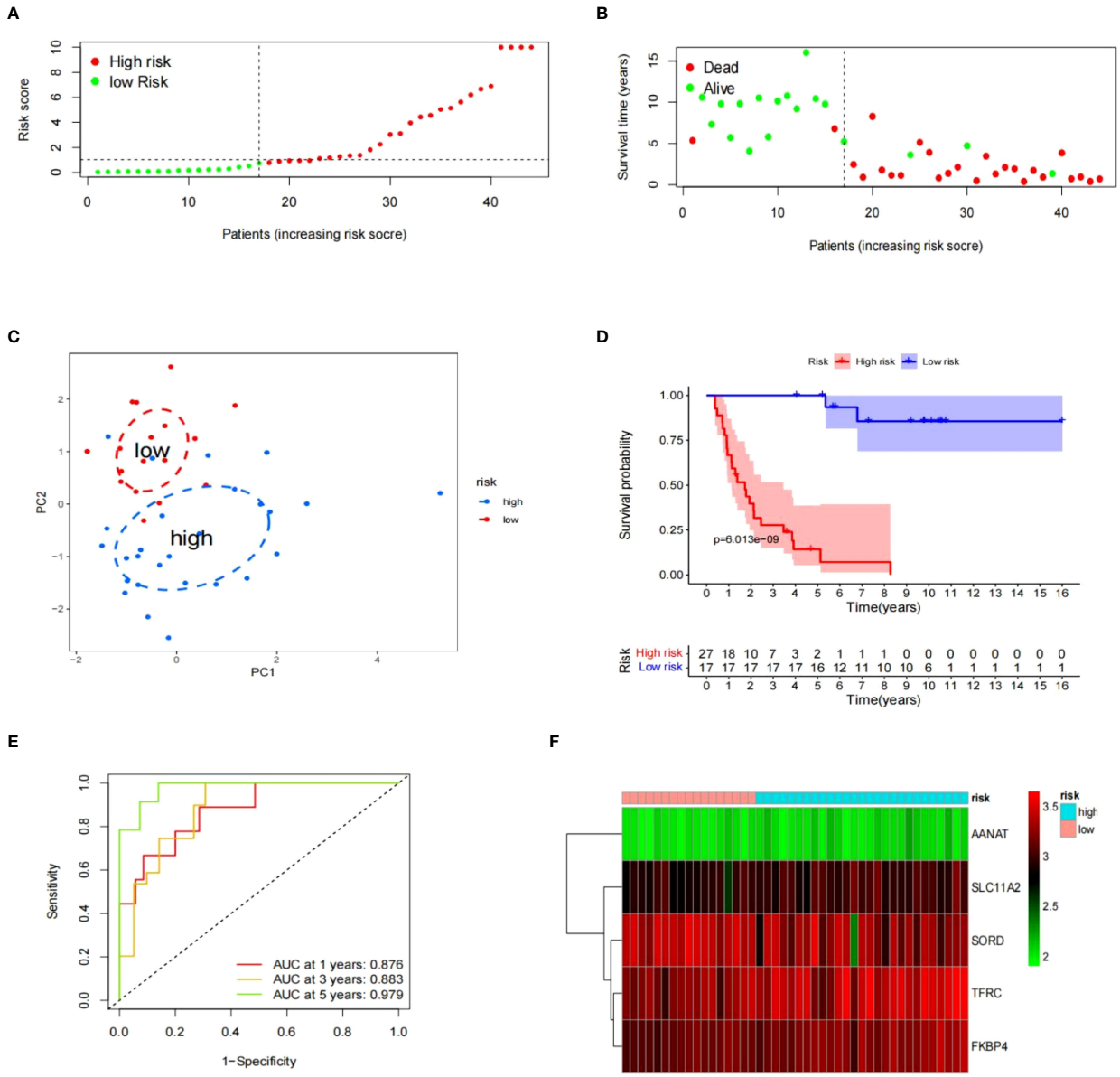

FIGURE 5
The prognostic significance of signatures in GSE17674. **(A–F)** The data includes the distribution of risk scores, survival status, PCA analysis results, K-M survival analysis results, time-ROC analysis results, and a heatmap of the signature.

3.4 Risk model construction and validation

Utilizing Lasso regression, we reduced the number of PR-CMRGs to 10, and subsequently, 5 genes (TFRC, SORD, SLC11A2, FKBP4, and AANAT) were identified as the prognostic signature through stepwise regression, which yielded the lowest AIC (n=144.54) (Figure 4A). The forest plot visualization of the prognostic model indicated that TFRC, SLC11A2, FKBP4, and AANAT with HR > 1 were associated with worse survival, whereas SORD with HR < 1 correlated with favorable survival (Figures 4B, C). All signatures had p-values < 0.05, indicating the independence of each gene as a prognostic indicator. The correlation of the risk signature was depicted (Figure 4D).

The risk score prediction model was formulated as follows: RS = TFRC * 0.649 + SORD * -0.503 + SLC11A2 * 0.886 + FKBP4 * 1.232 + AANAT * 2.867. This algorithm was used to computed each sample's risk score.

The "surv_cutpoint" function was used to generate a cutoff value, which was then applied to split the ES samples in GSE17674 into two risk groups. Upon examining risk scores distribution and survival status, the high-risk group exhibited a more dismal prognosis than the low-risk group, which became evident. (Figures 5A, B). This distinction between risk groups was validated using the PCA method (Figure 5C). The survival curve for Kaplan-Meier with a p-value of 6.013e-09 indicated a significant correlation between risk groups and survival rates

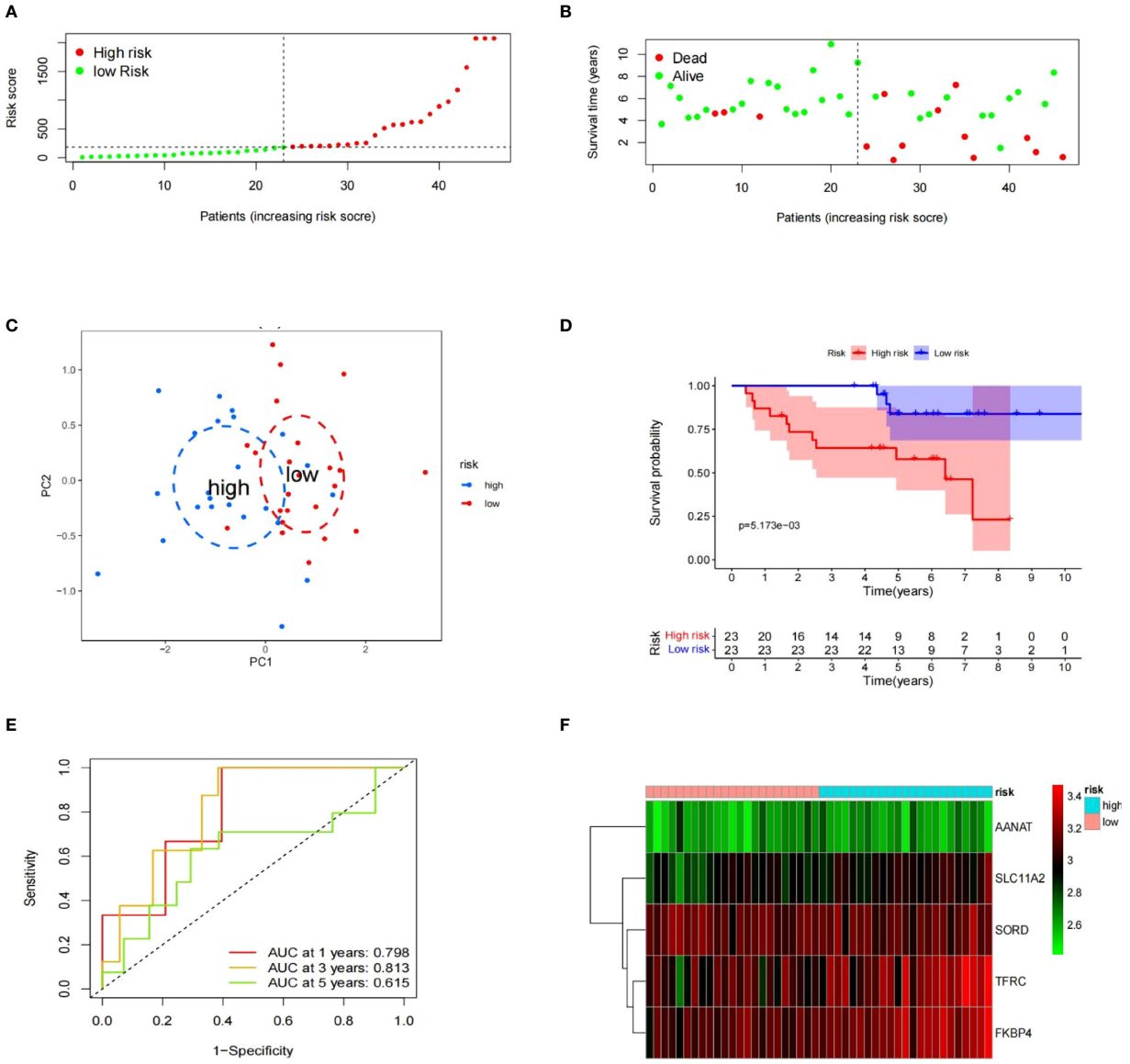

FIGURE 6
Prognostic value of signatures in GSE63155. **(A– F)** Distribution of the risk scores, survival status, PCA analysis, K-M survival analysis, time-ROC analysis, heatmap of the signature.

(Figure 5D). The time-dependent ROC curve with AUC values of 0.876, 0.883, and 0.979 at 1, 3, and 5 years respectively demonstrated the risk model's strong performance in terms of specificity and sensitivity (Figure 5E). A heatmap was created to provide a clear visualization of the signature profile between the two groups (Figure 5F).

To evaluate the risk model's accuracy, we utilized the signatures on three external datasets: GSE63155, GSE63156 and the ICGC dataset. Employing the RS formula, we calculated each sample's risk score in the three test datasets. Samples were classified as different risk groups based on the cutoff value produced by the "surv_cutpoint" function (Figures 6A, B). Risk scores and survival status distribution was visualized, highlighting worse outcome in the high-risk group. The PCA plot confirmed the clear separation in the two groups (Figure 6C). Subsequently, time ROC curves, heatmaps and K-M survival curves were generated using methods similar to those in the training dataset (Figures 6D-F). A parallel conclusion was drawn through Kaplan-Meier survival analysis, revealing p-values of 5.173e-03, 8.152e-03, and 3.701e-03 in GSE63155, GSE63156, and the ICGC dataset, respectively. The timeROC results reflected commendable AUC values for 1, 3, and 5 years in GSE63155 (0.798, 0.813, 0.815), GSE63156 (0.898, 0.843, 0.711) (Figures 7A-F), and the ICGC dataset (0.797, 0.619, 0.712) (Figures 8A-F). These results

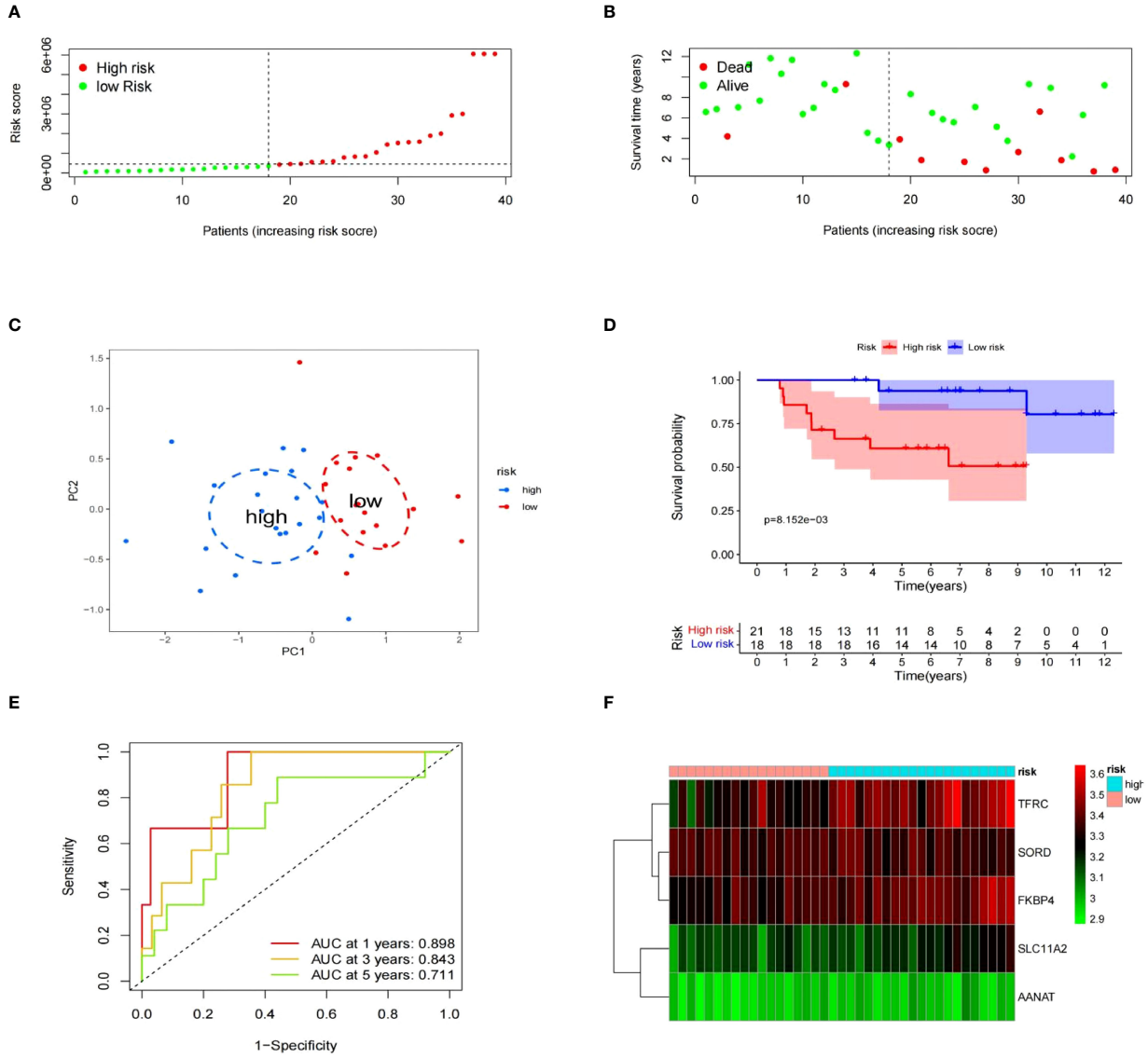

FIGURE 7
The prognostic significance of gene expression profiles in dataset GSE63156. **(A–F)** The information contains the distribution of risk scores, survival status, PCA analysis results, K-M survival analysis results, time-ROC analysis results, and a heatmap of the signature.

substantiated the model's ability to differentiate samples with favorable and worse prognoses, thereby demonstrating its potential for predictive prognosis.

3.5 Clinical features associated with risk model

Using Kaplan-Meier survival method, we tested the risk model's prediction effectiveness across different clinical subgroups. It demonstrated that the risk model was effective in predicting prognosis for certain subgroups, including individuals aged 14 years and older ($p<0.001$), individuals less than 14 years ($p=0.007$), females ($p<0.001$), males ($p<0.001$), individuals with primary stage cancer ($p<0.001$), and those with metastatic stage cancer ($p=0.002$) (Figure 9A). The fact that risk scores produced the greatest AUC values was confirmed by ROC curves that plotted risk scores against clinical variables (age, sex, and stage) for1,3, and 5 years (Figures 9B, C). Furthermore, a box plot was employed to display the distribution of risk scores across different molecular clusters and clinical subgroups (Figure 9D). An alluvial diagram showcased that samples associated with females, adults, metastasis, and cluster A exhibited elevated risk scores (Figure 9E).

3.6 Establishment and validation of nomogram

To assess the risk score prognostic independence, Cox regression analysis was performed. According to both the

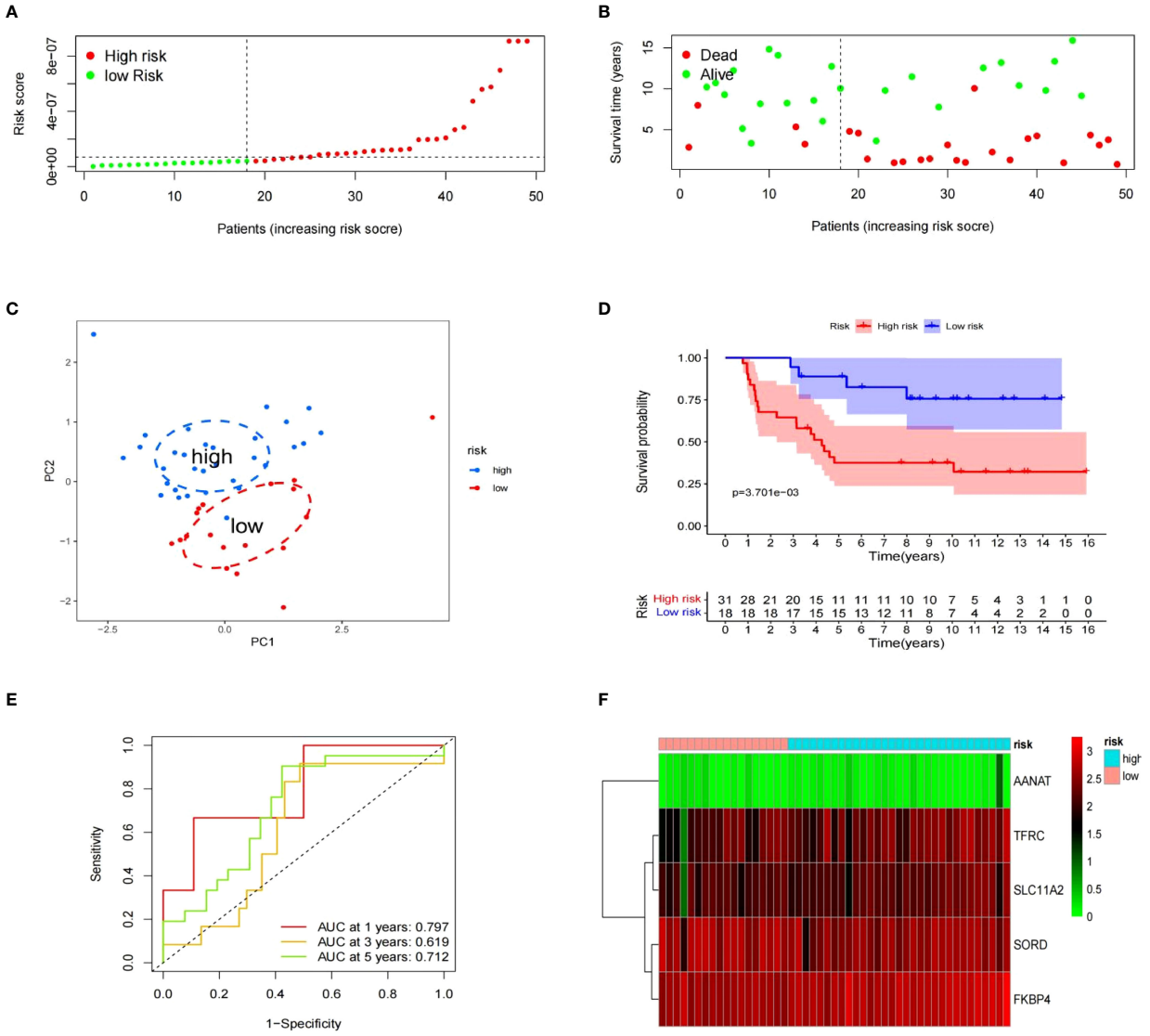

FIGURE 8
Value of signatures for prognosis ICGC dataset. **(A–F)** Risk score distribution, survival status, principal component analysis, K-M survival, time-ROC, and signature heatmap.

univariate and multivariate regression analysis, the risk score significantly affected ES prognosis, indicating that it was an independent prognostic factor ($p<0.05$).While no significant prognostic associations were observed with clinical features (Figures 10A, B). Subsequently, the risk level and clinical features were used to build a predictive nomogram. (Figure 10C). The 1-, 3-, and 5-year calibration curves showed that the ideal and predictive curves were well aligned (Figure 10D).

3.7 Immune infiltration analysis

Using ssGSEA analysis, we determined the abundance of different immune cells. The results showed that whereas activated CD4 T cells were more common in the high-risk group, central memory CD4 T cells and plasmacytoid dendritic cells were much more prevalent in the low-risk group (Figure 11A).

Further analysis indicated that Type 2 T helper cells and Activated CD4 T cells were significantly increasing in the high-expression group of TRFC and SORD, whereas Central memory CD4 T cells and Immature B cells were more abundant in the group with reduced expression of TRFC and SORD. In the case of FKBP4, the low-expression group exhibited enrichment of Gamma delta T cells, Type 1 T helper cells, Natural killer cells, and Central memory CD4 T cells. On the other hand, the group with high expression had elevated quantities of activated CD4 T cells. Low-expression of AANAT was associated with enriched Type 1 T helper cells. SLC11A2 groups did not exhibit differences in immune cells (Figures 11B-F) (Table 2).

The heatmap and lollipop plots highlighted correlations between immune cells and signatures (Figures 11G-I). Notably, the association between TFRC and Activated CD4 T cells was positive, with the highest r=0.73, while SORD displayed a negative correlation with T

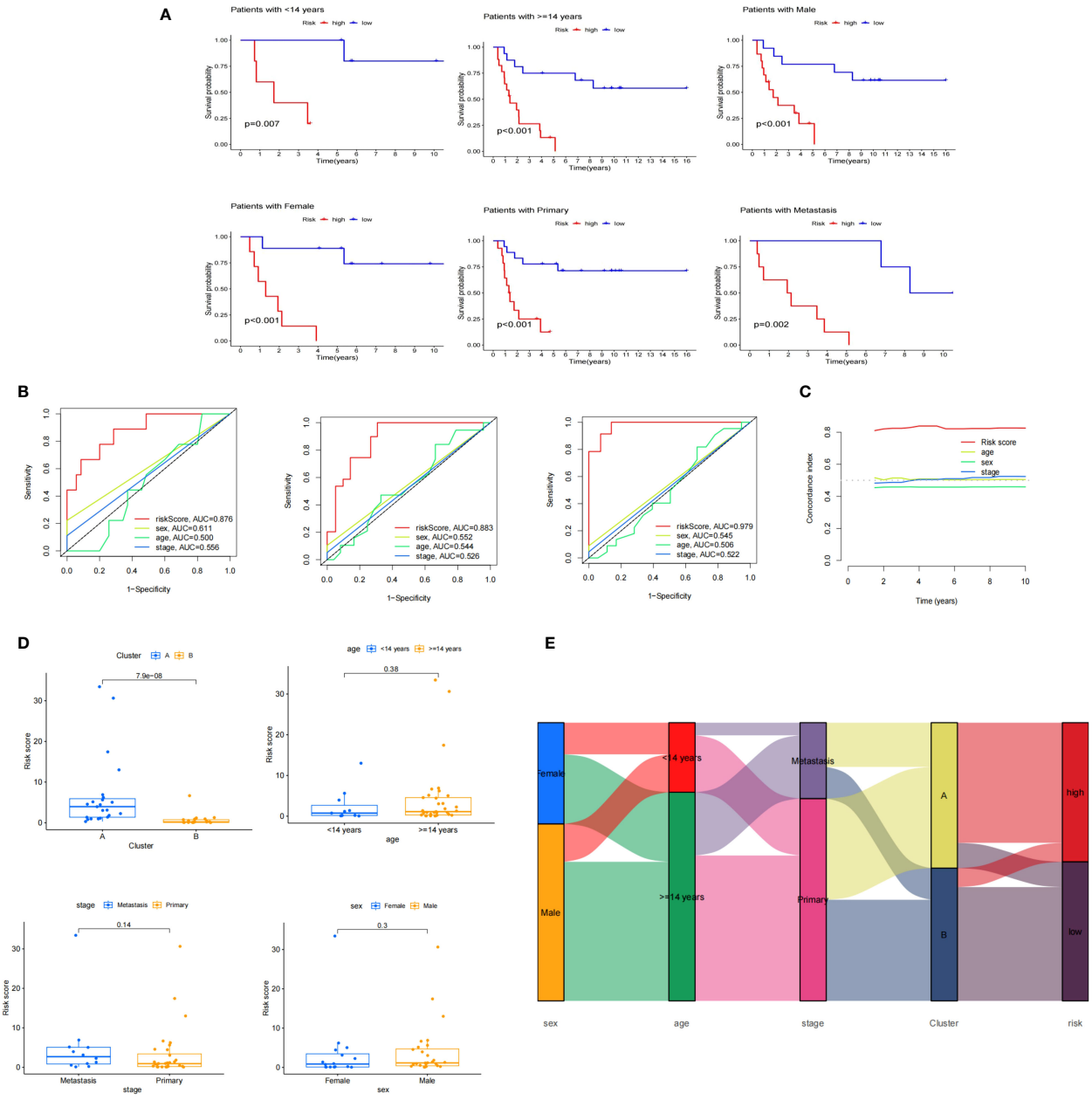

FIGURE 9
Clinical features associated with risk model. **(A)** Perform K-M survival analysis on age, sex, and stage subgroups; **(B)** Conduct ROC analysis to evaluate the risk score and clinical features (sex, age, stage) at 1, 3, and 5 years; **(C)** Calculate the C-index for the risk score and clinical features (sex, age, stage); **(D)** Examine the distribution of the risk score among clusters and clinical subgroups; **(E)** Create an alluvial diagram to visualize the relationship between molecular clusters, risk groups, and clinical features.

follicular helper cells and Neutrophils with r=-0.58. These findings imply a potential collaboration between risk signatures and immune cells in influencing ES clinical prognosis.

The findings presented above lend support to the notion that samples in the low-risk group exhibit better prognoses, likely due to heightened immune cell infiltration. These results offer potential evidence for the feasibility of immunotherapy in ES. However, further validation through additional studies is necessary to solidify these findings.

3.8 Sensitivity of chemotherapeutic drugs

Employing the "pRRophetic" package, clinical data was used to investigate the differential chemotherapeutic response in different risk groups. The findings showed that NU.7441 and ABT.263 were expected to be beneficial for the low-risk group, whereas exhibited greater benefit from AKT.inhibitor.VIII, AS601245, AUY922, Bleomycin, Tipifarnib, PHA.665752, MG.132, JNK.9L, BMS.708163, Erlotinib, and Imatinib in the high-risk group (Figure 12).

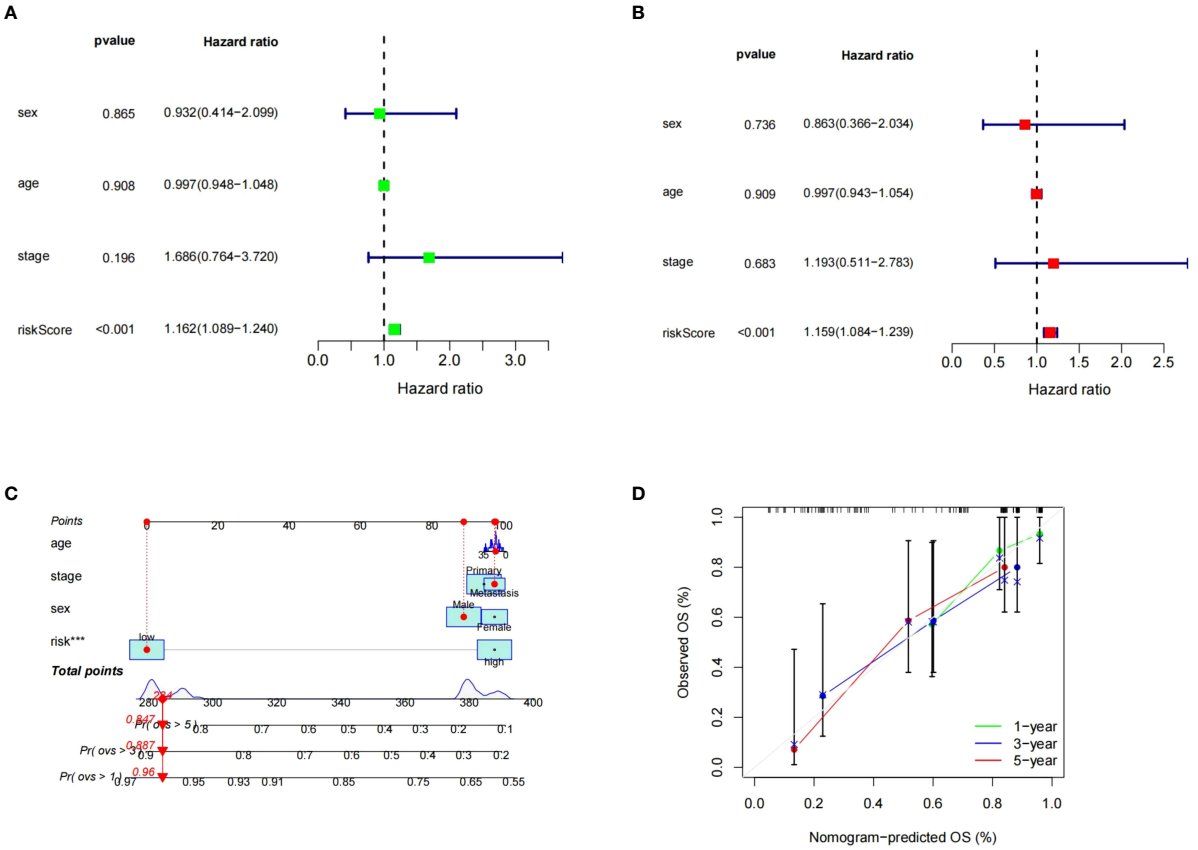

FIGURE 10
Independence of the risk model in GSE17674. **(A, B)** The results of univariate and multivariate COX regression analysis. **(C)** Nomogram for predicting 1, 3 and 5-year OS. **(D)** The calibration plots for predicting 1, 3, 5-years OS. *** means $p < 0.001$.

3.9 Differentially expressed genes between risk groups and functional enrichment

A total of ninety genes that exhibited differential expression were discovered in the GSE17674 dataset, visualized through volcano and circular heatmap representations (Figures 13A, B).GO terms like Mitotic sister chromatid segregation, sister chromatid segregation, and chromosome, centromeric region were shown to be prevalent, according to functional enrichment analysis. In terms of KEGG pathways, the analysis was primarily associated with DNA replication, Cell cycle, and Ribosome biogenesis in eukaryotes (Figures 13C, D).

The GSVA results indicated that the high-risk group exhibited pathways enrichment, including pancreas_beta_cells, spermatogenesis,e2f_targets,g2m_checkpoint,ras_signaling_dn, and others. Conversely, pathways like heme_metabolism, tgf_beta_signaling,androgen_response,apoptosis,interferon_alpha_response,fatty_acid_metabolism,uv_response_dn,p53_pathway, xenobiotic_metabolism,adipogenesis,peroxisome,interferon_gamma_response,and kras_signaling_up,pancreas_beta_cells, spermatogenesis, e2f_targets, g2m_checkpoint, ras_signaling_dn were more prevalent in the group at low risk. (Figure 13E). Byheme_metabolism,tgf_beta_signaling,androgen_response,apoptosis, interferon_alpha_response,fatty_acid_metabolism,uv_response_dn, p53_pathway,xenobiotic_metabolism,adipogenesis,peroxisome, interferon_gamma_response,kras_signaling_up,and spermattogenesis e2f_targets g2m_checkpoint kras_signaling_dn were showed in the high risk group (Figure 13F).

4 Discussion

The prognosis of ES remains poor despite comprehensive treatment strategies (20). Proto-oncogenes and tumor suppressor genes undergo a number of genetic and epigenetic modifications over the course of Ewing's sarcoma development (21). As a vital micronutrient, copper is involved in many different physiological processes. According to earlier studies, altering copper metabolism may prevent the growth and invasion of cancer cells (22). Additionally, there have been the development of therapeutic strategies that specifically focus on copper or proteins involved in copper metabolism (23, 24).This work aims to examine the function of CMRGs in ES, Given the significance of copper in cancer.

The purpose of this study is to investigate the prognostic potential of CMRGs in ES. Using univariate Cox regression, we identified 22 CMRGs as prognostic indicators. The Kaplan-Meier analysis revealed notable disparities in survival rates between the groups with high and low expression of these PR-CMRGs. Notably,

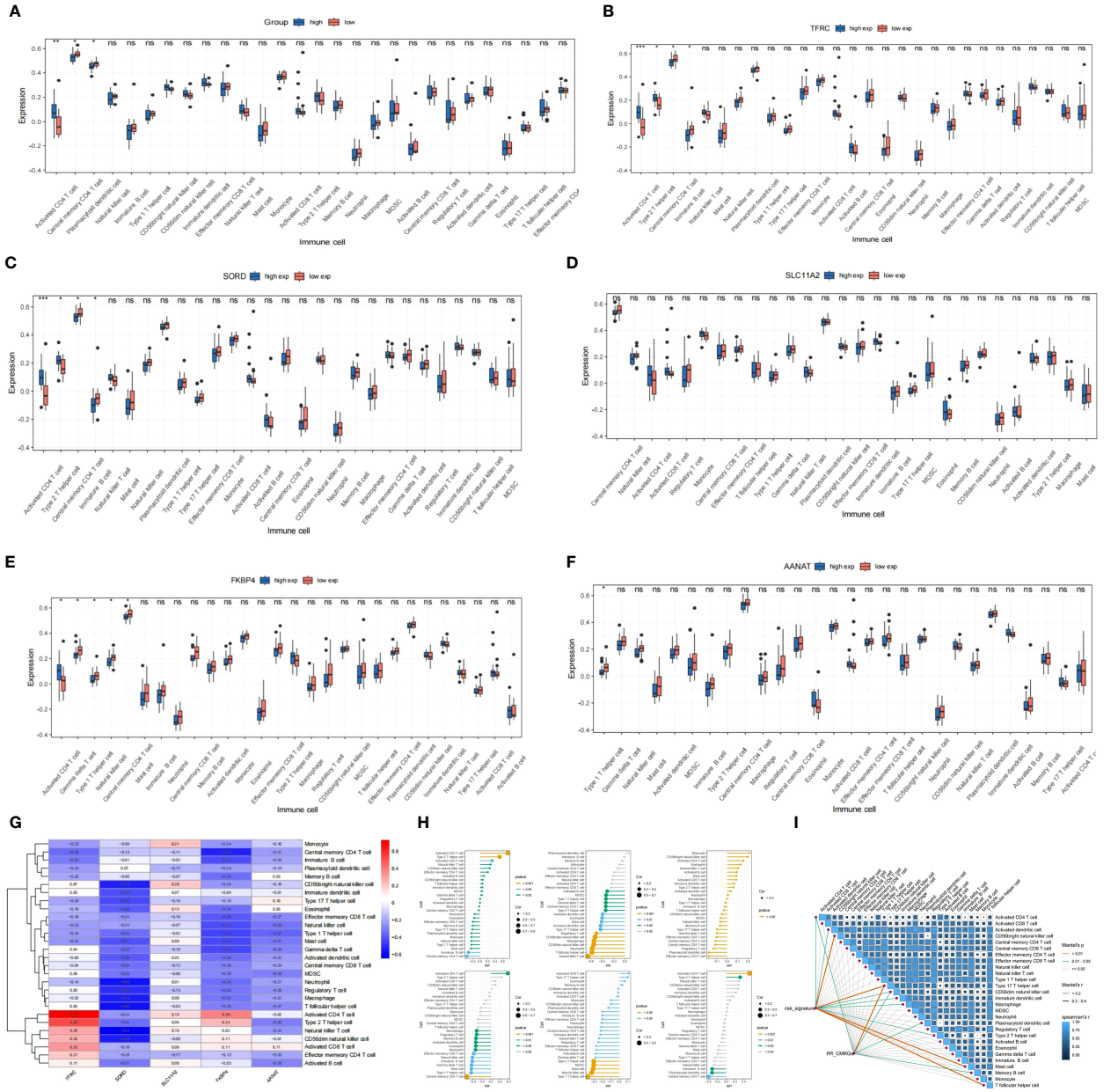

FIGURE 11
(A) Evaluation of immune cell infiltration between high and low risk groups (high: blue vs. low: red). **(B–F)** Boxplot of immune cell infiltration in differential TRFC,SORD,FKBP4,AANAT and SLC11A2 expression groups(high: blue vs. low: red). **(G–I)** Correlation of signatures and infiltrated immune cells, immune related pathways. * means p < 0.05, ** means p < 0.01, *** means p < 0.001 and ns means no significance (p>0.05).

seven PR-CMRGs—DAXX, CCS, MTF2, F8, SLC11A2, IL1A, and FKBP4—displayed differential expression in ES samples. Moreover, the expressions of seven PR-CMRGs were valided in MSCs, RD-ES and A673.Functional enrichment analysis, encompassing GO and KEGG pathways, revealed key functions and pathways through which these PR-CMRGs impact ES prognosis. These included responses to metal ions, transition metal ion transport, copper ion binding, and pathways related to various human cancers. These findings emphasized the link between copper metabolism and the formation and advancement of cancer.

To comprehend the molecular subtypes of ES based on PR-CMRGs, unsupervised clustering identified two distinct molecular clusters with differing survival rates. Additionally, these clusters exhibited distinct immune cell infiltration patterns, highlighting the potential involvement of the immune system in ES prognosis.

Prognostic risk models provide valuable insights into predicting cancer results. Such models can offer information about survival likelihood, risk of recurrence, and potential treatment responses, assisting clinicians in making well-informed treatment decisions. Given the significant role of CMRGs in ES, a risk model was established based on these genes.

There is no study suggested that the mechanism of TFRC, SORD, SLC11A2, FKBP4, and AANAT in cuproptosis. But in this

TABLE 2 Differential immune cell infiltration in differential TRFC,SORD,FKBP4,AANAT and SLC11A2 expression groups.

	TFRC		SORD		SLC11A2		FKBP4		ANNAT	
	High expression	low expression	High expression	low expression	High expression	low expression	High expression	low expression	High expression	low expression
Activated CD4 T cell	up		up				up			
Central memory CD4 T cell		up		up				up		
Gamma delta T cell								up		
Immature B cell		up								
Natural killer cell				up				up		
Type I Thelper cell								up		up
Type 2 Thelper cell	up	up								

study, it is demonstrated that TFRC, SORD, SLC11A2, FKBP4, and AANAT associated with survival and immune infiltration. The potential mechanism need further research. In this study, we identified TFRC, SORD, SLC11A2, FKBP4, and AANAT as a risk signature for ES. The prognostic model constructed using these genes demonstrated that TFRC, SLC11A2, FKBP4, and AANAT, each with a HR greater than 1, were associated with increased risk, while SORD, with an HR less than 1, was a favorable prognostic factor. The efficacy of the risk signature was comprehensively assessed through the utilization of Kaplan-Meier survival and ROC curves in training dataset and three validation datasets. The correlation between the risk group and survival rates was consistently observed, and the signature's specificity and sensitivity were robustly validated.

The TFRC gene in humans is responsible for encoding the transferrin receptor protein 1, controlling intracellular iron levels. Increased expression of TFRC promotes ferroptosis during CVB3 infection by recruiting Sp1 to the nucleus (25). TFR1, which mainly

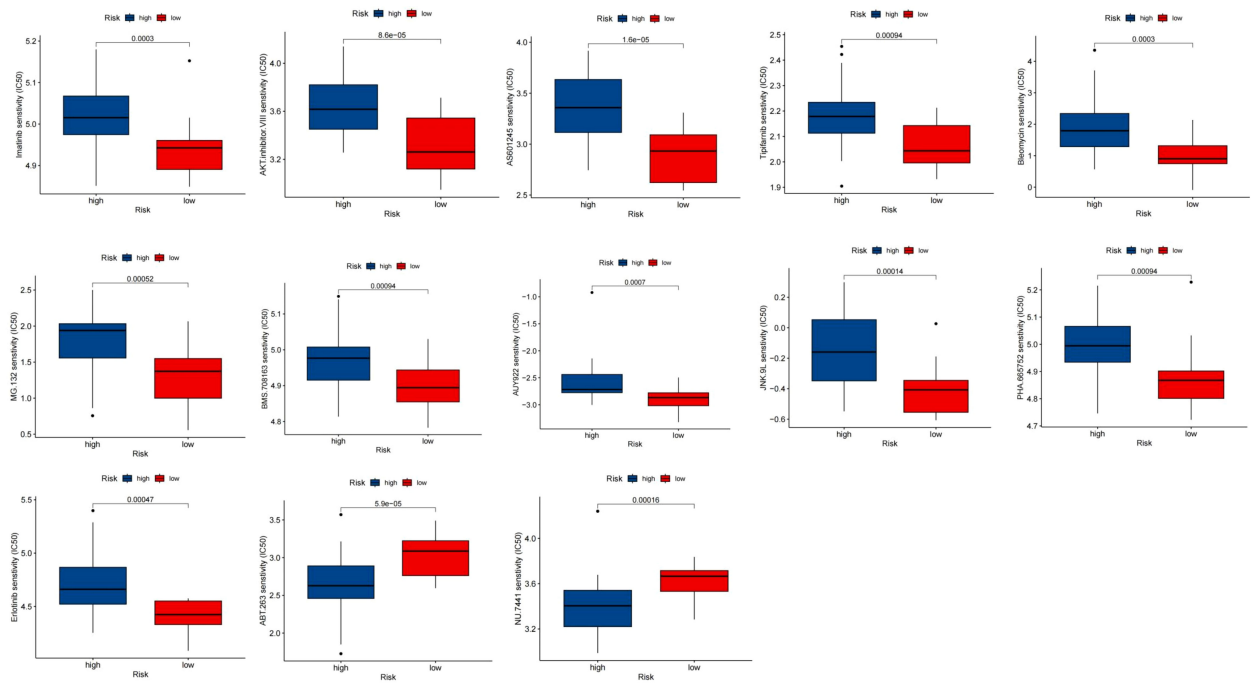

FIGURE 12
Chemotherapeutic response between risk groups. Boxplot of drugs benefited for samples in high and low risk groups.

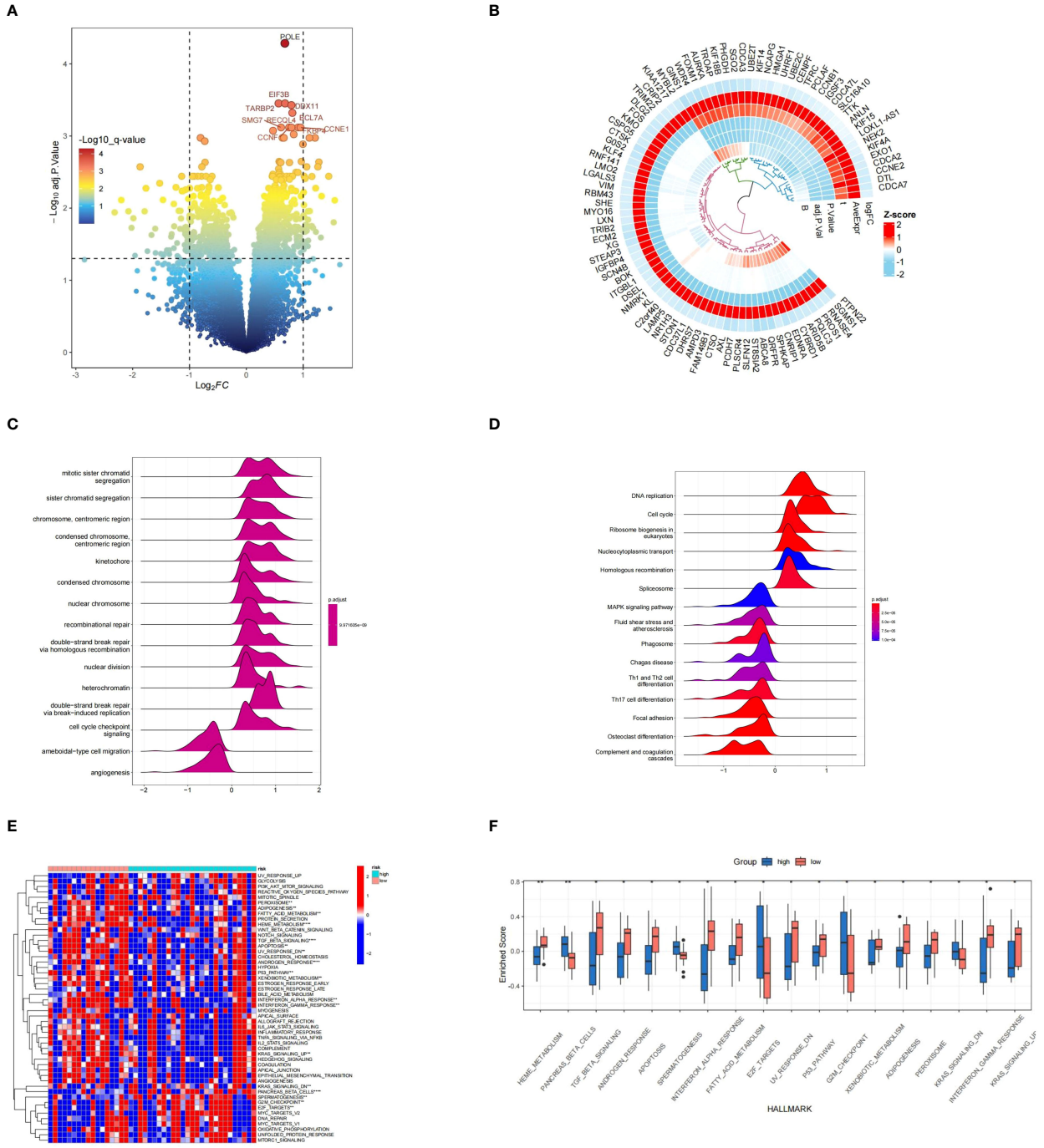

FIGURE 13
Analysis of differentially expressed genes (DEGs) and functional enrichment results. **(A, B)** Visualization of DEGs between various risk categories using a volcano plot and heatmap. **(C, D)** A ridgeplot displaying the GO and KEGG data by GSEA. **(E, F)** The results of GSVA analysis in groups classified as high and low risk. * means $p < 0.05$, ** means $p < 0.01$.

regulates cellular iron intake (26), binds to transferrin that is laden with iron, becomes surrounded by vesicles coated with clathrin, and then gets taken up by cells (27). TFR1 imports extracellular iron into cells, supporting the cellular iron store and being essential for ferroptosis (28). There is a close relationship between the iron and copper metabolic fares. The study demonstrated that the presence of Cu and Zn hindered the absorption of Fe, whereas the presence of Fe hindered the absorption of Cu (29). Thus, TFRC maybe change homeostasis of cellular iron to intervene copper metabolism. SORD is a dehydrogenase/reductase protein and plays a role in the metabolism of glucose (30). Studies have indicated SORD's involvement as a cuproptosis-related gene in coronary artery disease (31). SLC11A2 is a key protein that aids the absorption of iron and its influence extends to breast and colon cancer progression (32, 33). Divalent metal ion transporter 1 (DMT1; often referred to as SLC11A2) has the ability to transport several divalent metal ions such

as Fe2+, Mn2+, Cu2+, Zn2+, Cd2+, and Pb2+. It is possible that DMT1 also plays a role in the absorption of Cu. Therefore, maintaining an appropriate copper concentration is crucial for cellular function (34). The protein FKBP4, often referred to as FKBP52, is an immunophilin. Linked to HSP90, it aids in assembling various protein complexes (35, 36). Acting as a scaffold, FKBP4 promotes interactions among key components of multiple cancer-promoting signaling pathways (37, 38). FKBP52 is a constituent of the copper efflux mechanism, potentially contributing to neuroprotection against copper toxicity (39). AANAT serves as the rate-limiting enzyme in melatonin synthesis. However, it is unclear the role of AANAT in copper metabolism. According to current study, O-GlcNAcylation of YY1 targets SLC22A15 and AANAT, which promotes carcinogenesis in colorectal cancer cells (40). To sum up, our results showed that TFRC, SORD, SLC11A2, FKBP4, and AANAT maybe novel genes played significant roles in Ewing's sarcoma.

A nomogram visually presents a prediction model, forecasting a patient's prognosis based on clinical features. It also identifies significant prognosis-affecting factors by comparing patient survival rates. The risk score was validated as an independent prognostic factor by both univariate and multivariate Cox regression analysis. Subsequently, a nomogram was constructed for convenient ES prognosis prediction. The accuracy of survival prognosis prediction for ES was evaluated by calibration curves at 1, 3, and 5 years.

We use ssGSEA analysis to explore the functions of PR-CMRGs in different risk groups. Remarkably, a significant number of pathways connected to the immune system showed enrichment in the low-risk group. Copper chelation in tumor cells increased CD8+ T and NK cell influx, resulting in slowing tumor growth (41). Consequently, we hypothesized a close connection between copper metabolism and anti-tumor immunity. We then proceeded to scrutinize the variance in the TME between the two groups. Notably, augmented levels of immune cell infiltration correlated with a more favorable prognosis.

Given that the levels of immune checkpoints can predict immunotherapy response (42), we conducted a more in-depth examination of the differences in the levels of thirteen immunological checkpoints in the two groups. Our findings unveiled that NU.7441 and ABT.263 were benefit for the low-risk group, while AKT inhibitor VIII, AS601245, AUY922, Bleomycin, Tipifarnib, PHA.665752, MG.132, JNK.9L, BMS.708163, Erlotinib, and Imatinib showed greater advantages for the high-risk group. These results collectively pointed towards the potential of PR-CMRGs to offer guidance for immunotherapy in individuals diagnosed with ES.

Nonetheless, this study remains certain limitations merit. Initially, PR-CMRGs construction and validation depend on public databases, necessitating subsequent validation through future multicenter and prospective investigations. Secondly, further experimental endeavors are imperative to authenticate the individual and collective functions of the five genes encompassed within PR-CMRGs in ES.

To conclude, the study uncovered the significant influence of the interplay between copper metabolism and immunity on the progression of ES. For ES patients, the prognostic model based on 5 PR-CMRGs was developed and its prediction efficiency was well demonstrated. This model can be conducive to prognostic prediction and may provide a guidance on immunotherapy.

Data availability statement

The original contributions presented in the study are included in the article/Supplementary Material. Further inquiries can be directed to the corresponding authors.

Ethics statement

Ethical approval was not required for the studies on humans in accordance with the local legislation and institutional requirements because only commercially available established cell lines were used. Ethical approval was not required for the studies on animals in accordance with the local legislation and institutional requirements because only commercially available established cell lines were used.

Author contributions

YC: Conceptualization, Formal analysis, Investigation, Writing – original draft, Writing – review & editing. WZ: Conceptualization, Formal analysis, Methodology, Writing – original draft, Writing – review & editing. XX: Data curation, Software, Validation, Writing – original draft, Writing – review & editing. BX: Data curation, Software, Validation, Writing – original draft, Writing – review & editing. YY: Data curation, Software, Validation, Writing – original draft, Writing – review & editing. HY: Data curation, Software, Validation, Visualization, Writing – original draft, Writing – review & editing. KL: Data curation, Software, Writing – original draft, Writing – review & editing. ML: Data curation, Software, Writing – original draft, Writing – review & editing. LQ: Conceptualization, Funding acquisition, Investigation, Methodology, Project administration, Supervision, Writing – original draft, Writing – review & editing. XJ: Conceptualization, Investigation, Methodology, Project administration, Supervision, Writing – original draft, Writing – review & editing.

Funding

The author(s) declare financial support was received for the research, authorship, and/or publication of this article. This work was funded by the Shandong Provincial Natural Science Foundation, China. (grant number: ZR2023MH383).

Conflict of interest

The authors declare that the research was conducted in the absence of any commercial or financial relationships that could be construed as a potential conflict of interest.

Publisher's note

All claims expressed in this article are solely those of the authors and do not necessarily represent those of their affiliated organizations, or those of the publisher, the editors and the reviewers. Any product that may be evaluated in this article, or claim that may be made by its manufacturer, is not guaranteed or endorsed by the publisher.

Supplementary material

The Supplementary Material for this article can be found online at: https://www.frontiersin.org/articles/10.3389/fonc.2024.1388868/full#supplementary-material

References

1. Balamuth NJ, Womer RB. Ewing's sarcoma. *Lancet Oncol.* (2010) 11:184–92. doi: 10.1016/S1470-2045(09)70286-4

2. Eyre R, Feltbower RG, James PW, Blakey K, Mubwandarikwa E, Forman D, et al. The epidemiology of bone cancer in 0 - 39 year olds in northern England, 1981 - 2002. *BMC Cancer.* (2010) 10:357. doi: 10.1186/1471-2407-10-357

3. Grünewald TGP, Cidre-Aranaz F, Surdez D, Tomazou EM, Álava E, Kovar H, et al. Ewing sarcoma. *Nat Rev Dis Primers.* (2018) 4:6. doi: 10.1038/s41572-018-0007-6

4. Gorthi A, Romero JC, Loranc E, Cao L, Lawrence LA, Goodale E, et al. EWS-FLI1 increases transcription to cause R-loops and block BRCA1 repair in Ewing sarcoma. *Nature.* (2018) 555:387–91. doi: 10.1038/nature25748

5. Spriano F, Chung E, Gaudio E, Tarantelli C, Cascione L, Napoli S, et al. The ETS inhibitors YK-4–279 and TK-216 are novel antilymphoma agents. *Clin Cancer Res.* (2019) 25:5167–76. doi: 10.1158/1078-0432.CCR-18-2718

6. Chen L, Min J, Wang F. Copper homeostasis and cuproptosis in health and disease. *Signal Transduct Target Ther.* (2022) 7:378. doi: 10.1038/s41392-022-01229-y

7. Gromadzka G, Tarnacka B, Flaga A, Adamczyk A. Copper dyshomeostasis in neurodegenerative diseases-therapeutic implications. *Int J Mol Sci.* (2020) 21. doi: 10.3390/ijms21239259

8. Chen J, Jiang Y, Shi H, Peng Y, Fan X, Li C. The molecular mechanisms of copper metabolism and its roles in human diseases. *Pflugers Arch.* (2020) 472:1415–29. doi: 10.1007/s00424-020-02412-2

9. Rezaei A, Falahati-Pour SK, Mohammadizadeh F, Hajizadeh MR, Mirzaei MR, Khoshdel A, et al. Effect of a copper (II) complex on the induction of apoptosis in human hepatocellular carcinoma cells. *Asian Pac J Cancer Prev.* (2018) 19:2877–84. doi: 10.22034/APJCP.2018.19.10.2877

10. Gupte A, Mumper RJ. Elevated copper and oxidative stress in cancer cells as a target for cancer treatment. *Cancer Treat Rev.* (2009) 35:32–46. doi: 10.1016/j.ctrv.2008.07.004

11. Zhang G, Sun J, Zhang X. A novel Cuproptosis-related LncRNA signature to predict prognosis in hepatocellular carcinoma. *Sci Rep.* (2022) 12:11325. doi: 10.1038/s41598-022-15251-1

12. Capriotti G, Piccardo A, Giovannelli E, Signore A. Targeting copper in cancer imaging and therapy: A new theragnostic agent. *J Clin Med.* (2022) 12. doi: 10.3390/jcm12010223

13. Ge EJ, Bush AI, Casini A, Cobine PA, Cross JR, DeNicola GM, et al. Connecting copper and cancer: from transition metal signalling to metalloplasia. *Nat Rev Cancer.* (2022) 22:102–13. doi: 10.1038/s41568-021-00417-2

14. Wang X, Zhou M, Liu Y, Si Z. Cope with copper: From copper linked mechanisms to copper-based clinical cancer therapies. *Cancer Lett.* (2023) 561:216157. doi: 10.1016/j.canlet.2023.216157

15. Wang Z, Jin D, Zhou S, Dong N, Ji Y, An P, et al. Regulatory roles of copper metabolism and cuproptosis in human cancers. *Front Oncol.* (2023) 13:1123420. doi: 10.3389/fonc.2023.1123420

16. Li Y. Copper homeostasis: Emerging target for cancer treatment. *IUBMB Life.* (2020) 72:1900–8. doi: 10.1002/iub.2341

17. Chang W, Li H, Zhong L, Zhu T, Chang Z, Ou W, et al. Development of a copper metabolism-related gene signature in lung adenocarcinoma. *Front Immunol.* (2022) 13:1040668. doi: 10.3389/fimmu.2022.1040668

18. Liu B, Liu Z, Feng C, Li C, Zhang H, Li Z, et al. Identification of cuproptosis-related lncRNA prognostic signature for osteosarcoma. *Front Endocrinol (Lausanne).* (2022) 13:987942. doi: 10.3389/fendo.2022.987942

19. Tisato F, Marzano C, Porchia M, Pellei M, Santini C. Copper in diseases and treatments, and copper-based anticancer strategies. *Med Res Rev.* (2010) 30:708–49. doi: 10.1002/med.20174

20. Gaspar N, Hawkins DS, Dirksen U, Lewis IJ, Ferrari S, Deley Le M-C, et al. Ewing sarcoma: current management and future approaches through collaboration. *J Clin Oncol.* (2015) 33:3036–46. doi: 10.1200/JCO.2014.59.5256

21. Li Z, Yu X, Shen J, Wu WK, Chan MT. MicroRNA expression and its clinical implications in Ewing's sarcoma. *Cell Prolif.* (2015) 48:1–6. doi: 10.1111/cpr.12160

22. Ruiz LM, Libedinsky A, Elorza AA. Role of copper on mitochondrial function and metabolism. *Front Mol Biosci.* (2021) 8:711227. doi: 10.3389/fmolb.2021.711227

23. Daniel KG, Gupta P, Harbach RH, Guida WC, Dou QP. Organic copper complexes as a new class of proteasome inhibitors and apoptosis inducers in human cancer cells. *Biochem Pharmacol.* (2004) 67:1139–51. doi: 10.1016/j.bcp.2003.10.031

24. Trackman PC. Lysyl oxidase isoforms and potential therapeutic opportunities for fibrosis and cancer. *Expert Opin Ther Targets.* (2016) 20:935–45. doi: 10.1517/14728222.2016.1151003

25. Yi L, Hu Y, Wu Z, Li Y, Kong M, Kang Z, et al. TFRC upregulation promotes ferroptosis in CVB3 infection via nucleus recruitment of Sp1. *Cell Death Dis.* (2022) 13:592. doi: 10.1038/s41419-022-05027-w

26. Fisher AL, Wang CY, Xu Y, Joachim K, Xiao X, Phillips S, et al. Functional role of endothelial transferrin receptor 1 in iron sensing and homeostasis. *Am J Hematol.* (2022) 97:1548–59. doi: 10.1002/ajh.26716

27. Cao H, Krueger EW, McNiven MA. Hepatocytes internalize trophic receptors at large endocytic "Hot Spots". *Hepatology.* (2011) 54:1819–29. doi: 10.1002/hep.24572

28. Feng H, Schorpp K, Jin J, Yozwiak CE, Hoffstrom BG, Decker AM, et al. Transferrin receptor is a specific Ferroptosis marker. *Cell Rep.* (2020) 30:3411–23.e7. doi: 10.1016/j.celrep.2020.02.049

29. Arredondo M, Martínez R, Núñez MT, Ruz M, Olivares M. Inhibition of iron and copper uptake by iron, copper and zinc. *Biol Res.* (2006) 39:95–102. doi: 10.4067/S0716-97602006000100011

30. El-Kabbani O, Darmanin C, Chung RP. Sorbitol dehydrogenase: structure, function and ligand design. *Curr Med Chem.* (2004) 11:465–76. doi: 10.2174/0929867043455927

31. Zhang B, He M. Identification of potential biomarkers for coronary artery disease based on cuproptosis. *Cardiovasc Ther.* (2023) 2023:5996144. doi: 10.1155/2023/5996144

32. Li Y, Pan K, Chen L, Ning J-L, Li X, Yang T, et al. Deferoxamine regulates neuroinflammation and iron homeostasis in a mouse model of postoperative cognitive dysfunction. *J Neuroinflammation.* (2016) 13:268. doi: 10.1186/s12974-016-0740-2

33. Chen C, Liu P, Duan X, Cheng M, Xu LX. Deferoxamine-induced high expression of TfR1 and DMT1 enhanced iron uptake in triple-negative breast cancer cells by activating IL-6/PI3K/AKT pathway. *Onco Targets Ther.* (2019) 12:4359–77. doi: 10.2147/OTT

34. Gunshin H, Mackenzie B, Berger UV, Gunshin Y, Romero MF, Boron WF, et al. Cloning and characterization of a mammalian proton-coupled metal-ion transporter. *Nature.* (1997) 388:482–8. doi: 10.1038/41343

35. Xue X, Ramakrishnan SK, Weisz K, Triner D, Xie L, Attili D, et al. Iron uptake via DMT1 integrates cell cycle with JAK-STAT3 signaling to promote colorectal tumorigenesis. *Cell Metab.* (2016) 24:447–61. doi: 10.1016/j.cmet.2016.07.015

36. Martinez NJ, Chang HM, Borrajo Jde R, Gregory RI. The co-chaperones Fkbp4/5 control Argonaute2 expression and facilitate RISC assembly. *RNA*. (2013) 19:1583–93. doi: 10.1261/rna.040790.113

37. Zong S, Jiao Y, Liu X, Mu W, Yuan X, Qu Y, et al. FKBP4 integrates FKBP4/Hsp90/IKK with FKBP4/Hsp70/RelA complex to promote lung adenocarcinoma progression via IKK/NF-κB signaling. *Cell Death Dis*. (2021) 12:602. doi: 10.1038/s41419-021-03857-8

38. Mangé A, Coyaud E, Desmetz C, Laurent E, Béganton B, Coopman P, et al. FKBP4 connects mTORC2 and PI3K to activate the PDK1/Akt-dependent cell proliferation signaling in breast cancer. *Theranostics*. (2019) 9:7003–15. doi: 10.7150/thno.35561

39. Sanokawa-Akakura R, Dai H, Akakura S, Weinstein D, Fajardo JE, Lang SE, et al. A novel role for the immunophilin FKBP52 in copper transport. *J Biol Chem*. (2004) 279:27845–8. doi: 10.1074/jbc.C400118200

40. Zhu G, Qian M, Lu L, Chen Y, Zhang X, Wu Q, et al. O-GlcNAcylation of YY1 stimulates tumorigenesis in colorectal cancer cells by targeting SLC22A15 and AANAT. *Carcinogenesis*. (2019) 40:1121–31. doi: 10.1093/carcin/bgz010

41. Voli F, Valli E, Lerra L, Kimpton K, Saletta F, Giorgi FM, et al. Intratumoral copper modulates PD-L1 expression and influences tumor immune evasion. *Cancer Res*. (2020) 80:4129–44. doi: 10.1158/0008-5472.CAN-20-0471

42. Ren D, Hua Y, Yu B, Ye X, He Z, Li C, et al. Predictive biomarkers and mechanisms underlying resistance to PD1/PD-L1 blockade cancer immunotherapy. *Mol Cancer*. (2020) 19:19. doi: 10.1186/s12943-020-1144-6

frontiers | Frontiers in Oncology

TYPE Original Research
PUBLISHED 01 October 2024
DOI 10.3389/fonc.2024.1428802

OPEN ACCESS

EDITED BY
Shivendra Vikram Singh,
St. Jude Children's Research Hospital,
United States

REVIEWED BY
Sanjay Pandey,
Albert Einstein College of Medicine,
United States
Arig Ibrahim-Hashim,
Moffitt Cancer Center, United States
Uri Nir,
Bar-Ilan University, Israel
Amit Kumar,
University of Maryland, United States

*CORRESPONDENCE
Randall J. Kimple
rkimple@humonc.wisc.edu

RECEIVED 07 May 2024
ACCEPTED 10 September 2024
PUBLISHED 01 October 2024

CITATION
Gurel Z, Luy MS, Luo Q, Arp NL, Erbe AK, Kesarwala AH, Fan J and Kimple RJ (2024) Metabolic modulation of melanoma enhances the therapeutic potential of immune checkpoint inhibitors.
Front. Oncol. 14:1428802.
doi: 10.3389/fonc.2024.1428802

Metabolic modulation of melanoma enhances the therapeutic potential of immune checkpoint inhibitors

Zafer Gurel[1], Michael S. Luy[1], Qianyun Luo[1], Nicholas L. Arp[2], Amy K. Erbe[1], Aparna H. Kesarwala[3], Jing Fan[2,4,5] and Randall J. Kimple[1,6]*

[1]Department of Human Oncology, University of Wisconsin School of Medicine and Public Health, Madison, WI, United States, [2]Morgridge Institute for Research, Madison, WI, United States, [3]Department of Radiation Oncology, Winship Cancer Institute, Emory University School of Medicine, Atlanta, GA, United States, [4]Cellular and Molecular Biology Graduate Program, University of Wisconsin-Madison, Madison, WI, United States, [5]Department of Nutritional Sciences, University of Wisconsin-Madison, Madison, WI, United States, [6]University of Wisconsin (UW) Carbone Cancer Center, University of Wisconsin School of Medicine and Public Health, Madison, WI, United States

Introduction: Lactate is a pivotal molecule with diverse functions in the metabolic reprogramming of cancer cells. Beyond its role in metabolism, lactate exerts a modulatory effect within the tumor microenvironment; it is utilized by stromal cells and has been implicated in the suppression of the immune response against the tumor.

Methods: Using *in vitro* assays (including flow cytometry, live-cell imaging and metabolic analyses), the impact of lactate dehydrogenase inhibitors (LDHIs) on melanoma cells were assessed. The therapeutic potential of LDHIs with immune checkpoint inhibitors (ICIs) were tested *in vivo* in murine models of melanoma tumors.

Results: A potent anti-proliferative effect (via both cell cycle alterations and enhanced apoptosis) of LDHIs, Oxamate (Oxa) and methyl 1-hydroxy-6-phenyl-4-(trifluoromethyl)-1H-indole-2-carboxylate (NHI-2), was found upon treatment of melanoma cell lines. Using a combination of Oxa and NHI-2, a synergistic effect to inhibit proliferation, glycolysis, and ATP production was observed. Metabolic analysis revealed significant alteration in glycolysis and oxidative phosphorylation, while metabolite profiling emphasized consequential effects on lactate metabolism and induced energy depletion by LDHIs. Detection of increased RANTES and MCP-1, with Oxa and NHI-2 treatment, prompted the consideration of combining LDHIs with ICIs. *In vivo* studies using a murine B78 melanoma tumor model revealed a significant improvement in treatment efficacy when LDHIs were combined with ICIs.

Conclusions: These findings propose the potential of targeting lactate metabolism to enhance the efficacy of ICI treatments in patients with melanoma.

KEYWORDS

melanoma, cancer metabolism, lactate, LDH, oxamate, NHI-2, immune checkpoint inhibitors

1 Introduction

The metabolism of cancer cells differs markedly from that of non-malignant cells. One of the major metabolic hallmarks of cancer cells, the Warburg effect, was reported almost a century ago (1). The Warburg effect is defined as an increased dependence on glycolysis for ATP synthesis, even in the presence of oxygen, diverging from the conventional oxidative phosphorylation pathway (2). Subsequent studies have revealed that the metabolic adaptations in tumors extend beyond the Warburg effect (3). Cancer cells demonstrate notable metabolic plasticity, enabling them to swiftly adjust to the dynamically changing tumor microenvironment (TME) (4). This metabolic plasticity, coupled with genetic and epigenetic alterations contributes to heterogeneity within the tumor, resulting in chemo/radio-resistance, immune escape, and tumor recurrence (5–7).

Lactate is a metabolic byproduct that has long been considered a waste product of glycolysis. Although the initial reports of lactate accumulation in muscles date back to the early 1900s (8, 9), it is only within the last two decades that we have started to unravel novel biological functions associated with this molecule. Lactate is now recognized as both an important carbon source for cellular metabolism and as a signaling molecule, particularly in chronically inflamed and cancerous tissues (10). However, the cellular response to lactate in the TME is quite different to that occurring in the context of chronic inflammation. Therefore, further studies are required to understand the role of lactate in the TME.

Given the metabolic diversity among tumor cells, there is a postulation that glycolytic and oxidative cells engage in symbiotic interactions. Glycolytic cells export lactate to the TME, while oxidative cells import it and utilize lactate as an energy source (11). This symbiotic relationship becomes particularly crucial as tumors grow, leading to a hypoxic microenvironment in the tumor center and better oxygenation near blood vessels (12). The utilization of lactate as an energy source by perivascular cells in tumors could elucidate the correlation between elevated lactate concentrations in the TME and the subsequent development of nodal or distant metastases in various cancers (13–19).

Moreover, high TME lactate levels play a crucial role in modulating immune cell function and fostering immune escape within tumors by suppressing the tumor-specific $CD8^+$ T lymphocytes and macrophages (20–22). Additionally, lactate-driven immune cell modulation includes an influx of suppressive immune subsets, with Treg cells adapting to the high-lactate/low-glucose environment by upregulating FOXP3 expression (23). This multilayered impact of lactate highlights its significance in tumor progression and immune response modulation.

In the landscape of melanoma treatment, immune checkpoint inhibitors (ICI) have emerged as a cornerstone over the past decade, revolutionizing therapeutic strategies for many patients. However, both innate and acquired resistance to ICI treatment present substantial challenges, limiting the therapeutic impact of ICI therapy in melanoma. Several checkpoint inhibitors, including the anti-CTLA-4 and the anti-PD-1 monoclonal antibodies, are approved for the treatment of advanced melanoma. Studies dedicated to melanoma treatment report response rates of 20% for anti-CTLA-4 and 40% for anti-PD-1, accompanied by 5-year progression-free survival (PFS) rates of 8% and 20%, respectively (24–27). These insights highlight the existing challenges and emphasize the need for innovative approaches to enhance the efficacy of ICI treatments in melanoma. Several clinical trials are in progress to evaluate the efficacy of combining glycolysis inhibitors with immune modulator therapies, predominantly focusing on the AKT/mTOR pathway (NCT03190174, NCT03772561, NCT04895748, NCT04591431). However, none of these clinical trials focus on melanoma patients and there are only a limited number of pre-clinical studies that utilize lactate dehydrogenase inhibitors (LDHIs) with ICIs in animal tumor models (28, 29).

Lactate dehydrogenase (LDH) is a critical enzyme in the metabolic process, serving a pivotal role in the interconversion of lactate and pyruvate, alongside the concomitant interconversion of NADH and NAD+ (30). LDH comprises multiple isoenzymes, among which LDHA and LDHB are the primary subunits that combine to form the various LDH isoforms present in human tissues (31). These subunits are encoded by distinct genes, LDHA and LDHB, respectively, and their expression and activity are finely tuned according to the metabolic demands and oxygen availability of specific tissues. The link between elevated serum LDH levels and poor prognosis in melanoma is well established, indicating the significance of LDH as a prognostic biomarker (32–35). Additionally, high baseline LDH levels and lactic acid accumulation have been correlated with less favorable outcomes in patients receiving ICIs, indicating that targeting LDH could enhance the efficacy of ICI therapies in melanoma (36–39).

This study aimed to disrupt the energy metabolism within melanoma tumors by targeting LDH enzymes, specifically LDHA and LDHB, with the goal of enhancing the efficacy of ICI treatments. We observed strong anti-proliferative effects of two LDHIs, namely Oxamate (Oxa) and Methyl 1-hydroxy-6-phenyl-4-(trifluoromethyl)-1H-indole-2-carboxylate (NHI-2), on melanoma cell lines. Oxa, acting as a pyruvate analog inhibits LDHA (40), whereas NHI-2 functions as a NADH competitor to inhibit both LDHA and LDHB (41). The observed synergistic interaction between Oxa and NHI-2 revealed an impact on melanoma cell metabolism that extends beyond glycolysis inhibition, including oxidative phosphorylation and macromolecule synthesis. These findings point to a more complex mechanism of action, underscoring the potential significance of this drug combination in targeting melanoma cells. Additionally, screening for changes in cytokines and chemokines showed an elevation in the release of specific chemokines, including regulated upon activation, normal T cell expressed and secreted (RANTES), and monocyte chemoattractant protein-1 (MCP-1) in the B78 melanoma cell line following LDHI treatment. *In vivo* studies showed a significant improvement in treatment efficacy when Oxa and NHI-2 were combined with immune checkpoint inhibitors

(aPD-L1+aCTL4) in a B78 melanoma tumor model. Therefore, this study not only indicated the potential strategy of disrupting melanoma cell metabolism through LDHIs but also emphasized the innovative approach of enhancing ICI efficacy through this combination.

2 Results

2.1 Synergistic anti-proliferative effects of LDH inhibitors on melanoma cell lines

The impact of LDHIs, specifically Oxa and NHI-2, on the proliferation of B78 (mouse amelanotic melanoma B78-D14), B16-F10 (mouse skin melanoma), and M21 (human metastatic melanoma) cell lines, was screened via real-time cell counting through an IncuCyte™ S3 live cell imaging system. The anti-proliferative effects of Oxa and NHI-2 became evident within 12 hours. Higher concentrations of Oxa (30 and 60 mM) led to a complete blockade of B78 cell proliferation (Figure 1A), and EC50 value was calculated as 20 mM for Oxa (Figure 1B). NHI-2 was effective in μM levels and 40 μM NHI-2 led to a complete blockade of B78 cell proliferation (Figure 1C). The EC50 value was calculated as 25 μM for NHI-2, according to inhibition of B78 cell proliferation (Figure 1D). Consistent outcomes were replicated in B16 and M21 cell lines (Supplementary Figure S1). At lower doses, such as 15 mM Oxa or 18 μM NHI-2, their combined application demonstrated an effective suppression of B78 cell proliferation, surpassing the outcomes observed with either vehicle control or single-drug treatments (Figure 1E).

The synergistic effects of the combination treatment of Oxa and NHI-2 on melanoma cell proliferation were assessed by subjecting cells to various concentrations of these inhibitors, administered either individually or in combination. Normalized results were analyzed using the SynergyFinderPlus tool, incorporating diverse models such as highest single agent (HAS), Bliss independence, Loewe additivity, and zero interaction potency (ZIP) to compute the synergy score (42). The recently developed ZIP model combines the strengths of the Loewe and Bliss models, assuming that non-interacting medicines cause modest modifications in their dose-response curves (43). The ZIP model analysis revealed an average synergy score of 20.88 ($p < 2e{-}324$) for the interaction between Oxa and NHI-2 in B78 cells (Figure 1F). Scores exceeding 10 indicated a synergistic effect. The synergy score reached up to 40 for certain concentrations, such as a combination of 15 mM Oxa and 18 μM NHI-2. Consistent with this, both the HSA and Bliss models affirmed the synergistic impact of the Oxa and NHI-2 combination treatment in B78 cells (Supplementary Figure S2). While M21 cells displayed less sensitivity to LDHIs than B78 cells, the combination of Oxa and NHI-2 still exhibited a synergistic effect, with an average ZIP score of 14.17 ($p = 1.08e{-}23$) (Supplementary Figure S3).

Overall, the interaction landscape indicates that the combined treatment of Oxa and NHI-2 exerts a synergistic effect on the survival of melanoma cell lines.

2.2 Impact of LDH inhibitors on cell viability and cell cycle in B78 melanoma cells

To assess the impact of LDHIs on apoptosis, apoptotic cell ratios were calculated using NucView® caspase-3 substrate. This substrate allows the detection of caspase-3/7 activity in live cells via the IncuCyte® imaging system. While individual administration of Oxa and NHI-2 did not induce a notable rise in caspase-3/7 activation, a significant increase in apoptosis was observed when 40 μM NHI-2 was combined with either 30 or 60 mM Oxa in B78 cells (Figure 2A). Specifically, 24 hours after treatment, the apoptotic cell ratio increased to 8.88% in the 30 mM Oxa + 40 μM NHI-2 group and to 9.12% in the 60 mM Oxa + 40 μM NHI-2 group, compared with 0.14% in the vehicle control group. Lower doses of the drugs, even in combination, did not significantly alter the apoptotic cell ratio, according to caspase-3/7 activity (Supplementary Figure S4).

To further investigate apoptosis and cell death, cells were treated with various concentrations of Oxa and NHI-2 for 24 hours. Subsequently, Annexin V/PI staining and flow cytometric analysis were conducted. The flow data, consistent with caspase-3/7 results, demonstrated an increase in early apoptotic (Annexin V positive) cell ratios, particularly with the combination of 40 μM NHI-2 with either 30 or 60 mM Oxa (Figure 2B). The early apoptotic cell ratio was 1.25% for the vehicle treatment, 5.82% for 30 mM Oxa + 40 μM NHI-2, and 3.09% for 60 mM Oxa + 40 μM NHI-2. Furthermore, the late apoptotic/dead (Annexin V + PI positive) cell ratio moderately increased in the 40 μM NHI-2 group to 23.64%, and it significantly increased in the 30 mM Oxa + 40 μM NHI-2 to 48.53% and 60 mM Oxa + 40 μM NHI-2 to 67.15% groups compared to the vehicle control, which was at 12.98%.

Furthermore, alterations in cell cycle distribution in B78 cells were analyzed after 24 hours of treatment with Oxa and NHI-2 either alone or in combination. Flow cytometry was employed to analyze changes in the cell cycle after PI staining. The results demonstrated that Oxa induced accumulation in the G1 phase of the cell cycle, whereas NHI-2 led to an increased cell population in the S and G2 phases, as evidenced by the gating strategy and quantification model employed (Figures 2C, D).

Together, these findings suggested that Oxa and NHI-2 may affect distinct pathways, and their combination has detrimental effects on B78 cells.

2.3 Metabolic impacts of Oxa and NHI-2 on glycolytic and oxidative pathways

To elucidate the metabolic alterations induced by Oxa and NHI-2 in B78 cells, the extracellular acidification rate (ECAR) and mitochondrial oxygen consumption rate (OCR) were quantified using a Seahorse XFe96 analyzer. Oxa treatment at 7.5- and 15-mM concentrations resulted in a dose-dependent decrease in ECAR, indicating reduced glycolytic activity. Furthermore, cells pre-treated with Oxa displayed a diminished ECAR upsurge in response to the ATP synthase inhibitor oligomycin, suggesting a compromised

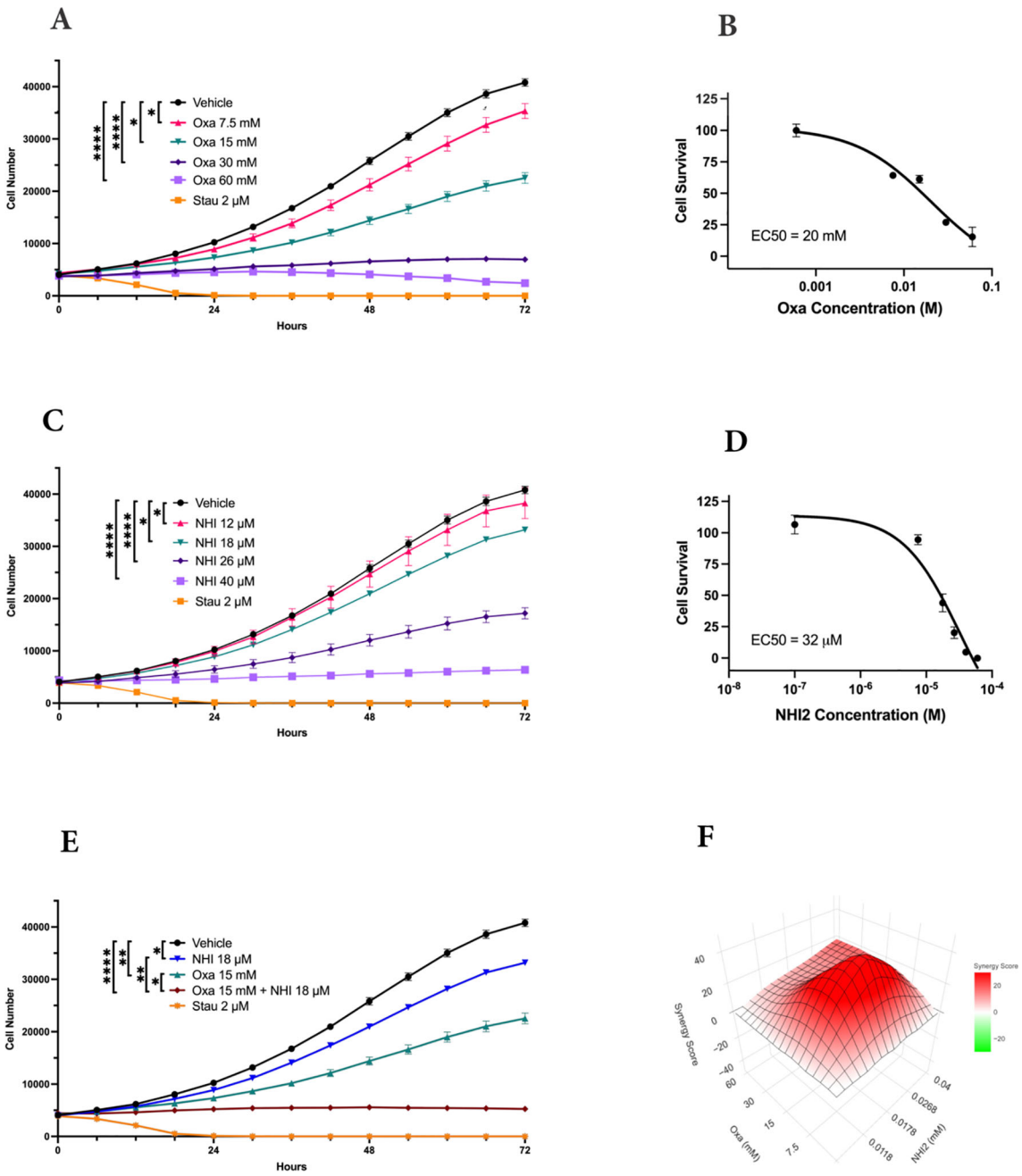

FIGURE 1
LDH-inhibitors oxamate and NHI-2 exhibit potent and synergistic anti- proliferative effects on B78-D14 melanoma cells. Cell proliferation was monitored in real time with the continuous presence of **(A)** Oxa (Oxamate) and **(C)** NHI-2 treatments for 72 hours using an IncuCyte ® S3 instrument. The changes in cell number are used as a surrogate marker of cell proliferation. Data shown are the mean ± SEM (n = 3). Cell viability curves and EC50 values for B78 cell lines treated with **(B)** Oxa and **(D)** NHI-2 for 48 h at various concentrations. EC50 values were calculated in GraphPad Prism using the non-linear fit curve method. **(E)** The graph and statistical analysis demonstrate the enhanced effectiveness of Oxa and NHI-2 combination treatments on B78 cell proliferation compared to single-agent usage, as indicated by the concentrations on the graph (Two-way ANOVA; ****$p < 0.0001$; **$p < 0.01$; *$p < 0.05$). Stau (Staurosporine) was used as positive control. **(F)** Synergy analysis for the Oxa and NHI-2 combination treatment in the B78 cell line, conducted using synergyfinderplus.org. The results are compared using three distinct synergy correlation method: ZIP (zero interaction potency) model, with a synergy score Mean of 20.88 ($p < 2e{-}324$). A synergy score exceeding 10 indicates a pronounced synergistic effect.

glycolytic compensatory mechanism (Figure 3A). NHI-2 at 12-and 18-µM concentrations elevated the basal glycolytic rate as reflected by ECAR measurements. However, at a 25 µM concentration, NHI-2 significantly decreased both basal and oligomycin-stimulated glycolytic processes (Figure 3B). Crucially, co-treatment with Oxa and NHI-2 led to an effective suppression of glycolysis at even lower doses, as evidenced by the ECAR data (Figure 3C, Supplementary Figure S5).

OCR data demonstrated that Oxa moderately increased both basal and maximal mitochondrial respiration (Figure 3D). NHI-2

significantly inhibited basal respiration in a dose-dependent manner, rendering cells unresponsive to FCCP (carbonylcyanide-p-trifluo romethoxy-phenyl-hydrazone) stimulation (Figure 3E). The combination of low doses of Oxa (7.5 mM) and NHI-2 (12 µM) resulted in a modest additional reduction in basal respiration compared to NHI-2 alone, likely due to the already substantial efficacy of NHI-2 in inhibiting basal respiration even at low doses as a single agent (Figure 3F).

Overall, ECAR measurements indicated the enhanced anti-glycolytic efficacy of the combination of Oxa and NHI-2, particularly at lower doses, surpassing the outcomes of individual treatments. Additionally, OCR data reveals that NHI-2 may also suppress oxidative phosphorylation (OXPHOS), suggesting its broader impact on cellular energy production.

2.4 Metabolic profile alterations in B78 cells treated with Oxa and NHI-2

To understand the effects of Oxa and NHI-2 treatments on metabolic pathways, metabolite levels in B78 cells were analyzed using liquid chromatography–mass spectrometry (LC-MS). This approach enabled the detection and quantification of sixty-six intracellular metabolites (Figure 4A). Only the combination

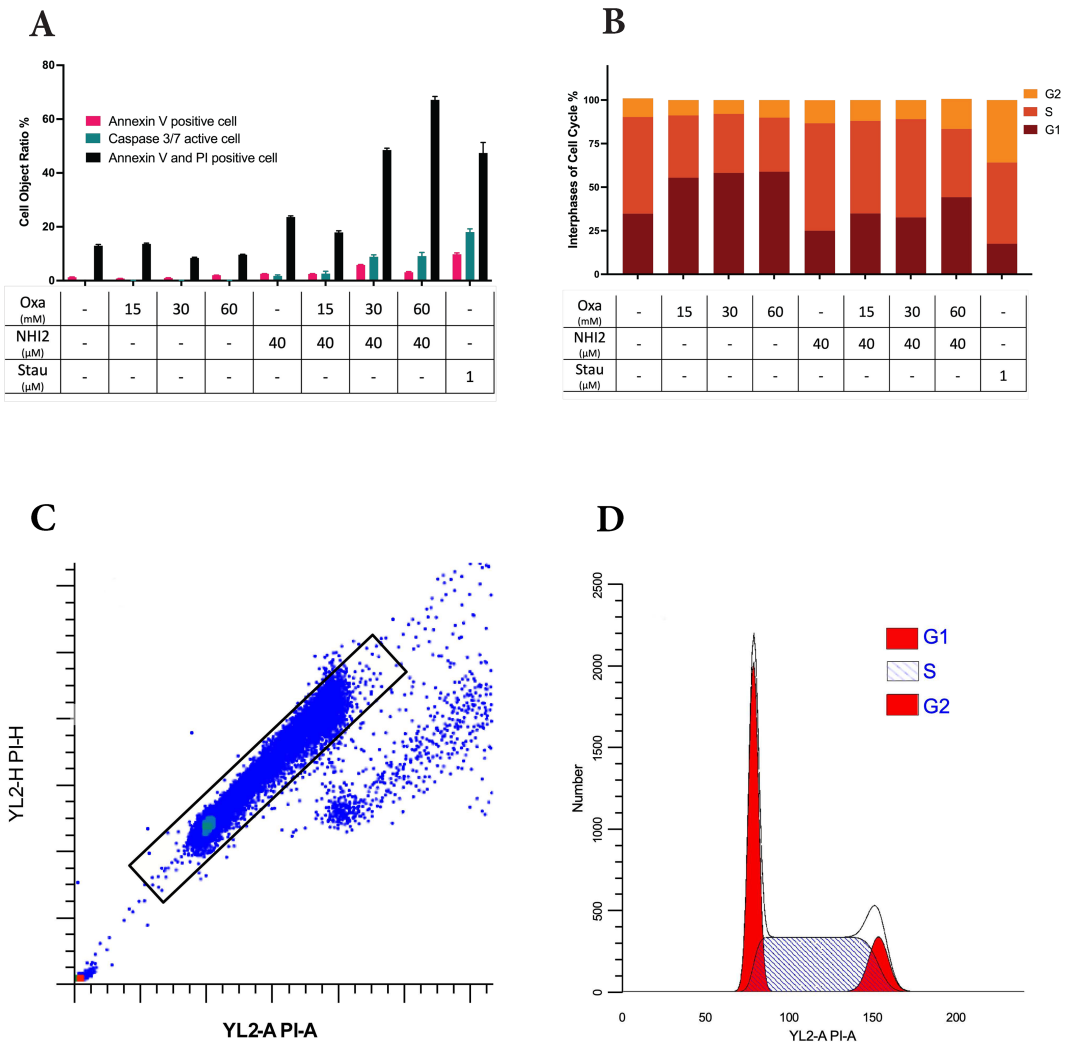

FIGURE 2
Higher doses of Oxamate and NHI-2 are required to induce apoptosis and disrupt the cell cycle in B78 cells. **(A)** Caspase-3/7 activation was assessed using the IncuCyte® live-cell analysis system, and apoptotic cell percentages were calculated alongside total cell numbers. Annexin V and/or PI-positive cell ratios were determined in non-fixed B78 cells at 24 hours post-treatment via flow cytometry analysis. Data represents the mean of 3 independent wells per condition ± SEM, with a noticeable increase in apoptotic and dead cell ratios observed only at higher doses of Oxa and NHI-2 combined treatment. **(B)** Cell cycle phases were assessed by flow cytometry analysis after PI staining of fixed cells. Data represents the mean of 3 independent repeats per time condition ± SEM. The untreated control sample serves as a reference for **(C)** the gating strategy and **(D)** the quantification model for the G1, S, and G2/M phases of the cell cycle. Analysis was performed using ModFit LT V5.0.9 software. Notably, Oxa treatment led to the accumulation of cells primarily in the G1 phase, whereas NHI-2 treatment resulted in the accumulation of cells in the S phase of the cell cycle.

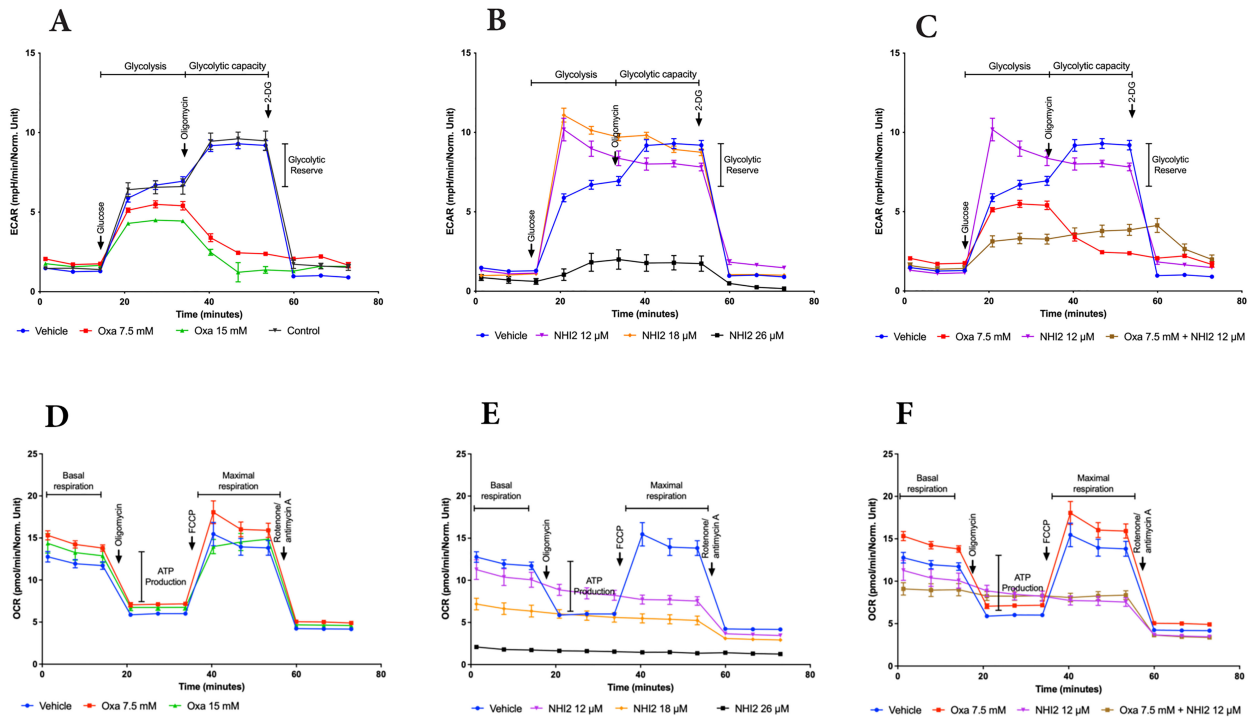

FIGURE 3
Oxamate and NHI-2 represent distinct effects on cellular bioenergetics. The continuous extracellular acidification rate (ECAR) values were monitored and analyzed employing a Seahorse XFe96 extracellular flux analyzer. B78 cells were treated with Oxa and NHI-2 one hour prior to loading the plate into the analyzer. The arrows indicate the time points of injections by the instrument. Sequential injections of 5 mM glucose, 1 µM oligomycin, and 50 mM 2-deoxy-D-glucose (2-DG) were introduced into the medium. Representative data are presented for the application of **(A)** Oxa, **(B)** NHI-2 as single agents, and **(C)** the combination of both. The continuous oxygen consumption rate (OCR) values were monitored and analyzed employing an XF94 extracellular flux analyzer. B78 cells were treated with Oxa and NHI-2 one hour prior to loading the plate into the analyzer. The arrows indicate the time points of injections by the instrument. Sequential injections of 1 µM oligomycin, and 0.5 µM FCCP (and 0.5 µM Rotenone/Antimycin A were introduced into the medium. Representative data are presented for the application of **(D)** Oxa, **(E)** NHI-2 as single agents, and **(F)** the combination of both. Error bars represent the mean ± standard error of the mean (SEM) (n = 5).

treatment of Oxa (15 mM) and NHI-2 (18 µM) resulted in a significant reduction in intracellular lactate levels, underscoring the importance of inhibiting LDHA and LDHB enzymes concurrently for efficient suppression of lactate production (Figure 4B). Increased ratios of ADP/ATP and AMP/ATP, especially evident in the combination treatment group when compared to the untreated control, suggest cellular energy depletion (Figures 4C, D). This state of energy depletion could account for the observed significant inhibition of cell proliferation. The KEGG pathway analysis of altered metabolites revealed that Oxa and NHI-2 had an impact not just on glycolysis but also on other related metabolic processes such as the tricarboxylic acid (TCA)cycle, arginine biosynthesis, pyrimidine metabolism, aminoacyl-tRNA biosynthesis, and alanine, aspartate, and glutamate metabolism (Figures 4E-G). The combination treatment of Oxa and NHI-2 exhibited greater significance scores for numerous pathways, as highlighted in Supplementary Table S1. The extensive inhibition of metabolic pathways, spanning from energy generation to macromolecule production, likely underlies the robust impact of the Oxa and NHI-2 combination on B78 cells.

2.5 Cytokine and chemokine profile modulation following LDH inhibitors treatment

Considering the data that highlight the potent anti-proliferative effects of LDHIs but also emphasizing the need for high concentrations to induce cell death, the study explored the potential of using LDHIs in combination to enhance the efficacy of current melanoma treatment regimens. In line with this approach, screening of cytokines, chemokines, and growth factors was conducted to assess potential alterations with LDHI treatments, employing Luminex xMAP technology. The results indicated the modulation of a group of components under LDHI treatments (Figure 5A). Particularly noteworthy was the substantial increase observed in RANTES and MCP-1 (Figures 5B, C). The elevation of these chemokines holds significant promise due to their positive effects on the recruitment of various immune cells (44, 45). The concurrent increase in these chemokines induced by LDHIs suggests the potential for enhancing immune cell response, making LDHIs promising

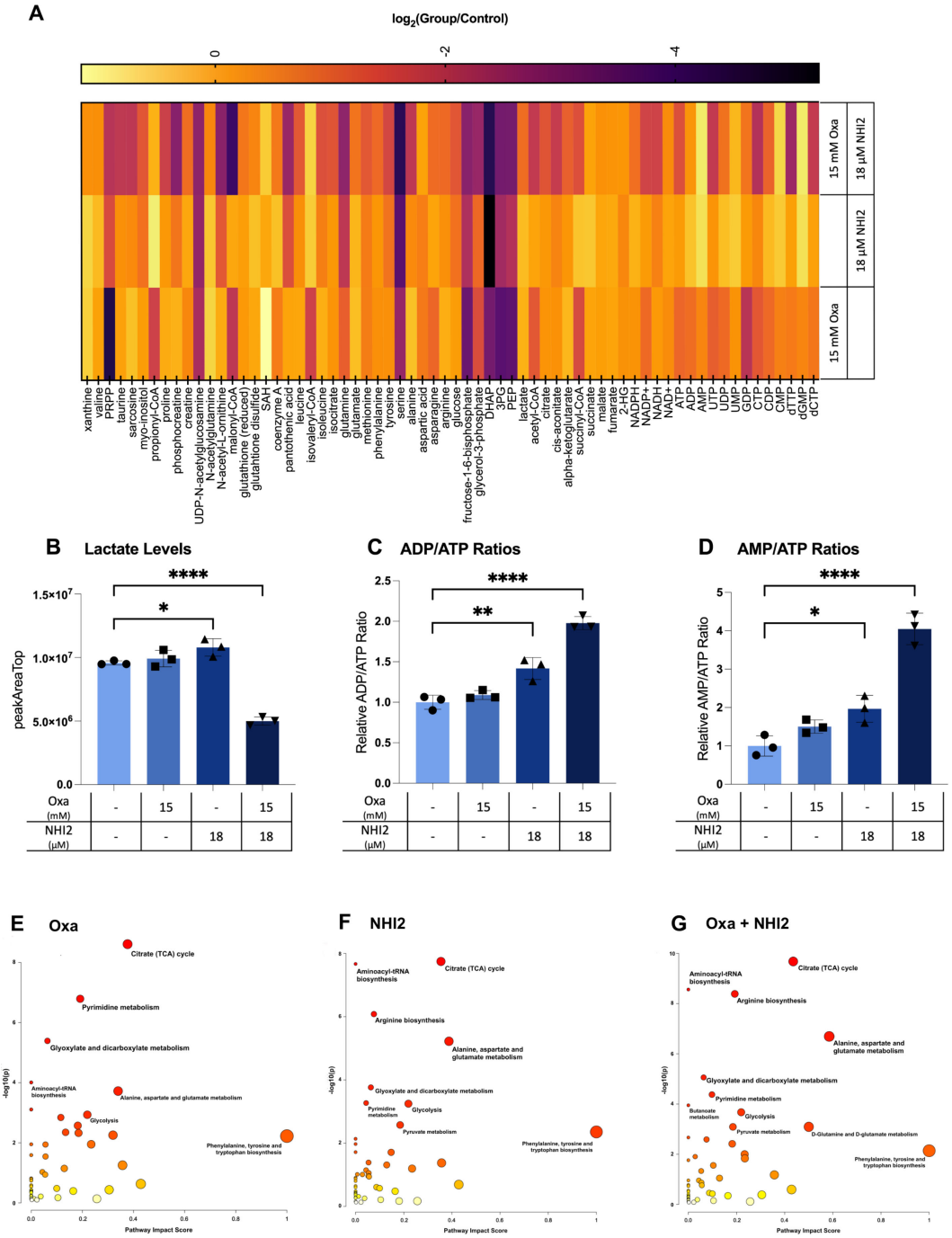

FIGURE 4
Oxamate and NHI-2 alter metabolite profiles and synergistically impair lactate and ATP production. B78 cells were exposed to drugs 24 hours prior to harvest. Metabolite samples were analyzed using a Thermo Q-Exactive mass spectrometer coupled to a Vanquish Horizon UHPLC. The metabolites reported were identified based on exact m/z and retention times determined with chemical standards. Data were analyzed with MAVEN. To quantify changes in relative metabolite levels, metabolite abundance measured by ion count in LCMS analysis were normalized to total protein content determined by BCA. **(A)** Log2 fold changes between the treatment and control groups represented in heatmap. Intracellular lactate, AMP, ADP, and ATP levels were quantified using LC-MS. Relative levels of **(B)** lactate, ATP, ADP, and AMP in B78 cells were expressed as peak areas normalized to the protein content. **(C)** ADP/ATP and **(D)** AMP/ATP ratios were calculated using the peak area data normalized to the protein content. Values represent the mean +/- SD of three technical runs for each sample. Statistical analysis was performed using one-way ANOVA; tititi $p < 0.0001$; titi$p < 0.01$; ti$p < 0.05$. The web-based platorm, MetaboAnalyst 5.0, was employed for pathway analysis, with enriched pathways predicted through the mummichog algorithm. Graphs illustrate the impacted pathways for **(E)** 15 mM Oxa, **(F)** 18 µM NHI-2, and **(G)** combination treatment groups. The sizes of the data points are based on their x values, while the colors correspond to their y values.

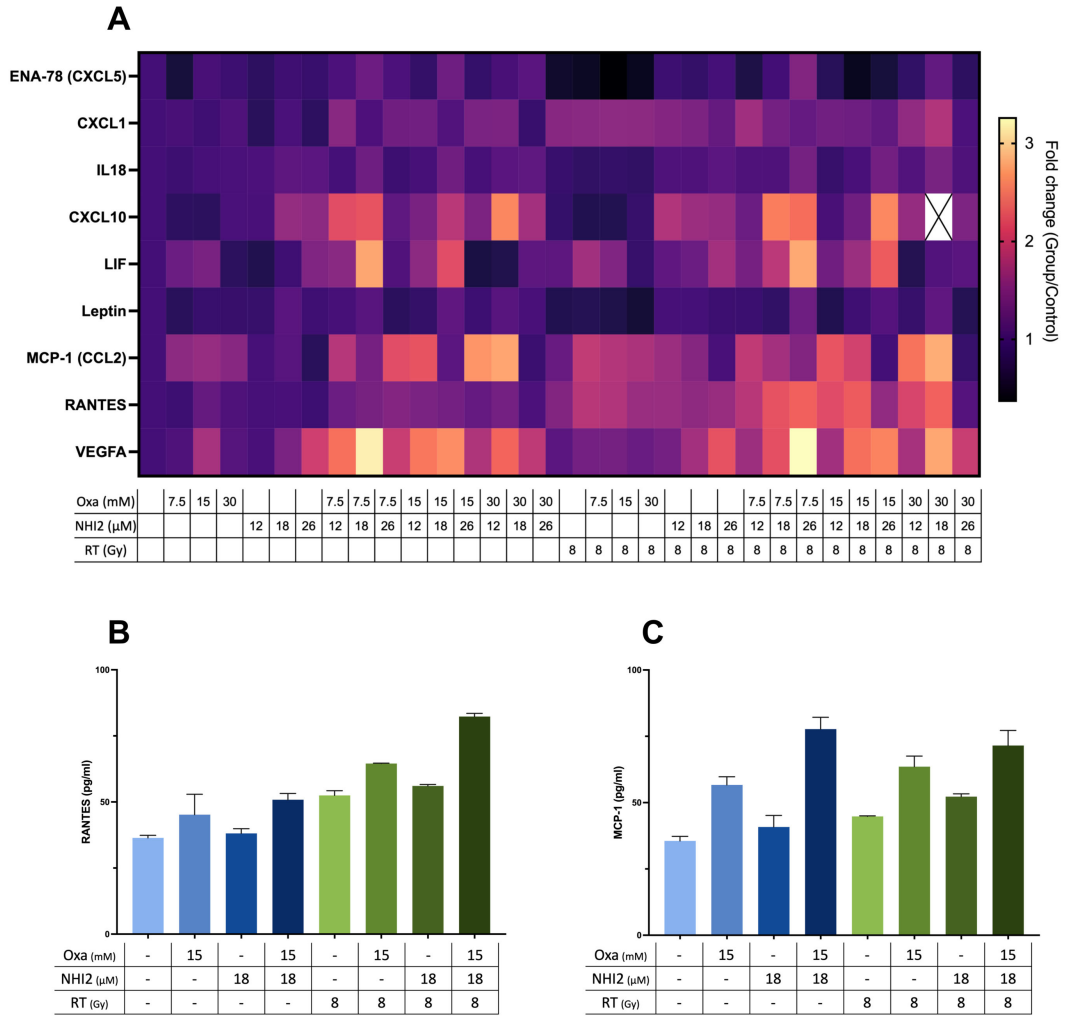

FIGURE 5
Combined Oxamate and NHI-2 treatment with ionizing radiation upregulates RANTES and MCP-1 expression in B78 cells. Multiplex analysis was conducted using the ProcartaPlex Mouse Immune Monitoring Panel 48plex, allowing for the simultaneous assessment of 48 cytokines, chemokines, and growth factors in B78 cell media following a 24-hour incubation with Oxamate (Oxa), NHI-2, and/or radiation therapy (RT). The data presented show the fold changes in detectable targets relative to the vehicle control. **(A)** Heatmap illustrating alterations in cytokine and chemokine levels in B78 cell media after 24-hour incubation with Oxa, NHI-2, and/or RT. Representative data highlight the levels of **(B)** RANTES and **(C)** MCP-1 in response to different treatments, including Oxa, NHI-2, and RT. Error bars represent the mean ± SEM (n = 2).

candidates for further investigation to elevate the efficacy of current immune therapies in the treatment of melanoma.

2.6 Enhanced efficacy of immune checkpoint inhibitors via LDH inhibitors

Because we observed increased levels of specific chemokines following Oxa and NHI-2 treatment, the potential of LDHIs to enhance the efficacy of current melanoma treatment regimens, namely ICIs, was tested. The LDHIs+ICIs regimen was assessed using an established B78 melanoma tumor model (Figure 6A), where the combination of ICIs and radiation therapy (RT) has previously demonstrated a reduction in tumor development without achieving complete eradication (46). In this study, we administered ICIs at intervals of 6 to 7 days. This dosing schedule was intentionally selected based on recent evidence suggesting that extending the intervals between ICI treatments can reduce adverse effects while maintaining their therapeutic effectiveness (47–51). Additionally, the timing of ICI administration was evaluated using current murine model. The results suggest that a 7-day interval between doses is as effective, if not more effective, than a more frequent 3-day schedule (data not shown). These findings support the feasibility of extending dosing intervals without compromising therapeutic efficacy.

The combined analysis of data from two distinct experiments yielded a total sample size of n=16 per group. In comparison to the RT alone group, the treatment of either LDHIs or ICIs alongside RT individually showed a modest inhibition of tumor growth. However, the treatments combining RT with LDHIs, and RT with LDHIs and ICIs (RT+LDHIs+ICIs) exhibited significantly greater efficacy in reducing tumor growth (Figure 6B) and led to the cure of

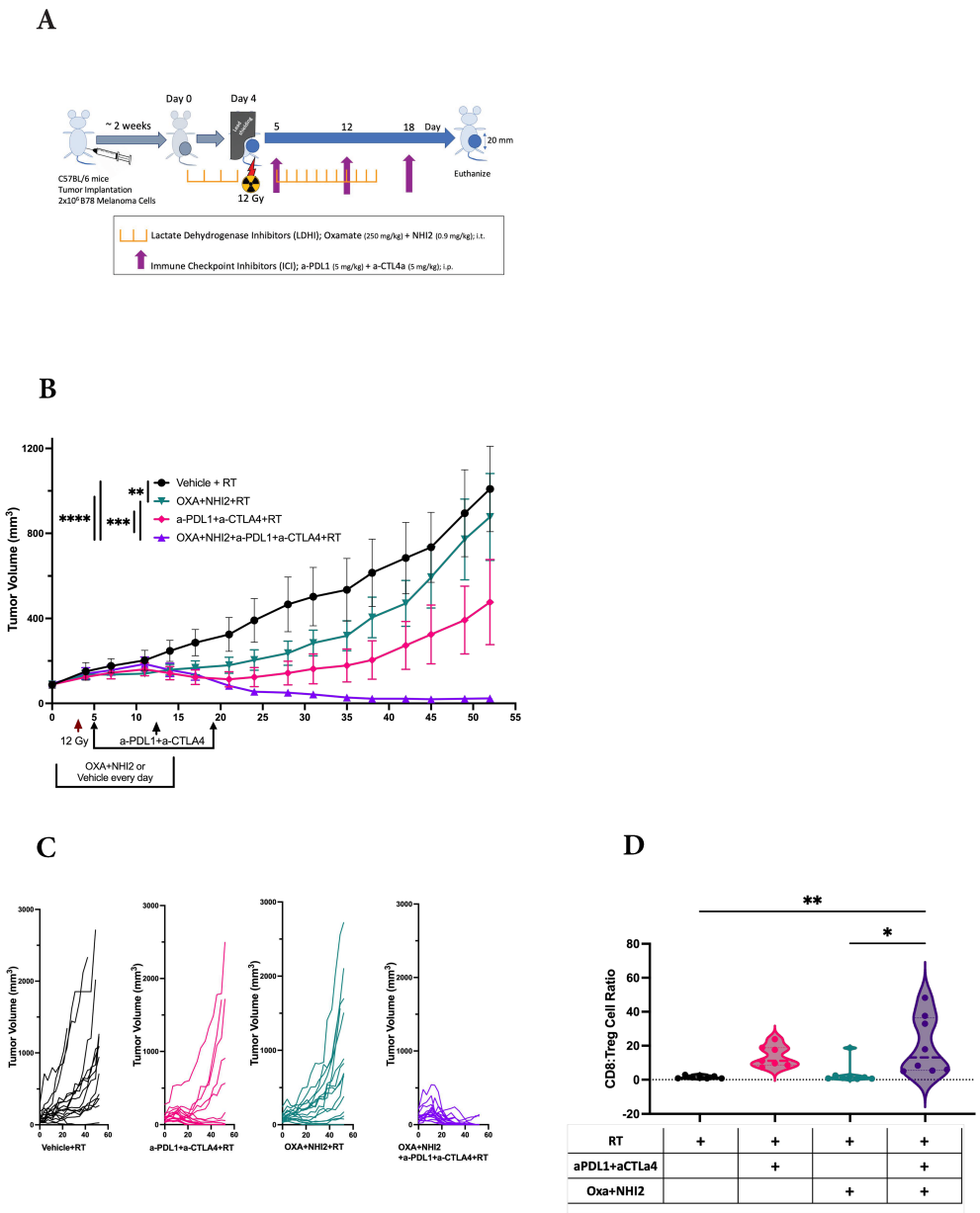

FIGURE 6
LDH inhibitors increase the therapeutic efficacy of immune checkpoint inhibitors in B78 tumors. **(A)** Schematic representation of the single-tumor mouse model and the treatment protocol. C57BL/6 mice were intradermally implanted with B78 syngeneic melanoma cells. When tumors reached an average volume of ~80 mm3, mice were randomized for intra-tumoral injections of Oxa and NHI-2 (depicted in purple and pink) or PBS (depicted in black and green) daily from day 0 to 15. On day 4, all mice received a 12Gy radiation therapy (RT) applied to the right flank. Anti-PDL1 and anti- CTLA4 (depicted in green and pink) or PBS (depicted in black and purple) were injected intraperitoneally on days 5, 12, and 18. **(B)** Average +/- SEM tumor volume from two individual experiments, total n=16 mice/group. Statistical analysis was performed using one-way ANOVA tests with Tukey *Post-Hoc* test; ****$p < 0.0001$; ***$p < 0.001$; **$p < 0.01$. **(C)** Individual tumor volumes from two individual experiments. **(D)** While no significant differences were observed in the CD8:Treg cell count ratio following RT+ICIs (pink) compared to RT alone (black) or following RT+LDHIs (green) compared to RT alone, the combination of RT+LDHIs+ICIs (purple) led to a significantly increased CD8:Treg cell ratio compared to RT +LDHIs (tip < 0.05) and to RT alone (titip < 0.01). Flow cytometry data represent the compilation of n=8 mice/group. One-way ANOVA tests with Tukey *Post-Hoc* test.

13 out of 16 mice compared to RT+ICIs (7/16, $p < 0.05$) or RT +LDHIs (2/16, $p < 0.0001$) (Figure 6C).

Furthermore, in the evaluation of the immune landscape on day 8 after treatment, only minor changes in the myeloid populations were observed following RT+LDHIs or RT+LDHIs+ICIs treatments (Supplementary Figure S6). Similarly, no significant alterations were detected in NK and NKT cell populations with any treatment groups compared to RT alone (Supplementary Figure S7). However, a significant enhancement of the ratio of CD8 to T regulatory cells (CD8:Tregs) was detected in the tumor samples of the combination of RT+LDHI+ICIs group compared to RT alone (Figure 6D). No significant differences were observed in any other treatment groups compared to RT alone. These data suggest that the addition of LDHIs to RT+ICIs (i.e., RT+LDHIs+ICIs) enhances CD8 effector infiltration

—potentially linked to increased RANTES stimulation from B78 melanoma cells—while reducing immunosuppressive Treg cells in the TME. Taken together, these *in vivo* studies demonstrated that the combination of ICIs (a-PDL1 and a-CTLA4) with LDHIs (Oxa and NHI-2) enhances the efficacy of ICIs in a melanoma tumor model.

3 Discussion

Cancer metabolism has emerged as a significant area of focus in the development of new treatment regimens for various malignancies. Unlike their non-cancerous counterparts, most cancer cells exhibit a remarkable ability to withstand oxidative and nutritional stresses through metabolic reprogramming. This reprogramming enables cancer cells to meet the high energy and biosynthetic requirements for tumor formation while also playing a role in the development of resistance to various treatments in tumors (17, 52, 53).

This study aimed to target the LDH enzyme, considering the preference of cancer cells to utilize glycolysis for energy production even in the presence of oxygen (Warburg effect) (1) and their ability to adapt their metabolism to changing TME conditions. The results indicated that the LDHA inhibitor Oxa alone could reduce the rate of ECAR but not completely halt it (Figure 3A), so it could not block lactate production completely in B78 cells (Figure 4A). This aligns with recent findings suggesting that both LDHA and LDHB contribute to pyruvate-to-lactate conversion, requiring the simultaneous knockout of both LDHA and LDHB to stop lactate production in LS174T (human colorectal adenocarcinoma) and B16-F10 (mouse melanoma) cell lines (54). Indeed, NHI-2, an LDHA and LDHB inhibitor, demonstrated significant inhibition of ECAR (Figure 3B) and ATP production (Figures 4C, D) when applied at a dose of 26 μM in B78 cells. However, NHI-2 was not effective at reducing ECAR levels at lower concentrations (12 and 18 μM). Similarly, NHI-2 exhibited no effect on B78 cell proliferation at lower concentrations. However, a marked decrease in cell proliferation was observed at concentrations beginning from 26 μM. The observed threshold effect, coupled with the low solubility of NHI-2, poses challenges in achieving its effective concentration within tumors. To address this, our study explored the combined application of Oxa and NHI-2, revealing synergistic interactions between the two compounds. This combination effectively inhibited cell proliferation and the production of glycolysis, lactate, and ATP, even at lower concentrations of each compound that were not effective when each compound was applied individually.

Cell cycle analysis revealed that Oxamate induced arrest in the G1 phase, while NHI-2 caused cell accumulation in the S and G2 phases (Figure 2B). The energy shortage and altered metabolic environment caused by Oxamate may lead to cell cycle arrest in the G1 phase as the cells are unable to accumulate the necessary energy and biosynthetic precursors required for DNA replication. However, NHI-2, as an LDH inhibitor and NADH competitor, not only affects glycolysis but also impacts mitochondrial metabolism and the NAD+/NADH balance, which are critical during DNA synthesis and cell division. The disruption of these processes during the S phase (DNA replication) and G2 phase (preparation for mitosis) can lead to cell cycle arrest at these points. These results indicated that using Oxa and NHI-2 together could be a promising therapeutic strategy because they exert complementary effects on the cell cycle and metabolism. Oxamate impedes the initial commitment to DNA synthesis, while NHI-2 disrupts later stages of cell division, leading to a comprehensive blockade of cancer cell proliferation. This dual approach could potentiate the effects of each inhibitor, making it more difficult for tumor cells to escape therapy.

Furthermore, metabolic flux analysis and metabolomic results demonstrated that NHI-2 not only inhibited ECAR but also had an impact on OXPHOS. This may be explained by a close link between glycolysis and the TCA cycle, and disruptions in one pathway often have downward effects on the other. Inhibition of LDH can lead to a bottleneck in glycolysis, reducing the supply of substrates (e.g., acetyl-CoA) and cofactors (NAD+) necessary for optimal TCA cycle function. Additionally, NHI-2 acts as a NADH competitor, directly impacting the NAD+/NADH cycle, which may further disrupt enzyme activities within the TCA cycle. Given the ability of cancer cells to alter their metabolic pathways and the cellular heterogeneity within tumors, this dual effect of NHI-2 can be advantageous for therapeutic purposes. Metabolite profiling further confirmed the enhanced effects of the combination treatment on lactate metabolism and revealed broader impacts on other metabolic pathways, providing insights into the mechanisms underlying the anti-proliferative effects of Oxa and NHI-2.

Besides disturbing the energy flow in cancer cells, LDHIs also possess the potential to regulate the immune response within the TME. Recent studies have highlighted that lowering lactate levels in the tumor can enhance immune responses, primarily by boosting the activity of immune cells through the reduction of acidity in the TME (21, 28, 55). Studies have also shown that metabolically active tumor cells can outcompete T cells for essential nutrients such as glucose and glutamine, leading to T cell exhaustion and reduced efficacy of immune responses (56, 57). NHI-2, through its dual effects, may disrupt the metabolic activity of tumor cells, thereby reducing this metabolic competition and enhancing T cell-mediated immune responses. Furthermore, a recent study has introduced a novel perspective, suggesting that LDHIs may directly regulate the immune response by inhibiting suppressive immune subsets (23). Given the observed outcomes, this study explored the potential of targeting LDH to improve the TME for ICI treatments in melanoma. The B78 melanoma tumor model was employed to evaluate the combination treatment of LDHIs and ICIs, revealing a significant enhancement in treatment efficacy upon the incorporation of LDHIs into the ICIs treatment regimen.

While ICIs have revolutionized cancer treatment, the resistance to these therapies remains a significant challenge. Therefore, novel approaches to enhance ICI efficacy are needed. The findings of this study have important implications for the development of new therapeutic strategies for melanoma. Targeting LDH could enhance the efficacy of ICIs and RT, potentially leading to more robust and durable patient responses. By understanding the complex interplay between lactate metabolism and immune cell modulation, new

approaches can be explored to overcome the limitations of current treatments and improve patient outcomes.

The development and utilization of more specific LDHIs will further validate the specificity and safety of the effects observed in this study, opening the way for clinical trials. Such trials could assess the efficacy of combining LDHIs with ICIs and RT in a clinical setting, potentially leading to the approval of new treatment protocols. Moreover, these findings provide valuable insights into novel therapeutic strategies for cancer management, not only for melanoma but potentially for other cancer types that exhibit similar metabolic characteristics.

The integration of anti-metabolic approaches with immunotherapy holds great promise for advancing cancer treatment. This combination strategy could be particularly beneficial in overcoming resistance mechanisms that limit the effectiveness of current therapies. As such, our study lays the foundation for future research exploring the therapeutic potential of targeting lactate metabolism, which could ultimately lead to improved clinical outcomes for a broader range of cancer patients.

4 Materials and methods

4.1 Study design

The study was designed to evaluate how LDHIs both directly hinder melanoma cell growth and enhance anti-tumor immunity when combined with ICIs in a preclinical model. This objective was addressed by (i) detecting the impact of Oxamate and NHI-2, individually or combined, on melanoma cell proliferation, viability, and cycle by further exploring changes in metabolic pathways, metabolites, and cytokine profiles in B78 melanoma *in vitro*, and (ii) assessing the efficacy of the combination of LDHIs and ICIs on a B78 melanoma tumor model.

Sample sizes were determined with the Biostatistics and Bioinformatics Core at University of Wisconsin-Madison to ensure that all studies were sufficiently powered, and that data were properly analyzed and interpreted. The exact sample size (n numbers) and statistic methods used in each experiment are indicated in the respective figure legends. The drug concentrations presented in the manuscript were determined by the authors based on preliminary cell-based experiments and initial findings from a pilot animal study. Cell-based assays were conducted in triplicate to ensure reproducibility, whereas animal studies were replicated twice, with the resulting data being aggregated for analysis. In the animal experiments, mice were randomized according to tumor volume at the initiation of the treatment protocol (about 80 mm^3). Body weights were measured on a weekly basis. Tumor dimensions and overall health assessments were performed twice weekly, and mice were euthanized when any mean tumor diameter reached or exceeded 20 mm. The study tasks — including randomization, administration of treatments, tumor sizing, and health evaluations — were conducted by different individuals under a double-blind arrangement. All animal experiments were in accordance with the guidelines of the Institutional Animal Care and Use Committee at the University of Wisconsin-Madison. Immune profiling experiments were performed blinded by a person without the knowledge of the treatment conditions.

4.2 Cell lines

B16-F10 [Mouse skin melanoma], M21 [Human metastatic melanoma] and the B78-D14 cell line were obtained from Dr. Paul Sondel (University of Wisconsin-Madison). Cells were grown in RPMI 1640 or DMEM (Gibco) media and supplemented with 10% fetal bovine serum (FBS), 2 mM L- glutamine, 100 U/mL penicillin, and 100 µg/mL streptomycin. Cells were maintained in culture below 80% confluence for all passages, and early passages after thaw (3–8) were used for all experiments. Cell authentication was performed per American Type Culture Collection guidelines using morphology, growth curves, and mycoplasma testing within 6 months of use.

4.3 IncuCyte imaging for dynamic cell proliferation and apoptosis analysis

To facilitate tracking of cell proliferation, a lentivirus-based method was employed to introduce a nuclear-localized fluorescent protein/mKate2, into the target cells, ensuring bright and consistent labeling throughout (Supplementary Figure S4). Subsequently, cells were cloned to obtain a population with uniformly labeled nuclei. Proliferation assays were performed using the IncuCyte live cell imaging system (Sartorius, Germany). This system enables real-time cell counting by analyzing florescence-labelled cell images over time. Briefly, 2×10^3 cells were seeded in 96-well TC-treated microplates in 100 µL culture medium containing 5 mM glucose and grown for 24 h. The next day, the cells were exposed to LDH inhibitors and subsequently placed in the IncuCyte live cell imaging system. Simultaneously, NucView®488 Caspase-3 Enzyme Substrate (Biotium, Fremont, CA) were added to wells to determine the rate of apoptotic cells. Entire well images were captured at 6-hour intervals over the course of 4 consecutive days. This continuous imaging provided a dynamic view of total and apoptotic cell numbers over time. Each experiment consisted of three independent replicates. The cell numbers were plotted and analyzed by GraphPad Prism software.

4.4 Flow cytometric detection of apoptosis and cell death

FITC Annexin V Apoptosis Detection Kit I (BD Biosciences, San Jose, CA) was used to detect apoptosis by flow cytometry. Briefly, cells were trypsinized and washed twice with cold PBS, and then resuspended in 1X Binding Buffer at a concentration of 1 x 10^6 cells/mL. Next, 100 µl of this cell suspensions (equivalent to 1 x 10^5 cells) were transferred to a 5-mL culture tube, and 5 µl each of FITC Annexin V and PI were added and then were incubated

for 15 min at room temperature in the dark. 400 µl of 1X Binding Buffer was added, and the cells were promptly analyzed by flow cytometry using an Attune NxT flow cytometer and analyzed using FlowJo version 10.7.1. Annexin V is a calcium-dependent phospholipid-binding protein that has a high affinity for the membrane phospholipid phosphatidylserine (PS) and is useful for identifying apoptotic cells with exposed PS. Propidium Iodide (PI) is a standard flow cytometric viability probe and is used to distinguish viable from nonviable cells. Viable cells with intact membranes exclude PI, whereas the membranes of dead and damaged cells are permeable to PI. Cells that stain positive for FITC Annexin V and negative for PI are undergoing apoptosis. Cells that stain positive for both FITC Annexin V and PI are either in the end stage of apoptosis, are undergoing necrosis, or are already dead. Cells that stain negative for both FITC Annexin V and PI are alive and not undergoing measurable apoptosis.

4.5 Flow cytometric detection of cell cycle

Cells were harvested and then resuspended in PBS. Cold ethanol was added dropwise to the pelleted cells to achieve a final concentration of 70% and fixed on ice for two hours. Cells were washed in PBS and were resuspended in staining buffer [0.1% Triton X-100, RNase A (100 µg/mL) and PI (50 µg/mL)]. Samples were incubated overnight at 4°C in the dark. Data acquisition was carried out on an Attune NxT flow cytometer and analyzed using ModFit 5.

4.6 Real-time cell metabolic analysis

Metabolic characterization of B78 cells was performed using a Seahorse XFe96 Extracellular Flux Analyzer (Agilent Technologies, Santa Clara, CA). Mitochondrial stress and glycolytic parameters were measured via Oxygen Consumption Rate (OCR) and ECAR, respectively. Briefly, 2×10^3 cells were seeded into the Seahorse XF Cell Culture Microplate in 100 µL RPMI-1640 medium containing 5 mM glucose, one day before the experiment. For analysis, cells were resuspended in seahorse XF RPMI medium supplemented with 5 mM glucose (Sigma-Aldrich), 1 mM pyruvate (Sigma-Aldrich), and 2 mM glutamine (Sigma-Aldrich). In this step, LDH inhibitors were added to the designated wells with medium. After incubating the plate in a 37°C non-CO_2 incubator for 45 min, The Cell Mito Stress Test was performed using 1.5 µM oligomycin, 0.5 µM FCCP, 0.5 µM rotenone, and 0.5 µM antimycin A (RotAA) purchased from Agilent Technologies.

Another plate was prepared as described above, but Seahorse XF Base Medium was used for Glycolysis Stress Test. After incubating the plate in a 37°C non-CO_2 incubator for 45 min, Glycolysis Stress Test was performed using 5 mM Glucose, 1.0 µM oligomycin, and 50 mM 2-Deoxy-D-glucose purchased from Agilent Technologies. Metabolic parameters were exported and calculated according to the manufacturer's instructions using the Seahorse Wave desktop software (Agilent Technologies).

4.7 Metabolite extraction and liquid chromatography-mass spectrometry analysis

B78 cells were washed three times with Phosphate Buffer Saline (PBS) and intracellular metabolites were extracted with cold 80% (v/v) LC-MS grade methanol. Samples were dried under nitrogen gas and resuspended in LC-MS-grade water. Metabolite samples were analyzed using a Thermo Q-Exactive mass spectrometer coupled to a Vanquish Horizon UHPLC. Analytes were separated on a 100 x 2.1 mm, 1.7 µM Acquity UPLC BEH C18 Column (Waters), with a gradient of solvent A (97:3 H2O: methanol, 10 mM TBA, 9 mM acetate, pH 8.2) and solvent B (100% methanol) at 0.2 mL/min flow rate. The gradient was: 0 min, 5% B; 2.5 min, 5% B; 17 min, 95% B; 21 min, 95% B; 21.5 min, 5%. Data were collected in full-scan negative mode. Setting for the ion source were: 10 aux gas flow rate, 35 sheath gas flow rate, 2 sweep gas flow rate, 3.2kV spray voltage, 320°C capillary temperature, and 300°C heater temperature.

The metabolites reported were identified based on exact m/z and retention times determined with chemical standards. Data were analyzed with MAVEN. To quantify changes in relative metabolite levels, metabolite abundance measured by ion count in LC-MS analysis were normalized to total protein content determined by bicinchoninic acid (BCA) assay. The web-based platform, MetaboAnalyst 5.0, was employed for pathway analysis, with enriched pathways predicted through the mummichog algorithm.

4.8 Comprehensive profiling of immune factors in B78 cell culture medium

B78 cell culture media, collected after 24 hours of Oxa ± NHI-2 treatment, underwent cytokine, chemokine, and growth factor measurement using the ProcartaPlex™ Mouse Immune Monitoring Panel 48-Plex (ThermoFisher) protocol. Briefly, cell culture supernatants were prepared by centrifuging samples at 1,400 rpm for 10 min at 4°C. The plate was prepped by adding the capture bead mix and washing it using a hand-held magnetic plate washer. Standards and samples were then added to the wells based on the plate map. The plate was shaken at 600 rpm overnight at 4°C. The next day, a washing step was followed by the addition of the biotinylated detection antibody mix to the plate. After shaking at 600 rpm for 30 min at room temperature and washing off unbound antibodies, Streptavidin-PE (SA-PE) was added, and the plate was shaken at 600 rpm for 30 min at room temperature. Final washes were performed before adding reading buffers to the wells. The plate was run on a xMAP™ instrument and analyzed following the operation manual for the Luminex™ instrument.

4.9 Animal study

All mouse procedures were conducted in accordance with the Institutional Animal Care and Use Committee at the University of Wisconsin-Madison. C57BL/6 female mice aged 6 to 8 weeks were purchased from The Jackson Laboratory. B78 flank tumors were

engrafted by intradermal flank injection of 2 x 10^6 cells diluted in 100 µL PBS (58). Tumor volume was assessed twice weekly by a blinded observer, and mice were euthanized when tumors exceeded 20 mm in any direction, or mice were assessed to be in distress by changes to posture, activity, or grooming. Tumor size was determined by precision caliper measurement and tumor volume was approximated using the formula (tumor volume in mm^3) = [(tumor width in mm)^2 x (tumor length in mm)]/2. Mice were randomized to treatment groups when tumors reached enrollment size (80 mm^3), which normally required 2-4 weeks following initial tumor implantation. Approximately 10% of mice failed to develop a suitable tumor, and these mice were excluded from randomization. A course of LDHIs was integrated into an ICIs treatment regimen, as described previously (46, 59). The protocol was further optimized by updating the ICI administration strategy, extending the dosing intervals to 6-7 days, based on recent evidence supporting the efficacy of this approach (47–50). The first day of treatment with LDH inhibitors was defined as "day 1". Intra-tumoral (IT) injections of LDH inhibitors (given daily on days 1-15) were performed via a single percutaneous needle puncture followed by injection of a 100 µL volume with needle redirection to distribute the injected material in the tumor. Oxa and NHI-2 dosages were 250 mg/kg and 1 mg/kg, respectively. radiation therapy (RT) (12 Gy) was delivered to primary B78 tumors using an Xstrahl Small Animal Radiation Research Platform on day 3. Mice were immobilized using custom lead jigs that exposed the dorsal right flank as previously described. Radiation was delivered in one fraction to a maximum dose of 12 Gy. Anti-CTLA-4 (2.5 mg/kg) and anti-programmed cell death-ligand 1 (anti-PD-L1) (5 mg/kg) were administered in 100 µL PBS by intraperitoneal (IP) injection on days 5, 12, and 18.

4.10 Flow cytometry method

Tumors were harvested from euthanized mice on day 15 and minced into 1–2 mm pieces. The small tumor pieces were collected into a 50-mL conical tube containing 5 mL of RPMI 1640 + 10% fetal bovine serum, protein transport inhibitors (ThermoFisher), 100µL of DNAse I (2.5 mg/mL, Sigma-Aldrich) and 100 µL collagenase IV (25 mg/mL, Gibco) and placed in an incubator/shaker at 200 RPM at 37°C for 30 min. After dissociation, the tumors were filtered through a 70 µM cell strainer, washed with 10 mL PBS, and centrifuged at 350 x g for 5 min. Cells were resuspended in 500µL PBS, transferred to flow tubes, and incubated with 0.5 µL GhostRed780 (Tonbo Biosciences) at 4°C for 30 min. Samples were then washed with 2 mL of flow buffer (PBS +2% FBS) and centrifuged at 350 x g for 5 min. TruStain FcX™ PLUS (BioLegend) was added to each sample, and samples were divided into 2 separate flow tubes for analysis of a myeloid antibody panel or a T/NK cell antibody panel. The myeloid master mix antibody markers included: CD45-FITC, CD206-PE, F4/80-PE-Dazzle594, CD3-PE-Cy5, Ly6g-PE-Cy7, MHCII-BV510, Ly6C-BV605, CD11b-BV711, CD11c-APC. The T/NK cell antibody panel included a surface stain of: CD45-FITC, CD4-AF700, CD8-BV605, CD25-BV711, NK1.1-PE-Dazzle594, CD3-PECy5; and an internal stain with: FoxP3-PE Cy7 (ThermoFisher). Cells were stained with surface markers for 30 min at 4°C in the dark and then washed in flow buffer. The myeloid panel data were acquired after wash was performed. For the T/NK cell antibody samples after surface staining the cells were then fixed using eBioscience™ Foxp3/Transcription Factor Staining Buffer Set (ThermoFisher) following the manufacturers protocol. Cells were washed in 1X permeabilization buffer and were then incubated in overnight with FoxP3 antibody in the dark at 4°C. The following day, samples were washed once with permeabilization buffer, centrifuged at 500 x g for 5 min, followed by a wash with flow buffer and centrifugation at 500 x g for 5 min. All data were acquired on an Attune™ NxT flow cytometer (Thermo Fisher) with manufacturer provided acquisition software. Data were analyzed using FlowJo version 10.7.1 (FlowJo LLC, Becton Dickinson & Company (BD) 2006-2020). Gates were determined using Fluorescence Minus One (FMOs).

4.11 Statistical analysis

Cell proliferation and tumor volume curves were analyzed by simple linear regression followed by one-way ANOVA with Tukey's *post-hoc* test for statistical considerations. One-way ANOVA followed by Tukey's *post-hoc* test for multiple comparisons were performed in flow cytometry studies of immune subsets, and to determine statistical differences for cell count and intracellular lactate levels.

Data availability statement

The raw data supporting the conclusions of this article will be made available by the authors, without undue reservation.

Ethics statement

The animal study was approved by Institutional Animal Care and Use Committee of the University of Wisconsin-Madison. The study was conducted in accordance with the local legislation and institutional requirements.

Author contributions

ZG: Conceptualization, Data curation, Formal analysis, Investigation, Methodology, Software, Validation, Visualization, Writing – original draft, Writing – review & editing. ML: Data curation, Investigation, Writing – review & editing, Methodology. QL: Data curation, Investigation, Methodology, Writing – review & editing. NA: Investigation, Writing – review & editing. AE: Conceptualization, Data curation, Formal analysis, Investigation, Methodology, Visualization, Writing – review & editing. AK: Funding acquisition, Resources, Supervision, Writing – review & editing. JF: Investigation, Methodology, Resources, Supervision,

Writing – review & editing. RK: Conceptualization, Funding acquisition, Resources, Supervision, Writing – review & editing.

Funding

The author(s) declare financial support was received for the research, authorship, and/or publication of this article. The authors acknowledge support from the University of Wisconsin Carbone Cancer Center Support Grant P30 CA014520 (RK), the University of Wisconsin Head and Neck SPORE Grant P50 DE026787 (RK), the University of Wisconsin Institute for Clinical and Translational Research 1UL1TR002373 (RK), and the Melanoma Research Alliance 695862 (AK).

Acknowledgments

The authors express their gratitude to Professors Paul Sondel and Zachary Morris from the University of Wisconsin-Madison for their generous contribution of melanoma cell lines and the anti-CTLA-4 monoclonal antibody. The authors thank James P. Zacny for manuscript preparation and formatting assistance.

Conflict of interest

The authors declare that the research was conducted in the absence of any commercial or financial relationships that could be construed as a potential conflict of interest.

Publisher's note

Supplementary material

The Supplementary Material for this article can be found online at: https://www.frontiersin.org/articles/10.3389/fonc.2024.1428802/full#supplementary-material

References

1. Warburg O, Wind F, Negelein E. The metabolism of tumors in the body. *J Gen Physiol*. (1927) 8:519–30. doi: 10.1085/jgp.8.6.519

2. Warburg O. On the origin of cancer cells. *Science*. (1956) 123:309–14. doi: 10.1126/science.123.3191.309

3. Pavlides S, Whitaker-Menezes D, Castello-Cros R, Flomenberg N, Witkiewicz AK, Frank PG, et al. The reverse Warburg effect: aerobic glycolysis in cancer associated fibroblasts and the tumor stroma. *Cell Cycle*. (2009) 8:3984–4001. doi: 10.4161/cc.8.23.10238

4. Niu N, Ye J, Hu Z, Zhang J, Wang Y. Regulative roles of metabolic plasticity caused by mitochondrial oxidative phosphorylation and glycolysis on the initiation and progression of tumorigenesis. *Int J Mol Sci*. (2023) 24:7076. doi: 10.3390/ijms24087076

5. Sharma P, Borthakur G. Targeting metabolic vulnerabilities to overcome resistance to therapy in acute myeloid leukemia. *Cancer Drug Resist*. (2023) 6:567–89. doi: 10.20517/cdr.2023.12

6. Cadenas-De Miguel S, Lucianer G, Elia I. The metabolic cross-talk between cancer and T cells. *Trends Biochem Sci*. (2023) 48:597–609. doi: 10.1016/j.tibs.2023.03.004

7. Singh B, Patwardhan RS, Jayakumar S, Sharma D, Sandur SK. Oxidative stress associated metabolic adaptations regulate radioresistance in human lung cancer cells. *J Photochem Photobiol B*. (2020) 213:112080. doi: 10.1016/j.jphotobiol.2020.112080

8. Stiven D. Lactic acid formation in muscle extracts. *Biochem J*. (1928) 22:867–73. doi: 10.1042/bj0220882

9. Wells HG. The pathogenesis of waxy degeneration of striated muscles (zenker's degeneration). *J Exp Med*. (1909) 11:1–9. doi: 10.1084/jem.11.1.1

10. Nakajima EC, Van Houten B. Metabolic symbiosis in cancer: refocusing the Warburg lens. *Mol Carcinog*. (2013) 52:329–37. doi: 10.1002/mc.21863

11. Sonveaux P, Végran F, Schroeder T, Wergin MC, Verrax J, Rabbani ZN, et al. Targeting lactate-fueled respiration selectively kills hypoxic tumor cells in mice. *J Clin Invest*. (2008) 118:3930–42. doi: 10.1172/JCI36843

12. Hensley CT, Faubert B, Yuan Q, Lev-Cohain N, Jin E, Kim J, et al. Metabolic heterogeneity in human lung tumors. *Cell*. (2016) 164:681–94. doi: 10.1016/j.cell.2015.12.034

13. Kennedy KM, Scarbrough PM, Ribeiro A, Richardson R, Yuan H, Sonveaux P, et al. Catabolism of exogenous lactate reveals it as a legitimate metabolic substrate in breast cancer. *PLoS One*. (2013) 8:e75154. doi: 10.1371/journal.pone.0075154

14. Walenta S, Salameh A, Lyng H, Evensen JF, Mitze M, Rofstad EK, et al. Correlation of high lactate levels in head and neck tumors with incidence of metastasis. *Am J Pathol*. (1997) 150:409–15.

15. Vlachostergios PJ, Oikonomou KG, Gibilaro E, Apergis G. Elevated lactic acid is a negative prognostic factor in metastatic lung cancer. *Cancer biomark*. (2015) 15:725–34. doi: 10.3233/CBM-150514

16. Brizel DM, Schroeder T, Scher RL, Walenta S, Clough RW, Dewhirst MW, et al. Elevated tumor lactate concentrations predict for an increased risk of metastases in head-and-neck cancer. *Int J Radiat Oncol Biol Phys*. (2001) 51:349–53. doi: 10.1016/s0360-3016(01)01630-3

17. Walenta S, Wetterling M, Lehrke M, Schwickert G, Sundfør K, Rofstad EK, et al. High lactate levels predict likelihood of metastases, tumor recurrence, and restricted patient survival in human cervical cancers. *Cancer Res*. (2000) 60:916–21.

18. Walenta S, Chau T-V, Schroeder T, Lehr H-A, Kunz-Schughart LA, Fuerst A, et al. Metabolic classification of human rectal adenocarcinomas: a novel guideline for clinical oncologists? *J Cancer Res Clin Oncol*. (2003) 129:321–6. doi: 10.1007/s00432-003-0450-x

19. Quennet V, Yaromina A, Zips D, Rosner A, Walenta S, Baumann M, et al. Tumor lactate content predicts for response to fractionated irradiation of human squamous cell carcinomas in nude mice. *Radiotherapy Oncol*. (2006) 81:130–5. doi: 10.1016/j.radonc.2006.08.012

20. Calcinotto A, Filipazzi P, Grioni M, Iero M, De Milito A, Ricupito A, et al. Modulation of microenvironment acidity reverses anergy in human and murine tumor-infiltrating T lymphocytes. *Cancer Res*. (2012) 72:2746–56. doi: 10.1158/0008-5472.CAN-11-1272

21. Pilon-Thomas S, Kodumudi KN, El-Kenawi AE, Russell S, Weber AM, Luddy K, et al. Neutralization of tumor acidity improves antitumor responses to immunotherapy. *Cancer Res*. (2016) 76:1381–90. doi: 10.1158/0008-5472.CAN-15-1743

22. Bohn T, Rapp S, Luther N, Klein M, Bruehl T-J, Kojima N, et al. Tumor immunoevasion via acidosis-dependent induction of regulatory tumor-associated macrophages. *Nat Immunol*. (2018) 19:1319–29. doi: 10.1038/s41590-018-0226-8

23. Angelin A, Gil-de-Gómez L, Dahiya S, Jiao J, Guo L, Levine MH, et al. Foxp3 reprograms T cell metabolism to function in low-glucose, high-lactate environments. *Cell Metab*. (2017) 25:1282–93.e7. doi: 10.1016/j.cmet.2016.12.018

24. Schachter J, Ribas A, Long GV, Arance A, Grob J-J, Mortier L, et al. Pembrolizumab versus ipilimumab for advanced melanoma: final overall survival results of a multicentre, randomised, open-label phase 3 study (KEYNOTE-006). *Lancet*. (2017) 390:1853–62. doi: 10.1016/S0140-6736(17)31601-X

25. Carlino MS, Long GV, SChadendorf D, Robert C, Ribas A, Richtig E, et al. Outcomes by line of therapy and programmed death ligand 1 expression in patients with advanced melanoma treated with pembrolizumab or ipilimumab in KEYNOTE-006: A randomised clinical trial. *Eur J Cancer*. (2018) 101:236–43. doi: 10.1016/j.ejca.2018.06.034

26. Long GV, Luke JJ, Khattak MA, de la Cruz Merino L, Del Vecchio M, Rutkowski P, et al. Pembrolizumab versus placebo as adjuvant therapy in resected stage IIB or IIC melanoma (KEYNOTE-716): distant metastasis-free survival results of a multicentre, double-blind, randomised, phase 3 trial. *Lancet Oncol.* (2022) 23:1378–88. doi: 10.1016/S1470-2045(22)00559-9

27. Larkin J, Chiarion-Sileni V, Gonzalez R, Grob J-J, Rutkowski P, Lao CD, et al. Five-year survival with combined nivolumab and ipilimumab in advanced melanoma. *N Engl J Med.* (2019) 381:1535–46. doi: 10.1056/NEJMoa1910836

28. Cascone T, McKenzie JA, Mbofung RM, Punt S, Wang Z, Xu C, et al. Increased tumor glycolysis characterizes immune resistance to adoptive T cell therapy. *Cell Metab.* (2018) 27:977–87.e4. doi: 10.1016/j.cmet.2018.02.024

29. Qiao T, Xiong Y, Feng Y, Guo W, Zhou Y, Zhao J, et al. Inhibition of LDH-A by oxamate enhances the efficacy of anti-PD-1 treatment in an NSCLC humanized mouse model. *Front Oncol.* (2021) 11:632364. doi: 10.3389/fonc.2021.632364

30. Nance WE, Claflin A, Smithies O. Lactic dehydrogenase: genetic control in man. *Science.* (1963) 142:1075–7. doi: 10.1126/science.142.3595.1075

31. Read JA, Winter VJ, Eszes CM, Sessions RB, Brady RL. Structural basis for altered activity of M- and H-isozyme forms of human lactate dehydrogenase. *Proteins.* (2001) 43:175–85. doi: 10.1002/1097-0134(20010501)43:2<175::aid-prot1029>3.0.co;2-

32. Perrotta R, Bevelacqua Y, Malaguarnera G, Paladina I, Giordano M, Malaguarnera M. Serum markers of cutaneous melanoma. *Front Biosci (Elite Ed).* (2010) 2:1115–22. doi: 10.2741/e170

33. Ho J, de Moura MB, Lin Y, Vincent G, Thorne S, Duncan LM, et al. Importance of glycolysis and oxidative phosphorylation in advanced melanoma. *Mol Cancer.* (2012) 11:76. doi: 10.1186/1476-4598-11-76

34. Rozendorn N, Shutan I, Feinmesser G, Grynberg S, Hodadov H, Alon E, et al. Real-world outcomes of inoperable and metastatic cutaneous head and neck melanoma patients. *Laryngoscope.* (2024) 134:2762–70. doi: 10.1002/lary.31290

35. Baschnagel AM, Kaushik S, Durmaz A, Goldstein S, Ong IM, Abel L, et al. Development and characterization of patient-derived xenografts from non-small cell lung cancer brain metastases. *Sci Rep.* (2021) 11:2520. doi: 10.1038/s41598-021-81832-1

36. Brand A, Singer K, Koehl GE, Kolitzus M, Schoenhammer G, Thiel A, et al. LDHA-associated lactic acid production blunts tumor immunosurveillance by T and NK cells. *Cell Metab.* (2016) 24:657–71. doi: 10.1016/j.cmet.2016.08.011

37. Badami S, Upadhaya S, Velagapudi RK, Mikkilineni P, Kunwor R, Al Hadidi S, et al. Clinical and molecular characteristics associated with survival in advanced melanoma treated with checkpoint inhibitors. *J Oncol.* (2018) 2018:6279871. doi: 10.1155/2018/6279871

38. Stukalin I, Navani V, Gupta M, Ruan Y, Boyne DJ, O'Sullivan DE, et al. Development and validation of a prognostic risk model for patients with advanced melanoma treated with immune checkpoint inhibitors. *Oncologist.* (2023) 28:812–22. doi: 10.1093/oncolo/oyad073

39. Wagner NB, Lenders MM, Kühl K, Reinhardt L, André F, Dudda M, et al. Pretreatment metastatic growth rate determines clinical outcome of advanced melanoma patients treated with anti-PD-1 antibodies: a multicenter cohort study. *J Immunother Cancer.* (2021) 9:e002350. doi: 10.1136/jitc-2021-002350

40. Nisselbaum JS, Packer DE, Bodansky O. Comparison of the actions of human brain, liver, and heart lactic dehydrogenase variants on nucleotide analogues and on substrate analogues in the absence and in the presence of oxalate and oxamate. *J Biol Chem.* (1964) 239:2830–4. doi: 10.1016/s0021-9258(18)93821-4

41. Granchi C, Calvaresi EC, Tuccinardi T, Paterni I, Macchia M, Martinelli A, et al. Assessing the differential action on cancer cells of LDH-A inhibitors based on the N-hydroxyindole-2-carboxylate (NHI) and malonic (Mal) scaffolds. *Org Biomol Chem.* (2013) 11:6588. doi: 10.1039/c3ob40870a

42. Zheng S, Wang W, Aldahdooh J, Malyutina A, Shadbahr T, Tanoli Z, et al. SynergyFinder plus: toward better interpretation and annotation of drug combination screening datasets. *Genomics Proteomics Bioinf.* (2022) 20:587–96. doi: 10.1016/j.gpb.2022.01.004

43. Yadav B, Wennerberg K, Aittokallio T, Tang J. Searching for drug synergy in complex dose-response landscapes using an interaction potency model. *Comput Struct Biotechnol J.* (2015) 13:504–13. doi: 10.1016/j.csbj.2015.09.001

44. Bhat H, Zaun G, Hamdan TA, Lang J, Adomati T, Schmitz R, et al. Arenavirus induced CCL5 expression causes NK cell-mediated melanoma regression. *Front Immunol.* (2020) 11:1849. doi: 10.3389/fimmu.2020.01849

45. Conti I, Rollins BJ. CCL2 (monocyte chemoattractant protein-1) and cancer. *Semin Cancer Biol.* (2004) 14:149–54. doi: 10.1016/j.semcancer.2003.10.009

46. Patel RB, Hernandez R, Carlson P, Grudinski J, Bates AM, Jagodinsky JC, et al. Low-dose targeted radionuclide therapy renders immunologically "cold" tumors responsive to immune checkpoint blockade. *Sci Transl Med.* (2021) 13:eabb3631. doi: 10.1126/scitranslmed.abb3631

47. Jiang M, Hu Y, Lin G, Chen C. Dosing regimens of immune checkpoint inhibitors: attempts at lower dose, less frequency, shorter course. *Front Oncol.* (2022) 12:906251. doi: 10.3389/fonc.2022.906251

48. Hirata T, Uehara Y, Hakozaki T, Kobayashi T, Terashima Y, Watanabe K, et al. Brief report: clinical outcomes by infusion timing of immune checkpoint inhibitors in patients with locally advanced NSCLC. *JTO Clin Res Rep.* (2024) 5:100659. doi: 10.1016/j.jtocrr.2024.100659

49. Kwon M, Jung H, Nam G-H, Kim I-S. The right Timing, right combination, right sequence, and right delivery for Cancer immunotherapy. *J Control Release.* (2021) 331:321–34. doi: 10.1016/j.jconrel.2021.01.009

50. Sehgal K, Costa DB, Rangachari D. Extended-interval dosing strategy of immune checkpoint inhibitors in lung cancer: will it outlast the COVID-19 pandemic? *Front Oncol.* (2020) 10:1193. doi: 10.3389/fonc.2020.01193

51. Feng Y, Masson E, Dai D, Parker SM, Berman D, Roy A. Model-based clinical pharmacology profiling of ipilimumab in patients with advanced melanoma. *Br J Clin Pharmacol.* (2014) 78:106–17. doi: 10.1111/bcp.12323

52. Hensley CT, Faubert B, Yuan Q, Lev-Cohain N, Jin E, Kim J, et al. Metabolic heterogeneity in human lung tumors. *Cell.* (2016) 164(4):681–94. doi: 0.1016/j.cell.2015.12.034

53. Costa ASH, Frezza C. Metabolic reprogramming and oncogenesis: one hallmark, many organelles. *Int Rev Cell Mol Biol.* (2017) 332:213–31. doi: 10.1016/bs.ircmb.2017.01.001

54. Ždralević M, Brand A, Di Ianni L, Dettmer K, Reinders J, Singer K, et al. Double genetic disruption of lactate dehydrogenases A and B is required to ablate the "Warburg effect" restricting tumor growth to oxidative metabolism. *J Biol Chem.* (2018) 293:15947–61. doi: 10.1074/jbc.RA118.004180

55. Damgaci S, Ibrahim-Hashim A, Enriquez-Navas PM, Pilon-Thomas S, Guvenis A, Gillies RJ. Hypoxia and acidosis: immune suppressors and therapeutic targets. *Immunology.* (2018) 154:354–62. doi: 10.1111/imm.12917

56. Chang C-H, Qiu J, O'Sullivan D, Buck MD, Noguchi T, Curtis JD, et al. Metabolic competition in the tumor microenvironment is a driver of cancer progression. *Cell.* (2015) 162:1229–41. doi: 10.1016/j.cell.2015.08.016

57. Qiu X, Li Y, Zhang Z. Crosstalk between oxidative phosphorylation and immune escape in cancer: a new concept of therapeutic targets selection. *Cell Oncol (Dordr).* (2023) 46:847–65. doi: 10.1007/s13402-023-00801-0

58. Carlson PM, Mohan M, Rodriguez M, Subbotin V, Sun CX, Patel RB, et al. Depth of tumor implantation affects response to in *situ* vaccination in a syngeneic murine melanoma model. *J Immunother Cancer.* (2021) 9:e002107. doi: 10.1136/jitc-2020-002107

59. Morris ZS, Guy EI, Francis DM, Gressett MM, Werner LR, Carmichael LL, et al. *In situ* tumor vaccination by combining local radiation and tumor-specific antibody or immunocytokine treatments. *Cancer Res.* (2016) 76:3929–41. doi: 10.1158/0008-5472.CAN-15-2644

frontiers | Frontiers in Endocrinology

TYPE Review
PUBLISHED 05 December 2024
DOI 10.3389/fendo.2024.1457943

OPEN ACCESS

EDITED BY
Parmanand Malvi,
University of Alabama at Birmingham, United States

REVIEWED BY
Ashish Toshniwal,
The University of Utah, United States
Meghna Saxena,
University of Minnesota Medical Center, United States

*CORRESPONDENCE
Bing Yan
ybwcy@163.com
Chenghao Zhanghuang
736564145@qq.com

†These authors have contributed equally to this work and share first authorship

RECEIVED 01 July 2024
ACCEPTED 19 November 2024
PUBLISHED 05 December 2024

CITATION
Yao G, Wang Z, Xie R, Zhanghuang C and Yan B (2024) Trace element zinc metabolism and its relation to tumors.
Front. Endocrinol. 15:1457943.
doi: 10.3389/fendo.2024.1457943

Trace element zinc metabolism and its relation to tumors

Guiping Yao[1†], Zhiwei Wang[1†], Rui Xie[2†], Chenghao Zhanghuang[1,3,4*] and Bing Yan[1,3,4*]

[1]Department of Urology, Kunming Children's Hospital, Kunming, Yunnan, China, [2]Department of Orthopedics, Kunming Children's Hospital, Kunming, Yunnan, China, [3]Yunnan Province Clinical Research Center for Children's Health and Disease, Kunming Children's Solid Tumor Diagnosis and Treatment Center, Kunming, Yunnan, China, [4]Yunnan Key Laboratory of Children's Major Disease Research, Yunnan Clinical Medical Center for Pediatric Diseases, Kunming Children's Hospital, Kunming, Yunnan, China

Zinc is an essential trace element in the human body, playing a crucial role in cellular metabolism.Dysregulation of zinc homeostasis can lead to abnormal cellular metabolism, contributing to diseases and closely related to tumor development. Adequate zinc intake can maintain zinc homeostasis in the body and support normal cellular metabolism. This review discusses the metabolic processes of zinc in the human body and its close relationship with tumorigenesis. It briefly describes zinc absorption, transport, storage, and release, as well as its important role in gene expression, signal transduction, oxidative stress, immune response, and apoptosis. It focuses on the abnormal cellular metabolism caused by excessive or insufficient zinc, the relationship between zinc homeostasis disruption and metabolic syndrome, and the mechanisms involved in tumor development. It analyzes how changes in the expression and activity of zinc transporters may lead to disrupted zinc homeostasis in tumor tissues. It points out that zinc deficiency is associated with various cancers, including prostate cancer, hepatocellular carcinoma, pancreatic cancer, lung cancer, ovarian cancer, esophageal squamous cell carcinoma, and breast cancer. The summary emphasizes that zinc metalloproteins could serve as potential targets for cancer therapy, and regulating the expression and activity of zinc transport proteins may offer new methods and strategies for clinical cancer treatment.

KEYWORDS

zinc, zinc metabolism, metabolic syndrome, cancer therapy, controversy

1 Introduction

Zinc is a vital trace element for the human body, playing a key role in protein composition within cells and participating in metabolic processes. Zinc is involved in the conformation and function of nuclear transcription factors, facilitating protein synthesis, and it also acts as a component of superoxide dismutase (SOD), providing strong

antioxidant activity. Additionally, zinc plays a role in processes such as apoptosis and immune response (1). Dysregulation of zinc homeostasis can lead to disturbances in cellular metabolic functions and human diseases, with the relationship between zinc metabolism disorders and metabolic syndrome and tumors needing further investigation. However, there is currently no definitive conclusion regarding the correlation between zinc metabolism and metabolic syndrome, as existing studies show contradictory results, and the specific mechanisms supporting their relationship remain unclear. More research is needed to explore this issue, as numerous studies have proposed a link between zinc homeostasis disruption and cancer (2). This article briefly summarizes zinc absorption, transport, and its involvement in metabolic processes within the human body. It summarizes diseases related to abnormal zinc metabolism and focuses on the relationship between zinc homeostasis disruption, metabolic syndrome, and tumors. It discusses issues and controversies regarding zinc in cancer treatment, offering insights for cancer diagnosis and therapy.

2 Zinc absorption, transport, and its functions

The main source of zinc in the human body is from dietary intake, and it can also be transported from reserves in the liver, muscles, and other tissues to other parts of the body. In the stomach, zinc forms complexes with proteins in food under the action of gastric acid. It is mainly absorbed in the upper part of the small intestine through zinc transporters on the apical membrane of intestinal epithelial cells, particularly the ZIP4 transporter. After absorption, zinc is transported into the plasma through zinc ion channels and the ZnT1 transport protein located on the basolateral membrane of intestinal epithelial cells, and subsequently delivered to body tissues (3). Zinc participates in vital cellular activities (4). It is primarily found in the liver, pancreas, muscles, bones, and prostate, playing significant roles in human health.

Zinc is transported across membranes via transporters ZnT or ZIP (as shown in Figure 1), with ZIP family proteins facilitating the influx of zinc ions from the extracellular space or from intracellular vesicles and organelles into the cytoplasm (5). Currently, at least 14 types of ZIP proteins and 10 types of ZnT proteins have been identified in the human body, which exhibit tissue-specific differential expression (6). These zinc transporters exhibit structural homology as well as differences, and their varying tissue distribution and functions have been a popular research topic (7). Zinc binds to metallothioneins (MT) in the cytoplasm, which consist of four subtypes; MT-1 and MT-2 are present in all cells of the body, regulating intracellular levels and flux of zinc and copper while detoxifying heavy metals. MTs are also involved in nuclear transcription and play a role in immune function through their chelation of metals (8).

Zinc homeostasis within cells is maintained by the ZIP (zinc transporter) and ZnT (zinc transport protein) families, as well as metallothioneins (1, 9). These proteins are all regulated during their functions and interact with other metabolic and signaling pathways. Once zinc ions enter the cells, they are transported to various organelles, with a significant presence in mitochondrial metalloproteins. Many zinc metalloproteins are secreted or reside in organelles such as the endoplasmic reticulum, Golgi apparatus, and secretory vesicles (1). Zinc ion signaling regulates cellular

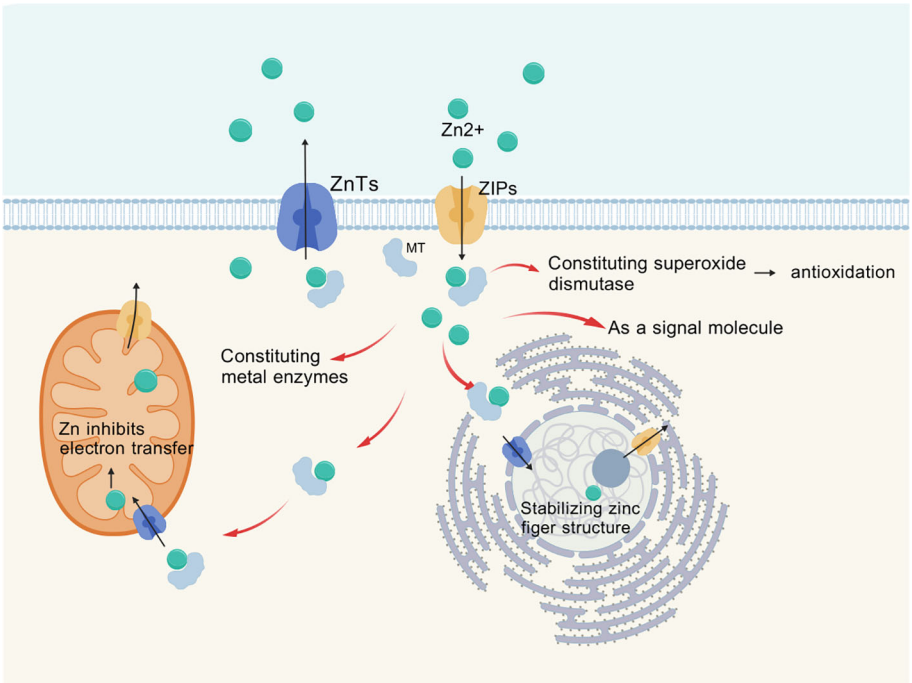

FIGURE 1
Transmembrane transport of Zinc via ZIPs, ZnTs.

proliferation, differentiation, ion transport, and secretory functions (10).

Zinc exists in two forms within human cells (11). One form of zinc is bound to proteins, serving as an essential component of many proteins in the human body (12). It can chelate with negatively charged parts of molecules, such as cysteine and histidine, providing structural bridges to maintain the three-dimensional conformation of polypeptides, known as zinc metalloproteins or zinc metallozymes. Currently, over 3,000 types of such metalloproteins have been identified (1). This includes oxidoreductases, transferases, hydrolases, lyases, isomerases, and ligases, which are involved in processes such as oxidative stress, apoptosis, and immune responses within cells (12). The other form is mobile zinc bound to non-protein ligands, the nature of which is still unknown (13). This type of zinc ion forms a loose association with non-protein ligands, known as free zinc ions, which serve as a pool for exchangeable zinc (11).

Zinc plays a crucial role in metabolic processes such as gene expression, signal transduction, oxidative stress, immune response, and apoptosis. It is involved in the conformation and function of nuclear transcription factors, such as zinc fingers and nuclear receptors, both of which are stabilized by four coordinated zinc ions. By stabilizing zinc finger structures, zinc executes important functions in cells, playing significant roles in DNA replication and repair, transcription and translation, cellular proliferation and maturation, as well as apoptosis regulation (14). Zinc, as a component of superoxide dismutase (SOD), exhibits strong antioxidant activity. SOD exists in three isoenzymatic forms in the body: copper-zinc superoxide dismutase, found in the cytoplasm; manganese superoxide dismutase (Mn SOD), located in the mitochondria; and extracellular superoxide dismutase (EC-SOD), which is present in extracellular spaces and fluids (15). These three forms of SOD work together to protect cells from the toxic effects of excessive reactive oxygen species. Zinc also acts as a cofactor in the formation of active thymosin (Zn FTS) released by thymocytes (9). Zn FTS regulates the differentiation of mature T cells in the thymus and the function of mature T cells in peripheral blood, having less impact on B cell development compared to T cells (16). It promotes the host defense functions of the immune system.

3 Disorders related to zinc homeostasis imbalance

Both excess and deficiency of zinc can lead to dysregulation of zinc homeostasis, and ultimately resulting in human diseases. Excessive zinc intake releases soluble zinc salts in acidic gastric fluid, which can directly irritate the gastrointestinal mucosa and lead to ulcer formation (17). This condition manifests as symptoms such as nausea, vomiting, decreased appetite, abdominal cramps, and headaches (18). Excessive zinc, once absorbed into the bloodstream, inhibits normal metabolic processes involving zinc (19). For example, high levels of zinc in the blood can suppress the antioxidant pathways in red blood cells, leading to oxidative damage to the cell membranes, which increases the risk of hemolysis, coagulopathy, and even triggers disseminated intravascular coagulation (DIC) (20). Systemic hypoxemia can then lead to liver dysfunction, pancreatitis, coagulation-related disorders, acute renal failure associated with tubular damage, and neurological abnormalities (19).

Mild micronutrient deficiencies in the human body can lead to chronic and subtle metabolic disturbances, resulting in DNA or mitochondrial damage, which may accelerate aging and contribute to cancer and degenerative diseases (21). Zinc deficiency is associated with diabetes, cirrhosis, inflammatory bowel disease, malabsorption syndrome, and sickle cell anemia (22–28). Zinc deficiency can lead to or exacerbate issues such as immune deficiencies, gastrointestinal problems, endocrine disorders, neurological dysfunction, cancer, aging, and degenerative diseases (19). Zinc deficiency affects all metabolic processes involving zinc (Figure 2), as evidenced by several aspects: first, certain intracellular transcription factors, hormone receptors, and many enzymes require zinc to maintain structural integrity. Zinc stabilizes the tertiary folding of smaller proteins, thereby contributing to the maintenance of their functional activity (29). Zinc also plays a structural role in ribosomes, cell membranes, and nucleic acids (30). Zinc deficiency can lead to protein structural abnormalities and impaired enzyme activity. Secondly, like calcium or nitric oxide (NO), zinc acts as an intracellular and intercellular messenger, activating intracellular signaling pathways and altering gene expression patterns. Free or exchangeable zinc (loosely bound zinc) can serve as a second messenger to control various functions, including gastric acid secretion, hormone release, and cardiac electrophysiology (31). Zinc, as a signaling molecule, functions similarly to other neurotransmitters and possesses neuromodulatory capabilities (32). In the immune system, zinc plays a role in intracellular, extracellular, and intercellular signaling. A classic sign of zinc deficiency in humans is impaired innate and cell-mediated immune functions, characterized by thymic atrophy, lymphopenia, reduced leukocyte function, and recurrent infections (33). Zinc deficiency leads to abnormalities in cellular signaling and neuromodulatory functions. Thirdly, redox reactions and antioxidant activities become dysregulated. Zinc can directly protect cell membranes from oxidative damage (34). Zinc can also indirectly reduce potential free radical formation and lipid peroxidation, as well as oxidative damage to proteins and DNA (34). Zinc deficiency is associated with increased oxidative stress factors and inflammatory biomarkers. Zinc supplementation can reduce biomarkers of oxidative stress, such as thiobarbituric acid reactive substances (TBARS) and malondialdehyde (MDA) levels (35). Most reactive oxygen species (ROS) are produced by NADPH oxidase (NOX), and zinc can scavenge ROS, exerting antioxidant effects. Zinc levels influence the activity and levels of copper-zinc superoxide dismutase (36). Zinc deficiency leads to abnormal thiol redox status in cell membranes, resulting in increased permeability and fragility of red blood cell membranes, as well as inactivation of calcium channel proteins in the membranes (30). The activities of antioxidant enzymes such as Cu/Zn superoxide dismutase, catalase, and peroxidase are affected, leading to weakened antioxidant defenses and accelerating the process of mitochondrial oxidative aging (37). Fourth, the processes of cell growth, development, proliferation, and apoptosis become dysregulated. Zinc deficiency

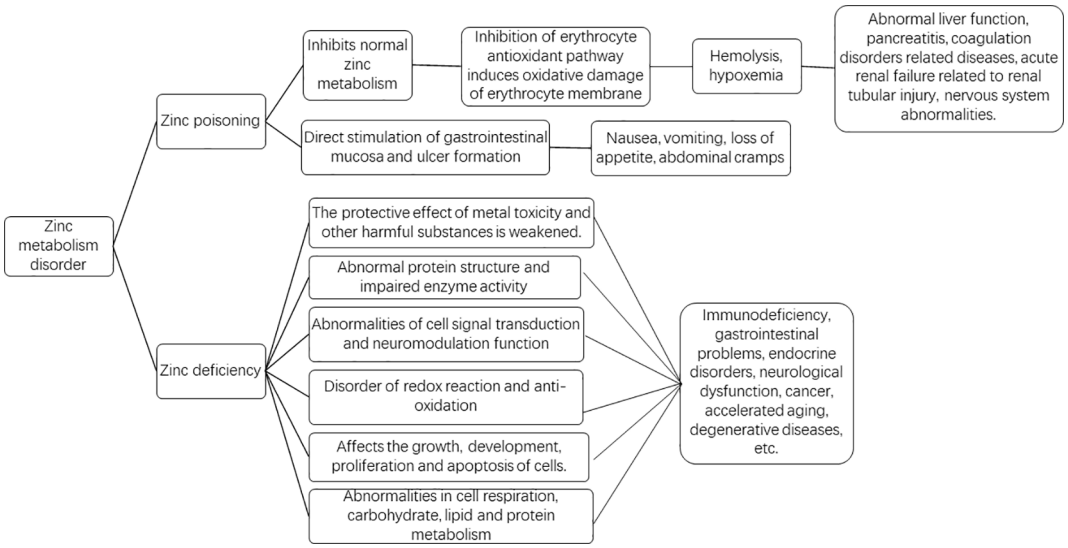

FIGURE 2
Graphic abstract of metabolic abnormalities caused by Zinc homeostasis disorder.

affects the structure of key enzymes and transcription factors involved in DNA repair and replication, including DNA polymerases, DNA-dependent RNA polymerases, and reverse transcriptases (38). Abnormal formation of zinc finger proteins, such as transcription factors, transcriptional repressors, steroid receptors, thyroid receptors, vitamin D receptors, and retinoic acid receptors occurs (39). These enzyme and protein abnormalities contribute to disruptions in cellular growth, development, and proliferation. Zinc deficiency also promotes apoptosis, primarily in rapidly growing tissues such as intestinal crypt cells, the thymus, and other embryonic and fetal tissues (40). Fifth, the metabolism of carbohydrates, lipids, and proteins, as well as cellular respiration, becomes abnormal. Within mitochondria, zinc inhibits mitochondrial respiration, terminal oxidation, and ATP production by altering the function of mitochondrial enzymes and the cytochrome electron transport chain (41). Zinc-containing enzymes and proteins participate in the metabolism of nucleic acids, proteins, carbohydrates, and lipids by interacting with hormone receptors, transcription factors, and enzyme systems (19). When zinc is deficient, the functions of the aforementioned metabolic enzymes are hindered. Additionally, zinc deficiency affects the regulatory roles of zinc-dependent metalloproteins or their antioxidant membrane-stabilizing effects, leading to diminished protection against metal toxicity and other harmful substances (42).

Currently, there is no definitive conclusion regarding the relationship between zinc metabolism-related diseases and metabolic syndrome. Metabolic syndrome is a cluster of conditions associated with obesity, hypertension, hyperglycemia, hyperlipidemia, and hyperuricemia (43). Some animal studies have suggested that zinc nanoparticles improve obesity-induced cardiovascular diseases by reducing blood pressure, oxidative stress, cardiac iron accumulation, insulin resistance, and inflammatory markers (44). Althanoon Zeina et al. also suggested that zinc supplementation in patients with metabolic syndrome is associated with improvements in systolic blood pressure, body mass index, and metabolic parameters, recommending the correction of zinc deficiency in these patients (45). These studies suggest that there may be a connection between zinc and factors associated with metabolic syndrome. However, current research remains controversial regarding whether there is a link between zinc metabolism and metabolic syndrome (46). Research shows that adequate dietary zinc consumption is linked to a decrease in the risk of MetS (47–49). A study in China has also indicated that zinc levels in children are indeed associated with components of metabolic syndrome (50). A meta-analysis of observational studies by Ding J et al. indicated that dietary zinc intake is negatively correlated with metabolic syndrome (46). Wu Y et al. found that higher blood zinc concentrations are associated with adverse changes in metabolic risk factors related to metabolic syndrome, particularly concerning BMI and LDL-c, and this relationship exhibits gender differences, mainly affecting women (51). In Aydogdu A's study, serum zinc levels were significantly elevated in children with metabolic syndrome (52). Due to limited evidence, more well-designed prospective cohort studies are needed to clarify the relationship between serum zinc levels and metabolic syndrome. The specific mechanisms linking zinc to metabolic syndrome remain unclear; a case-control study suggested that higher serum zinc levels might be related to the number of metabolic factors, independent of BMI and insulin resistance (48). Research on this issue is limited, necessitating further studies to clarify the role of zinc status in the mechanisms associated with metabolic syndrome and to determine the optimal range of blood zinc levels in the body (51). In contrast, a cross-sectional study conducted in Iran on the relationship between serum zinc levels and metabolic syndrome in children and adolescents suggested that there is no association between serum zinc levels and metabolic syndrome in children (53). A case-control study by Ennes Dourado Ferro F et al. also indicated that there is no relationship between zinc nutritional status and biochemical

markers of metabolic syndrome (54). In summary, current research on the relationship between zinc metabolism and metabolic syndrome is contradictory, and the specific mechanisms in studies supporting their correlation remain unclear, necessitating further investigation into this issue.

4 Zinc metabolism abnormalities and tumor

Approximately two-thirds of tumors in the human body are related to addictive behaviors, diet, lack of exercise, excessive sun exposure, or infections. Zinc can protect cells from damage caused by inflammation and oxidative stress, leading to the hypothesis that zinc has anti-cancer properties (55). As mentioned earlier, zinc stabilizes the structure of proteins, DNA, RNA, and ribosomes within cells, and regulates gene expression through zinc finger transcription factors, thereby altering the expression of different components in the DNA damage response (DDR) (56). Zinc deficiency is involved in various aspects of cancer cell generation and growth. Changes in zinc ion concentration can directly and specifically affect the activity of YY1 (YY1 is an intrinsically disordered transcription factor, a protein regulator of gene expression that has been shown to be related to the progression of many cancers), leading to altered gene expression patterns and potentially resulting in tumor transformation or progression (57). Zinc deficiency (ZD) is present in various tumors and affects their occurrence and progression. For instance, zinc levels in the serum or plasma of breast cancer patients are significantly reduced (58–61). The serum zinc levels are significantly reduced in patients with acute leukemia (62). Similarly, serum zinc levels are also significantly lower in bladder cancer patients, as well as in those with esophageal squamous cell carcinoma (ESCC), malignant prostate cancer, and ovarian cancer (63). This decrease in serum zinc levels may be due to the increased uptake by tumor cells and enhanced enzyme activity, leading to a higher demand for zinc in cancerous tissues (64). Conversely, some studies have found that higher toenail zinc levels in men are associated with an increased risk of prostate cancer (65).

4.1 Zinc metabolic abnormalities and tumor-related mechanisms

Disruption of zinc homeostasis is associated with tumor development, and the role of zinc varies across different types of cancer (66). Zinc indirectly affects tumor cells by influencing gene expression and cell survival, and directly impacts tumor cells by regulating the activation, function, and/or survival of immune cells (67). Under physiological conditions, Th2 and Th1 cells collaboratively engage in anti-tumor immunity, with cytokines like IL-4, IL-5, and IL-6 promoting B lymphocyte antibody synthesis and contributing to cancer prevention, and zinc is essential for activating this series of responses (67). Zinc deficiency disrupts processes such as oxidative stress, DNA damage, DNA repair, cell cycle, apoptosis, metabolic changes, microRNA expression, and inflammatory factors, thereby promoting cancer development (36). Zinc deficiency reduces the number of T and B cells in the thymus and bone marrow, increasing the body's susceptibility to infections and weakening its defenses, which results in a higher incidence of tumors. Another potential mechanism by which zinc inhibits tumor growth is closely related to its suppression of the activity of the nuclear transcription factor NF-κB (68, 69). NF-κB in its active form induces the expression of approximately 200 genes, which are related to angiogenesis, metastasis, and cell proliferation. Zinc influences gene expression at the nuclear level by stabilizing structures and regulating various transcription factors, including NF-κB (69). The NF-κB transcription factor can enhance inflammatory responses, particularly by boosting the production of pro-inflammatory cytokines by macrophages. Zinc ions negatively regulate NF-κB activity through proteins like A20 with zinc finger structures and by reversibly inhibiting phosphodiesterase (PDE), thus suppressing inflammatory responses and cancer development. The tumor-suppressing effect of zinc is also related to its antioxidant properties. Established cancer cells generate large amounts of reactive oxygen species (ROS), and the clearance of these ROS relies on the activity of antioxidant enzymes. However, zinc can protect healthy cells from the cytotoxic and genotoxic effects of hydrogen peroxide, but in tumor tissues, it can exacerbate the toxicity of H2O2, leading to oxidative stress dysregulation in cancer cells (70). The mechanism of zinc and cancer is shown in Table 1.

Altered expression levels of zinc transporters are one of the reasons for zinc homeostasis disruption in tumor tissues (85). For example, current studies show that zinc levels are high in prostate tissue cells, and this elevated intracellular zinc level facilitates the production and secretion of citrate in prostatic fluid, as well as aids normal cells in exerting cytotoxic effects to eliminate harmful cells. In contrast, prostate tumor cells exhibit reduced zinc levels, which may be due to low expression of the ZIP1 transporter protein, leading to low intracellular zinc and consequently promoting tumor cell proliferation (86, 87). In ER-positive breast cancer, elevated expression levels of ZIP7 increase zinc levels in ER-positive breast cancer cells. ZIP7 is activated by serine phosphorylation and is involved in the pathways that promote the progression of ER-positive breast cancer (88).

4.2 Zinc and tumor therapeutic targets

The mechanisms by which zinc homeostasis dysregulation leads to tumors have given rise to different anticancer targets for various cancers. Zinc transport proteins may serve as potential targets for cancer therapy, as modulating their function or zinc levels could offer new strategies for cancer treatment (89). Zinc transport proteins serve as targets for cancer therapy. Messenger RNA analysis in pancreatic cancer cells shows overexpression of ZIP4, while other ZIP variants are downregulated. ZIP4 promotes cell proliferation and tumor progression, and interfering with the RNA involved in the generation of ZIP4 can inhibit tumor cell proliferation and invasion; however, more research is needed to further explore the related mechanisms (90). Excess zinc

TABLE 1 Literature summary table on the relationship between zinc and cancer.

Relationship between zinc and cancer	Zinc proteins	Action mechanism	Reference
Carcinogenic effect of zinc	Zinc finger protein(ZNFs)	Overexpression of ZNF322A activates genes related to metastasis, tumor stemness and angiogenesis, thereby promoting the progression of lung cancer.	(71)
		Oncogenic zinc finger protein ZNF687 activates PI3K/Akt/mTOR signaling pathway to accelerate lung adenocarcinoma cell proliferation and tumor progression.	(72)
		Zinc finger protein CXXC5 promotes breast cancer by regulating TSC1/mTOR signaling pathway.	(73)
		GATA zinc finger protein p66β acts as a co-activator of Snail to promote breast cancer cell migration	(74)
		ZNF692 promotes proliferation, migration and invasion of osteosarcoma cells through TNK2-mediated MEK/ERK pathway activation.	(75)
		ZNF554 inhibits the progression of endometrial cancer by regulating RBM5 and inactivating WNT/β-Catenin signaling pathway.	(76)
		Zinc finger protein 263 promotes the malignant progression of non-small cell lung cancer by up-regulating interleukin 33 and inhibiting autophagy.	(77)
The anti-cancer effect of zinc	Metallothionein(MTs)	Activation of esterase D (ESD) promotes its interaction with MT2 A, reduces the protein level of MT2 A, up-regulates the concentration of free zinc ions, and inhibits the migration of A549 lung cancer cells *in vitro*.	(78)
		Metallothionein family proteins act as zinc ion regulators to synergistically enhance the anticancer effect of cannabidiol in human colorectal cancer cells.	(79)
	Zinc finger protein(ZNFs)	Zinc finger protein ZNF575 promotes the transcription of p53 to inhibit the growth of colorectal cancer.	(80)
		The protein expression of ZNF746 is significantly increased in colorectal cancer. ZNF746 plays an important role in the invasion and migration of colorectal cancer (CRC) cells.	(81)
		Zinc finger protein 671 plays a tumor suppressor role in colorectal cancer by inhibiting Notch signaling pathway.	(82)
	–	Zinc exerts its anti-tumor effect by acting on the central cytotoxic T cells of cellular immunity.	(83)
		Zinc deficiency promotes the proliferation, migration and invasion of esophageal squamous cell carcinoma EC109 cells.	(84)

accumulates in breast tumor cells, and this excess zinc has a toxic effect on them. Breast tumor cells increase the expression levels of ZnT2, which transports the excess zinc into vesicles, thereby reducing its toxic effects. Inhibiting the activity of ZnT2 in breast tumor cells can release excess zinc from these vesicles, resulting in cytotoxic effects on malignant breast cancer cells (91). In esophageal squamous cell carcinoma (ESCC), ZIP6 promotes cancer cell proliferation, invasion, and metastasis by increasing intracellular zinc levels, thereby activating the PI3K/AKT and MAPK/Erk pathways. Targeting ZIP6 may represent a potential strategy for treating the aggressiveness of ESCC (92). In various tumor cells, the expression levels of zinc transporters differ (see Table 2), and regulating the expression or activity of these transporters could also serve as a strategy for cancer treatment. The increased expression of MT has been linked to the proliferation rate of tumor cells (93), indicating that MT could be a potential target for future cancer suppression research (93). Zinc finger proteins (ZNFs) regulate the expression of various target genes, influencing tumor occurrence, progression, and patient prognosis. ZNFs are also expected to serve as new biological markers or therapeutic targets for malignant tumors (94).

4.3 The controversy of zinc supplementation in tumor treatment

Zinc supplementation is beneficial for the treatment of many tumors. Studies have found that zinc supplementation can induce cytotoxicity in pancreatic cancer cells and reduce their invasiveness (95). Zinc oxide nanoparticles can also promote apoptosis in liver and ovarian cancer cells by inducing autophagy (96, 97). Metal chelators can form stable complexes with metals, reducing the consumption of metal ions. The antibiotic chloroquine is a metal chelator that can chelate zinc, increasing intracellular zinc levels in tumor cells and enhancing anti-cancer effects (98). Metal chelating compounds (such as disulfiram, chloroquine, and dithiocarbamate

TABLE 2 Expression of zinc transporters in different types of cancer.

Type of cancer	Expression of zinc transporters	Potential tumor markers
Pancreatic cancer	ZIP4 increased	ZIP4
Prostate cancer	ZIP1 ZIP4 decreased.	MTs
ER-positive breast cancer	ZIP7 increased	ZIP7
non-small cell lung cancer	ZIP4 increased, ZnTs decreased	ZIP4
Hepatocarcinoma	ZIP14 ZIP2 ZIP9 decreased	ZIP14
stomach and colon cancer	ZIP10 increased	
ovarian cancer	ZIP4 increased	ZIP4
advanced kidney cancer	ZIP10 increased	ZIP10
cervical cancer	ZIP7 increased	ZIP7
Nasopharyngeal carcinoma	ZIP4 increased	ZIP4
bladder cancer	ZnT1 increased	ZnT1
oral squamous cell carcinoma	ZIP4 increased	

derivatives) serve as coordination complexes targeting metals like copper, zinc, and gold in the ubiquitin-proteasome pathway, potentially acting as anti-cancer drugs (99). However, zinc chelation may also produce side effects. Some studies suggest that ferroptosis is a cell death mechanism that can be targeted for cancer treatment, but zinc chelation may inhibit this mechanism (100). This presents a major controversy in the use of metal chelates for cancer treatment, and further research is needed to confirm the impact of these side effects. The use of metal chelators should consider the specific characteristics of the cancer being treated. The benefits and risks of targeted therapies involving zinc in different types of tumors still require further investigation.

The application of zinc supplementation in cancer treatment is becoming increasingly common, but there remains significant controversy regarding its therapeutic use and effects for some tumors. Current studies have many shortcomings, and the benefits and risks of zinc supplementation for cancer treatment require further investigation. A study examining whether a combination of antioxidant vitamins and minerals can reduce the risk of skin cancer (SC) randomly assigned 7,876 French women and 5,141 French men to receive either a daily antioxidant capsule (containing 20 mg of zinc) or a matched placebo. With a median follow-up time of 7.5 years, the results indicated that zinc-containing antioxidant supplements had differential effects on SC incidence, increasing the risk in women but not in men (101). Taking prostate cancer, which has been extensively studied, as an example, there is considerable controversy regarding the therapeutic and preventive roles of zinc in this context. Numerous experimental studies have confirmed that the application of zinc derivatives and supplements can inhibit the proliferation, migration, and invasion of prostate cancer cells. However, some studies suggest that the efficacy of zinc supplementation in any form appears to be limited (87), primarily because malignant tumor cells with ZIP1 deficiencies cannot uptake and accumulate zinc from increased plasma zinc concentrations. Additionally, zinc supplementation formulations, especially those containing cadmium and lead, may have potential contaminants, and the bioavailability of different zinc compounds (such as sulfates, gluconates, and less commonly used citrates) varies (102). Some research has suggested that direct intratumoral injection of zinc can inhibit the growth of prostate cancer cells in xenograft mice (103), but the practicality of this intratumoral administration method in humans remains to be debated. Another controversial aspect of zinc's use in prostate cancer treatment is that zinc levels in metastatic and late-stage hormone-independent prostate cancer have not been established, and effective treatments for advanced malignant prostate tumors and metastases are lacking. A large prospective cohort study found that low-dose zinc supplementation (1 to 24 mg/d) after diagnosis was associated with a reduced risk of lethal prostate cancer in men with non-metastatic prostate cancer (104). Conversely, another 30-year follow-up study indicated that daily supplementation of more than 75 mg of zinc or supplementation for more than 15 years could significantly increase the risk of lethal and aggressive prostate cancer (102). Therefore, the potential risks and benefits of low-dose zinc supplementation after diagnosis, as well as the duration of supplementation, require further investigation regarding prostate cancer survival.

In summary, the trace element zinc is involved in the formation of intracellular proteins and plays a crucial role in cellular processes such as gene expression, signal transduction, oxidative stress, immune response, and apoptosis. Both excess and deficiency of zinc can lead to metabolic abnormalities in cells, resulting in disease; therefore, it is essential to ensure an appropriate zinc intake to maintain zinc homeostasis and normal cellular metabolism. Current research on the relationship between zinc metabolism and metabolic syndrome is contradictory, and the specific mechanisms supporting their correlation remain unclear, necessitating further studies to explore this issue. Cancer is a major disease impacting human health, and zinc homeostasis is closely related to cancer; zinc deficiency can disrupt cellular immune responses and oxidative stress, thereby promoting cancer development. Zinc supplementation has been shown to be beneficial for various cancers, including pancreatic, colorectal,

liver, ovarian, and cervical cancers. The role of zinc in cancer varies by cancer type, allowing for the selection of different therapeutic targets based on specific mechanisms of action. The expression levels of zinc transport proteins vary across different cancer cells; thus, regulating the expression or activity of these transport proteins is also a therapeutic approach for cancer treatment. Many studies currently focus on zinc transport proteins as targets for cancer therapy, but further exploration is needed. Other proteins involved in zinc metabolism, such as metallothioneins and zinc finger structures, may also serve as potential research directions for future tumor suppressive targets, providing new approaches for clinical cancer treatment.

Author contributions

GY: Conceptualization, Data curation, Formal analysis, Funding acquisition, Investigation, Methodology, Project administration, Writing – original draft, Writing – review & editing. ZW: Data curation, Formal analysis, Writing – original draft. RX: Conceptualization, Investigation, Methodology, Writing – original draft. CZ: Writing – original draft, Writing – review & editing. BY: Writing – review & editing.

Funding

The author(s) declare financial support was received for the research, authorship, and/or publication of this article. The study was supported by: Scientific Research Foundation of Education Department of Yunnan Province (No. 2020J0228, 2023J0295), Kunming Medical University Joint Project of Department of Science and Technology of Yunnan Province (No. 202301AY070001-108); Kunming City Health Science and Technology Talent "1000" training Project (No. 2020-SW (Reserve)-112), Kunming Health Personnel Training Project Technology Center Construction Project (No. 2020-SW (Tech) -15) and Yunnan Province Clinical Research Center for Children's Health and Disease. The funding bodies played no role in the study's design and collection, analysis and interpretation of data, and writing the manuscript.

Conflict of interest

The authors declare that the research was conducted in the absence of any commercial or financial relationships that could be construed as a potential conflict of interest.

Publisher's note

References

1. Maret W. Zinc and the zinc proteome. *Met Ions Life Sci.* (2013) 12:479–501. doi: 10.1007/978-94-007-5561-1_14

2. Sugimoto R, Lee L, Tanaka Y, Morita Y, Hijioka M, Hisano T, et al. Zinc deficiency as a general feature of cancer: a review of the literature. *Biol Trace Elem Res.* (2024) 202:1937–47. doi: 10.1007/s12011-023-03818-6

3. Stiles LI, Ferrao K, Mehta KJ. Role of zinc in health and disease. *Clin Exp Med.* (2024) 24:38. doi: 10.1007/s10238-024-01302-6

4. Liu H, Li L, Lu R. ZIP transporters-regulated Zn2+ homeostasis: A novel determinant of human diseases. *J Cell Physiol.* (2024) 239:e31223. doi: 10.1002/jcp.v239.5

5. Wang X, Zhang M, Ma J, Tie Y, Wang S. Biochemical markers of zinc nutrition. *Biol Trace Elem Res.* (2024) 202(12):5328–38. doi: 10.1007/s12011-024-04091-x

6. Cousins RJ, Liuzzi JP, Lichten LA. Mammalian zinc transport, trafficking, and signals. *J Biol Chem.* (2006) 281:24085–9. doi: 10.1074/jbc.R600011200

7. Kambe T, Tsuji T, Hashimoto A, Itsumura N. The physiological, biochemical,and molecular roles of zinc transporters in zinc homeostasis and metabolism. *Physiol Rev.* (2015) 95:749–84. doi: 10.1152/physrev.00035.2014

8. Solomons NW. Update on zinc biology. *Ann Nutr Metab.* (2013) 62 Suppl 1:8–17. doi: 10.1159/000348547

9. Fukada T. [Zinc transporters and zinc signaling]. *Nihon Rinsho.* (2016) 74:1087–93.

10. Levaot N, Hershfinkel M. How cellular Zn2+ signaling drives physiological functions. *Cell Calcium.* (2018) 75:53–63. doi: 10.1016/j.ceca.2018.08.004

11. Costello LC, Fenselau CC, Franklin RB. Evidence for operation of the direct zinc ligand exchange mechanism for trafficking, transport, and reactivity of zinc in mammalian cells. *J Inorg Biochem.* (2011) 105:589–99. doi: 10.1016/j.jinorgbio.2011.02.002

12. Vallee BL, Galdes A. The metallobiochemistry of zinc enzymes. *Adv Enzymol Relat Areas Mol Biol.* (1984) 56:283–430. doi: 10.1002/9780470123027.ch5

13. Maret W. Metals on the move: zinc ions in cellular regulation and in the coordination dynamics of zinc proteins. *Biometals.* (2011) 24:411–8. doi: 10.1007/s10534-010-9406-1

14. Krishna SS, Majumdar I, Grishin NV. Structural classification of zinc fingers: survey and summary. *Nucleic Acids Res.* (2003) 31:532–50. doi: 10.1093/nar/gkg161

15. Zelko IN, Mariani TJ, Folz RJ. Superoxide dismutase multigene family: a comparison of the CuZn-SOD (SOD1), Mn-SOD (SOD2), and EC-SOD (SOD3) gene structures, evolution, and expression. *Free Radic Biol Med.* (2002) 33:337–49. doi: 10.1016/S0891-5849(02)00905-X

16. Rink L, Kirchner H. Zinc-altered immune function and cytokine production. *J Nutr.* (2000) 130:1407S–11S. doi: 10.1093/jn/130.5.1407S

17. Meurs KM, Breitschwerdt EB. CVT update: zinc toxicity. In: Bonagura JD, editor. *Kirk's Current Veterinary Therapy XII Small Animal Practice.* W.B. Saunders, Philadelphia, PA (1995). p. 238239.

18. Walsh CT, Sandstead HH, Prasad AS, Newberne PM, Fraker PJ. Zinc: health effects and research priorities for the 1990s. *Environ Health Perspect.* (1994) 102 Suppl 2:5–46. doi: 10.1289/ehp.941025

19. Cummings JE, Kovacic JP. The ubiquitous role of zinc in health and disease. *J Vet Emerg Crit Care (San Antonio).* (2009) 19:215–40. doi: 10.1111/j.1476-4431.2009.00418.x

20. Khan SA. Zinc toxicosis. In: Cote E, editor. *Clinical Veterinary Advisor Dogs and Cats.* Mosby, St Louis, MO (2007). p. 1171–3.

21. Ames BN. Supplements and tuning up metabolism. *J Nutr.* (2004) 134:3164S–8S. doi: 10.1093/jn/134.11.3164S

22. Sun W, Yang J, Wang W, Hou J, Cheng Y, Fu Y, et al. The beneficial effects of Zn on Akt-mediated insulin and cell survival signaling pathways in diabetes. *J Trace Elem Med Biol.* (2018) 46:117–27. doi: 10.1016/j.jtemb.2017.12.005

23. Barman S, Srinivasan K. Diabetes and zinc dyshomeostasis: Can zinc supplementation mitigate diabetic complications? *Crit Rev Food Sci Nutr.* (2022) 62:1046–61. doi: 10.1080/10408398.2020.1833178

24. Barman S, Srinivasan K. Zinc supplementation alleviates hyperglycemia and associated metabolic abnormalities in streptozotocin-induced diabetic rats. *Can J Physiol Pharmacol*. (2016) 94:1356–65. doi: 10.1139/cjpp-2016-0084

25. Himoto T, Yoneyama H, Kurokochi K, Inukai M, Masugata H, Goda F, et al. Contribution of zinc deficiency to insulin resistance in patients with primary biliary cirrhosis. *Biol Trace Elem Res*. (2011) 144:133–42. doi: 10.1007/s12011-011-9049-2

26. Himoto T, Masaki T. Associations between zinc deficiency and metabolic abnormalities in patients with chronic liver disease. *Nutrients*. (2018) 10:88. doi: 10.3390/nu10010088

27. Ullah MI, Alameen AAM, Al-Oanzi ZH, Eltayeb LB, Atif M, Munir MU, et al. Biological role of zinc in liver cirrhosis: an updated review. *Biomedicines*. (2023) 11:1094. doi: 10.3390/biomedicines11041094

28. Barman S, Srinivasan K. Attenuation of oxidative stress and cardioprotective effects of zinc supplementation in experimental diabetic rats. *Br J Nutr*. (2017) 117:335–50. doi: 10.1017/S0007114517000174

29. Berg JM, Shi Y. The galvanization of biology: a growing appreciation for the roles of zinc. *Science*. (1996) 271:1081–5. doi: 10.1126/science.271.5252.1081

30. O'Dell BL. Role of zinc in plasma membrane function. *J Nutr*. (2000) 130:1432S–6S. doi: 10.1093/jn/130.5.1432S

31. Hershfinkel M, Silverman WF, Sekler I. The zinc sensing receptor, a link between zinc and cell signaling. *Mol Med*. (2007) 13:331–6. doi: 10.2119/2006-00038.Hershfinkel

32. Frederickson CJ, Suh SW, Silva D, Frederickson CJ, Thompson RB. Importance of zinc in the central nervous system: the zinc-containing neuron. *J Nutr*. (2000) 130:1471S–83S. doi: 10.1093/jn/130.5.1471S

33. Shankar AH, Prasad AS. Zinc and immune function: the biological basis of altered resistance to infection. *Am J Clin Nutr*. (1998) 68:447S–63S. doi: 10.1093/ajcn/68.2.447S

34. Bray TM, Bettger WJ. The physiological role of zinc as an antioxidant. *Free Radic Biol Med*. (1990) 8:281–91. doi: 10.1016/0891-5849(90)90076-U

35. Zarezadeh M, Faghfouri AH, Aghapour B, Rostamkhani H, Malekahmadi M, Naemi Kermanshahi M, et al. Investigation of the clinical efficacy of Zn supplementation in improvement of oxidative stress parameters: A systematic review and dose-response meta-analysis of controlled clinical trials. *Int J Clin Pract*. (2021) 75:e14777. doi: 10.1111/ijcp.v75.12

36. Zhang Y, Tian Y, Zhang H, Xu B, Chen H. Potential pathways of zinc deficiency-promoted tumorigenesis. *BioMed Pharmacother*. (2021) 133:110983. doi: 10.1016/j.biopha.2020.110983

37. Beckman KB, Ames BN. The free radical theory of aging matures. *Physiol Rev*. (1998) 78:547–81. doi: 10.1152/physrev.1998.78.2.547

38. Frassinetti S, Bronzetti G, Caltavuturo L, Cini M, Croce CD. The role of zinc in life: a review. *J Environ Pathol Toxicol Oncol*. (2006) 25:597–610. doi: 10.1615/JEnvironPatholToxicolOncol.v25.i3.40

39. Berg JM, Shi Y. The galvanization of biology: a growing appreciation for the roles of zinc. *Science*. (1996) 271:1081–5. doi: 10.1126/science.271.5252.1081

40. Truong-Tran AQ, Carter J, Ruffin RE, Zalewski PD. The role of zinc in caspase activation and apoptotic cell death. *Biometals*. (2001) 14:315–30. doi: 10.1023/A:1012993017026

41. Lemire J, Mailloux R, Appanna VD. Zinc toxicity alters mitochondrial metabolism and leads to decreased ATP production in hepatocytes. *J Appl Toxicol*. (2008) 28:175–82. doi: 10.1002/jat.v28:2

42. Coyle P, Philcox JC, Carey LC, Rofe AM. Metallothionein: the multipurpose protein. *Cell Mol Life Sci*. (2002) 59:627–47. doi: 10.1007/s00018-002-8454-2

43. Engin A. The definition and prevalence of obesity and metabolic syndrome. *Adv Exp Med Biol*. (2017) 960:1–17. doi: 10.1007/978-3-319-48382-5

44. Bashandy SAE, El-Seidy AMA, Ibrahim FAA, Abdelrahman SS, Abdelmottaleb Moussa SA, ElBaset MA. Zinc nanoparticles ameliorated obesity-induced cardiovascular disease: role of metabolic syndrome and iron overload. *Sci Rep*. (2023) 13:16010. doi: 10.1038/s41598-023-42550-y

45. Althanoon Z, Merkhan M. Effects of zinc supplementation on metabolic status in patients with metabolic syndrome. *Acta Poloniae Pharm - Drug Res*. (2021) 78:521–26. doi: 10.32383/appdr/141348

46. Ding J, Liu Q, Liu Z, Guo H, Liang J, Zhang Y. Association between dietary zinc intake and metabolic syndrome. *A Meta-Analysis Observational Stud Front Nutr*. (2022) 9:825913. doi: 10.3389/fnut.2022.825913

47. Qu R, Jia Y, Liu J, Jin S, Han T, Na L. Dietary flavonoids, copper intake, and risk of metabolic syndrome in Chinese adults. *Nutrients*. (2018) 10:991. doi: 10.3390/nu10080991

48. Lu CW, Lee YC, Kuo CS, Chiang CH, Chang HH, Huang KC. Association of serum levels of zinc, copper, and iron with risk of metabolic syndrome. *Nutrients*. (2021) 13:548. doi: 10.3390/nu13020548

49. Yang S, Chen Q, Wang L. Association of zinc intake, tobacco smoke exposure, with metabolic syndrome: evidence from NHANES 2007-2018. *Biol Trace Elem Res*. (2024) 202(12):5429–37. doi: 10.1007/s12011-024-04120-9

50. Zhang H, Man Q, Song P, Li S, Liu X, Wang L, et al. Association of whole blood copper, magnesium and zinc levels with metabolic syndrome components in 6-12-year-old rural Chinese children: 2010-2012 China National Nutrition and Health Survey. *Nutr Metab (Lond)*. (2021) 18:67. doi: 10.1186/s12986-021-00593-w

51. Wu Y, Xu G, Bai R, Yu P, He Z, Chen M, et al. Association between circulating zinc levels and risk factors of metabolic syndrome: insights from a bi-directional Mendelian randomization analysis and cross-sectional study. *Biol Trace Elem Res*. (2023) 202(7):3051–61. doi: 10.1007/s12011-023-03918-3

52. Aydogdu A, Unal Ö, Baltaci SB, Menevse E, Mogulkoc R, Erdem SS, et al. Plasma leptin, nesfatin 1, NPY, and zinc levels in obese and metabolic syndrome children. *Eur J Ther*. (2023) 29:856–65. doi: 10.58600/eurjther1760

53. Qorbani M, Movasaghi N, Mohammadian Khonsari N, Daneshzad E, Shafiee G, Ashraf H, et al. Association of zinc serum level with metabolic syndrome in Iranian children and adolescents: The CASPIAN-V study. *Front Nutr*. (2022) 9:932746. doi: 10.3389/fnut.2022.932746

54. Ennes Dourado Ferro F, de Sousa Lima VB, Mello Soares NR, Franciscato Cozzolino SM, do Nascimento Marreiro D. Biomarkers of metabolic syndrome and its relationship with the zinc nutritional status in obese women. *Nutr Hosp*. (2011) 26:650–4. doi: 10.1590/S0212-16112011000300032

55. Skrajnowska D, Bobrowska-Korczak B. Role of zinc in immune system and anti-cancer defense mechanisms. *Nutrients*. (2019) 11:2273. doi: 10.3390/nu11102273

56. Samavarchi Tehrani S, Mahmoodzadeh Hosseini H, Yousefi T, Abolghasemi M, Qujeq D, Maniati M, et al. The crosstalk between trace elements with DNA damage response, repair, and oxidative stress in cancer. *J Cell Biochem*. (2019) 120:1080–105. doi: 10.1002/jcb.v120.2

57. Figiel M, Górka AK, Górecki A. Zinc ions modulate YY1 activity: relevance in carcinogenesis. *Cancers (Basel)*. (2023) 15:4338. doi: 10.3390/cancers15174338

58. Jouybari L, Kiani F, Akbari A, Sanagoo A, Sayehmiri F, Aaseth J, et al. A meta-analysis of zinc levels in breast cancer. *J Trace Elem Med Biol*. (2019) 56:90–9. doi: 10.1016/j.jtemb.2019.06.017

59. Tu K, Liu K, Wang Y, Jiang Y, Zhang C. Association of dietary intake of zinc and selenium with breast cancer risk: A case-control study in Chinese women. *Nutrients*. (2023) 15:3253. doi: 10.3390/nu15143253

60. Laya A. Trace elements homeostasis in biological samples as new candidate biomarkers for early diagnosis and prognosis of female breast cancer and therapeutic response: systematic review. *Arch Breast Cancer*. (2023) 10:26–37. doi: 10.32768/abc.202310126-37

61. Feng Y, Zeng JW, Ma Q, Zhang S, Tang J, Feng JF. Serum copper and zinc levels in breast cancer: A meta-analysis. *J Trace Elem Med Biol*. (2020) 62:126629. doi: 10.1016/j.jtemb.2020.126629

62. Kim S, Freeland-Graves JH, Babaei M, Sachdev PK, Beretvas SN. Quantifying the association between acute leukemia and serum zinc, copper, and selenium: a meta-analysis. *Leuk Lymphoma*. (2019) 60:1548–56. doi: 10.1080/10428194.2018.1540043

63. Mao S, Huang S. Zinc and copper levels in bladder cancer: a systematic review and meta-analysis. *Biol Trace Elem Res*. (2013) 153:5–10. doi: 10.1007/s12011-013-9682-z

64. Drake EN2nd, Sky-Peck HH. Discriminant analysis of trace element distribution in normal and Malignant human tissues. *Cancer Res*. (1989) 49:4210–5.

65. Gutiérrez-González E, Pastor-Barriuso R, Castelló A, Castaño-Vinyals G, Fernández de Larrea-Baz N, Dierssen-Sotos T, et al. Toenail zinc and risk of prostate cancer in the MCC-Spain case-control study. *Environ Res*. (2024) 245:118065. doi: 10.1016/j.envres.2023.118065

66. Bendellaa M, Lelièvre P, Coll JL, Sancey L, Deniaud A, Busser B. Roles of zinc in cancers: From altered metabolism to therapeutic applications. *Int J Cancer*. (2024) 154:7–20. doi: 10.1002/ijc.v154.1

67. John E, Laskow TC, Buchser WJ, Pitt BR, Basse PH, Butterfield LH, et al. Zinc in innate and adaptive tumor immunity. *J Transl Med*. (2010) 8:118. doi: 10.1186/1479-5876-8-118

68. Rink L, Kirchner H. Zinc-altered immune function and cytokine production. *J Nutr*. (2000) 130:1407S–11S. doi: 10.1093/jn/130.5.1407S

69. Skrajnowska D, Bobrowska-Korczak B. Role of zinc in immune system and anti-cancer defense mechanisms. *Nutrients*. (2019) 11:2273. doi: 10.3390/nu11102273

70. Sliwinski T, Czechowska A, Kolodziejczak M, Jajte J, Wisniewska-Jarosinska M, Blasiak J. Zinc salts differentially modulate DNA damage in normal and cancer cells. *Cell Biol Int*. (2009) 33:542–7. doi: 10.1016/j.cellbi.2009.02.004

71. Huang SH, Hsieh HC, Shieh JM, Su WC, Wang YC. Downregulation of microRNA-326 enhances ZNF322A expression, transcriptional activity and tumorigenic effects in lung cancer. *Biofactors*. (2024) 50:214–27. doi: 10.1002/biof.v50.1

72. Li M, Liu Z, Hou Z, Wang X, Shi H, Li Y, et al. Oncogenic zinc finger protein ZNF687 accelerates lung adenocarcinoma cell proliferation and tumor progression by activating the PI3K/AKT signaling pathway. *Thorac Cancer*. (2023) 14:1223–38. doi: 10.1111/1759-7714.14856

73. Wang W, Zhang Z, Zhao M, Wang Y, Ge Y, Shan L. Zinc-finger protein CXXC5 promotes breast carcinogenesis by regulating the TSC1/mTOR signaling pathway. *J Biol Chem*. (2023) 299:102812. doi: 10.1016/j.jbc.2022.102812

74. Zou X, Ma L, Zhang Y, Zhang Q, Xu C, Zhang D, et al. GATA zinc finger protein p66β promotes breast cancer cell migration by acting as a co-activator of Snail. *Cell Death Dis*. (2023) 14:382. doi: 10.1038/s41419-023-05887-w

75. Zheng D, Wei Z, Zhang C, Liu W, Gong C, Wu F, et al. ZNF692 promotes osteosarcoma cell proliferation, migration, and invasion through TNK2-mediated activation of the MEK/ERK pathway. *Biol Direct*. (2024) 19:28. doi: 10.1186/s13062-024-00472-3

76. Zhu CC, Sun HL, Long TF, Lyu YY, Liu JL, Ni GT. ZNF554 inhibits endometrial cancer progression via regulating RBM5 and inactivating WNT/β-catenin signaling pathway. *Curr Med Sci*. (2024) 44:406–18. doi: 10.1007/s11596-024-2845-7

77. Xu J, Zhou Y, Wang Q, Liu Y, Tang J. Zinc finger protein 263 upregulates interleukin 33 and suppresses autophagy to accelerate the Malignant progression of non-small cell lung cancer. *Clin Transl Oncol*. (2024) 26:924–35. doi: 10.1007/s12094-023-03325-z

78. Yao W, Chen X, Cui X, Zhou B, Zhao B, Lin Z, et al. Esterase D interacts with metallothionein 2A and inhibits the migration of A549 lung cancer cells in vitro. *J Cell Biochem*. (2023) 124:373–81. doi: 10.1002/jcb.v124.3

79. Kwon IS, Hwang YN, Park JH, Na HH, Kwon TH, Park JS, et al. Metallothionein family proteins as regulators of zinc ions synergistically enhance the anticancer effect of cannabidiol in human colorectal cancer cells. *Int J Mol Sci*. (2023) 24:16621. doi: 10.3390/ijms242316621

80. An N, Peng H, Hou M, Su D, Wang L, Shen X, et al. The zinc figure protein ZNF575 impairs colorectal cancer growth via promoting p53 transcription. *Oncol Res*. (2023) 31:307–16. doi: 10.32604/or.2023.028564

81. Huang CR, Chu YT, Chang CL, Yip HK, Chen HH. ZNF746 plays cardinal roles on colorectal cancer (CRC) cell invasion and migration and regulates mitochondrial dynamics and morphological changes of CRC cells-Role of combined melatonin and 5-FU regimen. *J Cell Biochem*. (2024) 125:e30507. doi: 10.1002/jcb.v125.2

82. Wang Y, Chen FR, Wei CC, Sun LL, Liu CY, Yang LB, et al. Zinc finger protein 671 has a cancer-inhibiting function in colorectal carcinoma via the deactivation of Notch signaling. *Toxicol Appl Pharmacol*. (2023) 458:116326. doi: 10.1016/j.taap.2022.116326

83. Nishida K, Nakagawa N. Zinc suppresses colorectal cancer development through cell-mediated immunity. *Yakugaku Zasshi*. (2024) 144:475–81. doi: 10.1248/yakushi.23-00154-1

84. Yang P, Li H, Sun M, Guo X, Liao Y, Hu M, et al. Zinc deficiency drives ferroptosis resistance by lactate production in esophageal squamous cell carcinoma. *Free Radic Biol Med*. (2024) 213:512–22. doi: 10.1016/j.freeradbiomed.2024.01.041

85. Pan Z, Choi S, Ouadid-Ahidouch H, Yang JM, Beattie JH, Korichneva I. Zinc transporters and dysregulated channels in cancers. *Front Biosci (Landmark Ed)*. (2017) 22:623–43. doi: 10.2741/4507

86. Costello LC, Franklin RB. A comprehensive review of the role of zinc in normal prostate function and metabolism; and its implications in prostate cancer. *Arch Biochem Biophys*. (2016) 611:100–12. doi: 10.1016/j.abb.2016.04.014

87. To PK, Do MH, Cho JH, Jung C. Growth modulatory role of zinc in prostate cancer and application to cancer therapeutics. *Int J Mol Sci*. (2020) 21:2991. doi: 10.3390/ijms21082991

88. Taylor KM, Hiscox S, Nicholson RI, Hogstrand C, Kille P. Protein kinase CK2 triggers cytosolic zinc signaling pathways by phosphorylation of zinc channel ZIP7. *Sci Signal*. (2012) 5:ra11. doi: 10.1126/scisignal.2002585

89. Wang J, Zhao H, Xu Z, Cheng X. Zinc dysregulation in cancers and its potential as a therapeutic target. *Cancer Biol Med*. (2020) 17:612–25. doi: 10.20892/j.issn.2095-3941.2020.0106

90. Hoeller D, Dikic I. Targeting the ubiquitin system in cancer therapy. *Nature*. (2009) 458:438–44. doi: 10.1038/nature07960

91. Lopez V, Foolad F, Kelleher SL. ZnT2-overexpression represses the cytotoxic effects of zinc hyper-accumulation in Malignant metallothionein-null T47D breast tumor cells. *Cancer Lett*. (2011) 304:41–51. doi: 10.1016/j.canlet.2011.01.027

92. Cheng X, Wei L, Huang X, Zheng J, Shao M, Feng T, et al. Solute carrier family 39 member 6 gene promotes aggressiveness of esophageal carcinoma cells by increasing intracellular levels of zinc, activating phosphatidylinositol 3-kinase signaling, and up-regulating genes that regulate metastasis. *Gastroenterology*. (2017) 152:1985–1997.e12. doi: 10.1053/j.gastro.2017.02.006

93. Dziegiel P. Expression of metallothioneins in tumor cells. *Pol J Pathol*. (2004) 55:3–12.

94. Zhao J, Wen D, Zhang S, Jiang H, Di X. The role of zinc finger proteins in Malignant tumors. *FASEB J*. (2023) 37:e23157. doi: 10.1096/fj.202300801R

95. Jayaraman AK, Jayaraman S. Increased level of exogenous zinc induces cytotoxicity and up-regulates the expression of the ZnT-1 zinc transporter gene in pancreatic cancer cells. *J Nutr Biochem*. (2011) 22:79–88. doi: 10.1016/j.jnutbio.2009.12.001

96. Padmanabhan A, Kaushik M, Niranjan R, Richards JS, Ebright B, Venkatasubbu GD. Zinc Oxide nanoparticles induce oxidative and proteotoxic stress in ovarian cancer cells and trigger apoptosis Independent of p53-mutation status. *Appl Surf Sci*. (2019) 487:807–818. doi: 10.1016/j.apsusc.2019.05.099

97. Yang R J, Wu R, Mei J, Hu FR, Lei CJ. Zinc oxide nanoparticles promotes liver cancer cell apoptosis through inducing autophagy and promoting p53. *Eur Rev Med Pharmacol Sci*. (2021) 25:1557–63.

98. Ding WQ, Liu B, Vaught JL, Yamauchi H, Lind SE. Anticancer activity of the antibiotic clioquinol. *Cancer Res*. (2005) 65:3389–95. doi: 10.1158/0008-5472.CAN-04-3577

99. Schmitt SM, Frezza M, Dou QP. New applications of old metal-binding drugs in the treatment of human cancer. *Front Biosci (Schol Ed)*. (2012) 4:375–91. doi: 10.2741/s274

100. Lei G, Zhuang L, Gan B. Targeting ferroptosis as a vulnerability in cancer. *Nat Rev Cancer*. (2022) 22:381–96. doi: 10.1038/s41568-022-00459-0

101. Hercberg S, Ezzedine K, Guinot C, Preziosi P, Galan P, Bertrais S, et al. Antioxidant supplementation increases the risk of skin cancers in women but not in men. *J Nutr*. (2007) 137:2098–105. doi: 10.1093/jn/137.9.2098

102. Zhang Y, Song M, Mucci LA, Giovannucci EL. Zinc supplement use and risk of aggressive prostate cancer: a 30-year follow-up study. *Eur J Epidemiol*. (2022) 37:1251–60. doi: 10.1007/s10654-022-00922-0

103. Shah MR, Kriedt CL, Lents NH, Hoyer MK, Jamaluddin N, Klein C, et al. Direct intra-tumoral injection of zinc-acetate halts tumor growth in a xenograft model of prostate cancer. *J Exp Clin Cancer Res*. (2009) 28:84. doi: 10.1186/1756-9966-28-84

104. Zhang Y, Stopsack KH, Wu K, Song M, Mucci LA, Giovannucci E. Post-diagnostic zinc supplement use and prostate cancer survival among men with nonmetastatic prostate cancer. *J Urol*. (2023) 209:549–56. doi: 10.1097/JU.0000000000003080

frontiers | Frontiers in Oncology

TYPE Original Research
PUBLISHED 13 January 2025
DOI 10.3389/fonc.2024.1499580

OPEN ACCESS

EDITED BY
Shivendra Vikram Singh,
St. Jude Children's Research Hospital,
United States

REVIEWED BY
Amilcare Barca,
University of Salento, Italy
Jianrong Lu,
University of Florida, United States

*CORRESPONDENCE
Yongli Zhao
13606305788@163.com
Jigang Dong
djg0107@163.com

†These authors have contributed equally to this work and share senior authorship

RECEIVED 21 September 2024
ACCEPTED 06 December 2024
PUBLISHED 13 January 2025

CITATION
Xu X, Fa L, Sun X, Yang F, Liu Y, Song J, Zhao Y and Dong J (2025) Integrative analysis of ferroptosis in the hypoxic microenvironment of gastric cancer unveils the immune landscape and personalized therapeutic strategies. *Front. Oncol.* 14:1499580. doi: 10.3389/fonc.2024.1499580

Integrative analysis of ferroptosis in the hypoxic microenvironment of gastric cancer unveils the immune landscape and personalized therapeutic strategies

Xiao Xu[1], Liangling Fa[2], Xiaoxiao Sun[1], Fangfang Yang[3], Yongrui Liu[4], Jifu Song[1], Yongli Zhao[1*†] and Jigang Dong[1,5*†]

[1]Department of Radiation Oncology, Qingdao People's Hospital Group (Jiaozhou), Jiaozhou Central Hospital of Qingdao, Qingdao, China, [2]Department of Pathology, Qingdao People's Hospital Group (Jiaozhou), Jiaozhou Central Hospital of Qingdao, Qingdao, China, [3]Cancer Precision Medical Center, Qingdao University, Qingdao, China, [4]Department of Oncology, Linyi Cancer Hospital, Linyi, China, [5]Tianjin Medical University Cancer Institute & Hospital, National Clinical Research Center for Cancer, Tianjin's Clinical Research Center for Cancer, Key Laboratory of Cancer Prevention and Therapy, Tianjin, China

Background: Ferroptosis is a cell death mode caused by excessive accumulation of lipid peroxides caused by disturbance of intracellular metabolic pathway, which is closely related to iron and cholesterol metabolism homeostasis. Its regulation within the hypoxic metabolic tumor microenvironment (TME) has the potential to improve the effectiveness of tumor immunotherapy. The predictive role of ferroptosis in gastric cancer (GC) hypoxia TME, particularly in relation to TME immune cell infiltration, has not been fully explained.

Methods: By analyzing the mRNA expression data of ferroptosis and hypoxia-related genes, a prediction model was constructed to evaluate further the predictive value of immune cell infiltration, clinical characteristics, and immunotherapy efficacy of gastric cancer, and the essential genes were validated.

Results: Two distinct molecular states of ferroptosis-hypoxia were identified in GC. Notably, patients with high ferroptosis-hypoxia risk scores (FHRS) displayed significant levels of hypoxia and epithelial-mesenchymal transition (EMT), which were associated with unfavorable prognosis, increased chemoresistance, and heightened immunosuppression.

Conclusions: This study demonstrates that ferroptosis under hypoxic conditions significantly affects the modulation of the tumor immune microenvironment. The FHRS can independently predict prognosis in gastric cancer. Assessing the molecular status of ferroptosis-hypoxia in individual patients will help in selecting more suitable immunotherapy regimens by providing a better understanding of TME characteristics and predicting immunotherapeutic outcomes.

KEYWORDS

ferroptosis, immune landscape, immunotherapy, hypoxia microenvironment, tumor metabolism

1 Introduction

The latest global cancer statistics report highlights gastric cancer as one of the top five prevalent malignancies worldwide. The far-reaching public health impact of gastric cancer underscores the urgent need for an in-depth study of molecular biological mechanisms and improved treatment outcomes (1). Although chemotherapy and molecular targeted therapy have effectively prolonged the survival of gastric cancer patients, drug resistance remains a significant challenge. The molecular mechanism of drug resistance in gastric cancer remains incompletely understood, resulting in a lack of effective prevention and intervention in clinical practice (2). The advent of immunotherapy has led to a notable improvement in the survival rate of patients with advanced gastric cancer, challenging the dominance of chemotherapy and targeted therapy. Nevertheless, the efficacy of immune checkpoint blockade (ICB) therapy is constrained by the complicated tumor microenvironment and the inactivation of the immune system, which results in disparate outcomes. Consequently, there is a pressing necessity to develop more precise markers to assess the malignant process and forecast treatment response. Identifying these markers will facilitate the development of personalized therapeutic approaches, thereby enhancing patient outcomes and survival rates.

The concept of ferroptosis was initially developed in the context of tumor research (3). Researchers discovered this particular form of cell death, searching for a method to selectively induce death in cancer cells carrying RAS mutations. Recent evidence indicates that drug-induced ferroptosis can reverse drug resistance, a crucial tumor suppressor mechanism (4). In addition, ferroptosis enhances the infiltration and activity of tumor immune cells and decreases the recruitment and function of immunosuppressive cells, thereby reducing immunosuppression and promoting tumor immunosurveillance and immune-mediated tumor clearance. The study by Li Y et al. proposes a novel strategy to enhance immunogenic cell death (ICD) and the cascade effect of T-cell activity through ferroptosis for effective tumor therapy (5, 6). Although the mechanisms of interaction between ferroptosis and ICB therapy are still under investigation, current evidence suggests that the facilitating role of ferroptosis may provide a new strategy for enhancing the response to ICBs in certain refractory tumors. Further studies are required to elucidate the specific mechanisms of these interactions and to validate the efficacy of the combination strategy of ferroptosis inducers and ICB therapy in clinical trials.

Hypoxia profoundly affects tumor metabolism and microenvironment, including angiogenesis, cell proliferation, invasion, and metastasis. These processes reduce apoptosis, differentiation, and ferroptosis, thereby promoting tumor immunosuppression and escape (7–9). Ameliorating hypoxia can reshape the immunosuppressive tumor microenvironment by reducing the intratumoral invasion of M2-type tumor-associated macrophages and decreasing PD-L1 expression in tumor cells (10). Furthermore, hypoxia can induce EMT in cancer cells, which promotes the stem-like features of cancer cells and leads to tumor therapy resistance. In human cancer cell lines and organoids, a highly mesenchymal state unequivocally implies a selective susceptibility associated with ferroptosis (3, 11). The central molecule in the cellular response to hypoxia is the hypoxia-inducible factor (HIF). The HIF signaling pathway senses metabolic changes due to cellular hypoxia, regulates cell proliferation, and induces inflammatory responses (12). It was found that HIF-1α upregulates SLC1A1 to enhance glutamate-cystine transport efficiency, thereby driving solid tumor resistance to ferroptosis (13). Additionally, LDHA-activated lactate accumulation is promoted by HIF-1α to enhance ferroptosis resistance (14, 15). Another researcher prepared nanoparticles (CI@HSA NPs) encapsulating capsaicin (CAP) and the photosensitizer IR780 to enhance the efficacy of photodynamic therapy (PDT) on osteosarcoma. The nanoparticles were designed to release capsaicin, which has been demonstrated to promote osteosarcoma ferroptosis and improve the hypoxic microenvironment (16). Combining HIF-1α inhibitors with ferroptosis inducers represents a novel strategy for solid tumor therapy. These findings elucidate the molecular mechanism of hypoxia-induced ferroptosis resistance in solid tumors and provide new theories and strategies for solid tumor treatment.

This study integrated genomic and clinical data from gastric cancer samples from four datasets to identify and comprehensively evaluate two ferroptosis clusters. Additionally, two hypoxia molecular subtypes were identified using the same method. Both molecular types were closely associated with the prognosis and immune cell infiltration signaling pathway in gastric cancer patients, suggesting that both ferroptosis and hypoxia play an integral role in shaping the specific characteristics of the individual tumor microenvironment. Consequently, these molecular subtypes were combined into a two-dimensional index, designated the ferroptosis-hypoxia subtypes. Further analysis demonstrated that the ferroptosis-hypoxia subtypes were closely associated with prognosis, tumor immune cell infiltration, and mesenchymal characteristics of gastric cancer patients. Based on these findings, we developed a scoring system that quantifies the ferroptosis-hypoxia status of individual patients. The scoring system enables the selection of individualized treatment regimens for patients and the optimization of treatment strategies by assessing the ferroptosis-hypoxia status.

2 Materials and methods

2.1 Data preparation

The gastric cancer gene expression data and clinical annotations were acquired from The Cancer Genome Atlas (TCGA) database, which is publicly accessible at https://portal.gdc.cancer.gov/repository. Validation cohort data from GSE112302, GSE84437, and ACRG/GSE62254 were downloaded from the Gene Expression Omnibus (GEO, https://www.ncbi.nlm.nih.gov/geo) database. TCGA-STAD copy number variation (CNV) data were also extracted from the UCSC Xena database (https://xena.ucsc.edu/). The anti-pd-1 treatment cohort PRJEB25780 data was obtained from the Tumor Immune Dysfunction and Exclusion Database (TIDE, http://tide.dfci.harvard.edu/) (17). The clinical information,

including microsatellite instability (MSI) status, remission, and Lauren typing, was extracted from the manuscript of Mayakonda et al. (18). A total of 1,121 GC patient samples were included in this study.

The "ComBat" function provided by the R package "sva" removed the batch effect. "ComBat" is a classical Bayesian-based analysis that utilizes known batch information for the correction of high-throughput data, ensuring that the comparisons across datasets are accurate and meaningful (19, 20).

Ferroptosis-related genes (FRGs) were obtained from the FerrDb website (http://www.zhounan.org/ferrdb), which is the first database of ferroptosis regulatory factors, biomarkers, and ferroptosis disease associations (21). We removed duplicate genes and obtained 380 FRGs for subsequent analyses (Supplementary Table 1). Hypoxia-related genes (HRGs) were obtained from the Molecular Signatures Database (MSigDB, https://www.gsea-msigdb.org/gsea/msigdb) (22). HIF-1 pathway target genes were downloaded from the Kyoto Encyclopedia of Genes and Genomes database (KEGG, https://www.kegg.jp/; ID:map04066), including genes associated with "increasing oxygen delivery" and "decreasing oxygen consumption". The negative and positive regulator genes of ferroptosis were downloaded from the Gene Ontology database (GO, https://geneontology.org/; GO: 0160020, GO: 0110076).

All data in TCGA, GEO, TIDE, FerrDb, KEGG, GO, and MSigDB are publicly available and adhere to the data access and release policies of the respective databases.

2.2 Detection of ferroptosis molecular subtypes and hypoxia molecular subtypes

The FPKM values of the RNA sequencing data from the TCGA-STAD dataset were transformed into TPM using the R package "TCGAbiolinks" (23). The differentially expressed FRGs and HRGs (FDR<0.01, |logFC|>1) were analyzed and screened from gastric cancer and para-carcinoma samples utilizing the R package "limma" (24). Unsupervised cluster analysis was performed with the "ConsensusClusterPlus" package to identify ferroptosis and hypoxia molecular subtypes based on the mRNA expression profiles of the differentially expressed genes (DEGs) (25). A consensus clustering algorithm was used to determine cluster number and stability. The analysis was repeated 1000 times to ensure classification stability. Subsequently, patients from the TCGA-STAD, GSE84437, GSE62254, GSE112302, and PRJEB25780 cohorts were categorized for subsequent analysis.

2.3 Tumor microenvironment characterization and functional enrichment analysis

To further enhance comprehension of how ferroptosis impacts the tumor immunological microenvironment, we applied the CIBERSORT analysis (http://cibersort.stanford.edu/) (26). The publication of CIBERSORT was released in the scientific journal Nature Methods in 2015. It is the most commonly referenced instrument for estimating and analyzing the infiltration of immune cells. We utilized CIBERSORT computations to conduct analyses on immune cell infiltration to identify the properties of the immunological microenvironment.

The ESTIMATE algorithm, which estimates the level of infiltrating stromal and immune cells in malignant tumor tissues, employs expression data to generate scores. These scores are used to calculate the level of infiltrating stromal cells and immune cells, as well as tumor purity.

GO and KEGG analyses were conducted on DEGs (FDR<0.05) using the "clusterProfiler" R package (27). To investigate the biological processes, we downloaded the gene set "c2.cp.kegg.v7.4" from the MSigDB database to perform Gene Set Variation Analysis (GSVA) enrichment analysis. GSVA is an unsupervised approach for quantifying alterations in biological pathways and processes within expression dataset samples. A collection of signaling pathways was examined to investigate the matrix state within the tumor microenvironment, including TGF-EMT, MAPK, NOTCH, KRAS, HALLMARK HYPOXIA, and HIF-1 (28). Subsequently, we employed single-sample Gene Set Enrichment Analysis (ssGSEA) to investigate the mechanisms underlying the generation of TME features (29). We acquired a collection of genes associated with EMT markers from Mariathasan et al., including EMT1, EMT2, EMT3, angiogenic signature, TGF-β response signature of pan-fibroblasts (Pan-FTBRS), and WNT targets (30).

2.4 Identification of characteristic molecular subtypes of ferroptosis-hypoxia

We proceeded to combine the above ferroptosis and hypoxia status into a two-dimensional index. The patients were classified into three groups: the ferroptosis-hypoxia (F-H) molecular subtypes A, B, and Mix. Patients belonging to both the ferroptosis cluster A and the hypoxia cluster A were identified as F-H subtype A, patients belonging to both the ferroptosis cluster B and the hypoxia cluster B were classified as F-H subtype B, and the remaining patients were classified as F-H subtype Mix. The F-H subtype expression profiles in groups A and B were compared to identify DEGs(FDR<0.001, |log FC|>1). Unsupervised clustering analysis was performed on the DEGs mentioned above to construct gene subtypes related to the F-H molecular subtypes.

The DEGs were overlaid with FRGs and HRGs and subjected to univariate Cox analysis. The ferroptosis-hypoxia-related prognostic DEGs were identified for further analysis (p<0.05). In order to reduce overfitting, we constructed a prognostic model utilizing Lasso-penalized Cox regression analysis (31). The Lasso algorithm was employed for variable selection and shrinkage, and the R package "glmnet" was utilized to filter out variables with less information. The model was constructed using the TCGA dataset as the training set and the GSE62254 dataset as the independent test set to obtain the optimal combination of variables. The regression model used the normalized expression matrix of candidate prognostic DEGs as independent factors. Meanwhile, OS and patient status in the TCGA were considered response variables. The penalty parameter (λ) of the model was chosen using tenfold

cross-validation according to the minimal criteria, which corresponds to the value of λ that minimizes the partial likelihood deviation. Risk scores for patients were computed by utilizing the normalized expression levels of each gene and their related regression coefficients. The formula is as follows: score = $e^{\text{sum (each gene's expression} \times \text{its corresponding coefficient)}}$. Subsequently, patients were divided into high-risk and low-risk groups based on the median risk score. Time-dependent ROC curve analysis of subjects at 1, 3, and 5 years was performed using the "timeROC" R package to assess the predictive power of the gene signature. Additionally, the AUC values of survival ROC curves were calculated to assess the performance of prognostic prediction models. Regression models were constructed by integrating risk scores and other clinical factors. Nomogram plots were employed to visually represent the relationship between variables in the prediction model. These plots were displayed on the same plane and at a specific scale. Prognostic calibration plots were used to analyze the fit of the model to the actual situation, with the objective of testing the consistency of the nomogram survival probability prediction with the actual observation.

2.5 Assessment of the correlation between clinical characteristics and predictive risk scores

The Kruskal-Wallis test assessed the disparities between clinical characteristics and risk scores generated by multiple data analyses. Spearman correlation analysis was employed to determine the correlation between risk scores. Furthermore, a Kaplan-Meier survival analysis (log-rank test) was conducted to evaluate the impact of patients on overall survival.

2.6 Analysis of the association between somatic mutations and risk scores

The WES data, obtained from the TCGA portal and analyzed using VarScan2, included single nucleotide variants (SNVs), insertions (INS), single nucleotide polymorphisms (SNPs), and deletions (DEL). The somatic mutation data were displayed employing the "maftools" software package, which is capable of processing Mutation Annotation Format (MAF) files (18). The calculation method for the tumor mutation burden (TMB) of each patient is as follows: the total number of variants was divided by the total exon length.

2.7 Therapeutic strategies based on ferroptosis-hypoxia risk scores

Jiang et al. established the Tumor Immune Dysfunction and Exclusion (TIDE) to mimic tumor immune escape mechanisms, including T-cell dysfunction and T-cell rejection (32). Consequently, TIDE can be employed to forecast the efficacy of immunotherapy. A higher TIDE score reflects an immune escape phenotype in the tumor and a poorer response to ICBs.

The Immunophenoscore (IPS) was obtained from The Cancer Immunome Atlas (TCIA, https://tcia.at/home). As a molecular marker of the immune response, the IPS provides an excellent indication of the immune landscape within the tumor. It was determined that a scoring scheme could be created by identifying genes related to the immune system. A higher IPS score is indicative of higher immunogenicity levels. In this context, IPS can be employed to assess immunotherapy efficacy in GC patients.

The Genomics of Drug Sensitivity in Cancer (GDSC) database was utilized to evaluate the susceptibility of ferroptosis-hypoxia states to chemotherapeutic drugs. The IC_{50} is calculated based on the "pRRophetic" software and represents the concentration at which the inhibitory effect reaches half the maximum value (33, 34).

2.8 Pan-cancer analysis

We further systematically summarized the clinical relevance and immunological characteristics of risk scores in pan-cancer to externally validate the general applicability of risk scores. Gene expression and associated clinical information for 33 tumors were downloaded from the TCGA database.

2.9 Quality control and standardization of scRNA-seq data

Download the six samples of the GSE112302 dataset from the GEO website, which includes scRNA-seq data from 402 GC cells. Then, create a "Seurat" object containing basic information about the single-cell dataset using the "CreateSeuratObject" function in the "Seurat" R package. Subsequently, data quality control was conducted. The scRNA-seq data underwent normalization applying the "LogNormalize" method, and a variance analysis was performed to identify the top 1500 genes with highly variable characteristics. Subsequently, the dimensionality of the data was reduced through the application of principal component analysis (PCA). The dimensions exhibiting significant separation were subjected to PCA at a false discovery rate (FDR) of less than 0.05, and the first 15 principal components (PCs) were subsequently downscaled by the t-distributed stochastic neighbor embedding (tSNE) algorithm to yield principal component clusters. The marker genes in each cluster were identified using the criteria of log2 [fold change (FC)] >0.5 and FDR<0.05. The clusters were annotated using the marker gene-based "Single" R package.

2.10 Immunohistochemical analysis of clinical validation cohort

A total of 30 surgical specimens of GC, along with 25 matched paracancerous tissues, were collected from Qingdao People's Hospital Group (Jiaozhou) (hereafter referred to as our hospital). In order to

evaluate the levels of expression of central genes (SDC2, RGS4, SERPINE1, DUSP1, and CAV1), immunohistochemistry (IHC) was conducted using GTVisionTM III Detection System. According to the instructions from the manufacturer, the following antibodies were used for immunohistochemical staining: 67088-1-Ig, 14530-1-AP, 66261-1-Ig, T56588S, and 16447-1-AP. Two pathologists, unaware of the patient's clinical information, evaluated the immunohistochemical staining. In case of a discrepancy in the assessments, a third pathologist conducted an independent review. Ten optical fields were examined in each diseased region using a high-power lens (×400). The IHC staining score was used as the definitive criterion for judging the staining. The IHC staining score is calculated by multiplying the staining area score by the staining intensity score. The score for the staining area was assessed on a scale ranging from 0 to 4, with 0 representing a staining area of ≤10%, 1 representing a staining area of 11 to 25%, 2 representing a staining area of 26 to 50%, 3 representing a staining area of 51 to 75%, and 4 representing a staining area of >75%. The staining intensity score was categorized as 0: negative, 1: weak, 2: moderate, or 3: strong. The IHC staining scores were dichotomized as follows: scores below six were defined as low expression, while scores above six were defined as high expression.

2.11 Statistical analysis

A student t-test was employed to assess differential gene expression between tumor and adjacent non-tumor tissues. Comparisons between the two groups were conducted via the Wilcoxon rank-sum test. Additionally, multiple comparisons were performed by the Kruskal-Wallis test. Cut-off points for each subgroup were determined using the "survminer" R software package. The Kaplan-Meier method was employed to analyze overall survival (OS) between subgroups, with the log-rank test used to assess the significance of the results. The chi-squared test was utilized to compare proportion differences. Univariate and multivariate Cox regression analyses were performed to determine the independent factors that predict OS.

3 Results

3.1 Identification of molecularly characterized subtypes of ferroptosis and hypoxia in GC

The flow chart shows our research procedure (Figure 1). In the TCGA-STAD cohort, we have found 59 FRGs that are expressed differently across tumor tissues and adjacent non-tumor tissues (FDR<0.001, |logFC|>1; Supplementary Figure 1A, Supplementary Table 2) using the "limma" R package. In KEGG and GO analysis, these DEGs were found to be enriched in several pathways, including positive regulation of MAP kinase (MAPK) activity, response to TGF-β, enhancement of cell-cell adhesion, and promotion of T-cell activation, activation of immune response, fibroblast proliferation, platinum resistance, apoptotic process of inflammatory cells, oxidoreductase complex, p53 signaling pathway, HIF-1 signaling pathway, and many other oncology-related pathways (Figure 2A). The same identification method was employed to screen for 26 HRGs that exhibited differential expression between gastric cancer tumors and normal tissues (FDR<0.001, |log FC|>1; Supplementary Figure 1B, Supplementary Table 2). These HRGs were enriched in many biological functions related to angiogenesis, modulation of extracellular matrix components, modulation of cell adhesion, chemotaxis of immune cells, and a variety of oncogenesis-related pathways (MAPK, Ras, Rap1, insulin-like growth factor receptor, p53, HIF-1) (Figure 2B).

It is reasonable to hypothesize that ferroptosis and hypoxia play a significant role in tumor progression. Subsequently, a consensus

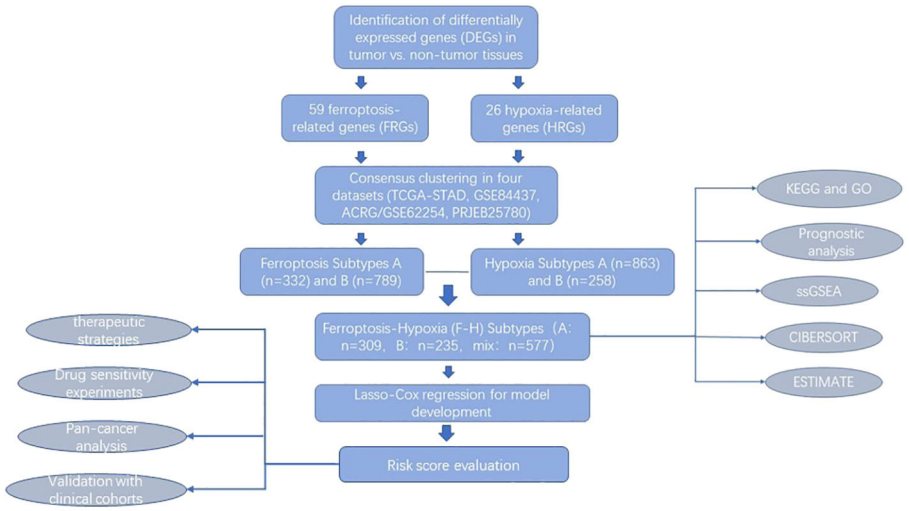

FIGURE 1
Flow chart of our study.

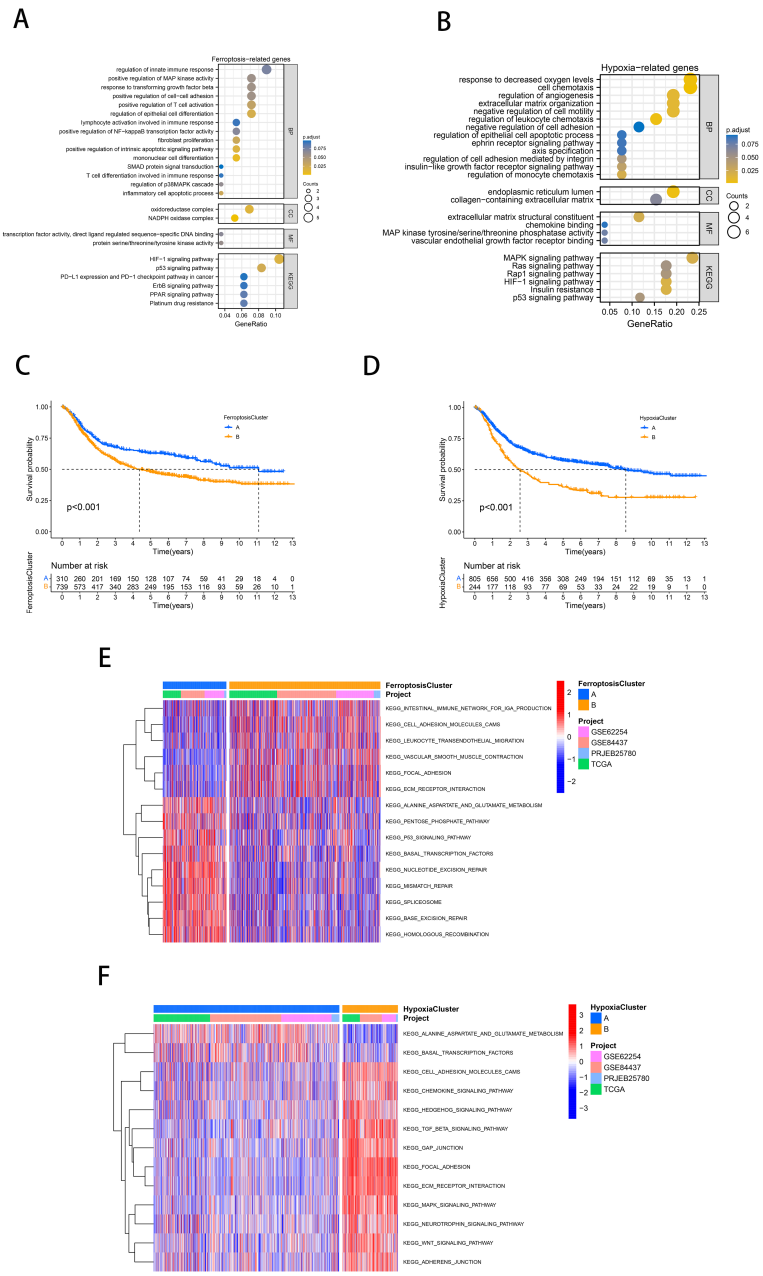

FIGURE 2
Identification of molecularly characterized subtypes of ferroptosis and hypoxia in GC. **(A, B)** GO and KEGG analysis based on FRGs **(A)** and HRGs **(B)**. **(C, D)** Kaplan-Meier curves of GC patients for ferroptosis molecular subtypes **(C)** and hypoxia molecular subtypes **(D)**. **(E, F)** GSVA analysis revealed distinct activations of biological pathways in ferroptosis clusters **(E)** and hypoxia clusters **(F)**. Blue represented the inhibition pathway, and red represented the activation pathway.

clustering approach was used to identify characteristic molecular subtypes of ferroptosis in gastric cancer. Based on the mRNA expression profiles of 59 FRGs, GC patients from 4 cohorts were clustered into two ferroptosis clusters, A and B (A: n=332, B: n=789; Supplementary Figure 1C). PCA confirmed that these two subtypes could be altogether distinguished (Supplementary Figure 1D). Prognostic analysis showed a significant survival advantage for ferroptosis cluster A compared to subtype B (p<0.001; Figure 2C). Following the same approach, we classified the gastric cancer samples from the four cohorts into two hypoxia molecular subtypes, A and B (A: n=863, B: n=258; Supplementary Figure 1E). PCA confirmed that these two subtypes could be fully distinguished (Supplementary Figure 1F). Similarly, prognostic analyses showed that hypoxia cluster A exhibited a notable survival benefit (p<0.001; Figure 2D).

As illustrated in Figure 2E, ferroptosis cluster A was significantly enriched in the pentose phosphate pathway, alanine aspartate and glutamate metabolism, DNA repair, and p53 signaling pathway. Subtype B was significantly enriched in the influence of the intestinal immune network for IgA production,

cell adhesion molecules (CAMs), and Extracellular matrix and (ECM) receptor interaction. According to Figure 2F, hypoxia cluster B was significantly enriched in the stromal activation and oncogenic pathways (ECM receptor interaction, CAMs, TGF-β signaling pathway, MAPK signaling pathway, WNT signaling pathway).

3.2 Identification of molecular subtypes for combined ferroptosis-hypoxia

The preceding analysis demonstrated that both the ferroptosis and hypoxia molecular subtypes exhibit favorable prognostic value and distinctive tumor-related biological characteristics. Therefore, based on the above ferroptosis and hypoxia status, we further combined them into a two-dimensional metric and categorized patients into ferroptosis-hypoxia (F-H) subtypes A, B, and mix (A: n=309, B: n=235, mix: n=577; Figure 3A). The survival analysis revealed that patients with F-H subtype A exhibited the highest survival rate, while those with F-H subtype B exhibited the poorest prognosis (p<0.001; Figure 3B).

The heatmap demonstrated the ESTIMATE score of F-H subtypes and the enrichment of multiple biological pathways (Figure 3C). Notably, we found that the NOTCH signaling pathway, MAPK signaling pathway, hypoxia, and activation of TGF-EMT signaling pathway were highly expressed in F-H subtype B, while TGF-EMT signaling down regulation were highly expressed in F-H subtype A. In 2018, Oh et al. conducted an analysis of genomic and proteomic data to distinguish between two separate categories of gastric cancer: mesenchymal phenotype (MP) and epithelial phenotype (EP) (35). These two subtypes showed markedly different survival and chemotherapy sensitivity. Based on their study, we found that the interstitial features of F-H subtype B were more prominent (Figure 3D). The EMT analysis was conducted using the single sample Gene Set Enrichment Analysis (ssGSEA) method, demonstrating significantly enhanced stromal activity in F-H subtype B. This was evidenced by the enrichment of EMT, pan-fibroblast TGF-β response signature (Pan-F-TBRS), and angiogenic pathways, which supported our hypothesis (Figure 3E). CIBERSORT analysis revealed a significant enrichment of immune-activated cells in F-H subtype A, including CD8+ T cells, M1 macrophages, and CD4+ T cells. The immunosuppressive cells, such as M2 macrophages, are abundant in subtype B (Figure 3F).

We further compared the expression profiles of F-H subtype A and F-H subtype B. A total of 520 DEGs were identified (FDR<0.001, |log FC|>1; Supplementary Figure 1G). In order to further verify this regulatory mechanism, an unsupervised clustering was performed on the basis of these DEGs. The patients were categorized into two F-H genomic patterns, referred to as gene clusters A and B (A: n=342; B: n=201). The prognosis for gene cluster A was demonstrably superior to that of gene cluster B (Figure 3G). We overlapped 520 DEGs with FRGs and HRGs to identify 25 ferroptosis-hypoxia (F-H) marker genes (Supplementary Figure 1H). Univariate Cox analysis was performed to select 14 F-H prognostic genes (p<0.05; Figure 3H). The heatmap demonstrated that the gene clusters were similar to the F-H molecular subtypes. Furthermore, the expression of the 14 prognostic DEGs was found to be significantly upregulated in gene cluster B and F-H subtype B (Figure 3I).

3.3 Construction and validation of a prognostic model based on ferroptosis-hypoxia genes

Considering the heterogeneity and complexity of individual gastric cancer patients, analyses based on patient groups alone are insufficient for accurately predicting the prognosis of individual GC patients. Therefore, we established a prognostic model by Lasso-Cox regression analysis using the expression profiles of the above 14 genes. A signature consisting of five genes was identified utilizing the optimum value of λ (Figures 4A, B). The risk score was computed employing the following methodology: e $^{(0.0029 \ *}$ expression level of CAV1 + 0.2445 * expression level of SDC2 + 0.0168 * expression level of RGS4 + 0.0485 * expression level of DUSP1 + 0.1873 * expression level of SERPINE1). Patients in TCGA (training cohort) were divided into high-risk (n=159) and low-risk (n=159) groups. Kaplan-Meier curves demonstrated that patients in the high-risk group exhibited a notably lower OS than patients in the low-risk group (Figure 4C). Time-dependent ROC curves further confirmed the excellent sensitivity and specificity of the risk score in predicting GC survival outcomes (1-year AUC=0.631, 3-year AUC=0.670, 5-year AUC=0.736; Figure 4D). The above conclusions were also validated in the GSE62254 cohort (Supplementary Figures 2A, B). The prognosis calibration chart was employed to assess the alignment between the model and the actual situation, with calibration curves for 1-, 3-, and 5-year OS analyzed. Figures 4E, F demonstrated that the risk score in the TCGA and GSE62254 cohorts had a predictive effect on the outcome of gastric cancer patients aligned with the actual situation. Subsequently, univariate and multivariate Cox analysis demonstrated the independent prognostic value of the risk score (p<0.001; Figure 4G). Nomograms were employed to visualize the risk score in conjunction with other clinical risk factors (grade, gender, age, stage) to construct a predictive multivariate regression model (Figure 4H). Figures 4I, J illustrated the calibration curves and time-dependent ROC curves for 1-year, 3-year, and 5-year OS. These figures demonstrate that the risk score has excellent predictive efficacy for the outcome of gastric cancer patients. This conclusion was similarly validated in the GSE62254 cohort (Supplementary Figures 2C–H).

3.4 The landscape of genetic variation of ferroptosis-hypoxia risk scores

The study of copy number variation (CNV) demonstrated that CNV was prevalent among the 25 ferroptosis-hypoxia genes, with a significant number concentrated on copy number amplification (Figure 5A). Figure 5B depicts the chromosomal location of CNV in ferroptosis-hypoxia genes. The somatic mutation data indicated that both the ferroptosis cluster A and the hypoxia cluster A

10.3389/fonc.2024.1499580

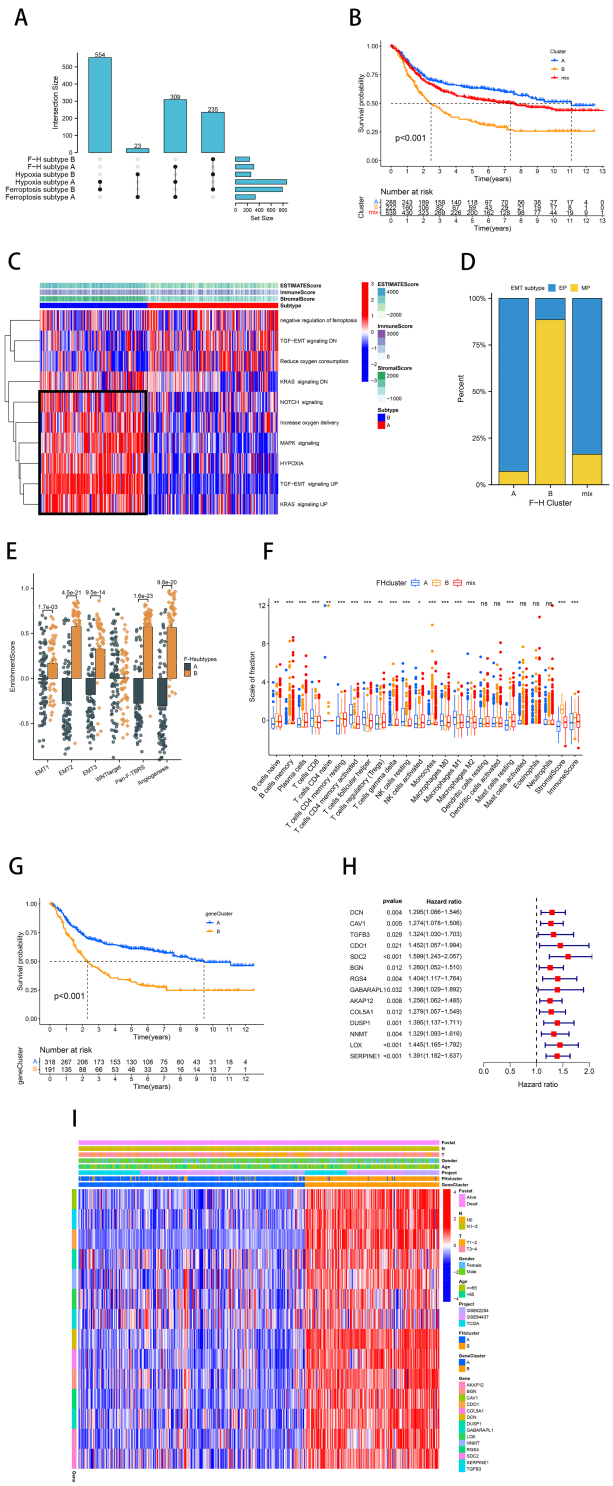

FIGURE 3
Identification of molecular subtypes for combined ferroptosis-hypoxia. **(A)** The upSet diagram shows the composition of ferroptosis-hypoxia subtypes. **(B)** Kaplan-Meier curves of GC patients for ferroptosis-hypoxia subtypes. **(C)** Heat map illustrating the relationship between ferroptosis-hypoxia subtypes, ESTIMATE score, and biological pathways. **(D)** Differences in ferroptosis-hypoxia subtypes for EMT typing. **(E)** Box plot showing ssGSEA analysis of EMT differences between ferroptosis-hypoxia subtypes. **(F)** Box plots of immune infiltration levels in ferroptosis-hypoxia subtypes. ns, not significant; *p<0.05; **p<0.01; ***p<0.001. **(G)** Kaplan-Meier curves for the gene clusters of GC patients. **(H)** Forest plots illustrating the Univariate Cox regression analysis of ferroptosis-hypoxia marker genes. **(I)** Heat map illustrating the relationship between ferroptosis-hypoxia subtypes associated gene expression, ferroptosis-hypoxia clusters, and various clinicopathological features.

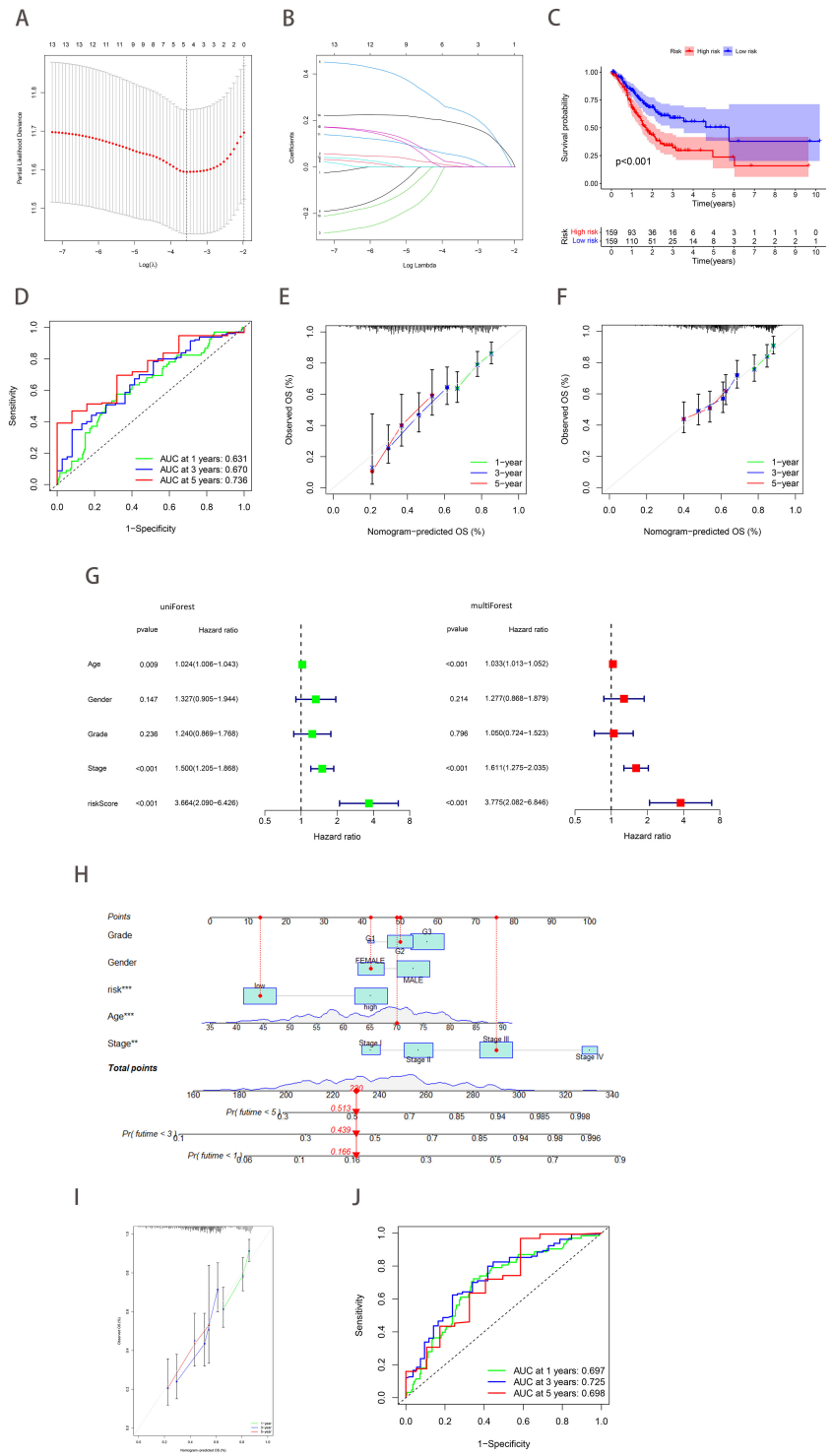

FIGURE 4
Construction and validation of a prognostic model based on ferroptosis-hypoxia genes. **(A)** The log value of the independent variable lambda (the abscissa represents the confidence interval of each lambda, and the ordinate represents errors in cross-validation). **(B)** The changing trajectory of each independent variable (the abscissa represents the corrected lambda, and the ordinate represents the coefficient of the independent variable). **(C)** The K-M curve of the five-gene signature-based stratification in TCGA training cohort. **(D)** The 1-, 3-, and 5-year ROC curve is based on five-gene signature stratification. **(E, F)** The calibration plot evaluates the fit analysis of the model to the actual situation in TCGA **(E)** and GSE62254 **(F)**. **(G)** Univariate and multivariate Cox analysis of risk score. **(H)** Nomogram plot of the prognostic multivariate regression model. **(I)** Prognostic Calibration plot evaluating the fit analysis of the model to the actual situation. **(J)** The 1-, 3-, and 5-year ROC curve is based on the prognostic multivariate regression model.

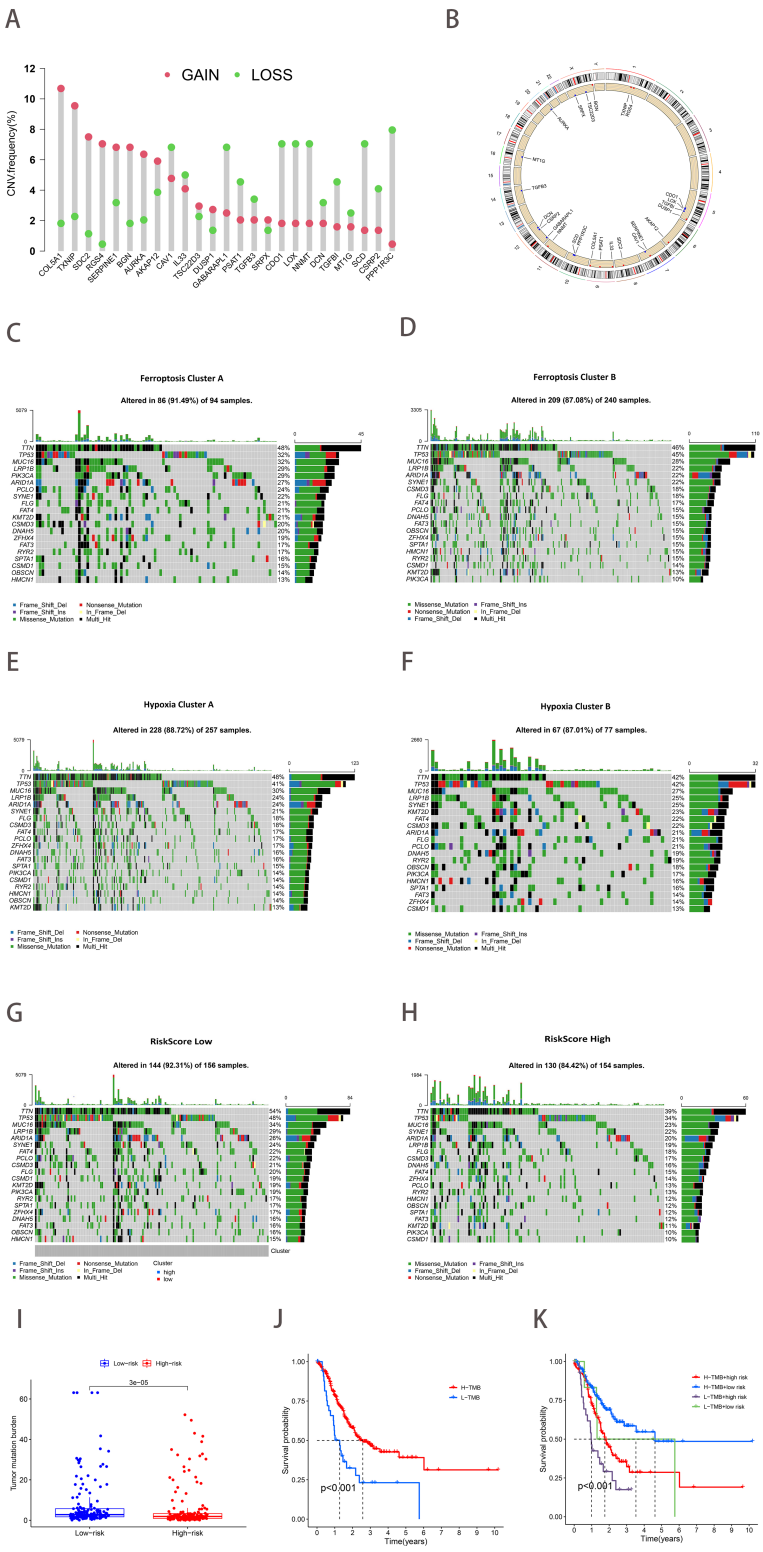

FIGURE 5
The landscape of genetic variation of ferroptosis-hypoxia risk scores. **(A)** The frequency of CNV variation of 25 ferroptosis-hypoxia genes. The height of the column represented alteration frequency. Green dots indicate deletions; red dots indicate amplifications. **(B)** CNV alteration locations for 25 ferroptosis-hypoxia genes. **(C–H)** Waterfall plots of tumor somatic mutations in patients with low ferroptosis subtypes A **(C)**, ferroptosis subtypes B **(D)**, hypoxia subtypes A **(E)**, hypoxia subtypes B **(F)**, low-risk group **(G)**, high-risk group **(H)**. Each column represents one patient. The top bar indicates the degree of tumor mutation. The numbers on the right indicate the frequency of mutations in each gene. The bars on the right show the proportion of different types of mutations. Stacked bar graphs show the conversion rate for each sample. **(I)** Boxplots illustrating the difference in tumor mutation burden between risk score groups. **(J)** Kaplan-Meier curve for tumor mutation burden groupings. **(K)** Kaplan-Meier curve for risk score and tumor mutation burden.

exhibited higher mutation frequencies than cluster B. Furthermore, when applying the risk score for grouping, the difference in mutation frequency between the low and high groups became more significant (Figures 5C–H). The quantification analysis of TMB demonstrated that, among patients with gastric cancer, those with a low-risk score exhibited a relatively higher TMB, and a higher TMB was associated with improved survival, which is consistent with our results (Figures 5I–J). In light of the possible synergistic impact of TMB and risk score on evaluating prognosis for patients, we proceed with performing stratified prognostic analysis. A significant survival advantage was observed in patients with low-risk scores and high TMB (p<0.001; Figure 5K). These data suggest that the combination of risk scores and TMB can further enhance the prognostic value for patients.

3.5 Association of ferroptosis-hypoxia risk score with clinical characteristics and other classical gastric cancer classification features

We proceeded to investigate the correlation between gastric cancer risk scores and clinical characteristics. The Kruskal-Wallis test demonstrated that risk scores exhibited a statistically significant difference between the F-H subtypes (p<0.05; Figure 6A). The results were consistent with the prediction, with F-H subtype B exhibiting the highest median risk score and the most unfavorable prognosis, whereas the opposite was true for the A subtype. Patients with a more favorable prognosis exhibited recognized clinical characteristics, including stage I-II and grade 1-2. These patients exhibited relatively low-risk scores (Figures 6B, C). Furthermore, risk scores were found to be significantly higher in patients with recurrent gastric cancer (Figure 6D). Patients in the diffuse category of the Lauren pathology classification exhibited relatively high-risk scores (Figure 6E). Subsequently, the relationship between other molecular features used to classify GC and the risk scores was examined. The TCGA study categorized primary gastric cancer into four distinct subtypes: Epstein-Barr virus (EBV) infection, microsatellite instability (MSI), chromosomal instability (CIN), and genomic stability (GS). In our analysis, patients with the GS type exhibited the highest risk score, while those with the EBV type exhibited the lowest risk score, in accordance with our anticipated results (Figure 6F). Figure 6G demonstrated that risk scores exhibited a statistically significant difference between EMT and other ACRG subtypes (p<0.001). Similarly, the MP subtype exhibited a markedly elevated risk score compared to the EP subtype (p<0.001; Figure 6H).

3.6 Tumor immune microenvironment associated with the ferroptosis-hypoxia risk score

The immune score, stromal score, and ESTIMATE score of the GC samples were calculated using the ESTIMATE algorithm to facilitate the assessment of the immune and stromal components of the TME. Higher ESTIMATE scores represent lower tumor purity, which means higher tumor progression and worse prognosis. The high-risk scoring group exhibited notably elevated levels of the stromal score, immune score, and ESTIMATE score (Figure 6I). As anticipated, subsequent ssGSEA analysis revealed that the high-risk score group was associated with stromal activation-related signaling pathways and hypoxia-associated pathways (TGF-EMT, MAPK, NOTCH, Hallmark hypoxia, and HIF-1). In contrast, the low-risk group was enriched in the negative regulation of ferroptosis (Figure 6J). Pathologically activated neutrophils (PMNs), called myeloid-derived suppressor cells (PMN-MDSCs), are major negative regulators of anti-tumor immunity. Figure 6K showed the significant enrichment of PMN-MDSCs in high-risk group samples (p=0.01). Subsequently, we conducted correlation analyses between the risk score and immune cell infiltration (Figure 6L). The risk score was found to be positively correlated with macrophage M2 infiltration and negatively correlated with T cells follicular helper, macrophages M1 infiltration. Moreover, the expression of the five key genes was also positively correlated with many immunogenic genes, especially macrophage M2 (Figure 6M). These data suggested that the ferroptosis-hypoxia risk score may influence tumor growth and progression by regulating immune cells and matrix activation within the tumor microenvironment.

3.7 Therapeutic strategies based on ferroptosis-hypoxia risk scores

The IPS immunotherapy prediction analysis demonstrated that the low-risk group exhibited favorable therapeutic outcomes in both anti-CTLA-4 and anti-PD-1 immune checkpoint treatment (p<0.01; Figure 7A). Considering the pivotal role of immunotherapy in cancer treatment, we further investigated the relationship between the risk score and ICBs response by using clinical data from TCGA-STAD and PRJEB25780 (a pembrolizumab-treated clinical trial cohort with metastatic gastric cancer). The risk score in the ICBs treatment response group was demonstrably lower than that in the non-response group (p<0.01; Figure 7B). Moreover, the TIDE algorithm assessed patients in the PRJEB25780 cohort, and it was found that the risk score was positively correlated with the TIDE score (p <0.01; Figure 7C). This finding was also validated in the TCGA-STAD cohort (p<0.01; Figure 7D).

A review of the clinical data on GC patients revealed that those with MSI-H had a lower risk score (p=0.04; Figure 7E). The MSI MANTIS score is positively correlated with MSI-H status probability (36, 37). By utilizing standard tumor-normal paired sequencing data, the MSI Sensor provides accurate MSI status determination (38). As anticipated, the MSI scores were found to be higher in the low-risk score group (p<0.01; Figures 7F, G). In conclusion, the evidence presented collectively provides strong support for the predictive efficacy of the risk score in relation to immunotherapy outcomes.

Furthermore, we sought to ascertain the relationship between the IC_{50} of chemotherapeutic agents and risk scores. The findings

revealed a significant positive correlation between the IC_{50} of several agents, including 5-fluorouracil, cetuximab, doxorubicin, gefitinib, tipifarnib, and veliparib, and the risk scores. Conversely, the IC_{50} of Cytarabine and Sunitinib demonstrated a strong inverse relationship with the risk score (Figure 7H).

3.8 Pan-cancer analysis

Forest plots from univariate Cox analysis demonstrated that when the clinical outcome was OS, risk scores were predictive of survival for nine cancer types (p<0.05; Figure 8A). However, when

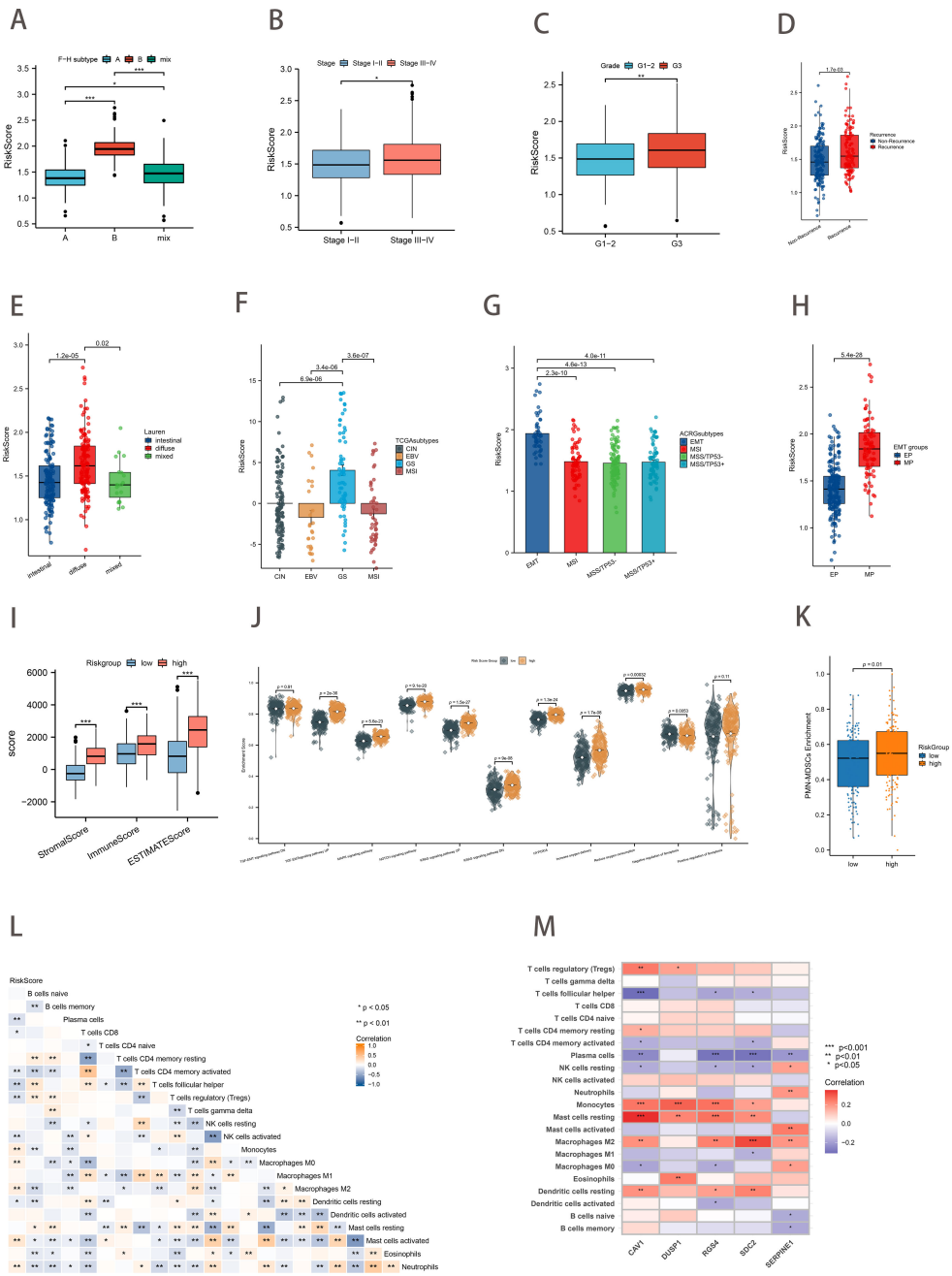

FIGURE 6
Association of Risk Score with Clinical Characteristics, Other Classification, and Tumor Immune Microenvironment. **(A)** Differences in risk scores between the ferroptosis-hypoxia subtypes **(B–E)** Relationship between risk scores and clinical features such as Stage **(B)**, Grade **(C)**, recurrence **(D)**, and Lauren classification **(E)**. **(F)** Differences in risk scores for TCGA types. **(G)** Differences in risk scores between ACRG types. **(H)** Differences in risk scores for EMT types. **(I)** Differences in ESTIMATE score between risk score groups. **(J)** Differences in biological pathways enrichment between risk score groups. **(K)** Differences in PMN-MDSCs enrichment between risk score groups. **(L)** Heat map of the correlation between risk score and immune cell infiltration; *p<0.05; **p<0.01. **(M)** Heat map of the correlation between five hub genes and immune cell infiltration t; *p<0.05; **p<0.01; ***p<0.001.

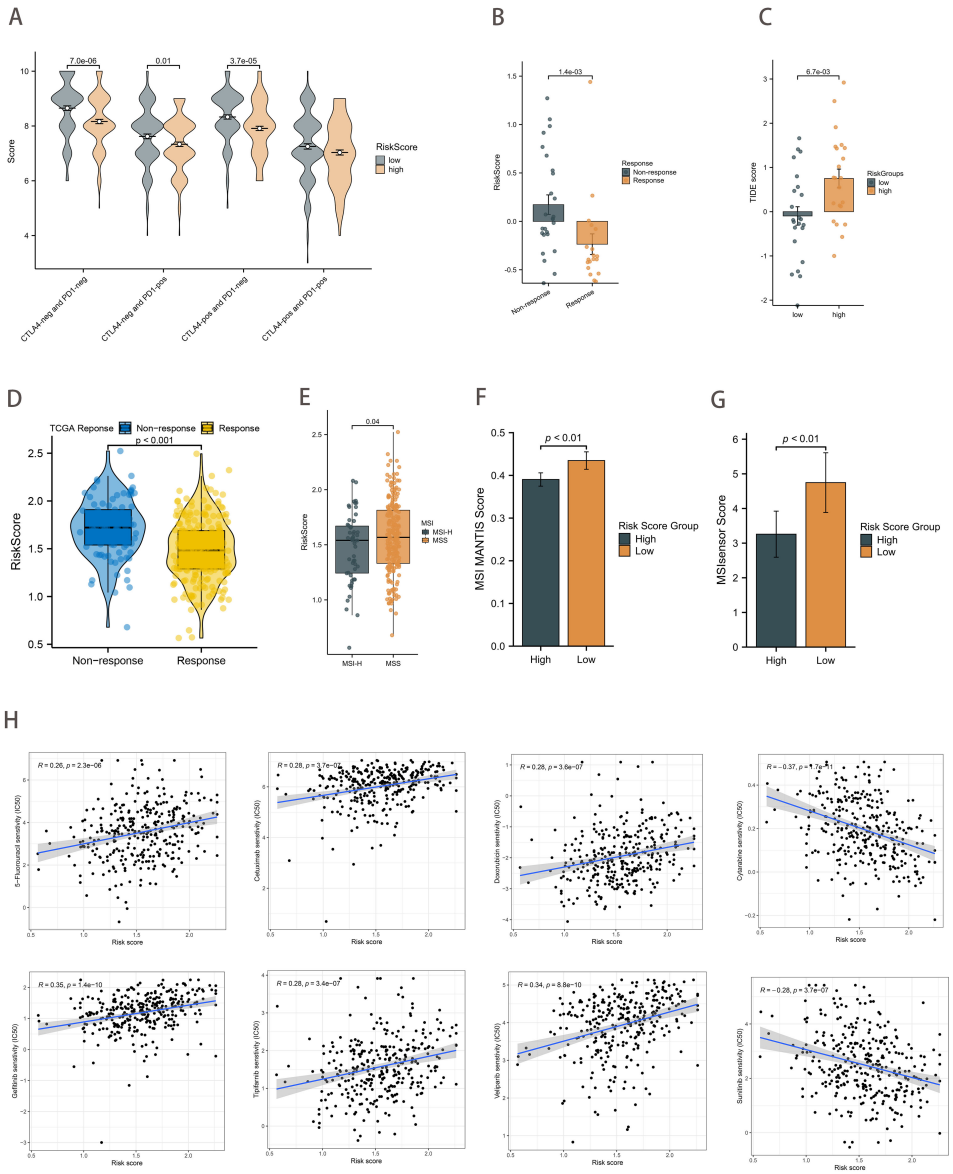

FIGURE 7
Therapeutic strategies based on risk scores. **(A)** Boxplot showing differences in IPS scores between risk score groups. **(B)** Differences in risk scores between the ICB treatment response and non-response groups in the PRJEB25780 cohort. **(C)** Differences in TIDE scores between the risk score groups from the PRJEB25780 cohort. **(D)** Differences in risk scores between the ICB treatment response and non-response groups from the TCGA cohort. **(E)** Differences in risk scores between MSI states. **(F, G)** Differences in risk score groups between MSI MANTIS score **(F)** and MSIsensor score **(G)**. **(H)** Correlation of risk scores with chemotherapeutic drug sensitivity.

the clinical outcome was disease-free survival (DFS), the risk score was only predictive of 4 cancer types (p<0.05; Figure 8B). In addition, Spearman rank correlation analysis between risk score and tumor mutational load (TMB) for 33 cancers showed that risk score was positively correlated with TMB in 3 cancers and negatively correlated with TMB in 11 cancers (p<0.05; Figure 8C). The correlation between risk score and MSI was positive in 2 cancers and negative in 6 cancers (p<0.05; Figure 8D). We found that risk scores were associated with immune cells in the majority of cancer types (Figure 8E). Additionally, ESTIMATE analysis revealed a strong correlation between risk scores and stromal and immune scores (Figure 8F).

3.9 Validation of ferroptosis-hypoxia related genes expression using scRNA-seq data

The study collected 402 cells from 6 GC samples sourced from GSE112302. After undergoing quality control and normalization, two cells that did not meet the required standards were removed from the study. There was no observed link between the depth of sequencing and the sequences of mitochondrial genes. However, sequencing depth showed a significant positive correlation with total intracellular sequences (R=0.38, Supplementary Figure 3A). Analysis of 16,288 genes revealed that 1,500 had substantial

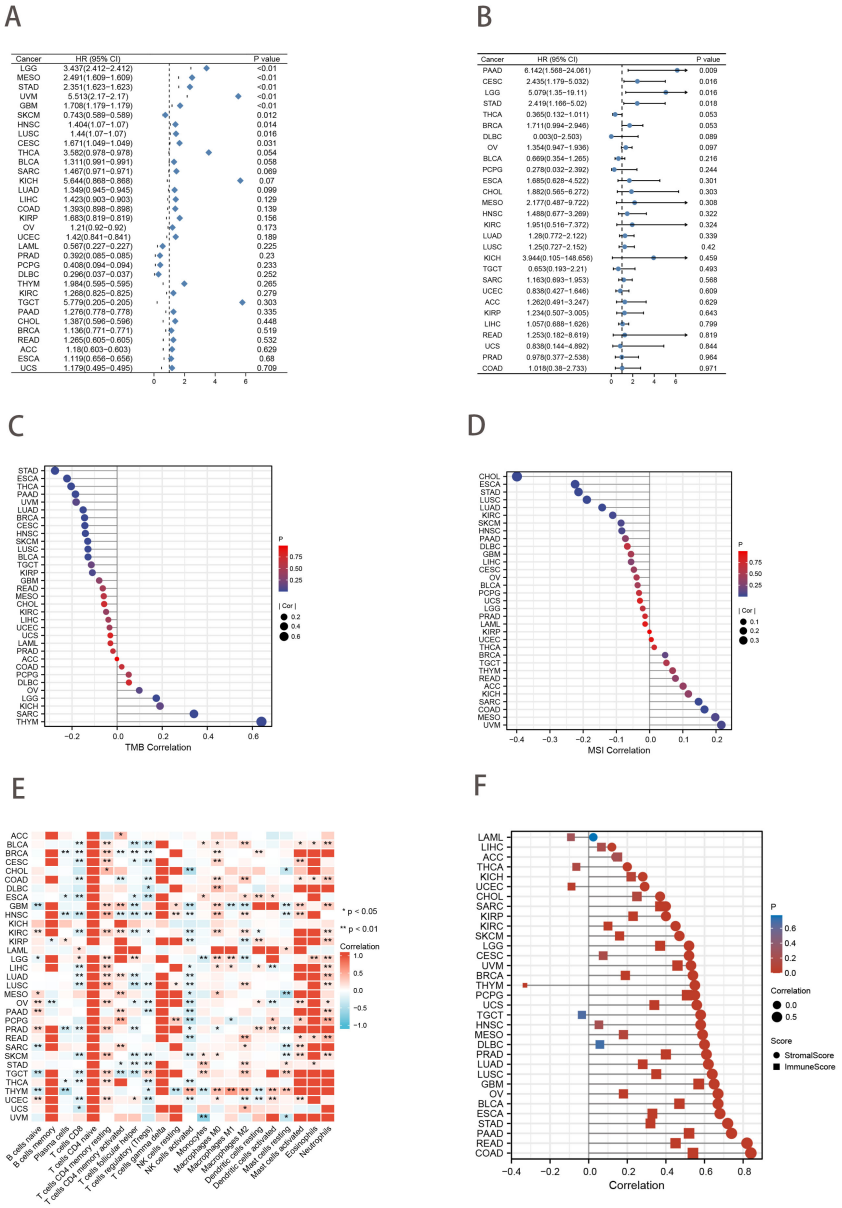

FIGURE 8
Pan-cancer analysis. **(A, B)** Univariate Cox analysis of risk score when the clinical outcome was OS **(A)** and DFS **(B)**. **(C, D)** Lollipop charts of the Spearman's Rank Correlation between risk score and TMB **(C)** and MSI **(D)**. **(E)** Pan-cancer landscape associated with risk score and immune cell infiltration. *p<0.05; ***p<0.01. **(F)** Lollipop charts describe the correlation of the risk score in pan-cancer with the ESTIMATE score.

intercellular variation and 14,788 had low variation (Supplementary Figure 3B).

PCA downscaling results showed no significant separation between GC cells (Supplementary Figure 3C). The top 15 principal components (PCs) with substantial distinctions were chosen for further research (Supplementary Figure 3D). The 400 GC cells were clustered into 6 clusters according to the tSNE algorithm (Supplementary Figure 3E). The 6 clusters were categorized based on marker genes. Clusters 0, 1, 2, 3, and 4 consisted of cancer cells, whereas cluster 5 was linked to macrophages (Supplementary Figure 3F). Figures 9A, B illustrated the expression levels of five ferroptosis-hypoxia-related genes across the 6 clusters. CAV1 increased in cluster 0, while SERPINE1 and RGS4 demonstrated an increase in cluster 1. Conversely, DUSP1 and SDC2 exhibited an increase in cluster 5.

3.10 Clinical cohort verification

An immunohistochemical (IHC) investigation assessed the expression levels of hub genes (SDC2, RGS4, SERPINE1, DUSP1, and CAV1) in gastric cancer. The majority of specimens from the validation cohort at our hospital exhibited positive expression of SDC2, RGS4, SERPINE1, DUSP1, and CAV1. Among the aforementioned genes, CAV1 was strongly stained in 13 (43.3%) specimens, SDC2 in 25 (83.3%) specimens, SERPINE1 in 27

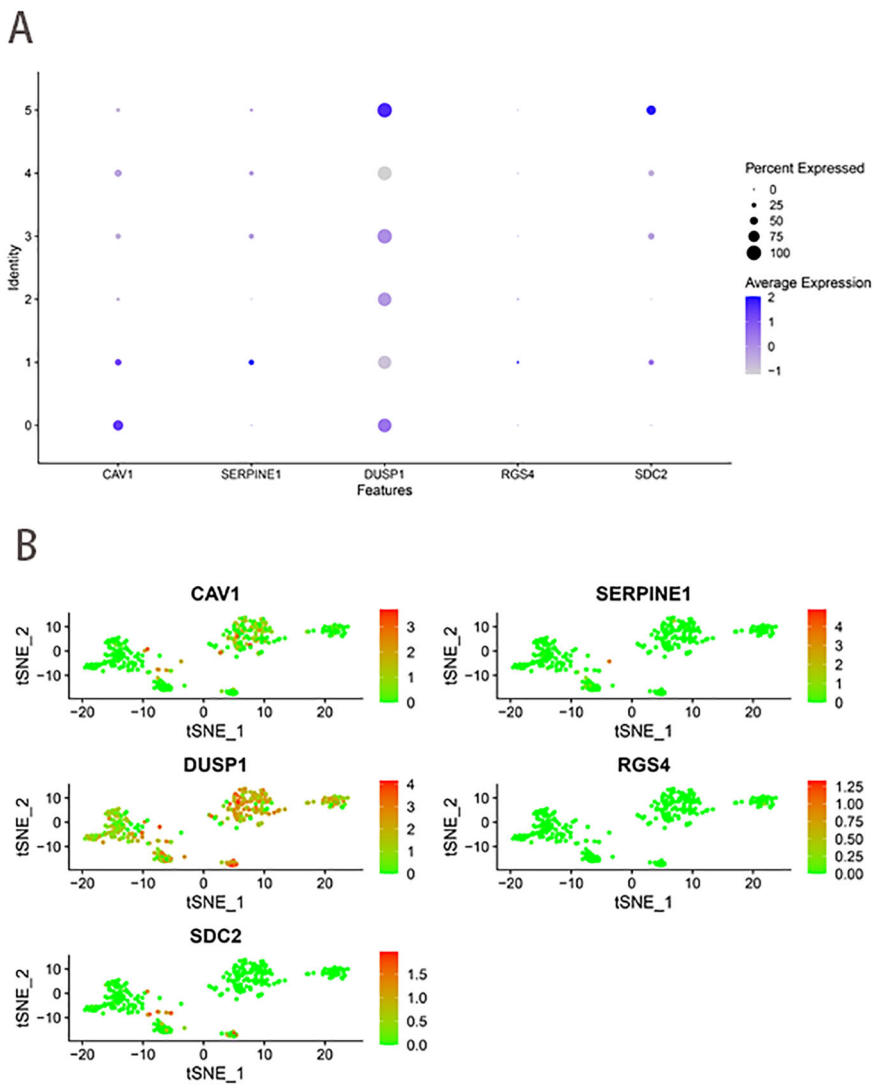

FIGURE 9
scRNA-seq data analysis. **(A)** The expression levels of five ferroptosis-hypoxia-related genes across the 6 clusters. **(B)** The t-SNE diagrams display expression levels of ferroptosis-hypoxia-related genes.

(90.0%) specimens, DUSP1 in 28 (93.3%) specimens, and RGS4 in 23 (76.7%) specimens (Figure 10). Furthermore, IHC results of candidate genes expression in gastric cancer tissues were found in the HPA database (Supplementary Figure 4).

4 Discussion

During the development of gastric cancer, metabolic reprograming, genomic instability and differences in the tumor microenvironment can result in the formation of cell clones with entirely different biological behaviors. These cell subsets exhibit notable heterogeneity in proliferation rate, invasion, and metastasis ability and also display varying sensitivities to drugs. The advancement of molecular analysis reveals that even under the same histological diagnosis, there are different genomic changes among patients (39). In recent years, with the advancement of immunotherapy and the identification of novel targets in gastric cancer, considerable progress has been made in treating gastric cancer (40, 41). With the diversification of systemic treatment options for advanced gastric cancer, the accurate selection of composite target inhibitors and personalized immunotherapy regimens has become a research priority. In the future, the exploration direction of advanced gastric cancer is to subclassify patients, identify personalized and efficient whole-course treatment strategies based on molecular typing, and accurately identify the population that may profit from immunotherapy to enhance long-term survival.

In this study, we initially identified genes related to ferroptosis and hypoxia that exhibited differential expression between gastric cancer and normal tissues. The identified DEGs were enriched in immune activation, p53 signaling pathway, HIF-1, angiogenesis regulation, extracellular matrix component regulation, and various tumor-related pathways. By unsupervised cluster analysis of these

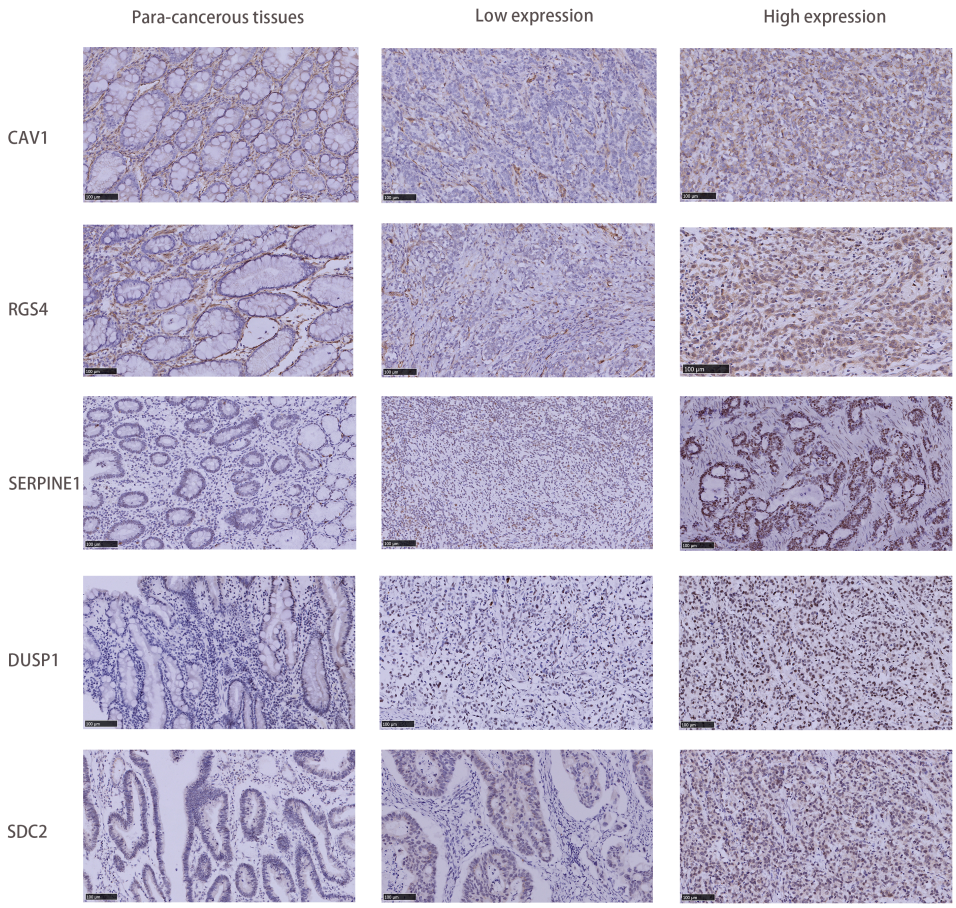

FIGURE 10
Comparison of SDC2, RGS4, SERPINE1, DUSP1, and CAV1 IHC expression in GC tissues and adjacent tissues.

DEGs, we classified gastric cancer patients into ferroptosis and hypoxia subtypes that differed significantly in prognostic and biological characteristics. The preceding analysis indicates that both the ferroptosis and hypoxia molecular subtypes exhibit favorable prognostic value and possess distinctive tumor-related biological characteristics. Given the close association between ferroptosis and hypoxia, we proceeded to combine the above ferroptosis and hypoxia status into a two-dimensional index classifying patients into three ferroptosis-hypoxia (F-H) subtypes. Our findings indicate that multiple oncogenic classical pathways are activated in the F-H subtype B. Furthermore, F-H subtypes B have increased matrix activity and more notable interstitial features (MP). This indicates that the F-H subtype B may be closely related to the EMT. These mechanisms are thought to suppress the activity of immune cells, and subsequent analysis of immune infiltration also verified the enrichment of immunosuppressive cells in subtype B. In addition, F-H subtype A exhibited increased immune activation, including elevated concentrations of CD8+ T cells, macrophages M1, and CD4+ T cells. The negative regulation of ferroptosis and downregulation of the TGF-EMT signaling pathway were highly expressed in the F-H subtype A. This suggests that two distinct ferroptosis-hypoxia subtypes may profoundly affect the biological behavior and immune microenvironment of GC.

Two gene clusters were identified based on the characteristic DEGs associated with the ferroptosis-hypoxia subtypes. Our findings indicate that the genomic pattern largely correlates with the molecular pattern associated with ferroptosis and hypoxia. Consequently, an extensive evaluation of the molecular characteristics of ferroptosis-hypoxia is crucial for gaining a deep comprehension of GC. Given the heterogeneity of GC, we employed Lasso-Cox regression analysis to identify five characteristic genes based on the expression profiles of the aforementioned genes. This analysis established a prognostic model and risk score, which were subsequently used to divide GC patients into high- and low-risk groups. There was a notable difference in OS between patients in the high-risk group and those in the low-risk group, suggesting that risk score demonstrated favorable predictive efficacy in prognosticating the outcomes of patients with gastric cancer.

As a crucial indicator of ICB efficacy, TMB represents the immunogenicity of the tumor itself. In patients with gastric cancer, higher TMB is associated with improved survival (42). The low-risk group exhibited relatively higher TMB, which is consistent with the results of our study. Furthermore, the correlation between risk scores and clinical features was investigated. Patients with a more favorable prognosis tend to exhibit recognized clinical features, including stage I-II, grade 1-2, and non-recurrent. These patients tend to have relatively low-risk

scores. Combined with several previous large-scale classical molecular typing studies of gastric cancer, we found that higher risk scores were significantly associated with diffuse of the Lauren category, GS subtype, EMT subtype, and MP subtype. All of these subtypes represent poorer prognosis and aggressive biological behaviors. The correlation between risk score and EMT phenotype also indicates that a higher risk score may be indicative of stromal activation. In addition, the high-risk score group was associated with lower tumor purity, matrix activation-related signaling pathways, hypoxia-related pathways, and abundant infiltration of M2 macrophages and PMN-MDSCs. Kim et al. proposed that hypoxia-mediated ferroptosis in tumor PMN-MDSCs is a unique targeted immunosuppressive mechanism in the tumor microenvironment. Inhibition of ferroptosis by using genes and drugs can eliminate the inhibitory activity of PMN-MDSCs, slow down tumor progression, and synergize with immune checkpoint blocking to increase the sensitivity of immunotherapy, thereby inhibiting tumor growth (43). The data manifest that the ferroptosis-hypoxia risk score may influence tumor growth and progression by modulating immune cell and matrix activation in the tumor microenvironment. It is, therefore, postulated that risk scores may be helpful for the prediction of immunotherapy. Therefore, we subsequently performed immunotherapy prediction analyses by multiple routes.

Pabolizumab has received approval for treating solid cancers characterized by high microsatellite instability (MSI-H) or mismatch repair defects (dMMR), making it the first ICBs to receive full approval as "pan-cancer" treatments (44, 45). A higher response rate to ICBs has been observed in patients with MSI-high (MSI-H) tumors compared with patients with microsatellite instability low (MSI-L) cancers (46). Among the numerous molecular markers for predicting the efficacy of immunotherapy, the clinical value of MSI has been consistently demonstrated in various clinical studies of gastric cancer (47). A review of the clinical data of GC patients revealed that MSI-H patients exhibited a lower risk score. Furthermore, the low-risk group exhibited higher MSI MANTIS and MSIsensor scores. The IPS analysis demonstrated that the low-risk group exhibited a favorable therapeutic response to both anti-CTLA-4 and anti-PD-1 immune checkpoint therapy. The predictive role of risk scores on immunotherapy response was validated in the TCGA-STAD and PRJEB25780 cohorts. The risk score of the ICB treatment response group was found to be significantly lower than that of the non-response group using multiple methods.

The results of the drug sensitivity analysis indicated a clear positive correlation between the IC_{50} and the risk score of various gastric cancer treatments, including 5-fluorouracil, cetuximab, doxorubicin, and gefitinib. One potential avenue for future research is the stratification of patients based on risk-scoring systems, the screening of immunotherapy-sensitive patients, and the identification of novel strategies to overcome chemotherapy resistance. These endeavors could provide invaluable insights for the advancement of more efficacious treatment modalities. Moreover, the risk score was extended to a pan-cancer analysis. The risk score exhibited varying degrees of sensitivity across different cancers. This provides a foundation for further research.

Finally, the expression of the five critical genes identified through the screening process was verified. Batch RNA sequencing (RNA-Seq) techniques provide transcriptional profiles of cell populations or average expression levels of tissues but lack the capacity to identify gene expression patterns in individual cells (48, 49). The advent of single-cell RNA sequencing (scRNA-seq) has enabled researchers to provide a comprehensive characterization of genetic complexity at the cellular level, thereby contributing to a more profound comprehension of cellular heterogeneity (50). Single-cell sequencing analysis revealed that the expression of these five genes was significantly enriched in cancer cells. In addition, DUSP1 and SDC2 exhibited an increase in macrophages in the tumor microenvironment. In clinical gastric cancer (GC) specimens without chemotherapy or targeted therapy, the expression of these five genes was significantly higher in cancerous tissues than in paracancerous tissues.

To improve the reliability and generalization of our study, we utilized gene expression files from 1121 samples across four datasets. We employed the ComBat method to eliminate the batch effect of gene expression data. The accuracy of the dataset is contingent upon the quality and availability of the original data. Additionally, some studies had limitations in the number of marker genes utilized, excluding some meaningful molecular targets in gastric cancer, such as *Claudin18.2*. Consequently, it is imperative to continuously enhance research methods and broaden the scope of research to improve model accuracy and effectiveness. Our current work consists of preliminary validation experiments, and the experimental results require validation in a large multicenter GC cohort. Moreover, further functional and mechanistic studies are necessary to elucidate hypoxic-ferroptosis interactions and potential cancer pathogenesis. Despite these limitations, this study's results may still offer new treatment strategies for GC. The challenges of chemotherapy resistance and immunotherapy insensitivity in treating gastric cancer are pressing issues. Researchers have been working on developing new therapies based on hypoxic-ferroptosis and have shown promising results in preclinical studies. It is believed that delving into hypoxic-ferroptosis in the tumor immune microenvironment will offer a new treatment strategy for advanced gastric cancer patients.

5 Conclusions

This study conducted a comprehensive assessment of the molecular patterns of ferroptosis-hypoxia in GC. To assess the ferroptosis-hypoxia condition of each patient, we have also furthermore developed a risk score. According to the results, risk scores could effectively assess the genetic mutation landscape of cancer, tumor microenvironment, survival prognosis, and immunotherapy response. In light of these findings, we might consider applying the risk score as a basis for categorizing GC. This could help in the development of targeted medicines and designed clinical trials.

Data availability statement

The datasets presented in this study can be found in online repositories. The names of the repository/repositories and accession number(s) can be found in the article/Supplementary Material.

Ethics statement

The studies involving humans were approved by The Institutional Review Board of Qingdao People's Hospital Group (Jiaozhou). The studies were conducted in accordance with the local legislation and institutional requirements. The participants provided their written informed consent to participate in this study.

Author contributions

XX: Conceptualization, Data curation, Formal analysis, Investigation, Software, Validation, Writing – original draft. LF: Conceptualization, Investigation, Project administration, Writing – review & editing. XS: Investigation, Methodology, Supervision, Writing – review & editing. FY: Data curation, Software, Supervision, Writing – review & editing. YL: Conceptualization, Data curation, Investigation, Writing – review & editing. JS: Conceptualization, Investigation, Methodology, Writing – review & editing. YZ: Conceptualization, Data curation, Funding acquisition, Investigation, Writing – review & editing. JD: Investigation, Methodology, Writing – review & editing.

Funding

The author(s) declare that financial support was received for the research, authorship, and/or publication of this article. Funding for this research was provided by the Qingdao Medical and Health Research Project (2024-WJKY104).

Conflict of interest

The authors declare that the research was conducted in the absence of any commercial or financial relationships that could be construed as a potential conflict of interest.

Publisher's note

Supplementary material

The Supplementary Material for this article can be found online at: https://www.frontiersin.org/articles/10.3389/fonc.2024.1499580/full#supplementary-material

References

1. Bray F, Laversanne M, Sung H, Ferlay J, Siegel RL, Soerjomataram I, et al. Global cancer statistics 2022: globocan estimates of incidence and mortality worldwide for 36 cancers in 185 countries. *CA Cancer J Clin*. (2024) 74:229–63. doi: 10.3322/caac.21834

2. Cao T, Zhang W, Wang Q, Wang C, Ma W, Zhang C, et al. Cancer slc6a6-mediated taurine uptake transactivates immune checkpoint genes and induces exhaustion in cd8(+) T cells. *Cell*. (2024) 187:2288–304.e27. doi: 10.1016/j.cell.2024.03.011

3. Chen X, Kang R, Kroemer G, Tang D. Broadening horizons: the role of ferroptosis in cancer. *Nat Rev Clin Oncol*. (2021) 18:280–96. doi: 10.1038/s41571-020-00462-0

4. Wang Y, Wu X, Ren Z, Li Y, Zou W, Chen J, et al. Overcoming cancer chemotherapy resistance by the induction of ferroptosis. *Drug Resist Update*. (2023) 66:100916. doi: 10.1016/j.drup.2022.100916

5. Hugo W, Zaretsky JM, Sun L, Song C, Moreno BH, Hu-Lieskovan S, et al. Genomic and transcriptomic features of response to anti-pd-1 therapy in metastatic melanoma. *Cell*. (2016) 165:35–44. doi: 10.1016/j.cell.2016.02.065

6. Li Y, Cao Y, Ma K, Ma R, Zhang M, Guo Y, et al. A triple-responsive polymeric prodrug nanoplatform with extracellular ros consumption and intracellular H(2) O(2) self-generation for imaging-guided tumor chemo-ferroptosis-immunotherapy. *Adv Healthc Mater*. (2024) 13(16):e2303568. doi: 10.1002/adhm.202303568

7. Harris AL. Hypoxia–a key regulatory factor in tumour growth. *Nat Rev Cancer*. (2002) 2:38–47. doi: 10.1038/nrc704

8. Gilkes DM, Semenza GL, Wirtz D. Hypoxia and the extracellular matrix: drivers of tumour metastasis. *Nat Rev Cancer*. (2014) 14:430–9. doi: 10.1038/nrc3726

9. Barsoum IB, Smallwood CA, Siemens DR, Graham CH. A mechanism of hypoxia-mediated escape from adaptive immunity in cancer cells. *Cancer Res*. (2014) 74:665–74. doi: 10.1158/0008-5472.Can-13-0992

10. He M, Zhang M, Xu T, Xue S, Li D, Zhao Y, et al. Enhancing photodynamic immunotherapy by reprograming the immunosuppressive tumor microenvironment with hypoxia relief. *J Control Release*. (2024) 368:233–50. doi: 10.1016/j.jconrel.2024.02.030

11. Fuhrmann DC, Mondorf A, Beifuß J, Jung M, Brüne B. Hypoxia inhibits ferritinophagy, increases mitochondrial ferritin, and protects from ferroptosis. *Redox Biol*. (2020) 36:101670. doi: 10.1016/j.redox.2020.101670

12. Jayaprakash P, Vignali PDA, Delgoffe GM, Curran MA. Hypoxia reduction sensitizes refractory cancers to immunotherapy. *Annu Rev Med*. (2022) 73:251–65. doi: 10.1146/annurev-med-060619-022830

13. Yang Z, Su W, Wei X, Qu S, Zhao D, Zhou J, et al. Hif-1α Drives resistance to ferroptosis in solid tumors by promoting lactate production and activating slc1a1. *Cell Rep*. (2023) 42:112945. doi: 10.1016/j.celrep.2023.112945

14. Pan T, Sun S, Chen Y, Tian R, Chen E, Tan R, et al. Immune effects of pi3k/akt/hif-1α-regulated glycolysis in polymorphonuclear neutrophils during sepsis. *Crit Care*. (2022) 26:29. doi: 10.1186/s13054-022-03893-6

15. Chen M, Cen K, Song Y, Zhang X, Liou YC, Liu P, et al. Nusap1-ldha-glycolysis-lactate feedforward loop promotes warburg effect and metastasis in pancreatic ductal adenocarcinoma. *Cancer Lett*. (2023) 567:216285. doi: 10.1016/j.canlet.2023.216285

16. Wang Y, Zhou X, Yao L, Hu Q, Liu H, Zhao G, et al. Capsaicin enhanced the efficacy of photodynamic therapy against osteosarcoma via a pro-death strategy by inducing ferroptosis and alleviating hypoxia. *Small*. (2024) 20(26):e2306916. doi: 10.1002/smll.202306916

17. Jiang P, Gu S, Pan D, Fu J, Sahu A, Hu X, et al. Signatures of T cell dysfunction and exclusion predict cancer immunotherapy response. *Nat Med*. (2018) 24:1550–8. doi: 10.1038/s41591-018-0136-1

18. Mayakonda A, Lin DC, Assenov Y, Plass C, Koeffler HP. Maftools: efficient and comprehensive analysis of somatic variants in cancer. *Genome Res*. (2018) 28 (11):1747–56. doi: 10.1101/gr.239244.118

19. Leek JT, Johnson WE, Parker HS, Jaffe AE, Storey JD. The sva package for removing batch effects and other unwanted variation in high-throughput experiments. *Bioinformatics*. (2012) 28:882–3. doi: 10.1093/bioinformatics/bts034

20. Zindler T, Frieling H, Neyazi A, Bleich S, Friedel E. Simulating combat: how batch correction can lead to the systematic introduction of false positive results in DNA

methylation microarray studies. *BMC Bioinf*. (2020) 21(1):271. doi: 10.1186/s12859-020-03559-6

21. Zhou N, Yuan X, Du Q, Zhang Z, Shi X, Bao J, et al. Ferrdb V2: update of the manually curated database of ferroptosis regulators and ferroptosis-disease associations. *Nucleic Acids Res*. (2023) 51:D571–d82. doi: 10.1093/nar/gkac935

22. Subramanian A, Tamayo P, Mootha VK, Mukherjee S, Ebert BL, Gillette MA, et al. Gene set enrichment analysis: A knowledge-based approach for interpreting genome-wide expression profiles. *Proc Natl Acad Sci U.S.A*. (2005) 102:15545–50. doi: 10.1073/pnas.0506580102

23. Colaprico A, Silva TC, Olsen C, Garofano L, Cava C, Garolini D, et al. Tcgabiolinks: an R/bioconductor package for integrative analysis of tcga data. *Nucleic Acids Res*. (2016) 44:e71. doi: 10.1093/nar/gkv1507

24. Ritchie ME, Phipson B, Wu D, Hu Y, Law CW, Shi W, et al. Limma powers differential expression analyses for rna-sequencing and microarray studies. *Nucleic Acids Res*. (2015) 43:e47. doi: 10.1093/nar/gkv007

25. Wilkerson MD, Hayes DN. Consensusclusterplus: A class discovery tool with confidence assessments and item tracking. *Bioinformatics*. (2010) 26:1572–3. doi: 10.1093/bioinformatics/btq170

26. Yoshihara K, Shahmoradgoli M, Martínez E, Vegesna R, Kim H, Torres-Garcia W, et al. Inferring tumour purity and stromal and immune cell admixture from expression data. *Nat Commun*. (2013) 4:2612. doi: 10.1038/ncomms3612

27. Yu G, Wang LG, Han Y, He QY. Clusterprofiler: an R package for comparing biological themes among gene clusters. *Omics*. (2012) 16:284–7. doi: 10.1089/omi.2011.0118

28. McFaline-Figueroa JL, Hill AJ, Qiu X, Jackson D, Shendure J, Trapnell C. A pooled single-cell genetic screen identifies regulatory checkpoints in the continuum of the epithelial-to-mesenchymal transition. *Nat Genet*. (2019) 51:1389–98. doi: 10.1038/s41588-019-0489-5

29. Bindea G, Mlecnik B, Tosolini M, Kirilovsky A, Waldner M, Obenauf AC, et al. Spatiotemporal dynamics of intratumoral immune cells reveal the immune landscape in human cancer. *Immunity*. (2013) 39:782–95. doi: 10.1016/j.immuni.2013.10.003

30. Mariathasan S, Turley SJ, Nickles D, Castiglioni A, Yuen K, Wang Y, et al. Tgfβ Attenuates tumour response to pd-L1 blockade by contributing to exclusion of T cells. *Nature*. (2018) 554:544–8. doi: 10.1038/nature25501

31. van Houwelingen HC, Bruinsma T, Hart AA, Van't Veer LJ, Wessels LF. Cross-validated cox regression on microarray gene expression data. *Stat Med*. (2006) 25:3201–16. doi: 10.1002/sim.2353

32. Bass AJ, Thorsson V, Shmulevich I, Reynolds SM, Miller M, Bernard B. Comprehensive molecular characterization of gastric adenocarcinoma. *Nature*. (2014) 513:202–9. doi: 10.1038/nature13480

33. Geeleher P, Cox N, Huang RS. Prrophetic: an R package for prediction of clinical chemotherapeutic response from tumor gene expression levels. *PloS One*. (2014) 9:e107468. doi: 10.1371/journal.pone.0107468

34. Yang W, Soares J, Greninger P, Edelman EJ, Lightfoot H, Forbes S, et al. Genomics of drug sensitivity in cancer (Gdsc): A resource for therapeutic biomarker discovery in cancer cells. *Nucleic Acids Res*. (2013) 41:D955–61. doi: 10.1093/nar/gks1111

35. Oh SC, Sohn BH, Cheong JH, Kim SB, Lee JE, Park KC, et al. Clinical and genomic landscape of gastric cancer with a mesenchymal phenotype. *Nat Commun*. (2018) 9:1777. doi: 10.1038/s41467-018-04179-8

36. Bonneville R, Krook MA, Kautto EA, Miya J, Wing MR, Chen HZ, et al. Landscape of microsatellite instability across 39 cancer types. *JCO Precis Oncol*. (2017) 2017:PO.17.00073. doi: 10.1200/po.17.00073

37. Lu M, Zhao B, Liu M, Wu L, Li Y, Zhai Y, et al. Pan-cancer analysis of setd2 mutation and its association with the efficacy of immunotherapy. *NPJ Precis Oncol*. (2021) 5:51. doi: 10.1038/s41698-021-00193-0

38. Niu B, Ye K, Zhang Q, Lu C, Xie M, McLellan MD, et al. Msisensor: microsatellite instability detection using paired tumor-normal sequence data. *Bioinformatics*. (2014) 30:1015–6. doi: 10.1093/bioinformatics/btt755

39. Lee J, Kim ST, Kim K, Lee H, Kozarewa I, Mortimer PGS, et al. Tumor genomic profiling guides patients with metastatic gastric cancer to targeted treatment: the viktory umbrella trial. *Cancer Discovery*. (2019) 9:1388–405. doi: 10.1158/2159-8290.Cd-19-0442

40. Şenbabaoğlu Y, Gejman RS, Winer AG, Liu M, Allen EV, Velasco GD, et al. Tumor immune microenvironment characterization in clear cell renal cell carcinoma identifies prognostic and immunotherapeutically relevant messenger rna signatures. *Genome Biol*. (2016) 18(1):46. doi: 10.1186/s13059-016-1092-z

41. Nishino M, Ramaiya NH, Hatabu H, Hodi FS. Monitoring immune-checkpoint blockade: response evaluation and biomarker development. *Nat Rev Clin Oncol*. (2017) 14:655–68. doi: 10.1038/nrclinonc.2017.88

42. Yarchoan M, Albacker LA, Hopkins AC, Montesion M, Murugesan K, Vithayathil TT, et al. Pd-L1 expression and tumor mutational burden are independent biomarkers in most cancers. *JCI Insight*. (2019) 4(6):e126908. doi: 10.1172/jci.insight.126908

43. Kim R, Hashimoto A, Markosyan N, Tyurin VA, Tyurina YY, Kar G, et al. Ferroptosis of tumour neutrophils causes immune suppression in cancer. *Nature*. (2022) 612:338–46. doi: 10.1038/s41586-022-05443-0

44. Maio M, Ascierto PA, Manzyuk L, Motola-Kuba D, Penel N, Cassier PA, et al. Pembrolizumab in microsatellite instability high or mismatch repair deficient cancers: updated analysis from the phase ii keynote-158 study. *Ann Oncol*. (2022) 33:929–38. doi: 10.1016/j.annonc.2022.05.519

45. Le DT, Diaz LA Jr., Kim TW, Van Cutsem E, Geva R, Jäger D, et al. Pembrolizumab for previously treated, microsatellite instability-high/mismatch repair-deficient advanced colorectal cancer: final analysis of keynote-164. *Eur J Cancer*. (2023) 186:185–95. doi: 10.1016/j.ejca.2023.02.016

46. Asaoka Y, Ijichi H, Koike K. Pd-1 blockade in tumors with mismatch-repair deficiency. *N Engl J Med*. (2015) 373:1979. doi: 10.1056/NEJMc1510353

47. Andrė T, Shiu KK, Kim TW, Jensen BV, Jensen LH, Punt C, et al. Pembrolizumab in microsatellite-instability-high advanced colorectal cancer. *N Engl J Med*. (2020) 383:2207–18. doi: 10.1056/NEJMoa2017699

48. Kalisky T, Blainey P, Quake SR. Genomic analysis at the single-cell level. *Annu Rev Genet*. (2011) 45:431–45. doi: 10.1146/annurev-genet-102209-163607

49. Wang Y, Navin NE. Advances and applications of single-cell sequencing technologies. *Mol Cell*. (2015) 58:598–609. doi: 10.1016/j.molcel.2015.05.005

50. Lovett M. The applications of single-cell genomics. *Hum Mol Genet*. (2013) 22:R22–6. doi: 10.1093/hmg/ddt377

frontiers | Frontiers in Oncology

TYPE Perspective
PUBLISHED 22 January 2025
DOI 10.3389/fonc.2024.1524651

OPEN ACCESS

EDITED BY
Parmanand Malvi,
University of Alabama at Birmingham, United States

REVIEWED BY
Ashish Toshniwal,
The University of Utah, United States
Raj Kumar,
University of Alabama at Birmingham, United States

*CORRESPONDENCE
Medhi Wangpaichitr
mwangpaichitr@med.miami.edu

†These authors have contributed equally to this work

RECEIVED 08 November 2024
ACCEPTED 23 December 2024
PUBLISHED 22 January 2025

CITATION
Kang I, Theodoropoulos G and Wangpaichitr M (2025) Targeting the kynurenine pathway: another therapeutic opportunity in the metabolic crosstalk between cancer and immune cells. *Front. Oncol.* 14:1524651. doi: 10.3389/fonc.2024.1524651

Targeting the kynurenine pathway: another therapeutic opportunity in the metabolic crosstalk between cancer and immune cells

Irene Kang[1,2†], George Theodoropoulos[1†] and Medhi Wangpaichitr[1,2,3,4*]

[1]Department of Veterans Affairs, Miami VA Healthcare System, Miami, FL, United States, [2]South Florida VA Foundation for Research and Education, Miami, FL, United States, [3]Department of Surgery, Division of Thoracic Surgery, University of Miami, Miami, FL, United States, [4]Sylvester Comprehensive Cancer Center, University of Miami, Miami, FL, United States

The pivotal role of metabolic reprogramming in cancer-related drug resistance, through the tryptophan-catabolized kynurenine pathway (KP), has been particularly underscored in recent research. This pathway, driven by indoleamine 2,3-dioxygenase 1 (IDO1), facilitates immune evasion and promotes tumor progression by fostering an immunosuppressive environment. In Phase III investigation of the combination of IDO1 inhibition with immune checkpoint inhibitors (ICIs), the combination therapy was not efficacious. In this review, we revisit current advances, explore future directions, and emphasize the importance of dual inhibition of the KP rate-limiting enzymes IDO1 and tryptophan 2,3-dioxygenase-2 (TDO2) in appropriate patient populations. We propose that dual inhibition may maximize the therapeutic potential of KP inhibition. Additionally, we delve into the complex cellular interactions in cancer and metabolic dependencies within the tumor microenvironment (TME). Insights from preclinical studies, recent clinical trials, and promising therapeutic combinations will be discussed to elucidate and promote a clear path forward for the direction of KP research into cancer-related outcomes.

KEYWORDS

lung cancer, metabolism, immunometabolism, drug resistance, kynurenine, dual inhibitors

Introduction

Drug resistance in cancer remains a formidable challenge in modern oncology, severely limiting the efficacy of treatments across a wide spectrum of malignancies. Resistance mechanisms are multifaceted, often involving genetic mutations, epigenetic alterations, or modifications in signaling pathways that protect cancer cells from cytotoxic agents. These

mechanisms vary from tissue to tissue and within tumor types in the same tissue. Hence, while treatments like chemotherapy, radiation, and immunotherapy initially showed promise, the emergence of resistant tumor cells decreased therapeutic effectiveness.

These developments increase the challenges in the application of therapies to the most appropriate patient cohort, treatment combination, and timing. This challenge is exemplified in cisplatin, one of the most used chemotherapy drugs. Initially effective in treating a variety of solid tumors, including non-small cell lung cancer (NSCLC), ovarian, and bladder cancers, cisplatin's effectiveness diminishes as tumor cells develop mechanisms to evade its cytotoxic effects. These mechanisms include enhanced DNA repair capabilities, increased efflux of the drug, and profound alterations in cellular metabolism promoting tumor survival (1, 2).

The reprogramming of cellular metabolism was proposed as a common type of tumor resistance decades ago, but the complexities and uniqueness of certain alterations in a tissue specific manner have only been described in the last decade. Altered metabolism has now emerged as a central factor in cancer resistance, particularly as tumors shift metabolic reliance to sustain growth after treatment. Based on these concepts, our lab has extensively investigated and characterized tumor metabolic pathways in hypoxic [hypoxia-inducible factor (HIF1α)] and normoxic (oxidative phosphorylation) conditions (3–5). This work led to the reporting of various metabolic components that tumor cells relied on for survival. One metabolic pathway that gained attention for promoting survival under treatment pressures is the kynurenine pathway (KP) of tryptophan degradation (6, 7). By degrading tryptophan into immunosuppressive metabolites like kynurenine, cancer cells create an environment that suppresses the activity of effector immune cells. This promotes the expansion of regulatory T cells (Tregs) and myeloid-derived suppressor cells (MDSCs) (8–10), enabling cancer cells to escape immune surveillance and contributing to therapy resistance.

This perspective review will explore the latest advances in targeting metabolic crosstalk with a particular focus on inhibiting the tryptophan-catabolized KP. We will discuss why current therapeutic strategies aimed at disrupting this crosstalk often fail and propose ways to enhance anti-tumor immunity and overcome drug resistance, offering a promising pathway for developing new cancer treatments.

The role of the kynurenine pathway in cancer metabolism

Tryptophan (TRP) is an essential amino acid required for protein synthesis as a precursor to serotonin and melatonin (11, 12). However, the majority of TRP (about 99%) not used for protein synthesis—is broken down via the kynurenine pathway (KP) to generate kynurenine (KYN) (13). The KP pathway involves rate-limiting key enzymes, including indoleamine 2,3-dioxygenase 1 (IDO1), tryptophan 2,3-dioxygenase (TDO), and indoleamine 2,3-dioxygenase 2 (IDO2). The first step in the pathway is the conversion of tryptophan to N-formyl kynurenine by either IDO1, TDO, or IDO2. N-formyl kynurenine is then rapidly converted into kynurenine, which serves as the precursor for several biologically active metabolites, such as kynurenic acid, xanthurenic acid, and anthranilic acid (14).

In cancer, IDO1 is overexpressed and has been linked to poor prognosis in several tumor types, including lung, ovarian, and pancreatic cancers (15). Studies also showed significantly shorter survival among patients with high expression of IDO1 or TDO2 (16). The overexpression of IDO1/TDO2 and the consequent accumulation of KYN suppress anti-tumor immunity by promoting the differentiation of Tregs and MDSCs, which in turn, inhibit the activity of effector CD8+T cells and NK cells (Figure 1A). We found that the key driver of this inhibition is the level of reactive oxygen species (ROS)-dependent IDO1 activity, rather than IDO1 expression (17). Cisplatin-resistant lung cancer cells possessed higher basal levels of ROS when compared to cisplatin-sensitive cells. Together, this immunosuppressive environment facilitates tumor immune evasion and contributes to the resistance of immunotherapies such as immune checkpoint inhibitors (ICIs).

Beyond its role in immune evasion, the KP also supports cancer cell survival and proliferation by supplying essential metabolic intermediates. KYN can activate signaling pathways that promote cancer cell survival, proliferation, and metastasis. KYN has been shown to activate the aryl hydrocarbon receptor (AHR), a transcription factor involved in cell growth and immune regulation (18). This activation promotes tumor growth, so we investigated inhibition in this context. Indeed, exposure to AHR inhibitors (DMF or CH-223191) resulted in the suppression of IDO1 activities, whereas the addition of KYN increased IDO1 activity in cisplatin-resistant cells (17).

Kynurenine–hypoxia inducible-1α – aryl hydrocarbon receptor axis

ARNT (AHR nuclear translocator) or HIF1β (hypoxia-inducible factor 1β) is a known binding partner of both HIF1α and AHR (Figure 2) (19, 20). We reported that HIF1α levels are low in cisplatin-resistant lung cancer cells. Downregulation of HIF1α allows ARNT to preferentially bind with activated AHR rather than HIF1, shifting the metabolic balance towards AHR-driven pathways (17, 21). This pathway enhances immune suppression by increasing FoxP3 (master regulator in the development and function of Tregs) expression and creating an immunosuppressive TME. The extensive characterization of these molecular pathways in lung cancer has led us to promote the concept that the components of these paths could be therapeutic targets helping eliminate resistant cells.

Minhas et al. recently reported that IDO1 is upregulated in response to amyloid and tau pathology in astrocytes, leading to increased production of kynurenine (KYN); these findings are consistent with our model (Figure 2B). This upregulation

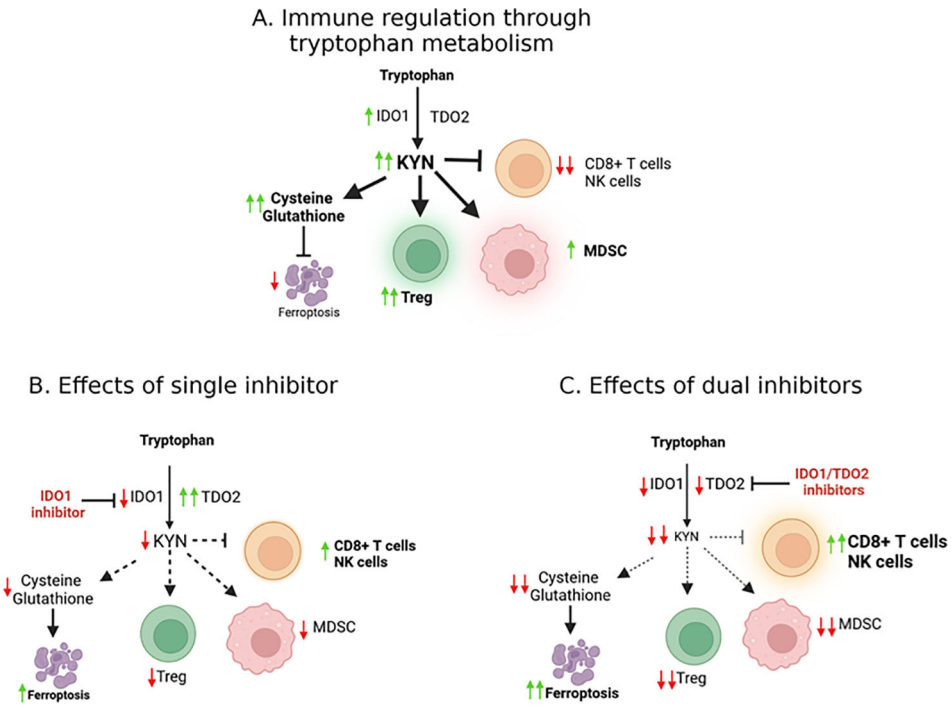

FIGURE 1
Molecular effects of IDO/TDO signaling. **(A)** The IDO1 enzyme catalyzes the conversion of tryptophan into kynurenine, an oncometabolite. Kynurenine production contributes to an immunosuppressive tumor microenvironment (TME), facilitating cancer progression as well as suppressing ferroptosis. **(B)** TDO2 can potentially compensate when IDO1 is inhibited, suggesting that effective targeting may require simultaneous inhibition of both IDO and TDO to overcome this compensatory mechanism and reduce immunosuppression in the TME **(C)**.

activates AHR and disrupts the balance between AHR and HIF1α signaling in astrocytes, suppressing astrocytic glycolysis and reducing lactate production. Astrocytic glycolysis is essential for neuronal support and disrupting this metabolic pathway contributes to neurodegeneration in Alzheimer's disease (AD) (22).

In both cancer and neurodegeneration, the IDO1/TDO2-KYN-AHR axis is central to metabolic alterations and immune evasion, highlighting its significance as a therapeutic target. This disruption of normal cellular metabolism and promotion of an immune-suppressive environment makes the KP a possible therapeutic target for both cancerous and neurodegenerative conditions.

Kynurenine and immune evasion: mechanistic insights

The immune system's ability to recognize and eliminate tumor cells is a critical component of effective cancer therapy (ICIs and others). In certain patients with tumors that escape immune surveillance, treatment is not effective. One of the central mechanisms by which tumors achieve this immune evasion is through the induction of IDO1 activity and the subsequent depletion of tryptophan and accumulation of kynurenine (Figure 1A) (23, 24).

Tryptophan depletion alone has significant effects on immune cell function since T cells, particularly effector T cells, are highly sensitive to tryptophan availability. In low tryptophan conditions, T cell proliferation is inhibited, and cells become functionally anergic. Moreover, kynurenine directly inhibits T cell proliferation and induces the differentiation of naïve T cells into Tregs, further suppressing the immune response (25–27). Tryptophan depletion and the resultant kynurenine accumulation favor immunosuppression over activation in the TME.

IDO1 and kynurenine also promote the expansion of MDSCs, a population of immune cells that suppresses both innate and adaptive immune responses (Figure 1A). MDSCs inhibit the activation of effector T cells and NK cells; additionally, they produce high levels of reactive oxygen species (ROS) and nitric oxide, which inhibit T cell receptor signaling and promote tumor progression (28, 29). Higher ROS levels generated by MDSCs may also further enhance IDO1 activity.

Crosstalk between cancer cells and immune cells in the TME

The metabolic crosstalk between cancer cells and immune cells in the TME is a key determinant of tumor progression and therapy resistance. By reprogramming their metabolism, cancer cells create an environment that is hostile to immune effector cells but supportive of immunosuppressive cells. This crosstalk can be mediated by a variety of metabolic pathways, including glycolysis, glutamine metabolism, and the KP.

In addition to the direct effects of TRP depletion and KYN accumulation on immune cells, cancer cells also engage in

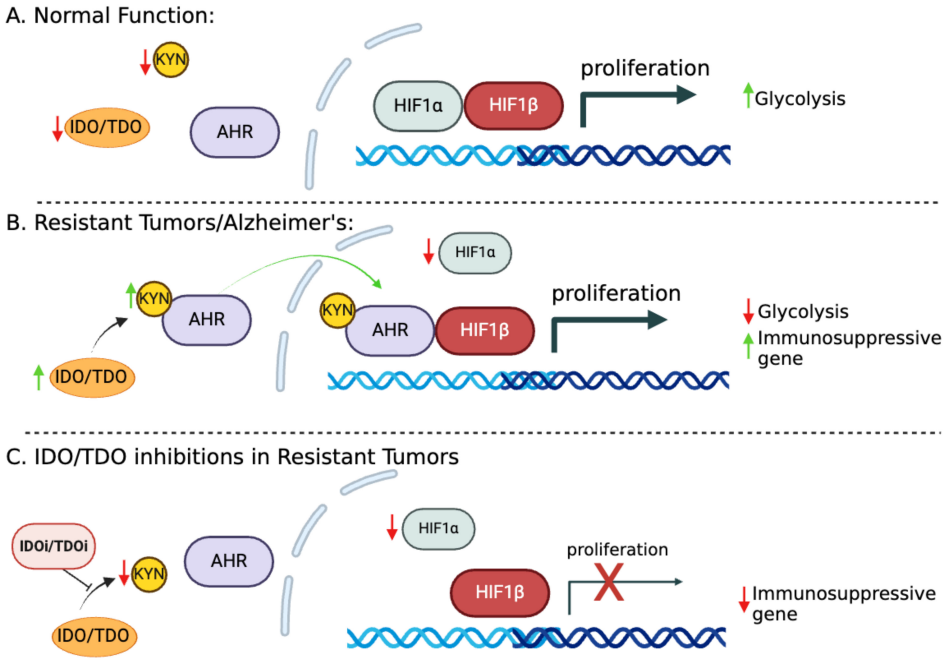

FIGURE 2
The IDO1-KYN-AHR axis and its role in promoting immunosuppression. **(A)** HIF1α and HIF1β facilitate the transcription of genes essential for glucose metabolism and cell proliferation/survival. **(B)** In cisplatin-resistant cells, increased KYN serves as a ligand for AHR, which becomes activated and translocated to the nucleus. Metabolic reprogramming in resistant cells leads to HIF1α downregulation, allowing ARNT to preferentially bind with activated AHR. This switch to AHR-driven pathways enhances the expression of immunosuppressive genes, fostering tumor immune evasion. **(C)** Targeting KYN could potentially reverse the immunosuppressive tumor microenvironment (TME), offering a therapeutic strategy to enhance antitumor immunity.

metabolic competition with immune cells. Effector T cells, for example, rely on glycolysis to support their rapid proliferation and production of cytokines (30). However, in the nutrient-deprived environment of the TME, cancer cells outcompete T cells for glucose, limiting the availability of this critical nutrient for immune cell function (31–33). Similarly, cancer cells' reliance on glutamine for the tricarboxylic acid (TCA) cycle also depletes the available glutamine for immune cell activity.

One of the most intriguing aspects of this metabolic crosstalk is the role of kynurenine in the ferroptosis of cancer cells, a form of programmed cell death characterized by the accumulation of lipid peroxides. KYN has an anti-ferroptosis effect that not only supports cancer cell survival but also creates an environment that is resistant to oxidative stress, further promoting immune evasion and drug resistance. Ferroptosis is regulated by the cystine/glutamate antiporter system (xCT), which imports cystine into cells in exchange for glutamate (34). Cystine is then reduced to cysteine, which is required for the synthesis of glutathione, a critical antioxidant that protects cells from ferroptosis. Unlike apoptosis, which is often inhibited in cancer cells, ferroptosis is regulated by the availability of cysteine and the function of the xCT antiporter. By disrupting the cystine/glutamate exchange, cancer cells can be sensitized to ferroptosis, making it an interesting and promising new target for therapy (34, 35).

KYN has been shown to inhibit ferroptosis by upregulating the expression of xCT, thereby enhancing cystine import and glutathione synthesis (34, 36, 37). This protects cancer cells from oxidative stress and ferroptosis (37). By inhibiting the kynurenine pathway, it may be possible to disrupt this protective mechanism and re-sensitize cancer cells to ferroptosis, offering a new avenue for cancer therapy (Figure 1B). Preclinical studies have shown that combining ferroptosis inducers with KP inhibitors can enhance the anti-tumor effects of both therapies. In a recent study by Fiore et al., inhibition of IDO1 sensitized cancer cells to ferroptosis, leading to increased cell death *in vitro* and reduced tumor growth *in vivo* (37) by inducing cell death and enhancing the immune response.

Inhibition of IDO1 and TDO2: a promising therapeutic strategy

The failure of single-agent IDO1 inhibitors, such as epacadostat, in clinical trials highlighted the limitations of targeting a single enzyme in the kynurenine pathway (Table 1). One of the key challenges is the compensatory upregulation of other enzymes, such as TDO2, which can maintain kynurenine production in the presence of IDO1 inhibitors (Figure 1B) (26, 38). To overcome this challenge, researchers have begun exploring the potential of dual

TABLE 1 IDO1 and TDO therapies in clinical development.

Drug name	Target	Description/Effects
Epacadostat (INCB024360)	IDO1	Studied with ICIs (such as pembrolizumab and nivolumab) for advanced melanoma tumors; failed to meet primary endpoints and trials were suspended
Indoximod (1-methyl-D-tryptophan)	IDO1	Acts as a tryptophan mimetic, evaluated for breast cancer and melanoma (alongside other therapies)
Linrodostat (BMS-986205)	IDO1	Tested in combination with nivolumab for non-small lung, head, and neck cancers; stopped in Phase III trials dur to industry challenges
Navoxiimod (GDC-0919)	IDO1	Assessed in early-phase clinical trials (as a monotherapy and with other agents) for advanced solid tumors
PF-06840003	IDO1	Went through clinical trials for safety and efficacy against advanced malignancies
KHK2455	IDO1	Investigated for potential in treating advanced solid tumors (both along and with other treatments)
M4112	IDO1/ TDO2	Demonstrated safety and efficacy as a monotherapy in Phase I trials, though plasma kynurenine levels were not significantly reduced in a steady state
AT-0174	IDO1/ TDO2	Showed significant tumor growth suppression in platinum-resistant non-small lung cancer models, especially with anti-PD-1 therapy

Green denotes IDO1 inhibitors. Blue denotes IDO1/TDO2 inhibitors.

inhibitors targeting both IDO1 and TDO2 (Figure 1C), thereby reducing the likelihood of compensatory metabolic pathways sustaining kynurenine production (39, 40).

In our recent preclinical studies, dual inhibition of IDO1 and TDO2 with the novel agent AT-0174 effectively reduced KYN levels, increased tumor infiltration with natural killer cells, and reduced regulatory T cells in cisplatin-resistant lung cancer models (38). In these studies, dual inhibition of IDO1 and TDO2 as monotherapy was similarly effective on overall survival as anti-PD1 monotherapy. Moreover, AT-0174 was synergistic when combined with anti-PD1 therapy on significant reduction of tumor growth, enhanced infiltration of CD8+ T cells into the TME, and improved survival time in animal models of treatment-resistant NSCLC tumors. This combination therapy not only reduced the immunosuppressive effects of KYN but also promoted immune-mediated tumor clearance.

These mechanisms were further substantiated in an aggressive model of glioblastoma where AT-0174 monotherapy increased natural killer cell infiltration, reduced Treg cells in tumor tissues, and was synergistic with Temozolomide (TMZ), an alkylating agent, in significantly prolonging animal survival (41). Glioblastoma is a highly aggressive brain cancer with limited treatment options and rapid resistance development to TMZ. These results suggest that AT-0174 administered at the time of Temozolomide initiation may, through synergistic mechanisms, aid in immune-mediated elimination of emergent tumor variants with resistance to Temozolomide, thereby improving patient survival.

In another study of high-grade serous carcinoma (HGSC), which is known to exhibit poor outcomes due to therapy resistance and an immunosuppressive TME, Crump et al. reported that HGSC tumors are driven predominantly by TDO2 in promoting tumor progression and immune evasion via kynurenine (KYN) production. High IL6 levels, linked to poor prognosis, correlate with elevated KYN in patient samples. Dual inhibition of IDO1/TDO2 using AT-0174 reduced tumor growth, diminished tumor-associated macrophages (TAMs), and suppressed PD-L1 expression. Cisplatin in combination with AT-0174 extended survival in preclinical models (42).

Together, these studies highlighted the potential of metabolic reprogramming of the TME to overcome immunotherapy resistance and provide a basis for advancing dual IDO1/TDO2 inhibitors in clinical settings.

Clinical trials

The first dual IDO1 and TDO2 inhibitor Phase I clinical trial (NCT03306420) was completed with 15 enrolled patients with advanced solid tumors (43). Another potent dual-inhibitor, AT-0174, is currently being tested across multiple sites in an initial clinical trial (ACTRN12623000956606), evaluating the efficacy in patients also with advanced metastatic solid cancers with promising preliminary results (Figure 3) (44). M4112, another IDO1/TDO2 inhibitor, did not present any serious safety concerns at doses up to 800 mg twice daily, though the best overall response observed was stable disease in nine patients (60%) with a progression-free survival of 3.7 months; it is noteworthy, however, that most of these patients had tumor types that are typically unresponsive to immunotherapy (43, 45). Unfortunately, due to the early termination of the study, neither the maximum tolerated dose (MTD) nor the recommended phase 2 dose (RP2D) was established. Another limitation of this study was that patient tumor biopsies were not obtained, but now, a KYN antibody is commercially available that could have been used to conduct immunohistochemistry staining. Therefore, neither changes in IDO/TDO expression nor changes in the tumor microenvironment could be evaluated. The termination of this study points to the potential for the appropriate patient cohort to have been investigated, possibly by characterizing patient KYN levels prior to treatment.

While the final results from the *ACTRN* trial are still pending, findings from the *NCT* trial suggest that dual inhibition of IDO1 and TDO2 may enhance the effectiveness of immunotherapies by

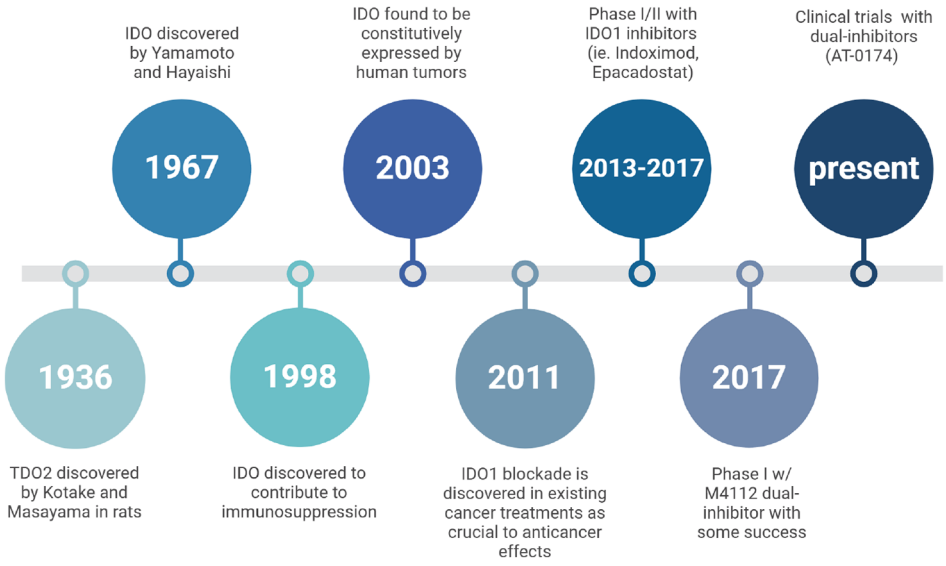

FIGURE 3
A historical timeline tracing research milestones on the physiology of IDO and TDO. It highlights key discoveries in the understanding of these enzymes' roles, particularly in immune regulation and cancer, and the development of inhibitors targeting IDO/TDO pathways to explore therapeutic potential.

reversing the immunosuppressive environment created by the KP. Therefore, further research into the pharmacodynamics, safety, and efficacy of dual inhibitors in combination with immune checkpoint inhibitors (ICIs) is of prime importance and warrants further investigation.

Inhibition of the kynurenine pathway combined with immune checkpoint blockade

Immune checkpoint inhibitors, such as anti-PD1 and anti-CTLA4 antibodies, have revolutionized the treatment of certain cancers by unleashing the immune system to attack tumor cells. However, many patients do not respond to these therapies, particularly those with tumors that have developed mechanisms of immune evasion. One of the primary mechanisms of immune evasion is the upregulation of the kynurenine pathway, which suppresses the activation and proliferation of effector immune cells (10, 46).

By combining KP inhibitors with immune checkpoint blockade, it may be possible to enhance the effectiveness of immunotherapy in these resistant tumors. Inhibiting the KP restores tryptophan levels and reduces the accumulation of immunosuppressive metabolites, thereby allowing effector T cells to proliferate and attack the tumor. Preclinical studies from our group and others have demonstrated that dual inhibition of IDO1 and TDO2, especially when combined with anti-PD1 therapy, can significantly improve survival in mouse models of lung cancer (47, 48). This combination therapy not only reduces tumor growth but also enhances the immune response, leading to durable tumor regression.

Future directions

While the KP represents a promising therapeutic target, it is unlikely that a one-size-fits-all approach will be effective for all patients. The expression of IDO1, TDO2, and other enzymes in the kynurenine pathway varies widely among different tumor types and even among patients with the same type of cancer (49–52). Testing (e.g. KYN levels) and additional characterization of expression levels in sensitive and resistant tumor types is warranted among all patient populations. Therefore, personalized approaches that tailor therapy based on specific metabolic tumor profiles are likely to be more effective in improving outcomes. Biomarker-driven approaches could help identify patients who are most likely to benefit from KP inhibitors and other combination therapies. Future clinical trials should evaluate the use of new and existing tests to assess biomarkers, such as IDO1/TDO2 expression and kynurenine levels, to guide treatment decisions. Another logical combination treatment could involve the use of AHR inhibitors to suppress IDO1 activities.

While preclinical studies have demonstrated the potential of targeting the KP to overcome drug resistance, translating these findings into clinical practice will require carefully designed trials. One of the key challenges in clinical translation is identifying the optimal combination of therapies that can effectively target the kynurenine pathway while minimizing toxicity. Combining IDO1/

TDO2 inhibitors with ICIs has shown promise in preclinical models, but the safety and efficacy of this combination need to be validated in clinical trials.

Conclusion

Mechanisms of cancer resistance mediated by metabolic alterations point to the kynurenine pathway as a critical metabolic axis in the TME that supports cancer cell survival and immune evasion. By targeting and decreasing the metabolic crosstalk between cancer cells and immune cells, particularly through dual inhibition of IDO1 and TDO2, new therapeutic strategies can be developed to overcome drug resistance and improve patient outcomes. These targets can not only be used to identify tumors that may be sensitive to inhibitors but also offer the potential for combining kynurenine pathway inhibition with immune checkpoint blockade as a promising approach to treating resistant cancers. As research into the metabolic vulnerabilities of cancer cells continues to evolve, the kynurenine pathway will likely remain a key target for future therapeutic interventions.

Data availability statement

The raw data supporting the conclusions of this article will be made available by the authors, without undue reservation.

Author contributions

MW: Conceptualization, Data curation, Formal analysis, Funding acquisition, Investigation, Methodology, Project administration, Resources, Software, Supervision, Validation, Visualization, Writing – original draft, Writing – review & editing. GT: Conceptualization, Formal analysis, Validation, Writing – review & editing. IK: Formal analysis, Validation, Visualization, Writing – review & editing.

Funding

The author(s) declare financial support was received for the research, authorship, and/or publication of this article. This work is supported by the BLR&D Merit Review Award (2I01BX004371) to MW and the South FL VA Foundation Research & Education fund to MW.

Conflict of interest

AT-0174 was manufactured and provided for study by Antido Therapeutics Australia Pty Ltd.

The authors declare that the research was conducted in the absence of any commercial or financial relationships that could be construed as a potential conflict of interest.

Generative AI statement

The author(s) declare that no Generative AI was used in the creation of this manuscript.

Publisher's note

References

1. Galluzzi L, Senovilla L, Vitale I, Michels J, Martins I, Kepp O, et al. Molecular mechanisms of cisplatin resistance. *Oncogene*. (2012) 31:1869–83. doi: 10.1038/onc.2011.384

2. Muggia FM, Bonetti A, Hoeschele JD, Rozencweig M, Howell SB. Platinum antitumor complexes: 50 years since Barnett Rosenberg's discovery. *J Clin Oncol*. (2015) 33:4219–26. doi: 10.1200/JCO.2015.60.7481

3. Wangpaichitr M, Savaraj N, Maher J, Kurtoglu M, Lampidis TJ, Intrinsically lower AKT. mammalian target of rapamycin, and hypoxia-inducible factor activity correlates with increased sensitivity to 2-deoxy-D-glucose under hypoxia in lung cancer cell lines. *Mol Cancer Ther*. (2008) 7:1506–13. doi: 10.1158/1535-7163.MCT-07-2334

4. Maher JC, Wangpaichitr M, Savaraj N, Kurtoglu M, Lampidis TJ. Hypoxia-inducible factor-1 confers resistance to the glycolytic inhibitor 2-deoxy-D-glucose. *Mol Cancer Ther*. (2007) 6:732–41. doi: 10.1158/1535-7163.MCT-06-0407

5. Long Y, Tsai WB, Chang JT, Estecio M, Wangpaichitr M, Savaraj N, et al. Cisplatin-induced synthetic lethality to arginine-starvation therapy by transcriptional suppression of ASS1 is regulated by DEC1, HIF-1alpha, and c-Myc transcription network and is independent of ASS1 promoter DNA methylation. *Oncotarget*. (2016) 7:82658–70. doi: 10.18632/oncotarget.12308

6. Gouasmi R, Ferraro-Peyret C, Nancey S, Coste I, Renno T, Chaveroux C, et al. The kynurenine pathway and cancer: why keep it simple when you can make it complicated. *Cancers (Basel)*. (2022) 14:1–15. doi: 10.3390/cancers14112793

7. León-Letelier RA, Dou R, Vykoukal J, Sater AHA, Ostrin E, Hanash S, et al. The kynurenine pathway presents multi-faceted metabolic vulnerabilities in cancer. *Front Oncol*. (2023) 13:1256769. doi: 10.3389/fonc.2023.1256769

8. Della Chiesa M, Carlomagno S, Frumento G, Balsamo M, Cantoni C, Conte R, et al. The tryptophan catabolite L-kynurenine inhibits the surface expression of NKp46- and NKG2D-activating receptors and regulates NK-cell function. *Blood*. (2006) 108:4118–25. doi: 10.1182/blood-2006-03-006700

9. Holmgaard RB, Zamarin D, Li Y, Gasmi B, Munn DH, Allison JP, et al. Tumor-expressed IDO recruits and activates MDSCs in a treg-dependent manner. *Cell Rep*. (2015) 13:412–24. doi: 10.1016/j.celrep.2015.08.077

10. Platten M, von Knebel Doeberitz N, Oezen I, Wick W, Ochs K. Cancer immunotherapy by targeting IDO1/TDO and their downstream effectors. *Front Immunol*. (2014) 5:673. doi: 10.3389/fimmu.2014.00673

11. Richard DM, Dawes MA, Mathias CW, Acheson A, Hill-Kapturczak N, Dougherty DM. L-tryptophan: basic metabolic functions, behavioral research and therapeutic indications. *Int J Tryptophan Res*. (2009) 2:45–60. doi: 10.4137/IJTR.S2129

12. Szczepanik M. Melatonin and its influence on immune system. *J Physiol Pharmacol*. (2007) 58:115–24.

13. Peters JC. Tryptophan nutrition and metabolism: an overview. *Adv Exp Med Biol*. (1991) 294:345–58. doi: 10.1007/978-1-4684-5952-4_32

14. Badawy AA. Kynurenine pathway of tryptophan metabolism: regulatory and functional aspects. *Int J Tryptophan Res*. (2017) 10:1178646917691938. doi: 10.1177/1178646917691938

15. Prendergast GC, Malachowski WJ, Mondal A, Scherle P, Muller AJ. Indoleamine 2,3-dioxygenase and its therapeutic inhibition in cancer. *Int Rev Cell Mol Biol*. (2018) 336:175–203. doi: 10.1016/bs.ircmb.2017.07.004

16. Du L, Xing Z, Tao B, Li T, Yang D, Li W, et al. Both IDO1 and TDO contribute to the Malignancy of gliomas via the Kyn-AhR-AQP4 signaling pathway. *Signal Transduct Target Ther*. (2020) 5:10. doi: 10.1038/s41392-019-0103-4

17. Nguyen DJM, Theodoropoulos G, Li YY, Wu C, Sha W, Feun LG, et al. Targeting the kynurenine pathway for the treatment of cisplatin-resistant lung cancer. *Mol Cancer Res*. (2020) 18:105–17. doi: 10.1158/1541-7786.MCR-19-0239

18. Bessede A, Gargaro M, Pallotta MT, Matino D, Servillo G, Brunacci C, et al. Aryl hydrocarbon receptor control of a disease tolerance defence pathway. *Nature*. (2014) 511:184–90. doi: 10.1038/nature13323

19. Denison MS, Nagy SR. Activation of the aryl hydrocarbon receptor by structurally diverse exogenous and endogenous chemicals. *Annu Rev Pharmacol Toxicol*. (2003) 43:309–34. doi: 10.1146/annurev.pharmtox.43.100901.135828

20. Semenza GL, Wang GL. A nuclear factor induced by hypoxia via *de novo* protein synthesis binds to the human erythropoietin gene enhancer at a site required for transcriptional activation. *Mol Cell Biol*. (1992) 12:5447–54. doi: 10.1128/mcb.12.12.5447

21. Schlichtner S, Yasinska IM, Klenova E, Abooali M, Lall GS, Berger SM, et al. L-Kynurenine participates in cancer immune evasion by downregulating hypoxic signaling in T lymphocytes. *Oncoimmunology*. (2023) 12:2244330. doi: 10.1080/2162402X.2023.2244330

22. Minhas PS, Jones JR, Latif-Hernandez A, Sugiura Y, Durairaj AS, Wang Q, et al. Restoring hippocampal glucose metabolism rescues cognition across Alzheimer's disease pathologies. *Science*. (2024) 385:eabm6131. doi: 10.1126/science.abm6131

23. Zhai L, Bell A, Ladomersky E, Lauing KL, Bollu L, Sosman JA, et al. Immunosuppressive IDO in cancer: mechanisms of action, animal models, and targeting strategies. *Front Immunol*. (2020) 11:1185. doi: 10.3389/fimmu.2020.01185

24. Passarelli A, Pisano C, Cecere SC, Di Napoli M, Rossetti S, Tambaro R, et al. Targeting immunometabolism mediated by the IDO1 Pathway: A new mechanism of immune resistance in endometrial cancer. *Front Immunol*. (2022) 13:953115. doi: 10.3389/fimmu.2022.953115

25. Rad Pour S, Morikawa H, Kiani NA, Yang M, Azimi A, Shafi G, et al. Exhaustion of CD4+ T-cells mediated by the kynurenine pathway in melanoma. *Sci Rep*. (2019) 9:12150. doi: 10.1038/s41598-019-48635-x

26. Stone TW, Williams RO. Modulation of T cells by tryptophan metabolites in the kynurenine pathway. *Trends Pharmacol Sci*. (2023) 44:442–56. doi: 10.1016/j.tips.2023.04.006

27. Kim M, Tomek P. Tryptophan: A rheostat of cancer immune escape mediated by immunosuppressive enzymes IDO1 and TDO. *Front Immunol*. (2021) 12:636081. doi: 10.3389/fimmu.2021.636081

28. Huang J, Zhao Y, Zhao K, Yin K, Wang S. Function of reactive oxygen species in myeloid-derived suppressor cells. *Front Immunol*. (2023) 14:1226443. doi: 10.3389/fimmu.2023.1226443

29. Ohl K, Tenbrock K. Reactive oxygen species as regulators of MDSC-mediated immune suppression. *Front Immunol*. (2018) 9:2499. doi: 10.3389/fimmu.2018.02499

30. Cao J, Liao S, Zeng F, Liao Q, Luo G, Zhou Y. Effects of altered glycolysis levels on CD8(+) T cell activation and function. *Cell Death Dis*. (2023) 14:407. doi: 10.1038/s41419-023-05937-3

31. Chang CH, Qiu J, O'Sullivan D, Buck MD, Noguchi T, Curtis JD, et al. Metabolic competition in the tumor microenvironment is a driver of cancer progression. *Cell*. (2015) 162:1229–41. doi: 10.1016/j.cell.2015.08.016

32. Cadenas-De Miguel S, Lucianer G, Elia I. The metabolic cross-talk between cancer and T cells. *Trends Biochem Sci*. (2023) 48:597–609. doi: 10.1016/j.tibs.2023.03.004

33. Yin Z, Bai L, Li W, Zeng T, Tian H, Cui J. Targeting T cell metabolism in the tumor microenvironment: an anti-cancer therapeutic strategy. *J Exp Clin Cancer Res*. (2019) 38:403. doi: 10.1186/s13046-019-1409-3

34. Koppula P, Zhuang L, Gan B. Cystine transporter SLC7A11/xCT in cancer: ferroptosis, nutrient dependency, and cancer therapy. *Protein Cell*. (2021) 12:599–620. doi: 10.1007/s13238-020-00789-5

35. Dixon SJ, Patel DN, Welsch M, Skouta R, Lee ED, Hayano M, et al. Pharmacological inhibition of cystine-glutamate exchange induces endoplasmic reticulum stress and ferroptosis. *Elife*. (2014) 3:e02523. doi: 10.7554/eLife.02523

36. Lin W, Wang C, Liu G, Bi C, Wang X, Zhou Q, et al. SLC7A11/xCT in cancer: biological functions and therapeutic implications. *Am J Cancer Res*. (2020) 10:3106–26.

37. Fiore A, Zeitler L, Russier M, Groß A, Hiller MK, Parker JL, et al. Kynurenine importation by SLC7A11 propagates anti-ferroptotic signaling. *Mol Cell*. (2022) 82:920–932.e7. doi: 10.1016/j.molcel.2022.02.007

38. Wu C, Spector SA, Theodoropoulos G, Nguyen DJM, Kim EY, Garcia A, et al. Dual inhibition of IDO1/TDO2 enhances anti-tumor immunity in platinum-resistant non-small cell lung cancer. *Cancer Metab*. (2023) 11:7. doi: 10.1186/s40170-023-00307-1

39. Peng X, Zhao Z, Liu L, Bai L, Tong R, Yang H, et al. Targeting indoleamine dioxygenase and tryptophan dioxygenase in cancer immunotherapy: clinical progress and challenges. *Drug Des Devel Ther*. (2022) 16:2639–57. doi: 10.2147/DDDT.S373780

40. Yoshioka S, Ikeda T, Fukuchi S, Kawai Y, Ohta K, Murakami H, et al. Identification and characterization of a novel dual inhibitor of indoleamine 2,3-dioxygenase 1 and tryptophan 2,3-dioxygenase. *Int J Tryptophan Res*. (2022) 15:11786469221138456. doi: 10.1177/11786469221138456

41. Bickerdike MJ, Nafia I, Bessede A, Chen CB, Wangpaichitr M. AT-0174, a novel dual IDO1/TDO2 enzyme inhibitor, synergises with temozolomide to improve survival in an orthotopic mouse model of glioblastoma. *BMC Cancer*. (2024) 24:889. doi: 10.1186/s12885-024-12631-w

42. Crump LS, Floyd JL, Kuo LW, Post MD, Bickerdike M, O'Neill K, et al. Targeting tryptophan catabolism in ovarian cancer to attenuate macrophage infiltration and PD-L1 expression. *Cancer Res Commun*. (2024) 4:822–33. doi: 10.1158/2767-9764.CRC-23-0513

43. Naing A, Eder JP, Piha-Paul SA, Gimmi C, Hussey E, Zhang S, et al. Preclinical investigations and a first-in-human phase I trial of M4112, the first dual inhibitor of indoleamine 2,3-dioxygenase 1 and tryptophan 2,3-dioxygenase 2, in patients with advanced solid tumors. *J Immunother Cancer*. (2020) 8:1–10. doi: 10.1136/jitc-2020-000870

44. AntidoTherapeutics, A phase I study to evaluate the safety, tolerability, pharmacology, and preliminary efficacy of AT-0174 in subjects with advanced solid Malignancies(2024). Available online at: https://trials.cancervic.org.au/details/vctl_actrn12623000956606 (Accessed February 20, 2024).

45. Ventola CL. Cancer immunotherapy, part 3: challenges and future trends. *P T*. (2017) 42:514–21.

46. Jennings MR, Munn D, Blazeck J. Immunosuppressive metabolites in tumoral immune evasion: redundancies, clinical efforts, and pathways forward. *J Immunother Cancer*. (2021) 9:1–19. doi: 10.1136/jitc-2021-003013

47. Opitz CA, Somarribas Patterson LF, Mohapatra SR, Dewi DL, Sadik A, Platten M, et al. The therapeutic potential of targeting tryptophan catabolism in cancer. *Br J Cancer*. (2020) 122:30–44. doi: 10.1038/s41416-019-0664-6

48. Fujiwara Y, Kato S, Nesline MK, Conroy JM, DePietro P, Pabla S, et al. Indoleamine 2,3-dioxygenase (IDO) inhibitors and cancer immunotherapy. *Cancer Treat Rev*. (2022) 110:102461. doi: 10.1016/j.ctrv.2022.102461

49. Hoffmann I, Dragomir MP, Monjé N, Keunecke C, Kunze CA, Schallenberg S, et al. Increased expression of IDO1 is associated with improved survival and increased number of TILs in patients with high-grade serous ovarian cancer. *Neoplasia*. (2023) 44:100934. doi: 10.1016/j.neo.2023.100934

50. Meireson A, Devos M, Brochez L. IDO expression in cancer: different compartment, different functionality? *Front Immunol*. (2020) 11:531491. doi: 10.3389/fimmu.2020.531491

51. Bessede A, Peyraud F, Le Moulec S, Cousin S, Cabart M, Chomy F, et al. Upregulation of indoleamine 2,3-dioxygenase 1 in tumor cells and tertiary lymphoid structures is a hallmark of inflamed non-small cell lung cancer. *Clin Cancer Res*. (2023) 29:4883–93. doi: 10.1158/1078-0432.CCR-23-1928

52. Fujiwara Y, Kato S, Nishizaki D, Miyashita H, Lee S, Nesline MK, et al. High indoleamine 2,3-dioxygenase transcript levels predict better outcome after front-line cancer immunotherapy. *iScience*. (2024) 27:109632. doi: 10.1016/j.isci.2024.109632

frontiers | Frontiers in Oncology

TYPE Original Research
PUBLISHED 17 March 2025
DOI 10.3389/fonc.2025.1522910

OPEN ACCESS

EDITED BY
Balkrishna Chaube,
Indian Institute of Technology Dharwad, India

REVIEWED BY
Ashish Toshniwal,
The University of Utah, United States
Meghna Saxena,
University of Minnesota Medical Center,
United States

*CORRESPONDENCE
Ting Zhang
3100102395@zju.edu.cn

RECEIVED 05 November 2024
ACCEPTED 19 February 2025
PUBLISHED 17 March 2025

CITATION
Huang Q, Xu Y-f, Li H-p and Zhang T (2025) Bioinformatics and experimental approach reveal potential prognostic and immunological roles of key mitochondrial metabolism-related genes in cervical cancer.
Front. Oncol. 15:1522910.
doi: 10.3389/fonc.2025.1522910

Bioinformatics and experimental approach reveal potential prognostic and immunological roles of key mitochondrial metabolism-related genes in cervical cancer

Qing Huang[1], Yang-feng Xu[1], Hui-ping Li[1] and Ting Zhang[2]*

[1]Gynecology Department, Ningbo Medical Center Lihuili Hospital, Ningbo, Zhejiang, China, [2]Orthopedics Department, Ningbo Medical Center Lihuili Hospital, Ningbo, Zhejiang, China

Background: Metabolic remodeling is the hallmark of cancer. In recent years, mitochondrial metabolism (MM) has been considered essential in tumorigenesis and cancer progression. Understanding the role of MM in cervical cancer (CC) can provide insights into disease progression and potential therapeutic targets.

Methods: Clinical data of CC patients was downloaded from the UCSC Xena dataset, and differentially expressed genes (DEGs) were identified between tumor and normal samples. MM-related genes (MMRGs) were screened from the MSigDB database. DEGs and MMRGs were then intersected to identify differentially expressed MMRGs. A prognostic risk model was constructed based on these intersecting genes through Cox regression analysis, and its association with the tumor microenvironment and immune checkpoint-related genes was evaluated. Hub genes' expression was evaluated in cells through qRT-PCR. Additionally, drug sensitivity analysis was conducted to explore potential therapeutic drugs.

Results: We identified 259 overlapping genes between DEGs and MMRGs, with 55 being prognosis-related. Two molecular clusters were revealed, with C1 exhibiting poorer prognosis. A prognostic risk model comprising five genes (BDH1, MIR210, MSMO1, POLA1, and STARD3NL) was established, showing significant associations with survival outcomes of CC patients. Functional enrichment analysis revealed that DEGs between high- and low-risk groups were tightly associated with the immune system. Analysis of the immune microenvironment showed significant differences between different risk groups, with higher immune and ESTIMATE scores observed in the low-risk

group. Additionally, expression levels of immune checkpoint-related genes were significantly correlated with the risk score. Drug sensitivity analysis identified potential therapeutic agents correlated with the expression of the five prognostic genes.

Conclusion: Our findings underscore the importance of MM in CC progression and provide potential therapeutic targets for CC.

KEYWORDS

cervical cancer, mitochondrial metabolism, risk score, prognosis, immunity

1 Introduction

Cervical cancer (CC) is one of the most prevalent gynecologic cancers, with an incidence of approximately 6.5% of all female cancer cases worldwide (1, 2). It is primarily caused by persistent infection with high-risk human papillomavirus (HPV) types (3). Despite advancements in screening programs and HPV vaccination efforts, CC remains a leading cause of cancer-related deaths among women globally (4). For patients with early or locally advanced CC, the 5-year survival rate exceeds 50% following surgical or chemoradiotherapy interventions (5, 6). However, the metastasis or recurrence significantly reduces survival rates, with a 5-year survival rate of only 10% for patients under such circumstances (4, 5). Therefore, it is urgent to delve deeper into the biological mechanisms of CC progression and identify novel prognostic biomarkers to enhance therapeutic strategies and patient outcomes.

Mitochondria, responsible for cellular energy generation, provide energy through the tricarboxylic acid (TCA) cycle and oxidative phosphorylation (OXPHOS) (7). Cellular energy imbalance is a recognized hallmark of cancer (8). In the 1920s, Otto Warburg postulated that cancer cells preferentially utilize glycolysis over OXPHOS for ATP production (9). For a long time, the major metabolic feature of tumor cells was considered to be the Warburg effect (10). However, in recent years, increasing evidence suggests that mitochondrial metabolism (MM) and function play a crucial role in tumorigenesis and cancer progression. Dysregulated mitochondrial function in cancer cells leads to alterations in energy production, metabolism, and redox balance, facilitating their proliferation, survival, and metastasis (11, 12). Moreover, mitochondria actively regulate apoptosis, allowing cancer cells to evade cell death signals and promote resistance to therapy (13–15). Therapeutic methods that target diverse pathways within MM, such as inhibiting cellular constituents engaged in mitochondrial synthesis, decreasing metabolite accumulation, or preventing energy production within mitochondria, have demonstrated therapeutic efficacy in various cancers (16–18). Several regents have been reported to alleviate CC by modulating MM. For example, Ginsenoside Rh2 induces CC cell apoptosis by suppressing mitochondrial electron transfer chain complex (19). Butyrate inhibited mitochondria-dependent apoptosis in CC cells (20). Therefore, MM could be a new therapeutic strategy for CC. Understanding the intricate interplay between MM and cancer biology holds promise for identifying novel therapeutic targets and developing personalized treatment strategies to combat CC.

This study aimed to elucidate the role of MM in CC progression and prognosis. Differentially expressed mitochondrial metabolism-related genes (MMRGs) in CC patients were identified and a prognostic risk model based on these genes was constructed. Through comprehensive bioinformatics analyses, we explored the clinical significance of MMRGs, as well as their association with tumor immune microenvironment and drug sensitivity, providing insights into potential therapeutic strategies for CC.

2 Methods

2.1 Acquirement of differentially expressed MMRGs

CC cohort was downloaded from the TCGA-UCSC Xena (http://xena.ucsc.edu). DEGs were identified between tumor samples (n = 305) and normal samples (n = 4) using the "limma" package in R software (version 4.1.3), with the criterion of |log2 fold change (FC)| > 1 and adjust p-value < 0.05. These DEGs were visualized in a volcano plot using "ggplot2". MMRGs were acquired from the MSigDB database (gsea-msigdb.org). Overlap genes in the DEGs and MMRGs were visualized through "upsetR" and "VennDiagram" packages.

2.2 Functional enrichment analysis

Gene ontology (GO) and Kyoto Encyclopedia of Genes and Genomes (KEGG) enrichment analyses were performed using the "clusterProfiler", with a criterion of $p < 0.05$. The results of GO and KEGG were visualized through the "Goplots" package in R.

2.3 Consensus clustering analysis

The MMRGs underwent univariate Cox regression analysis using the SPSS ($p < 0.05$). Consensus clustering analysis was then performed using R package ConsensusClusterPlus.

2.4 Establishment and evaluation of prognostic risk model

To mitigate overfitting, LASSO regression analysis was conducted on genes selected through univariate Cox regression utilizing the R package "glmnet", with the penalty function lambda (0.5765) employed via cross-validation to identify and eliminate overfitting genes. Finally, a multivariate Cox regression analysis was performed on the retained genes using SPSS to establish a prognostic risk model for MMRGs in CC. The risk score was calculated using the obtained regression coefficients from the multivariate Cox regression analysis, with a formula as follows:

$$risk\ score = \sum_{i=1}^{n} exp_{RNAi} * Coef_{RNAi}$$

Subsequently, the risk score for each sample in the TCGA dataset was calculated. Based on their RiskScore values, samples were categorized into high- and low-risk groups, with the median RiskScore serving as the threshold. Kaplan-Meier (K-M) curves and receiver operating characteristic (ROC) curves were then generated for both groups using the R packages "survival" and "survminer" to assess the predictive performance of the model. The area under the ROC curve (AUC) for 1-, 3-, and 5-years overall survival was calculated. The expression of prognostic biomarkers in each sample was visualized in a heatmap using the "ggplot2" package in R.

2.5 Construction of nomogram

Clinical characteristics encompass age, TNM stage, and pathology stage. A nomogram was established based on these clinical features and risk scores. The calibration curve depicted the 45-degree dashed lines representing the best predictions of the nomogram. The nomogram and calibration curve was constructed using "rms", "regplot", and "survival" packages.

2.6 Evaluation of tumor immune microenvironment landscape

The stromal score, immune score, ESTIMATE score, and tumor purity were acquired using the ESTIMATE algorithm. They were then compared between different risk groups using the Wilcoxon rank-sum test. Immune cell abundance in the high- and low-risk groups was detected using the MCPcounter algorithm.

2.7 Immune checkpoint and immunotherapy response analysis

Immune checkpoint-related genes in CC were searched from the Checkpoint Therapeutic Target Database (CKTTD) (21). Expression levels of these genes in different risk groups were explored, and the correlation of them with risk score was visualized using the R package "ggplot2". Tumor immune dysfunction and exclusion (TIDE) score was determined using the TIDE algorithm. $p < 0.05$ indicates statistical significance.

2.8 Drug sensitivity analysis

CellMiner (https://discover.nci.nih.gov/cellminer) encompasses 60 distinct cell lines originating from 9 types of malignancies, serving as essential screens in the development of novel anti-tumor medications. It includes 262 drugs, either FDA-approved or undergoing clinical trials (22). NCI60 drug response data were acquired from the CellMiner tool. Drug sensitivity between different risk groups was evaluated, and the association between drug sensitivity and prognostic gene expression was assessed using Pearson's test.

2.9 Cell culture

Human cervical epithelial cells (Cat NO.: CP-H059) and cervical cancer cells Hela S3 (Cat NO.: CL-0350) were purchased from Wuhan Pricella Biotechnology Co., Ltd. All cells were cultured in a specialized medium containing Ham's F-12K supplemented with 10% FBS and 1% P/S in an incubator at 37°C with 5% CO_2. The medium was changed every 2–3 days.

2.10 Quantitative real-time (qRT)-PCR

Total RNA was extracted using TRIzol reagent (Invitrogen) according to the manufacturer's protocol. The concentration and purity of the extracted RNA were assessed using a NanoDrop spectrophotometer (Thermo Fisher Scientific, CA, USA). The isolated RNA was then reverse-transcribed into cDNA with the PrimeScript RT reagent kit (Takara, Dalian, China). The reaction conditions were as follows: 42°C for 15 min and 95°C for 3 min. For quantification, qRT-PCR was performed using the Hieff UNICON Universal Blue qPCR SYBR Green Master Mix (Yeasen, Shanghai, China) on the ABI7900HT System. The thermocycling program was set as follows: initial denaturation at 95°C for 30 s, followed by 40 cycles of 95°C for 3 s and 60°C for 20 s. The relative mRNA expression levels were determined using the $2^{-\Delta\Delta Ct}$ method, with GAPDH serving as the internal control. The primer sequences were designed by Gene Creat Bioengineering CO. (Wuhan, China) and were shown in Supplementary Table S1.

2.11 Statistical analysis

Statistical analyses were conducted using R software version 4.2.0 and GraphPad Prism 8.0.2. Student t-test was used to compare the differences between the two groups, and the Pearson method was used for correlation analysis. All experiments were performed in triplicate, and data were analyzed using GraphPad Prism software. Statistical significance was determined using a Student's t-test. Statistical significance was defined as $p < 0.05$.

3 Results

3.1 Identification of prognosis-related differentially expressed MMRGs in patients with CC

Based on the TCGA dataset, 4353 DEGs were identified between the tumor and normal samples. Volcano plot showed 1976 upregulated genes and 2377 downregulated genes in the tumor group (Figure 1A). Additionally, 1234 MMRGs were

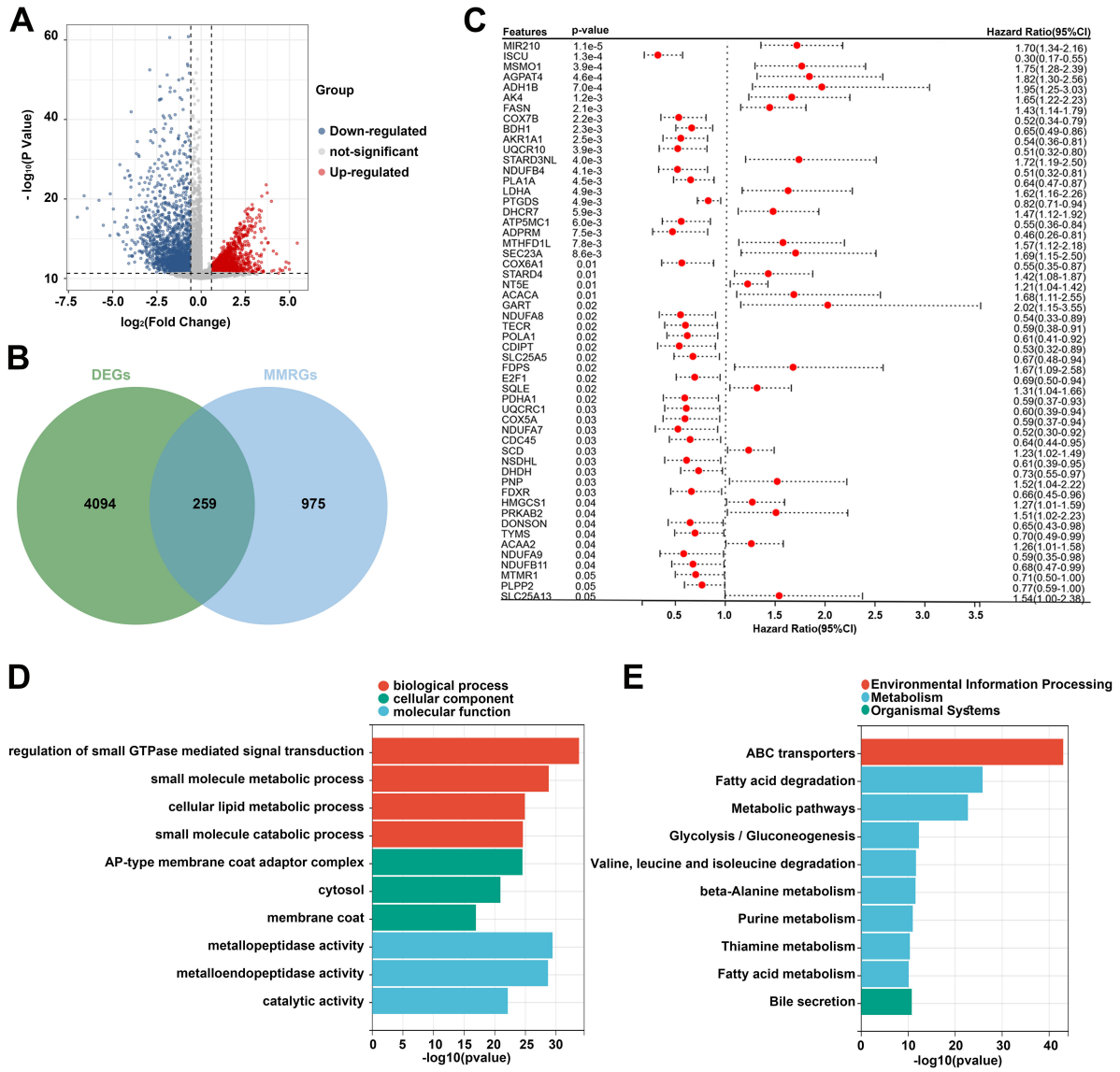

FIGURE 1
Identification of prognosis-related differentially expressed MMRGs in patients with CC. **(A)** Volcano plot of DEGs between tumor and normal samples in the TCGA database. The blue dots represent downregulated genes and the red dots represent upregulated genes. **(B)** A total of 4353 DEGs and 1234 MMRGs were screened from public databases, and 259 intersecting genes were identified between the DEGs and MMRGs using the Venn diagram. **(C)** Prognostic features were selected using the univariate Cox regression based on 259 differentially expressed MMRGs; $p < 0.05$. **(D, E)** GO and KEGG enrichment analysis was performed on the genes identified by univariate Cox regression analysis. CC, cervical cancer; DEG, differentially expressed gene; MMRG, mitochondrial metabolism-related gene; GO, Gene Ontology; KEGG, Kyoto Encyclopedia of Genes and Genomes.

screened from the MsigDB database (Figure 1B). Venn diagram revealed 259 overlapping genes in the DEGs and MMRGs (Figure 1B). Then, the overlapping genes were seeded on the univariate Cox regression, identifying 55 prognosis-related MMRGs (Figure 1C). GO enrichment analysis showed that these genes were associated with biological process, such as regulation of small GTPase mediated signal transduction, small molecule metabolic process, cellular lipid metabolic process, and small molecule catabolic process. They were also related to cellular components, including AP-type membrane coat adaptor complex, cytosol, and membrane coat. As for molecular functions, metallopeptidase activity, metalloendopeptidase activity, and catalytic activity were enriched (Figure 1D). The enriched KEGG pathways were related to environmental information processing, metabolism, and organismal systems, such as ABC transporters, fatty acid degradation, and bile secretion (Figure 1E).

3.2 Identification of two CC molecular subtypes

Subsequently, consensus clustering analysis was performed on the 55 prognosis-related MMRGs. The CDF curve showed that k = 2 is the optimal number of clusters (Figures 2A, B). Figure 2C displayed the consensus values for different k values, with the highest consensus value at k = 2. Therefore, all samples were clustered into two subtypes. The heatmap showed that the samples were well separated, with a clear distinction between the two subtypes (Figure 2D). K-M curves revealed that patients in C1 had significantly poorer OS than those in C2 (Figure 2E). Compared to C2, patients in C1 had higher pathological stages (Table 1). These results suggest that patients in C1 may have a worse prognosis and a higher degree of malignancy.

We then compared the expression levels of 55 prognosis-related MMRGs between C1 and C2. As shown in Figure 3A, 17 MMRGs were significantly overexpressed and 25 MMRGs were downregulated in C1. KEGG pathways analysis revealed that both overexpressed genes and downregulated genes in C1 were associated with metabolic pathways (Figures 3B, C). These results indicated that metabolic pathways may be involved in the imbalance of these differentially expressed prognosis-related genes to regulate the CC tumor microenvironment and progression.

3.3 Establishment of the MM-related risk model for patients with CC

To further explore the role of 55 MMRGs in CC prognosis, lasso regression was performed on these genes, and 10 MMRGs were identified (Figure 4A). The 10-round cross-validation was used to

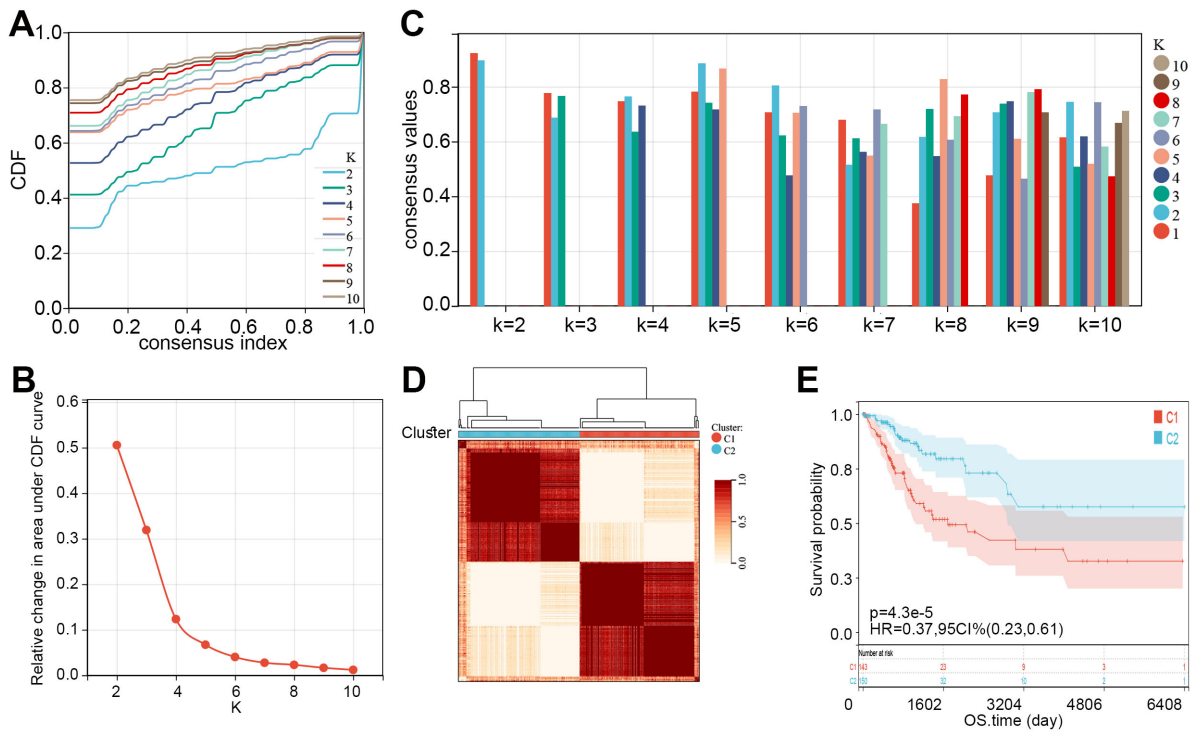

FIGURE 2
Two molecular subtypes of CC were identified. **(A)** Consensus CDF curves for different values of k (k = 2 to 10). **(B)** Relative change in the area under the CDF curve for different k values, indicating the optimal number of clusters. **(C)** Bar plot showing consensus values for different k values, with different colors representing varying cluster numbers. **(D)** Consensus clustering heatmap showing the division of samples into two clusters (C1 and C2) based on consensus matrix values. **(E)** K-M curve showed the overall survival time of CC patients between C1 and C2. CDF, cumulative distribution function; CC, cervical cancer; K-M, Kaplan-Meier; HR, hazard ratio; CI, confidence interval; OS, overall survival.

TABLE 1 Differences in stages and grades between two different subtypes.

Variables	Missing	Category	Total (n=293)	C1 (n=143)	C2 (n=150)	p
Stage, n(%)	6	I	158(55.052)	66(47.482)	92(62.162)	**0.029**
		II	65(22.648)	35(25.180)	30(20.270)	
		III	42(14.634)	22(15.827)	20(13.514)	
		IV	22(7.666)	16(11.511)	6(4.054)	
Grade, n(%)	28	1	19(7.170)	9(7.317)	10(7.042)	0.709
		2	129(48.679)	63(51.220)	66(46.479)	
		3	117(44.151)	51(41.463)	66(46.479)	

determine the optimal values of the penalty parameter (Figure 4B). Finally, using multivariate Cox regression, five genes, including BDH1, MIR210, MSMO1, POLA1, and STARD3NL were identified ($p < 0.05$, Figure 4C). Results revealed that BDH1 (HR = 0.71, 95%CI: 0.530-0.951) and POLA1 (HR = 0.581, 95%CI: 0.357-0.946) were protective features, while MIR210 (HR = 1.702, 95%CI: 1.326-2.186), MSMO1 (HR = 1.592, 95%CI: 1.158-2.189), and STARD3NL (HR = 1.776, 95% CI: 1.199-2.631) were harmful features (Figure 4C).

Furthermore, based on the expression levels of the above 5 prognostic genes, the risk score of each sample in the TCGA dataset

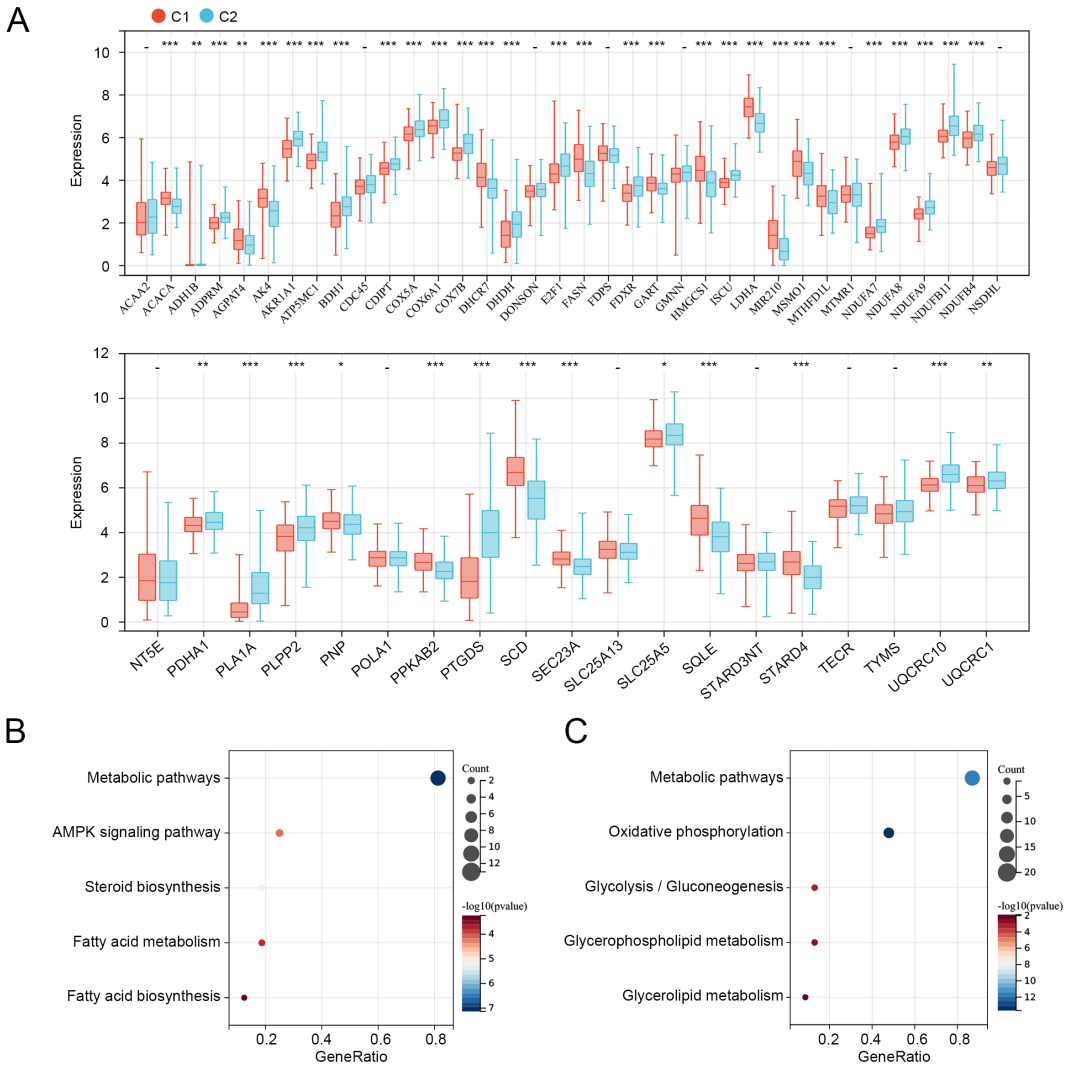

FIGURE 3
Expression and functions of prognosis-related genes in C1 and C2. **(A)** Expression levels of 55 prognosis-related genes in C1 and C2. **(B)** KEGG pathways related to overexpressed genes in C1. **(C)** KEGG pathways related to downregulated genes in C1. *p < 0.05, **p < 0.01, ***p < 0.001, "-"means no significant.

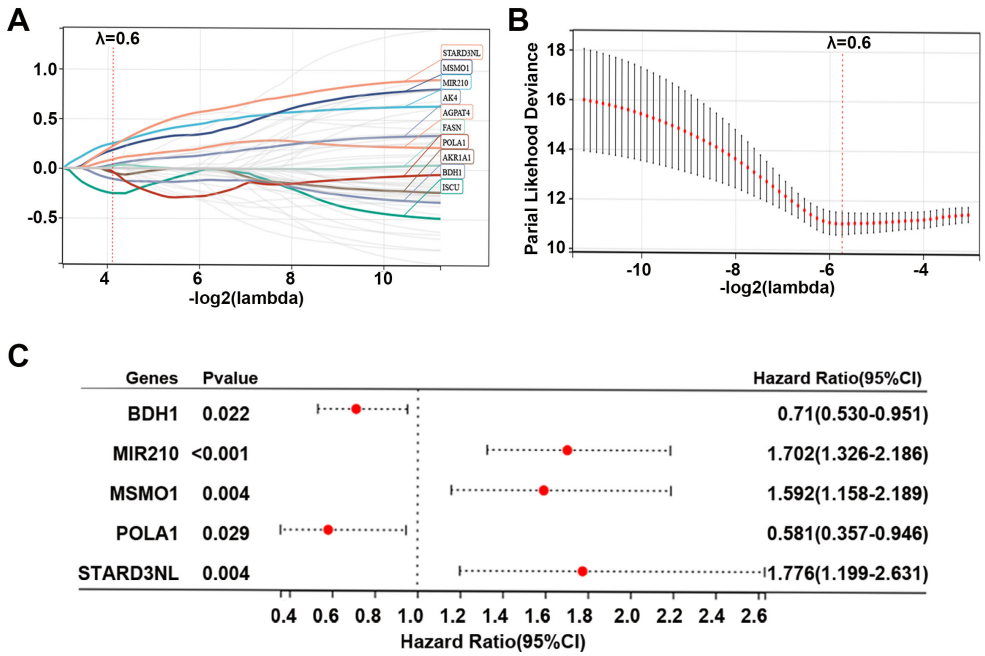

FIGURE 4
Identification of prognostic genes in CC. **(A, B)** Lasso Cox regression identified 10 genes related to the prognosis of patients with CC, and 10-round cross-validation was performed to detect the optimal values of the penalty parameter. **(C)** Multivariate Cox regression identified 5 prognostic genes based on the above 10 genes; $p < 0.05$. CC, cervical cancer; MMRG, mitochondrial metabolism-related gene.

was calculated as follows: risk score = -0.343*BDH1 + 0.532*MIR20 + 0.465*MSMO1 + -0.543*POLA1 + 0.575*STARD3NL. CC patients in the TCGA dataset were divided into high- and low-risk groups based on the median risk score. The risk score distribution of patients was visualized in Figure 5A. Our data indicated that patients with high risk scores had worse prognoses (Figure 5A). The expression of BDH1 and POLA1 was higher in the low-risk group, while the expression of MIR210, MSMO1, and STARD3NL was higher in the high-risk group (Figure 5A). The K-M survival curve demonstrated superior survival outcomes for the low-risk group compared to the high-risk group (Figure 5B). The AUCs of the enrolled patients at 1-, 3-, and 5-year were 0.78, 0.77, and 0.75, respectively (Figure 5C).

A nomogram was then constructed to show the performance of risk score and clinical features on CC prognosis. As shown in Figure 5D, the M stage, pathology stage, and risk score ranked in the top three in terms of contribution to predicting CC, followed by T stage, G stage, N stage, and age. The calibration curves of the nomogram for the probability at 3- and 5-year indicated a good clinical value (Figure 5E).

3.4 Functional enrichment analysis of DEGs between high-risk and low-risk groups

Subsequently, DEGs between high- and low-risk groups were identified, and the function of these genes was explored using GO and KEGG enrichment analyses. The top five enriched GO biological process terms were immune system process, response to stress, regulation of response to stimulus, response to chemical, and system development (Figure 6A). The top five GO cellular component terms included extracellular region, vesicle, endomembrane system, intrinsic component of membrane, and integral component of membrane (Figure 6B). The GO molecular function terms were mainly enriched in signaling receptor binding, protein-containing complex binding, molecular function regulator, anion binding, and small molecule binding (Figure 6C). The KEGG pathways were major enriched in cell adhesion molecules, Th17 cell differentiation, IL-17 signaling pathway, T cell receptor signaling pathway, and MAPK signaling pathway (Figure 6D). These results revealed that DEGs between high- and low-risk cohorts were tightly associated with tumor immune microenvironment.

3.5 Tumor immune microenvironment analysis

Given the above results that differentially expressed prognosis-related genes were related to metabolic pathways and that DEGs in high risk vs. low risk were related to the immune system process, we then explore the immune microenvironment between different risk groups. Our data showed that immune and ESTIMATE scores in the low-risk group were significantly higher than those in the high-risk group ($p < 0.05$, Figure 7A), and the high-risk group had a higher tumor purity (Figure 7B). Additionally, we observed five immune cells were significantly infiltrated in the low-risk group, including T cells, CD8 T cells, cytotoxic lymphocytes, B lineage, and myeloid dendritic cells (Figure 7C).

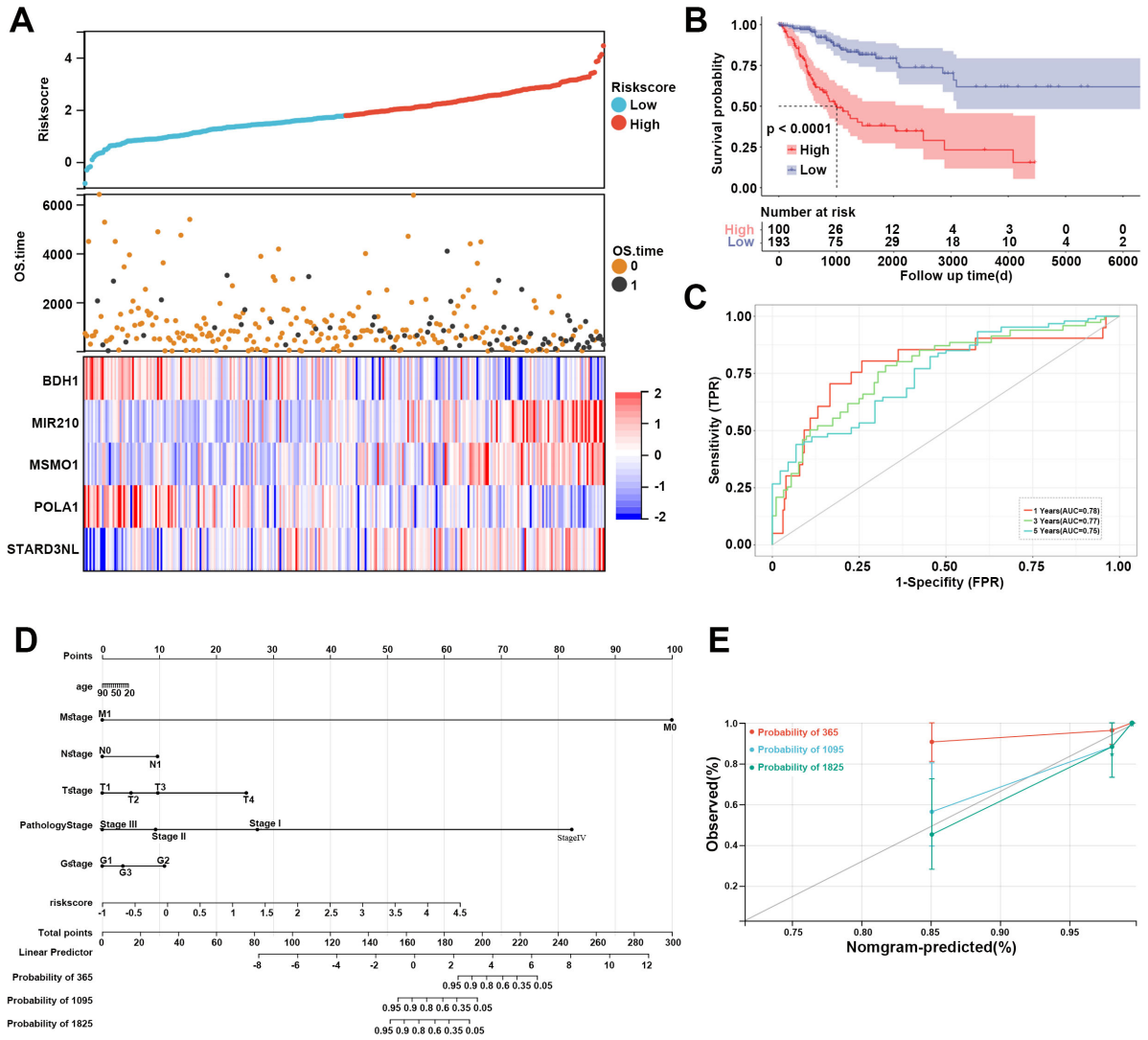

FIGURE 5
Assessment of MM-related risk model for CC. **(A)** Risk score distribution, OS time of each patient in the TCGA cohort, and heatmap of the five prognostic genes. **(B)** Kaplan-Meier curve revealed the survival probability of patients in different risk groups. **(C)** The ROC curve of the risk model at 1-, 3-, and 5-year. Red represents 1-year, green represents 3-year, and blue represents 5-year. **(D)** Nomogram for predicting 1-, 3-, and 5-year OS time for CC patients in the TCGA database. **(E)** Calibration curves of the nomogram observed 1-, 3-, and 5-year outcomes. MM, mitochondrial metabolism; CC, cervical cancer; OS, overall survival; ROC, receiver operating characteristic.

The effector function of CD8 T cells is regulated by immune checkpoints. Due to the differences in the levels of CD8 T cells between high and low risk groups, we further analyzed the differences in immune checkpoint gene expression between high and low risk groups. Among 13 checkpoint-related genes, 7 genes were observed to be significantly correlated to the risk score, and all of them were downregulated in the high-risk group, including CDK1, EZH2, ICOS, IDO1, PLK1, TIGIT, and TLR8 ($p < 0.05$, Figure 8A). Further research showed that the high-risk group had a higher TIDE score and exclusion score than the low-risk group (Figure 8B). These results suggest that the high risk group is associated with an immunosuppressive environment.

3.6 Expression of hub genes

To further explore whether the differences in the microenvironment between different groups are related to the hub genes, we examined the expression of these hub genes among different groups. Compared to the low-risk group, BDH1 and POLA1 were downregulated in the high-risk group, while MIR210, MSMO1, and STARD3NL were upregulated (Figure 9A). Similarly, in the C1 group, BDH1 and POLA1 were downregulated, while MIR210, MSMO1, and STARD3NL were upregulated (Figure 9B). These results are consistent with previous findings, indicating a higher mortality risk and therefore a poorer prognosis in the C1 group. Furthermore, we conducted cell

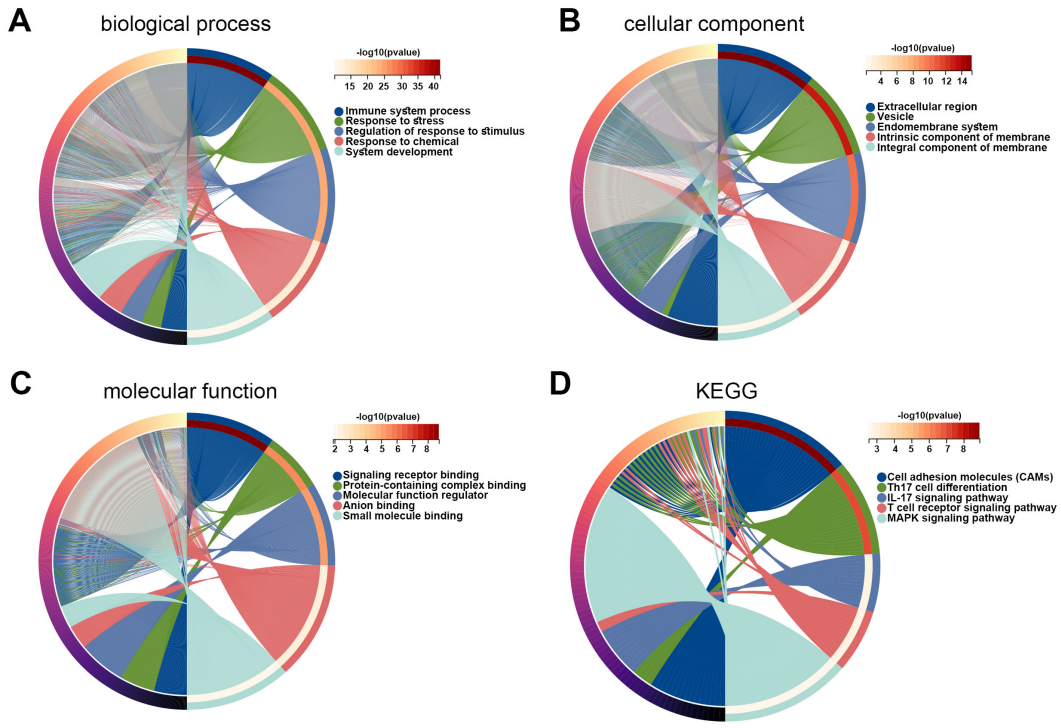

FIGURE 6
Functions of DEGs between high and low risk groups. **(A–C)** GO enrichment analysis was performed on DEGs in high and low risk groups, including biological process **(A)**, cellular component **(B)**, and molecular function **(C)**. **(D)** KEGG pathways related to DEGs in high and low risk groups. DEG, differentially expressed gene; GO, Gene Ontology; KEGG, Kyoto Encyclopedia of Genes and Genomes.

experiments to validate the expression of these genes. Compared to human cervical epithelial cells, BDH1 and POLA1 were downregulated, while MIR210, MSMO1, and STARD3NL were upregulated in the CC cell line Hela S3 cells (Figure 9C). These findings suggest that the expression of these five hub genes may be closely related to tumor immune-metabolic regulation.

3.7 Drug sensitivity analysis

The correlation between the expression levels of 5 prognostic genes and drug sensitivity was further investigated utilizing the CellMiner database. The top three drugs significantly correlated with the expression of each gene are shown in Supplementary Figure S1. BDH1 is positively associated with ciclosporin, Raloxifene, and Tamoxifen (Supplementary Figure S1A). MIR210 was positively associated with Cediranib, ergenyl, and Motesanib (Supplementary Figure S1B). Similarly, MSMO1 displayed a positive correlation with Amiodarone, uridin, and Zoledronate (Supplementary Figure S1C), and POLA1 was positively associated with Methylprednisolone, PX-316, and ZM-336372 (Supplementary Figure S1D). STARD3NL showed a positive association with JNJ-38877605 and Lovastatin while displaying a negative association with Fluorouracil (Supplementary Figure S1E). Among these drugs, the high-risk group was significantly sensitized to certain drugs, including ciclosporin, Raloxifene, Tamoxifen, Zoledronate, and Lovastatin (Supplementary Figure S2).

4 Discussion

Although advances in the treatment of CC have been made, its poor prognosis still poses a significant threat to women's health (4). Recent studies suggest that MM is essential for tumor growth, and some clinical trials have demonstrated the feasibility of modulating MM to treat cancer (23). The bioinformatic research on MM in CC is limited. Therefore, this study constructed a prognostic model based on five MMRGs for CC and explored their association with the immune microenvironment.

Metabolic remodeling is one of the hallmarks of cancer. Current evidence indicates that MM-related pathways are reprogrammed in cancer, playing crucial roles in bioenergetics, biosynthesis, and redox homeostasis (24). The regulation of redox balance in tumor cells is influenced by their significantly increased glucose uptake, which produces TCA cycle metabolites. These metabolites supply electrons to the mitochondrial electron transport chain (ETC) (25). Inhibiting ETC-related genes could heighten the vulnerability of cancer cells to glucose depletion, consequently impeding tumor progression (26). MMRGs have been considered prognostic markers for various cancers, including breast cancer (27), osteosarcoma (28), and ovarian cancer (29). Based on the MMRGs. the present study identified two molecular subtypes of CC, and C1 showed shorter OS time than C2. Additionally, 5 key prognostic MMRGs in CC were identified, including BDH1, MIR210, MSMO1, POLA1, and STARD3NL. BDH1 is a key catalytic enzyme in ketogenesis, catalyzing the reversible

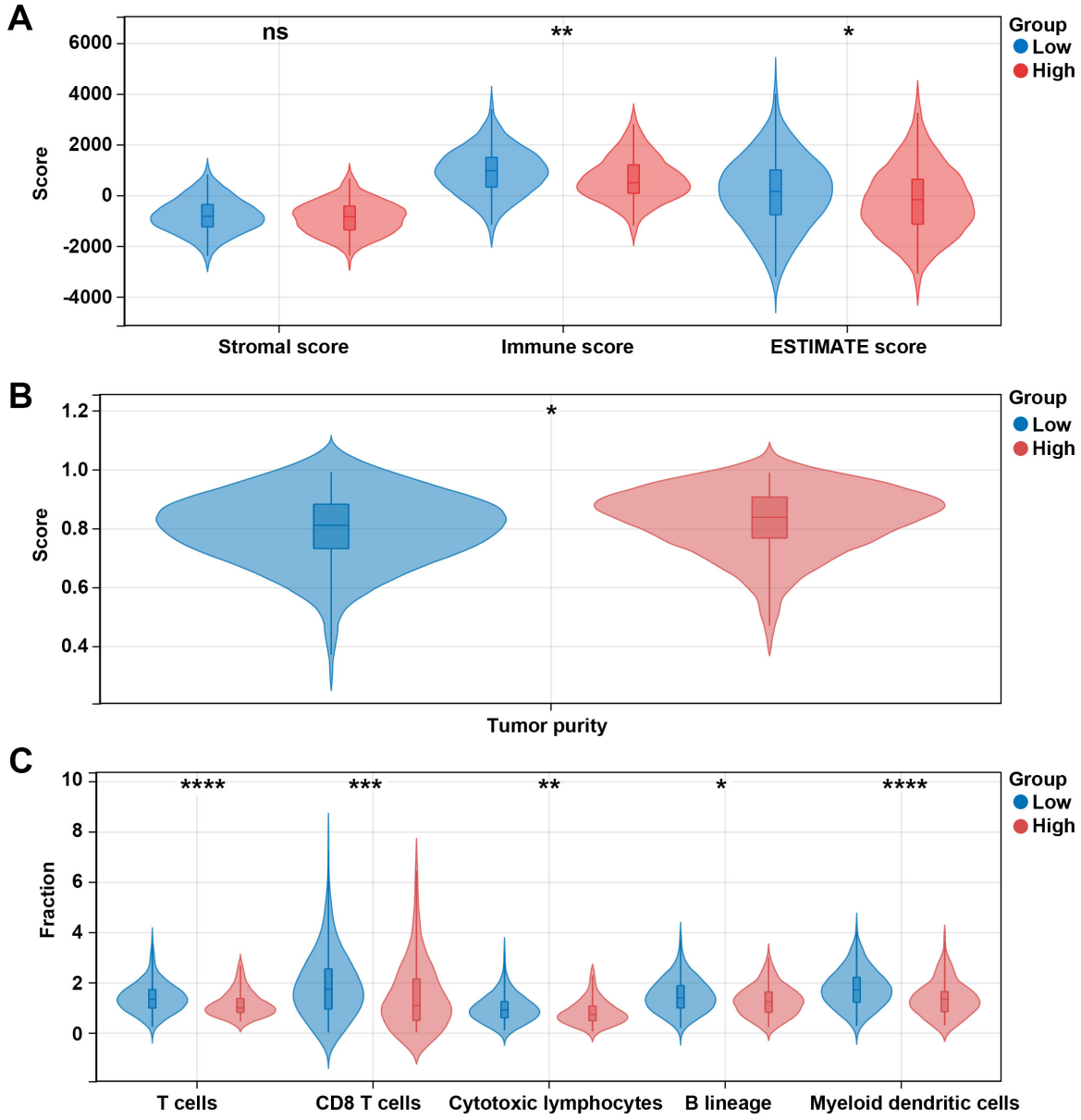

FIGURE 7
Different immune profiles between different risk groups in the TCGA dataset. **(A)** Stromal, immune, and ESTIMATE scores between the low- and high-risk groups. **(B)** Tumor purity between the low- and high-risk groups. **(C)** Cell fraction between the low- and high-risk groups. *p < 0.05, **p < 0.01, ***p < 0.001, ****p < 0.0001, ns, no significant.

conversion of acetoacetate to beta-hydroxybutyrate (30). Within the mitochondria, ketone bodies undergo oxidation via the TCA cycle, leading to the generation of acetyl-CoA and NADH. Downregulation of BDH1 is a prognostic marker in hepatocellular carcinoma (31). POLA1 encodes DNA polymerase, which facilitates DNA replication and repair, ensuring the maintenance of mitochondrial genome integrity. POLA1 has antitumor activity in inhibiting cancer cell proliferation and inducing apoptosis (32). A previous study demonstrates that POLA overexpression is associated with the poor prognosis of CC patients (33). MIR210 originates from mitochondria, its expression correlates with hypoxia gene signatures, and it could reduce the activity of proteins controlling MM (34). Nakada et al. points out that MIR210 induces energy metabolism shift from OXPHOS to glycolysis via acting on the mitochondrial inner membrane (35). MSMO1 catalyzes the demethylation of C4-methyl sterol, a critical step in cholesterol biosynthesis within mitochondria. Abnormal expression of MSMO1 would lead to CC (36). STARD3NL is involved in MM by mediating the transfer of cholesterol between membranes, potentially contributing to lipid metabolism and homeostasis within mitochondria (37). The risk score constructed using these five MMRGs exhibits good prognostic function for patients with CC. Patients within the low-risk group have longer survival time.

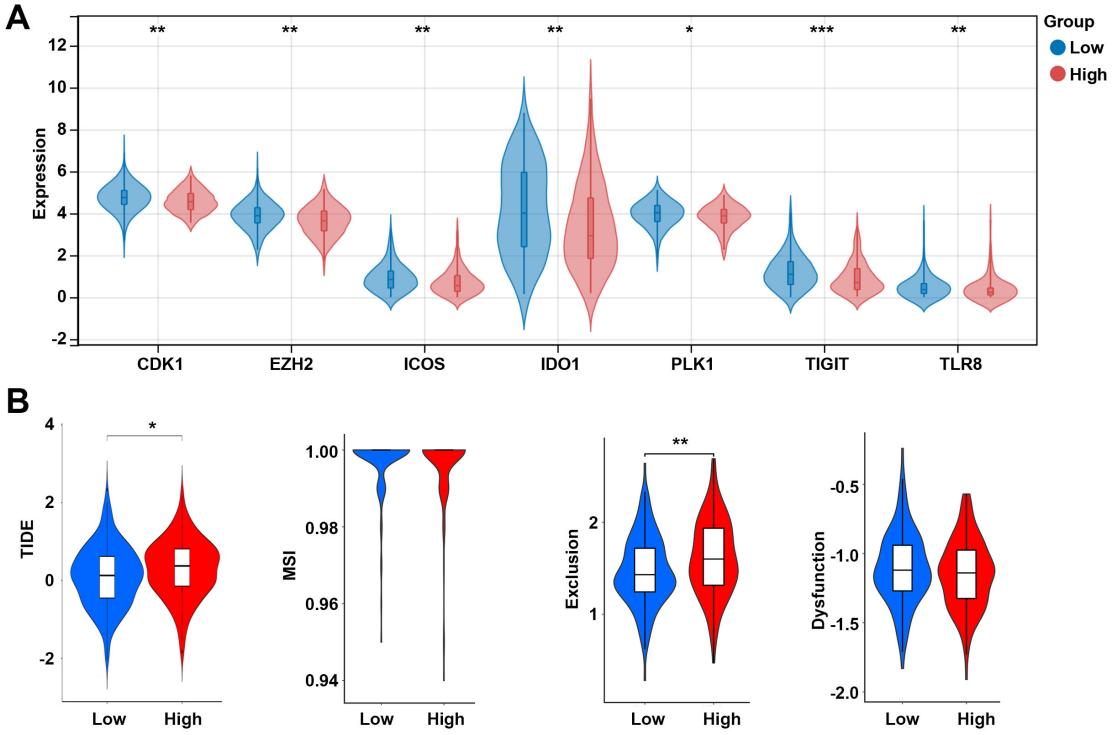

FIGURE 8
Analysis of immune checkpoints between the low- and high-risk groups. **(A)** Expression levels of immune checkpoint-related genes between the low- and high-risk groups. **(B)** TIDE score between the low- and high-risk groups. *p < 0.05, **p < 0.01, ***p < 0.001. TIDE, tumor immune dysfunction and exclusion; MSI, microsatellite instability.

Furthermore, KEGG analysis of DEGs in the normal and tumor groups was enriched for several metabolic pathways. Overexpressed genes and downregulated genes in C1 were also associated with metabolic pathways. Metabolism and immunity are usually inextricably linked. After further analyzing the function of DEGs in high- and low-risk populations, we found that these DEGs are primarily associated with the immune system, including the Th17 cell differential, IL-17 signaling pathway, and MAPK signaling pathway. Th17 cells are a subset of T-helper cells that produce IL-17, a pro-inflammatory cytokine (38). IL-17 acts on tumor cells and various components of the tumor microenvironment to promote tumor growth, angiogenesis, and metastasis (39). It can also induce the production of other pro-inflammatory cytokines and chemokines, creating a pro-tumor inflammatory environment (40). The MAPK signaling pathway is a crucial intracellular signaling cascade involved in cell proliferation, survival, and differentiation (41). Activation of MAPK signaling can occur downstream of IL-17 receptor engagement. In breast cancer, the Th17/IL-17/MAPK cascade signaling pathway plays a multifaceted role in cancer progression (42). Previous studies have indicated that MM abnormalities can influence tumor cell antigen presentation and processing, thereby aiding tumor cells in evading recognition and attack by the immune system (43). Activation of the IL-17/MAPK signaling pathway can lead to an increase in immunosuppressive cells such as regulatory T cells and myeloid-derived suppressor cells (MDSCs), thereby inhibiting the anti-tumor immune response. Additionally, activation of the IL-17/MAPK signaling pathway may result in changes in tumor cell surface antigens, making tumor cells less recognizable and susceptible to clearance by the immune system (44). Th17 and the MAPK signaling pathway have been demonstrated to play a pro-econogenic role in promoting CC (45, 46). Therefore, we hypothesize that MMRGs may enhance tumor immune evasion by modulating the IL-17/MAPK signaling pathway in cervical cancer.

Given the crucial role of the immune microenvironment in cancer progression, we further investigated differences in immune cell infiltration and immune scores among individuals at different risk groups. The results indicated that individuals at low risk had higher immune scores, and correspondingly, we observed more immune cell infiltration in the low-risk group, including T cells, CD8 T cells, cytotoxic lymphocytes, B lineage cells, and myeloid dendritic cells. These findings demonstrate the correlation between MM-related prognostic models and immune infiltration in CC. To regulate immune responses, PD-L1 was expressed in these immune cells to maintain immune homeostasis and protect the body from foreign pathogens (47). Furthermore, analysis of immune checkpoint-related genes revealed higher expression of immune checkpoints in the low-risk group, suggesting better efficacy of immune therapy in this group compared to the high-risk group. Among the identified immune checkpoint genes, TIGIT showed the most significant difference between the two groups. TIGIT is a crucial target in tumor immunotherapy, as it can prevent NK cells from releasing tumor antigens, impair dendritic cell-induced T cell priming, or inhibit CD8+ T cell-mediated killing of cancer cells

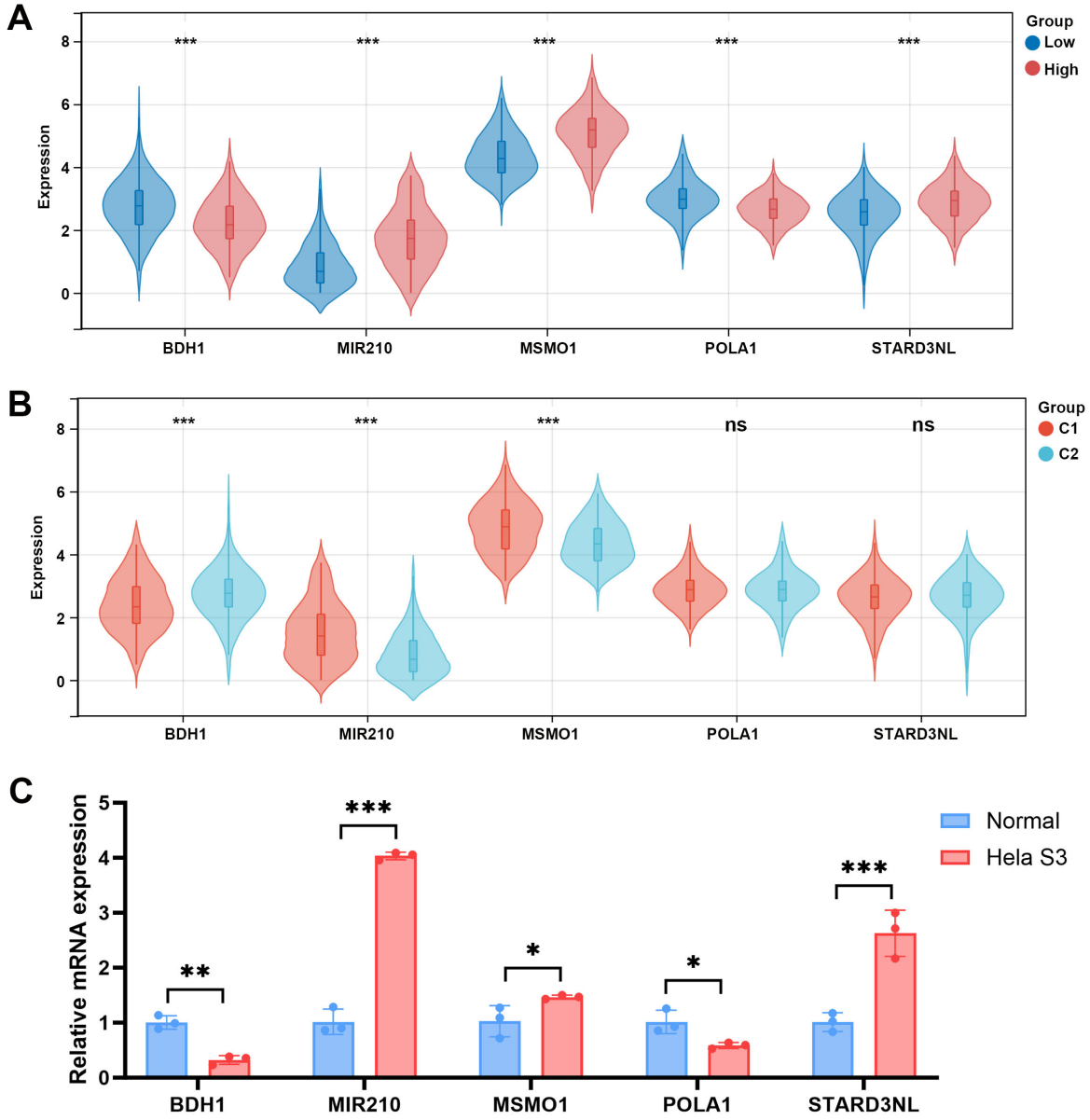

FIGURE 9
Expression levels of 5 MMRGs in different groups. **(A)** Expression levels of 5 prognostic genes in the low- and high-risk groups. **(B)** Expression levels of 5 prognostic genes in C1 and C2. **(C)** Expression levels of 5 prognostic genes in human cervical epithelial cells and CC cells. *p < 0.05, **p < 0.01, ***p < 0.001. MMRG, mitochondrial metabolism-related gene; CC, cervical cancer.

(48). This is consistent with the findings of Han et al., suggesting that TIGIT may kill cancer cells in the low-risk group by reducing dendritic cell-triggered T-cell priming (49). However, the specific mechanism of action of TIGIT in cervical cancer remains to be further elucidated. Additionally, Our results revealed that BDH1 expression is positively related to ciclosporin, a typical immunosuppressive drug with an anti-tumor effect (50). Importantly, the drug sensitivity of ciclosporin is higher in the high-risk group, indicating that CC patients have better outcomes with this drug. Research suggests that alterations in MM within cancer cells may also modulate drug sensitivity and resistance through the MAPK signaling pathway (51). Whether MM-modulated MAPK signaling influences the drug sensitivity of ciclosporin needs further research.

5 Conclusion

In conclusion, this study elucidated the significance of MM in CC progression and its interplay with the immune microenvironment. By constructing a prognostic model based on five MMRGs (BDH1, MIR210, MSMO1, POLA1, and STARD3NL) and exploring their association with immune infiltration, significant insights were gained into CC treatment. Furthermore, the study highlighted the potential

involvement of the Th17/IL-17/MAPK signaling pathway in mediating immune escape in CC, possibly influenced by MMRGs. Additionally, the analysis of immune checkpoint-related genes suggested a potential for improved efficacy of immune therapy in the low-risk group, with TIGIT emerging as a significant target. These findings underscore the intricate relationship between MM, immune regulation, and therapeutic outcomes in CC, providing valuable insights for the development of novel prognostic markers and therapeutic strategies.

Data availability statement

The raw data supporting the conclusions of this article will be made available by the authors, without undue reservation.

Ethics statement

Ethical approval was not required for the study involving humans in accordance with the local legislation and institutional requirements. Written informed consent to participate in this study was not required from the participants or the participants' legal guardians/next of kin in accordance with the national legislation and the institutional requirements.

Author contributions

QH: Conceptualization, Data curation, Formal analysis, Writing – original draft. Y-FX: Investigation, Methodology, Writing – original draft. H-PL: Data curation, Methodology, Writing – original draft. TZ: Formal analysis, Supervision, Writing – original draft, Writing – review & editing.

Funding

The author(s) declare that no financial support was received for the research and/or publication of this article.

Conflict of interest

The authors declare that the research was conducted in the absence of any commercial or financial relationships that could be construed as a potential conflict of interest.

Generative AI statement

The author(s) declare that no Generative AI was used in the creation of this manuscript.

Publisher's note

All claims expressed in this article are solely those of the authors and do not necessarily represent those of their affiliated organizations, or those of the publisher, the editors and the reviewers. Any product that may be evaluated in this article, or claim that may be made by its manufacturer, is not guaranteed or endorsed by the publisher.

Supplementary material

The Supplementary Material for this article can be found online at: https://www.frontiersin.org/articles/10.3389/fonc.2025.1522910/full#supplementary-material.

SUPPLEMENTARY FIGURE 1
Correlation between predicted drugs and prognostic genes. **(A)** Correlation of BDH1 with ciclosporin, Raloxifene, and Tamoxifen. **(B)** Correlation of MIR210 with Cediranib, ergenyl, and Motesanib. **(C)** Correlation of MSMO1 with Amiodarone, uridin, and Zoledronate. **(D)** Correlation of POLA1 with Methylprednisolone, PX-316, and ZM-336372. **(E)** Correlation of STARD3NL with JNJ-38877605, Lovastatin, and Fluorouracil.

SUPPLEMENTARY FIGURE 2
Drug sensitivity between different risk groups. *p < 0.05, **p < 0.01, ns, no significant.

References

1. Jha AK, Mithun S, Sherkhane UB, Jaiswar V, Osong B, Purandare N, et al. Systematic review and meta-analysis of prediction models used in cervical cancer. *Artif Intell Med.* (2023) 139:102549. doi: 10.1016/j.artmed.2023.102549

2. Ming C, Bai X, Zhao L, Yu D, Wang X, Wu Y. RPL24 as a potential prognostic biomarker for cervical cancer treated by Cisplatin and concurrent chemoradiotherapy. *Front Oncol.* (2023) 13:1131803. doi: 10.3389/fonc.2023.1131803

3. Schubert M, Bauerschlag DO, Muallem MZ, Maass N, Alkatout I. Challenges in the diagnosis and individualized treatment of cervical cancer. *Medicina (Kaunas).* (2023) 59:925. doi: 10.3390/medicina59050925

4. Han S, Wang S, Lv X, Li D, Feng Y. Ferroptosis-related genes in cervical cancer as biomarkers for predicting the prognosis of gynecological tumors. *Front Mol Biosci.* (2023) 10:1188027. doi: 10.3389/fmolb.2023.1188027

5. Li C, Cang W, Gu Y, Chen L, Xiang Y. The anti-PD-1 era of cervical cancer: achievement, opportunity, and challenge. *Front Immunol.* (2023) 14:1195476. doi: 10.3389/fimmu.2023.1195476

6. Lv X, Jia Y, Li J, Deng S, Yuan E. The construction of a prognostic model of cervical cancer based on four immune-related LncRNAs and an exploration of the correlations between the model and oxidative stress. *Front Pharmacol.* (2023) 14:1234181. doi: 10.3389/fphar.2023.1234181

7. Wang SF, Tseng LM, Lee HC. Role of mitochondrial alterations in human cancer progression and cancer immunity. *J BioMed Sci.* (2023) 30:61. doi: 10.1186/s12929-023-00956-w

8. Huang L, Wei B, Zhao Y, Gong X, Chen L. DYNLT1 promotes mitochondrial metabolism to fuel breast cancer development by inhibiting ubiquitination degradation of VDAC1. *Mol Med.* (2023) 29:72. doi: 10.1186/s10020-023-00663-0

9. Foo BJ, Eu JQ, Hirpara JL, Pervaiz S. Interplay between mitochondrial metabolism and cellular redox state dictates cancer cell survival. *Oxid Med Cell Longev.* (2021) 2021:1341604. doi: 10.1155/2021/1341604

10. Kubicka A, Matczak K, Labieniec-Watala M. More than meets the eye regarding cancer metabolism. *Int J Mol Sci.* (2021) 22:9507. doi: 10.3390/ijms22179507

11. Dong L, Gopalan V, Holland O, Neuzil J. Mitocans revisited: mitochondrial targeting as efficient anti-cancer therapy. *Int J Mol Sci*. (2020) 21:7941. doi: 10.3390/ijms21217941

12. Passaniti A, Kim MS, Polster BM, Shapiro P. Targeting mitochondrial metabolism for metastatic cancer therapy. *Mol Carcinog*. (2022) 61:827–38. doi: 10.1002/mc.23436

13. Dabravolski SA, Nikiforov NG, Zhuravlev AD, Orekhov NA, Mikhaleva LM, Orekhov AN. The role of altered mitochondrial metabolism in thyroid cancer development and mitochondria-targeted thyroid cancer treatment. *Int J Mol Sci*. (2021) 23:460. doi: 10.3390/ijms23010460

14. Sainero-Alcolado L, Liano-Pons J, Ruiz-Perez MV, Arsenian-Henriksson M. Targeting mitochondrial metabolism for precision medicine in cancer. *Cell Death Differ*. (2022) 29:1304–17. doi: 10.1038/s41418-022-01022-y

15. Li W, Zhang L. Rewiring mitochondrial metabolism for CD8(+) T cell memory formation and effective cancer immunotherapy. *Front Immunol*. (2020) 11:1834. doi: 10.3389/fimmu.2020.01834

16. Shrestha R, Johnson E, Byrne FL. Exploring the therapeutic potential of mitochondrial uncouplers in cancer. *Mol Metab*. (2021) 51:101222. doi: 10.1016/j.molmet.2021.101222

17. Mamouni K, Kallifatidis G, Lokeshwar BL. Targeting mitochondrial metabolism in prostate cancer with triterpenoids. *Int J Mol Sci*. (2021) 22:2466. doi: 10.3390/ijms22052466

18. Paragliola RM, Torino F, Papi G, Locantore P, Pontecorvi A, Corsello SM. Role of mitotane in adrenocortical carcinoma - review and state of the art. *Eur Endocrinol*. (2018) 14:62–6. doi: 10.17925/EE.2018.14.2.62

19. Liu Y, Yu S, Xing X, Qiao J, Yin Y, Wang J, et al. Ginsenoside Rh2 stimulates the production of mitochondrial reactive oxygen species and induces apoptosis of cervical cancer cells by inhibiting mitochondrial electron transfer chain complex. *Mol Med Rep*. (2021) 24:873. doi: 10.3892/mmr.2021.12513

20. Zhang K, Ji X, Song Z, Song W, Huang Q, Yu T, et al. Butyrate inhibits the mitochondrial complex Iota to mediate mitochondria-dependent apoptosis of cervical cancer cells. *BMC Complement Med Ther*. (2023) 23:212. doi: 10.1186/s12906-023-04043-3

21. Zhang Y, Yao Y, Chen P, Liu Y, Zhang H, Liu H, et al. Checkpoint therapeutic target database (CKTTD): the first comprehensive database for checkpoint targets and their modulators in cancer immunotherapy. *J Immunother Cancer*. (2020) 8:e001247. doi: 10.1136/jitc-2020-001247

22. Shankavaram UT, Varma S, Kane D, Sunshine M, Chary KK, Reinhold WC, et al. CellMiner: a relational database and query tool for the NCI-60 cancer cell lines. *BMC Genomics*. (2009) 10:277. doi: 10.1186/1471-2164-10-277

23. Vasan K, Werner M, Chandel NS. Mitochondrial metabolism as a target for cancer therapy. *Cell Metab*. (2020) 32:341–52. doi: 10.1016/j.cmet.2020.06.019

24. Boese AC, Kang S. Mitochondrial metabolism-mediated redox regulation in cancer progression. *Redox Biol*. (2021) 42:101870. doi: 10.1016/j.redox.2021.101870

25. Oliveira GL, Coelho AR, Marques R, Oliveira PJ. Cancer cell metabolism: Rewiring the mitochondrial hub. *Biochim Biophys Acta Mol Basis Dis*. (2021) 1867:166016. doi: 10.1016/j.bbadis.2020.166016

26. Sun L, Wan A, Zhou Z, Chen D, Liang H, Liu C, et al. RNA-binding protein RALY reprogrammes mitochondrial metabolism via mediating miRNA processing in colorectal cancer. *Gut*. (2021) 70:1698–712. doi: 10.1136/gutjnl-2020-320652

27. Lin Y, Huang Z, Zhang B, Yang H, Yang S. Construction and analysis of a mitochondrial metabolism-related prognostic model for breast cancer to evaluate survival and immunotherapy. *J Membr Biol*. (2024) 257:63–78. doi: 10.1007/s00232-024-00308-1

28. Yang S, Liu L, Liu X, Li X, Zheng Y, Ren Z, et al. The mitochondrial energy metabolism pathway-related signature predicts prognosis and indicates immune microenvironment infiltration in osteosarcoma. *Med (Baltimore)*. (2023) 102:e36046. doi: 10.1097/MD.0000000000036046

29. Fu Y, Huang Z, Huang J, Xiong J, Liu H, Wan X. Metabolism-related gene vaccines and immune infiltration in ovarian cancer: A novel risk score model of machine learning. *J Gene Med*. (2024) 26:e3568. doi: 10.1002/jgm.3568

30. Zhang Z, Bi X, Lian X, Niu Z. BDH1 promotes lung cancer cell proliferation and metastases by PARP1-mediated autophagy. *J Cell Mol Med*. (2023) 27:939–49. doi: 10.1111/jcmm.17700

31. Luo W, Wu S, Zhang F, Chen X, Ma Y, Mo Y. Decreased expression of 3-hydroxybutyrate dehydrogenase 1 is a prognostic marker and promotes tumor progression in hepatocellular carcinoma. *Pathol Res Pract*. (2022) 238:154111. doi: 10.1016/j.prp.2022.154111

32. Han T, Goralski M, Capota E, Padrick SB, Kim J, Xie Y, et al. The antitumor toxin CD437 is a direct inhibitor of DNA polymerase alpha. *Nat Chem Biol*. (2016) 12:511–5. doi: 10.1038/nchembio.2082

33. Yu L, Wei M, Li F. Longitudinal analysis of gene expression changes during cervical carcinogenesis reveals potential therapeutic targets. *Evol Bioinform Online*. (2020) 16:1176934320920574. doi: 10.1177/1176934320920574

34. Chan SY, Zhang YY, Hemann C, Mahoney CE, Zweier JL, Loscalzo J. MicroRNA-210 controls mitochondrial metabolism during hypoxia by repressing the iron-sulfur cluster assembly proteins ISCU1/2. *Cell Metab*. (2009) 10:273–84. doi: 10.1016/j.cmet.2009.08.015

35. Nakada C, Hijiya N, Tsukamoto Y, Yano S, Kai T, Uchida T, et al. A transgenic mouse expressing miR-210 in proximal tubule cells shows mitochondrial alteration: possible association of miR-210 with a shift in energy metabolism. *J Pathol*. (2020) 251:12–25. doi: 10.1002/path.5394

36. Zheng G, Wang Z, Fan Y, Wang T, Zhang L, Wang M, et al. The clinical significance and immunization of MSMO1 in cervical squamous cell carcinoma based on bioinformatics analysis. *Front Genet*. (2021) 12:705851. doi: 10.3389/fgene.2021.705851

37. Xu Y, Bao X, Chen X, Wu P, Chen S, Zhang B, et al. STARD3NL inhibits the osteogenic differentiation by inactivating the Wnt/beta-catenin pathway via binding to Annexin A2 in osteoporosis. *J Cell Mol Med*. (2022) 26:1643–55. doi: 10.1111/jcmm.17205

38. Yasuda K, Takeuchi Y, Hirota K. The pathogenicity of Th17 cells in autoimmune diseases. *Semin Immunopathol*. (2019) 41:283–97. doi: 10.1007/s00281-019-00733-8

39. Nalbant A. IL-17, IL-21, and IL-22 cytokines of T helper 17 cells in cancer. *J Interferon Cytokine Res*. (2019) 39:56–60. doi: 10.1089/jir.2018.0057

40. Salazar Y, Zheng X, Brunn D, Raifer H, Picard F, Zhang Y, et al. Microenvironmental Th9 and Th17 lymphocytes induce metastatic spreading in lung cancer. *J Clin Invest*. (2020) 130:3560–75. doi: 10.1172/JCI124037

41. Wei J, Liu R, Hu X, Liang T, Zhou Z, Huang Z. MAPK signaling pathway-targeted marine compounds in cancer therapy. *J Cancer Res Clin Oncol*. (2021) 147:3–22. doi: 10.1007/s00432-020-03460-y

42. Shibabaw T, Teferi B, Ayelign B. The role of Th-17 cells and IL-17 in the metastatic spread of breast cancer: As a means of prognosis and therapeutic target. *Front Immunol*. (2023) 14:1094823. doi: 10.3389/fimmu.2023.1094823

43. Guo Y, Luo C, Sun Y, Guo W, Zhang R, Zhang X, et al. Inhibition of mitochondrial fusion via SIRT1/PDK2/PARL axis breaks mitochondrial metabolic plasticity and sensitizes cancer cells to glucose restriction therapy. *BioMed Pharmacother*. (2023) 166:115342. doi: 10.1016/j.biopha.2023.115342

44. Lin Z, Huang Q, Liu J, Wang H, Zhang X, Zhu Z, et al. Interleukin-17D promotes lung cancer progression by inducing tumor-associated macrophage infiltration via the p38 MAPK signaling pathway. *Aging (Albany NY)*. (2022) 14:6149–68. doi: 10.18632/aging.204208

45. Liu Y, Guo QF, Chen JL, Li XR, Hou F, Liu XY, et al. Correlations between alterations of T-helper 17 cells and treatment efficacy after concurrent radiochemotherapy in locally advanced cervical cancer (stage IIB-IIIB): a 3-year prospective study. *Chin Med J (Engl)*. (2021) 134:954–62. doi: 10.1097/CM9.0000000000001475

46. Sun HN, Xie DP, Ren CX, Guo XY, Zhang HN, Xiao WQ, et al. Ethyl beta-carboline-3-carboxylate increases cervical cancer cell apoptosis through ROS-p38 MAPK signaling pathway. *In Vivo*. (2022) 36:1178–87. doi: 10.21873/invivo.12817

47. Sun C, Mezzadra R, Schumacher TN. Regulation and function of the PD-L1 checkpoint. *Immunity*. (2018) 48:434–52. doi: 10.1016/j.immuni.2018.03.014

48. Liang JY, Wang DS, Lin HC, Chen XX, Yang H, Zheng Y, et al. A novel ferroptosis-related gene signature for overall survival prediction in patients with hepatocellular carcinoma. *Int J Biol Sci*. (2020) 16:2430–41. doi: 10.7150/ijbs.45050

49. Ge X, Su Z, Wang Y, Zhao X, Hou K, Zheng S, et al. Identifying the intervention mechanisms of polydatin in hyperuricemia model rats by using UHPLC-Q-Exactive Orbitrap mass spectroscopy metabonomic approach. *Front Nutr*. (2023) 10:1117460. doi: 10.3389/fnut.2023.1117460

50. Wu PJ, Hsin IL, Hung WL, Lee MS, Wang PH, Ko JL. Combination treatment with cyclosporin A and arsenic trioxide induce synergistic cell death via non-apoptotic pathway in uterine cervical cancer cells. *Chem Biol Interact*. (2022) 368:110177. doi: 10.1016/j.cbi.2022.110177

51. Vu MH, Iswanto ABB, Lee J, Kim JY. The role of plasmodesmata-associated receptor in plant development and environmental response. *Plants (Basel)*. (2020) 9:216. doi: 10.3390/plants9020216

frontiers | Frontiers in Oncology

TYPE Original Research
PUBLISHED 04 April 2025
DOI 10.3389/fonc.2025.1552506

OPEN ACCESS

EDITED BY
Balkrishna Chaube,
Indian Institute of Technology Dharwad, India

REVIEWED BY
Ashish Toshniwal,
The University of Utah, United States
Ishan Pandey,
Moti Lal Nehru Medical College, India
Meghna Saxena,
University of Minnesota Medical Center, United States

*CORRESPONDENCE
Stefano Indraccolo
stefano.indraccolo@unipd.it

RECEIVED 28 December 2024
ACCEPTED 17 March 2025
PUBLISHED 04 April 2025

CITATION
Dal Maso A, Ferrarini F, Esposito G, Minuzzo SA, Puggia AM, Pezzuto F, Zulato E, Bao LC, De Nuzzo M, Ferro A, Frega S, Pasello G, Calabrese F, Fassan M, Rea F, Guarneri V, Indraccolo S and Bonanno L (2025) Liver kinase B1 expression is associated with improved prognosis and tumor immune microenvironment features in small cell lung cancer. *Front. Oncol.* 15:1552506. doi: 10.3389/fonc.2025.1552506

Liver kinase B1 expression is associated with improved prognosis and tumor immune microenvironment features in small cell lung cancer

Alessandro Dal Maso[1], Federica Ferrarini[2], Giovanni Esposito[3], Sonia Anna Minuzzo[4], Anna Maria Puggia[5], Federica Pezzuto[6], Elisabetta Zulato[2], Loc Carlo Bao[1,4], Mattia De Nuzzo[1,4], Alessandra Ferro[1], Stefano Frega[1], Giulia Pasello[1,4], Fiorella Calabrese[6], Matteo Fassan[7,8], Federico Rea[6,9], Valentina Guarneri[1,4], Stefano Indraccolo[2,4]* and Laura Bonanno[1,4]

[1]Medical Oncology 2, Veneto Institute of Oncology IOV - IRCCS, Padova, Italy, [2]Basic and Translational Oncology, Veneto Institute of Oncology IOV - IRCCS, Padova, Italy, [3]Immunology and Molecular Oncology Diagnostics, Veneto Institute of Oncology IOV - IRCCS, Padova, Italy, [4]Department of Surgery, Oncology and Gastroenterology, University of Padova, Padova, Italy, [5]Anatomy and Pathological Histology, Veneto Institute of Oncology IOV - IRCCS, Castelfranco Veneto, Italy, [6]Department of Cardiac, Thoracic, Vascular Sciences and Public Health, University of Padova, Padova, Italy, [7]Department of Medicine, University of Padua, Padua, Italy, [8]Veneto Institute of Oncology IOV - IRCCS, Padua, Italy, [9]Thoracic Surgery Unit, Padova University Hospital, Padova, Italy

Background: Small cell lung cancer (SCLC) is characterized by early metastatic potential and poor prognosis. Liver kinase B1 (LKB1) is a tumor suppressor and a cell metabolism regulator. LKB1 downregulation has been associated with a cold tumor immune microenvironment (TIME). We aimed to analyze the role of LKB1 in SCLC in relation to its association with overall survival (OS) and TIME components.

Methods: We retrospectively evaluated SCLC patients consecutively treated at our institution from 1996 to 2020 with available tissue. LKB1, PD-L1 on tumor cells and on tumor immune-infiltrating cells, CD8, and FOXP3 were evaluated by immunohistochemistry (IHC), categorized according to predefined cutoffs. The primary endpoint was the description of LKB1 expression, and the secondary endpoints were the association with prognosis and TIME features.

Results: Tissue samples of 138 out of 481 SCLCs were adequate for molecular analyses. Eighty patients had limited stage (LS) at diagnosis and 58 had extended stage (ES). The median LKB1 IHC score was 4. Patients with IHC score >4 (n = 67) were classified as LKB1-positive. The probability of LKB1 positivity was higher in LS [odds ratio 2.78, 95% confidence interval (95% CI) 1.18–7.14]. At the data cutoff (2 January 2024), 123 patients died. The median OS (mOS) was 14.0 months (95% CI 11.5–19.4). mOS was significantly longer in patients with LKB1-positive expression [32.4 months (95% CI 13.6–62.4) vs. 11.2 months (95% CI 8.7–14.7); p < 0.001]. At multivariate analysis, positive LKB1 expression, LS, and no weight

loss at diagnosis were confirmed as independent positive prognostic factors. TIME features were evaluated in 70 patients. Unexpectedly, LKB1-negative samples were more likely to show $CD8^+$ tumor-infiltrating lymphocytes (TILs; $p = 0.013$). No association with PD-L1 expression nor the presence of $FOXP3^+$ TILs was found.

Conclusion: LKB1 expression is a potential positive prognostic marker in SCLC. In this series, LKB1 expression was negatively associated with the presence of $CD8^+$ TILs.

KEYWORDS

small cell lung cancer, liver kinase B1, serine/threonine kinase 11, immunohistochemistry, overall survival, tumor immune microenvironment

1 Introduction

Lung cancer represents the leading cause of cancer-related deaths worldwide (1). Small cell lung cancer (SCLC) accounts for nearly 15% of lung cancer diagnoses and is a high-grade neuroendocrine cancer, associated with a dismal prognosis (2). Limited stage (LS) SCLC is defined as a tumor confined to one hemithorax and regional lymph nodes, eligible for curative intent treatment. Radical intent radiotherapy (RT) and concurrent chemotherapy (ChT) are the standard of care for LS, although, in selected cases, surgery followed by adjuvant platinum and etoposide (PE) is considered, in the absence of lymph node involvement at clinical staging (2, 3). The upfront treatment of extended stage (ES) SCLC has been unchanged for decades and consisted of PE ChT (2, 3). Recently, several randomized phase III trials demonstrated the superiority of first-line chemoimmunotherapy, showing a similar rate of overall survival (OS) improvement versus standard ChT alone (3–10). A comparable benefit was shown in real-world studies including patients with relevant comorbidities, older age, and high-symptom burden (11, 12). Despite a statistically significant difference, clinical outcome improvement is only modest and only approximately 15% are alive after 3 years of chemoimmunotherapy treatment (5, 7, 13).

The study of the molecular features of SCLC is one key element in order to finally improve clinical outcome (14). Recently, transcriptomic profiling has led to a new molecular classification of SCLC, based on the deregulation of key cellular pathways. No clear prognostic impact was found for the classification, whereas an inflamed subtype, characterized by overexpression of human leukocyte antigens, immune checkpoints, and cytokines, was suggested as a potential positive predictive factor for chemoimmunotherapy (15). Conversely, the SCLC-N subtype was characterized by overexpression of the *NEUROD1* transcription factor, and SCLC-N cell lines were highly sensitive to multiple aurora kinase (AURK) inhibitors (15). AURK is a serine/threonine kinase localized to the centrosome, which is crucial during the cell cycle to guarantee the right chromosome segregation, but has also tumor-promoting roles unrelated to mitosis (16–19). AURK has been involved in phosphorylating liver kinase B1 (LKB1, also known as serine/threonine kinase 11, STK11) resulting in the suppression of the LKB1/adenosine monophosphate-activated protein kinase (AMPK) signaling pathway and the proliferation, invasion, and migration of non-small cell lung cancer (NSCLC) cells (20).

LKB1 is a tumor suppressor and cell metabolism regulator and has been shown to modulate tumor immune microenvironment (TIME) features in NSCLC (21–28). *LKB1* alterations have been described in approximately 30% of NSCLCs, including nonsense mutations, frameshift mutations, large exonic deletions, and intronic mutations in conserved splice sites (29, 30). These mutations translate into either a truncated, inactive protein or the absence of the protein. Epigenetic inactivation has also been demonstrated, with promoter hypermethylation detected in up to 13% of the specimens (31, 32).

Few data are available for *LKB1* alterations in SCLC and mostly concerning *LKB1* mutations (33–36). Based on these premises, we aimed to describe LKB1 expression in SCLC and investigate its potential prognostic role and association with TIME features.

2 Materials and methods

2.1 Study patients and endpoints

We retrospectively evaluated all SCLC cases consecutively treated at Veneto Institute of Oncology IOV - IRCCS with available tissue, from 1996 to 2020. The inclusion criteria were pathological diagnosis of SCLC, availability of clinical data and adequate follow-up, and availability of pathological samples.

Histological diagnosis was obtained by formalin-fixed paraffin-embedded (FFPE) samples that were collected before starting the primary treatment. Staging included brain, neck, chest, and

abdomen computed tomography (CT) scan with iodine contrast, bone scan and, in selected cases, brain magnetic resonance imaging and/or total body ^{18}F-fluorodeoxyglucose positron emission tomography/CT scans.

A multidisciplinary team, including dedicated medical oncologists, radiation oncologists, thoracic surgeons, pneumologists, a radiologist, and a nuclear medicine physician evaluated all the patients and decided on the treatment plan, according to guidelines. Patients with limited stage disease received radical chemoradiotherapy and, in selected cases, surgery followed by adjuvant ChT. ChT consisted of four to six PE cycles, while 3D conformal RT was started as early as possible. After upfront surgery, four cycles of adjuvant PE were administered, when clinically feasible. If the patient responded to radical treatment, prophylactic cranial irradiation was discussed with the patient. Extended SCLC cases received upfront ChT with PE (up to six cycles) and palliative RT was administered when indicated. ChT and RT were administered at Veneto Institute of Oncology IOV - IRCCS. Surgery was carried out at the Thoracic Surgery Unit of Padova University Hospital and histological diagnosis at the Pathology Unit of Padova University Hospital.

Clinical variables collected from electronic medical records were sex, age at diagnosis, smoking status, Eastern Cooperative Oncology Group (ECOG) performance status (PS) at diagnosis, presence of symptoms at diagnosis, presence of weight loss at diagnosis, stage at diagnosis, central nervous system (CNS) metastases at diagnosis, and primary treatment.

The Ethics Committee of Veneto Institute of Oncology IOV - IRCCS in Padova evaluated and approved the study and informed consent that was required, whenever feasible, for the collection, analysis, and publication of data, according to the Helsinki Declaration and Italian Data Protection Authority dispositions (approval number: IOV-MICRO-2017).

The primary endpoint of the study was the description of LKB1 expression by immunohistochemistry (IHC), and the secondary endpoints were the association with prognosis and TIME features.

2.2 Immunohistochemistry

Four-micrometer-thick FFPE tissue slices were used for IHC testing. IHC staining was performed automatically using the BOND RX system (Leica Biosystems, Nussloch, Germany).

The primary antibodies were as follows: Ley 37D/G6 (Santa Cruz Biotechnology, Dallas, TX, USA) for LKB1, C8/144B clone (DAKO, Carpinteria, CA, USA) for cluster of differentiation 8 (CD8), 236A/E7 clone (Abcam, Cambridge, UK) for forkhead box P3 (FOXP3), and 22C3 clone (DAKO, Carpinteria, CA, USA) for programmed death-ligand 1 (PD-L1). The semiquantitative score for LKB1 expression was calculated: the proportion of cell staining was scored 1 to 6 (0%–4%: 1, 5%–20%: 2, 21%–40%: 3, 41%–60%: 4, 61%–80%: 5, 81%–100%: 6), whereas intensity was scored 0 to 3+. The two scores were multiplied to obtain the final score (ranging from 0 to 18). The median LKB1 score was calculated and chosen as the cutoff for LKB1 expression positivity (37, 38).

TILs were described using semiquantitative criteria: absent or sporadic (0), moderate (1+), abundant (2+), and highly abundant (3+). A specimen was considered negative for $CD8^+$ TILs presence when scoring 0–2+ and positive when scoring 3+, whereas a case was considered negative for $FOXP3^+$ TILs when IHC scored 0 and positive when IHC scored 1–3+ (39). PD-L1 expression in TC and TIIC was considered negative when 0% and positive when ≥1% (39).

2.3 Statistical analysis

Qualitative clinical and biological variables were described with counts and proportions, whereas quantitative variables were described with median and range. Associations between qualitative variables were evaluated using chi-squared or Fisher exact test, as appropriate; odds ratios (ORs) were calculated along with the 95% confidence interval (95% CI), and multivariate analysis was performed with logistic regression. Kaplan–Meier survival curves were built to estimate median OS with 95% CI, and the log-rank test was used to compare survival curves. Cox regression analysis was carried out to estimate univariate and multivariate hazard ratios (HRs) for death, along with 95% CI. The significance level was set at $p < 0.05$. Statistical analysis was performed with the R software, version 4.3.0 (The R Foundation, Vienna, Austria).

3 Results

3.1 Study population

All pathological samples were revised by an experienced pathologist, and 138 out of 481 cases were judged adequate for molecular testing and included in the analysis. The clinical features of the study population considered for analysis are summarized in Table 1. Eighty-seven of 138 patients (63.0%) were men and 51 (37.0%) were women, and the median age at diagnosis was 68 years (range: 47–82). One hundred and thirty-four patients (97.1%) were smokers, 125 (90.6%) had ECOG performance status (PS) ≤1, 99 (71.7%) had any symptom at diagnosis, and 24 (17.4%) had weight loss at diagnosis.

Eighty (58.0%) patients had LS disease at diagnosis: 31 (22.5%) were treated with radical RT concomitantly with ChT and 49 (35.5%) received surgery followed by adjuvant ChT. Fifty-eight (42.0%) patients had ES disease and received chemotherapy. Thirteen of 58 (22.4%) patients with ES had CNS metastases at diagnosis.

3.2 LKB1 expression and association with clinical features

LKB1 IHC was performed in all cases considered adequate for molecular analyses. In our series, the staining for LKB1 was

10.3389/fonc.2025.1552506

TABLE 1 Study population.

Variable	*n* = 138
Sex	
Male	87 (63.0%)
Female	51 (37.0%)
Age	
Median (range)	68 (47–82)
<70	81 (58.7%)
≥70	57 (41.3%)
Smoker	
Yes (current/former)	134 (97.1%)
No	4 (2.9%)
ECOG PS	
≤1	125 (90.6%)
>1	13 (9.4%)
Symptoms at diagnosis	
Yes	99 (71.7%)
No	39 (28.3%)
Weight loss at diagnosis	
Yes	24 (17.4%)
No	114 (82.6%)
Stage at diagnosis	
Limited	80 (58.0%)
Extended	58 (42.0%)
CNS metastases at diagnosis	13 (22.4%)
Treatment	
Surgery followed by adjuvant ChT	49 (35.5%)
Concurrent ChT-RT	31 (22.5%)
Palliative ChT	58 (42.0%)

ECOG PS, Eastern Cooperative Oncology Group performance status; CNS, central nervous system; ChT, chemotherapy; RT, radiotherapy.

localized exclusively in the cytoplasm of tumor cells, with varying intensities observed (Figure 1). The median LKB1 IHC score was 4 (range: 0–18; first quartile: 0, third quartile: 10). The median score was chosen as a positivity cutoff for LKB1 expression: 67 (48.5%) cases scored >4 and were considered positive, whereas 71 (51.5%) cases scored ≤4 and were considered negative.

We evaluated the association between LKB1 expression and clinical features, i.e., sex, age at diagnosis, smoking status, PS at diagnosis, symptoms at diagnosis, weight loss at diagnosis, and stage at diagnosis (Table 2). At univariate analysis, LKB1 expression was significantly correlated with PS ≤1 and LS disease. LKB1 expression was positive in 47 out of 80 (58.8%) patients with limited SCLC and in 20 out of 58 (34.5%) patients with extended SCLC. Multivariate analysis confirmed a significant positive association of LKB1 expression only with LS disease (OR 2.78, 95% CI 1.18–7.14, $p = 0.023$) (Table 2).

3.3 LKB1 expression and association with prognosis

At the data cutoff (2 January 2024), 123 patients (89.1%) had a death event. The median OS of the study population was 14.0 months (95% CI 11.5–19.4, Figure 2).

At univariate analysis, PS >1, weight loss, symptoms at diagnosis, female sex, and ES disease were significantly correlated to a worse prognosis (Table 3). Positive LKB1 expression was significantly associated with better prognosis: median OS was significantly longer in patients with LKB1 expression >4 (32.4 months, 95% CI 13.6–62.4 vs. 11.2 months, 95% CI 8.7–14.7, $p < 0.001$) (Figure 2).

At multivariate analysis, positive LKB1 expression, LS at diagnosis, and the absence of weight loss at diagnosis were confirmed as independent positive prognostic factors (Table 3).

3.4 TIME subset: clinical features and molecular results

We evaluated TIME features in 20 of 138 cases (TIME subset), due to the limited availability of the specimens. In this subset, 48 (68.6%) patients were men and 22 (31.4%) were women, and the median age at diagnosis was 68 years (range: 47–81). Sixty-seven (95.7%) patients were smokers, all had PS ≤1, 47 (67.1%) had any symptom at diagnosis, and 10 (14.3%) had weight loss at diagnosis. Fifty-four (77.1%) patients were diagnosed with LS disease, of which 45 (64.3%) were treated with surgery and 9 (12.9%) with chemoradiotherapy; 16 patients (22.9%) had ES at diagnosis and were administered ChT (Supplementary Table S1).

TIME features were investigated by IHC. PD-L1 expression on TCs was positive in 23 out of 70 cases (32.9%), whereas PD-L1 expression on TIIC was positive in 35 cases (50.0%). Nine (12.9%) cases were deemed positive (3+) for $CD8^+$ TIL presence, and 54 cases (77.1%) were positive (1–3+) for $FOXP3^+$ TILs (Supplementary Table S2).

We investigated the association between TIME features and clinical features. No TIME feature significantly correlated with sex, age, smoking status, PS, symptoms at diagnosis, weight loss, or stage at diagnosis (Supplementary Table S3).

We further explored the association between LKB1 expression and TIME features. A significant negative association was found between LKB1 expression and the presence of $CD8^+$ TILs (OR 0.14, 95% CI 0.03–0.63, $p = 0.013$). No association was found between LKB1 expression and PD-L1 expression or the presence of $FOXP3^+$ TILs (Table 4).

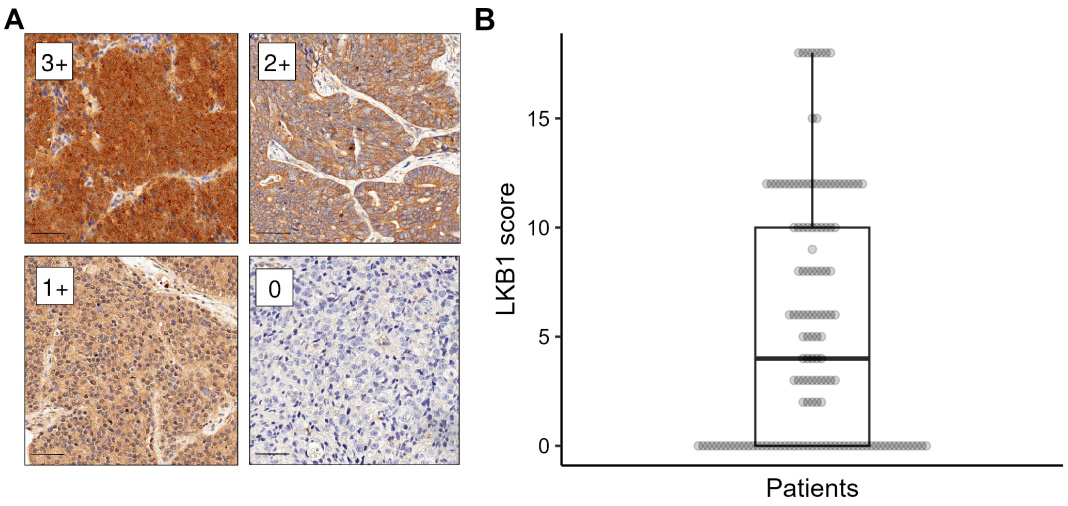

FIGURE 1
LKB1 immunohistochemistry (IHC). **(A)** Different levels of LKB1 IHC staining intensity (labeled as 0–3+) magnified at ×200, scale bar 50 μm. **(B)** Distribution of LKB1 IHC expression score in the study population.

At the data cutoff, 64 (91.4%) of 70 patients in the TIME subset had a death event. In the TIME subset, the median OS was 32.4 months (95% CI 16.3–62.4) (Supplementary Figure S1). At univariate analysis, the presence of weight loss, symptoms at diagnosis, and extended stage were significantly associated with a worse OS, while the presence of FOXP3$^+$ TILs in tumor specimens associated with a significantly better OS. LKB1-positive expression showed a trend toward a better prognosis. Multivariate analysis confirmed FOXP3$^+$ TILs and LS as independent positive prognostic factors (Supplementary Figure S1, Supplementary Table S4).

4 Discussion

SCLC is a recalcitrant cancer characterized by a dismal prognosis. The study of biomarkers in SCLC is highly challenging due to limited tissue availability, and currently, no predictive biomarker is available in clinical practice to tailor treatments.

In the depicted project, we explored the expression of LKB1 in SCLC and evaluated its prognostic role and relationship with TIME features. We chose to evaluate the potential biomarkers by using IHC, because the testing is relatively feasible, requires a

TABLE 2 Association between LKB1 expression and clinical features.

Variable		LKB1 > 4	LKB1 ≤ 4	Univariate OR (95% CI)	Multivariate OR (95% CI)
Sex	Male	45 (51.7)	42 (48.3)	1.41 (0.71–2.85, p = 0.331)	–
	Female	22 (43.1)	29 (56.9)	–	–
Age	<70	37 (45.7)	44 (54.3)	0.76 (0.38–1.49, p = 0.421)	–
	≥70	30 (52.6)	27 (47.4)	–	–
Smoker	Yes	64 (47.8)	70 (52.2)	0.30 (0.01–2.45, p = 0.309)	–
	No	3 (75.0)	1 (25.0)	–	–
ECOG PS	≤1	65 (52.0)	60 (48.0)	5.96 (1.52–39.53, **p = 0.024**)	4.57 (0.98–34.14, p = 0.080)
	>1	2 (15.4)	11 (84.6)	–	–
Symptoms at diagnosis	Yes	46 (46.5)	53 (53.5)	0.74 (0.35–1.56, p = 0.435)	–
	No	21 (53.8)	18 (46.2)	–	–
Weight loss at diagnosis	Yes	12 (50.0)	12 (50.0)	1.07 (0.44–2.61, p = 0.876)	–
	No	55 (48.2)	59 (51.8)	–	–
Stage at diagnosis	Limited	47 (58.8)	33 (41.2)	2.70 (1.37–5.55, **p = 0.005**)	2.78 (1.18–7.14, **p = 0.023**)
	Extended	20 (34.5)	38 (65.5)	–	–

OR, odds ratio; ECOG PS, Eastern Cooperative Oncology Group performance status. Bold text represents statistically significant differences.

10.3389/fonc.2025.1552506

TABLE 3 Survival analysis in the study population.

Variable		mOS, months (95% CI)	*p* (log rank)	Univariate HR (95% CI)	*p*	Multivariate HR (95% CI)	*p*
PS	>1	7.9 (3.1–NC)	**0.007**	2.28 (1.24–2.28)	**0.007**	1.83 (0.90–3.75)	0.096
	≤1	14.7 (11.9–20.6)					
Weight loss at diagnosis	No	16.3 (12.7–27.4)	**0.001**	0.48 (0.30–0.75)	**0.001**	0.57 (0.33–0.97)	**0.038**
	Yes	8.2 (4.9–13.6)					
Symptoms at diagnosis	No	60.2 (30.5–77.2)	**<0.001**	0.45 (0.30–0.69)	**<0.001**	0.72 (0.45–1.13)	0.161
	Yes	10.1 (8.1–13.0)					
Sex	Female	11.9 (8.4–17.6)	**0.032**	1.50 (1.03–2.18)	**0.033**	1.30 (0.87–1.95)	0.198
	Male	16.9 (11.7–31.7)					
Age	≥70	12.7 (8.2–20.8)	0.700	1.07 (0.74–1.55)	0.705	–	
	<70	14.7 (11.5–22.4)					
LKB1	≤4	11.2 (8.7–14.7)	**<0.001**	2.22 (1.52–3.26)	**<0.001**	1.73 (1.15–2.61)	**0.008**
	>4	32.4 (13.6–62.4)					
Stage at diagnosis	Extended	7.8 (6.7–10.1)	**<0.001**	4.82 (3.15–7.37)	**<0.001**	3.65 (2.24–5.94)	**<0.001**
	Limited	32.4 (20.3–65.7)					

HR, hazard ratio; 95% CI, 95% confidence interval; mOS, median overall survival. Bold text represents statistically significant differences.

relatively low amount of tissue, and accounts for the presence of *LKB1* epigenetic alterations (37, 40). In our cohort, LKB1 expression was deemed positive in 48.5% of cases. Limited data are available in the literature about LKB1 in SCLC. While no LKB1 mutations were reported in 11 SCLC cell lines (34, 35), a previous paper by Amin and colleagues reported a lower (13.3%) LKB1 IHC expression in 30 SCLC patients, of which 27 received surgery, but LKB1 expression was studied with a different antibody (D-19) and different scoring system (36). On the other hand, a recent retrospective work by Sivakumar and colleagues aimed at genotyping 3,600 SCLCs with FoundationOne CDx next-generation sequencing (NGS) panel, identified 62 *LKB1* mutant tumors, representing 1.7% of the entire cohort, which is a lower prevalence of LKB1 loss compared to our study. However, the prevalence of LKB1 loss may be underestimated because of the composition of the NGS panel and because the FoundationOne CDx panel does not account for epigenetic causes of LKB1 loss (33).

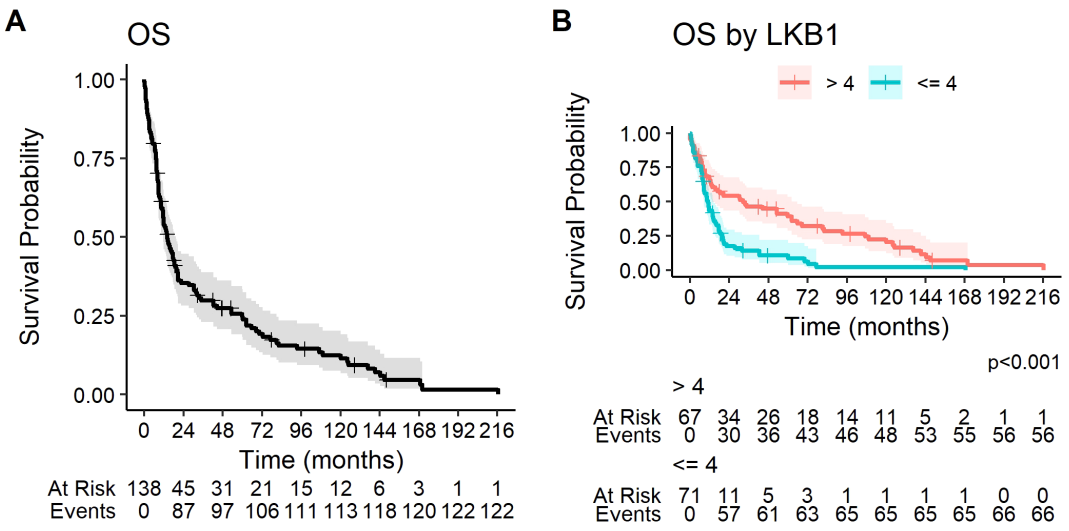

FIGURE 2
Kaplan–Meier curves for overall survival **(A)** in the overall study population and **(B)** according to LKB1 IHC expression.

10.3389/fonc.2025.1552506

TABLE 4 Tumor immune microenvironment features and association with LKB1 expression.

Variable	LKB1 > 4 *n* = 50	LKB1 ≤ 4 *n* = 20	*p*
$CD8^+$ TILs			**0.013**
0–2+	47 (94.0%)	14 (70.0%)	
3+	3 (6.0%)	6 (30.0%)	
$FOXP3^+$ TILs			0.8
1–3+	39 (78.0%)	15 (75.0%)	
0	11 (22.0%)	5 (25.0%)	
PD-L1 TIIC			0.4
0%	35 (70.0%)	12 (60.0%)	
≥1%	15 (30.0%)	8 (40.0%)	
PD-L1 TC			>0.9
0%	25 (50.0%)	10 (50.0%)	
≥1%	25 (50.0%)	10 (50.0%)	

TILs, tumor-infiltrating lymphocytes; TIIC, tumor immune-infiltrating cells; TC, tumor cells. Bold text represents statistically significant differences.

Our study identifies a strong association between LKB1 positivity and LS-SCLC. Given that LKB1 status was assessed prior to treatment, this association likely reflects inherent biological differences between LS and ES disease, which warrants further investigation.

In our study, we described significantly longer OS for patients expressing LKB1. This is consistent with the well-recognized LKB1 tumor suppressor functions and previous observations in NSCLC and other cancers (21, 27, 29, 30, 37). Importantly, in a previous broad molecular evaluation, Sivakumar and colleagues found only 7 *LKB1*-mutant patients out of 678, and a statistically significant worse overall survival for patients with *LKB1* mutations was reported, consistent with our results (33). Our data also confirm the prognostic significance of LKB1 impairment, demonstrating that its loss of expression is relatively frequent and can be detected in clinical practice using IHC, a simple and cost-effective method. Importantly, while our findings suggest LKB1 as a prognostic marker, we did not provide mechanistic validation through functional assays with SCLC cells, such as gene knockdown models, cytokine profiling, or immune response assays, as these were beyond the scope of our study. Nevertheless, the prognostic value of LKB1 in SCLC aligns with the well-established tumor suppressor functions of this gene, which encodes a master kinase that regulates cell migration, polarity, proliferation, and metabolism, primarily through downstream AMPK and AMPK-related kinase signaling, as extensively documented in prior studies (21, 41).

LKB1 mutant/*KRAS* mutant NSCLCs showed significantly decreased tumor-associated macrophages, tumor-infiltrating lymphocytes, and PD-L1 expression and increased tumor-associated neutrophils compared to *KRAS* mutant only tumors (26). In order to understand the potential role in immunotherapy response, we focused on the expression of PD-L1, $CD8^+$, and $FOXP3^+$ TILs to study TIME. In a previous study by our team, consisting of 66 LS and 38 ES SCLCs, PD-L1 was expressed on TCs and TIICs in 25% and 40% of the cases, respectively. The proportion of PD-L1-positive cases was significantly higher in LS versus ES patients. $CD8^+$ and $FOXP3^+$ TILs were present in 59% and 72% of the samples, respectively. The presence of $FOXP3^+$ TILs was associated with improved prognosis among LS patients, in univariate and multivariate analyses (39). In the present study, we were able to evaluate TIME features only in 50.7% of cases, due to limited tissue availability, but we confirmed the prognostic role of the $FOXP3^+$ infiltrate. Positive cases of PD-L1 on tumor cells were 32.9%. The prevalence was similar to other larger studies with extended SCLCs (42, 43).

Moreover, we explored the association between LKB1 and TIME features. Previous studies described LKB1 as a promoter of a hot TIME in mouse models of NSCLC and other tumor types as well as clinical samples, with *LKB1* mutant tumors being characterized by decreased $CD8^+$ TILs (26, 44, 45). However, in our cohort, LKB1 IHC positivity was negatively associated with the presence of $CD8^+$ TILs. This aspect, partially contrasting the idea of LKB1 loss association with a cooler immune microenvironment, might be explained by a more complex role in modulating TIME and the involvement of TIME components. Interestingly, Best and colleagues showed that murine models of lung adenocarcinoma harboring *KRAS* and *LKB1* mutations exhibit increased glutaminase expression by tumor cells and increased glutamate in the tumor microenvironment, compared to *KRAS* mutant/*KEAP1* mutant lung adenocarcinomas. Glutamate abundance was associated with increased granzyme and interferon genes in *KRAS* mutant/*LKB1* mutant tumors, suggesting an increased activation of $CD8^+$ cells (46). Whether this pathway could explain the negative association between LKB1 expression and $CD8^+$ TILs in SCLC has to be elucidated. At the same time, a recent work by Qian and colleagues highlighted the role of lactate as the link between LKB1 metabolic roles and TIME modulation: in murine lung adenocarcinoma models, *LKB1* loss resulted in increased glycolysis and enhanced lactate production and export via the monocarboxylate transporter 4; this caused increased M2 macrophage polarization, which in turn resulted in hypofunctional T cells (47). Consistently, *LKB1* mutant lung adenocarcinomas from patients demonstrated a similar phenotype of enhanced M2 macrophage polarization and hypofunctional T cells (47). Further investigation of this pathway and M2 macrophage polarization in SCLC could explain our findings and should be warranted, especially considering that consolidation with immune checkpoint inhibitors would likely be the new standard of care in LS-SCLC, and in this context, it seems to have a higher impact on the outcome (48).

To the best of our knowledge, this is the first large series of SCLCs studied for the expression of LKB1. We were able to demonstrate that LKB1 impairment is likely to be associated with ES and worse prognosis, and its role in TIME modulation warrants further investigation.

The strengths of the study are the number of cases, particularly the high number of limited SCLC cases. This point is rather difficult to reach due to the clinical presentation of SCLC, and this allowed us to enhance the differential distribution of LKB1 expression according to stage. Finally, we were able to study LKB1 expression with IHC,

which is a simple and inexpensive method, able to detect the consequences of mutational and also epigenetic *LKB1* alterations.

The weak points of the study are its retrospective nature, the lack of validation in a parallel cohort, and the lack of ES patients treated with chemoimmunotherapy combinations. Moreover, due to the limited availability of FFPE archival specimens, it was not possible to proceed with *LKB1* mutational analysis, metabolic profile analysis, and evaluation of their association with IHC status. Anyway, future analyses in patients treated with chemoimmunotherapy are ongoing, and parallel prospective tissue and liquid biopsy collection might be useful, in order to increase our knowledge about the role and pathway of LKB1 in SCLC.

Data availability statement

The raw data supporting the conclusions of this article will be made available by the authors, without undue reservation.

Ethics statement

The studies involving humans were approved by Ethics Committee of Veneto Institute of Oncology IOV - IRCCS. The studies were conducted in accordance with the local legislation and institutional requirements. The participants provided their written informed consent to participate in this study.

Author contributions

ADM: Data curation, Formal Analysis, Investigation, Resources, Visualization, Writing – original draft, Writing – review & editing. FF: Writing – original draft, Writing – review & editing, Data curation, Investigation, Resources, Visualization. GE: Resources, Writing – original draft, Writing – review & editing, Data curation, Investigation, Visualization. SAM: Data curation, Investigation, Resources, Writing – original draft, Writing – review & editing. AP: Data curation, Investigation, Resources, Writing – original draft, Writing – review & editing. FP: Resources, Writing – original draft, Writing – review & editing. EZ: Data curation, Investigation, Methodology, Resources, Writing – original draft, Writing – review & editing. LCB: Resources, Writing – original draft, Writing – review & editing. MDN: Resources, Writing – original draft, Writing – review & editing. AF: Resources, Writing – original draft, Writing – review & editing. SF: Resources, Writing – original draft, Writing – review & editing. GP: Resources, Writing – original draft, Writing – review & editing. FC: Resources, Writing – original draft, Writing – review & editing. MF: Data curation, Investigation, Resources, Writing – original draft, Writing – review & editing. FR: Resources, Writing – original draft, Writing – review & editing. VG: Resources, Supervision, Writing – original draft, Writing – review & editing. SI: Conceptualization, Resources, Supervision, Writing – original draft, Writing – review & editing. LB: Conceptualization, Resources, Supervision, Writing – original draft, Writing – review & editing.

Funding

The author(s) declare that financial support was received for the research and/or publication of this article. This work was supported by Ricerca Corrente with funding from the Italian Ministry of Health (Grant ID: L02P03).

Conflict of interest

The authors declare that the research was conducted in the absence of any commercial or financial relationships that could be construed as a potential conflict of interest.

The author(s) declared that they were an editorial board member of Frontiers, at the time of submission. This had no impact on the peer review process and the final decision.

Generative AI statement

The author(s) declare that no Generative AI was used in the creation of this manuscript.

Publisher's note

Supplementary material

The Supplementary Material for this article can be found online at: https://www.frontiersin.org/articles/10.3389/fonc.2025.1552506/full#supplementary-material

References

1. Siegel RL, Miller KD, Wagle NS, Jemal A. Cancer statistics, 2023. *CA Cancer J Clin*. (2023) 73:17–48. doi: 10.3322/caac.21763

2. Rudin CM, Brambilla E, Faivre-Finn C, Sage J. Small-cell lung cancer. *Nat Rev Dis Primer*. (2021) 7:1–20. doi: 10.1038/s41572-020-00235-0

3. Dingemans AMC, Früh M, Ardizzoni A, Besse B, Faivre-Finn C, Hendriks LE, et al. Small-cell lung cancer: ESMO Clinical Practice Guidelines for diagnosis, treatment and follow-up. *Ann Oncol Off J Eur Soc Med Oncol*. (2021) 32:839–53. doi: 10.1016/J.ANNONC.2021.03.207

4. Horn L, Mansfield A, Szczesna A, Havel L, Krzakowski M, Hochmair M, et al. First-line atezolizumab plus chemotherapy in extensive-stage small-cell lung cancer. *N Engl J Med*. (2018) 379:2220–9. doi: 10.1056/NEJMOA1809064

5. Liu SV, Reck M, Mansfield AS, Mok T, Scherpereel A, Reinmuth N, et al. Updated overall survival and PD-L1 subgroup analysis of patients with extensive-stage small-cell lung cancer treated with atezolizumab, carboplatin, and etoposide (IMpower133). *J Clin Oncol Off J Am Soc Clin Oncol*. (2021) 39:619–30. doi: 10.1200/JCO.20.01055

6. Paz-Ares L, Dvorkin M, Chen Y, Reinmuth N, Hotta K, Trukhin D, et al. Durvalumab plus platinum-etoposide versus platinum-etoposide in first-line treatment of extensive-stage small-cell lung cancer (CASPIAN): a randomised, controlled, open-label, phase 3 trial. *Lancet*. (2019) 394:1929–39. doi: 10.1016/S0140-6736(19)32222-6

7. Paz-Ares L, Chen Y, Reinmuth N, Hotta K, Trukhin D, Statsenko G, et al. Durvalumab, with or without tremelimumab, plus platinum-etoposide in first-line treatment of extensive-stage small-cell lung cancer: 3-year overall survival update from CASPIAN. *ESMO Open*. (2022) 7:100408. doi: 10.1016/J.ESMOOP.2022.100408

8. Rudin CM, Awad MM, Navarro A, Gottfried M, Peters S, Csoszi T, et al. Pembrolizumab or placebo plus etoposide and platinum as first-line therapy for extensive-stage small-cell lung cancer: randomized, double-blind, phase III KEYNOTE-604 study. *J Clin Oncol Off J Am Soc Clin Oncol*. (2020) 38:2369–79. doi: 10.1200/JCO.20.00793

9. Cheng Y, Han L, Wu L, Chen J, Sun H, Wen G, et al. Effect of first-line serplulimab vs placebo added to chemotherapy on survival in patients with extensive-stage small cell lung cancer: the ASTRUM-005 randomized clinical trial. *JAMA*. (2022) 328:1223. doi: 10.1001/jama.2022.16464

10. Wang J, Zhou C, Yao W, Wang Q, Min X, Chen G, et al. Adebrelimab or placebo plus carboplatin and etoposide as first-line treatment for extensive-stage small-cell lung cancer (CAPSTONE-1): a multicentre, randomised, double-blind, placebo-controlled, phase 3 trial. *Lancet Oncol*. (2022) 23:739–47. doi: 10.1016/S1470-2045(22)00224-8

11. Rittberg R, Leung B, Al-Hashami Z, Ho C. Real-world eligibility for platinum doublet plus immune checkpoint inhibitors in extensive-stage small-cell lung cancer. *Front Oncol*. (2022) 12:1002385. doi: 10.3389/fonc.2022.1002385

12. Bonanno L, Calvetti L, Dal Maso A, Pavan A, Bao LC, De Nuzzo M, et al. Real-world impact of the introduction of chemo-immunotherapy in extended small cell lung cancer: a multicentric analysis. *Front Immunol*. (2024) 15:1353889. doi: 10.3389/fimmu.2024.1353889

13. Bonanno L, Pavan A, Attili I, Pasello G, Guarneri V. Immunotherapy in SCLC: exceptional clinical benefit and abscopal pneumonitis after radiotherapy. *J Thorac Oncol Off Publ Int Assoc Study Lung Cancer*. (2019) 14:e5–7. doi: 10.1016/j.jtho.2018.08.2033

14. Lorenzi M, Resi MV, Bonanno L, Frega S, Dal Maso A, Ferro A, et al. Tissue and circulating biomarkers of benefit to immunotherapy in extensive-stage small cell lung cancer patients. *Front Immunol*. (2024) 15:1308109. doi: 10.3389/fimmu.2024.1308109

15. Gay CM, Stewart CA, Park EM, Diao L, Groves SM, Heeke S, et al. Patterns of transcription factor programs and immune pathway activation define four major subtypes of SCLC with distinct therapeutic vulnerabilities. *Cancer Cell*. (2021) 39:346–360.e7. doi: 10.1016/J.CCELL.2020.12.014

16. Willems E, Dedobbeleer M, Digregorio M, Lombard A, Lumapat PN, Rogister B. The functional diversity of Aurora kinases: a comprehensive review. *Cell Div*. (2018) 13:7. doi: 10.1186/s13008-018-0040-6

17. Yang S, He S, Zhou X, Liu M, Zhu H, Wang Y, et al. Suppression of Aurora-A oncogenic potential by c-Myc downregulation. *Exp Mol Med*. (2010) 42:759. doi: 10.3858/emm.2010.42.11.077

18. Takahashi Y, Sheridan P, Niida A, Sawada G, Uchi R, Mizuno H, et al. The AURKA/TPX2 axis drives colon tumorigenesis cooperatively with MYC. *Ann Oncol*. (2015) 26:935–42. doi: 10.1093/annonc/mdv034

19. Bertolin G, Tramier M. Insights into the non-mitotic functions of Aurora kinase A: more than just cell division. *Cell Mol Life Sci*. (2020) 77:1031–47. doi: 10.1007/s00018-019-03310-2

20. Zheng X, Chi J, Zhi J, Zhang H, Yue D, Zhao J, et al. Aurora-A-mediated phosphorylation of LKB1 compromises LKB1/AMPK signaling axis to facilitate NSCLC growth and migration. *Oncogene*. (2018) 37:502–11. doi: 10.1038/onc.2017.354

21. Shackelford D, Shaw R. The LKB1-AMPK pathway: metabolism and growth control in tumour suppression. *Nat Rev Cancer*. (2009) 9:563–75. doi: 10.1038/NRC2676

22. Kullmann L, Krahn MP. Controlling the master—upstream regulation of the tumor suppressor LKB1. *Oncogene*. (2018) 37:3045–57. doi: 10.1038/s41388-018-0145-z

23. Bonanno L, Zulato E, Pavan A, Attili I, Pasello G, Conte P, et al. LKB1 and tumor metabolism: the interplay of immune and angiogenic microenvironment in lung cancer. *Int J Mol Sci*. (2019) 20:1874. doi: 10.3390/ijms20081874

24. Hu L, Liu M, Tang B, Li Q, Pan B-S, Xu C, et al. Posttranslational regulation of liver kinase B1 in human cancer. *J Biol Chem*. (2023) 299:104570. doi: 10.1016/j.jbc.2023.104570

25. Ndembe G, Intini I, Perin E, Marabese M, Caiola E, Mendogni P, et al. LKB1: can we target an hidden target? Focus on NSCLC. *Front Oncol*. (2022) 12:889826. doi: 10.3389/fonc.2022.889826

26. Koyama S, Akbay EA, Li YY, Aref AR, Skoulidis F, Herter-Sprie GS, et al. STK11/LKB1 deficiency promotes neutrophil recruitment and proinflammatory cytokine production to suppress T-cell activity in the lung tumor microenvironment. *Cancer Res*. (2016) 76:999–1008. doi: 10.1158/0008-5472.CAN-15-1439

27. Skoulidis F, Goldberg ME, Greenawalt DM, Hellmann MD, Awad MM, Gainor JF, et al. STK11/LKB1 mutations and PD-1 inhibitor resistance in KRAS-mutant lung adenocarcinoma. *Cancer Discovery*. (2018) 8:822–35. doi: 10.1158/2159-8290.CD-18-0099

28. Mazzaschi G, Leonetti A, Minari R, Gnetti L, Quaini F, Tiseo M, et al. Modulating tumor microenvironment: A review on STK11 immune properties and predictive vs prognostic role for non-small-cell lung cancer immunotherapy. *Curr Treat Options Oncol*. (2021) 22:1–25. doi: 10.1007/S11864-021-00891-8/xxxS/2

29. Sanchez-Cespedes M, Parrella P, Esteller M, Nomoto S, Trink B, Engles J, et al. Inactivation of LKB1/STK11 is a common event in adenocarcinomas of the lung. *Cancer Res*. (2002) 62:3659–62.

30. Sanchez-Cespedes M. A role for LKB1 gene in human cancer beyond the Peutz-Jeghers syndrome. *Oncogene*. (2007) 26:7825–32. doi: 10.1038/SJ.ONC.1210594

31. Esteller M, Avizienyte E, Corn PG, Lothe RA, Baylin SB, Aaltonen LA, et al. Epigenetic inactivation of LKB1 in primary tumors associated with the Peutz-Jeghers syndrome. *Oncogene*. (2000) 19:164–8. doi: 10.1038/SJ.ONC.1203227

32. Lee SM, Choi JE, Na YK, Lee EJ, Lee WK, Choi YY, et al. Genetic and epigenetic alterations of the LKB1 gene and their associations with mutations in TP53 and EGFR pathway genes in Korean non-small cell lung cancers. *Lung Cancer*. (2013) 81:194–9. doi: 10.1016/j.lungcan.2013.04.013

33. Sivakumar S, Moore JA, Montesion M, Sharaf R, Lin DI, Colón CI, et al. Integrative analysis of a large real-world cohort of small cell lung cancer identifies distinct genetic subtypes and insights into histologic transformation. *Cancer Discovery*. (2023) 13:1572–91. doi: 10.1158/2159-8290.CD-22-0620

34. Carretero J, Medina PP, Pio R, Montuenga LM, Sanchez-Cespedes M. Novel and natural knockout lung cancer cell lines for the LKB1/STK11 tumor suppressor gene. *Oncogene*. (2004) 23:4037–40. doi: 10.1038/SJ.ONC.1207502

35. Onozato R, Kosaka T, Achiwa H, Kuwano H, Takahashi T, Yatabe Y, et al. LKB1 gene mutations in Japanese lung cancer patients. *Cancer Sci*. (2007) 98:1747–51. doi: 10.1111/J.1349-7006.2007.00585.X

36. Amin RMS, Hiroshima K, Iyoda A, Hoshi K, Honma K, Kuroki M, et al. LKB1 protein expression in neuroendocrine tumors of the lung. *Pathol Int*. (2008) 58:84–8. doi: 10.1111/J.1440-1827.2007.02194.X

37. Bonanno L, De Paoli A, Zulato E, Esposito G, Calabrese F, Favaretto A, et al. LKB1 expression correlates with increased survival in patients with advanced non–small cell lung cancer treated with chemotherapy and bevacizumab. *Clin Cancer Res Off J Am Assoc Cancer Res*. (2017) 23:3316–24. doi: 10.1158/1078-0432.CCR-16-2410

38. Zulato E, Bergamo F, De Paoli A, Griguolo G, Esposito G, De Salvo G, et al. Prognostic significance of AMPK activation in advanced stage colorectal cancer treated with chemotherapy plus bevacizumab. *Br J Cancer*. (2014) 111:25–32. doi: 10.1038/BJC.2014.274

39. Bonanno L, Pavan A, Dieci M, Di Liso E, Schiavon M, Comacchio G, et al. The role of immune microenvironment in small-cell lung cancer: Distribution of PD-L1 expression and prognostic role of FOXP3-positive tumour infiltrating lymphocytes. *Eur J Cancer*. (2018) 101:191–200. doi: 10.1016/J.EJCA.2018.06.023

40. Calles A, Sholl LM, Rodig SJ, Pelton AK, Hornick JL, Butaney M, et al. Immunohistochemical loss of LKB1 is a biomarker for more aggressive biology in KRAS-mutant lung adenocarcinoma. *Clin Cancer Res Off J Am Assoc Cancer Res*. (2015) 21:2851–60. doi: 10.1158/1078-0432.CCR-14-3112

41. Trelford CB, Shepherd TG. LKB1 biology: assessing the therapeutic relevancy of LKB1 inhibitors. *Cell Commun Signal CCS*. (2024) 22:310. doi: 10.1186/s12964-024-01689-5

42. Antonia SJ, López-Martin JA, Bendell J, Ott PA, Taylor M, Eder JP, et al. Nivolumab alone and nivolumab plus ipilimumab in recurrent small-cell lung cancer (CheckMate 032): a multicentre, open-label, phase 1/2 trial. *Lancet Oncol*. (2016) 17:883–95. doi: 10.1016/S1470-2045(16)30098-5

43. Schultheis AM, Scheel AH, Ozretić L, George J, Thomas RK, Hagemann T, et al. PD-L1 expression in small cell neuroendocrine carcinomas. *Eur J Cancer*. (2015) 51:421–6. doi: 10.1016/j.ejca.2014.12.006

44. Granado-Martínez P, Garcia-Ortega S, González-Sánchez E, McGrail K, Selgas R, Grueso J, et al. STK11 (LKB1) missense somatic mutant isoforms promote tumor growth, motility and inflammation. *Commun Biol*. (2020) 3: 366. doi: 10.1038/S42003-020-1092-0

45. Hsu H-P, Wang C-Y, Kuo Y-L, Lee K-T, Chen P-S, Cheung CHA, et al. Modulating tumor immune microenvironment by the STK11/LKB1 signaling in breast cancer. *J Clin Oncol Off J Am Soc Clin Oncol*. (2020) 38:e15185–5. doi: 10.1200/JCO.2020.38.15_suppl.e15185

46. Best SA, Gubser PM, Sethumadhavan S, Kersbergen A, Negrón Abril YL, Goldford J, et al. Glutaminase inhibition impairs CD8 T cell activation in STK11-/Lkb1-deficient lung cancer. *Cell Metab*. (2022) 34:874–887.e6. doi: 10.1016/j.cmet.2022.04.003

47. Qian Y, Galan-Cobo A, Guijarro I, Dang M, Molkentine D, Poteete A, et al. MCT4-dependent lactate secretion suppresses antitumor immunity in LKB1-deficient lung adenocarcinoma. *Cancer Cell*. (2023) 41:1363–1380.e7. doi: 10.1016/j.ccell.2023.05.015

48. Cheng Y, Spigel DR, Cho BC, Laktionov KK, Fang J, Chen Y, et al. Durvalumab after chemoradiotherapy in limited-stage small-cell lung cancer. *N Engl J Med*. (2024) 391:1313–27. doi: 10.1056/NEJMoa2404873

frontiers | Frontiers in Oncology

TYPE Original Research
PUBLISHED 26 May 2025
DOI 10.3389/fonc.2025.1570873

OPEN ACCESS

EDITED BY
Balkrishna Chaube,
Indian Institute of Technology Dharwad, India

REVIEWED BY
Ishan Pandey,
Moti Lal Nehru Medical College, India
Meghna Saxena,
University of Minnesota Medical Center, United States

*CORRESPONDENCE
Ben Liu
benliu100@tmu.edu.cn
Kexin Chen
chenkexin@tmu.edu.cn

†These authors have contributed equally to this work

RECEIVED 04 February 2025
ACCEPTED 28 April 2025
PUBLISHED 26 May 2025

CITATION
Liu H, Hu X, Zhang X, Yao Y, Wu L, Tian Y, Dai H, Chen K and Liu B (2025) Unveiling fatty acid subtypes: immunometabolic interplay and therapeutic opportunities in gastric cancer.
Front. Oncol. 15:1570873.
doi: 10.3389/fonc.2025.1570873

Unveiling fatty acid subtypes: immunometabolic interplay and therapeutic opportunities in gastric cancer

Huahuan Liu[1†], Xin Hu[1,2†], Xiangnan Zhang[1†], Yanxin Yao[1], Liuxing Wu[1], Ye Tian[1], Hongji Dai[1], Kexin Chen[1*] and Ben Liu[1*]

[1]Department of Epidemiology and Biostatistics, Key Laboratory of Molecular Cancer Epidemiology, Key Laboratory of Prevention and Control of Human Major Diseases, Ministry of Education, National Clinical Research Center for Cancer, Tianjin Medical University Cancer Institute and Hospital, Tianjin Medical University, Tianjin, China, [2]Center for Single-Cell Omics and Tumor Liquid Biopsy, Zhongnan Hospital of Wuhan University, Wuhan, China

Background: The goal of this study was to develop a predictive signature using genes associated with fatty acid metabolism to evaluate the prognosis of individuals with gastric cancer (GC).

Method: A total of 24 prognostic-related genes were identified by intersecting differentially expressed genes with 525 fatty acid metabolism (FAM) -related genes and applying a univariate Cox proportional hazards model. By performing consensus clustering of 24 genes associated with FAM, two distinct clusters of GC patients were identified. Subsequently, a risk model was constructed using 39 differentially expressed mRNAs from the two clusters through a random forest model and univariate Cox regression.

Results: An R package, "GCFAMS", was developed to assess GC patients' prognosis based on FAM gene expression. The low-risk group exhibited a more favorable prognosis compared to the high-risk group across various datasets ($P < 0.05$). The model demonstrated strong predictive performance, with AUC values of 0.86, 0.623, and 0.508 for 5-year survival prediction in the training and two validation datasets. The high-risk group displayed lower IC50 values for embelin and imatinib, suggesting the potential efficacy of these drugs in this subgroup. Conversely, the low-risk group demonstrated an elevated response to immune checkpoints blockade therapy and a higher immunophenoscore, which was further validated in additional cancer cohorts. Public data from single-cell RNA sequencing confirmed that the characterized genes were predominantly expressed in endothelial cells and fibroblasts. Furthermore, the integration of transcriptomics and metabolomics revealed notable variations in fatty acid levels between the clusters, underscoring the

clinical relevance of our fatty acid metabolism signature in shaping the metabolic profiles of GC patients.

Conclusion: This developed FAM signature demonstrated potential as a biomarker for guiding treatment and predicting prognosis in GC.

KEYWORDS

gastric cancer, fatty acid metabolism, multi-omics technologies, immunotherapy, single-cell transcriptomics

1 Introduction

Gastric cancer (GC) is a common form of cancer worldwide, with nearly 1 million new cases and over half a million deaths reported in 2022 based on the most recent data from the World Health Organization International Agency for Research on Cancer (1). This places GC as the fifth most prevalent form of cancer and the fifth leading contributor to cancer-related deaths on a global scale. The risk factors contributing to developing of GC include infection by Helicobacter pylori, advanced age, high salt intake, and inappropriate dietary habits (2).

Lipids play a crucial role in the composition of cellular membranes and structural units of cells. In addition, lipids are also used for energy storage and metabolism and play essential roles as signaling molecules in various cell activities. Cancer is characterized by significant alterations in lipid metabolism, including fatty acids (FAs) and cholesterol (3). Cancer cells rely on lipid metabolism to obtain the energy, components for biological membranes, and signaling molecules needed for their growth, survival, spread, metastasis, and reaction to the tumor microenvironment and cancer therapy (4).

Malignant tumors primarily rely on *de novo* synthesis for necessary FAs, whereas normal cells typically obtain them through external sources (5–8). The increased production of saturated and monounsaturated FAs from *de novo* FA synthesis in cancer cells increase cell membrane saturation and resistance to chemotherapeutic drugs (9). Certain important enzymes involved in fatty acid synthesis, including ATP citrate lyase (ACLY), acetyl-CoA carboxylase (ACC), and fatty acid synthase (FASN), are upregulated in tumors and linked to aggressive tumor behavior and unfavorable prognosis (10–12). Moreover, the fatty acid transporter CD36, which is upregulated in cancer cells, facilitates the spread and resistance to treatment of tumor cells through increased absorption of long-chain FAs (13, 14).

FAs and lipid storage can also impact various types of immune cells, often leading to suppression of the immune system. Lipid buildup inside bone marrow cells promotes oxidative metabolism and supports immune-suppressing capabilities (15). The abnormal accumulation of lipids in tumor-infiltrating DCs (TIDCs) hinders their ability to present antigens (16). FA oxidation (FAO) is necessary to form CD8+ memory T cells (17). It is also crucial for differentiating Tregs and blocking FAO to avoid aggregation of immunosuppressive effector T-cell populations (18, 19). In conclusion, fatty acid metabolism (FAM) has impacts on immune cell function in the tumor microenvironment.

In recent years, the specific phenotype of abnormal FAM in tumor cells has gradually attracted great attention. Exploring the role of abnormal FAM in tumor biology and strategies to treat malignant tumors by targeting FAM pathways is receiving much attention. The role of FAM in GC in its clinical treatment is unknown and deserves further exploration. To evaluate the relationship between the FAM-related gene expression pattern and clinical outcomes of GC patients, 347 TCGA GC samples were collected and divided into two clusters. A FAM-related risk score was constructed to evaluate the prognosis of GC patients and assess the biological characteristics.

2 Materials and methods

2.1 Data acquisition

Gene expression patterns and detailed clinical information were acquired from The Cancer Genome Atlas database (TCGA), accessible through the Genomic Data Commons portal (GDC) (https://portal.gdc.cancer.gov/). Individuals within the dataset who did not have detailed survival records were not considered for further study. The training dataset consisted of a total of 347 clinical samples from GC (The Cancer Genome Atlas-Stomach Adenocarcinoma, TCGA-STAD). To validate our results, we included the GC dataset from the Gene Expression Omnibus (GEO) with the accession number GSE34942, consisting of 56 samples, and the Tianjin GC cohort, which served as validation sets and included 90 cases (20). Raw RNA-seq data from TCGA and Tianjin GC cohort were normalized to Transcripts Per Million

Abbreviations: CNV, copy number variations; DEGs, differentially expressed genes; FAM, fatty acid metabolism; FAO, fatty acid oxidation; GC, gastric cancer; IPS, immunophenoscore; OS, overall survival; PCA, principal component analysis; AUC, area under the curve; ROC, receiver operator characteristic; SsGSEA, single-sample genome enrichment analysis; CDF, cumulative distribution function.

(TPM) values. Microarray data from the GEO dataset (GSE34942, GSE13861, GSE15459, GSE26901, GSE26899, GSE28541) were normalized using the Robust Multi-array Average (RMA) method. To minimize potential batch effects across datasets, we applied the ComBat algorithm. Quality control measures were applied to remove low-quality samples and exclude those with incomplete survival data. Additionally, TCGA mutation data and copy number variation (CNV) data were extracted from the GDC, which hosts TCGA data alongside other genomic datasets.

2.2 Identification of the FAM clusters in GC

525 genes associated with FAM were compiled from the Gene Set Enrichment Analysis (GSEA) database. Differentially expressed genes (DEGs) between cancer and paracancerous tissue were identified by applying the criteria (21) |log2 Fold Change (FC)| > 1 and $P < 0.05$ using the R package 'edgeR', and then intersected with FAM-related genes. Afterwards, the univariate Cox proportional hazards model was used to identify 24 genes linked to the survival time of GC patients. The gene expression levels of 24 genes were used to uniformly categorize the GC samples into clusters. The ConsensusClusterPlus package (version 1.58.0) in R was employed to perform the consensus clustering algorithm, repeated 1000 times to ensure the stability of clusters (22). This process identified two clusters, labeled as "cluster1" and "cluster2". Principal component analysis (PCA) confirmed the stability and reliability of the subtype classification. The operating system of the identified clusters was evaluated utilizing the Kaplan-Meier technique, with the log-rank test employed to examine any statistical disparities.

2.3 Conducting pathway enrichment analysis on genes that are expressed differently across clusters

To identify DEGs in two clusters, we used differential expression analysis based on an empirical Bayesian approach, which is implemented in the 'limma' package of the R language (23). DEGs were considered significant if their |log2FC| was greater than 1 and the adjusted P value was less than 0.05 (24). To adjust for multiple testing, we applied the Benjamini method and then conducted Kyoto Encyclopedia of Genes and Genomes (KEGG) and Gene Ontology (GO) enrichment analyses using the 'clusterProfiler' R package to investigate variations in biological processes between clusters. The findings were considered statistically significant, as the adjusted p-value was below 0.05.

2.4 Estimation of immune cell infiltration between clusters

The single-sample genome enrichment analysis (ssGSEA) algorithm (25) to perform a detailed analysis of 28 immune cell types in the tumor microenvironment. This analysis was based on specific gene panels defined in the literature for each immune cell subpopulation (26). To fully evaluate the immune status of cancer patients, we utilized the 'estimate' R package to determine the immune score, stroma score, and tumor purity. In addition, we employed the CIBERSORT, MCPcounter and TIMER algorithms to quantitatively assess the level of immune cell infiltration in the two clusters. The ssGSEA score indicated the proportional presence of different types of immune cells. Normalization of these scores to a unity distribution ensures that the minimum score is zero and the maximum is one, allowing for a standardized comparison across different immune cell types.

2.5 Changes in gene landscapes and mutation patterns in the two clusters are of great importance

Utilizing the GenVisR tool, version 1.26.0, within the R package, we identified the significantly mutated genes (SMGs). Afterward, two groups were analyzed for mutation patterns using MutationalPatterns version 3.4.0 and maftools version 2.10.0 from R packages. We then extracted the mutational signature from the GC dataset and performed a comparative analysis against the COSMIC V2 mutation database (https://cancer.sanger.ac.uk/cosmic), employing the cosine similarity method.

2.6 Construction and evaluation of the FAM-related risk signature

DEGs were selected to create a set of signature genes using the R software 'limma', based on the conditions of |log2FC| > 0.5 and $P < 0.05$ (27, 28). Volcano plots were used to demonstrate differential genes. The R package "randomForest" was used to identify key mRNAs, miRNAs, and lncRNAs contributing to the construction of the FAM signature. Model performance was optimized using 10-fold cross-validation, with 5 repeated runs to ensure stability and reduce overfitting. The mean error rate and cross-validation error were recorded for model selection. Genes significantly associated with survival risk were identified through univariate Cox regression analysis, and significant candidates ($P < 0.05$) were used to construct prognostic signatures. A multivariate Cox proportional hazards model was then applied to the selected genes, with the best model determined via stepwise regression. The model's predictive ability was evaluated using the concordance index (C-index) and log-rank test. A risk score for each sample was computed using the coefficients derived from the multivariate Cox model. The correlation between risk scores and survival time was assessed using the Kaplan-Meier method and log-rank test. Additionally, the risk models were assessed using receiver operating curves (ROC). Multivariate Cox regression was used to assess the difference between this risk signature and traditional risk factors such as sex and age on the prognosis of GC patients.

2.7 Immunotherapy response prediction with FAM prognosis signature

Two groups undergoing immunotherapy were chosen to confirm the effectiveness of the FAM signature: one with advanced urothelial cancer (UC) treated with atezolizumab (IMvigor210 cohort, N = 298) (29) and the other with melanoma receiving anti-PD1 immunotherapy (Mela cohort, N = 121 (30). Data on clinical information and gene expression from the IMvigor210 cohort were obtained from the IMvigor210 dataset. Gene expression data of the anti-PD1 melanoma cohort were obtained from previous studies (30). Gene expression and prognosis data for the Mela cohorts (GSE78220, N = 26; GSE100797, N = 21) (31, 32) and the bladder cancer cohort (GSE176307, N = 90) (33), all treated with immunotherapy, were obtained from publicly available datasets.

2.8 Immunophenoscore analysis and chemotherapeutic response between different risk groups

The immunophenoscore (IPS), a highly effective molecular indicator of immune response, was employed for profiling the immune environments within tumors and cancer antigen profiles. Previous research involved gathering data on the weights of groupings of genes associated with the immune system, categorized into four main groups: major histocompatibility complex (MHC) molecules, suppressor cells, effector cells, and immune checkpoints or immunomodulatory factors. Weighted average Z-scores were computed using the gene expression levels. Additionally, we calculated the IPS by adding together the weighted average Z-scores of the four gene categories, resulting in a score between 0 and 10. The score measures the amount and behavior of immune cells in the tumor's immune system, thus forecasting how the tumor will respond to immunotherapy. A higher IPS represents a higher immunotherapy response rate (26).

The study utilized the R package 'pRRophetic' to forecast the sensitivity of chemotherapeutic drugs in GC patients (34), determining IC50 through ridge regression and evaluating prediction accuracy with 10-fold cross-validation (35).

2.9 Cluster analysis of single-cell RNA-sequencing data

Data from individual cells (GSE167297) in five STAD samples underwent preprocessing and analysis using the 'Seurat' R package. To filter out low-quality cells, only cells with transcript counts between 300 and 10,000, detected in at least three cells per transcript, and with mitochondrial read fractions below 5% were retained for further analysis. For clustering, we employed the Louvain algorithm with a resolution parameter of 0.5, which was selected to effectively capture major cell populations while avoiding over-segmentation. This choice was validated through dimensionality reduction techniques (UMAP and t-SNE) and marker gene expression analysis, confirming that the clusters aligned with known major cell types. This resolution also aligned with commonly used thresholds in published scRNA-seq studies (36, 37). Primary cell categories were identified based on established cell markers obtained from published sources or the CellMarker database.

2.10 Study participants

A total of 42 individuals were included in the study, sourced from the Tumor Tissue Bank at Tianjin Cancer Hospital. Illumina NovaSeq 6000 was utilized for the RNA sequencing of every sample. METWARE performed untargeted metabolomics measurements in plasma. All the samples came from individuals diagnosed with GC with accurate histological and pathological assessments. All cases in the study were handled anonymously in compliance with legal and medical standards, as approved by the Ethics Committee of Tianjin Medical University Cancer Hospital and Institute, with informed consent obtained from all patients.

2.11 Collection and preparation of serum samples

Blood samples were obtained between 6:00 and 8:00 in the morning following a period of fasting to minimize the impact of food intake. Subsequently, all specimens were promptly placed in a freezer at -80°C. Prior to initiating the process, take out the samples from the -80°C freezer and allow them to thaw on ice until they are completely free of ice (all following steps should be carried out on ice). After thawing, vortexed the samples for 10 s and mix well. Pipetted 50 µL of the sample into a numbered centrifuge tube. Next, 300 microliters of an internal standard extract containing 20% acetonitrile and methanol in a 1:4 volume-to-volume ratio was mixed vigorously for 3 minutes, followed by centrifugation at 12000 rotations per minute for 10 minutes at 4°C. Following centrifugation, transfer 200 µL of the liquid above the sediment into a separate centrifuge tube with the same number, then store it in a freezer at -20°C for half an hour. After being spun at 12000 revolutions per minute for 3 minutes at 4 degrees Celsius, 180 microliters of the liquid above the sediment were transferred into a tube equipped with the appropriate injection vial for analysis using liquid chromatography-mass spectrometry. All sample extracts were mixed in equal parts to form a QC sample.

2.12 LC-MS analysis

2.12.1 T3 UPLC conditions

The sample extracts were analyzed using an LC-ESI-MS/MS system (38–40) (UPLC, ExionLC AD, https://sciex.com.cn/; MS, QTRAP® System, https://sciex.com/). The analysis parameters included the use of a UPLC column, specifically the Waters

ACQUITY UPLC HSS T3 C18 (1.8 μm, 2.1 mm*100 mm), with the column temperature set at 40°C, a flow rate of 0.4 mL/min, and an injection volume of either 2 μL or 5 μL. The solvent system consisted of a mixture of water (0.1% formic acid) and acetonitrile (0.1% formic acid) with a gradient program starting at 95% acetonitrile and 5% water at 0 min, transitioning to 10% acetonitrile and 90% water at 10.0 min, maintaining that ratio until 11.0 min, then returning to 95% acetonitrile and 5% water at 11.1 min and staying at that ratio until 14.0 min.

2.12.2 QTOF-MS/MS

The Triple TOF mass spectrometer was utilized for its capability to collect MS/MS spectra in an information-dependent manner (IDA) while conducting an LC/MS analysis. The TripleTOF 6600 acquisition software from AB SCIEX continuously assesses the complete scan survey MS data in this setting. It gathers and initiates the collection of MS/MS spectra based on predetermined conditions. During every iteration, 12 precursor ions with an intensity exceeding 100 were selected for fragmentation using a collision energy (CE) of 30 V, resulting in 12 MS/MS events with a product ion accumulation time of 50 msec each. The ESI source parameters were established with Ion source gas 1 and Ion source gas 2 set at 50 Psi each, Curtain gas at 25 Psi, source temperature at 500°C, and Ion Spray Voltage Floating (ISVF) at 5500 V or -4500 V in positive or negative modes, respectively.

Electrospray ionization quadrupole time-of-flight mass spectrometry.

Triple quadrupole (QQQ) and LIT scans were obtained using a QTRAP mass spectrometer, specifically the QTRAP® LC-MS/MS System. This instrument is equipped with an ESI Turbo Ion-Spray interface and operates in both positive and negative ion mode. Analyst 1.6.3 software (Sciex) controls the system. The parameters for operating the ESI source were temperature of the source at 500° C; ion spray voltage at 5500 V (positive) and -4500 V (negative); gas I (GSI), gas II (GSII), and curtain gas (CUR) set at 50, 50, and 25.0 psi, respectively; high collision gas (CAD) was used. Calibration of the instruments was carried out using solutions of polypropylene glycol at concentrations of 10 and 100 μmol/L in QQQ and LIT modes, respectively. Each period was monitored for a distinct group of MRM transitions based on the metabolites that were eluted during that time frame.

2.13 Statistical analysis

Consensus clustering was utilized to perform clustering in order to identify robust structure across multiple clustering iterations (41). Survival curve for prognosis analysis was generated using the Kaplan-Meier method, with significance of differences determined by performing the log-rank test. Hazard ratios (HR) were calculated using univariate and multivariate Cox regression models, and their coefficients were displayed in forest plots. The Wilcoxon rank-sum test was used to compare continuous variables between two groups, while the chi-square test was employed for comparing classified variables. Spearman coefficients were applied to evaluate correlations among variables. Unsupervised clustering was performed to detect unique clusters based on the 39 genes' expression in the signature of FAM. Orthogonal Partial Least Squares Discriminant Analysis (OPLS-DA) was utilized to confirm the efficacy of the clustering process (42). Chi-square tests were used to analyze the variations in baseline characteristics between cases and controls for categorical variables, while paired t-tests or Wilcoxon's signed-rank tests were used for continuous variables. Significance was established with a P value less than 0.05, and all P values reported were calculated for both sides of the distribution. R 4.0.0 software was used for all statistical analyses.

3 Results

3.1 Development and validation of FAM clusters

We devised a systematic flowchart to illustrate our study methodology (Figure 1). A total of 525 genes related to FAM were obtained from GO, Hallmark, KEGG, and Reactome databases (Figure 2A, Supplementary Table S1). After screening the DEGs in cancer and paracancerous tissues, intersected with 525 genes in FAM, and 24 prognostic-related genes were further screened using a univariate Cox proportional hazards model (Supplementary Table S2).

Subsequently, consensus clustering based on the expression patterns of the 24 FAM-related genes indicated that the most suitable number of clusters was two. This finding was confirmed by Cumulative Distribution Function (CDF) curves (Figures 2B, C). PCA revealed significant differences in gene expression between the two identified groups (Figure 2D). The expression patterns of the genes used for consensus clustering in the two clusters were visualized in Figure 2E, showing that cluster2 exhibited higher gene expression levels compared to cluster1.

Survival analysis revealed a significant difference in outcomes between the two clusters, as indicated by the log-rank test with a P-value of 0.021 (Figure 2F). Importantly, the observed prognostic differences were validated across three independent GEO GC datasets: GSE26899 (N = 93, P = 0.039), GSE26901 (N = 109, P = 0.0015), and GSE28541 (N = 40, P = 0.0011) (Supplementary Figures S1A–C). These findings demonstrated that GC samples could be classified into two groups based on 24 FAM-associated genes, revealing a distinct variation in prognosis between the groups.

3.2 Immune cell infiltration between FAM clusters

We evaluated the presence of immune cells in the two groups by analyzing the tumor immune environment through the immune score, stromal score, tumor purity score, and the abundance of 28 different immune cell types. A heatmap was used to illustrate the distribution of immune cell infiltration based on the four algorithms

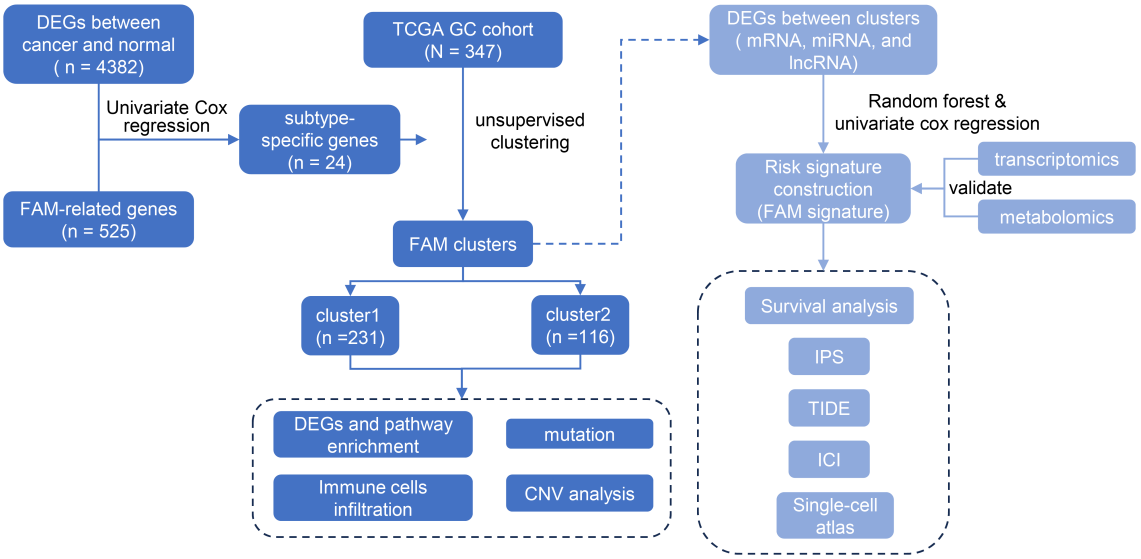

FIGURE 1
Flow chart of the experimental design and analysis of FAM related signature.

mentioned (Figure 3A). Compared to cluster2, which had a poorer prognosis, cluster1 exhibited a lower immune score and stromal score but a higher tumor purity score (Figure 3B). The degree of immune infiltration varied between the clusters, with cluster2 displaying more pronounced immune cell infiltration than cluster1 (Figure 3C).

3.3 Analysis of mutation patterns between FAM clusters

To investigate the relationship between FAM clusters and mutation patterns, we conducted SMG analysis. In our analysis of the top 20 mutated genes in GC, we found various mutated genes that differed between clusters, such as TTN, LRBP1, SYNE1, FAT4, and additional genes (Figure 4A). Four mutated signatures were derived from the COSMIC database by analyzing GC genomic somatic mutation data in order to explore differences in the mutational processes between the two subtypes. From the mutation data, four mutational patterns (signatures 6, 10, 17, and 21) were identified in cluster1, while cluster2 showed four different mutational patterns (signatures 3, 6, 17, and 1) as depicted in Figures 4B, C. Signatures 10 and 21 were unique in cluster1, and signatures 3 and 1 were distinctive in cluster2. The findings indicated that the mutation feature of cluster2 was linked to DNA damage and repair processes, like homologous recombination, resulting in the inability to repair DNA double-strand breaks.

We further investigated the differential somatic CNV alterations between FAM subtypes. CNV analysis identified 12 copy number gains, including 1q21.3 ($P < 0.05$), 5p15.33 ($P < 0.001$), 8q24.21 ($P < 0.01$) and 17q12 ($P < 0.05$) amplifications, and seven copy number losses, including 1p36.11 ($P < 0.05$), 3p14.2 ($P < 0.05$), and 5q12.1 ($P < 0.001$) (Figure 4D). The focal and arm level CNVs were compared through the GISTIC 2.0 approach. Cluster1 exhibited a greater overall load of copy number amplifications and deletions compared to cluster2 (Figure 4E).

3.4 Enrichment analysis between FAM clusters

To further explore the effects of DEGs between the two clusters, we analyzed the signaling pathways of DEGs using KEGG and GO enrichment analysis. The findings indicated that the DEGs in the two groups were predominantly involved in various well-known signaling pathways such as the PI3K-Akt and MAPK pathways, as well as metabolic pathways, cell growth, and immune response (Figures 5A, B), and the PIA3K-Akt signaling pathway was associated with metabolism. All these results indicate that the two clusters exhibit differences in metabolism, immunity, and proliferation.

3.5 Development of a prognostic signature related to FAM

We screened for DEGs between the two clusters that could be used to construct a GC prognosis signature. First, we identified 3594 mRNAs, 402 lncRNAs, and 196 miRNAs differentially expressed between FAM clusters (Figures 5C–E, Supplementary Table S3).Then, the above genes were further screened, and 165 mRNAs, 22 lncRNAs, and 10 miRNAs were selected through the "randomForest" package (Figures 5F–K, Supplementary Table S4). Finally, 39 mRNAs, 4 lncRNAs, and 1 miRNA were further selected by univariate Cox regression analysis for GC prognosis signature construction (Supplementary Table S5). The cutoff values of high- and low-risk mRNAs, miRNAs, and lncRNAs were 0.414, 2.166, and

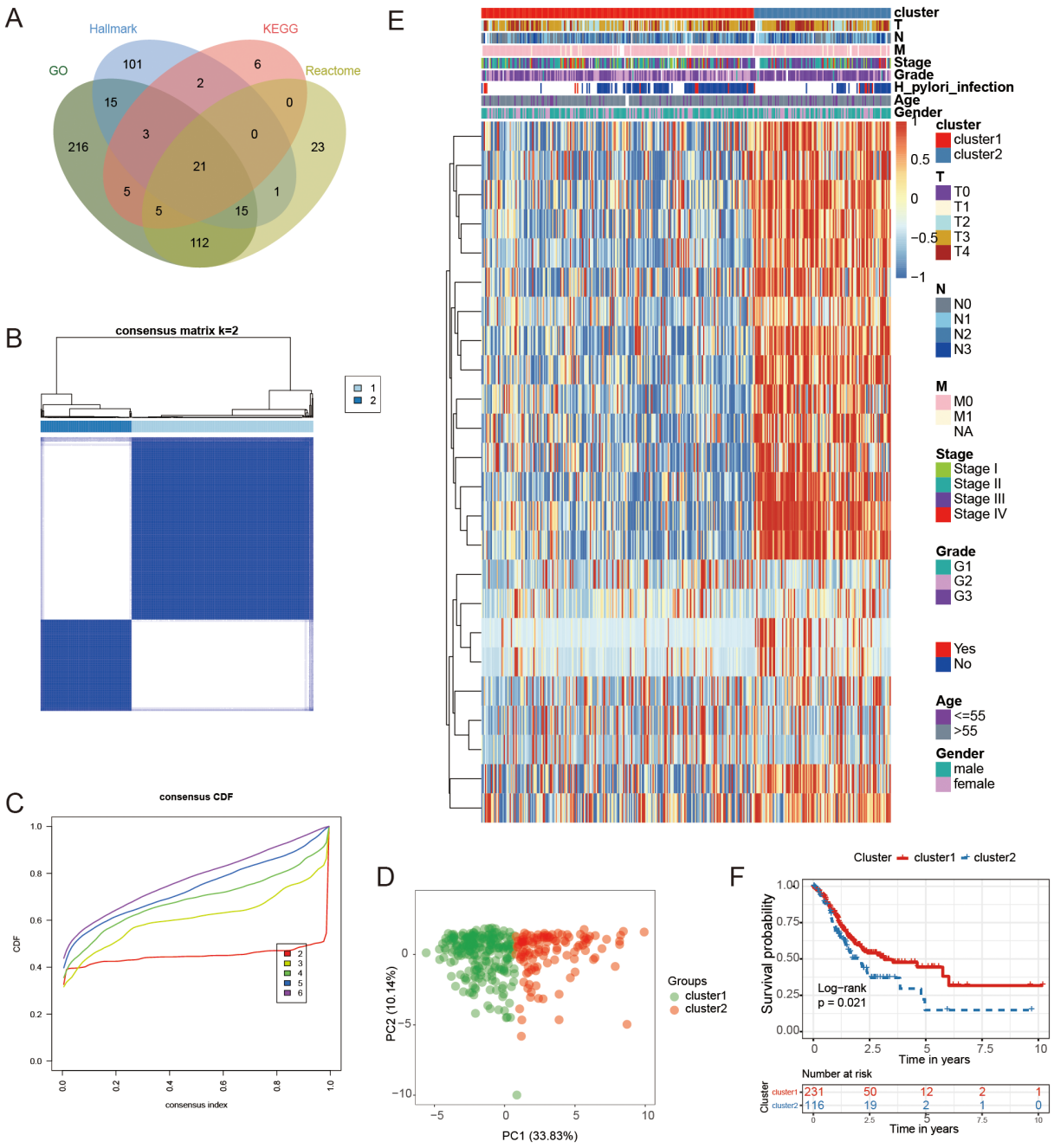

FIGURE 2
Classification and analysis of FAM subtypes. **(A)** The diagram illustrating the overlap of genes related to FAM from databases such as KEGG, GO, Hallmark, and Reactome. **(B, C)** The best classification effect was achieved by determining the optimal number of clusters (K=2) from CDF curves. **(D)** PCA was conducted on samples from GC using the principal component analysis method. **(E)** A heatmap illustrating the expression levels of 24 genes specific to each subtype. **(F)** Kaplan-Meier curves were used to forecast survival rates in individuals categorized into two clusters.

0.052, respectively, which were calculated by the R package "survminer". Prognosis models built using mRNAs, lncRNAs, and miRNAs indicated a greater likelihood of survival for the low-risk group compared to the high-risk group ($P < 0.0001$, $P < 0.0001$, $P = 0.0032$; Figures 6A, C, E). The area under the curve values for the 5-year survival rates in the three categories were 0.860, 0.569, and 0.666, as shown in the Figures 6B, D, F, indicating that the 39 mRNAs constructed FAM risk signature could better predict the prognosis of GC patients. The heatmap showed the visualization of the expression level of the mRNAs in GC patient samples (Figure 6G).

The validation dataset (GSE34942) was utilized to confirm the accuracy of the GC prognosis signature constructed by 39 FAM-related mRNAs. The high-risk group, as determined by the risk signature in the TCGA GC cohort, had a worse outcome compared to the low-risk group ($P = 0.035$, Figure 6H). Nevertheless, the AUC values for 1-, 3-, and 5- years were lower compared to the training

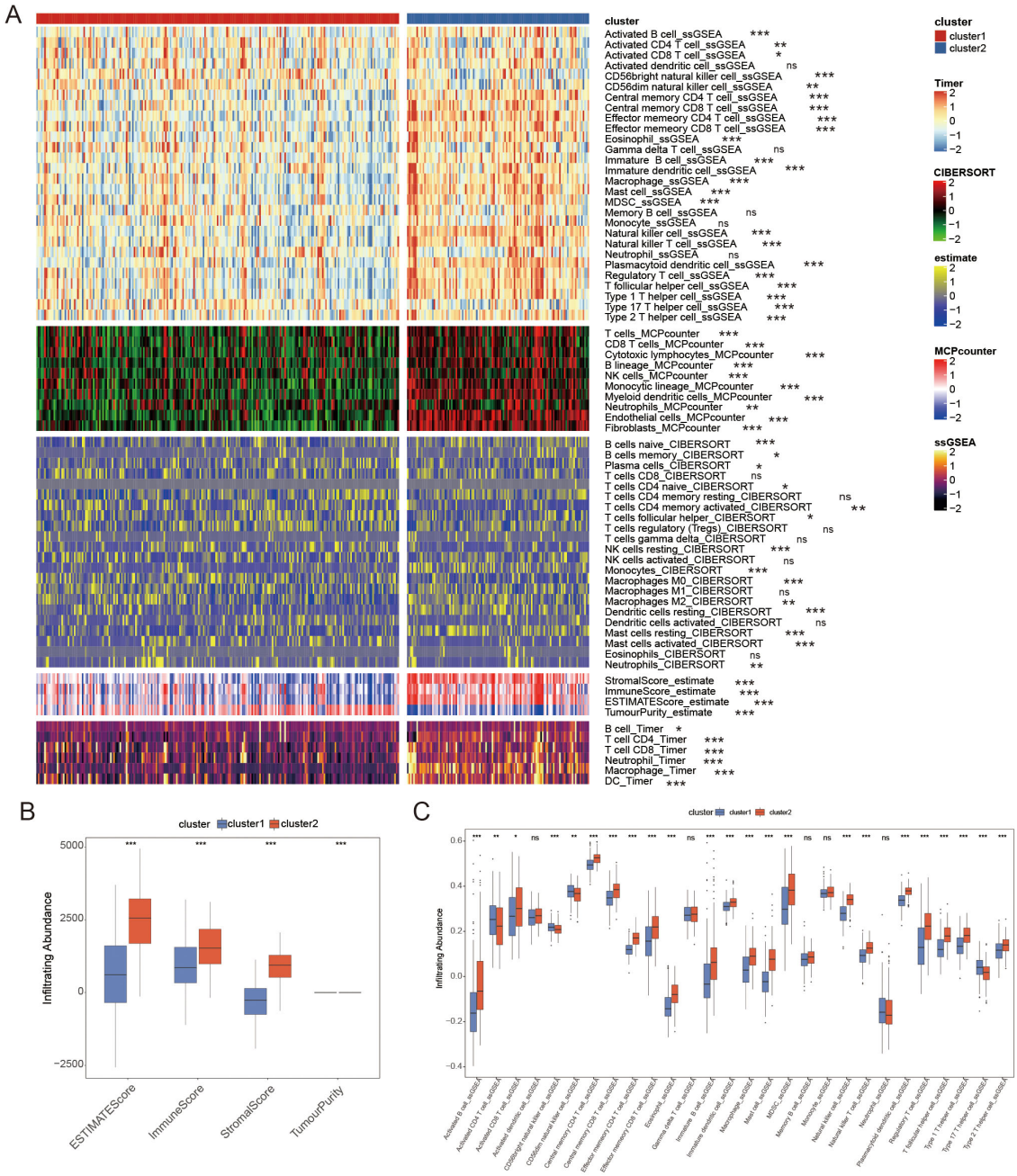

FIGURE 3
The distribution of immune cell infiltration as determined by four different algorithms. **(A)** Comparing the infiltration of immune cells in cluster1 and cluster2 using a Heatmap. **(B)** Tumor immune microenvironment scores between clusters. **(C)** There was a difference in the number of immune cells infiltrating between the two groups. * P < 0.05, ** P < 0.01, *** P < 0.001, ns P ≥ 0.05.

dataset (Figure 6I). The internal GC dataset we analyzed (Tianjin GC dataset, N = 90) showed that the low-risk group had a greater survival rate compared to the high-risk group (P = 0.037, Figure 6J). Furthermore, the AUC values were still lower than those in the training dataset (Figure 6K). Furthermore, to strengthen the generalizability of our risk signature, we included three additional external validation cohorts (GSE13861, GSE15459, GSE26901) (Supplementary Figure S2; P = 0.041, P =9e-04, P = 0.0027). The results further confirmed the prognostic utility of the 39-mRNA FAM risk signature in independent patient populations.

3.6 Assessment of the GC prognosis signature constructed by FAM-related mRNAs

The AUC values of this constructed signature and common risk factors for GC were compared to further validate the validity of this signature. In the TCGA GC cohort, the risk score (AUC = 0.749) was more effective in predicting GC prognosis compared to traditional risk factors like pathological stage (AUC = 0.595), age (AUC = 0.540), and sex (AUC = 0.458) (Figure 7A), which

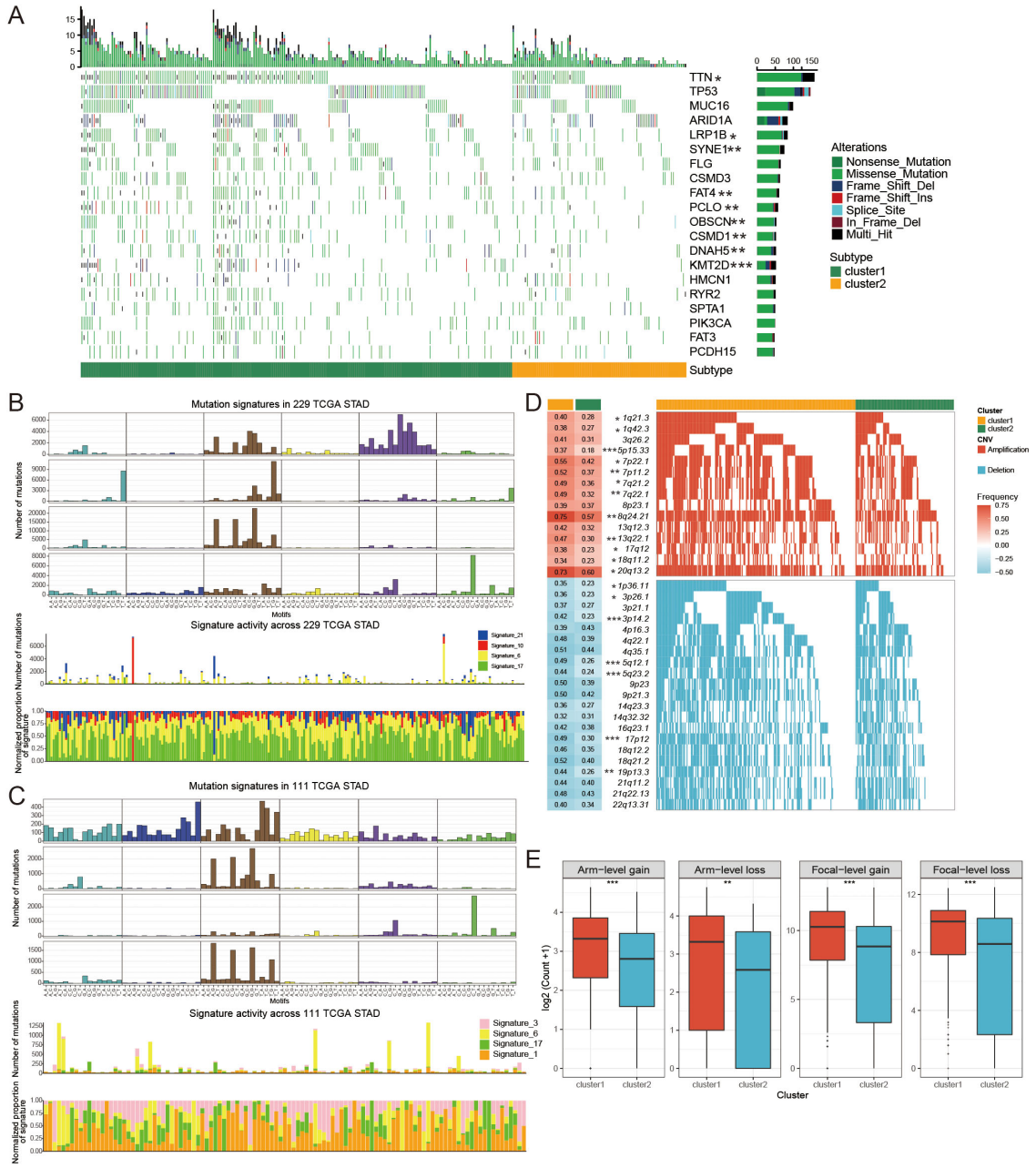

FIGURE 4
The mutational patterns and signatures of two FAM clusters. **(A)** Individuals in cluster1 and cluster2 created the graphical representation of tumor somatic mutations in the form of a waterfall plot. **(B, C)** Mutation signature identified in cluster1 **(B)** and cluster2 **(C)**. **(D)** Detailed charts showing copy number amplifications (increases) and copy number deletions (decreases) between different subtypes of FAM. **(E)** Distribution of specific and general changes in copy numbers between different subtypes of FAM. Significance levels were denoted as follows: *for P < 0.05, **for P < 0.01, ***for P < 0.001, and ns for non-significant results.

suggested that the signature had a better prognostic ability for GC. Furthermore, there were differences in the risk scores of the four pathological stages in patients with GC (P = 0.023, Figure 7B). Multivariate Cox regression was employed to determine whether the signature has a prognostic value in GC independent of clinicopathological indicators such as age, pathological stage, and sex. In the multivariate Cox regression, the risk score had a hazard ratio (HR) of 5.037 with a 95% confidence interval (CI) of 3.523-7.202, showing statistical significance (P < 0.001, Figure 7C). A nomogram, created using a combination of the risk score and traditional risk factors, was utilized to forecast the chances of survival at 3- and 5- year for a patient with GC (Figure 7D). In addition, we developed an R package called "GCFAMS" (Gastric Cancer Fatty Acid Metabolism Score) for calculating the prognostic score of FAM in GC patients based on fatty acid metabolism gene expression (https://github.com/huxintmu/GCFAMS).

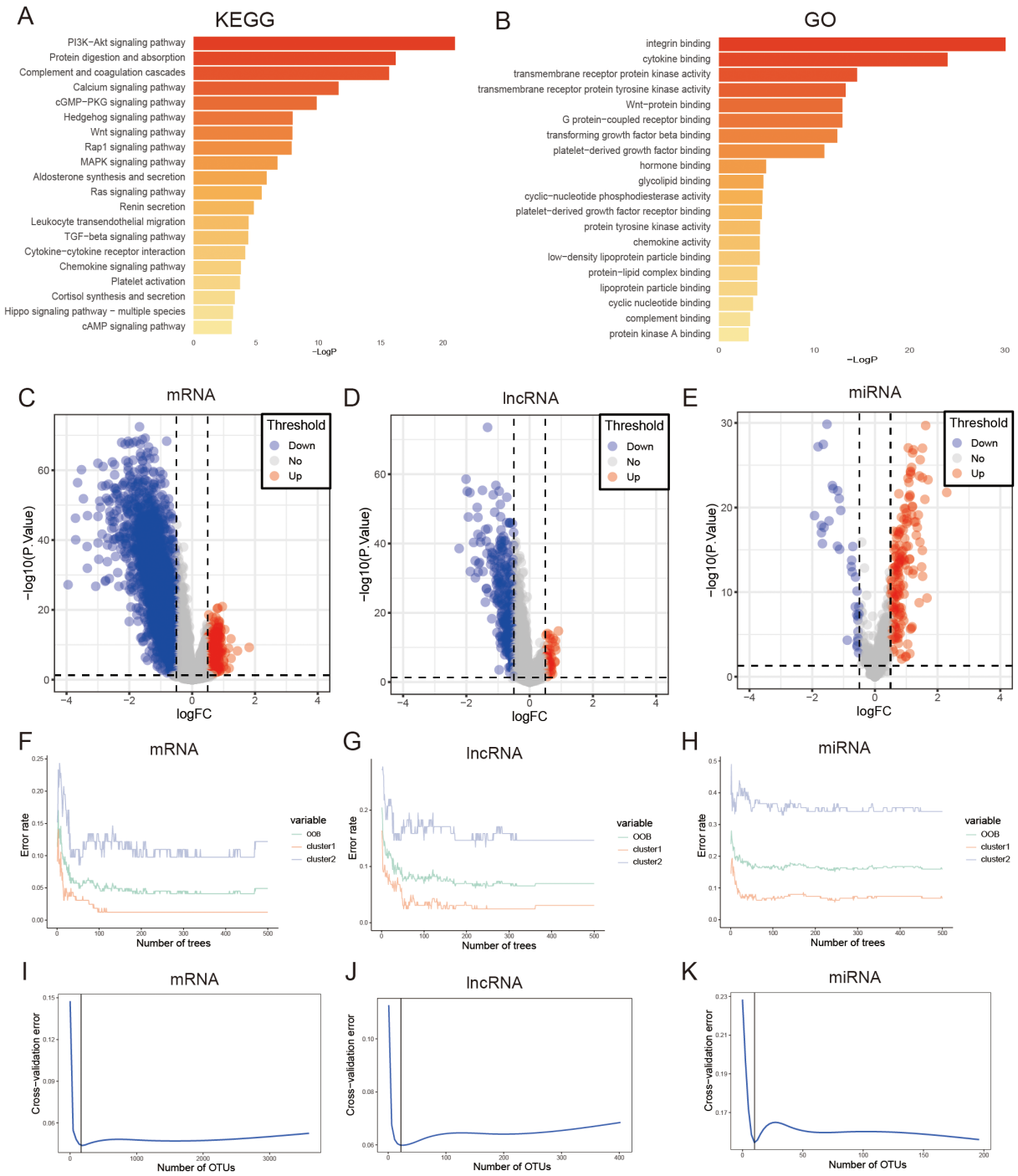

FIGURE 5
Performing enrichment analysis on DEGs between clusters of FAM using KEGG pathways. **(A)** and GO pathways **(B)**. **(C)** The volcano plot indicates that there were 3594 mRNAs that exhibited differential expression in the two subtypes of FAM. **(D)** The volcano plot indicates that there were 402 lncRNAs that exhibited differential expression in the two subtypes of FAM. **(E)** The volcano plot indicates that there were 196 miRNAs that showed differential expression in the two subtypes of FAM. **(F–H)** Error rate of the random forest model. **(I–K)** Cross-validation error of random forest model.

3.7 FAM-related mRNA signature predicts the response to immunotherapy and chemotherapy

We utilized the Tumor Immune Dysfunction and Exclusion (TIDE) analysis to investigate the potential of the FAM risk model in predicting immunotherapy response within the GC cohort (43). The findings indicated that individuals in the low-risk category exhibited a more favorable reaction to immunotherapy (Figure 8A). The findings indicated that the IPS was higher in the low-risk group compared to the high-risk group, as shown in Figure 8B. The study found that individuals with a low-risk score may have higher

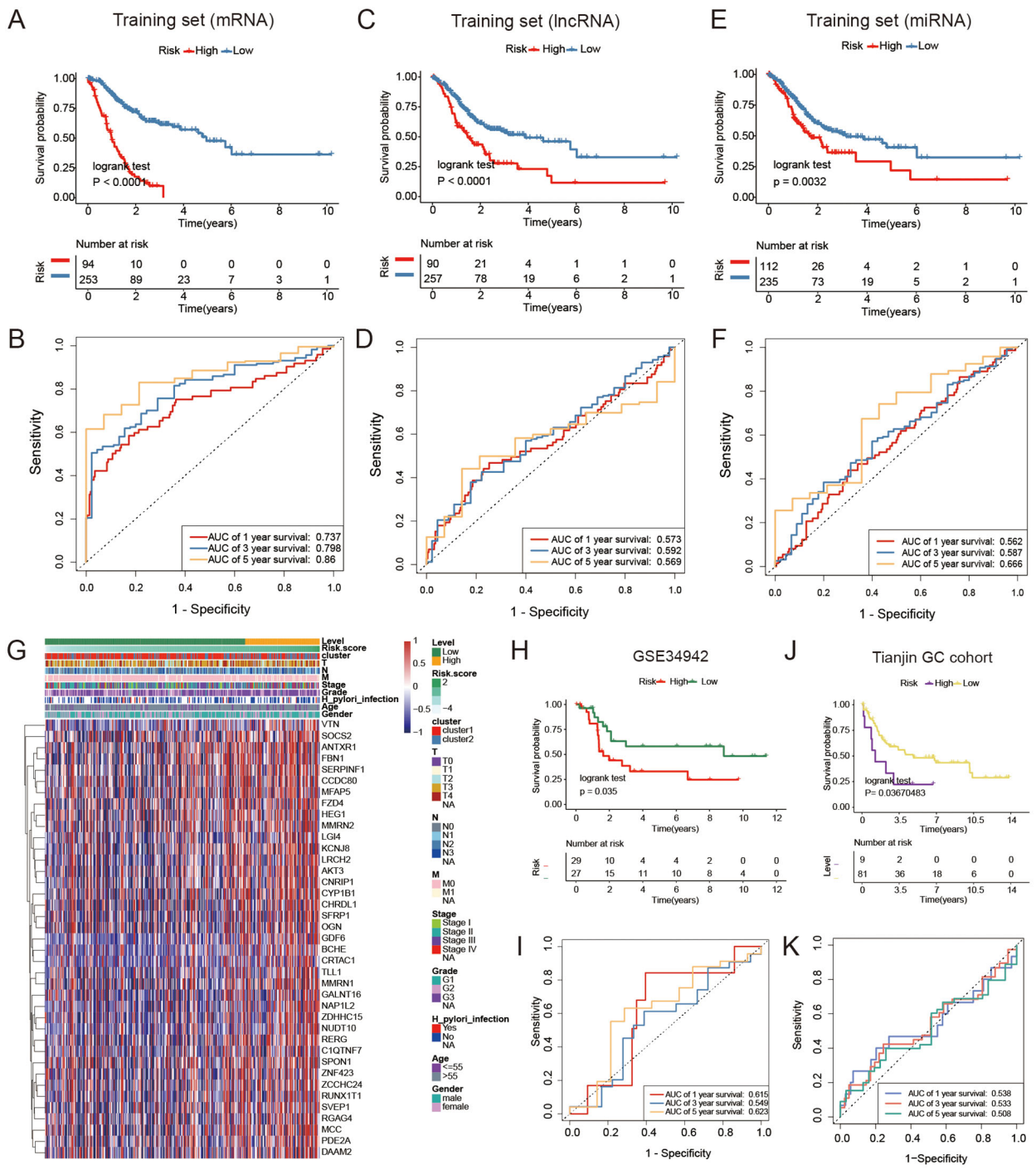

FIGURE 6
Comparison of different FAM risk models. **(A, C, E)** Kaplan-Meier plots were generated for GC patients based on their risk scores derived from a combination of mRNAs, lncRNAs, and miRNAs. Individuals classified as high-risk (red) had a lower overall survival rate (OS) compared to those classified as low-risk (blue). **(B, D, F)** ROC curves were generated to forecast the sensitivity and specificity of survival at 1-, 3-, and 5- years based on the risk scores derived from mRNA, lncRNA, and miRNA signatures. **(G)** The expression of mRNAs used to construct signature model in GC patients. **(H)** Kaplan-Meier analysis was performed on a group categorized as high- or low-risk based on 39 mRNAs in the GEO validation dataset (GSE34942, N = 56). **(I)** ROC curves to forecast the sensitivity and specificity of survival at 1-, 3-, and 5-years in the GEO validation dataset containing 56 subjects. **(J)** A Kaplan-Meier analysis was performed on the high-risk and low-risk groups created based on 39 mRNAs in the Tianjin GC dataset (N = 90). **(K)** ROC curves were utilized to forecast the sensitivity and specificity of survival at 1-, 3-, and 5- years in the Tianjin GC dataset (N = 90).

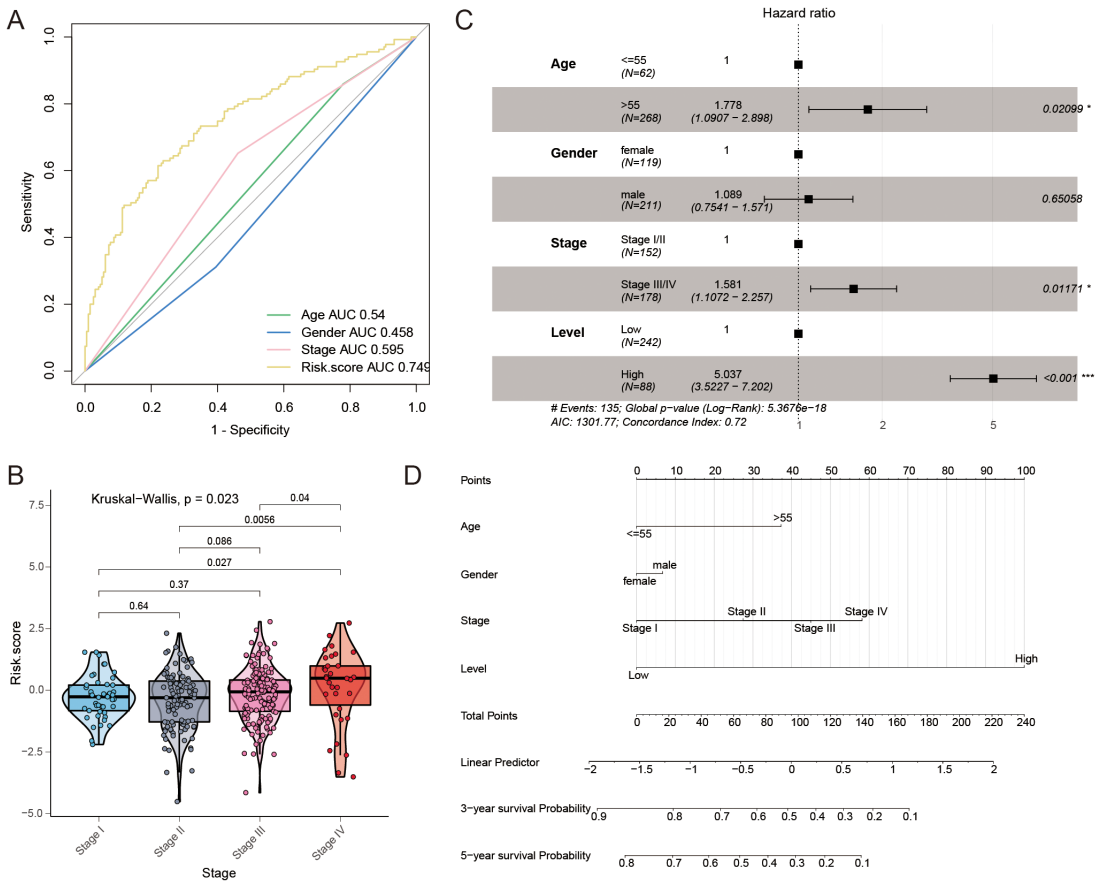

FIGURE 7
The predictive significance of the risk model for FAM. **(A)** ROC curves were used to evaluate the predictive ability of age, gender, stage, and risk score in determining sensitivity and specificity in GC patients, along with clinicopathological factors and a 39-mRNA signature-derived risk scores. **(B)** Comparing risk scores for FAM across various clinical stages. **(C)** Multivariate Cox regression was performed to analyze the relationship between clinicopathological factors and overall survival in patients with GC. **(D)** A nomogram was created utilizing the risk score for FAM along with established risk factors.

possibility of responding positively to immunotherapy. Next, we conducted a Spearman correlation analysis to investigate the connection between the FAM score and the infiltration of immune cells. As shown in Figure 8C, there was a relationship observed between the FAM risk score and immune cells.

Moreover, we found that the FAM score had the strongest positive correlation with mast cells (r = 0.220, P < 0.0001; Figure 8D) and a negative correlation with CD56dim natural killer cells (r = -0.12, P = 0.02; Figure 8E). In order to confirm the significance of the FAM score in immunotherapy, cohorts of malignant melanoma (Mela) and urothelial carcinoma (UC, the most prevalent form of bladder cancer) were utilized to investigate which individuals derive benefits from immunotherapy. Validation set results indicated that the low-risk group exhibited a greater response rate to immune-checkpoint blockade (ICB) in the Mela and UC cohorts (P < 0.05, Figures 8F–I). The findings indicated that individuals in the low-risk group were more likely to benefit from immunotherapy. To further confirm the robustness and real-world applicability of the FAM risk model, we performed external validation using an independent bladder cancer cohort (GSE176307) and two Mela cohorts (GSE78220, GSE100797). The results showed that low-risk patients had a significantly higher likelihood of responding to ICB (P = 0.033, P = 0.067, P = 0.032; Supplementary Figure S3), consistent with our findings in UC and Mela cohorts.

Furthermore, we evaluated the impact of chemotherapy drug reactions in both the high-risk and low-risk categories of the GC dataset. Chemotherapy drugs had distinct impacts on the high-risk and low-risk groups. In the high-risk group, embelin (P = 0.0023) and imatinib (P = 0.0048) showed lower IC50 values compared to the low-risk group (Supplementary Figure S4). The findings indicated variations in the effectiveness of immunotherapy and chemotherapy among different groups, with immunotherapy showing greater efficacy in the low-risk group and chemotherapy being more effective in the high-risk group.

3.8 Single-cell atlas distribution of genes that make up the signature for FAM

The single cells of GC were clustered unsupervised by hypervariable genes, and the single-cell atlas comprised 21

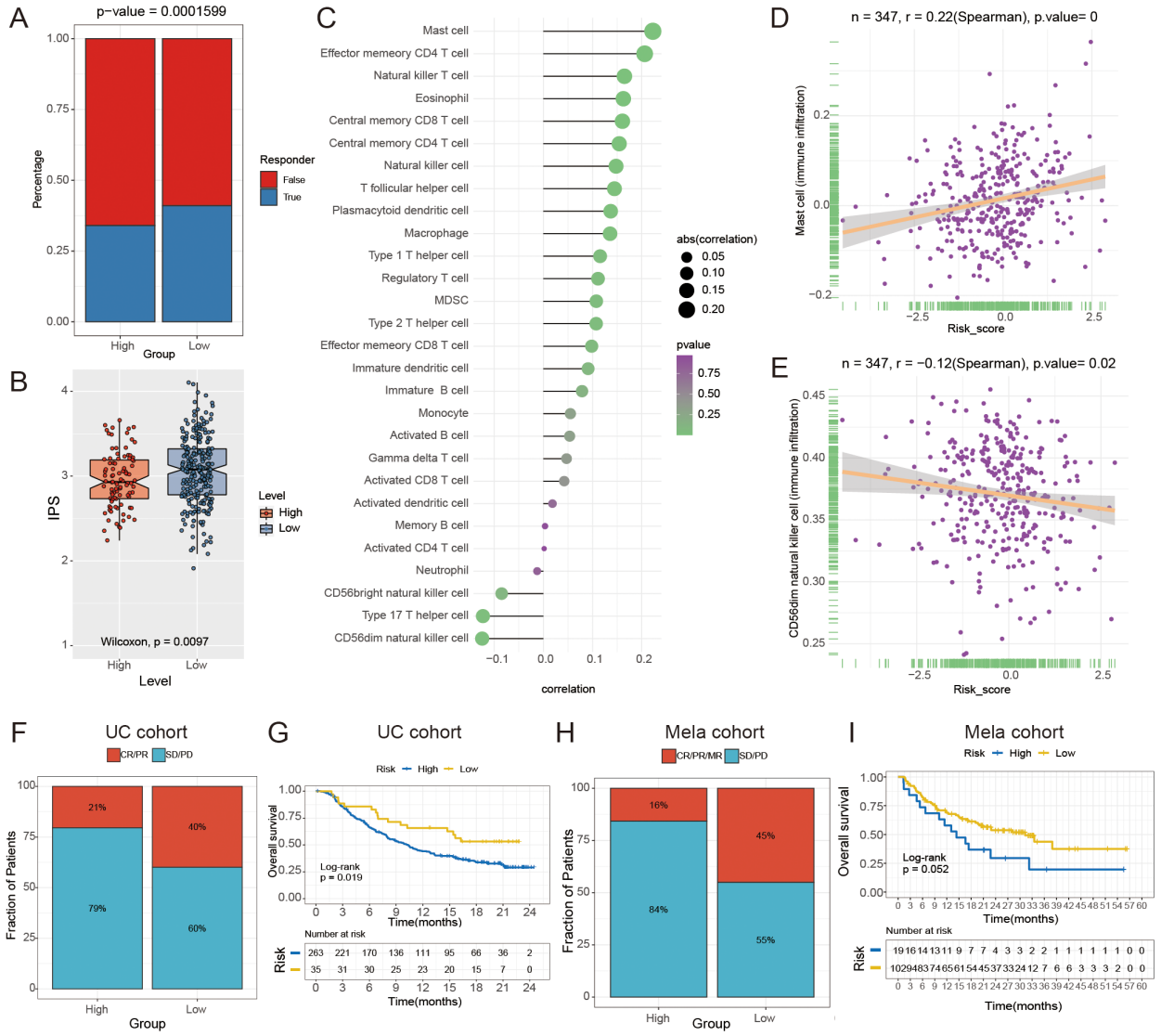

FIGURE 8
The relationship between the risk score for FAM and the effectiveness of immunotherapy. **(A)** The Tumor Immune Dysfunction and Exclusion (TIDE) analysis was used to forecast the response to immunotherapy in GC patients with high- and low- risk groups. **(B)** The boxplot indicates a notable contrast in IPS between the high- and low-risk groups (P = 0.0097). **(C)** The lollipop chart displays the correlation between the score of FAM and 28 different types of immune cells. **(D, E)** Spearman correlation between FAM score and mast cells **(D)** and activated CD56dim natural killer cells **(E)**. **(F, H)** Comparison of immune response to immunotherapy between high- and low- risk subgroups. CR indicates complete response, PR indicates partial response, SD indicates stable disease, and PD indicates progressive disease. **(G, I)** Kaplan-Meier analysis and the percentage of immune response to immunotherapy were compared between high- and low-risk groups in the UC **(G)** and Mela cohorts **(I)**.

clusters, as shown with a UMAP plot (Figures 9A, B). A single-cell atlas of multi-region GC cells included nine major cell populations (Figure 9C). T cells, B cells, macrophages, plasma cells, mast cells, epithelial cells, endothelial cells, fibroblasts, and others were included in the single-cell atlas. Detailed expression profiles and gene features of single gene markers are shown in Figure 9D. The expression heatmap of the marker genes of the major cell lineages is shown in Figure 9E. The gene enrichment analysis of FAM signature genes indicated that the genes were predominantly expressed in fibroblasts and endothelial cells, as shown in Figures 9F, G. Above all, single-cell analysis revealed that FAM signature genes were predominantly expressed in fibroblast cells and endothelial cells.

3.9 Joint analysis using transcriptomic and fatty acid metabolomic data to validate signature

We enrolled 42 GC samples and performed a consensus clustering analysis based on FAM signature expression, showing the optimal number of clusters was two (cluster1 and clsuter2,

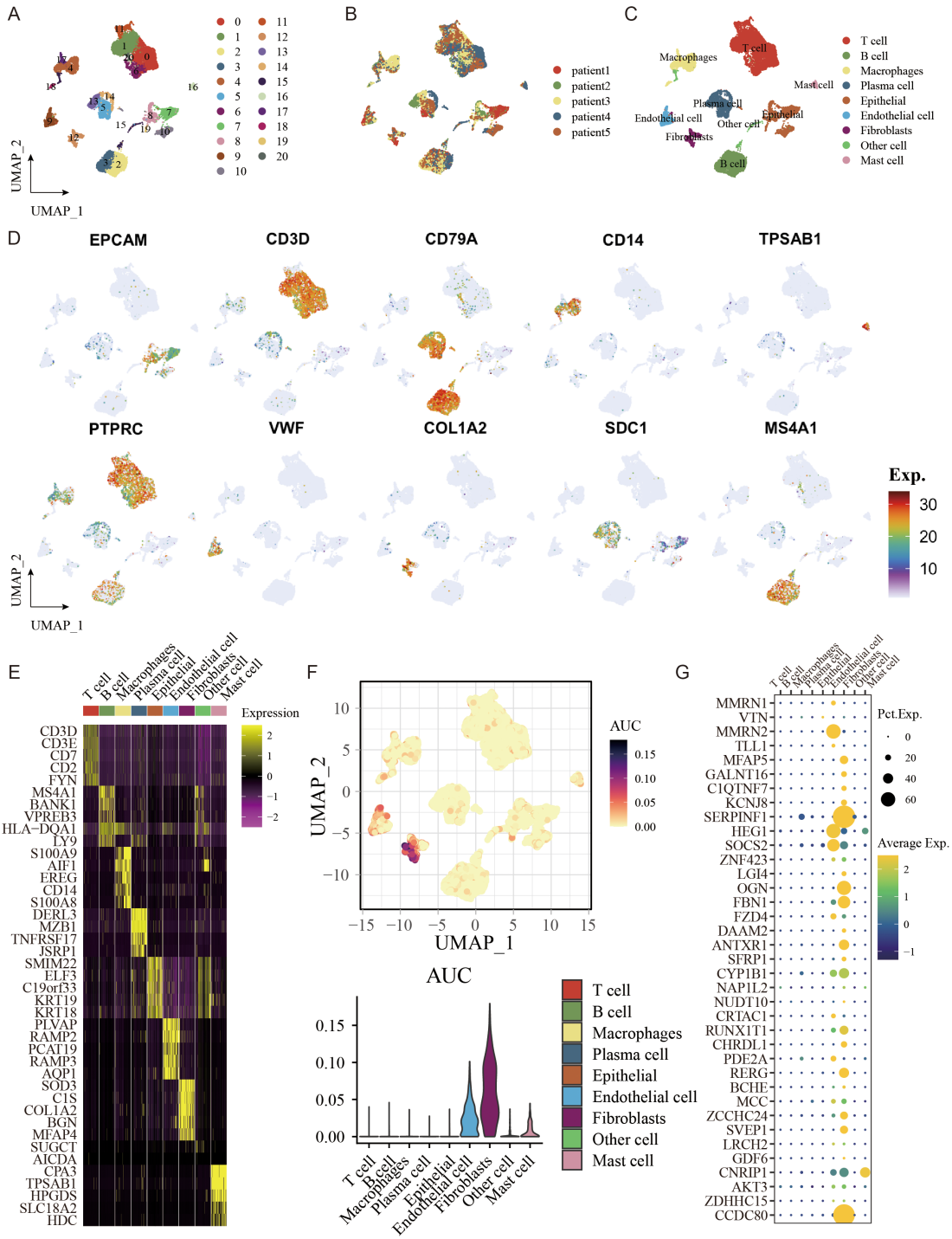

FIGURE 9
The single-cell atlas shows major cell lineages. **(A)** UMAP analysis was conducted to visualize and group 21 distinct cell clusters. **(B)** The distribution of cells with respect to the five patients (Patient1 to Patient5) is shown. **(C)** A UMAP plot displays nine primary lineages consisting of 23,060 cells. **(D)** UMAP feature plots were selected to display RNA expression of seven primary cell lineages. **(E)** Heatmap of the marker genes of the seven major cell lineages. **(F)** AUCell was used to analyze the gene enrichment of genes related to FAM that were used to create the signature. **(G)** FAM-related genes were utilized to create signatures in seven primary cell lineages.

Figures 10A, E), which was also defined by OPLS-DA analysis and CDF curves (Figure 10C, Supplementary Figure S5). Kaplan-Meier curves indicated that compared to cluster1, cluster2 had a better prognosis (log-rank test, P = 0.054, Figure 10B).

We identified the metabolites in the samples based on a broadly targeted metabolomic technique. A total of 1669 metabolites were detected using a non-targeted metabolomic technique for the detection of 42 mixed samples. Metabolomic variances among

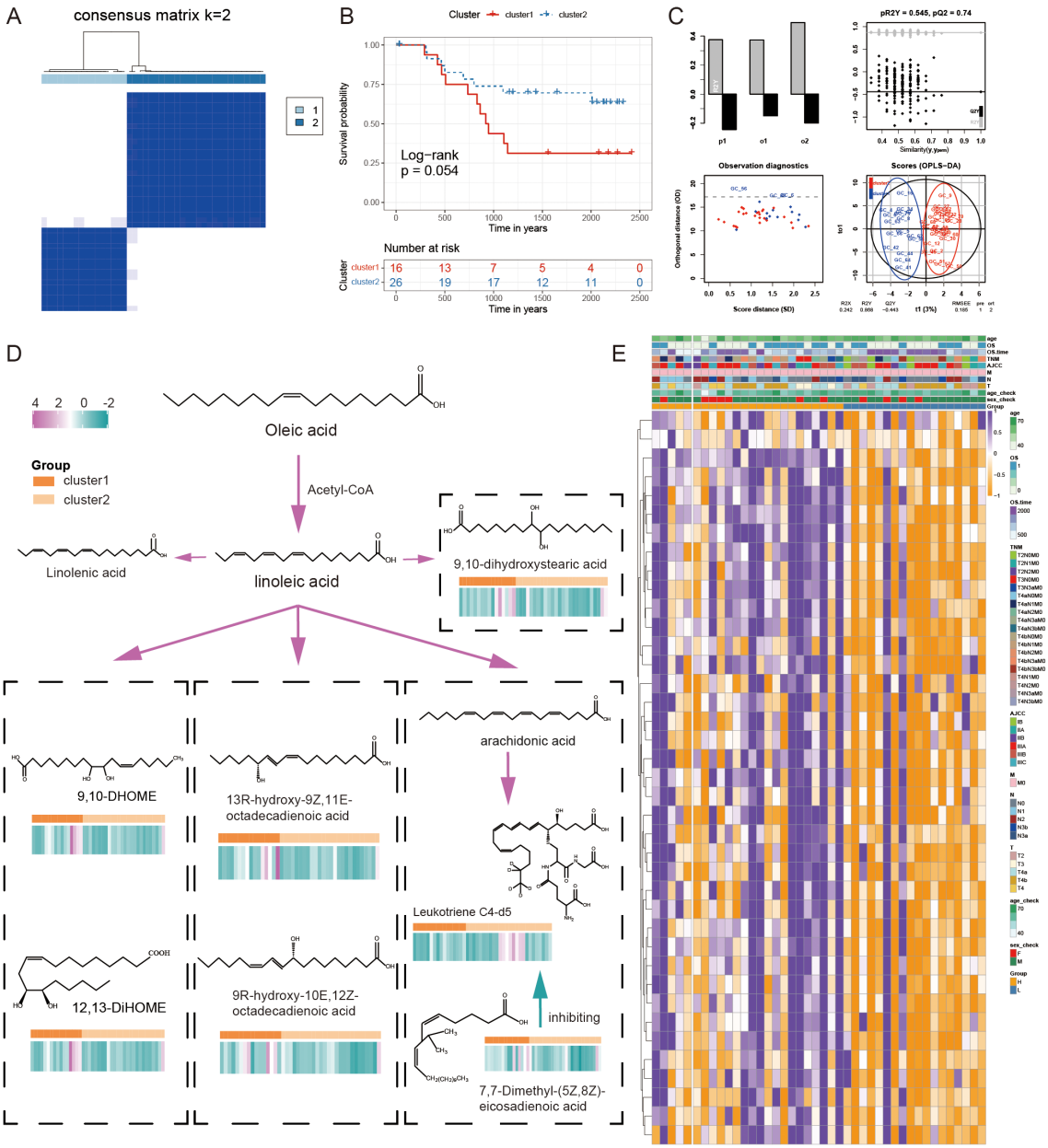

FIGURE 10
The combined examination of gene expression and metabolites in relation to the FAM pattern. **(A)** The ideal cluster number (K = 2) was identified based on the expression of signature genes related to FAM in 42 samples of GC. **(B)** Survival prediction of samples from two clusters was analyzed using Kaplan-Meier curves. **(C)** The OPLS-DA analysis of two clusters. **(D)** The differential FAM pathway diagram with content level differences. **(E)** A heatmap illustrating the levels of expression for 39 genes associated with FAM.

samples were explored through the utilization of a UPLC-MS/MS detection system, a custom-built database, and multivariate statistical techniques. Analysis of the variations between the two groups of metabolites revealed that a total of seven fatty acid-related metabolites exhibited statistically significant differences in expression, including '12,13-DiHOME', '13R-hydroxy-9Z,11E-octadecadienoic acid', '7,7-Dimethyl-(5Z,8Z)-eicosadienoic acid', '9,10-DHOME', '9,10-dihydroxystearic acid', '9R-hydroxy-10E,12Z-octadecadienoic acid', and 'Leukotriene C4-d5'. In addition to Leukotriene C4-d5, other fatty acid-related metabolites showed higher levels in cluster1. The differential FAM pathway diagram was displayed with the content level differences in Figure 10D. The combined transcriptomic and metabolomic analysis of the same GC samples further revealed the importance of signature in FAM.

4 Discussion

Extensive evidence indicates that metabolic reprogramming plays a critical role in tumor progression (44). Tumor cells

demonstrate increased FA production and uptake to support their needs, such as proliferation. A previous study utilized a FAM signature constructed from FAM-related genes to classify and evaluate the clinical therapies for colorectal cancer patients (45). In this study, a unique FAM profile was developed to personalize the evaluation of patients' FAM levels, aiming to investigate how these levels influence the clinical outcomes and therapeutic strategies of GC patients.

To explore the clinical and biological implications of FAM in GC, we conducted unsupervised clustering based on FAM-related gene expression, categorizing the TCGA GC cohort into two distinct clusters. This stratification revealed a significant survival disparity between the two groups. Additionally, we identified altered genes and differences in immune cell infiltration between the two subgroups, and we performed a functional enrichment analysis of DEGs associated with the FAM subtypes. Subsequently, DEGs at different levels (mRNA, lncRNA, and miRNA) between the two clusters were identified for further analysis.

In the analysis of somatic mutations and CNVs, we identified several gene mutations and CNVs associated with FAM genes. Among them, LRP1B, a potential tumor suppressor gene (46), has been shown to enhance responses to immune checkpoint inhibitors (ICIs) in cancers with mutations in this gene (47). LRP1B mutation could potentially be used as a biomarker to anticipate the immune response and is linked to extended survival in melanoma and NSCLC immunotherapy groups (47). A comprehensive study across multiple cancer types demonstrated that patients with pathogenic or likely pathogenic LRP1B alterations experienced significantly improved outcomes with ICI treatment compared to those with alterations of unknown significance, regardless of their TMB/MSI status (48). Furthermore, research indicated that a solitary LRP1B mutation is associated with a poor response to ICI therapy and adverse outcomes in patients with HCC (49). In our study, cluster1 exhibited a higher LRP1B mutation rate compared to cluster2, suggesting that GC patients in cluster1 might achieve better outcomes with immunotherapy.

Additionally, SETDB1, located in the 1q21.3 region of human tumors, acts as an epigenetic barrier that suppresses the intrinsic immunity of tumors, making it a promising target for immunotherapy (50). Furthermore, a higher amplification of 8q24.21 was observed in cluster1 compared to cluster2. This region contains the C-MYC oncogene, which is associated with the development and progression of numerous types of cancers (51). Studies have shown that the activation of MYC signaling enables cancer cells to disrupt the surrounding microenvironment, allowing them to evade the body's immune response (52). Amplification of 8q24.21 has been linked to tumor development and immune system modulation.

The ARID1A gene, located on 1p36.11, is the fourth most commonly mutated gene in GC. Han et al. demonstrated that ARID1A deficiency impairs fatty acid oxidation (FAO) by downregulating PPARα and altering the epigenetic landscape of specific metabolism-related genes (53). In our study, a higher deletion frequency of 1p36.11 was identified in cluster1 compared to cluster2. This finding suggests that patients in cluster2 may exhibit enhanced FAO capabilities.

PIK3CA initiates pathways that regulate cell growth, viability, division, movement, and morphology. It also promotes increased arachidonic acid metabolism through downstream mTORC2 signaling to sustain cell proliferation (54, 55). The PI3K-AKT-mTOR pathway plays a role in FAM in cancer, contributing to molecular heterogeneity and oncogenic signal transduction (44). The PI3Kδ enzyme complex is primarily found in the immune system, and its dysregulation-whether overactivation or insufficient activity-can lead to impaired and uncontrolled immune responses (56, 57). In this study, KEGG and GO analyses revealed that the two FAM clusters exhibited distinct differences in both FAM and immune activity.

Numerous studies have demonstrated a strong correlation between FAM and cancer progression, treatment, and immunity (58–60). FAs released by cancer cells influence immune cell infiltration within the tumor microenvironment. Disrupted lipid processing, such as upregulated FAO and *de novo* lipid synthesis, provides tumors with a competitive advantage against chemotherapy and radiation therapy, while also mitigating cellular stress associated with metastasis.

Additionally, T-cell activation requires *de novo* FA synthesis (61–63), and like other cell types, T cells rely on β-oxidation to degrade FAs as an energy source. FAO has been linked to various cell types, including CD8+ memory T cells and CD4+ regulatory T cells (19). Furthermore, the growth of B cells depends on monounsaturated FAs to sustain mitochondrial function and mTOR activity, thereby preventing excessive autophagy and endoplasmic reticulum stress (60).

In our research, cluster2 exhibited better survival outcomes compared to cluster1, potentially due to differences in immune cell infiltration. Previous study has also demonstrated that a high-fat diet increases FA uptake by cancer cells without significantly affecting tumor-infiltrating CD8+ T cells. This imbalance in FA distribution impairs the infiltration and function of CD8+ T cells, suggesting that optimizing metabolism could enhance tumor immunotherapy (64).

The observed AUC reduction in validation cohorts reflects real-world clinical complexity. Despite this, the model maintained significant survival stratification ($P < 0.05$) across all cohorts, demonstrating preserved clinical utility. Future multi-center studies with standardized protocols will further validate its robustness.

To assess the prognosis and effectiveness of immunotherapy and chemotherapy in patients with GC, we analyzed specific genes using various statistical methods, developed a signature consisting of 39 mRNAs, and confirmed its utility in guiding treatment decisions for immunotherapy and chemotherapy. Our study demonstrates that the FAM risk model is significantly associated with immune cell infiltration and immunotherapy response prediction. Specifically, the low-risk group exhibited a higher IPS and an improved response to immunotherapy, as validated in both GC and independent cohorts of Mela and UC. These findings

suggest that the FAM score could serve as a potential biomarker to stratify patients for immunotherapy selection.

Moreover, we found that the FAM score was positively correlated with mast cells and negatively correlated with CD56dim natural killer cells, indicating that immune cell infiltration characteristics could influence treatment efficacy. Given that mast cells can promote an immunosuppressive tumor microenvironment (65, 66), while CD56dim NK cells play a critical role in tumor surveillance (67, 68), these correlations provide mechanistic insights into how the FAM signature may reflect tumor immune evasion strategies.

Furthermore, the integration of the FAM score with TIDE analysis revealed that patients in the low-risk category exhibited a higher likelihood of responding positively to ICB therapies (43), reinforcing the potential clinical utility of this model. By incorporating the FAM score into patient stratification strategies, clinicians may be able to better identify individuals who are most likely to benefit from immunotherapy, thereby improving personalized treatment approaches for GC.

The combination of transcriptome data with single-cell analysis provides a more comprehensive understanding of the mechanisms underlying cell heterogeneity in GC. A single-cell analysis was conducted to further investigate the expression of FAM-associated genes used in constructing the signature. Our results demonstrated that the genes incorporated into the signature were primarily expressed in endothelial cells and fibroblasts. Previous studies have suggested that fibroblasts contribute to the progression of GC (69), implying that they play a role in the malignancy of the cancer.

We performed an integrated transcriptomic and metabolomic analysis of the FAM signature to obtain multiple key differential fatty acid metabolites in the fatty acid metabolic pathway. Previous research has indicated that the imbalance in FAM processing can promote the proliferation of cancer cells, which usually exhibiting increased lipid storage compared to normal cells (70). An analysis using Mendelian randomization indicated that stearic acid was linked to a higher likelihood of developing colorectal cancer (71). In our study, cluster1 exhibited significantly higher levels of most fatty acid-related metabolites, except for Leukotriene C4-d5, and was associated with a relatively poorer prognosis compared to cluster2. The Leukotriene D4- Cysteinyl Leukotriene 2 receptor (CysLT2R) signaling pathway plays a key role in colorectal cancer, where CysLT2R has shown antitumor activity in intestinal epithelial cells. Since CysLT2R is a receptor for both Leukotriene C4 and Leukotriene D4, it is plausible that Leukotriene C4 may possess tumor-suppressive properties through its interaction with CysLT2R (72). The seven metabolites identified in our study are all metabolites of linoleic acid, which as a polyunsaturated fatty acid (PUFA) and an essential fatty acid, regulates cancer development by participating in a variety of *in vivo* metabolic pathways, including apoptosis, oxidative stress, and cell proliferation (73). A metabolomic investigation of hepatocellular carcinoma (HCC) revealed decreased levels of linoleic acid in portal vein and fecal samples of HCC patients compared to healthy controls (74). Further research has demonstrated that linoleic acid can stimulate CD8 T cells to boost their anti-tumor functions in both *in vivo* and *in vitro* settings (75). Furthermore, it was shown that intestinal-type GC could not produce arachidonic acid (AA) and adrenic acid (AdA) from linoleic acid, making GC cells immune to ferroptosis (76), indicating that polyunsaturated fatty acids might impact GC via the ferroptosis pathway. Therefore, various fatty acid-related metabolites can influence cancer development, progression, and therapeutic efficacy in various ways, while FAM signature, as a vital cancer biomarker, contributes to guiding the prediction of FAM levels in the human body.

Our study provided a comprehensive computational analysis of the FAM signature and its potential role in immune infiltration and therapeutic response. Using publicly available datasets and statistical models, we identified key genes associated with survival risk and validated the prognostic significance of the FAM-based risk score.

However, we acknowledge certain limitations in our study. First, our findings were based on bioinformatics analyses without direct experimental validation. Future studies should include *in vitro* and *in vivo* experiments to confirm the biological role of the identified genes. Second, prospective clinical validation is needed to confirm the clinical relevance of the FAM signature. One promising approach is the use of GC 3D models (77). GC organoids could be used to functionally validate the FAM signature, assess its impact on immune cell infiltration and test its predictive value for drug response. This would help bridge the gap between computational predictions and clinical applications.

Despite these limitations, our study provides a valuable framework for identifying prognostic biomarkers and generating hypotheses for future experimental research.

5 Conclusion

We developed a FAM signature to guide treatment and evaluate the prognosis of GC patients. Nevertheless, this study still has certain limitations. Further expansion of the sample size is required to confirm the findings of this research. Moreover, experiments still need to verify the relationship between FAM, immune cell infiltration, and outcomes of GC patients.

Data availability statement

This study analyzed datasets that were accessible to the public. The data involved in this article could be downloaded directly from TCGA and GEO datasets (GSE34942, GSE26899, GSE26901, GSE28541, GSE167297, GSE13861, GSE15459). Genome-wide microRNA and mRNA expression profiling of 90 Tianjin GC samples included a validation set of Tianjin GC data (20). For further information on this research, please contact the corresponding author.

Ethics statement

The studies involving humans were approved by the Medical Ethics Committee of Tianjin Medical University Cancer Institute and Hospital. The studies were conducted in accordance with the local legislation and institutional requirements. The participants provided their written informed consent to participate in this study.

Author contributions

HL: Writing – review & editing, Conceptualization, Resources, Writing – original draft. XH: Conceptualization, Writing – original draft, Formal analysis, Methodology. XZ: Writing – original draft, Visualization. YY: Writing – original draft, Formal analysis, Validation. LW: Data curation, Investigation, Writing – original draft. YT: Data curation, Writing – original draft. HD: Writing – review & editing. KC: Funding acquisition, Project administration, Supervision, Writing – review & editing. BL: Funding acquisition, Project administration, Supervision, Writing – review & editing.

Funding

The author(s) declare that financial support was received for the research and/or publication of this article. This work was supported by the following grants: National Key R&D Program of China (2021YFC2500400) to KC; National Natural Science Foundation of China (8237258, 82073028) to BL; National Natural Science Foundation of China (82172894) to KC; The 14th five-year Special Project of Cancer Prevention and Treatment for the Youth Talents of Tianjin Cancer Institute and Hospital (YQ-04) to BL; Beijing-Tianjin-Hebei Basic Research Cooperation Special Project (20JCZXJC00090) to KC; Tianjin Key Medical Discipline (Specialty) Construction Project (TJYXZDXK-009A) to KC.

Acknowledgments

We are thankful to the TCGA platform and other opening access GC cohort provider.

Conflict of interest

The authors declare that the research was conducted in the absence of any commercial or financial relationships that could be construed as a potential conflict of interest.

Generative AI statement

The author(s) declare that no Generative AI was used in the creation of this manuscript.

Publisher's note

Supplementary material

The Supplementary Material for this article can be found online at: https://www.frontiersin.org/articles/10.3389/fonc.2025.1570873/full#supplementary-material

References

1. Bray F, Laversanne M, Sung H, Ferlay J, Siegel RL, Soerjomataram I, et al. Global cancer statistics 2022: GLOBOCAN estimates of incidence and mortality worldwide for 36 cancers in 185 countries. *CA Cancer J Clin*. (2024) 74:229–63. doi: 10.3322/caac.21834

2. Smyth EC, Nilsson M, Grabsch HI, van Grieken NC, Lordick F. Gastric cancer. *Lancet*. (2020) 396:635–48. doi: 10.1016/s0140-6736(20)31288-5

3. Santos CR, Schulze A. Lipid metabolism in cancer. *FEBS J*. (2012) 279:2610–23. doi: 10.1111/j.1742-4658.2012.08644.x

4. Bian X, Liu R, Meng Y, Xing D, Xu D, Lu Z. Lipid metabolism and cancer. *J Exp Med*. (2021) 218:e20201606. doi: 10.1084/jem.20201606

5. Medes G, Thomas A, Weinhouse S. Metabolism of neoplastic tissue. IV. A study of lipid synthesis in neoplastic tissue slices *in vitro*. *Cancer Res*. (1953) 13:27–9.

6. Kinlaw WB, Baures PW, Lupien LE, Davis WL, Kuemmerle NB. Fatty acids and breast cancer: make them on site or have them delivered. *J Cell Physiol*. (2016) 231:2128–41. doi: 10.1002/jcp.25332

7. Flavin R, Zadra G, Loda M. Metabolic alterations and targeted therapies in prostate cancer. *J Pathol*. (2011) 223:283–94. doi: 10.1002/path.2809

8. Rohrig F, Schulze A. The multifaceted roles of fatty acid synthesis in cancer. *Nat Rev Cancer*. (2016) 16:732–49. doi: 10.1038/nrc.2016.89

9. Rysman E, Brusselmans K, Scheys K, Timmermans L, Derua R, Munck S, et al. *De novo* lipogenesis protects cancer cells from free radicals and chemotherapeutics by promoting membrane lipid saturation. *Cancer Res*. (2010) 70:8117–26. doi: 10.1158/0008-5472.CAN-09-3871

10. Luo X, Cheng C, Tan Z, Li N, Tang M, Yang L, et al. Emerging roles of lipid metabolism in cancer metastasis. *Mol Cancer*. (2017) 16:76. doi: 10.1186/s12943-017-0646-3

11. Menendez JA, Lupu R. Fatty acid synthase and the lipogenic phenotype in cancer pathogenesis. *Nat Rev Cancer*. (2007) 7:763–77. doi: 10.1038/nrc2222

12. Currie E, Schulze A, Zechner R, Walther TC, Farese RV Jr. Cellular fatty acid metabolism and cancer. *Cell Metab*. (2013) 18:153–61. doi: 10.1016/j.cmet.2013.05.017

13. Pascual G, Avgustinova A, Mejetta S, Martin M, Castellanos A, Attolini CS, et al. Targeting metastasis-initiating cells through the fatty acid receptor CD36. *Nature*. (2017) 541:41–5. doi: 10.1038/nature20791

14. Pascual G, Dominguez D, Elosua-Bayes M, Beckedorff F, Laudanna C, Bigas C, et al. Dietary palmitic acid promotes a prometastatic memory via Schwann cells. *Nature*. (2021) 599:485–90. doi: 10.1038/s41586-021-04075-0

15. Le Bourgeois T, Strauss L, Aksoylar HI, Daneshmandi S, Seth P, Patsoukis N, et al. Targeting T cell metabolism for improvement of cancer immunotherapy. *Front Oncol*. (2018) 8:237. doi: 10.3389/fonc.2018.00237

16. Herber DL, Cao W, Nefedova Y, Novitskiy SV, Nagaraj S, Tyurin VA, et al. Lipid accumulation and dendritic cell dysfunction in cancer. *Nat Med*. (2010) 16:880–6. doi: 10.1038/nm.2172

17. Weinberg SE, Chandel NS. Futility sustains memory T cells. *Immunity*. (2014) 41:1–3. doi: 10.1016/j.immuni.2014.06.009

18. Beier UH, Angelin A, Akimova T, Wang L, Liu Y, Xiao H, et al. Essential role of mitochondrial energy metabolism in Foxp3(+) T-regulatory cell function and allograft survival. *FASEB J*. (2015) 29:2315–26. doi: 10.1096/fj.14-268409

19. Michalek RD, Gerriets VA, Jacobs SR, Macintyre AN, MacIver NJ, Mason EF, et al. Cutting edge: distinct glycolytic and lipid oxidative metabolic programs are essential for effector and regulatory CD4+ T cell subsets. *J Immunol*. (2011) 186:3299–303. doi: 10.4049/jimmunol.1003613

20. Song F, Yang D, Liu B, Guo Y, Zheng H, Li L, et al. Integrated microRNA network analyses identify a poor-prognosis subtype of gastric cancer characterized by the miR-200 family. *Clin Cancer Res*. (2014) 20:878–89. doi: 10.1158/1078-0432.CCR-13-1844

21. Zhao J, He K, Du H, Wei G, Wen Y, Wang J, et al. Bioinformatics prediction and experimental verification of key biomarkers for diabetic kidney disease based on transcriptome sequencing in mice. *PeerJ*. (2022) 10:e13932. doi: 10.7717/peerj.13932

22. Wilkerson MD, Hayes DN. ConsensusClusterPlus: a class discovery tool with confidence assessments and item tracking. *Bioinformatics*. (2010) 26:1572–3. doi: 10.1093/bioinformatics/btq170

23. Ritchie ME, Phipson B, Wu D, Hu Y, Law CW, Shi W, et al. limma powers differential expression analyses for RNA-sequencing and microarray studies. *Nucleic Acids Res*. (2015) 43:e47. doi: 10.1093/nar/gkv007

24. Zanjirband M, Baharlooie M, Safaeinejad Z, Nasr-Esfahani MH. Transcriptomic screening to identify hub genes and drug signatures for PCOS based on RNA-Seq data in granulosa cells. *Comput In Biol Medicine*. (2023) 154:106601. doi: 10.1016/j.compbiomed.2023.106601

25. Barbie DA, Tamayo P, Boehm JS, Kim SY, Moody SE, Dunn IF, et al. Systematic RNA interference reveals that oncogenic KRAS-driven cancers require TBK1. *Nature*. (2009) 462:108–12. doi: 10.1038/nature08460

26. Charoentong P, Finotello F, Angelova M, Mayer C, Efremova M, Rieder D, et al. Pan-cancer immunogenomic analyses reveal genotype-immunophenotype relationships and predictors of response to checkpoint blockade. *Cell Rep*. (2017) 18:248–62. doi: 10.1016/j.celrep.2016.12.019

27. Zhou H, Mu L, Yang Z, Shi Y. Identification of a novel immune landscape signature as effective diagnostic markers related to immune cell infiltration in diabetic nephropathy. *Front In Immunol*. (2023) 14:1113212. doi: 10.3389/fimmu.2023.1113212

28. Loring KE, Mattiske T, Lee K, Zysk A, Jackson MR, Noebels JL, et al. Early 17β-estradiol treatment reduces seizures but not abnormal behaviour in mice with expanded polyalanine tracts in the Aristaless related homeobox gene (ARX). *Neurobiol Disease*. (2021) 153:105329. doi: 10.1016/j.nbd.2021.105329

29. Mariathasan S, Turley SJ, Nickles D, Castiglioni A, Yuen K, Wang Y, et al. TGFbeta attenuates tumour response to PD-L1 blockade by contributing to exclusion of T cells. *Nature*. (2018) 554:544–8. doi: 10.1038/nature25501

30. Liu D, Schilling B, Liu D, Sucker A, Livingstone E, Jerby-Arnon L, et al. Integrative molecular and clinical modeling of clinical outcomes to PD1 blockade in patients with metastatic melanoma. *Nat Med*. (2019) 25:1916–27. doi: 10.1038/s41591-019-0654-5

31. Hugo W, Zaretsky JM, Sun L, Song C, Moreno BH, Hu-Lieskovan S, et al. Genomic and transcriptomic features of response to anti-PD-1 therapy in metastatic melanoma. *Cell*. (2017) 168:542. doi: 10.1016/j.cell.2017.01.010

32. Lauss M, Donia M, Harbst K, Andersen R, Mitra S, Rosengren F, et al. Mutational and putative neoantigen load predict clinical benefit of adoptive T cell therapy in melanoma. *Nat Communications*. (2017) 8:1738. doi: 10.1038/s41467-017-01460-0

33. Rose TL, Weir WH, Mayhew GM, Shibata Y, Eulitt P, Uronis JM, et al. Fibroblast growth factor receptor 3 alterations and response to immune checkpoint inhibition in metastatic urothelial cancer: a real world experience. *Br J Cancer*. (2021) 125:1251–60. doi: 10.1038/s41416-021-01488-6

34. Geeleher P, Cox N, Huang RS. pRRophetic: an R package for prediction of clinical chemotherapeutic response from tumor gene expression levels. *PloS One*. (2014) 9:e107468. doi: 10.1371/journal.pone.0107468

35. Geeleher P, Cox NJ, Huang RS. Clinical drug response can be predicted using baseline gene expression levels and *in vitro* drug sensitivity in cell lines. *Genome Biol*. (2014) 15:R47. doi: 10.1186/gb-2014-15-3-r47

36. Butler A, Hoffman P, Smibert P, Papalexi E, Satija R. Integrating single-cell transcriptomic data across different conditions, technologies, and species. *Nat Biotechnol*. (2018) 36:411–20. doi: 10.1038/nbt.4096

37. Maynard A, McCoach CE, Rotow JK, Harris L, Haderk F, Kerr DL, et al. Therapy-induced evolution of human lung cancer revealed by single-cell RNA sequencing. *Cell*. (2020) 182:1232–1251.e22. doi: 10.1016/j.cell.2020.07.017

38. Chen W, Gong L, Guo Z, Wang W, Zhang H, Liu X, et al. A novel integrated method for large-scale detection, identification, and quantification of widely targeted metabolites: application in the study of rice metabolomics. *Mol Plant*. (2013) 6:1769–80. doi: 10.1093/mp/sst080

39. Fraga CG, Clowers BH, Moore RJ, Zink EM. Signature-discovery approach for sample matching of a nerve-agent precursor using liquid chromatography-mass spectrometry, XCMS, and chemometrics. *Anal Chem*. (2010) 82:4165–73. doi: 10.1021/ac1003568

40. Shen X, Wang R, Xiong X, Yin Y, Cai Y, Ma Z, et al. Metabolic reaction network-based recursive metabolite annotation for untargeted metabolomics. *Nat Commun*. (2019) 10:1516. doi: 10.1038/s41467-019-09550-x

41. Liu Z, Liu L, Jiao D, Guo C, Wang L, Li Z, et al. Association of RYR2 mutation with tumor mutation burden, prognosis, and antitumor immunity in patients with esophageal adenocarcinoma. *Front Genet*. (2021) 12:669694. doi: 10.3389/fgene.2021.669694

42. Thevenot EA, Roux A, Xu Y, Ezan E, Junot C. Analysis of the human adult urinary metabolome variations with age, body mass index, and gender by implementing a comprehensive workflow for univariate and OPLS statistical analyses. *J Proteome Res*. (2015) 14:3322–35. doi: 10.1021/acs.jproteome.5b00354

43. Jiang P, Gu S, Pan D, Fu J, Sahu A, Hu X, et al. Signatures of T cell dysfunction and exclusion predict cancer immunotherapy response. *Nat Medicine*. (2018) 24:1550–8. doi: 10.1038/s41591-018-0136-1

44. Koundouros N, Poulogiannis G. Reprogramming of fatty acid metabolism in cancer. *Br J Cancer*. (2020) 122:4–22. doi: 10.1038/s41416-019-0650-z

45. Ding C, Shan Z, Li M, Chen H, Li X, Jin Z. Characterization of the fatty acid metabolism in colorectal cancer to guide clinical therapy. *Mol Ther Oncolytics*. (2021) 20:532–44. doi: 10.1016/j.omto.2021.02.010

46. Lu YJ, Wu CS, Li HP, Liu HP, Lu CY, Leu YW, et al. Aberrant methylation impairs low density lipoprotein receptor-related protein 1B tumor suppressor function in gastric cancer. *Genes Chromosomes Cancer*. (2010) 49:412–24. doi: 10.1002/gcc.20752

47. Chen H, Chong W, Wu Q, Yao Y, Mao M, Wang X. Association of LRP1B mutation with tumor mutation burden and outcomes in melanoma and non-small cell lung cancer patients treated with immune check-point blockades. *Front Immunol*. (2019) 10:1113. doi: 10.3389/fimmu.2019.01113

48. Brown LC, Tucker MD, Sedhom R, Schwartz EB, Zhu J, Kao C, et al. LRP1B mutations are associated with favorable outcomes to immune checkpoint inhibitors across multiple cancer types. *J Immunother Cancer*. (2021) 9:e001792. doi: 10.1136/jitc-2020-001792

49. Cheng Y, Tang R, Li X, Wang B, Cheng Y, Xiao S, et al. LRP1B is a potential biomarker for tumor immunogenicity and prognosis of HCC patients receiving ICI treatment. *J Hepatocell Carcinoma*. (2022) 9:203–20. doi: 10.2147/JHC.S348785

50. Griffin GK, Wu J, Iracheta-Vellve A, Patti JC, Hsu J, Davis T, et al. Epigenetic silencing by SETDB1 suppresses tumour intrinsic immunogenicity. *Nature*. (2021) 595:309–14. doi: 10.1038/s41586-021-03520-4

51. Dang CV. MYC on the path to cancer. *Cell*. (2012) 149:22–35. doi: 10.1016/j.cell.2012.03.003

52. Dhanasekaran R, Deutzmann A, Mahauad-Fernandez WD, Hansen AS, Gouw AM, Felsher DW. The MYC oncogene - the grand orchestrator of cancer growth and immune evasion. *Nat Rev Clin Oncol*. (2022) 19:23–36. doi: 10.1038/s41571-021-00549-2

53. Qu YL, Deng CH, Luo Q, Shang XY, Wu JX, Shi Y, et al. Arid1a regulates insulin sensitivity and lipid metabolism. *EBioMedicine*. (2019) 42:481–93. doi: 10.1016/j.ebiom.2019.03.021

54. Koundouros N, Karali E, Tripp A, Valle A, Inglese P, Perry NJS, et al. Metabolic fingerprinting links oncogenic PIK3CA with enhanced arachidonic acid-derived eicosanoids. *Cell*. (2020) 181:1596–1611 e1527. doi: 10.1016/j.cell.2020.05.053

55. Kudo Y, Tanaka Y, Tateishi K, Yamamoto K, Yamamoto S, Mohri D, et al. Altered composition of fatty acids exacerbates hepatotumorigenesis during activation of the phosphatidylinositol 3-kinase pathway. *J Hepatol*. (2011) 55:1400–8. doi: 10.1016/j.jhep.2011.03.025

56. Nunes-Santos CJ, Uzel G, Rosenzweig SD. PI3K pathway defects leading to immunodeficiency and immune dysregulation. *J Allergy Clin Immunol*. (2019) 143:1676–87. doi: 10.1016/j.jaci.2019.03.017

57. Lucas CL, Chandra A, Nejentsev S, Condliffe AM, Okkenhaug K. PI3Kdelta and primary immunodeficiencies. *Nat Rev Immunol*. (2016) 16:702–14. doi: 10.1038/nri.2016.93

58. Butler LM, Perone Y, Dehairs J, Lupien LE, de Laat V, Talebi A, et al. Lipids and cancer: Emerging roles in pathogenesis, diagnosis and therapeutic intervention. *Adv Drug Delivery Rev*. (2020) 159:245–93. doi: 10.1016/j.addr.2020.07.013

59. Corn KC, Windham MA, Rafat M. Lipids in the tumor microenvironment: From cancer progression to treatment. *Prog Lipid Res*. (2020) 80:101055. doi: 10.1016/j.plipres.2020.101055

60. Lochner M, Berod L, Sparwasser T. Fatty acid metabolism in the regulation of T cell function. *Trends Immunol*. (2015) 36:81–91. doi: 10.1016/j.it.2014.12.005

61. Berod L, Friedrich C, Nandan A, Freitag J, Hagemann S, Harmrolfs K, et al. *De novo* fatty acid synthesis controls the fate between regulatory T and T helper 17 cells. *Nat Med*. (2014) 20:1327–33. doi: 10.1038/nm.3704

62. Kidani Y, Elsaesser H, Hock MB, Vergnes L, Williams KJ, Argus JP, et al. Sterol regulatory element-binding proteins are essential for the metabolic programming of effector T cells and adaptive immunity. *Nat Immunol*. (2013) 14:489–99. doi: 10.1038/ni.2570

63. Yang K, Shrestha S, Zeng H, Karmaus PW, Neale G, Vogel P, et al. T cell exit from quiescence and differentiation into Th2 cells depend on Raptor-mTORC1-

mediated metabolic reprogramming. *Immunity*. (2013) 39:1043–56. doi: 10.1016/j.immuni.2013.09.015

64. Ringel AE, Drijvers JM, Baker GJ, Catozzi A, Garcia-Canaveras JC, Gassaway BM, et al. Obesity shapes metabolism in the tumor microenvironment to suppress anti-tumor immunity. *Cell*. (2020) 183:1848–1866 e1826. doi: 10.1016/j.cell.2020.11.009

65. Kalesnikoff J, Galli SJ. Antiinflammatory and immunosuppressive functions of mast cells. *Methods In Mol Biol (Clifton NJ)*. (2011) 677:207–20. doi: 10.1007/978-1-60761-869-0_15

66. Kalesnikoff J, Galli SJ. New developments in mast cell biology. *Nat Immunol*. (2008) 9:1215–23. doi: 10.1038/ni.f.216

67. Cao Y, Wang X, Jin T, Tian Y, Dai C, Widarma C, et al. Immune checkpoint molecules in natural killer cells as potential targets for cancer immunotherapy. *Signal Transduction Targeted Ther*. (2020) 5:250. doi: 10.1038/s41392-020-00348-8

68. Cichicki F, Schlums H, Theorell J, Tesi B, Miller JS, Ljunggren H-G, et al. Diversification and functional specialization of human NK cell subsets. *Curr Topics In Microbiol Immunol*. (2016) 395:63–94. doi: 10.1007/82_2015_487

69. Kang B, Camps J, Fan B, Jiang H, Ibrahim MM, Hu X, et al. Parallel single-cell and bulk transcriptome analyses reveal key features of the gastric tumor microenvironment. *Genome Biol*. (2022) 23:265. doi: 10.1186/s13059-022-02828-2

70. Li Z, Zhang H. Reprogramming of glucose, fatty acid and amino acid metabolism for cancer progression. *Cell Mol Life Sci*. (2016) 73:377–92. doi: 10.1007/s00018-015-2070-4

71. May-Wilson S, Sud A, Law PJ, Palin K, Tuupanen S, Gylfe A, et al. Pro-inflammatory fatty acid profile and colorectal cancer risk: A Mendelian randomisation analysis. *Eur J Cancer*. (2017) 84:228–38. doi: 10.1016/j.ejca.2017.07.034

72. Jiang M, Xu Y, Luan X, Wu K, Li Z, Xu HE, et al. Structural basis of the cysteinyl leukotriene receptor type 2 activation by LTD4. *Proc Natl Acad Sci United States America*. (2025) 122:e2417148122. doi: 10.1073/pnas.2417148122

73. Vangaveti VN, Jansen H, Kennedy RL, Malabu UH. Hydroxyoctadecadienoic acids: Oxidised derivatives of linoleic acid and their role in inflammation associated with metabolic syndrome and cancer. *Eur J Pharmacol*. (2016) 785:70–6. doi: 10.1016/j.ejphar.2015.03.096

74. Liu J, Geng W, Sun H, Liu C, Huang F, Cao J, et al. Integrative metabolomic characterisation identifies altered portal vein serum metabolome contributing to human hepatocellular carcinoma. *Gut*. (2022) 71:1203–13. doi: 10.1136/gutjnl-2021-325189

75. Nava Lauson CB, Tiberti S, Corsetto PA, Conte F, Tyagi P, Machwirth M, et al. Linoleic acid potentiates CD8(+) T cell metabolic fitness and antitumor immunity. *Cell Metab*. (2023) 35:633–650 e639. doi: 10.1016/j.cmet.2023.02.013

76. Lee JY, Nam M, Son HY, Hyun K, Jang SY, Kim JW, et al. Polyunsaturated fatty acid biosynthesis pathway determines ferroptosis sensitivity in gastric cancer. *Proc Natl Acad Sci U S A*. (2020) 117:32433–42. doi: 10.1073/pnas.2006828117

77. Farhat J, Pandey I, AlWahsh M. Transcending toward Advanced 3D-Cell Culture Modalities: A Review about an Emerging Paradigm in Translational Oncology. *Cells*. (2021) 10:1657. doi: 10.3390/cells10071657

frontiers | Frontiers in Oncology

TYPE Original Research
PUBLISHED 02 July 2025
DOI 10.3389/fonc.2025.1578419

OPEN ACCESS

EDITED BY
Balkrishna Chaube,
Indian Institute of Technology Dharwad, India

REVIEWED BY
Bharath Kumar Gajjela,
Icahn School of Medicine at Mount Sinai, United States
Ganesh Kumar Barik,
Dana–Farber Cancer Institute, United States

*CORRESPONDENCE
Ang Xuan
xuanang@zzu.edu.cn
Xinyu Wu
xinyu-wu2008@163.com
Junling Xu
xjlhzq@zzu.edu.cn
Yongju Gao
gaoyongju@zzu.edu.cn

†These authors have contributed equally to this work

RECEIVED 17 February 2025
ACCEPTED 30 May 2025
PUBLISHED 02 July 2025

CITATION
Jin H, Hu B, Zhang J, Long Y, Xuan A, Wu X, Xu J and Gao Y (2025) The predictive value of total body PET/CT in high PD-L1 expression and immunotherapy in advanced non-small cell lung cancer patients.
Front. Oncol. 15:1578419.
doi: 10.3389/fonc.2025.1578419

The predictive value of total body PET/CT in high PD-L1 expression and immunotherapy in advanced non-small cell lung cancer patients

Huibin Jin[1,2†], Bingxin Hu[1,2†], Jie Zhang[1,2], Ye Long[1,2], Ang Xuan[1,2*], Xinyu Wu[1,2*], Junling Xu[1,2*] and Yongju Gao[1,2*]

[1]Department of Nuclear Medicine of Henan Provincial People's Hospital and The People's Hospital of Zhengzhou University, Zhengzhou, China, [2]Henan Key Laboratory of Novel Molecular Probes and Clinical Translation in Nuclear Medicine, Henan Provincial People's Hospital, Zhengzhou, China

Introduction: Total-body positron emission tomography/computed tomography (PET/CT) using uEXPLORER scanners demonstrates superior imaging capabilities for assessing programmed death ligand 1 (PD-L1) expression heterogeneity between primary tumors (PTs) and metastatic tumors (MTs) in advanced nonsmall cell lung cancer (NSCLC).

Methods: This retrospective study of 99 treatment-naïve NSCLC patients revealed that metabolic parameters (SUVmax, SUR-L, and SUR-BP) derived from biopsy-correlated PET/CT sites significantly predicted high PD-L1 expression (TC ≥ 50% or IC ≥ 10% by IHC).

Results: SUR-L exhibited the highest diagnostic accuracy (AUC = 0.758, $p < 0.001$). Among 30 immunotherapytreated patients, PD-L1 positivity and SUR-BP ≥ 7.30 were associated with prolonged disease-free survival (DFS) ($p = 0.012$ and $p = 0.035$, respectively).

Discussion: Our findings establish SUR-BP as a novel non-invasive biomarker for immunotherapy prognosis in NSCLC, addressing spatial heterogeneity challenges in PD-L1 assessment.

KEYWORDS

NSCLC, SUR, PD-L1, immunotherapy, prognosis

Introduction

In recent years, immune checkpoint inhibitors (ICIs) targeting programmed death ligand 1 (PD-L1) have become an important additional cornerstone in the therapy of advanced non-small cell lung cancer (NSCLC) (1–5). Previous studies demonstrated that PD-L1 expression has two mechanisms: innate expression on tumor cells (TCs) and variable expression on tumor-infiltrating immune cells (ICs) (6, 7). Based on the European Medicines Agency (EMA) and the Food and Drug Administration (FDA), PD-L1 expression no less than 50% on TC or 10% on IC was defined as high expression, which implies that immunotherapy could be a first-line treatment for advanced NSCLC (8, 9). Therefore, it is important to get accurate PD-L1 expression levels when choosing proper treatments.

Immunohistochemistry (IHC) is widely used to detect PD-L1 expression. Generally, two kinds of specimens were tested in advanced NSCLC patients: biopsy of primary tumors (PTs) and biopsy of metastatic tumors (MTs). However, previous studies had reported the inconsistency of PD-L1 expression in different specimens (10, 11). Some studies had confirmed the temporal and spatial discordance of PD-L1 between PTs and metastases and found higher expression in PTs (12–15). However, other studies (16–18) obtained different results. The inconsistency of PD-L1 expression might be due to intramural heterogeneity in which biopsy samples could not show the panoramic view of the tumor and its microenvironment (10, 19).

β-2-^{18}F-fluoro-2-deoxy-D-glucose positron emission tomography/computed tomography (^{18}F-FDG PET/CT) plays a key role in tumor diagnosis, staging, re-staging, and response evaluation. Currently, the total-body PET/CT, uEXPLORER (United Imaging Healthcare, Shanghai, China) with an 194-cm-long FOV, dramatically improves image quality and the ability to detect small lesions (20, 21). Our previous studies had demonstrated that PET/CT-related parameters, including maximum standard uptake value (SUVmax) and standard uptake value ratio (SUR), had good consistency with PD-L1 expression (22–24).

Based on the above, to avoid differences between PTs and MTs in advanced NSCLC patients, we collected PD-L1 expression and PET-related parameters for both primary and metastatic sites. Thus, we conduct a retrospective study to analyze the relationship between PET/CT-related metabolic parameters obtained by the newest PET/CT machine and high PD-L1 expression in PT and MT. Furthermore, we explored the prognostic value of the expression and parameters with respect to patients' prognosis.

Methods

Ethics statement

The study protocol was approved by the Institutional Review Board of Henan Provincial People's Hospital. Our ethics committee waived the need for informed consent from the study participants. All methods were performed in accordance with the relevant guidelines and regulations in our analysis.

Patients

In this study, 99 patients with primary NSCLC from June 2020 to March 2022 in our hospital were enrolled. The screening criteria were as follows: (1) first diagnosis of NSCLC without other systemic diseases or treatments; (2) integrity of pathological data; (3) total body PET/CT images before biopsy; and (4) first treated at our hospital during the study period. Clinicopathological data included age, gender, maximum diameter, smoking history, histological subtype, the source of histologic samples, metastatic sites, and treatments. The study protocol was approved by the institutional review board, and the need for written informed consent was waived.

^{18}F-FDG PET/CT

All patients fasted no less than 6 h and serum glucose levels were no more than 10 mmol/L before intravenous injection of ^{18}F-FDG with a dosing regimen (3.7 MBq/kg). All patients rested approximately 60 min after injection and then underwent PET/CT imaging. All images were acquired on total-body PET/CT (uEXPLORER, United Imaging Healthcare, Shanghai, China). A low-dose CT scan (tube current, 10 mA; voltage, 100 kV; rotation time, 0.5 s; pitch, 1.0125; collimation, 80 × 0.5 mm) was conducted first for anatomical localization and reconstructed in a 512 × 512 matrix for attenuation correlation. Then, PET imaging was performed with 5-min acquisition.

Image analysis

All images were analyzed by two experienced nuclear medicine physicians with one of them having at least 10 years of experience. Region of interest (ROI) was drawn at lung primary lesions and metastatic lesions on PET/CT images and SUVmax was calculated based on body weight. Meanwhile, mean standard uptake value (SUVmean) of liver and blood pool were collected. A 30-mm-diameter ROI was placed at the normal right hepatic lobe to avoid intrahepatic lesions. A 10-mm-diameter ROI was placed at the middle of the descending aorta to avoid partial volume effects. SUR values were defined as the ratios of lung lesions/metastatic lesions SUVmax to liver and blood pool SUVmean (SUR-L and SUR-BP, respectively).

Immunohistochemical staining

All tissues were fixed with 10% formalin after no less than 6 h and embedded in paraffin, and then hematoxylin–eosin (HE) staining and IHC were conducted. All samples were analyzed on

an automated stainer with 22C3 (PD-L1 test kits, DAKO/Agilent, USA) (25). At least two pathologists evaluated the slides to determine the scores of PD-L1-positive cells on TC and/or IC. According to clinical trials (1, 2), PD-L1 high expression was defined as positive scores on TC of no less than 50% or IC no less than 10%.

Response assessment

All patients' treatment response information was retrospectively acquired from electronic medical records and patients' imaging and testing results. Disease-free survival (DFS) was used to conduct a response assessment over a median follow-up of 5.53 (0.17–34.07) months in our patients. DFS was defined as the time from diagnosis until disease progression (positive) or the last visit in our hospital where the patient was alive without recurrence (negative). All treatment protocols were the first line. As for the immunotherapy group, those patients were undergoing immunotherapy only or in combination with chemotherapy. As for the "others" group, those patients were undergoing chemotherapy, targeted therapy, or radiotherapy. The response to therapy was assessed on 4 August 2023.

Statistical analysis

Statistically significant differences were analyzed using chi-square test or Fisher's exact test for categorical variables and Mann–Whitney U test for continuous variables. Receiver operating characteristic (ROC) curve analyses were used to test the continuous variables and discriminate negative and positive PD-L1 expression; sensitivity (Se) and specificity (Sp) were collected to choose the optimal cutoff value, and the 95% confidence intervals (CIs) were calculated. The log-rank test with Kaplan–Meier analysis was used to make survival analysis. All statistical analyses were carried out with SPSS, version 23.0 (SPSS Inc., Chicago, IL, USA). Statistical significance was defined as $p < 0.05$.

Results

Patients' clinical characteristics

Clinical characteristics are shown in Table 1. There were 99 patients enrolled in the research with 20 squamous cell carcinoma (SCC) and 79 adenocarcinoma (ADC). Among these 99 patients, the biopsy of 62 patients was from the PTs and that of 37 patients was from the MTs. A total of 37 patients (37.4%) expressed PD-L1 positively with 23 (37.1%) in biopsy of PTs and 14 (37.8%) in MTs. As for MTs, 27 (73%) were from lymph nodes, 5 (13.5%) from bone, 2 (5.4%) from brain, 1 (2.7%) from pleura, and 2 (5.4%) from pleural fluid.

Among all the patients, a total of 30 patients received immunotherapy and 69 patients received other first-line treatments. A total of 47 patients (47.4%) had disease progression, with 18 (60%) patients receiving immunotherapy and 29 (42%) receiving the other treatments. Of the patients, 58 (58.6%) were younger than 63 years, 62 (62.6%) were male patients, 62 (62.6%) had a diameter of no less than 30 mm, and 48 (48.5%) were smokers. None of these characteristics were correlated with PD-L1 expression or DFS.

^{18}F-FDG PET parameters

The correlation between PET-related parameters and PD-L1 expression is shown in Table 2 and Figure 1. PET/CT parameters were acquired from both primary and metastatic lesions, ensuring spatial concordance with biopsy sites.

In our patients, those metabolic parameters were higher in positive than in negative, including SUVmax (16.29 ± 9.06 vs. 10.29 ± 5.50, $p < 0.001$), SUR-L (7.78 ± 4.17 vs. 4.67 ± 2.91, $p < 0.001$), and SUR-BP (11.51 ± 6.96 vs. 6.87 ± 4.36, $p = 0.001$). The best cutoff value of SUVmax determined by ROC was 13.29, and the area under curve (AUC) was 0.739 (95% CI: 0.642–0.836, $p < 0.001$) with a sensitivity (Se) of 64.9% (95% CI: 47.5%–79.8%) and a specificity (Sp) of 72.6% (95% CI: 59.8%–83.2%). The best cutoff value of SUR-L determined by ROC was 4.97, and the AUC was 0.758 (95% CI: 0.663–0.853, $p < 0.001$) with a Se of 75.7%(58.8%–88.2%) and a Sp of 67.7% (54.7%–79.1%). The best cutoff value of SUR-BP determined by ROC was 7.30, and the AUC was 0.735 (95% CI: 0.636–0.834, $p = 0.000$) with a Se of 70.3% (53.0%–84.1%) and a Sp of 67.7% (54.7%-79.1%). It could be seen that SUR-L, which had the largest AUC, demonstrated moderate diagnostic accuracy.

The PET/CT and IHC images are shown in Figure 2. The first patient (A–C) was a 68-year-old man with ADC. The biopsy site was from a rib metastasis and PD-L1 expression was negative. The SUVmax, SUR-L, and SUR-BP of PTs were 15.72, 6.89, and 9.14, and those of rib metastasis were 19.92, 8.74, and 11.58, respectively. The second patient (D–F) was a 66-year-old woman with SCC. The biopsy site was from lung PTs and PD-L1 expression was positive. The SUVmax, SUR-L, and SUR-BP of PTs were 14.76, 5.35, and 10.32 and those of lung PTs were 5.23, 1.89, and 3.66, respectively.

Prognostic value of PD-L1 expression and PET parameters

Kaplan–Meier survival curves for DFS based on PD-L1 expression and PET parameters are shown in Figures 3, 4. In our group, there were 30 patients undergoing immunotherapy only or combination with chemotherapy and 69 patients undergoing other treatments, including chemotherapy, targeted therapy, or radiotherapy. During our follow-up process, a total of 47 people had disease progression. PD-L1 expression was not related to DFS in all patients ($p = 0.622$) and it was the same with the other treatments ($p = 0.426$). However, PD-L1 positivity had a significantly longer DFS ($p = 0.012$) than PD-L1 negativity in patients who received immunotherapy.

TABLE 1 Characteristics of PD-L1 expression.

Characteristics	PD-L1				DFS			
	Negative (62)	Positive (37)	χ^2	P	Negative (52)	Positive (47)	χ^2	P
Age (year)			0.081	**0.775**			0.358	**0.550**
<63	25	16			23	18		
≥63	37	21			29	29		
Gender			0.126	**0.722**			0.356	**0.551**
Male	38	24			34	28		
Female	24	13			18	19		
Maximum Diameter (mm)			1.475	**0.225**			0.055	**0.814**
<30	26	11			20	17		
≥30	36	26			32	30		
Smoking history			0.001	**0.980**			0.518	**0.472**
Smoker	30	18			27	21		
Non-smoker	32	19			25	26		
Histologic subtype			3.327	**0.068**			0.562	**0.454**
ADC	53	26			40	39		
SCC	9	11			12	8		
Biopsy			0.005	**0.941**			0.033	**0.857**
Primary tumors	39	23			33	29		
Metastatic tumors	23	14			19	18		
Metastatic tumors			4.184	**0.382**			1.211	**0.876**
Lymph node	16	11			13	14		
Bone	3	2			3	2		
Brain	2	0			1	1		
Pleura	0	1			1	0		
Pleural fluid	2	0			1	1		
Treatments			2.932	**0.087**			2.708	**0.100**
Immunotherapy	15	15			12	18		
Others	47	22			40	29		

PD-L1, programmed death ligand 1; DFS, disease-free survival; NSCLC, non-small cell lung cancer; ADC, adenocarcinoma; SCC, squamous cell carcinoma; immunotherapy, immunotherapy only or combination with chemotherapy; others, chemotherapy, targeted therapy or radiotherapy.
Bold value, p value.

TABLE 2 The relationship between PET parameters and PD-L1 expression.

Parameters	Numerical value (mean±SD)			
	PD-L1(-)(62)	PD-L1(+)(37)	U	P
SUVmax	10.29±5.50	16.29±9.06	599	0.000*
SUR-L	4.67±2.91	7.78±4.17	555	0.000*
SUR-BP	6.87±4.36	11.51±6.96	608	0.000*

*: P<0.05; SD, standard deviation; U, Mann-Whitney U test; SUVmax, the maximum of standard uptake value; SUR-L, the ratio of lung lesion SUVmax to liver SUVmean; SUR-BP, the ratio of lung lesion SUVmax to blood pool SUVmean.

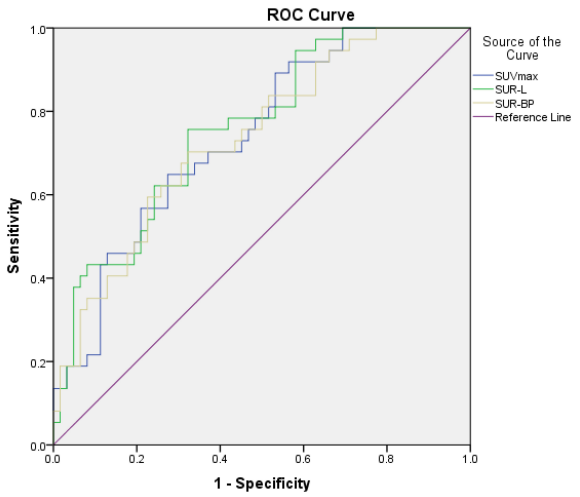

FIGURE 1
The relationship between PET parameters and high PD-L1 expression. The area under curve (AUC), cutoff value, sensitivity, and specificity of SUVmax were 0.739, 13.29, 64.9%, and 72.6%, respectively; those of SUR-L were 0.758, 4.97, 75.7%, and 67.7%, respectively; and those of SUR-BP were 0.735, 7.30, 70.3%, and 67.7%, respectively.

By applying a cutoff value of PD-L1-positive expression in SUVmax (13.29), SUR-L (4.97), and SUR-BP (7.30), we found that DFS was longer in SUR-BP ≥ 7.30 for those who received immunotherapy only or combination with chemotherapy. There was no significant difference in the other groups. SUR-BP ≥ 7.30 was the only correlating factor for DFS in our analysis.

Discussion

ICIs targeting PD-1/PD-L1 have prolonged the survival time in patients with advanced NSCLC, and PD-L1 is the only biomarker used for screening patients for ICIs. Previous studies had pointed out that PD-L1 expression was inconsistent in PT and MT. Based on these studies, PD-L1 expression data were collected from PTs and MTs of patients with advanced lung cancer, as well as the relevant PET parameters from PET/CT machines corresponding to the biopsy sites. To our knowledge, this represents the first investigation of the predictive value of PET/CT parameters for immunotherapy outcomes in patients with advanced NSCLC.

Some studies have investigated PD-L1 expression in NSCLC between PTs and MTs and found significant discrepancy between

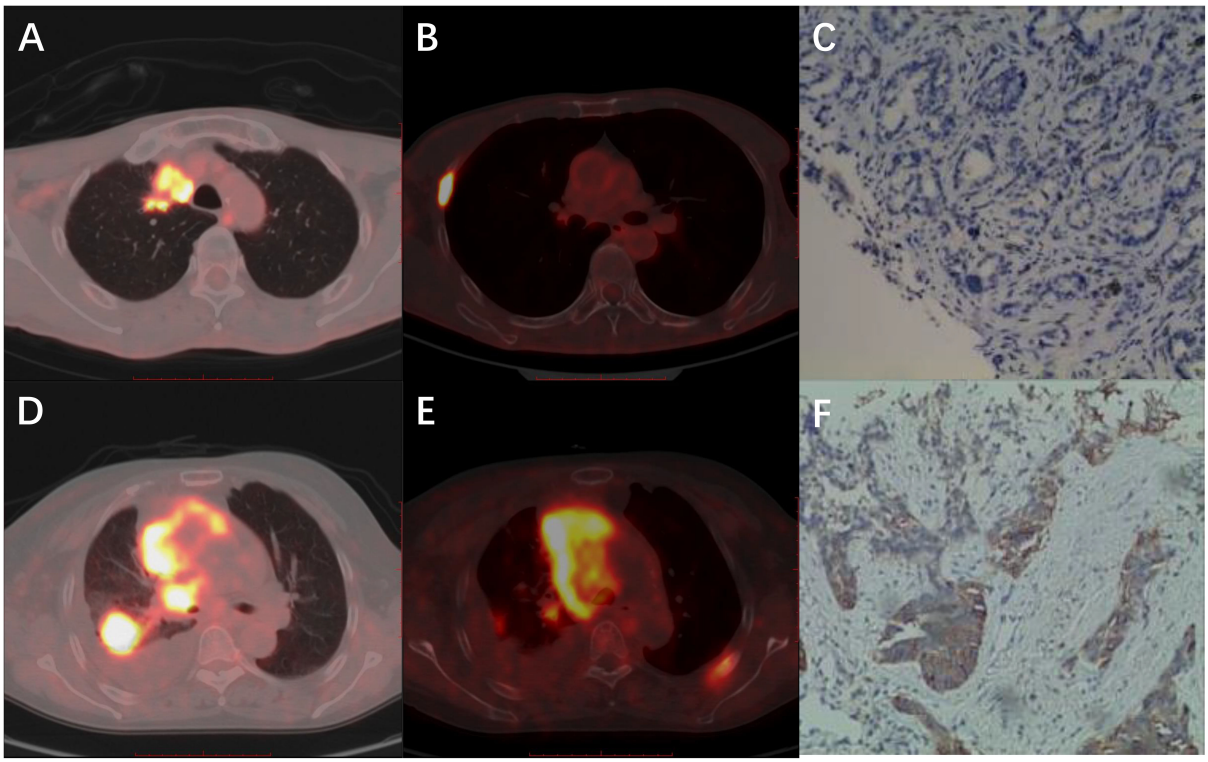

FIGURE 2
Representative images of PET/CT and IHC. **(A-C)** A 68-year-old man with ADC. The biopsy site was from rib metastasis and PD-L1 expression was negative. The SUVmax, SUR-L, and SUR-BP of primary tumors were 15.72, 6.89, and 9.14 and of rib metastasis were 19.92, 8.74, and 11.58. **(D-F)** A 66-year-old woman with SCC. The biopsy site was from lung primary tumors and PD-L1 expression was positive. The SUVmax, SUR-L, and SUR-BP of primary tumors were 14.76, 5.35, and 10.32, and those of lung primary tumors were 5.23, 1.89, and 3.66, respectively.

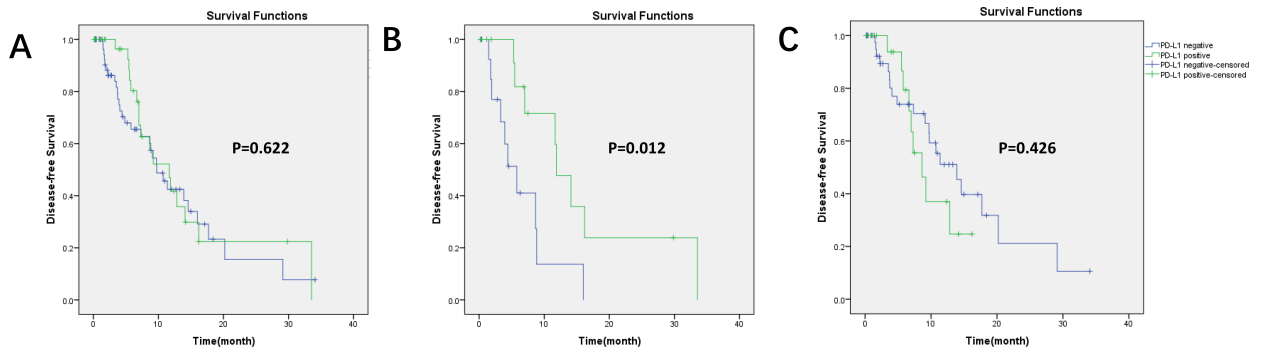

FIGURE 3
Kaplan–Meier survival curves for DFS based on PD-L1 expression. **(A)** In all patients (99 patients), p = 0.622; **(B)** in immunotherapy (30 patients), p = 0.012, PD-L1 positivity had longer DFS; **(C)** in other treatments (69 patients), p = 0.426.

the two (10–13, 16–18). Generally, the expression was higher in PTs than that in MTs. Previous studies (22, 23, 26–28) had confirmed that PET/CT parameters were related to PD-L1 expression in lung cancer. The PET/CT parameters included SUVmax, SUVmean, SUVpeak, SUR, metabolic tumor volume (MTV), and total lesion glycolysis (TLG). These studies included patients with stage I–IV disease, but the studies mentioned did not specifically distinguish the source of the specimens between the primary and metastatic lesions.

For better patient management, in our study, for patients whose biopsy sites were from MT, we collected PET/CT-related parameters from those biopsy sites to ensure sites' consistency between the PD-L1 expression and PET/CT parameters. In this regard, we found that SUVmax, SUR-L, and SUR-BP were associated with PD-L1 expression but not with clinical factors. In PET/CT data, SUR-L had the biggest AUC, which was 0.758. Therefore, our research indicated that the stability of SUR was superior to SUVmax, which was consistent with previous studies (29, 30).

In our study, all patients whose biopsy sites were from MT also had PET parameters from the corresponding MT. To compare with other studies, we also analyzed PET/CT parameters in those 99 patients' PTs with PD-L1 expression (regardless whether the biopsy sites were from PT or MT); the AUC of PT-SUVmax, PT-SUR-L, and PT-SUR-BP was 0.675, 0.696, and 0.683, respectively (not shown). These results were in line with previous studies (22–24, 31). However, it was clear that the PET/CT parameters corresponding to the biopsy sites had greater reference value, which indicated that PET/CT parameters had good correlation with PD-L1 expression. In our group, PET/CT parameters in primary lesions were higher than those in metastatic lesions (not shown). Kaira et al. pointed out that PD-L1 expression was linked to hypoxia-inducible factor alpha (HIF-α) and glucose transporter 1 (GLU1) (32). Hence, our metabolic values might support the idea that PD-L1 expression was lower in MT (12, 13).

Some studies concluded that both PD-L1 expression and PET/CT parameters were predictive factors to survival outcomes (32–36). However, others did not support the conclusion (26, 37–39). In our group, when we did not separate immunotherapy from the other treatments, the survival analysis showed no significant correlation between PD-L1 expression and DFS, as well as PET/CT parameters. Such different results might be related to several factors, such as treatment protocols, tumor types, patients' selection, and stage.

Kudura et al. (40) pointed out that PD-L1 expression and PET/CT parameters were very strong long-term outcome predictors

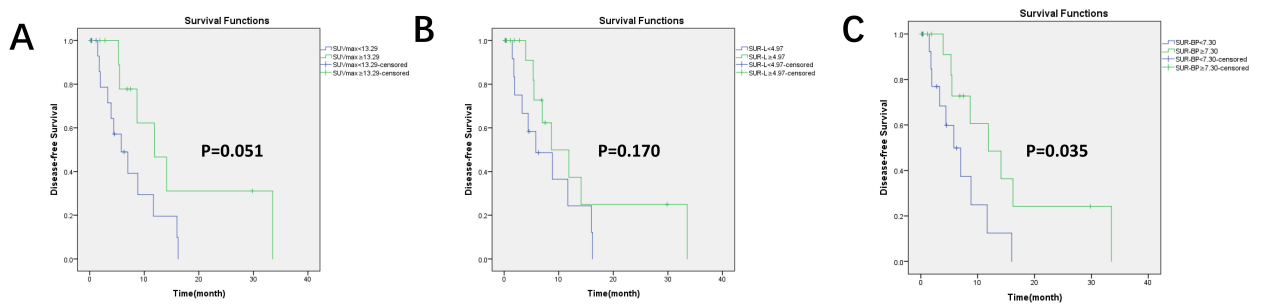

FIGURE 4
Kaplan–Meier survival curves for DFS based on the optimal value of PET/CT parameters in the immunotherapy group. There were 30 patients who received immunotherapy. **(A)** Based on the optimal cutoff value of SUVmax = 13.29, p = 0.051; **(B)** based on the optimal cutoff value of SUR-L = 4.97, p = 0.170; **(C)** based on the optimal cutoff value of SUR-BP = 7.30, p = 0.035; SUR-BP no less than 7.30 had longer DFS.

of patients treated with immunotherapy, while no significant outcome predictors could be found for the cohort with no immunotherapy. To avoid treatments bias, we performed analysis on immunotherapy and other treatments separately. Our results were in line with them. In patients who received immunotherapy as first line, we found that PD-L1 positivity and having a SUR-BP no less than 7.30 had favorable clinical outcomes, which was consistent with previous research (41). What was more important, we were the first to report that SUR-BP was associated with PD-L1 expression and immunotherapy outcomes.

In the immunotherapy subgroup, PET/CT parameters were acquired from both primary and metastatic lesions, ensuring spatial concordance with biopsy sites. In addition, we also analyzed the relationship between the primary lesion PET/CT parameters and prognosis. The *p*-value of PT-SUVmax, PT-SUR-L, and PT-SUR-BP was 0.384, 0.047, and 0.224 by Kaplan–Meier analysis, respectively. The results indicated that PT-SUR-L had a higher reference value for the prognosis of immunotherapy. In our follow-up, positive DFS was due to the progression of the metastatic lesions. This might explain the difference between the two sets of results.

There were some limitations in our study: First, the absence of paired PD-L1 measurements in PT–MT pairs limits our ability to characterize intrapatient heterogeneity. Future studies incorporating multi-site synchronous biopsies are warranted. Second, we only collected DFS without overall survival (OS) and progression-free survival (PFS). If we included these two factors, we could provide more comprehensive prognostic information. Third, as for PET/CT parameters, we lacked MTV and TLG, among other parameters (42, 43). They also had some influence on PD-L1 expression and clinical outcomes. More parameters should be included in future studies in order to obtain more accurate prognostic information. Fourth, our study was single-center, retrospective, and based on a Chinese cohort; thus, the results might have some limitations. Multi-center, prospective, and multi-population studies might yield more authoritative results.

Conclusion

SUVmax, SUR-L, and SUR-BP values were consistent with PD-L1 expression. PD-L1 expression and SUR-BP were related to DFS. In immunotherapy, PET/CT parameters could provide relevant reference values for PD-L1 expression and treatment prognosis, especially SUR-BP.

Data availability statement

The raw data supporting the conclusions of this article will be made available by the authors, without undue reservation.

Ethics statement

The studies involving humans were approved by the Institutional Review Board of Henan Provincial People's Hospital. The studies were conducted in accordance with the local legislation and institutional requirements. Written informed consent for participation in this study was provided by the participants' legal guardians/next of kin.

Author contributions

HJ: Writing – original draft, Funding acquisition. BH: Writing – original draft. JZ: Formal analysis, Methodology, Writing – original draft. YL: Formal analysis, Methodology, Writing – original draft. AX: Project administration, Supervision, Writing – review & editing. XW: Project administration, Supervision, Writing – review & editing. JX: Writing – review & editing. YG: Writing – review & editing, Funding acquisition.

Funding

The author(s) declare that financial support was received for the research and/or publication of this article. This work was supported by the Fund Program of the Science and Technology Research of Henan Provincial Health and Health Commission (SBGJ202102015) and the Program of Henan Provincial Medical Science and Technology Research (LHGJ20220064 and LHGJ20230066).

Conflict of interest

The authors declare that the research was conducted in the absence of any commercial or financial relationships that could be construed as a potential conflict of interest.

Generative AI statement

The author(s) declare that no Generative AI was used in the creation of this manuscript.

Publisher's note

References

1. Fehrenbacher LD, Spira AM, Ballinger MP, Kowanetz MP, Vansteenkiste JP, Mazieres JP, et al. Atezolizumab versus docetaxel for patients with previously treated non-small-cell lung cancer (POPLAR): a multicentre, open-label, phase 2 randomised controlled trial. *Lancet*. (2016) 387:1837–46. doi: 10.1016/S0140-6736(16)00587-0

2. Rittmeyer A, Barlesi F, Waterkamp D, Park K, Ciardiello F, von Pawel J, et al. Atezolizumab versus docetaxel in patients with previously treated non-small-cell lung cancer (OAK): a phase 3, open-label, multicentre randomised controlled trial. *Lancet*. (2017) 389:255–65. doi: 10.1016/S0140-6736(16)32517-X

3. Hellmann MD, Rizvi NA, Goldman JW, Gettinger SN, Borghaei H, Brahmer JR, et al. Nivolumab plus ipilimumab as first-line treatment for advanced non-small-cell lung cancer (CheckMate 012): results of an open-label, phase 1, multicohort study. *Lancet Oncol*. (2017) 18:31–41. doi: 10.1016/S1470-2045(16)30624-6

4. Mok TSK, Wu Y, Kudaba I, Kowalski DM, Cho BC, Turna HZ, et al. Pembrolizumab versus chemotherapy for previously untreated, PD-L1-expressing, locally advanced or metastatic non-small-cell lung cancer (KEYNOTE-042): a randomised, open-label, controlled, phase 3 trial. *Lancet*. (2019) 393:1819–30. doi: 10.1016/S0140-6736(18)32409-7

5. Herbst RS, Baas P, Kim DW, Felip E, Perez-Gracia JL, Han JY, et al. Pembrolizumab versus docetaxel for previously treated, PD-L1-positive, advanced non-small-cell lung cancer (KEYNOTE-010): a randomised controlled trial. *Lancet*. (2016) 387:1540–50. doi: 10.1016/S0140-6736(15)01281-7

6. Topalian SL, Taube JM, Anders RA, Pardoll DM. Mechanism-driven biomarkers to guide immune checkpoint blockade in cancer therapy. *Nat Rev Cancer*. (2016) 16:275–87. doi: 10.1038/nrc.2016.36

7. Diggs LP, Hsueh EC. Utility of PD-L1 immunohistochemistry assays for predicting PD-1/PD-L1 inhibitor response. *Biomarker Res*. (2017) 5. doi: 10.1186/s40364-017-0093-8

8. *TECENTRIQ ® (Atezolizumab)—EMA/234492/2021 EMEA/H/C/004143* (2021).

9. *TECENTRIQ ® (Atezolizumab) Injection, for Intravenous Use Initial U.S. Approval: 2016. Reference ID: 4748227* (2016).

10. Nakamura S, Hayashi K, Imaoka Y, Kitamura Y, Akazawa Y, Tabata K, et al. Intratumoral heterogeneity of programmed cell death ligand-1 expression is common in lung cancer. *PloS One*. (2017) 12:e186192. doi: 10.1371/journal.pone.0186192

11. Takamori S, Toyokawa G, Okamoto I, Takada K, Kozuma Y, Matsubara T, et al. Discrepancy in Programmed Cell Death-Ligand 1 Between Primary and Metastatic Non-small Cell Lung Cancer. *Anticancer Res*. (2017) 37:4223–8. doi: 10.21873/anticanres.11813

12. Mansfield AS, Aubry MC, Moser JC, Harrington SM, Dronca RS, Park SS, et al. Temporal and spatial discordance of programmed cell death-ligand 1 expression and lymphocyte tumor infiltration between paired primary lesions and brain metastases in lung cancer. *Ann Oncol*. (2016) 27:1953–8. doi: 10.1093/annonc/mdw289

13. Zhou J, Gong Z, Jia Q, Wu Y, Yang Z, Zhu B. Programmed death ligand 1 expression and CD8+ tumor-infiltrating lymphocyte density differences between paired primary and brain metastatic lesions in non-small cell lung cancer. *Biochem Bioph Res Co*. (2018) 498:751–7. doi: 10.1016/j.bbrc.2018.03.053

14. Ilie M, Long-Mira E, Bence C, Butori C, Lassalle S, Bouhlel L, et al. Comparative study of the PD-L1 status between surgically resected specimens and matched biopsies of NSCLC patients reveal major discordances: a potential issue for anti-PD-L1 therapeutic strategies. *Ann Oncol*. (2016) 27:147–53. doi: 10.1093/annonc/mdv489

15. Kian W, Roisman LC, Wallach N, Levitas D, Yakobson A, Dudnik Y, et al. Programmed death-ligand 1 expression discrepancy between primary tumor and metastatic lymph nodes in non-small cell lung cancer. *J Thoracic Dis*. (2020) 12:3918–20. doi: 10.21037/jtd.2020.04.45

16. Moutafi MK, Tao W, Huang R, Haberberger J, Alexander B, Ramkissoon S, et al. Comparison of programmed death-ligand 1 protein expression between primary and metastatic lesions in patients with lung cancer. *J ImmunoTherapy Cancer*. (2021) 9:e2230. doi: 10.1136/jitc-2020-002230

17. Liu Y, Dong Z, Jiang T, Hou L, Wu F, Gao G, et al. Heterogeneity of PD-L1 Expression Among the Different Histological Components and Metastatic Lymph Nodes in Patients With Resected Lung Adenosquamous Carcinoma. *Clin Lung Cancer*. (2018) 19:e421–30. doi: 10.1016/j.cllc.2018.02.008

18. Wu J, Sun W, Yang X, Wang H, Liu X, Chi K, et al. Heterogeneity of programmed death-ligand 1 expression and infiltrating lymphocytes in paired resected primary and metastatic non-small cell lung cancer. *Mod Pathol*. (2022) 35:218–27. doi: 10.1038/s41379-021-00903-w

19. Chao Li CHTS, Fan WZYH, Peisha Huang GL. Comparison of 22C3-PD-L1 expression between surgically resected specimens and paired tissue microarrays in non-small cell lung cancer. *J Thorac Oncol*. (2017), 1536–43.

20. Cherry SR, Jones T, Karp JS, Qi J, Moses WW, Badawi RD, et al. Maximizing Sensitivity to Create New Opportunities for Clinical Research and Patient Care. *J Nuclear Med (1978)*. (2018) 59:3–12. doi: 10.2967/jnumed.116.184028

21. Xiao J, Yu H, Sui X, Hu Y, Cao Y, Liu G, et al. Can the BMI-based dose regimen be used to reduce injection activity and to obtain a constant image quality in oncological patients by 18F-FDG total-body PET/CT imaging? *Eur J Nucl Med Mol I*. (2021) 49:269–78. doi: 10.1007/s00259-021-05462-5

22. Hu B, Chen W, Zhang Y, Shi H, Cheng D, Xiu Y. 18F-FDG maximum standard uptake value predicts PD-L1 expression on tumor cells or tumor-infiltrating immune cells in non-small cell lung cancer. *Ann Nucl Med*. (2020). doi: 10.1007/s12149-020-01451-0

23. Hu B, Xiao J, Xiu Y, Fu Z, Shi H, Cheng D. Correlation of PD-L1 expression on tumor cell and tumor infiltrating immune cell with 18F-fluorodeoxyglucose uptake on PET/computed tomography in surgically resected pulmonary adenocarcinoma. *Nucl Med Commun*. (2020) 41:252–9. doi: 10.1097/MNM.0000000000001136

24. Hu B, Jin H, Li X, Wu X, Xu J, Gao Y. The predictive value of total-body PET/CT in non-small cell lung cancer for the PD-L1 high expression. *Front Oncol*. (2022) 12:943933. doi: 10.3389/fonc.2022.943933

25. Yang X, Jiang L, Jin Y, Li P, Hou Y, Yun J, et al. PD-L1 Expression in Chinese Patients with Advanced Non-Small Cell Lung Cancer (NSCLC): A Multi-Center Retrospective Observational Study. *J Cancer*. (2021) 12:7390–8. doi: 10.7150/jca.63003

26. Lopci E, Toschi L, Grizzi F, Rahal D, Olivari L, Castino GF, et al. Correlation of metabolic information on FDG-PET with tissue expression of immune markers in patients with non-small cell lung cancer (NSCLC) who are candidates for upfront surgery. *Eur J Nucl Med Mol I*. (2016) 43:1954–61. doi: 10.1007/s00259-016-3425-2

27. Mitchell KG, Amini B, Wang Y, Carter BW, Godoy MCB, Parra ER, et al. 18F-fluorodeoxyglucose positron emission tomography correlates with tumor immunometabolic phenotypes in resected lung cancer. *Cancer Immunol Immunother*. (2020) 69:1519–34. doi: 10.1007/s00262-020-02560-5

28. Takada K, Toyokawa G, Okamoto T, Baba S, Kozuma Y, Matsubara T, et al. Metabolic characteristics of programmed cell death - ligand 1 - expressing lung cancer on 18F fluorodeoxyglucose positron emission tomography/computed tomography. *Cancer Med*. (2017) 6:2552–61. doi: 10.1002/cam4.1215

29. van den Hoff J, Lougovski A, Schramm G, Maus J, Oehme L, Petr J, et al. Correction of scan time dependence of standard uptake values in oncological PET. *EJNMMI Res*. (2014) 4:18. doi: 10.1186/2191-219X-4-18

30. van den Hoff J, Oehme L, Schramm G, Maus J, Lougovski A, Petr J, et al. The PET-derived tumor-to-blood standard uptake ratio (SUR) is superior to tumor SUV as a surrogate parameter of the metabolic rate of FDG. *EJNMMI Res*. (2013) 3:77. doi: 10.1186/2191-219X-3-77

31. Tien Cong B, Cam Phuong P, Thai P, Thuong V, Quang Hung N, Hang D, et al. Prognostic Significance of PD-L1 Expression and Standardized Uptake Values in the Primary Lesions of Stage IV Adenocarcinoma Lung Cancer. *Front Med*. (2022) 9:895401. doi: 10.3389/fmed.2022.895401

32. Kaira K, Shimizu K, Kitahara S, Yajima T, Atsumi J, Kosaka T, et al. 2-Deoxy-2-[fluorine-18] fluoro-d-glucose uptake on positron emission tomography is associated with programmed death ligand-1 expression in patients with pulmonary adenocarcinoma. *Eur J Cancer*. (2018) 101:181–90. doi: 10.1016/j.ejca.2018.06.022

33. Zhang M, Wang D, Sun Q, Pu H, Wang Y, Zhao S, et al. Prognostic significance of PD-L1 expression and (18)F-FDG PET/CT in surgical pulmonary squamous cell carcinoma. *Oncotarget*. (2017) 8:51630–40. doi: 10.18632/oncotarget.18257

34. Kasahara N, Kaira K, Bao P, Higuchi T, Arisaka Y, Erkhem-Ochir B, et al. Correlation of tumor-related immunity with 18F-FDG-PET in pulmonary squamous-cell carcinoma. *Lung Cancer*. (2018) 119:71–7. doi: 10.1016/j.lungcan.2018.03.001

35. Wang Y, Zhao N, Wu Z, Pan N, Shen X, Liu T, et al. New insight on the correlation of metabolic status on 18F-FDG PET/CT with immune marker expression in patients with non-small cell lung cancer. *Eur J Nucl Med Mol I*. (2020) 47:1127–36. doi: 10.1007/s00259-019-04500-7

36. Grizzi F, Castello A, Qehajaj D, Toschi L, Rossi S, Pistillo D, et al. Independent expression of circulating and tissue levels of PD-L1: correlation of clusters with tumor metabolism and outcome in patients with non-small cell lung cancer. *Cancer Immunol Immunother*. (2019) 68:1537–45. doi: 10.1007/s00262-019-02387-9

37. Kaira K, Higuchi T, Naruse I, Arisaka Y, Tokue A, Altan B, et al. Metabolic activity by 18F– FDG-PET/CT is predictive of early response after nivolumab in previously treated NSCLC. *Eur J Nucl Med Mol I*. (2018) 45:56–66. doi: 10.1007/s00259-017-3806-1

38. Castello A, Grizzi F, Toschi L, Rossi S, Rahal D, Marchesi F, et al. Tumor heterogeneity, hypoxia, and immune markers in surgically resected non-small-cell lung cancer. *Nucl Med Commun*. (2018) 39:636–44. doi: 10.1097/MNM.0000000000000832

39. Malet J, Ancel J, Moubtakir A, Papathanassiou D, Deslée G, Dewolf M. Assessment of the Association between Entropy in PET/CT and Response to Anti-PD-1/PD-L1 Monotherapy in Stage III or IV NSCLC. *Life*. (2023) 13:1051. doi: 10.3390/life13041051

40. Kudura K, Ritz N, Kutzker T, Hoffmann MHK, Templeton AJ, Foerster R, et al. Predictive Value of Baseline FDG-PET/CT for the Durable Response to Immune Checkpoint Inhibition in NSCLC Patients Using the Morphological and Metabolic Features of Primary Tumors. *Cancers*. (2022) 14:6095. doi: 10.3390/cancers14246095

41. Zhang F, Guo W, Zhou B, Wang S, Li N, Qiu B, et al. Three-Year Follow-Up of Neoadjuvant Programmed Cell Death Protein-1 Inhibitor (Sintilimab) in NSCLC. *J Thorac Oncol*. (2022) 17:909–20. doi: 10.1016/j.jtho.2022.04.012

42. Cui Y, Li X, Du B, Diao Y, Li Y. PD-L1 in Lung Adenocarcinoma: Insights into the Role of 18F-FDG PET/CT. *Cancer Manage Res*. (2020) 12:6385–95. doi: 10.2147/CMAR.S256871

43. Yamaguchi O, Kaira K, Hashimoto K, Mouri A, Shiono A, Miura Y, et al. Tumor metabolic volume by 18F-FDG-PET as a prognostic predictor of first-line pembrolizumab for NSCLC patients with PD-L1 ≥ 50%. *Sci Rep-UK*. (2020) 10. doi: 10.1038/s41598-020-71735-y

Frontiers in Oncology

Advances knowledge of carcinogenesis and tumor progression for better treatment and management

The third most-cited oncology journal, which highlights research in carcinogenesis and tumor progression, bridging the gap between basic research and applications to imrpove diagnosis, therapeutics and management strategies.

Discover the latest Research Topics

See more →

Frontiers

Avenue du Tribunal-Fédéral 34
1005 Lausanne, Switzerland
frontiersin.org

Contact us

+41 (0)21 510 17 00
frontiersin.org/about/contact